

# **INAUGRAL DISSERTATION**

Zur Erlangung der Doktorwürde  
Fakultät für Chemie und Geowissenschaften  
Institut für Geowissenschaften  
Ruprecht-Karls-Universität Heidelberg

Vorgelegt von

**Ross A. Elgin**

Tag der mündlichen Prüfung: 19th May 2014

# **Palaeobiology, Morphology, and Flight Characteristics of Pterodactyloid Pterosaurs**

**Ross Alexander Elgin**

---

Gutacher: Prof. Dr. Wolfgang Stinnesbeck

Prof. Dr. Eberhard Frey

# Palaeobiology, Morphology, and Flight Characteristic of Pterodactyloid Pterosaurs

This thesis is submitted to the Faculty of Chemistry and Geological Sciences of the University of Heidelberg for the degree of Doctorate of Philosophy (PhD).

I declare that all the information and data presented in the context of this thesis, except where due acknowledgement has been made, is my own original work.

Ross Alexander Elgin  
20-06-1981

Signed / Unterschrift \_\_\_\_\_

Oral Examination \_\_\_\_\_

This thesis and all work contained herein represent the original work of the author and conforms to all necessary requirements for the degree of Doctor of Philosophy within the Faculty of Chemistry and Geological Sciences, University of Heidelberg.

Primary Supervisor: Prof. Dr. Wolfgang Stinnesbeck  
Department of Geological Sciences  
Faculty of Chemistry and Geological Sciences  
University of Heidelberg  
Germany

Signed / Unterschrift \_\_\_\_\_

Date / Datum \_\_\_\_\_

Place / Ort \_\_\_\_\_

Secondary Supervisor: Prof. Dr. Eberhard Frey  
Department of Geological Sciences  
State Museum of Natural History Karlsruhe  
Erbprinzenstraße 13  
76133, Karlsruhe  
Germany

Signed / Unterschrift \_\_\_\_\_

Date / Datum \_\_\_\_\_

Place / Ort \_\_\_\_\_

## Acknowledgements – Danksagung

I am indebted to both **David Hone** and **Eberhard “Dino” Frey** for the opportunity to undertake this project and continue my work on the enigmatic and curious group of animals known as pterosaurs. Their help and encouragement over the years has been invaluable to this thesis being brought to a close. During the course of this work I have received assistance from a number of diverse sources and also wish to extend my thanks to these individuals. **René Kastner** for all his preparation work on the fossil specimens described herein as well as the construction of numerous models over the years. To several private collectors, most notably **Urs Oberli**, for allowing me to observe the pterosaurian specimens within their care. **Alexander Kellner**, **Taisa Rodrigues** and all the staff at the Museu Nacional (Rio de Janeiro, Brazil), as well as the Museums of Natural History of Stuttgart and Munich for permitting me to study the specimens within their collections.

In addition to these, **Wolf Krüger** and staff at the DLR helped greatly with the aerodynamics section of this work and the production of computer simulations. **Sebastian Rück** and **Torsten Schenkel** from the KIT worked on the CFD simulations of *Coloborhynchus* and were actively involved in the setup and operation of the wind tunnel. **Colin Palmer** for several useful discussions on aerodynamics and **Edina Prondvai** for all her help during my time in Karlsruhe.

To my parents for their encouragement, **Nicole** for the final push, and to **Kim**, for her years of continuous support and understanding, without which this project may never have been realised.

## Funding Declaration

The initial part of this thesis was funded by the Deutsche Forschungsgemeinschaft under the project grants FR1314/15 - 1 & 2 during which time the majority of the experiments detailed within this work were undertaken. Their support in this manner was invaluable to the success of the project.

## **Abstract:**

Several new specimens of pterodactyloid pterosaurs attributed to the Ornithocheiroidea and Azhdarchoidea and housed within the State Museum of Natural History Karlsruhe are described. Knowledge of their anatomy, morphometrics, joint mechanics, and extent of the soft tissue membrane were subsequently used to create models that tested the aerodynamic characteristics of the wing, body and head.

Two specimens are herein erected as holotypes, the ornithocheirid *Barbosania gracilirostris* and the azhdarchoid *Microtuban altivolans*. The former of these, uncovered from the Romualdo member of the Santana Formation of NE Brazil, preserves an unusually advanced state of skeletal fusion where the suture between the extensor tendon process and the proximal articular surface of the first wing finger phalanx is partially closed. The fossil further advances the cause that crestless ornithocheiroids should not be considered as juvenile morphs of pre-established taxa. The second specimen, *Microtuban altivolan* was unearthed from the Upper Cretaceous *Lagerstätten* of northern Lebanon and represents a non-azhdarchoid azhdarchoid displaying unusual proportions between the wing finger phalanges. The hyper reduction without loss of the fourth wing finger phalanx is shown to be more widespread within the Azhdarchoidea. Additional specimens presented here are attributed to the ornithocheirid *Coloborhynchus robustus* and the azhdarchoids *Tapejara wellnhoferi* and cf. *Tupuxuara*.

The “crocodilian-like” sequence of suture closure between the neural arches and vertebral bodies of the thoracic vertebrae is confirmed within the azhdarchoid pterosaurs, indicating that the developmental timing between the Azhdarchoidea and Ornithocheiroidea did not significantly differ. A possible sexual dimorphism, where the pelvic girdle lacks a symphysis and remains open even in large adults is observed within *Coloborhynchus robustus*, while a single preaxial metacarpal is observed to contact the distal carpus with cf *Tupuxuara*, indicating that this feature was widespread within Azhdarchoidea.

The primary flight membrane is reconstructed with an ankle attachment of the trailing edge, a configuration that was never fundamentally altered throughout the evolutionary history of the group. By adopting heavier estimates of mass and increasing wing load, horizontal/vertical flight velocities and circling radii are shown to increase. Maximum range speed for the study

subject *C. robustus* varies between 15 – 21 ms, depending on the methodology, along with maximum L/D ratios of 13-23. Body drag of the small azhdarchoid *Aurorazhdarcho micronyx* is estimated at <0.015 while a CFD analysis of *C. robustus* indicates a coefficient of 0.022 for the large ornithocheiroid. Despite the presence of an often enlarged head, this feature contributes only 13-16% of the total parasite drag coefficient when orientated directed into the flow. Yawing of the head, however, results in increases of up to 20-91% by the relatively low angle of 40°. The crest of *Nyctosaurus gracilis* is found to flutter in low to moderate flow velocities, resulting in higher than expected drag coefficients. While the head and crest are found to influence the aerodynamics of the animal a primarily aerodynamic function is rejected.

## **Zusammenfassung:**

Einige neue Spezies der Pterodactyloid Pterosaurier angehörig der Ornithocheiroidea und Azhdarchoidea, die im staatlichen Naturhistorischen Museum in Karlsruhe untergebracht sind, werden beschrieben. Das Wissen über ihre Anatomie, Morphometrie, Gelenkmechanik und das Ausmaß der Weichteilmembran wurden danach benutzt, um Modelle zu erstellen, mit denen die Charakteristiken der Aerodynamik der Flügel, des Körpers und des Kopfes getestet wurden.

Zwei Spezies, der Ornithocheiroid *Barbosania Gracilirostris* und der Azhdarchoid *Microtuban altivolans* sind hierin als Holotypen aufgerichtet. Letzterer wurde vom Romualdo Member der Santana Formation im Nordosten Brasiliens aufgedeckt und preserviert einen ungewöhnlich fortgeschrittenen Zustand der Skelettfusion, in welcher die Suture zwischen des Strecksehnenprozesses und die proximale Gelenkfläche des ersten Flügelfingergliedes partial geschlossen ist.

Das Fossil zeigt des weiteren, dass der haubenlose Ornithocheiroids nicht zu den jugentlichen Morphen der vorherbestimmten Taxa gezählt werden darf. Die zweite Spezies, *Microtuban altivolans* wurde aus den Oberen Kreidezeitlagerstätten im Norden von Lebanon ausgegraben und repräsentiert einen non-azhdarchid azhdarchoid, der ungewöhnliche Proportionen zwischen den Flügelfingerphalangen vorweist. Die Hyperreduktion ohne den Verlust des vierten Flügelfingergliedes zeigt sich als üblich bei den Azhdarchoidea.

Weitere Spezien, die hier präsentiert werden, sind auf den Ornithocheirid *Coloborhynchus robustus* zurückzuführen, und der Azhdarchoids *Tapejara wellnhoferi* und cf. *Tupuxuara*.

Die Primäre Fliegemembran ist mit einer Knöchelanhaftung der Hinterkante rekonstruiert, eine Konfiguration, die nie fundamental im Laufe der evolutionären Geschichte dieser Gruppe abgeändert wurde. Durch das Adoptieren von schwereren Schätzungen der Masse und steigender Flügelbelastung, zeigen sich horizontale/vertikale Fluggeschwindigkeit und Kreiseradien als erhöht. Der maximale Geschwindigkeitsumfang für das Studiensubjekt *C. robustus* variiert zwischen 15 – 21 ms, davon abhängig welche Methodologie verwendet wird, außerdem mit Maximum L/D Verhältnissen von 13-23.



# Table of Contents

## Chapter 1

|     |  |     |
|-----|--|-----|
| 1.0 | Introduction .....   | 1-2 |
| 1.1 | Aims and Goals .....   | 2   |
| 1.2 | Collections of the State Museum of Natural History Karlsruhe .....             | 4   |
| 1.3 | Note on the status of privately purchased fossils included in this study ..... | 4   |
| 1.4 | Introduction to the Pterosauria .....  | 6   |
| 1.5 | A short note on pterosaur phylogeny and relationships .....                    | 9   |

## Chapter 2

|      |  |       |
|------|--|-------|
| 2.0  | The description of a new specimen of <i>Coloborhynchus robustus</i> (SMNK PAL1133) .....         | 12-13 |
|      | 2.0.1 Introduction .....   | 13    |
|      | 2.0.2 Systematic Palaeontology .....   | 13    |
|      | 2.0.3 Specimen Details .....   | 14    |
|      | 2.0.4 Specimen Description .....   | 14    |
|      | 2.0.5 Discussion of the systematic palaeontology .....   | 49    |
|      | 2.0.6 Discussion of anatomical features .....  | 51    |
| 2.1. | The description of a novel genus and species <i>Barbosania gracilirostris</i> (MHNS/00/85) ..... | 64    |
|      | 2.1.1 Introduction .....   | 64    |
|      | 2.1.2 Systematic Palaeontology .....   | 65    |
|      | 2.1.3 Specimen Details .....   | 66    |
|      | 2.1.4 Specimen Description .....   | 66    |
|      | 2.1.5 Additional Remarks .....   | 66    |
| 2.2. | The description of a new ornithocheirid specimen (SMNK PAL 3854) ...                             | 75    |
|      | 2.2.1 Introduction .....   | 75    |
|      | 2.2.2 Systematic Palaeontology .....   | 75    |
|      | 2.2.3 Specimen Details .....   | 75    |
|      | 2.2.4 Specimen Description .....   | 76    |

## Chapter 3

|     |  |       |
|-----|--|-------|
| 3.0 | Further examination of an indeterminate azhdarchoid specimen (SMNK PAL 3830) ..... | 81-82 |
|     | 3.0.1 Introduction .....   | 82    |
|     | 3.0.2 Systematic Palaeontology .....   | 82    |
|     | 3.0.3 Specimen Details .....   | 82    |
|     | 3.0.4 Specimen Remarks .....   | 83    |
| 3.1 | Description of an indeterminate azhdarchoid (SMNK PAL 3900) .....                  | 87    |
|     | 3.1.1 Introduction .....   | 87    |
|     | 3.1.2 Systematic Palaeontology .....   | 87    |
|     | 3.1.3 Specimen Details .....   | 88    |
|     | 3.1.4 Specimen Description .....   | 88    |
|     | 3.1.5 Additional Remarks .....   | 92    |
| 3.2 | Description of an indeterminate azhdarchoid (SMNK PAL 3985) .....                  | 96    |
|     | 3.2.1 Systematic Palaeontology .....   | 96    |
|     | 3.2.2 Specimen Details .....   | 96    |
|     | 3.2.3 Specimen Remarks .....   | 97    |

|     |   |     |
|-----|---|-----|
| 3.3 | The description of a new specimen of <i>Tapejara wellnhoferi</i> (SMNK PAL 3986) .....          | 99  |
|     | 3.3.1 Introduction .....  | 99  |
|     | 3.3.2 Systematic Palaeontology .....  | 99  |
|     | 3.3.3 Specimen Details .....  | 100 |
|     | 3.3.4 Specimen Description .....  | 100 |
| 3.4 | Description of an indeterminate azhdarchoid (SMNK PAL 6409) .....                               | 102 |
|     | 3.4.1 Introduction .....  | 102 |
|     | 3.4.2 Systematic Palaeontology .....  | 102 |
|     | 3.4.3 Specimen Details .....  | 102 |
|     | 3.4.4 Specimen Description .....  | 102 |
|     | 3.4.5 Additional Remarks .....  | 106 |
| 3.5 | The description of a novel genus and species <i>Microtuban altivolans</i> (SMNK PAL 6595) ..... | 111 |
|     | 3.5.1 Introduction .....  | 111 |
|     | 3.5.2 Systematic Palaeontology .....  | 111 |
|     | 3.5.3 Specimen Details .....  | 112 |
|     | 3.5.4 Specimen Description .....  | 113 |
| 3.6 | The description of a new <i>Tupuxuara</i> –like azhdarchoid .....                               | 116 |
|     | 3.6.1 Introduction .....  | 116 |
|     | 3.6.2 Systematic Palaeontology .....  | 116 |
|     | 3.6.3 Specimen Details .....  | 117 |
|     | 3.6.4 Specimen Description .....  | 117 |
|     | 3.6.5 Specimen Comments .....   | 122 |

## Chapter 4

|     |  |         |
|-----|--|---------|
| 4.0 | Comments and analysis of pterosaurian joint mobility ..... | 134-135 |
| 4.1 | Material and Methods .....                                 | 135     |
| 4.2 | Current limits of joint mobility in pterosaurs .....       | 136     |
| 4.3 | Revised estimates of joint mobility .....                  | 154     |
| 4.4 | Position and mobility of the pteroid .....                 | 158     |

## Chapter 5

|     |  |         |
|-----|--|---------|
| 5.0 | Introduction to the aerodynamics of biological fliers .....    | 164-165 |
|     | 5.0.1 Aerodynamic forces .....                                 | 165     |
|     | 5.0.2 Gliding flight .....                                     | 173     |
|     | 5.0.3 Circling performance .....                               | 176     |
| 5.1 | Introduction to pterosaur aerodynamics and methodologies ..... | 178     |
| 5.2 | Methodologies .....  | 179     |
|     | 5.2.1 Skeletal Reconstruction .....                            | 179     |
|     | 5.2.2 Wing Reconstruction .....                                | 180     |
|     | 5.2.3 Mass Relationships .....                                 | 181     |
|     | 5.2.4 Theoretical Modelling .....                              | 182     |
|     | 5.2.5 Computer based modelling .....                           | 183     |
|     | 5.2.6 Calibration and operation of the wind tunnel .....       | 183     |
|     | 5.2.7 Set up of the mounting bracket .....                     | 184     |
|     | 5.2.8 Set up of the velocity control .....                     | 188     |
|     | 5.2.9 Construction of fixed wing model .....                   | 190     |
|     | 5.2.10 Construction of body casts .....                        | 190     |

|  |     |
|--|-----|
| 5.2.11 Construction of cranial models .....                  | 191 |
| 5.3 Wind tunnel experiments .....                            | 195 |
| 5.3.1 Aerodynamics of the pterosaurian body .....            | 195 |
| 5.3.2 Aerodynamics of cranial models .....                   | 196 |
| 5.3.3 Aerodynamics of fixed wing models .....                | 206 |
| 5.3.4 Discussion .....                                       | 216 |
| 5.3.5 Summary of experimental results .....                  | 219 |
| 5.4 Theoretical simulations .....                            | 221 |
| 5.4.1 Flat plate theoretical performance .....               | 221 |
| 5.4.2 Performance estimates of TORNADO models .....          | 228 |
| 5.4.3 Estimates from previous studies .....                  | 241 |
| 5.4.4 CFD simulation of <i>Coloborhynchus robustus</i> ..... | 245 |
| 5.4.5 Summary of theoretical data .....                      | 255 |
| 5.5 Chapter Summary .....                                    | 258 |
| Concluding Statement   | 261 |
| References   | 264 |
| Appendix   |     |

## Acronyms & Abbreviations:

### Aerodynamics

---

|   |   |
|---|---|
| <b>A</b> , surface area   | <b>M<sup>2</sup></b> , munk's span factor   |
| <b>AR</b> , aspect ratio ( $b^2/A$ )  | <b>M</b> , mass   |
| <b>b</b> , span   | <b>Re</b> , Reynolds number   |
| <b>CD</b> , coefficient of (total) drag   | <b>S</b> , surface area   |
| <b>CD<sub>par</sub></b> , parasite drag coefficient                               | <b>S<sub>w</sub></b> , wetted surface area  |
| <b>CD<sub>pro</sub></b> , profile drag coefficient                                | <b>V</b> , volume   |
| <b>CD<sub>i</sub></b> , induced drag coefficient                                  | <b>V</b> , horizontal velocity (ms)   |
| <b>CL</b> , coefficient of lift   | <b>V<sub>t</sub></b> , horizontal velocity during a turn (ms)                     |
| <b>Cp</b> , contours of the pressure coefficient                                  | <b>V<sub>s</sub></b> , vertical sinking velocity (ms)                             |
| <b>D</b> , drag (total)   | <b>V<sub>st</sub></b> , vertical sinking velocity during a turn (ms)              |
| <b>D<sub>par</sub></b> , parasite drag  | <b>V<sub>ms</sub></b> , horizontal velocity at the point of minimum vertical sink |
| <b>D<sub>pro</sub></b> , profile drag   | <b>α</b> , alpha (angle of attack in degrees)                                     |
| <b>D<sub>i</sub></b> , induced drag   | <b>p</b> , pressure   |
| <b>e</b> , power induced correction factor  | <b>ρ</b> , density of air (1.23)  |
| <b>F</b> , force  | <b>π</b> , pie (i.e. 3.14)  |
| <b>g</b> , gravity  | <b>ε</b> , glide ratio  |
| <b>k</b> , deviation of lift from an ideal elliptical pattern (usually 1.1 – 1.2) |   |
| <b>L</b> , lift   |   |

### Anatomical

---

|                                       |  |   |
|---------------------------------------|--|---|
| <b>act</b> , acetabulum               | <b>dsc</b> , distal syncarpal          | <b>m</b> , maxilla                        |
| <b>acf</b> , actinofibrils            | <b>dt</b> , distal tarsal              | <b>mas</b> , medial articular surface     |
| <b>ast</b> , astragalus               | <b>dtub</b> , distal tubercle          | <b>mc</b> , metacarpal                    |
| <b>av</b> , alveolus                  | <b>epy</b> , epiphysis                 | <b>mdr</b> , medial dorsal ridge          |
| <b>b. tub.</b> , biceps tubercle      | <b>etp</b> , extensor tendon process   | <b>mdt</b> , medial distal tarsal         |
| <b>c</b> , cervical                   | <b>f</b> , frontal                     | <b>mec</b> , medial epicondyles           |
| <b>cap</b> , capitulum                | <b>f</b> , foramina                    | <b>mf</b> , medial flange                 |
| <b>ccrp</b> , cranial carpal          | <b>fcpt</b> , femoral head             | <b>ms</b> , muscle scar                   |
| <b>cd</b> , caudal vertebrae          | <b>fcl</b> , femoral neck              | <b>msa</b> , medial scapular articulation |
| <b>cdcrp</b> , caudal carpal          | <b>fe</b> , femur                      | <b>msc</b> , mandibular sagittal crest    |
| <b>cdfc</b> , caudal facet            | <b>fov</b> , fovea                     | <b>mr</b> , muscle ridge                  |
| <b>cf</b> , cranial facet             | <b>g</b> , groove                      | <b>mr</b> , medial ridge                  |
| <b>cf</b> , coracoid facet            | <b>gb</b> , gastral basket             | <b>mt</b> , metatarsal                    |
| <b>cr</b> , cranium;                  | <b>gl</b> , glenoid                    | <b>n</b> , notarium                       |
| <b>co</b> , coracoid                  | <b>gr</b> , gastral rib                | <b>na</b> , nasal                         |
| <b>cpr</b> , caudal process           | <b>gtr</b> greater trochanter          | <b>naof</b> , nasoantorbital fenestra     |
| <b>cpr</b> , caudal process           | <b>hu</b> , humerus                    | <b>nc</b> , neural canal                  |
| <b>cr</b> , cranial rib               | <b>hcl</b> , humeral collum            | <b>ns</b> , neural spine                  |
| <b>cr</b> , cranial ridge             | <b>hcpt</b> , humeral caput            | <b>ob</b> , obturator foramen             |
| <b>crp</b> , carpus                   | <b>hu</b> , humerus                    | <b>ocd</b> , occipital condyle            |
| <b>crp</b> , carpus                   | <b>hl</b> , hind limb                  | <b>op</b> , opisthotic                    |
| <b>cs</b> , cristospine               | <b>hyp</b> , hypapophysis              | <b>or</b> , orbit                         |
| <b>cty</b> , cotyle                   | <b>ics</b> , inter condular sulcus     | <b>p</b> , process                        |
| <b>d</b> , dorsal                     | <b>il</b> , ilium                      | <b>p</b> , parietal                       |
| <b>dXpX</b> , digit X phalanx X       | <b>isc</b> , ischium                   | <b>part</b> , proximal articulation       |
| <b>das</b> , dorsal articular surface | <b>j</b> , jugal                       | <b>pac</b> , preaxial carpal              |
| <b>dcrp</b> , dorsal carpal           | <b>la</b> , lacrimal                   | <b>pact</b> , postacetabular process      |
| <b>dcty</b> , dorsal cotyle           | <b>las</b> , lateral articular surface | <b>pas</b> , preaxial carpal art surface  |
| <b>dp</b> , diapophysis               | <b>lec</b> , lateral epicondyles       | <b>pf</b> , pneumatic foramen             |
| <b>dp</b> , deltopectoral process     | <b>ld</b> , left dentary               | <b>pg</b> , pelvic girdle                 |
| <b>dp</b> , depression                | <b>ltr</b> , lesser trochanter         | <b>pm</b> , premaxilla                    |
| <b>dpc</b> , deltopectoral crest      | <b>m</b> , mandible                    |   |

**postzy**, postzygapophyses  
**pp**, parapophysis  
**pr**, position of radius  
**pre**, pre-exapophysis  
**prezy**, prezygapophysis  
**psc**, proximal syncarpal  
**dsc**, distal syncarpal  
**pt**, pteroid  
**pu**, pubis  
**postzy**, postzygapophyses  
**q**, quadrate  
**r**, ridge  
**rap**, right articular process  
**rb**, ribs  
**rd**, radius  
**s**, sacral

**s**, suture  
**sa**, sacral articulation  
**sac**, sacral  
**sca**, sternal articulation  
**sc**, scapulocoracoid  
**scp**, scapula  
**scr**, sclerotic ring  
**scp**, scapula  
**ses**, sesamoid  
**sf**, sacular furrow  
**snp**, supraneural plate  
**soc**, supraoccipital crest  
**sp**, sternal plate  
**sq**, squamosal  
**ss**, sagittal sulcus  
**sr**, sacral rib

**st**, soft tissue  
**sut**, suture  
**sy**, symphysis  
**tub**, tubercle  
**ti**, tibia  
**tp**, transverse process  
**tro**, trochlea  
**tub**, tubercle  
**wph**, wing finger phalanx  
**ul**, ulna  
**vas**, ventral articular surface  
**vc**, ventral condyle  
**vcty**, ventral cotyle  
**vf**, ventral flange  
**vmr**, ventral medial ridge

## Institutional

---

**AMNH**, American Museum for Natural History, New York, USA.  
**BMNH**, British Museum of Natural History, London, UK.  
**BPM**, Beipaio Paleontological Museum, Beipaio, China.  
**BSP**, Bayerische Staatssammlung für Paläontologie und Geologie, Munich, Germany.  
**DGM**, Department of Geology and Paleontology, Museu Nacional, Rio de Janeiro, Brazil.  
**DLR**, German Centre for Flight and Space Travel, Göttingen, Germany.  
**FHSM**, Fort Hays State Museum, Fort Hays State University, Hays, Kansas, USA. **FMNH**, Field Museum of Natural History, Chicago, USA.  
**GMV**, Geological Museum of Nanjing, Nanjing, China.  
**IMCF**, Iwaki Coal and Fossil Museum, Japan.  
**IVPP**, Institute of Vertebrate Palaeontology and Palaeoanthropology, Beijing, China.  
**JME**, Jura Museum Eichstätt, Eichstätt, Germany.  
**JSE**, Jura Museum, Eichstätt, Germany;  
**MCSNB**, Museo Civico di Scienze Naturali Bergamo, Bergamo, Italy.  
**MCT**, Museu de Ciências da Terra of the Departamento Nacional de Produção Mineral, Rio de Janeiro, Brazil.

**MN**, Museu Nacional, Rio de Janeiro, Brazil.  
**MNHS**, Museum of Natural History, Sintra, Portugal.  
**NHMW**, Natural History Museum of Vienna, Vienna, Austria.  
**NSM**, National Science Museum, Tokyo, Japan.  
**KUVP**, Museum of Natural History, University of Kansas, USA.  
**KIT**, Karlsruhe Institute of Technology, Karlsruhe, Germany;  
**KPM-NH**, Kanagawa Prefectural Museum of Natural History, Japan;  
**PIN**, Palaeontological Institute, Moscow, Russia.  
**RGM**, Rijksmuseum van Geologie en Mineralogie, Nationaal Natuurhistorisch Museum, Leiden, Netherlands.  
**SMNK**, State Museum of Natural History Karlsruhe, Karlsruhe, Germany.  
**TMM**, Texas Memorial Museum, University of Texas, Austin, USA.  
**TMP**, Tyrrell Museum of Palaeontology, Drumheller, Canada.  
**TTU**, Texas Tech University, Texas, USA;  
**YH**, Yizhou Museum, Yixian, Liaoning Province, China.  
**YPM**, Yale Peabody Museum, Yale University, New Haven, USA.

## Chapter 1

---

### INTRODUCTION

## **1.0. Introduction**

This body of work, presented as the culmination of several projects undertaken within the frame of Doctorate of Philosophy, focuses on the anatomy and palaeontological inferences of the Pterosauria, an extinct group of volant archosauromorphs that ruled the Mesozoic skies between the Middle / Late Triassic and the latest part of the Cretaceous.

The thesis focuses specifically on a large collection of undescribed Cretaceous pterosaurs that have been amassed by the Staatliches Museum für Naturkunde Karlsruhe (SMNK), due to the presence of both new genera and species, as well as the numerous palaeontological insights that they provide. These fossils are restricted taxonomically to two well known divisions of the Pterosauria, the Ornithocheiroidea and Azhdarchoidea (e.g. Unwin 2003; Lü et al. 2009).

Further to this, interdisciplinary collaborations with the Karlsruher Institut für Technologie (KIT, German Institute of Technology) and the Deutsches Zentrum für Luft und Raumfahrt (DLR, German Centre for Flight and Space Travel) permit the aerodynamic and flight capabilities of individual animals to be assessed based, in part, on the *bauplan* and joint mechanics of those specimens described herein. With these broader considerations in mind, several specific aims are proposed to be investigated herein, further increasing our knowledge of the palaeobiology, morphology, and flight characteristics of this unique group of flying reptiles.

## **1.1. Aims and Goals**

The primary goals of this thesis are divided between two major lines of investigation, firstly those of an anatomical and palaeontological theme, and secondly those of an aerodynamic nature. These two themes are intended to complement one another where a better understanding of the pterosaurian *bauplan*, the extent and shape of the wing membranes, scaling relationships, and joint mobility will allow the construction of the physical, digital, and mathematical models required for any subsequent aerodynamic assessment. The alteration of key variables in the experimental models,

in addition to adopting multiple lines of investigation is considered to provide a robust means of assessing the likely aerodynamic performance within the study taxa. Likewise this information will allow a better understanding of the palaeobiology and evolution of pterosaurian skeleton.

The principal aims proposed for this work are:

**Anatomical / Palaeontological Aims:**

- i) The description and taxonomic identification of several new specimens of Cretaceous pterodactyls.
- ii) Identification of the morphological and palaeontological inferences that such specimens provide, and their significance within a modern palaeontological context.
- iii) Determination of the long bone morphometric relationships between divisions of the Pterosauria.
- iv) Determination of joint mechanics and available degrees of freedom.

**Aerodynamic Aims:**

- v) Reconstruction of the pterosaurian *bauplan* and wing shape.
- vi) Estimation of aerodynamic performance in pterodactyl pterosaurs. These are to be established based on three methodologies: mathematical theory, computer simulations, and wind tunnel modelling.
- vii) Comparison between various methodologies to establish the most likely aerodynamic characteristics of each study taxon.



## **1.2. Collections of the State Museum of Natural History Karlsruhe.**

The Museum of Natural History Karlsruhe lies in the south-western province of Baden-Württemberg and represents one of major museums of palaeontological interest in Germany – where specialist collections contain Tertiary birds and crocodiles, Pleistocene mammals, Permian tetrapods, and fishes of various Periods. In addition to these, and of direct relevance to this project, it also holds one of the largest collections of pterosaurs in Western Europe and arguably the largest publicly accessible collections of Cretaceous pterodactyls from the Chapada do Araripe in NE Brazil; a region famous for the exceptional preservation of these, and other animals (Unwin and Martill 2007). The large numbers of specimens that at the time of writing lacked any full or proper description was one of the major influences in the creation of this body of work, creating a catalogue of fossils that increase our understanding of this enigmatic group and permitting ready access to photographs and descriptions for future workers – much as has been achieved for other collections (e.g. Veldmeijer 2006).

Material housed in these collections are assigned the pre-fix SMNK, for “Staatliches Museum für Naturkunde Karlsruhe,” followed by “PAL” where they belong within the palaeontological section of the museum. The museum is state owned rather than privately backed, and has a long and proud history of over 200 years of open public access. As such all specimens described within the context of this body of work are available for study and further evaluation through the curator of the Department of Earth Sciences. Further information may be found on the museum website in English, German, and Spanish at [www.smnk.de/](http://www.smnk.de/)

## **1.3. Note on the status of privately purchased fossil included in this study.**

While the SMNK conducts large amounts of fieldwork worldwide, a substantial number of specimens stem from private collectors who sell fossils directly to the museum. As all of the specimens described within this thesis were sourced in such a

way, primarily from Brazil which legislates against such practices, a brief foreword is required to cover this often controversial practice.

The collection of fossils for commercial sale has a very long history and has inevitably lead to a number of important specimens and discoveries that would otherwise gone unheeded. Furthermore with museum budgets under pressure and staff otherwise engaged, academic excursions dedicated to the collection and discover of new material are limited in both their time and scope, meaning that commercial quarrying can be seen as a positive means to offset these limitations – in addition to providing education and an addition source of wealth for those involved with the initial collections.

Many others, however, have highlighted the problems associated with commercial quarrying whereby locality data is unreliable (and often purposefully absent or incorrect), sites can be irreversibly damaged, and many museum and institutions can be out priced for scientifically valuable by private collectors – the specimens often disappearing from the academic community for generations at a time. Perhaps the most vocal critics of commercial fossil collecting also point out that greater rewards can be obtained by moving material unearthed in one country to another, leading to the development of an illicit trade in fossil material, as many countries restrict ownership of what they regard as “cultural patrimony” (Yates and Elgin 2013).

This latter point is directly relevant to the pterosaurs purchased by SMNK, as Brazil has banned the commercial sale of all fossil originating from its territories since 1942. In spite of this large numbers of fossils continue to make their way to the USA and Western Europe where they end up in public or private institutions. Although successive articles of legislation from UNSECO have attempted to address such problems, the current legal framework is weak as individual countries differ on their interpretation of fossil rights, legal consequences, and is the legislation itself remains non-binding. While one legislative article may offer some form of compensation, see UNIDROIT (1995), this has been criticised by Palmer (2000) and furthermore Germany is not one of the current signatories. As such current UNESCO guidelines indicate that Brazil (as the injured party) must prove that any specimen described herein was excavated from its soil post 1942 before it may be deemed to have been

illicitly smuggled – an impossible task as such specimens are provided with little documentation that would permit this to be determined. It also remains a matter of great debate within the scientific community as to whether fossils can, or indeed should, be regarded as the “cultural patrimony” of any state, given that they predate the evolution of human race by a considerable margin, but this is beyond the scope of this thesis. What is clear, however, is that national and international legislation governing palaeontological specimens require some degree of change to better reflect the modern world, and effectively decouple them from the archaeological practices to which they are often bound (Yates and Elgin 2013).

These considerations in mind, the pterosaurs described within this body of work are presented for the good of the scientific community. While discouraging illicit trafficking is to be encouraged, the fact that the featured specimens are interred within a registered museum, rather than ending up within a private institution as would have certainly been their fate otherwise, guarantees the continued and universal access to any and all persons, to the benefit of the international community.

#### **1.4. Introduction to the Pterosauria.**

The pterosaurs (“*ptero*” – wing, “*saur*” – reptile) are a volant group of archosauromorph reptiles that represent an important transition within the vertebrate fossil record. These animals were the first vertebrates to evolve an active system of powered flight and, based on fossil finds, ruled the Mesozoic skies for at a minimum of 45 Million Years prior to the evolution of the first paravians. Despite the lack of specimens the Pterosaurian lineage must have extended back to the earliest part of the Triassic, prior to their split with the Dinosauria, giving them an evolutionary range that approached 180 Million years – reaching its maxima during the Late Jurassic and Early Cretaceous (Wellnhofer 1991a; Barrett et al. 2008; Lockley et al. 2008) and terminating at close of the Cretaceous (Maastrichtian). During this period the pterosaurs achieved an almost worldwide distribution (Wellnhofer 1991a; Barrett et al. 2008) and diversified into a wide range of piscivorous (Wellnhofer 1991a; Unwin 2005; Kellner and Campos 2002; Veldmeijer et al. 2007) and insectivorous (Döderlein 1923; Wellnhofer 1975, 1991a; Bennett 2007a) taxa, with rarer examples

indicating that hard shelled organisms (Wellnhofer 1991a), small vertebrates (Witton and Naish 2008), and filtered prey were also captured (Codorniu et al. 2013).

The aerial performance of these animals has traditionally been regarded as exceptional, with even the largest individuals capable of slow stable flight, low sinking speeds, and capable of performing exceedingly tight turns relative to other animals of their size (Bramwell and Whitfield 1974; Brower 1981, 1983; Chatterjee and Templin 2004). As such pterosaurs have been inferred to spend much of their life travelling and feeding on the wing by snatching prey from the surface water (Veldmeijer et al. 2006).

Despite the lack of fossil material from the Middle to Early Triassic, even the most basal taxa are known to possess fully developed and functioning wings (Wild 1984a, b; Dalla Vecchia 2003; Wellnhofer 2003; Stecher 2008) indicating that flight, or an efficient method of gliding, must have evolved at a very early point within the lineage and predates their earliest occurrence within the fossil record. Indeed, all specimens are known to display numerous adaptations to a volant lifestyle (Figure 1.1), with notable features include the elongation of the first four phalanges of the fourth digit in the manus to form the distal wing spar, the presence of three distinct membranes that acted as the flight surfaces (Frey et al. 2003a), a well developed brain for sensory processing (Witmer et al. 2003; Eck et al. 2011), hollow long bones with paper thin cortices (Elgin and Hone 2013), and an invasive pneumatic system that became increasingly extensive in more derived genera (Claessens et al. 2009; Eck et al. 2011). At no point within the lineage was flight abandoned in favour of terrestrial locomotion as in the case for a number of birds, and instead derived pterosaurs became the largest flying animals of all time, with wing spans up to and likely in excess of 10 m (Lawson 1975). Although the flight capabilities of the largest of these has been questioned (Sato et al. 2009; Henderson 2010), even medium sized pterosaurs from the Cretaceous achieved wing spans well in excess of 5 m by late adulthood (Bennett 2001a, b; Kellner et al. 2013).

The appearance of these larger species throughout the Cretaceous, replacing the pre-existing fauna of typically small (< 2 m) species known from the Triassic and Jurassic has been demonstrated to conform to the criteria of Cope's Rule (Hone and Benton

2007). The result of such a trend, culminating in a low diversity of exceedingly large Late Cretaceous taxa, when contrasted against the wide diversity of taxa known from the Jurassic and Early Cretaceous (Wellnhofer 1991a,b; Wang et al. 2005; Unwin and Martill 2007), indicates that pterosaurs were already in steep decline by the terminal Cretaceous (Unwin 1987) – becoming extinct along with majority of other large bodied animals abruptly at the K-T boundary 65 Million year ago. Although fragmentary bones of pterosaurs have been unearthed from Tertiary deposits of the south of England, all are known to have been reworked from older Cretaceous aged sediments (Unwin 2001).

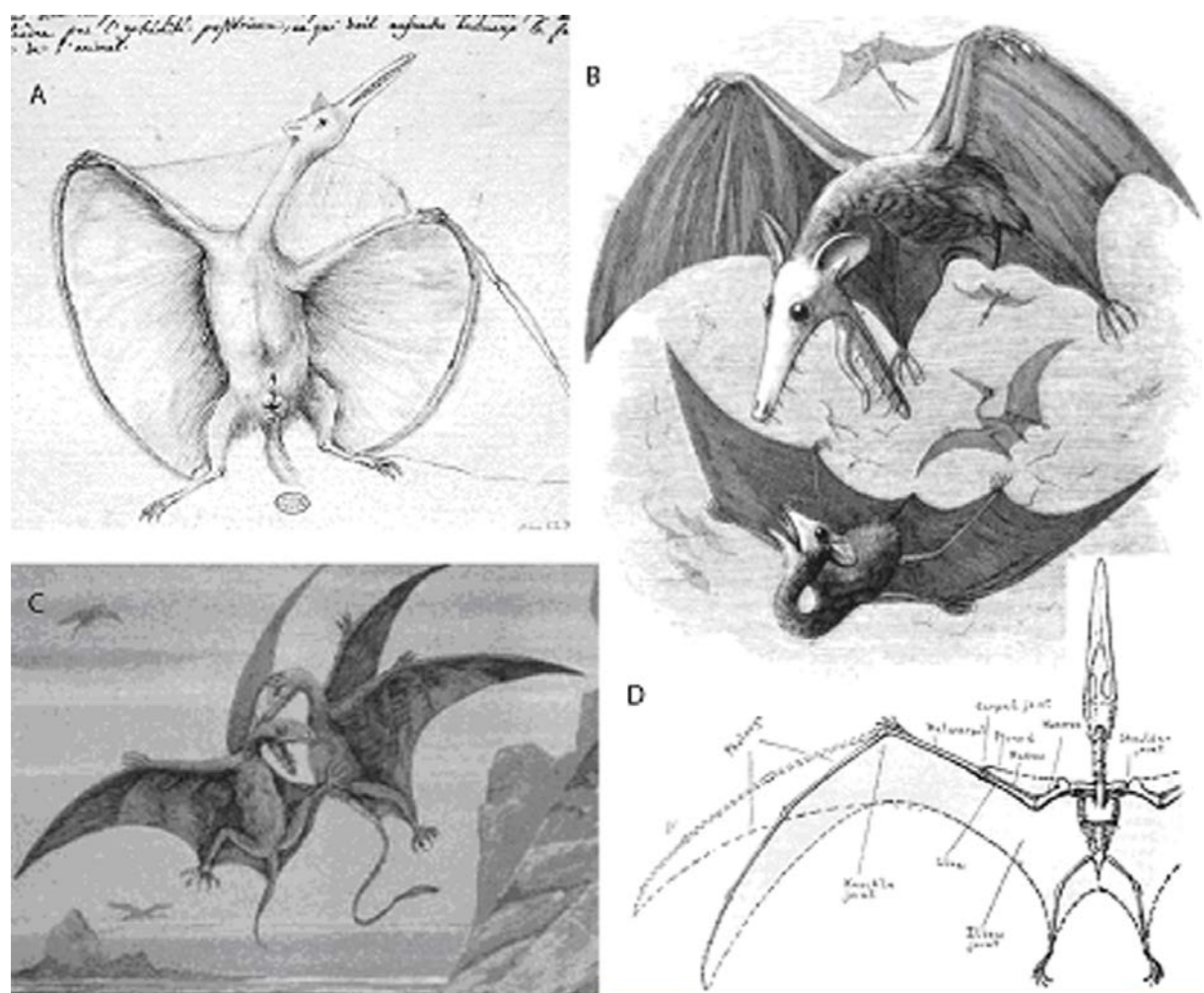


Figure 1.1. - Pterosaur reconstructions over the years. A, the earliest restoration from 1800 (see Taquet and Padian 2004) emphasising its supposed mammalian character; B, restoration of several pterosaurs from Seeley (1901), appearing very bat-like in character; C, two non-pterodactyloid pterosaurs also displaying a “bat-like” character to their anatomy and movement; D, a substantially more accurate reconstruction of a pterosaur (*Pteranodon*) by Marsh with the flight membrane extending down to the ankle.

## 1.5. A short note on pterosaur phylogeny and relationships.

The position of the Pterosauria within the vertebrate tree is complicated by the derived state of skeletal characters observed within Upper Triassic pterosaurs (i.e. *Eudimorphodon*, Wild 1973, 1978, 1984a; Wellnhofer 2003; *Peteinosaurus*, Wild 1984b; *Preondactylus*, Dalla Vecchia 1997; *Raeticodactylus*, Stecher 2008). Consequently even the earliest known animals possessed a highly modified skeleton for the dual purpose of terrestrial locomotion and flapping flight, resulting in few anatomical clues to their immediate ancestors. Despite initial arguments that pterosaurs represented a marine creature (Collini 1784), a type of bat (von Sömmering 1812), or an intermediate form between mammals and birds, it was Cuvier (1809) who recognised their reptilian nature and erected the term “*Ptero-dactyle*” to accommodate the original fossil of Collini (1784). Subsequent studies and cladistic analyses have supported pterosaurs as archosauromorph reptiles and as such are included with the ornithodirans (Padian 1984; Gauthier 1986; Sereno 1991; Benton 1999; Irmis et al. 2007; Hone and Benton 2007; Padian 2008; Andres et al. 2010); a group containing the Pterosauria, *Scleromochlus*, Dinosauria, and all their more recent decedents (see Padian 2008, Figure 1.2).

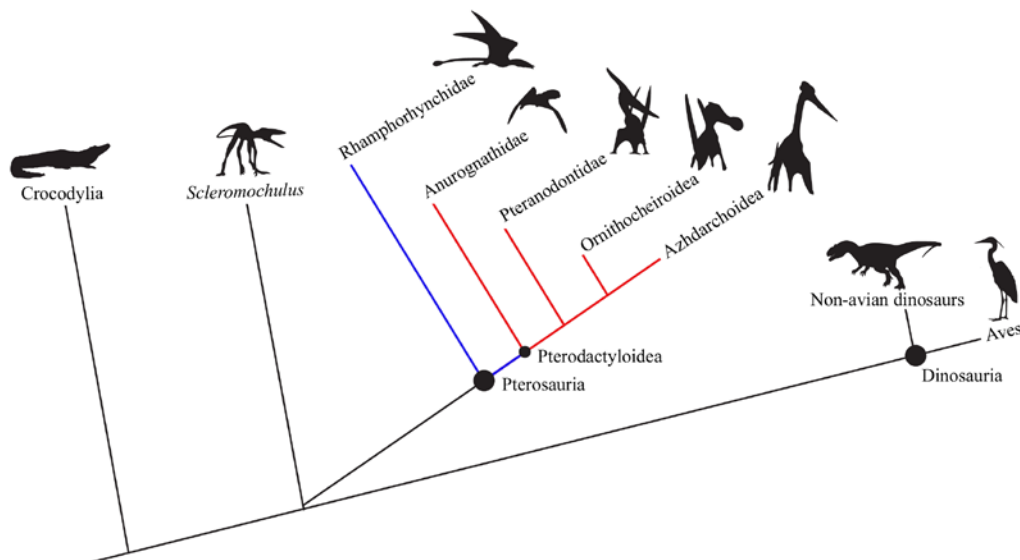


Figure 1.2. – Selected divisions of the Pterosauria and their potential relationship to other archosauromorph reptiles. The Pterosauria is divided into two major groups, the more basal non-pterodactyloids (blue lines), and the more derived pterodactyloid pterosaurs (red lines). Modified from Padian 2008.

Although alternative hypotheses exist, where pterosaurs have been suggested to have originated within the Prolacertiformes (Peters 2000), this has generated little support (see Hone and Benton 2007) and an ornithodiran placement is adopted for the remainder of this thesis.

The Pterosauria itself is a monophyletic group divided between a basal, paraphyletic group of non-pterodactyloids taxa (i.e. “Rhamphorhynchoidea”) and a derived group of short-tailed animals, the Pterodactyloidea. The discovery of *Darwinopterus modularis* (Lü et al. 2009), an animal intermediate between the two traditional divisions by possessing a combination of pterodactyloid and non-pterodactyloid characteristics including an elongate caudal series and single nasoantorbital fenestra, further divides the Pterosauria into monofenestratid (i.e. Pterodactyloidea + *Darwinopterus*) and the non-monofenestratid taxa (i.e. pterosaurs that do not possess a nasoantorbital fenestra). Although the major divisions within the Pterosauria have been identified through successive cladistic studies (e.g. Andres and Ji 2008; Andres et al. 2010; Bennett 1989, 1994; Kellner 1995, 1996a, 2003, 2004a; Lü and Ji 2006; Lü et al. 2006a, b, 2009; Unwin 1995, 2003; Wang and Zhou 2006; Wang et al. 2008, 2009), continued debate on the taxonomic position and content of these has resulted in an abundance of somewhat contradictory phylogenies within the published literature (Figure 1.3.). As this work neither investigates nor attempts to fundamentally alter the established phylogeny I will follow that laid out by Lü et al. (2009) and adopt the terms Ornithocheiroidea and Ornithocheiridae *sensu* Unwin (2003). While I accept that other studies utilise these specific divisions to cover a different selection of taxa (e.g. Kellner 2003) the major conclusions of this work are not altered by the use of a conflicting phylogeny.

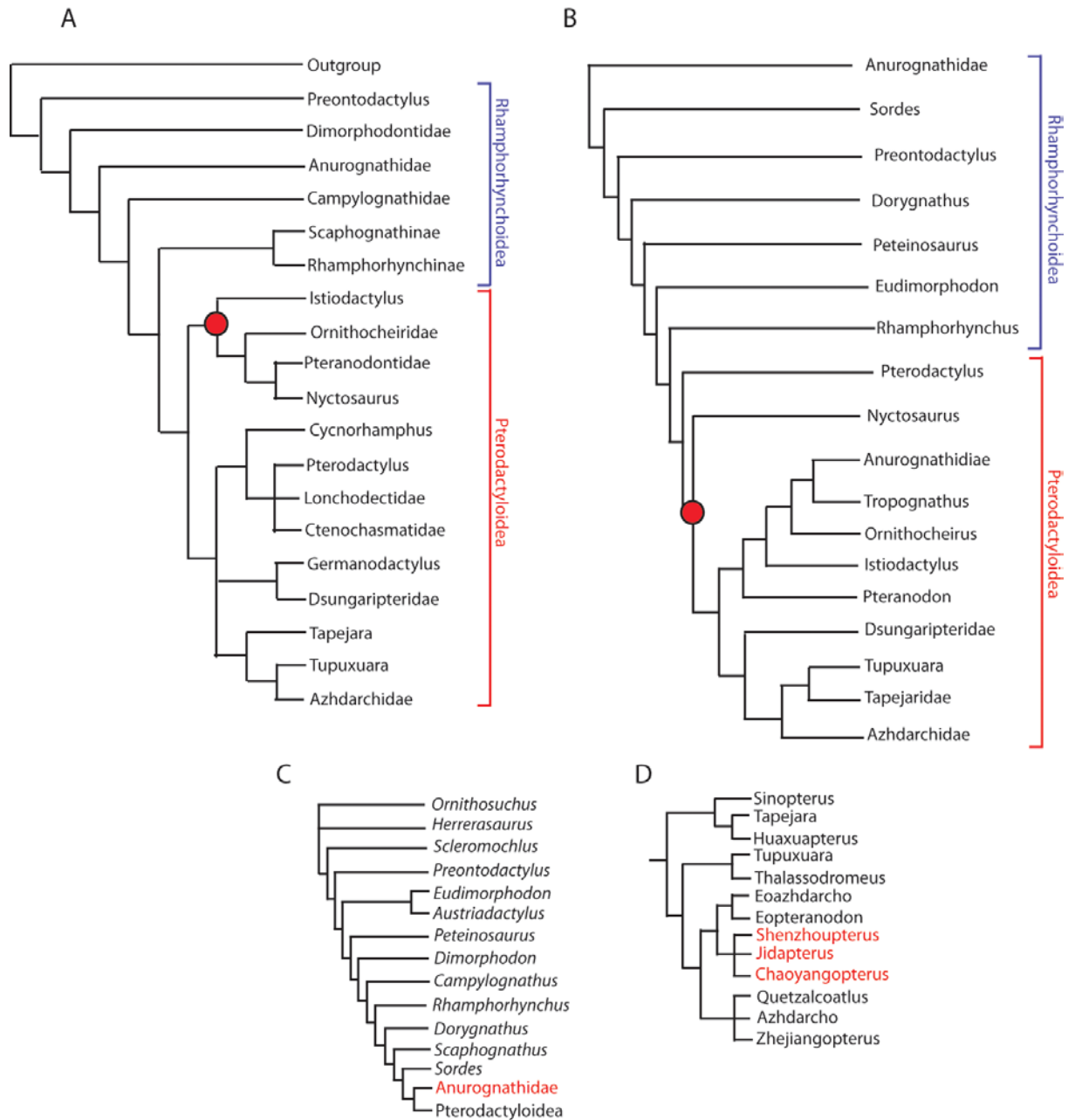


Figure 1.3. - Various phylogenies depicting the relationships between the pterosaurs. A, Unwin (2003), with the circle representing the Ornithocheiroidea (*sensu* Unwin 2003); B, Kellner (2003), circle representing the Ornithocheiroidea (*sensu* Kellner 2003); C, Andres et al. (2010), noting the more derived position of the Anurognathidae; D, Lü et al. (2008), detailing the relationships of the Azhdarchoidea.



## Chapter 2

---

### DESCRIPTIVE PALAEOLOGY OF THE ORNITHOCHIRIDAE

## **2.0. The description of a new specimen of *Coloborhynchus robustus* (SMNK PAL 1133).**

### **2.0.1 Introduction**

A near complete ornithocheiroid represents one of the most extensively preserved skeleton of these large pterodactyloids, matching those of other exceptional specimens known from the same region in NE Brazil (e.g. RGM 401880, Veldmeijer 2003; NSM-PV 19892, Kellner and Tomida 2000) but lacks the majority of the skull. The large number of postcranial elements and excellent three dimensional state of the bones permitted Wilkinson (2008) to reconstruct the joint mobility of the Ornithocheiridae, allowing a good comparison between these animals and *Pteranodon* (from which large amounts of good three dimensional material is known). In spite of this, the specimen lacks a formal and detailed description of its anatomy. It is therefore described as a new specimen of the ornithocheirid *Coloborhynchus robustus* (Wellnhofer 1987; Fastnacht 2001), by far the most complete skeleton of this species known to date, and is compared with other allied species from the Romualdo Member, Chapada do Araripe, NE Brazil..

### **2.0.2 Systematic Palaeontology**

Order Pterosauria Kaup 1834

Superfamily Ornithocheiroidea Seeley 1870

Family Ornithocheiridae Seeley 1870

Genus *Coloborhynchus* Owen 1874

**Diagnosis** (after Fastnacht 2001) - Median depression on the anterior margin of the upper jaw. Flattened anterior margin of the premaxilla triangular. Pair of teeth projecting anteriorly from the blunt anterior margin of the upper jaw at a significant elevation above the palate relative to subsequent teeth. Medial crest on upper jaw rises from the tip of the snout. Upper jaw laterally expanded in a spoon-shape in dorsal view from the second to the fourth pair of alveoli. Lower jaw with medial crest rising from its anterior end. Lower jaw laterally expanded in a spoon-shape from the first to

the third pair of alveoli. Second and third pair of alveoli of the upper and lower jaw enlarged relative to other alveoli.

*Tropeognathus robustus* Wellnhofer 1987

*Anhanguera robustus* Kellner 1989

*Coloborhynchus robustus* Fastnacht 2001

**Included Material** - BSP 1987 I 47 (Holotype), SMNK PAL 2303 (Paratype), SMNK PAL 1133.

**Diagnosis** (after Fastnacht 2001) - Facies rostralis anterior of upper jaw wider than high. Depressus medianus of facies rostralis anterior of the upper jaw triangular. Sagittal crest of the upper jaw rising with a straight dorsal crista from the anterior end of the jaw. Second pair of alveoli of the upper jaw projecting anteroventrally.

### **2.0.3 Specimen details**

**Collection number of the described specimen** - SMNK PAL 1133

**History & Locality Information** - The specimen originates from the Chapada do Araripe, NE of Brazil, and was purchased by the museum from a private collector. The specimen is inferred as being unearthed from the Romualdo Member (Albian, Lower Cretaceous) based on the excellent condition of the skeleton and the original concretions that surrounded these elements. No additional locality information is possible to provide.

**Preservation** - The described specimen is primarily represented by postcranial elements covering almost the entire skeleton. These bones are preserved in three dimensions with no noticeable crushing or distortion. Many elements are damaged and have been extensively repaired with white plaster of Paris.

### **2.0.4 Specimen Description**

**Cranial elements** – A partially complete, tri-radiate bone, interpreted as the caudal portion of the jugal is the only part of the skull preserved (Figure 2.1). The three radiations of the bone are very thin and blade-like in cross-section, representing the cranio- and caudoventral margins of the orbita and the lower temporal fenestra respectively. In lateral view the middle radiation is broadest, while the most cranially preserved radiation curves sharply medially and appears to terminate in an expanded concave articular surface. In cross-section the long axes of the most cranial and caudally preserved branches are offset at an angle of just less than 90°.

**Mandible** – The partial mandible is well preserved in three dimensions but is missing the left ramus and has suffered some damage to the rostral tip (Figure 2.2). The rostral tip, left ramus, and the caudal portion of the right dentary have all been restored with white plaster of Paris. Only one set of alveoli is thought to be missing due to the damage to the rostrum (see discussion). Further damage has occurred on the left flank of the bone, level with the start of the rostral expansion. All the alveoli in this localised region are missing.

The right dentary is elongate in its lateral aspect, the dorsoventral height does not taper and remains relatively constant for the entire length of the bone (i.e. 35 mm). Only a slight increase in height of up to 39 mm is observed immediately rostral to the symphysis. The right ramus is directed 16° against the midline of the mandible and has fused to the remaining part of the left ramus, creating a symphysis 40 mm in width. The total length between the start of the symphysis and the rostral termination is 250 mm. The dorsal face of the dentary is dominated by a large sagittal sulcus, situated between two large medial ridges, and tapers rostrally. The sulcus begins 9 mm rostral to the symphysis and terminates on the rostral expansion, the exact position of which is not visible due to the damage to the left side of the dentary. A large median sagittal crest begins ventral to the position of the 9<sup>th</sup> visible alveoli (i.e. 10<sup>th</sup> tooth socket) and although its true extent is not visible due to the damage of the rostroventral margin, it likely extended to the rostral tip of the dentary. The crest is sub-triangular in cross-section.

Seventeen tooth sockets are observed on the right dentary with thirteen of these positioned rostral to the symphysis. These are positioned dorsolaterally on the lateral

flank of the medial dentary ridge and are oval in shape, their long axes directed rostromedially. The 4<sup>th</sup> visible alveolus is the smallest and marks the beginning of a slight rostral expansion. This is interpreted as the 5<sup>th</sup> tooth socket.

A large adductor fossa is partially preserved on the medial side of the right dentary at the caudal termination of the bone.

**Cervical vertebrae** – Two vertebrae of the cervical column are present but have been partially repaired with plaster. The first of these has had the tip of the neural spine and the right postzygapophyses restored, while the second is missing the entire corpus and the non-articular section of the right prezygapophysis.

The first vertebra described here belongs to the middle portion of the cervical column and is regarded as the 6<sup>th</sup> cervical owing to its long and low profile, where the central body is approximately 2.3 times longer than it is wide (Figure 2.3). The prezygapophyses are directed laterally between 56 - 59° to the sagittal plane and in lateral view are located slightly ventral to the level of the postzygapophyses. The ventral margin of the corpus is sigmoidal in lateral view due to the development of a pronounced hypapophysis on the anteroventral margin of the vertebral body (Figure 2.3B & C). The lateral flank of the vertebra is occupied by a single large oval foramen approximately half way along its length. The postexapophyses are large and directed ventrolaterally in cranial view. The neural canal is small and sub-circular in outline.

The remaining vertebra is that of the 8<sup>th</sup> cervical due to the presence of a tall neural spine, and widely splayed branches of the prezygapophyses. Further to this it articulates perfectly with the ninth cervical which itself is incorporated into the notarium. The 8<sup>th</sup> cervical is large and robust, where the body is squatter than the more cranially positioned cervicals, the centrum being 1.5 times as long as it is wide. The cranial branches of the bone are widely splayed at an angle of 54° in dorsal view and therefore similar to those described above, however, in the 8<sup>th</sup> cervical they are more elongate, i.e. twice as long as they are wide. The neural spine is tall and directed slightly caudally, the lateral faces of which are heavily marked by a series of rough cranioventrally orientated scars. The postzygapophyses are located relatively high on the caudal margin of the vertebrae.

**Notarium** – Six elements, the 9<sup>th</sup> cervical and first five thoracic vertebrae, have fused together to form a notarium, where the neural spines of the thoracic vertebrae have developed into a supraneural plate (Figure 2.4). Fracture lines are observed between the individual elements and across the middle portion of the centra while damage has removed several pairs of pre- and postzygapophyses. The transverse processes of the 3<sup>rd</sup> thoracic vertebrae were broken and have been repaired with plaster, as has the corpus and ventral portion of the neural arch on the 5<sup>th</sup> thoracic vertebra.

The bodies of the vertebrae are similar in form to one another, relatively narrow about their middle point in ventral view but expand laterally to form the proximal and distal margins. The profile of the body of the 9<sup>th</sup> cervical is the same as these subsequent vertebrae but it is slightly larger in size. In lateral view the vertebral bodies are dorsoventrally compressed. A single large pneumatic foramen pierces the lateral face of the body on the 9<sup>th</sup> cervical and the first two thoracic vertebrae. In cranial view a pair of sutures extends diagonally across the cranial articular surface, terminating against the ventral margin of the neural canal and marking the division between the vertebral body and the transverse processes/neural arch. The neural canal is slightly dorsoventrally compressed and is flanked laterally by small foramina, situated ventral the prezygapophyses. The articular surfaces of the prezygapophyses are flat and orientated ~60° dorsolaterally against the transverse plane. The diapophyses of the first thoracic vertebrae are located on the craniolateral margin of the centrum, clearly ventral to the position of the parapophysis, which has developed on the lateral margin of the transverse process. The diapophyses of subsequent vertebrae are positioned more dorsally relative to those of each preceding element until the 5<sup>th</sup> thoracic vertebrae, where after the diapophyses and parapophysis are located at the same level on the transverse process. This indicates that the first four thoracic vertebrae would have supported large double headed ribs. The transverse processes are long and narrow, directed laterally, and show a decrease in length moving caudally along the vertebral series. The transverse processes of the 4<sup>th</sup> thoracic vertebra are broader than other vertebrae, giving them a square-like profile. At least one large foramen has developed on the ventral face of each of the transverse processes.

A natural contact between the pre- and postzygapophyses is retained between the 9<sup>th</sup> cervical and 1<sup>st</sup> – 2<sup>nd</sup> thoracic vertebrae but fusion between these features has not occurred. The neural spines of the first five thoracic vertebrae are tall but broad and have fused together to form a supraneural plate. The lateral margin of the 1<sup>st</sup> thoracic vertebra is marked by strong linear depressions for the insertion of muscles or the position of mineralized tendons (Bennett 2001a). The lateral face of the 4<sup>th</sup> thoracic vertebra is substantially broader than all others and has expanded craniocaudally to form the lateral articulation with the scapula.

**Dorsal vertebrae** - Three isolated vertebrae are present and would have been originally positioned between the notarium and the sacrum (Figure 2.5). These vertebrae are well preserved although both are missing the lateral half of the left transverse process and have sustained damage to the pre- and post-zygapophyses/exapophyses.

The vertebral bodies are procuneiform and only marginally longer than they are wide, narrowing in width towards the middle of the body. The lateral faces of the vertebral bodies are slightly concave and free of foramina. No sutures between the bodies and the neural arches are visible indicating that the vertebrae are fully fused.

The neural canal dominates the cranial faces of the vertebrae. The preexapophyses are positioned on the dorsolateral margin of the cranial cotyle and are large, with flat craniodorsally orientated articular surfaces. Dorsal to the preexapophysis sits a large foramen, positioned dorsolateral to the neural canal and ventrolateral to the remains of the prezygapophyses. The cranial face of the vertebrae between the prezygapophyses is strongly concave and merges smoothly with the neural spine. The neural spine is tall and narrow, approximately 1.7 times as tall as it is wide in lateral view. In lateral view the neural spines lie adjacent to one another while the left faces are marked by small ridges for the attachment of muscles. The transverse processes are long and narrow, approximately three times as long as they are wide, and are orientated slightly craniolaterally when viewed in their dorsal aspects. Three large foramina pierce the transverse process. The first of these is positioned immediately caudolateral to the prezygapophyses while the second lies adjacent to this, occupying the junction between the transverse processes and the neural spine. The third foramen occupies the

medial portion of the ventral surface. The postexapophyses are small, but slightly concave, and positioned on the dorsolateral margins of the distal condyle. Dorsolateral to the neural canal the two foramina observed on the cranial surface exit onto the caudal face of the bone. The caudal face of the neural spine is triangular, the base of which is formed by the remnants of the postzygapophyses. The central region of the neural spine is depressed relative to the level of the surround bone.

**Sacral vertebrae** – The sacral vertebrae are well preserved in an excellent three dimensional state with the exceptions of the neural spines, which are broken.

Four vertebrae have fused together into a synsacrum where the post- and prezygapophyses and the intercentral sutures have fully closed (Figure 2.6). The articular surfaces of the prezygapophyses are directed slightly caudolaterally. The neural canal dominates the cranial face of the bones. The ventral margins of the centra are flat rather than concave as is typically observed in the thoracic vertebrae. The neural spines, where present, are low and broad, giving them a square appearance in lateral view. Each of the vertebrae preserves a pair of large sacral ribs. These ribs are narrow medially but expand craniocaudally towards their lateral margins. In dorsal view the first three are directed caudolaterally while the fourth is directed laterally. The first rib has twisted so that in lateral view it is directed craniodorsally at an angle of  $26^\circ$  to the horizontal axis. The remaining ribs are also twisted, but in the opposite direction, the angle of which becomes progressively shallower in a caudal direction (i.e.  $57^\circ$ ,  $41^\circ$  and  $12^\circ$  for ribs 2, 3 and 4 respectively).

**Caudal vertebrae** – Six caudal vertebrae are present, the first of which lies in articulation with the four sacrals but is badly damaged and has been extensively repaired.

The remaining five caudals are found together (Figure 2.7), however, they have not sutured with one another and are instead held in place with glue. The dorsal margins of four of the caudal vertebrae have been broken and repaired with plaster. The difference in size between the articular surfaces of 1<sup>st</sup> caudal vertebrae and the 1<sup>st</sup> element of the articulated block suggests that the two do not represent a natural series.



When viewed from their dorsal aspects the two most cranially located vertebrae have a square outline with relatively high and narrow neural spines compared to the remaining caudals. Caudally, the vertebrae become progressively more elongate with lower and broader neural spines. A prominent neural canal has developed through each of the caudal vertebrae.

**Sternum** – The sternum is partially preserved but significant portions of the left side of the sternal plate, the right hand margin of this plate, and the cranial portion of the cristospine have been restored. As such the lateral margins and overall shape of the sternal plate is reconstructed.

Despite the level of reconstruction the lateral faces of the cristospine are concave, while in dorsal view the bone is sub-triangular and tapers cranially (Figure 2.8). A weak median dorsal ridge terminates caudally against the articulation facets for the coracoids, which are divided into two craniolaterally located surfaces on the large dorsal tubercle. The cristospine is widest level with these articular facets. The caudal-most portion of the articulation is formed by a prominent tubercle that is sub-triangular in cranial view. The articulation itself is divided into two individual surfaces, located dorsally and laterally on the cristospine, one for each of the medial forks of the coracoid. In lateral view the articulation is directed craniodorsally. The neck of the sternal plate, where it meets the cristospine, is narrow but immediately caudal to this point the bone expands laterally. The lateral margins are directed dorsally in cranial view so that caudal to the neck the sternal plate lies dorsal to the cristospine. The sternal plate is transversely concave and the dorsal surface pierced by a large pneumatic foramen immediately caudal to the neck. In ventral view a weak median crest extends caudally from the cristospine approximately half way along the sternal plate.

**Scapulocoracoid** – The right scapula and coracoid have fused together to form a scapulocoracoid that is well preserved in three dimensions, missing only the caudal portion of the medial scapular articulation and the central portion of the coracoid furca. The left element is represented only by a fragment of the scapula and has been restored based on the dimensions of the right.

The scapulocoracoid is a weakly U-shaped element where the coracoid is longer than the scapula (Figure 2.9). A comparison between the articular facet on the 4<sup>th</sup> thoracic vertebrae and the scapula indicates that in life the scapula was angled craniolaterally against the mid line of the vertebral column. The scapula forms the dorsal half of the scapulocoracoid body, including the dorsal half of the glenoid fossa. Dorsal to the glenoid fossa a large bulbous tubercle is present and marks the boundary between the medial portion of the scapula and the main body. On the ventral side of the scapula, below the large tubercle, a smaller and isolated tubercle is present. The medial section of the bone is dorsoventrally compressed and narrowest about its mid point but expands towards the medial articulation. In medial view the articular surface is oval, elongated craniocaudally, and displays a slight convex curvature. The cranial most portion is distinct from the remainder of the articular surface, its face being flatter and directed craniolaterally rather than flat against the sagittal plane.

The coracoid forms the ventral half of the scapulocoracoid, including the ventral half of the glenoid. A large tubercle (biceps tubercle after Bennett 2003a) is observed cranial to the glenoid fossa and a pneumatic foramen is present between this and the cranial margin of the glenoid fossa. A second and larger foramen occupies the medial face of the scapulocoracoid body, just ventral to the level of glenoid fossa. Medially, the coracoid body thins to form a narrow shaft that is sub-triangular in cross-section. A short, but pronounced, craniocaudally compressed ridge is visible on the ventral surface of the shaft close to the coracoid body. The caudal face of the coracoid shaft is slightly concave between a sharp central ridge and the caudal margin of the bone. Medially a long low ridge is adjacent to the articular surface of the sternum for the insertion of *M. sternocoracoideus* (Bennett 2003a). The medial articular surface of the coracoid is formed by a slight craniocaudal expansion of the shaft and the development of a shallow V-shaped furca, the cranial branch of which is considerably smaller than that of the caudal branch.

The glenoid fossa is wide and occupies the caudolateral face of the scapulocoracoid but does not extend onto either of the cranial or caudomedial faces. The dorsal half of the glenoid fossa is flat to slightly concave while the ventral half is convex. In its medial aspect the two halves meet at an angle only slightly greater than 90°. A small

furrow divides the dorsal and ventral halves of the glenoid fossa and marks the position of the former suture between the scapula and coracoid.

**Humerus** - Both humeri are present and well preserved in three dimensions. Only the right element is complete, with the left preserving only those regions of bone medial to the deltopectoral crest and the dorsal portion of the distal articulation. The missing shaft of the left humerus has been restored with plaster to mirror that of the right.

In cranial view the dorsal surface of the collum adjacent to the humeral caput is concave and directed dorsally at an angle of 31° to the long axis of the shaft (Figure 2.10). On the ventral face of the collum, immediately adjacent to the humeral head, the bone surface is sunken, creating a large depression. The proximal articular surface of the humerus with the scapulocoracoid is “kidney-bean” shaped with a short bulbous caudal process that supports a small medial protrusion. A short curved ridge originating on the cranioventral margin of the medial face separates the cranial half of the surface into dorsal and ventral faces. The ventral face is marked by a series of small ridges immediately adjacent the origin of the separating ridge. The caudal half of the medial face is regularly convex in dorsoventral section.

The deltopectoral crest is sub-triangular in cranial view and occupies approximately 36% the length of the humerus. In cranial view the deltopectoral crest expands ventrally and develops a strongly concave distal margin. In ventral view the crest is thin and blade-like medially but curves sharply caudally and expands until it is very large and robust. The ventral surface of the deltopectoral crest is concave and strongly marked by large scars that would have acted as the insertion for the powerful pectoral muscles. A pronounced ridge separates the cranial half of the crest from the caudal half and merges gradually with the caudoventral margin of the humeral shaft. The caudal process (or posterior tuberosity, Bennett 2001a) is small and grades smoothly into the humeral head, while on the ventral surface the process forms the caudal margin of the central depression. The shaft is narrowest at the distal termination of the deltopectoral crest but expands distally near to the articular surface. A large pneumatic foramen pierces the dorsal face of the bone at the junction of the humeral neck and the caudal process. In ventral view the shaft is marked by several rugose ridges, presumably for the attachment of muscles. Two of these ridges are located

along the caudoventral margin of the bone, the first positioned just distal to the mid shaft, while the second is more distal and merges with the caudal portion of the entepicondyle. A large craniocaudally compressed supracondylar process is observed on the cranioventral margin of the shaft approximately three quarters along its length.

The distal articular surface is D-shaped in its lateral aspect and dominated by a large central depression. The craniodorsal half of the surface is formed by two large condyles, the capitulum and trochlea, which are orientated and extend diagonally across the ventral face of the shaft. The caudoventral portion of the surface is formed by the development of an oval, convex entepicondyle, the dorsal margin of which is bordered by a large, distally orientated protrusion.

**Radius** – The left radius is represented by only the proximal half of the shaft while the right element is complete but has been fractured into three portions.

The radius is a long and narrow element with expanded proximal and distal regions (Figure 2.11). The shaft is bowed in a dorsal direction. The proximal articular surface is craniocaudally compressed and divided into three parts: a large dorsally located process, a flat articular surface directly ventral to this that forms the cranial articular surface with the capitulum of the humerus, and a small concave cotyle towards the caudoventral margin of the bone for the trochlea. A low ridge for the attachment of muscles is observed on the ventral margin of the radius only slightly distal to the proximal articulation. The distal expansion is craniocaudally compressed and is regularly convex to fit the articular surface on the proximal syncarpal.

**Ulna** – As with the radii the left element preserves only the proximal half of the shaft and although the right ulna is complete, it has been severely fractured in several places along its length.

The ulna is long and narrow, particularly about the mid shaft, while the proximal and distal margins have expanded (Figure 2.12). The dorsal portion of the proximal articular face is convex and articulates with the capitulum of the humerus while the most ventral portion of this convexity braced against the trochlea. There is no observed division of this surface. The dorsal cotyle is separated from a more ventrally

located cotyle, accommodating the entepicondyle of the humerus, by a bulbous ridge of bone that fits into the concavity of the ventral margin of the trochlea. The proximal surface is D-shaped in appearance and matches the distal face of the humerus. The dorsal margin of the cotyle for the capitulum extends onto the cranial face of the ulna as a short sharp ridge, marking the dorsal position of the radius, while a second ridge forms ventral and slightly distal to this, marking the section where the radius lay tight against the ulna. A single low ridge is present along the ventral margin of the ulna. In contrast to the proximal surface the distal expansion of the ulna is craniocaudally compressed. A rough but partially broken ridge marks the dorsal limit of a smooth region of bone on the cranial face where the radius would have lain in life. The ventral border of this region is formed by a blade-like ridge on the ventral margin ulna. Three features form the distal articular face of the ulna: a large, dorsally located and slightly convex articular surface, a tubercle located directly ventral to this, and finally a small rounded fovea near the ventral margin of the bone.

**Carpus** – The individual carpals of the right forearm have completely fused to form proximal and distal syncarpal units (Figures 2.13 - 14). The preaxial carpal is complete but loose from the distal syncarpal block while the pteroid is also present but was sectioned for study by Unwin et al. (1996). As such only the articulation and proximal most portion of the shaft remain. No elements from the left carpus are preserved.

The proximal syncarpal is narrow mediolaterally and shows a complex shape owing to the proximal and distal articular surfaces. The proximal face is divided between three features, the largest of which is the concave facet for the ulna and occupies the entire central region. At the cranioventral-most margin of this facet is a large tubercle that inserts into a fovea on the cranioventral margin of the ulna. A high ridge separates the smaller, but strongly concave articular surface for the radius from the articular surface for the ulna and the articular tubercle. A number of small foramina occupy a position immediately ventral to this ridge between the tubercle. The distal articular face is divided into two surfaces. The dorsal most of these surfaces is concave and sub-circular in profile, occupying a craniodorsal position, while the ventral most surface is elongate and extends diagonally from the caudodorsal to the cranioventral margin of the bone. A small, cranioventrally orientated ridge separates

the dorsal and ventral articular surfaces. The dorsal, ventral and cranial faces are all perforated by foramina.

The proximal face of the distal syncarpal is divided into two convex surfaces that are separated by a central furrow, allowing the syncarpal to fit tightly against the proximal elements. A very large circular foramen occupies the cranioventral face of the bone. A single large foramen occupies the central portion of the distal articular surface. Dorsal to this the articular surface of what would have been the dorsal distal carpal prior to fusion is predominantly flat. The junction between the dorsal carpal and the cranial carpal is marked by a deep pit that matches a step-like articular surface on the fourth metacarpal. In cranial view the cranial carpal has a smooth convex surface that protrudes craniodistally and acts as the articular surface for the preaxial carpal. The dorsal margin of this surface is marked by a small crescent ridge while a second but more pronounced ridge is located dorsal to this. A small tubercle is located on the distal face of the cranial carpal. The ventral carpal forms the majority of the articular surface and is gently concave, the curvature becoming stronger towards the caudal margin. The fourth distal carpal, suggested by Kellner & Tomida (2000) to lie immediately dorsal to the foramen, is not observed in this specimen as this location is broken.

The preaxial carpal has an oval, transversely compressed articular face that is concave to fit against the cranial protrusion of the cranial distal carpal. The middle portion of the carpal is narrower than the base, however, the bone expands both dorsoventrally and mediolaterally towards the cranial margin. The craniodorsal portion of the bone bears a wide V-shaped fovea that tapers distally and would have housed a sesamoid (pisiform after Bennett 2008). The medial face of the preaxial carpal contains a single foramen but no potential articular surface or ridge for the pteroid (see Bennett 2007b). The cranial face ventral to the fovea is bulbous, marked by a ridge on its proximal margin.

**Metacarpals** – All three of the preaxial metacarpals are also preserved but only one of these is complete. Both of the wing metacarpals (mc IV) are also incomplete, the left hand element represented by proximal and distal articular ends of the bone while

the right hand element preserves only the proximal half of the shaft. Both wing metacarpals have been reconstructed with plaster of Paris.

The single complete metacarpal, interpreted as mc I, has a diameter of 4 mm but has expanded at both the proximal and distal terminations to create the articular surfaces for the carpus and digits respectively (Figure 2.15). The distal expansion is bulbous but elongated in a craniocaudal orientation. The shaft of mc I is only just shorter than the reconstructed length of the fourth metacarpal.

The fourth metacarpal is elongate and narrow, reconstructed as being of a similar length to that of the humerus as supported by other more complete ornithocheiroids (e.g. AMNH 225555, SMNK PAL 1132, MHNS/00/85, NSM-PV 19892, RGM 401880). The proximal articulation is slightly expanded dorsally and divided into two surfaces by a small step of bone, matching the distal articular surface of the distal syncarpal. Originating by the proximal articulation, a thin flange of bone extends along the ventral margin of the cranial face of the shaft. The distal articular face is formed by two large condyles, the dorsal condyle of which is angled slightly dorsally in its cranial aspect. The intercondylar sulcus is therefore directed dorsally at an angle of 14° to the long axis of the shaft. A large depression is visible on the cranial face of the bone directly adjacent to the dorsal condyle for the attachment of muscles relating to the remaining metacarpals or digits. Directly ventral and slightly medial to this depression a small tuberosity is present on the ventral margin of the bone. In its caudal aspect a large depression is present on the shaft directly medial to the dorsal condyle that likely accommodates the flexor tendon or muscles of the fourth wing finger phalanx during flexion.

**Manus** – Only two elements of the manual digits are preserved. The proximal face of the bone is rhomboid in outline, the dorsal half of which is concave to accept the bulbous articular surface of the metacarpal (Figure 2.16). The ventral half is craniocaudally compressed. In cranial view a long flange runs from the proximal margin of the digit along the ventral margin and merges with the mid-shaft of the bone. The presence of this feature suggests that the bone may be the first phalanx of the third digit (see Bennett 2001a) and may have developed for the insertion of (?) *M. interosseus*. Adjacent to the dorsal margin of the cranial face the bone is marked by

small, circular scars. The shafts of all the phalanges are slightly curved in a cranial direction and distally form a wide, saddle-shaped joint that is offset slightly dorsocaudally, resulting in a ventral component of movement being introduced when the digits were flexed. The second phalanx is almost identical in form but lacks the ventral flange and the dorsally located scars of ligaments or tendons.

**Digit 4** - Only the proximal portion of the left first wing phalanx is preserved, the remainder having been restored with plaster. The second phalanx of the left wing is mostly complete while that of the right preserves only the distal half of the shaft. The third phalanx of the left wing preserves only the proximal portion of the bone while the right element is complete. The fourth phalanges of both wings are missing.

The proximal articular surface of the first phalanx is formed by two cotyles, one positioned dorsally and one ventrally (Figure 2.17). The dorsal cotyle of the articular surface is larger than that of the ventral cotyle and extends further caudally due to the development of a caudal process on the phalanx. The cranial halves of both of these cotyles are located on the extensor tendon process. The extensor tendon process is sub-triangular element in dorsal its dorsal aspect and firmly sutured to the main body of the phalanx. On the ventral face of the process a single large pneumatic foramen is observed.

**Prepubic bones** – The prepubic bones are mostly complete but both are missing their cranial margins and have been repaired with plaster. The articular surface with the pubis on the left element is also broken.

The articular surface with the pubis is dorsoventrally compressed and slightly concave as observed on the right element (Figure 2.18). The medial and lateral margins of the prepubes are concave with a much greater curvature being observed on the medial margins of the bones. As a result both elements show a pronounced expansion towards their cranial margins. A small blade-like process has developed on the medial margin of the bones, between the caudal articulation with the pubis and the cranial expansion of the prepubes. Although a deep depression is observed on the process of the left prepube, such a feature is not present on the right element. Two deep scars occupy the lateral margin of the dorsal surface of the right prepube but are likewise



not observed on the left. In lateral view the cranial blade of the prepubes are directed dorsally against the shaft to give the element a concave profile.

**Pelvic plate** - Only those elements of the left pelvic plate are present but the cranial and caudal margins of the ilium, and the caudoventral margin of the ischium are all broken and have been reconstructed in plaster. The cranioventral margin of the pubis is broken but has not been repaired.

The three individual bones of the pelvis, the pubis, ischium and ilium, have fully fused to form a single solid plate (Figure 2.19). While all sutures have closed slight ridges or scars define the original boundaries of the three elements, with a slightly raised region of bone marking the former position of the now closed suture between the pubis and ischium. This ridge terminates 8 mm ventral to the ventral margin of the acetabulum. A second ridge of raised bone, positioned level with middle region of the acetabulum, marks the former division between the ilium and the puboischiatic plate. The preacetabular process of the ilium is long, narrow and dorsoventrally compressed. The postacetabular process is mediolaterally compressed, the caudal half of which has twisted so that the long axis of the blade is directed dorsolaterally in caudal view. In lateral view a large oval acetabulum, 25 mm in diameter, occupies the central region of the pelvic plate, bounded by the pubis, ilium and ischium. Directly ventral to the acetabulum is a small foramen (obturator foramen) that pierces all the way through the puboischiadic plate. The obturator foramen is completely enclosed within the pubis. In cranial view the pubis is broadest where it forms the articular surface for the sacrals but narrows rapidly in a ventral direction to form a transversely compressed blade of bone. The cranial portion of the bone is twisted laterally with respect to the long axis of the pubic plate. In medial view a large trough located towards the dorsal margin of the plate represents the articular surface of the sacrals, the lowest point of this depression representing the division between the ilium and the puboischiatic plate. Surrounding the obturator foramen are four large pneumatic alveoli, two positioned within the pubis and two within the ischium. In caudal view the entire blade is strongly convex, causing the bone to be directed back towards the midline of the body.

**Femur** - The right femur is well preserved but missing part of the neck and head. The left femur is not present. What is preserved of the collum is offset against the shaft at

an angle of the 20° (Figure 2.20). The greater trochanter develops as a small, dorsally directed protrusion on the dorsolateral margin of the shaft. Immediately ventral to the base of the collum where it meets the shaft, a long rugose ridge, representing the lesser trochanter, is observed. The shaft of the femur is long and narrow with a lateral curvature and expands at its distal margin to create the articular surface with the tibia. The medial and lateral condyles of the femur are small. The intercondylar sulcus present between the two condyles is longer and more prominent on the cranial surface than that of the caudal.

**Digits of the pes** - Eight elements of the pes are preserved, these being the complete series of phalanges of digit 3, two additional unguals, and two isolated phalanges (Figure 2.21). The phalanges are short and delicate considering the large size of the animal and display a slight ventral curvature along the length of the shaft. The proximal and distal ends are slightly expanded towards the articular surfaces while the unguals are themselves also short and display only a slight curvature.

| Element       | Length (mm) | Element | Length (mm) |
|---------------|-------------|---------|-------------|
| Humerus       | 290         | Wph 1   | 620         |
| Ulna          | 390         | Wph 2   | 566         |
| Metacarpal IV | 285         | Wph 3   | 460         |
| Femur         | 277         | Wph 4   | 330         |
| Tibia         | 338*        |         |             |

Table 1. – Average length of long bone elements in *Coloborhynchus robustus* (SMNK PAL 1133). \* denotes estimated measurements.



Figure 2.1. - SMNK PAL 1133. Partial jugal.

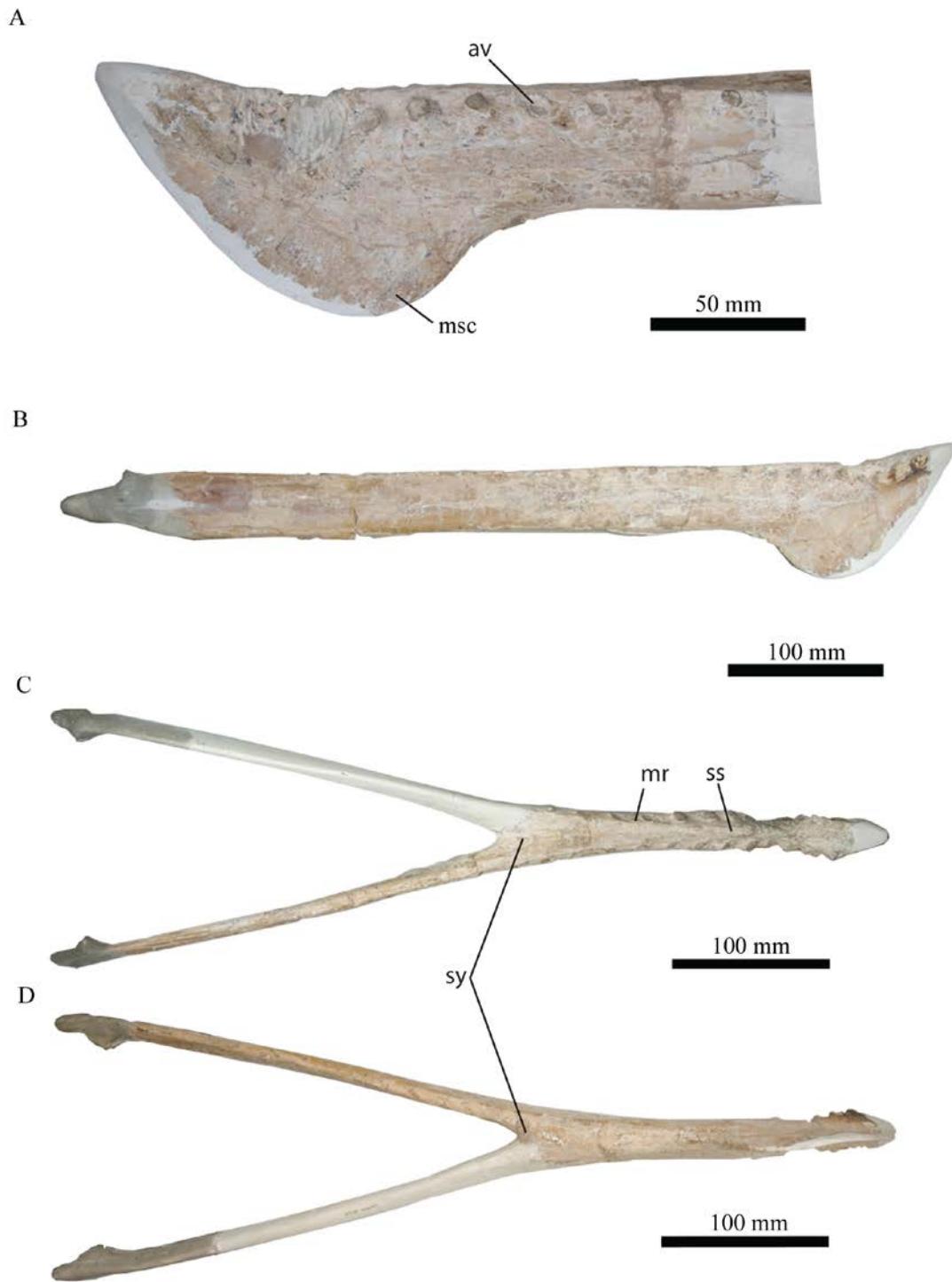


Figure 2.2. - SMNK PAL 1133. Mandible, where A, rostral section in its right lateral aspect; B, mandible in its left lateral aspect; C, dorsal aspect; D, ventral aspect.

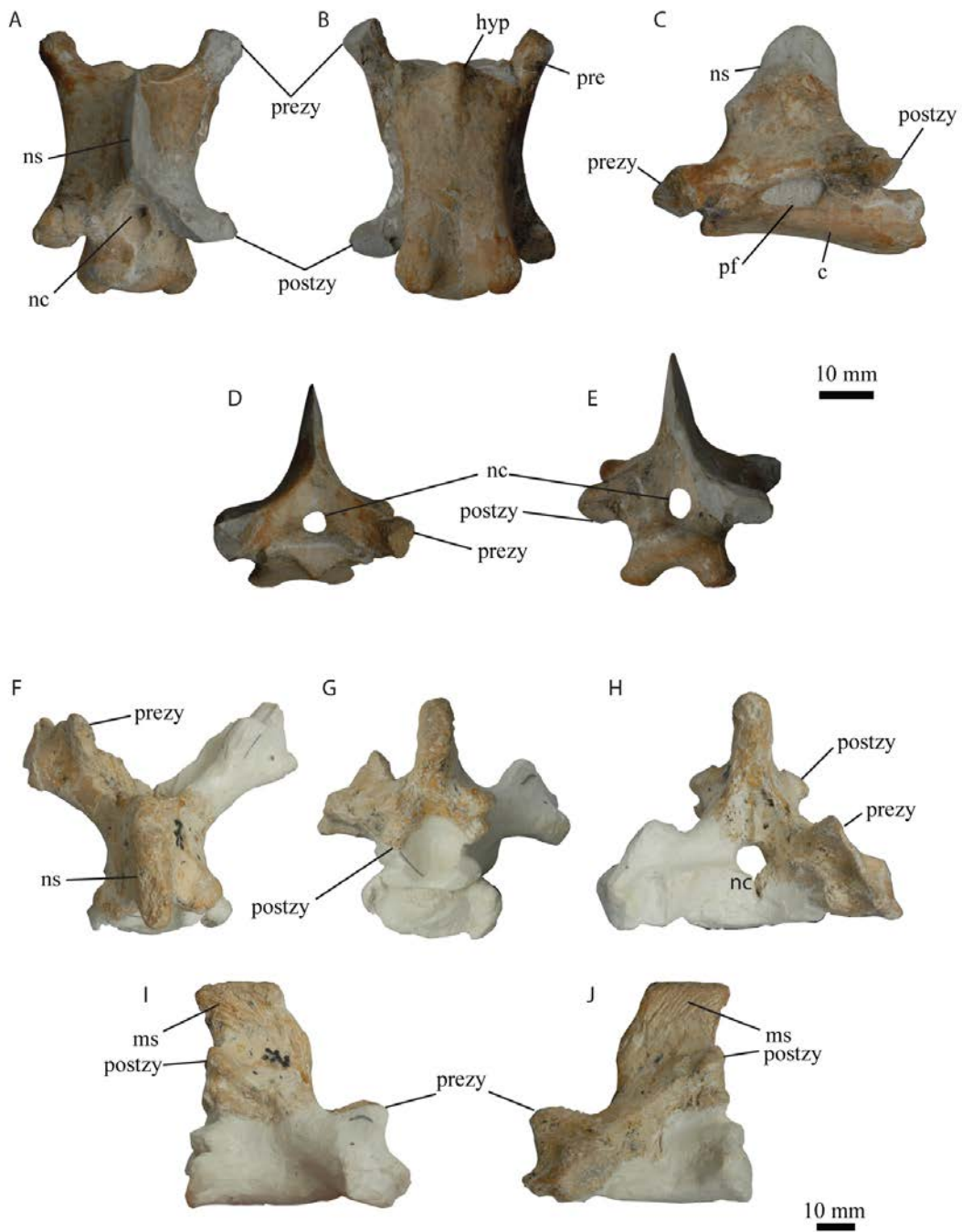


Figure 2.3. - SMNK PAL 1133. Cervical vertebrae. A-E, 6th cervical; F-J, 8th cervical. 6th cervical observed in its A, dorsal; B, ventral; C, lateral; and E, caudal aspects. 8th cervical observed in its F, dorsal; G, caudal; H, cranial; I right lateral; and J, left lateral aspects.

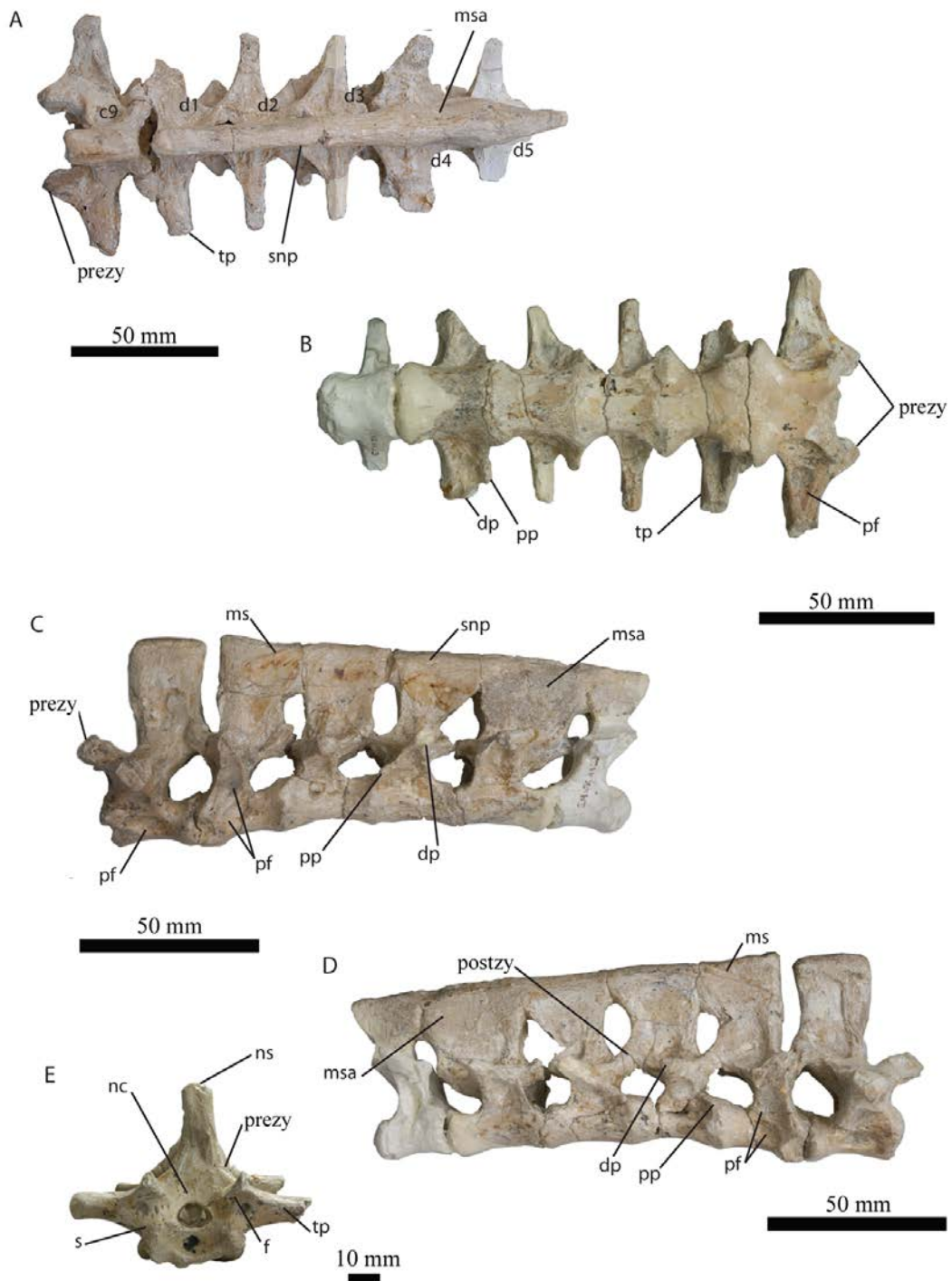


Figure 2.4. - Notarium of SMNK PAL 1133. A, dorsal; B, ventral; C, left lateral; D, right lateral; and E, cranial aspects.

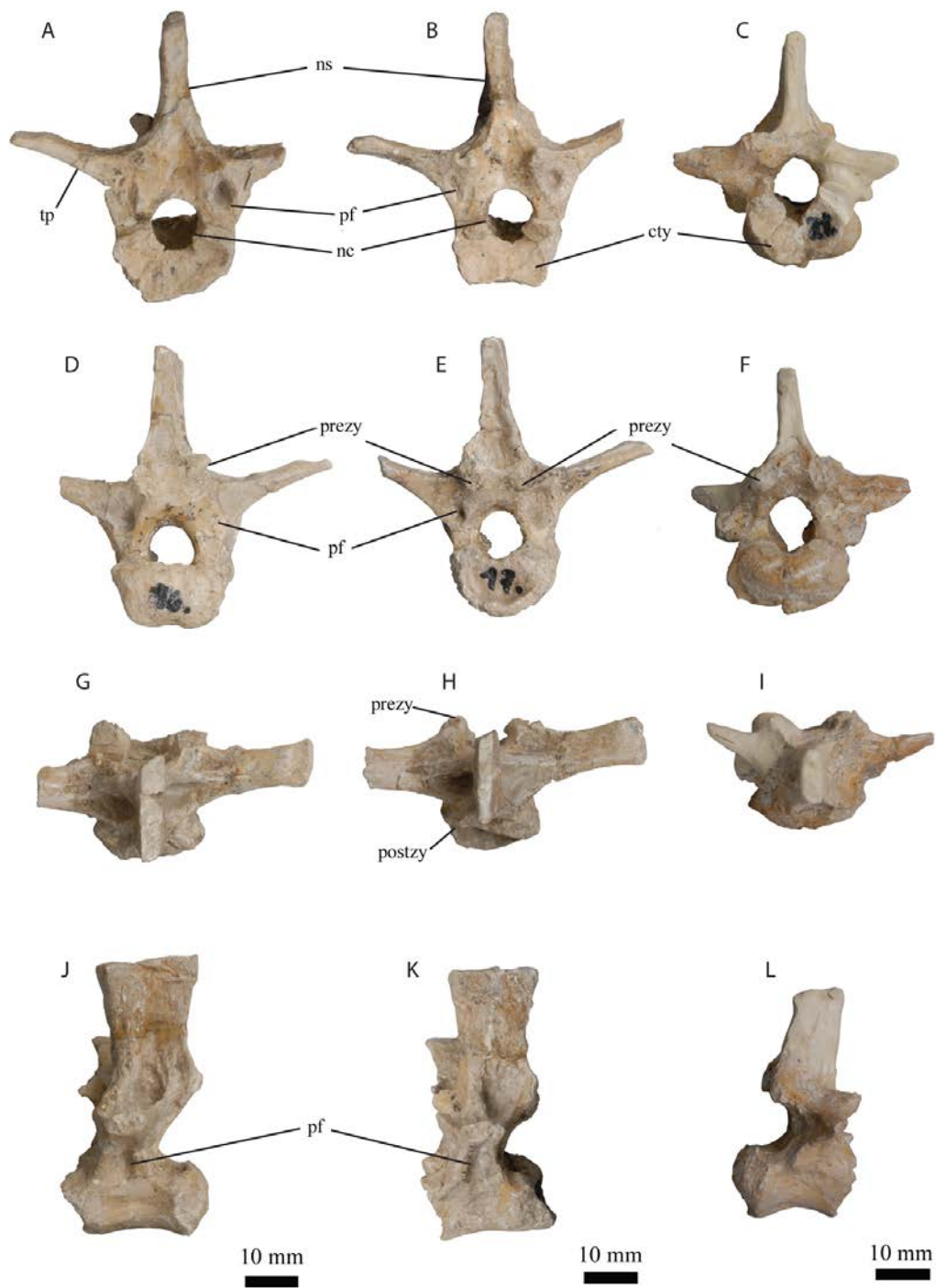
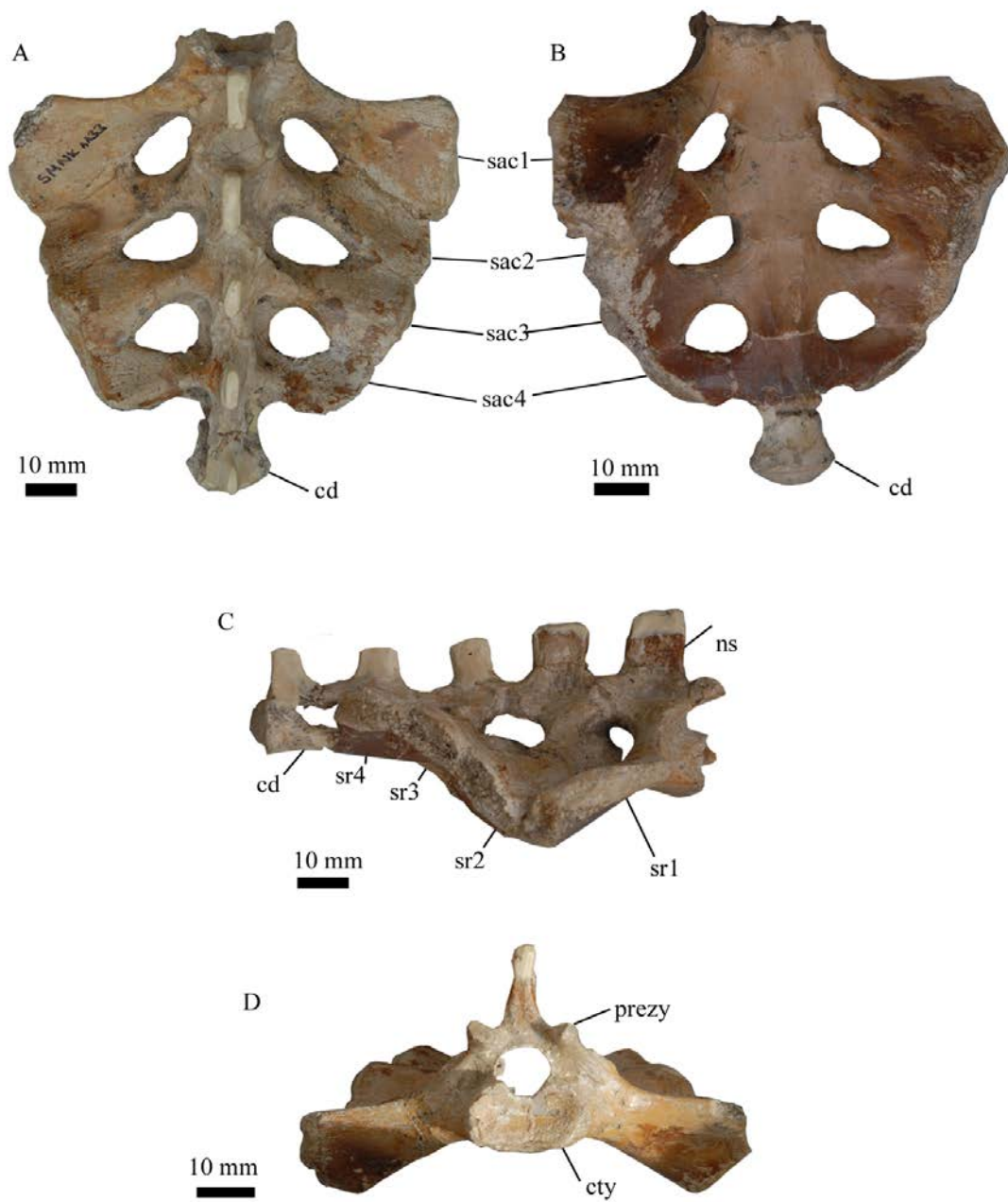


Figure 2.5. SMNK PAL 1133. Three dorsal vertebrae (positions uncertain). Elements are displayed in their cranial (A-C), caudal (D-E), dorsal (G-I), left lateral (J-K) and right lateral views (L). Scale bars are for all elements in that column.



Figures 2.6. SMNK PAL 1133. Sacrum. A, dorsal; B, ventral; C, left lateral; D, cranial aspects.



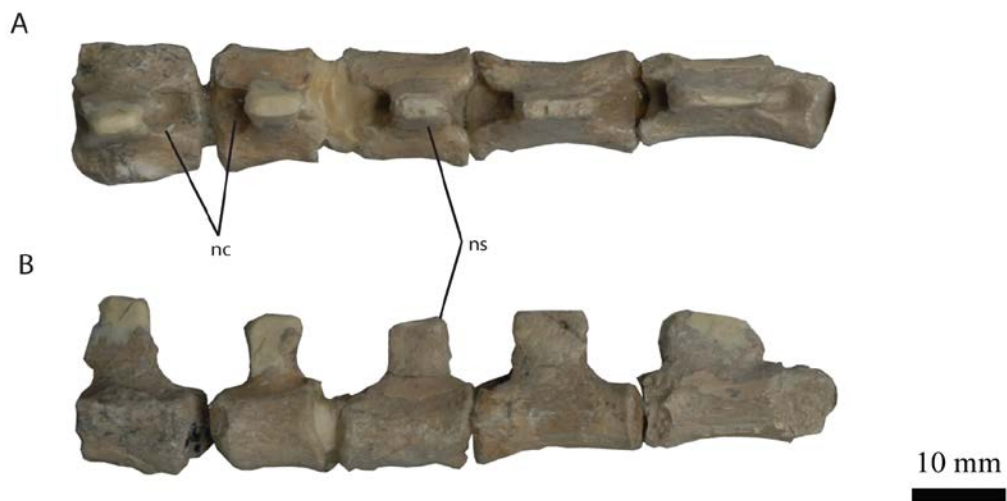


Figure 2.7 - SMNK PAL 1133. Caudal vertebrae. A, Dorsal, B, left lateral aspects. These vertebrae likely represent the anterior-most elements of the series, with the two right hand most elements illustrating the onset of a transition between short bodied bones with tall neural and those more elongate bones where the neural spine is depressed or absent.

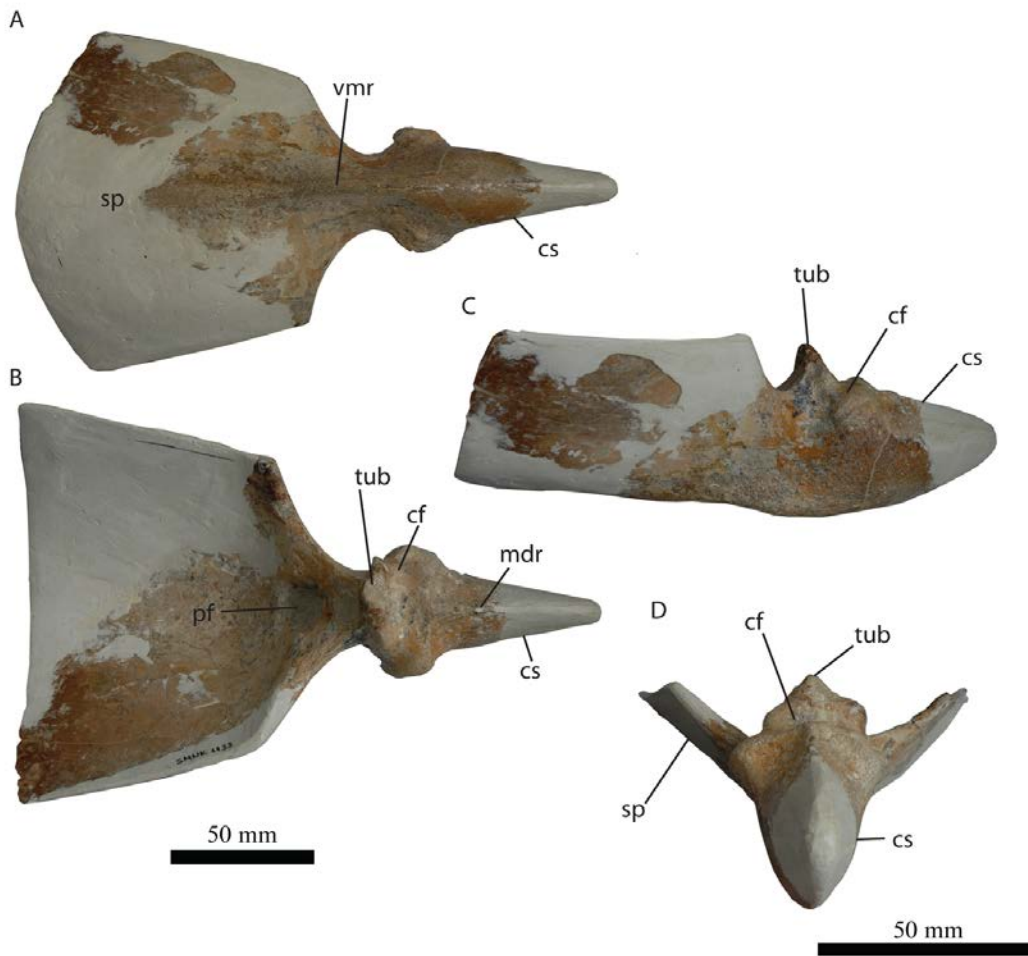


Figure 2.8. - SMNK PAL 1133. Sternal plate. A, ventral; B, dorsal; C, left lateral; D, cranial aspects.

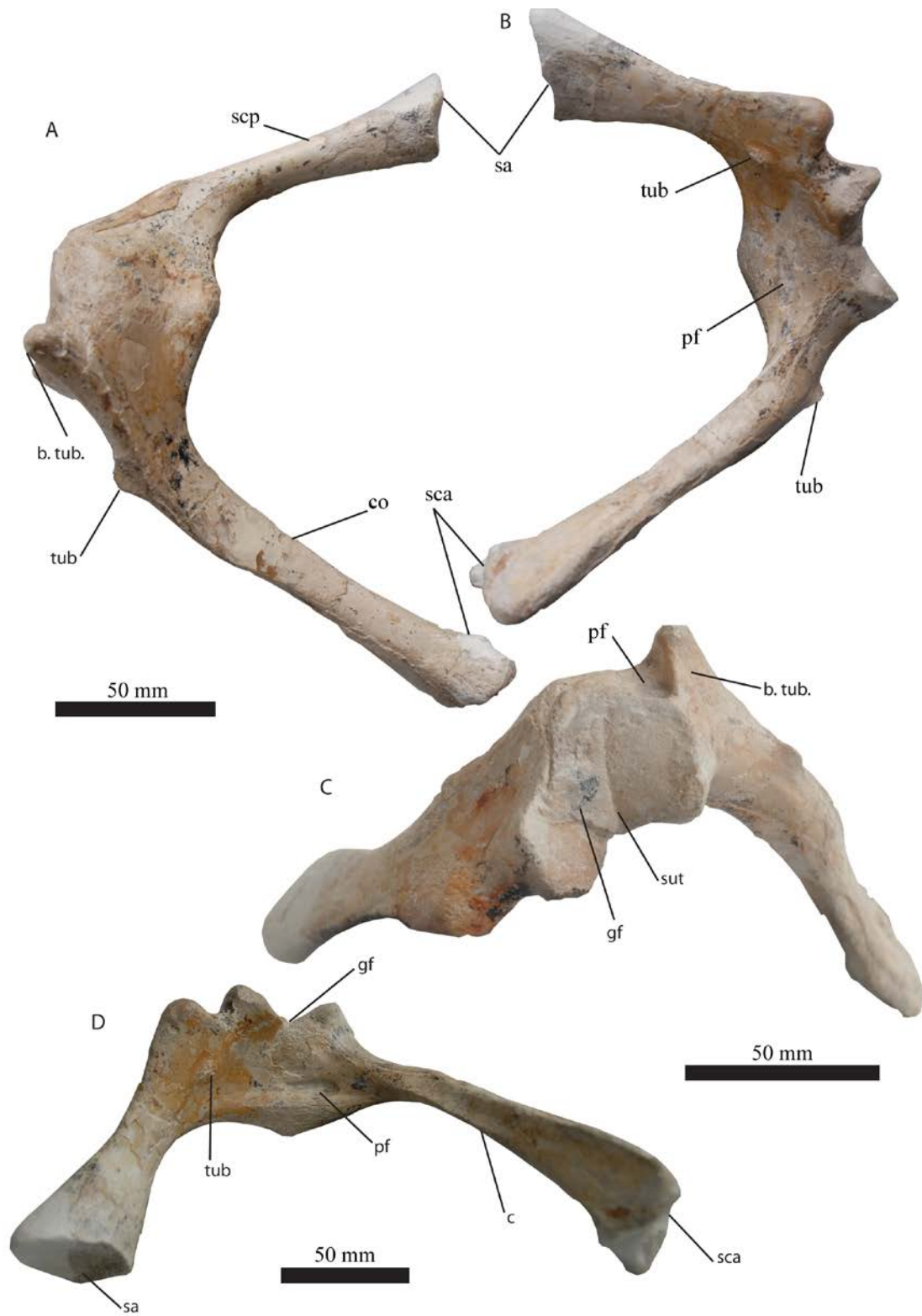


Figure 2.9. - SMNK PAL 1133. Right scapulocoracoid. A, cranial; B, caudal; C, lateral; D, medial aspects.

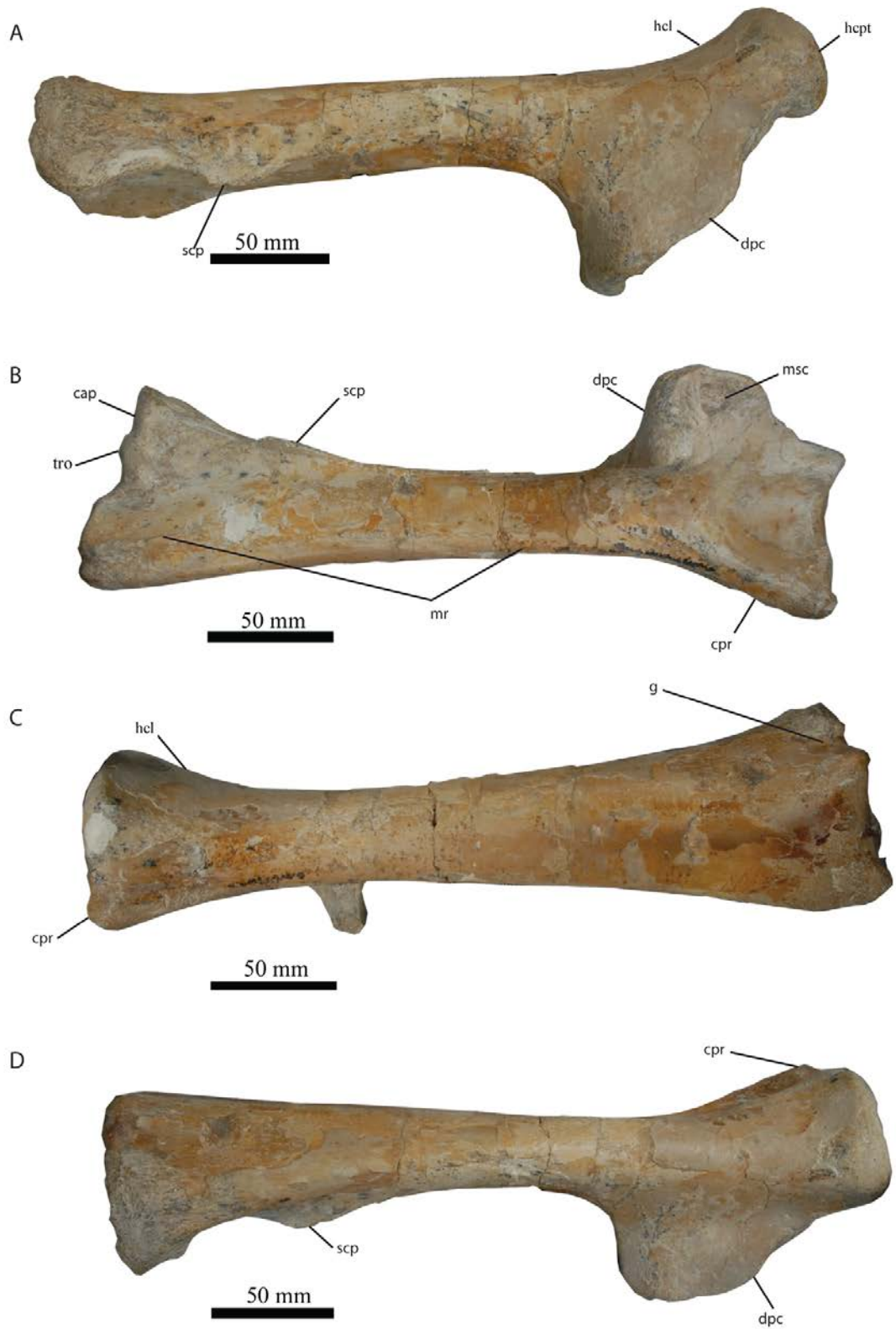


Figure 2.10. - SMNK PAL 1133. Right humerus. A, cranial; B, ventral; C, caudal; D, dorsal aspects.



Figure 2.11. - SMNK PAL 1133. Proximal portion of the right radius. A-C, proximal portion of the bone in: A, cranial; B, dorsal; C, caudal aspects. D-G, distal portion in D, caudal; E, dorsal; F, cranial; G, ventral aspects.

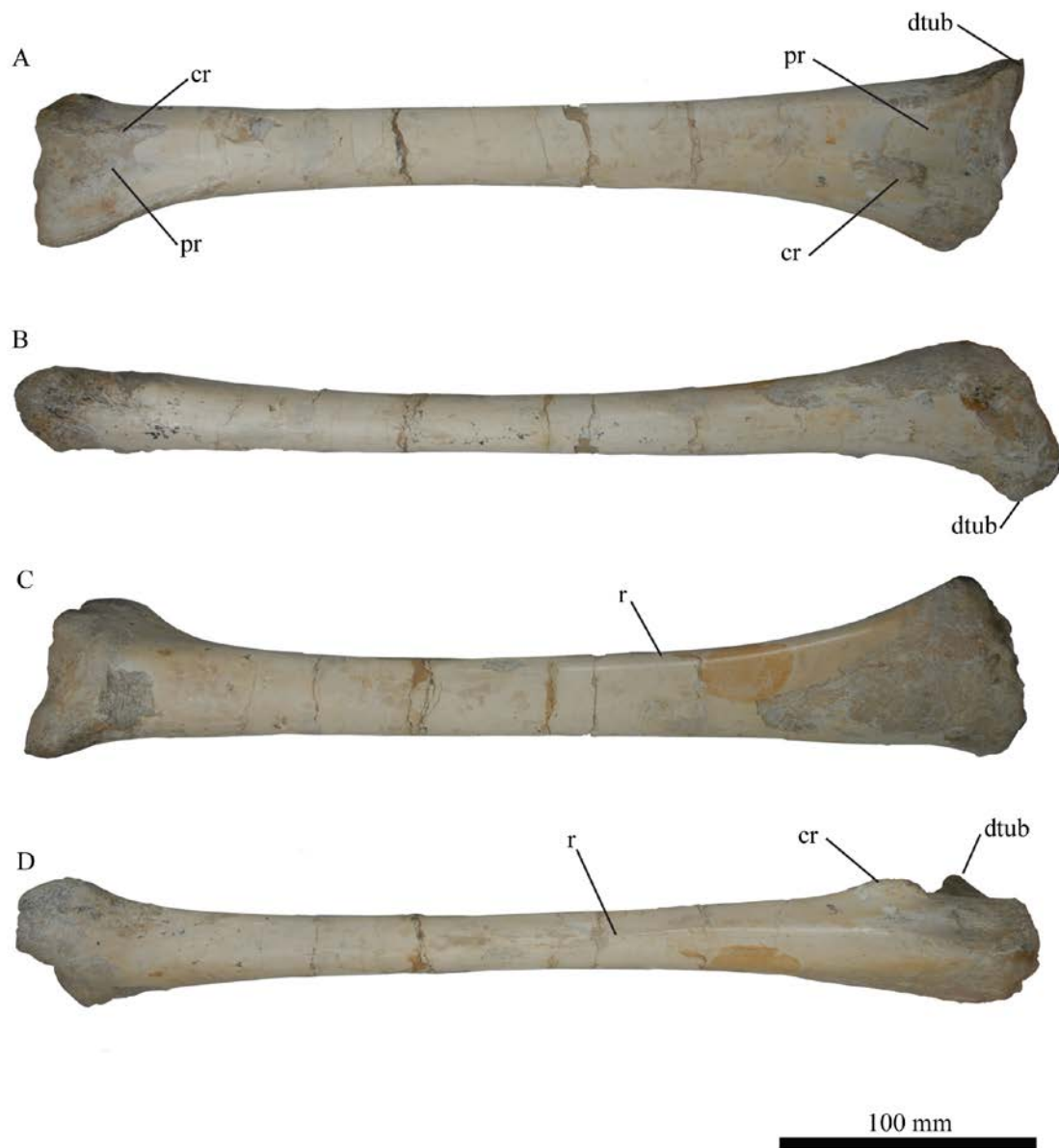


Figure 2.12. - SMNK PAL 1133. Right Ulna. A, cranial; B, dorsal; C, caudal; D, ventral aspects.

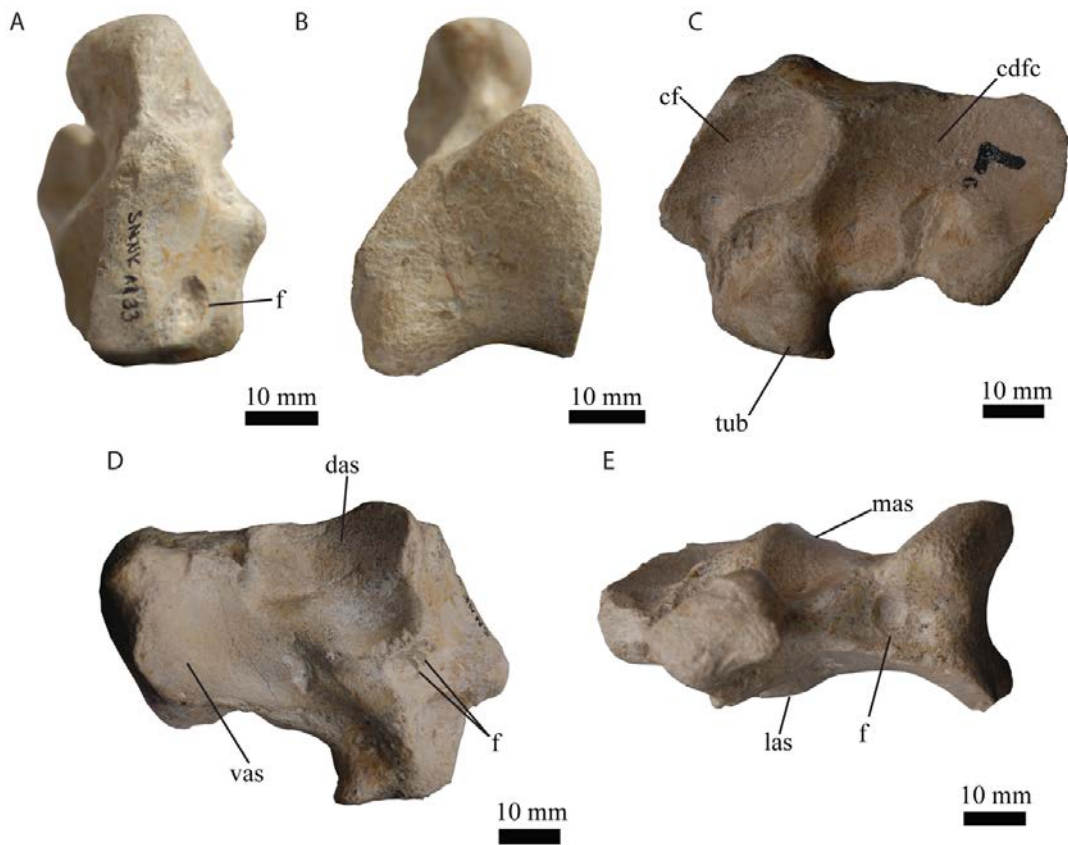


Figure 2.13. - SMNK PAL 1133. Proximal syncarpal. A, cranial; B, caudal; C, medial; D, lateral; E, ventral aspects.

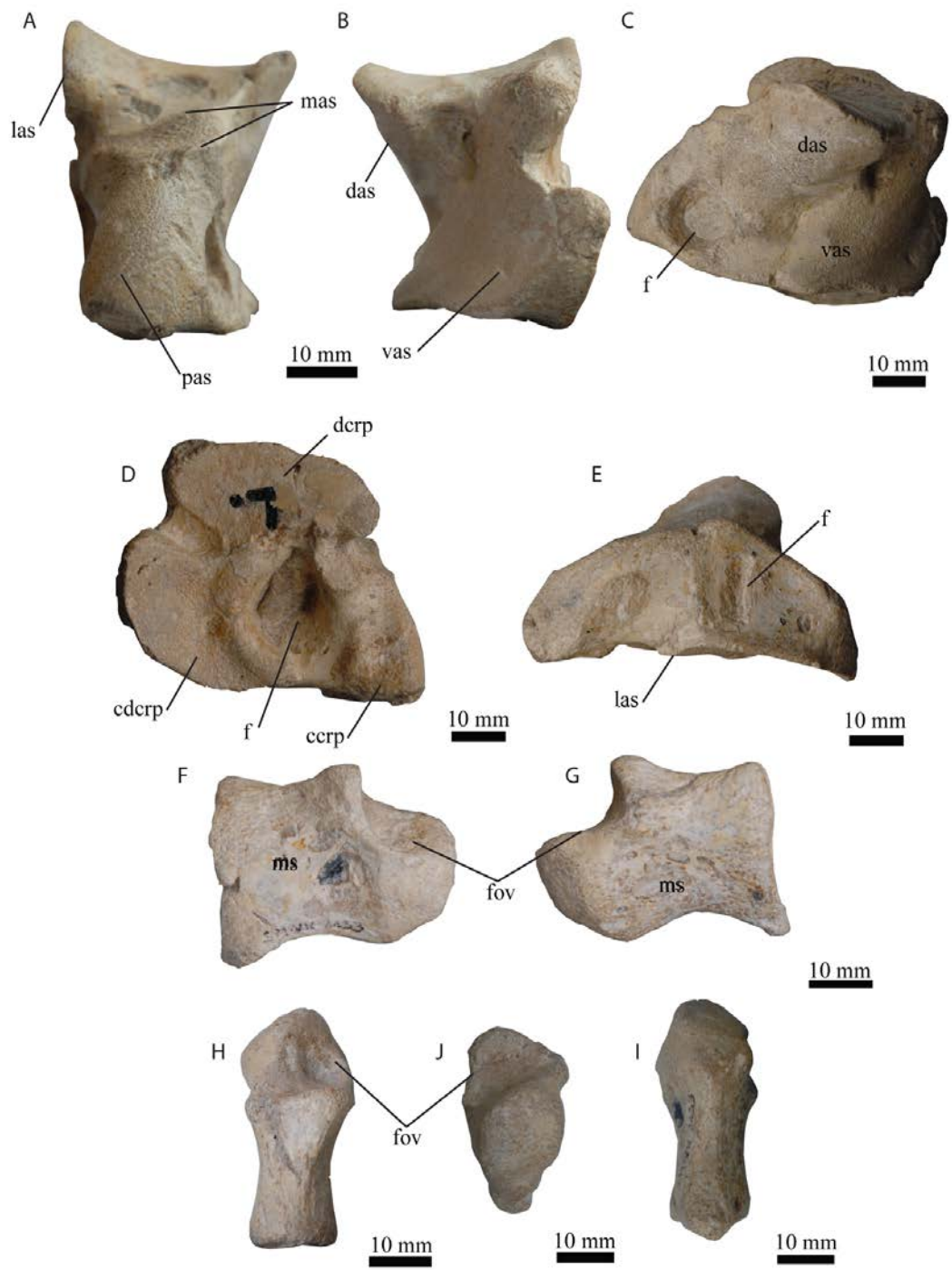


Figure 2.14. - SMNK PAL 1133. Distal syncarpal and preaxial carpal. A-E, Distal syncarpal in A, cranial; B, caudal; C, medial; D, lateral; E, ventral aspects. F-I, preaxial carpal in F, proximal; G, distal; H, dorsal; J, cranial; I, ventral aspects.



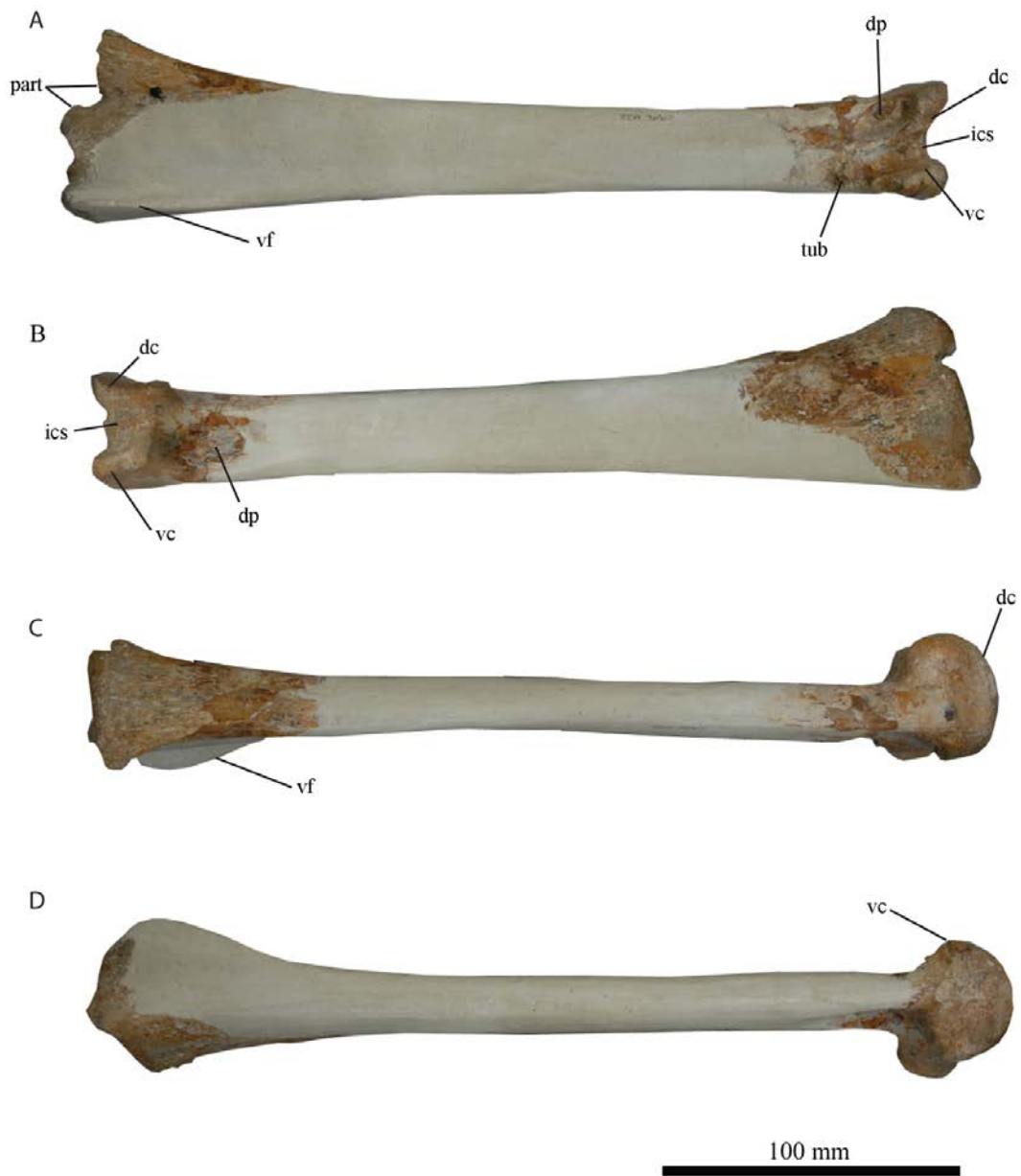


Figure 2.15. - SMNK PAL 1133. Left metacarpal IV. A, cranial; B, caudal; C, dorsal; D, ventral aspects.



Figure 2.16. - Manual digits of SMNK PAL 1133. Indeterminate phalanx in A, cranial and B, caudal aspects. First phalanx of the third digit in C, cranial and D, caudal aspects.

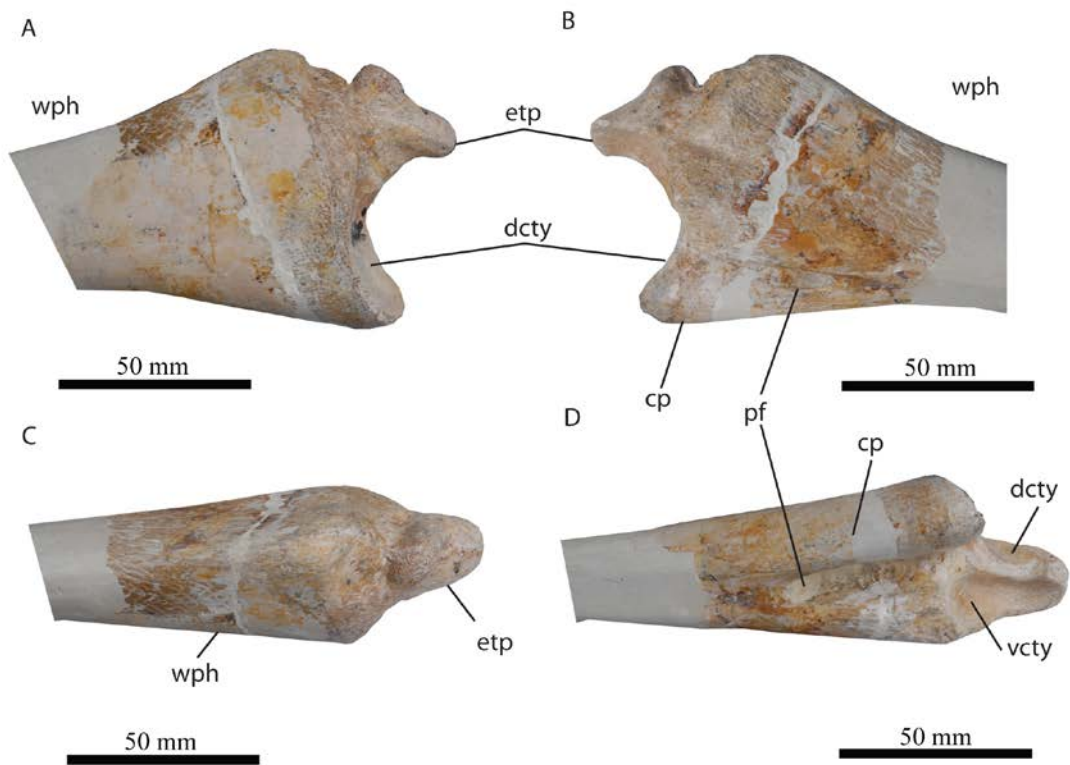


Figure 2.17. - Proximal 1st wing finger phalanx of SMNK PAL 1133 (left wing). A, dorsal; B, ventral; C, cranial; D, caudal aspects.

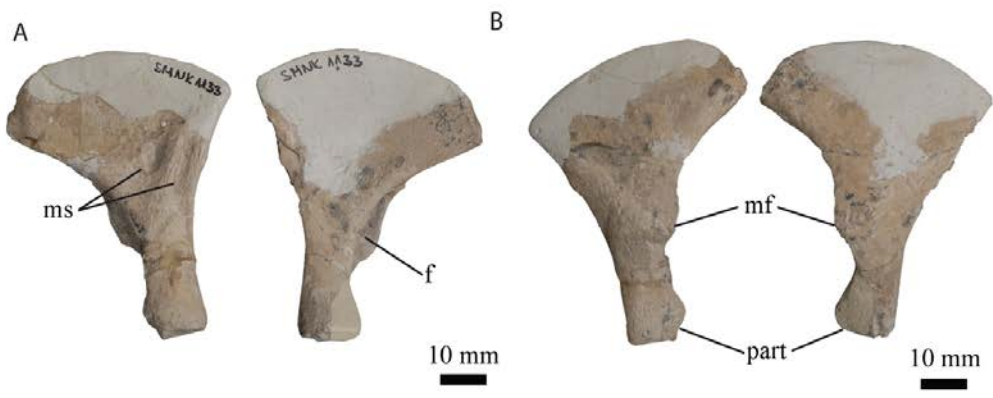


Figure 2.18. - SMNK PAL 1133. Prepubes. A, Dorsal; B, ventral aspects.

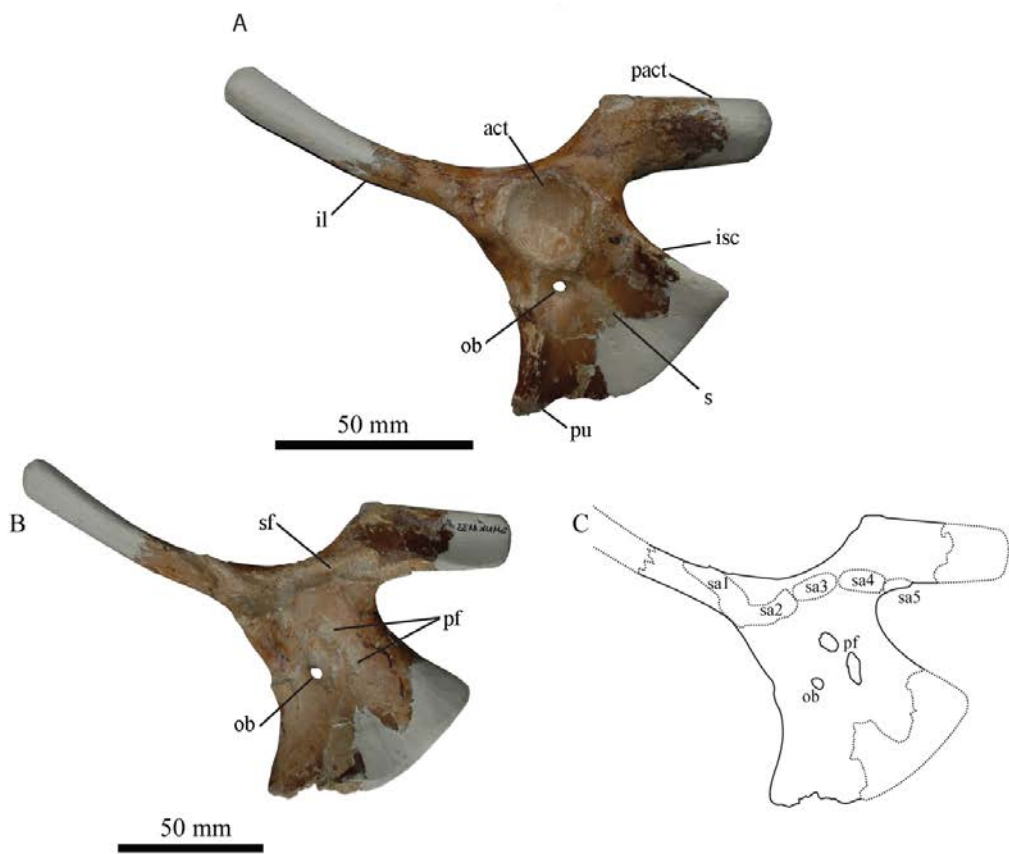


Figure 2.19. SMNK PAL 1133. Right pelvic plate. A, right lateral; B, medial view, C, line tracing of the medial aspect illustrating the sacral articular facets.



Figure 2.20. - SMNK PAL 1133. Right femur. A, cranial; B, medial; C, caudal; D, lateral aspects.

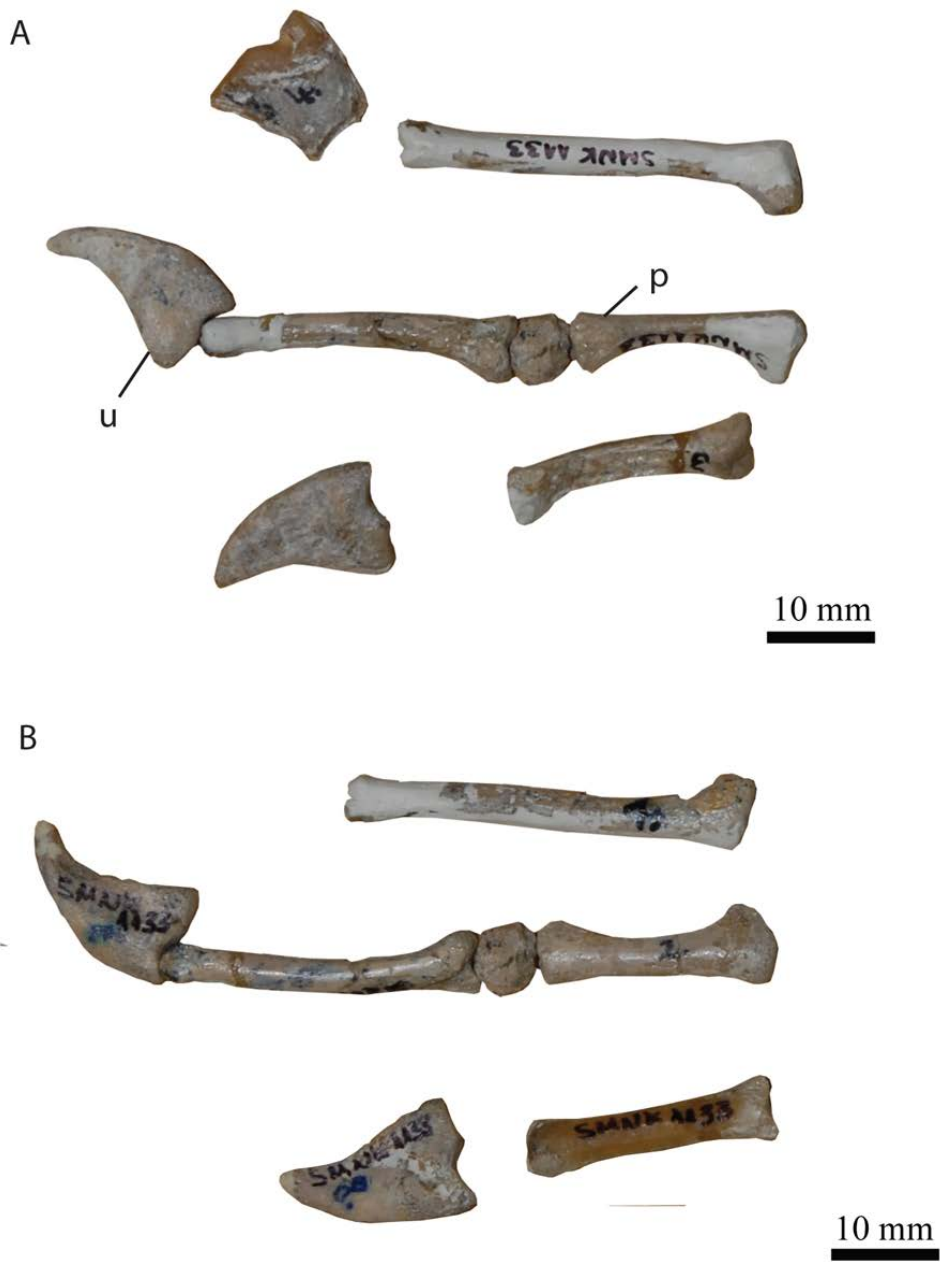


Figure 2.21. - SMNK PAL 1133. Phalanges of the pes. A, left lateral; B, right lateral aspects. The center series is complete and represents that of digit 3.

### **2.0.5 Discussion of the systematic palaeontology:**

The taxonomic history of much of the Ornithocheiroidea, is long and complex, with numerous examples of novel genera and species having been erected on some good, but some poor and ontogenetically variable characteristics, and specimens being first considered synonymous and later re-separated. As it is not necessary to re-state much of this history, interested parties are referred to, among others, Unwin (2001), Veldmeijer et al. (2006), Rodrigues and Kellner (2013) for summaries.

The described specimen SMNK PAL 1133 lacks any elements useful for diagnosis from the skull, reducing the number of specimens to which it can be adequately compared, however, the presence of a largely complete mandible permits an analysis of tooth and diastema patterns. The mandible preserves 17 laterally oriented alveoli, indicating that at least 18 teeth were present owing to the missing first alveoli, and occupy 65% of the total length of the mandible. While SMNK PAL 1133 is of a similar size to the blunt crested *Tropeognathus mesembrinus* (Wellnhofer 1987, Kellner et al. 2013), with mandibular lengths of 572 mm versus 540 mm respectively, they are clearly distinct as the later species has only 11 teeth of a rather uniform size that occupy 51% of the mandibular length.

Within SMNK PAL 1133 the 2<sup>nd</sup> and 3<sup>rd</sup> alveoli are the largest of the preserved features, the 5<sup>th</sup> is the smallest, while the 6<sup>th</sup> alveolus is notably larger than either 4 or 7, after which alveolus size typically increases up to the 9<sup>th</sup> alveolus. This pattern, however, is generally of limited value as similar traits are noted in specimens of *Anhanguera* (e.g. N40PZ-DBAV-UERJ; SAO 2006002), although alveolus size decreases again after the 8<sup>th</sup> feature, and *Coloborhynchus* (e.g. NSM-PV 19892). In spite of this the presence of a significant diastema between the 4<sup>th</sup> and 5<sup>th</sup> alveoli of the mandible is considered diagnostic for *Coloborhynchus robustus* (Wellnhofer 1987, Fastnacht 2001, Veldmeijer et al. 2006), indicating that the described specimen may be considered synonymous with this species.

Wellnhofer (1987) originally named BSP 1987 I 47 as *Tropeognathus robustus* although Kellner (1989) and Kellner and Tomida (2000) later regarded this specimen as *Anhanguera robustus*. Fastnacht (2001) subsequently rejected this conclusion and,

noting the diastema between the 4<sup>th</sup> and 5<sup>th</sup> alveoli in both BSP 1987 I 47 and SMNK PAL 2303, transferred these specimens to *Coloborhynchus* based on the diagnosis of Lee (1994), erecting SMNK PAL 2303 as the paratype of *C. robustus* and amending the diagnosis for the genus. Although Wellnhofer (1987) regarded the shape of the anterior margin of the mandibular crest, making a sharp angle of about 50° with the upper edge of the jaw as diagnostic for the species, the value of the form, shape, and size of the crest in pterosaurs remains controversial as the intraspecific variability of this feature throughout ontogeny remains largely unknown (Martill and Naish 2006). Fastnacht (2001), later supported by Veldmeijer et al (2006), did not regard it as a suitable feature as it is not present in SMNK PAL 2303 and was not included in his 2001 diagnosis. The anterior tip of the mandible in SMNK PAL 1133 has been broken off and thus the amount of information it can add to this debate is limited. The mandibular crest however is a deep feature, indicated by the steepness of its caudal margin, the convex curvature of which suggests a maximum depth of 75 mm occurred level with the 3<sup>rd</sup>-4<sup>th</sup> tooth diastema. While the caudal margin is much steeper than that observed within BSP 1987 I 47, where the maximum depth of the bone occurs beneath the 4<sup>th</sup> -5<sup>th</sup> tooth diastema, in both cases the anterior margin of the crest would have been required to turn dorsally at a very sharp angle before the anterior termination of the mandible. SMNK PAL 1133 and BSP 1987 I 47 are here suggested to have very similar crest forms, *contra* that present within SMNK PAL 2303 (Figure 2.22).

While the genus *Coloborhynchus* was first proposed by Owen (1874) who erected it to accommodate the single specimen of *C. clavirostris* (BMNH 1822) a specific diagnosis was not given, rather only a collection of notable characteristics. The subsequent discovery of another species of *Coloborhynchus* (*C. wadleighi*) from the Lower Cretaceous Paw Paw Formation permitted Lee (1994) to formalise a diagnosis for the genus. While Kellner (1989), Kellner and Tomida (2000) and Rodrigues et al. (2008) have argued that *Coloborhynchus* should be restricted only to these two specimens, with other proposed taxa (including *C. robustus*) assimilated into the genus *Anhanguera* as part of the Anhanguridea (Kellner), this approach has been rejected by a number of workers who hold that differences in dentition pattern (see Veldmeijer et al. 2006), and the blunt anterior margin of the rostrum, brought about by the upturning of the palate, are significant to warrant a split between *Anhanguera*

and *Coloborhynchus* (Lee 1994; Fastnacht 2001; Unwin 2003; Veldmeijer et al 2006). These conclusions are adopted herein and SMNK PAL 1133 is regarded as a further specimen of the species *C. robustus*.

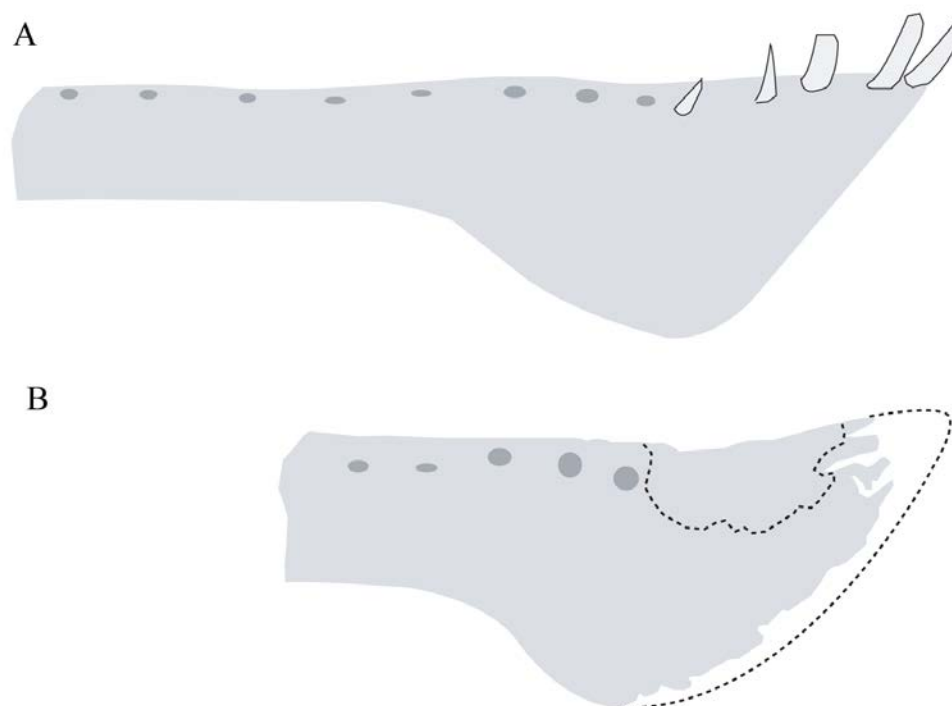


Figure 2.22 – Schematic outline of the anterior mandible in A, *C. robustus* (BSP 1987 I 47, Wellnhofer 1987), and B, SMNK PAL 1133. While SMNK PAL 1133 is badly damaged, mandibular crest is also confined to only the most anterior portion of the dentary, and must have been similarly short and angular. Dashed lines indicate parts of the specimen repaired by plaster. Drawings are not to scale.

### **2.0.6 Discussion of anatomical features:**

The preserved alveoli of SMNK PAL 1133 indicate a similarly large and robust dentition to that of SMNK PAL 2303 and other species within the Ornithocheiroidea that have an elongate mandible, with an expanded rostral end and interlocking teeth. Distal to these the alveoli are generally smaller and more widely spaced. This configuration is strongly indicative that prey capture occurred at the rostral expansion, incorporating the first four to five sets of teeth, and conforming to a “snap-and-kill” style of hunting (Frey et al. 2003a, see Veldmeijer et al. 2007), with the smaller teeth being used to prevent the slippery prey from falling as it was moved back to be swallowed.



Although most evidence now supports a primary role of the crests in sexual selection/display (Tomkins et al. 2010; Hone et al. 2011) it remains possible that this feature may have performed, or assisted, to minor degrees in other activities. Positioning the crest near the tip of the rostrum would have added extra mass to the section of the jaw responsible for killing its prey and created a more forceful bite, although it is noted that the crests are hollow and formed from splints of the premaxilla such that any increase in mass would have been small. Likewise Veldmeijer et al. (2007) advocated that the thin, wedge-shaped crest could have equally been deployed as a wave-cutter to reduce drag while the jaws were submerged during prey capture.

The remains of SMNK PAL 1133 add another three dimensional specimen to the growing number of skeletons that preserve an extensive number of postcranial remains (Wellnhofer 1991b, Kellner and Tomida 2000, Veldmeijer 2006, Kellner et al. 2013). Although postcranial remains are typically poor in diagnostic features (Naish et al. 2013) this nonetheless allows for robust comparisons between a variety of ornithocheirid taxa.

**Cervical vertebrae** - Three cervical vertebrae are known from SMNK PAL 1133, one from the middle portion of the series, while the remaining elements are confidently described as the 8<sup>th</sup> and 9<sup>th</sup> vertebrae – the latter of which is incorporated into the notarium. The condyle of the first of these elements is too narrow to make a firm articulation with the cotyle of the 8<sup>th</sup> cervical. The form of the bone is very similar to that of the 6<sup>th</sup> vertebrae of BSP 1991 I 27, both of which are elongate and narrow with dorsoventrally compressed vertebral bodies (Veldmeijer et al. 2009). The lack of a large pneumatic foramen on the caudal face of the neural spine, dorsal to the neural canal, further supports this interpretation; where in AMNH22555 (Wellnhofer 1991b) this foramen is present in all cervicals anterior to the 6<sup>th</sup>. The only minor differences between the two bones are that the prezygapophyses in SMNK PAL 1133 appear broader and less elongate in lateral view while the prezygapophyses are narrower but orientated in the same direction. The presence of a large pneumatic opening on the lateral flank of the bone is shared with specimens of *Brasileodactylus* (Veldmeijer et al. 2009), *A. santanae* (Wellnhofer 1991b), and *C. piscator* (Kellner

and Tomida 2000), the latter indicating that this feature extended all the way to the atlas-axis and was very likely universal throughout all ornithocheirids. As with *A. santanae* and *C. piscator* no pneumatic elements are located lateral to the neural canal.

The 8<sup>th</sup> cervical is typical in its form to those described from other specimens where it has a “partially dorsalised” (Kellner et al. 2013) appearance with its short, wide body and square neural spine. The rugose scars on the lateral flank of the spine are orientated anteroventrally to differing degrees, becoming more ventrally orientated towards the anterior margin of the spine, and indicate the insertion for muscles that would have acted to control the motions and stability of the neck. Damage to the body prevents any comparison with other specimens (see Veldmeijer et al. 2009) but the presence of bone within the ventral portion of neural canal suggest that the vertebral body and neural arch were fused, unlike NSM-PV 19892.

The 9<sup>th</sup> cervical vertebra is almost identical to the succeeding dorsals but slightly larger in size. As with specimens of *Santanadactylus brasiliensis* and *C. spielbergi* it forms part of the notarium and thus shows a contrasting configuration to *T. mesembrinus* (Kellner et al. 2013) in which only the dorsal vertebrae are included. The taxonomic significance of this observation, however, is debateable, as while genuine differences are observed, there are insufficient specimens to determine if this varies within individual species. The configuration of SMNK PAL 1133 where the cervical has fused its centrum and postzygapophyses with the first dorsal is intermediate between that of RGM 401 880 and MN 6594-V, as the neural spine remains separate from the supraneural plate between the first five dorsals. This, however, can be taken one of two ways, that *C. robustus* has developed an intermediate configuration where the 9<sup>th</sup> cervical only partially fuses with the 1<sup>st</sup> dorsal and thus represents a transitional state between being fully incorporated into the notarium (i.e. taxonomically significant), or further ontological development will eventually cause the neural spine to fuse into the supraneural plate. Although it is not possible to make any firm conclusions the presence of breaks between the individual neural spines that make up the supraneural plate suggests that the notarium is only weakly fused and that further development is likely.

Although the anteroventral margin of the cervical is damaged the presence of a prominent hypapophysis is confirmed where the right hand half of the feature is preserved along the ventral margin of the cotyle. Pneumatic features are present on the anterior face of the bone, ventral to the prezygapophyses, which are also noted in *Brasileodactylus* (BSP 1991 I 27, Veldmeijer et al. 2013). Similar features are noted in AMNH 22555, but are described as flanking the neural canal, while in NSV-PV 19892 Kellner and Tomida (2000) report that they have been reduced to two tiny foramina. Across the cotyle the remnants of the suture between the centum and neural spine is visible. Despite this the bones are firmly fused indicating that sufficient internal fusion has occurred to hold the bones together prior to the obliteration of this suture, and that this must disappear following the complete fusion of the postzygapophyses with the prezygapophyses of the first dorsal.

**Notarium** - The development of the notarium is clearly linked to ontogeny where relatively young ornithocheiroids, i.e. those demonstrating poor degrees of skeletal fusion, do not possess one, while in more mature individuals the notarium can be very robust. As indicated previously the number of vertebrae incorporated into the notarium is variable but it appears that 5-6 dorsals is normal (e.g. Bennett 2001a, b), although more elongate supraneural processes are known that can include much (if not all) of the thoracic column (e.g. SMNK PAL 6609).

The form of the vertebrae agree well with all other published accounts of good three dimensional material with double headed ribs extending up to and (presumably) including the 5<sup>th</sup> dorsal vertebrae. As in other specimens the fourth dorsal possesses a broader neural spine to act as the articulation for the scapula. Large muscle scars appear to be restricted to the first two dorsal vertebrae. While the five dorsal vertebrae form a single solid unit the large gaps between the neural spines, breaks across the divisions of the supraneural plate, visible sutures between accompanying sets of pre/postzygapophyses are contrasted against the notarium of RGM 401 880 in which all sutures (and almost all gaps within the supraneural plate) have closed. The poor/semi-fused state of the bones thus suggests that the condition observed within SMNK PAL 1133 is the more juvenile notarial state within large ornithocheiroids that subsequently develops to a form more similar to RGM 401 880 during later ontogeny.

**Dorsal Ribs** - The majority of the fragmented ribs can be assigned to the first five dorsal vertebrae on account of their widely spaced articulations, which correspond to the spacing between the diapophyses and parapophyses of the notarial vertebrae. As with those ribs attributed to *C. piscator* the caudal face of these is perforated by a single large pneumatic foramen situated between the tuberculum and capitulum, indicating that the pneumatic system extended into the thoracic ribs.

**Remaining Dorsals** - The form of those dorsal vertebrae that are not incorporated into the notarium generally agree well with other published accounts (Wellnhofer 1985, 1991a; Veldmeijer et al. 2009; Kellner and Tomida 2000) and there is little additional information to add. Kellner and Tomida (2000) commented that two pneumatic openings are located dorsolateral to the neural canal and these are also present here in two of the three vertebrae labelled as SMNK PAL 1133, exiting onto the posterior face of the bone. Unlike the previous vertebrae the smallest of the three preserved dorsals does not possess any pneumatic features and is most similar in appearance to dorsal number 11 of *C. spielbergi*, but appears too squat to articulate with the sacral series.

**Sacrals** - The sacrum of SMNK PAL 1133 consists of four fused sacral vertebrae, which is one fewer than reported in each of MN 6594-V, NSM-PV 19892, AMNH 22555 (Wellnhofer 1991b), and AMNH 22569 (Bennett 1990), and two fewer than noted for SMNK PAL 1132 (Frey and Martill 1994) and RGM 401 880 (Veldmeijer 2006), although Kellner et al. (2009) regard there as being only five in this latter specimen. The first element in SMNK PAL 1133 possesses large ribs that are directed strongly caudolaterally which is also the situation noted for the 1<sup>st</sup> sacral in both AMNH 22569 and RGM 401 880, with subsequent vertebrae having been shown to possess ribs that are directed in a more lateral direction. The twisting of the first sacral rib so that it is orientated strongly anterodorsally (*contra* to the subsequent ribs) is also present in AMNH 22555 (Wellnhofer 1991b) and appears to be a diagnostic characteristic of this bone. A different configuration, however, is noted in *Arthurdactylus conandoylei* (Frey and Martill 1994) where the first set of sacral ribs do not expand laterally. It is not certain if the pelvic plate would record the presence of these ribs due to the crushed nature of this specimen, however, the grooves on the medial face of the pelvic plate in SMNK PAL 1133 perfectly match the outline of the

sacral ribs indicating that this unit must represent the first four vertebrae, as well as a missing fifth element, as well as indicating that fusion of the individual sacral occur prior to the fusion of the pelvic plate the sacrum. The missing fifth sacral, with short broad ribs, close to the vertebral body (e.g. Kellner and Tomida 2000) has been replaced with a caudal vertebra during the preparation process, which has been erroneously glued into its place. As such it is not possible to determine if 5 or 6 vertebrae would have been originally present, however, the length of the pelvic plate strongly suggests that SMNK PAL 1133 would only have possessed five sacral, making it distinct from RGM 401 880 but conforming to that configuration noted for other large pterodactyls. As such the sacral of SMNK PAL 1133 are similar to those of other ornithocheiroids the only noticeable difference being that the sacral ribs of the 3<sup>rd</sup> vertebrae are directed anteroventrally at a much steeper angle than in NSM-PV 19892 (the condition in other taxa is uncertain due to the sacrum being fused to the pelvic plate).

**Caudals** - At least eleven caudal vertebrae were described from the ornithocheiroid *C. piscator* (Kellner and Tomida 2000) and indicated that the more anterior elements possessed short vertebral bodies (similar in size to their respective neural spines) which became progressively more elongate in the more posteriorly located bones. While another articulated caudal series considered by Bennett (2001a, UALVP 24238) had vertebrae that remained short and square in outline this likely represents a taxonomic difference as those of Bennett (2001a) belong to *Pteranodon* rather than *Coloborhynchus*. As such the latter are regarded as being of more relevance here. It is uncertain if the first preserved element described by Kellner and Tomida (2000) represents the first bone of the caudal series but the bones are of an identical form to those in SMNK PAL 1133, indicating that those in the latter specimen clearly represent the most anterior of these vertebrae. In NSM-PV 19892 the neural spine has become very low by the 5<sup>th</sup> element while in SMNK PAL 1133 there are at least four bones that possess a neural spine of a similar length to that of the vertebral body and two where these are shorter – indicating that the neural spines in the described specimen did not become very depressed until a more posterior position on the caudal series relative to NSM-PV 19892.

**Sternum** - Repair to the sternum of SMNK PAL 1133 has given it a very misleading outline where comparisons with other well preserved ornithocheirids (e.g. NSM-PV 19892 and RGM 401880) indicate that the plate itself should be more “D-shaped” in dorsal view. Otherwise, the preserved sections agree very well with both specimens and further indicate the presence of large pneumatic foramen on the anterior section of the plate, adjacent to the sternal neck, and supporting the inclusion of the sternum into the pneumatic system. A further foramen located anterior to the first (Veldmeijer 2006) is also observed in SMNK PAL 1133. One noticeable difference concerns the position of the coracoid facets, where Veldmeijer (2006) described these for RGM 401 880 as being located caudal to the large, dorsally located tubercle. In contrast, while Kellner and Tomida (2000) note the presence of a deep depression in NSM-PV 19892, not present in SMNK PAL 1133, they note that the coracoid facets are located anterior to this tubercle and is thus more similar to that of SMNK PAL 1133 than RGM 401 880.

**Scapulocoracoid** - While the scapula and coracoid have fused and represent a morphologically mature unit the suture line between the two bones is still visible running across the glenoid fossa. This feature indicates complete fusion but suggests the animal was only recently mature as in other specimens the suture line has been completely obliterated (e.g. Veldmeijer 2006). The scapulocoracoid is identical to that described by Veldmeijer (2006), the presence of a slit-like pneumatic foramen on the medial face of the bone, and would have undoubtedly extended across both scapula and coracoid indicates the connection of the element to the pneumatic system where it would have opened into a large open internal cavity as illustrated in numerous specimens where the one have not fused.

**Humerus** - The humerus of SMNK PAL 1133 illustrates the mature state of the bone where all epiphyses has fused to the distal end and deep scars have developed on the ventral face of the deltopectoral crest (*contra* to examples such as NSM-PV 19892). A single foramen located on the dorsal aspect of the humerus by the posterior process agrees with other accounts of ornithocheiroid specimens and indicates the only point where the humerus was incorporated into the pneumatic system. The large circular depression on the distal face of the humerus, while still filled with matrix, is not regarded as a pneumatic feature based on a comparison with RGM 401 880. Although

not always present (e.g. NSM-PV 19892, AMNH 22555), the ridge across the medial face of the caput is also noted within the humerus of RGM 401 880 (Veldmeijer 2006), suggesting that it may represent an ontogenetic character – only appearing in more mature skeletons.

**Ulna** - The ulna of SMNK PAL 1133 possess a prominent set of cotyles for articulating against the capitulum and trochlea of the humerus and a large biceps tubercle on the proximal articular face – similar to that observed in RGM 401 880 but lacking in more immature skeletons where epiphyses have yet to fuse. Only minor differences between these specimens are noted where the biceps tubercle is not located right on the cranial margin of bone but slight more on the articular face itself, and the articular face for the capitulum has a more narrow and pointed outline. As with RGM 401 880 and NSM-PV 19892, SMNK PAL 1133 lacks a pneumatic opening either on the shaft or the proximal and distal articular surfaces, contra to that noted in BSP 1982 I 89 where a pneumatic opening is observed on the distal articulation. This indicates that the number of elements incorporated into the pneumatic system appears to variable even within closely allied taxa.

**Carpus** - Kellner and Tomida (2000) suggested the presence of a fourth distal carpal that formed across the dorsal margin of the large depression (fovea carpalis) located on the distal articular face of the distal syncarpus based on NSM-PV 19892). While this observation cannot be firmly supported or rejected here, the top of this fovea is marked by a depression with rough edges in both SMNK PAL 1133 and SMNK PAL 1134 (an ossified proximal and distal syncarpus), suggesting that some element should have been positioned here during life. Both distal syncarpals are ontogenetically mature and fusion between all the carpalia is complete so there is no reason that the fourth carpal suggested by Kellner and Tomida (2000) should be missing. However, the roughness of the bone at this location in SMNK PAL 1133 and 1134 suggests that the bone has been forcibly broken (see Figure 2.14D). I can offer no good reason as to why this location should be broken in such a manner in mature ornithocheiroids.

**Metacarpals** - The fourth metacarpal is marked by two large depressions on the distal cranial and caudal sections of the bone for the insertion for extensor and flexor

muscles originating off the first metacarpal, however, none of these have developed to an extent that they pierce the compacta as noted in a number of taxa including the immature NSM-PV 19892 (Kellner & Tomida 2000) and *Pteranodon* (Bennett 2001a, b). While these foramina are small it seems likely that they represent the precursors to the development of fully pneumatic openings in the more derived azhdarchoids (Eck et al. 2011) and indicate that at least some pneumatic openings originated in more primitive taxa as deep excavations to support the insertion of muscles – a feature also noted for the femur.

**Digit IV** - The wing finger phalanges in almost all pterosaurs are similar in form with expanded proximal and distal margins, the shafts of which show various degrees of curvature. Those preserved in SMNK PAL 1133 are not exception and agree well with other descriptions of pterodactyls. The extensor tendon process is fused to the first wing finger phalanx, indicating that it is relatively more mature than specimens such as NSM-PV 19892 (*Coloborhynchus piscator*) and MHNS/00/85 (*Barbosania gracilirostris*), this feature being largely regarded as a reliable indicator of late ontogeny (although see Elgin and Frey 2011a). The presence of a large pneumatic foramen on the ventral face of the phalanx close to the proximal margin is a feature that is observed in all ornithocheiroids where the element is preserved, and indicates that this element must have formed part of the pneumatic system. The lack of any pneumatic elements on the fourth metacarpal of SMNK PAL 1133, suggest that subcutaneous air-sacs (as argued by Claessens et al. 2009) would have been required to connect the bone to those pneumatic elements of the antebrachium.

**Pelvis** - The pelvic plate in SMNK PAL 1133 is fully fused although the traces of where the individual elements meet are still visible, indicating that the skeletal state of the plate was not fully mature. The elongate ilium curves dorsally similar to that of *T. mesembrinus* (Kellner et al. 2013) while the postacetabular process is directed caudally and is identical to that of described for both NSM-PV 19892 and AMNH 22555 (Wellnhofer 1988; Kellner and Tomida 2000). The obturator foramen of SMNK PAL 1133 is fully incorporated into the pubis while the ischium is perforated by two very large pneumatic features on its medial face. These features all appear to be the primary way in which the pelvic girdle is incorporated into the pneumatic



system, as has been noted by Claessens et al. (2009) and in the azhdarchoid SMNK PAL 6609.

The formation of a symphysis in mature or sub-adult individuals, formed between the opposing pubes and ischia, have been observed in numerous specimens, e.g. AMNH 22569 (Bennett 1990), RGM 401 880 (Veldmeijer 2003), SMNK PAL 4331, or can be inferred in morphologically immature specimens by restoring the pelvic elements to their life positions (i.e. NSM-PV 19892, Kellner & Tomida 2000). A restoration of the pelvic girdle of SMNK PAL 1133 using casts to reconstruct the missing left hand pelvic plate, however, does not bring ventral margin of the ischium close to the midline, implying that the formation of a symphysis would not have been possible without substantial growth and elongation of the ischium (Figure 2.23). This observation results in two possible conclusions where either the pelvic symphysis is not universally present in pterodactyloid pterosaurs, or the pelvic girdle of SMNK PAL 1133 underwent an abnormal pattern of development, a conclusion that appears unlikely given the superb and otherwise normal preservation of the skeleton. If the former is true then the lack of a symphysis represents a taxonomic feature that separates *C. robustus* from its immediate relatives or represents a sexual dimorphism; the individual being a female with an open pelvic girdle to facilitate the passage of eggs. The lack of specimens that support this interpretation, however, means that it must be treated with caution and it is noted that in all the pelvic girdles examined by Bennett (1993), including those of putative females, the symphysis has formed.

**Femur** - The caput is offset against the shaft at an angle of 20° against the femoral shaft and is subsequently similar to the range of values noted for other ornithocheiroids (e.g. 28°- 32°, Kellner and Tomida 2000; Veldmeijer 2006). The “greater trochanter” (Bennett 2001a, b) or “lesser trochanter” (Hutchinson 2001) is little more than a small protrusion which is sharply contrasted against those known within the Azhdarchoidea for which terrestrial locomotion appears to have been a more commonly utilised mode of transport. The femur of SMNK PAL 1133 does not possess any pneumatic features indicating that, as with other ornithocheirids, the pneumatic system did not extend into the hind limbs.

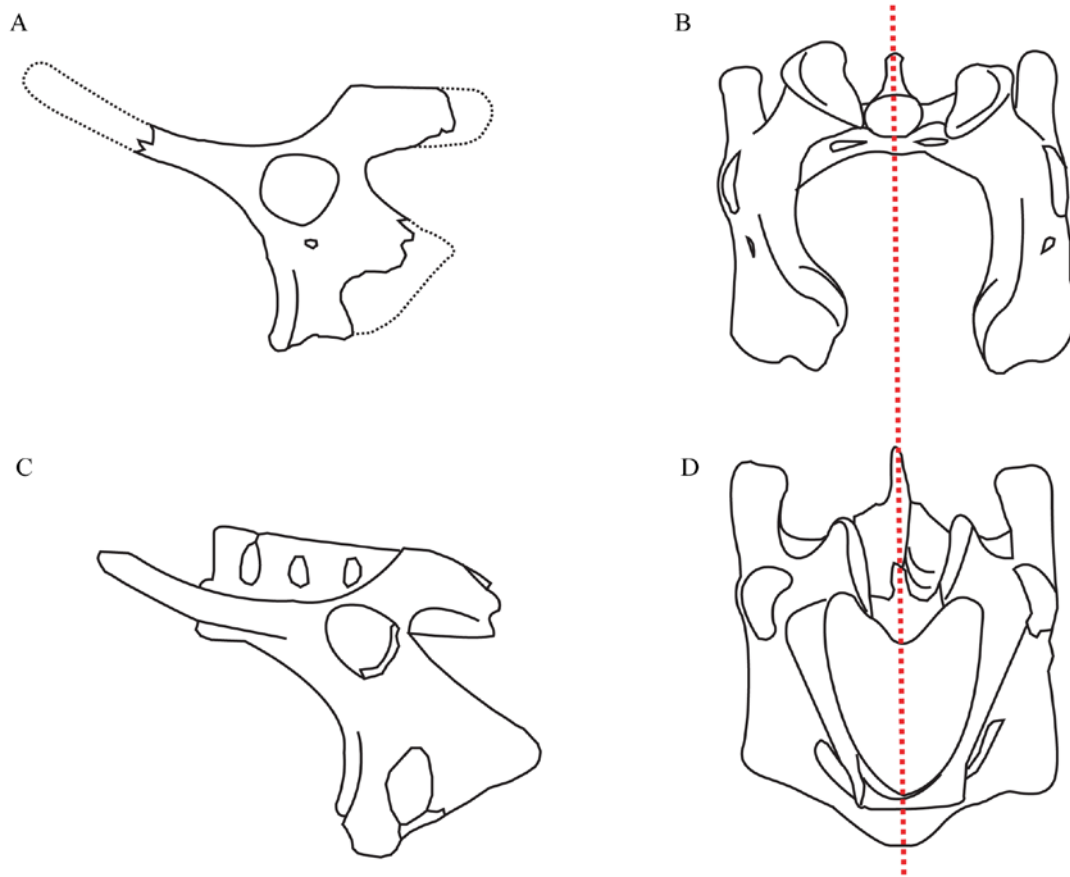


Figure 2.23. – Pelvic girdle in two ornithocheiroid taxa. A-B. *Coloborhynchus robustus* (SMNK PAL 1133); C-D, *C. speilbergi* (RGM 401880). A & C, illustrate the pelvic girdle in its left lateral aspect. B & D, illustrate the pelvic girdle in its caudal aspect. Pelvic girdle of SMNK PAL 1133 reconstructed from resin casts of the bones. Hatched line in B and D indicate the midline of the body. Ventral margin of the bone is open in SMNK PAL 1133 while a symphysis has formed in RGM 401880.

**Morphological maturity** –The described specimen of *C. robustus* represents an adult individual based on the extensive closure of bone sutures, well ossified articular surfaces, and a lack of pitting of the cortex, three features considered representative of mature pterosaurs (Bennett 1993). It is, however, inferred to be a relatively newly adult as several features known to fused together in later ontogeny remain either unfused, or display an incompletely closed sutures, where the lines of contact between elements have not yet been obliterated. As such the specimen provides a degree of information on the relative timing of suture closure in pterodactyloid pterosaurs (see Bennett 1993; Kellner and Tomida 2000), where the fusion of the pelvic plate to the sacral vertebrae to form the pelvic girdle as a single ossified unit, occurs very late in ontogeny. Likewise, fusion of the vertebral bodies to the neural spines appears to occur later in the more anterior located vertebrae, where the first element of the

notarium (i.e. the 9<sup>th</sup> cervical) still preserves the remains of the neurocentral suture, as to does the scapulocoracoid. Although each of these elements is considered mature it is apparent that further development to obliterate these sutures would have taken place in later adulthood. The notarium itself displays an interesting combination of suture states where the pre/postzygapophyses are fused but the neural plate, while fused, appears only weakly so, with cracks through the bone marking the contact between adjacent neural spines and evidently representing lines of weakness that fractured during the fossilization process.

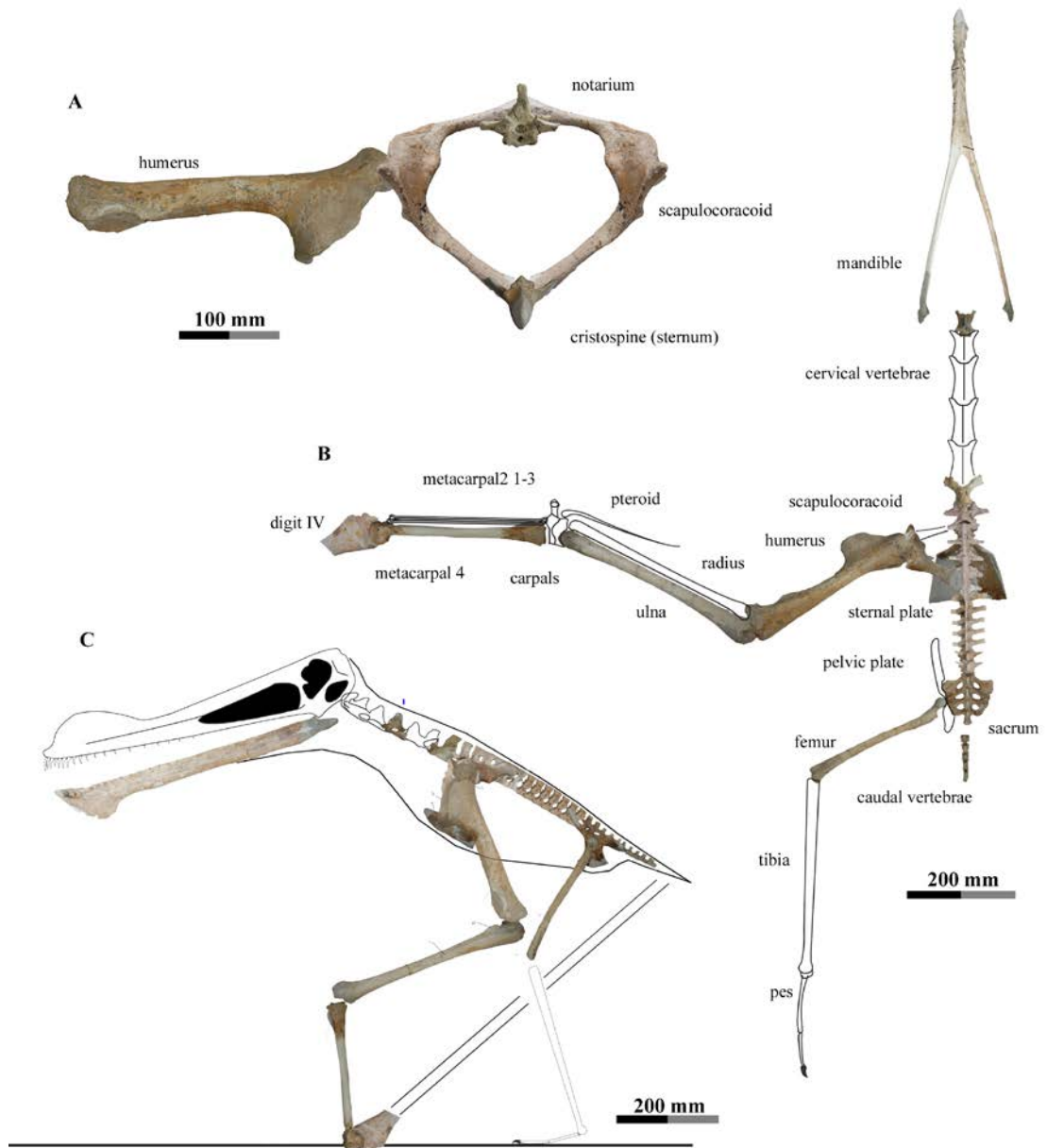


Figure 2.24 – Reconstructions of *Coloborhynchus robustus* (SMNK PAL 1133) based on the isolated bones of the prepared skeleton. A, cranial view of the pectoral girdle, indicating maximum girth of the animal, and level/position of the humerus when placed within the glenoid fossa. B, *C. robustus* in dorsal view with the skeleton arranged in the hypothetical glide position. The distal wing spar and reconstruction of the skull are omitted for clarity. C, *C. robustus* in left lateral view with the skeleton arranged into a hypothetical standing position. Wing finger is omitted for clarity.

## **2.1. The description of a novel genus and species *Barbosania gracilirostris* (MHNS/00/85).**

### **2.1.1 Introduction**

The function (or functions) of the cranial crests in pterosaurs are varied, with authors advocating a role in sexual selection, heat exchange, aerodynamic or hydrodynamic activities (e.g. Bramwell and Whitfield 1974; Kellner and Tomida 2000; Veldmeijer 2009; Tomkins et al. 2010; Hone et al. 2011). Their presence in a wide range of pterosaurs, including the more basal Triassic and Jurassic members (Stecher 2008), infer that crests formed an important function and were a common feature within the lineage. While the significance of the crest for taxonomic purposes has long been discussed with regards to the Ornithocheiroidea, several specimens lack this entirely and are attributed to the genus *Brasileodactylus*. While such specimens are morphologically immature, as too are many ornithocheirids for which a crest is also known.

Here a new specimen of crestless ornithocheirid was acquired by the Sintra Museum of Natural History, Portugal from the Romualdo Member of the Chapada do Araripe, NE Brazil. In addition to providing a detailed account of the skeleton of a well preserved, juvenile ornithocheirid, the specimen is sufficiently distinct from specimens of *Brasileodactylus* to warrant the erection of a new genus, *Barbosania*. The skeleton is unusual in that the extensor tendon process of the wing finger phalanx has partially fused.

The fossil was almost completely encased within its protective concretion and required extensive preparation to expose it. The Sintra museum requested that the SMNK prepare the specimen and generously allowed it to be described on completion of this work. A single cast of the specimen is retained by the SMNK while the original fossil was returned to Portugal where it is held under the collection number MHNS/00/85.

### **2.1.2 Systematic Palaeontology**

Order Pterosauria Kaup 1834

Superfamily Ornithocheiroidea Seeley 1870

Family Ornithocheiridae Seeley 1870

Genus *Barbosania* Elgin and Frey 2011a

**Diagnosis** - Ornithocheirid pterosaur with the following combination of diagnostic features. Only character 11 is considered truly apomorphic for this genus:

1. Keeled but crestless rostrum with a pointed termination.
2. Rostral-most pair of the mandibular and premaxillary alveoli positioned rostroventrally and rostr dorsally respectively.
3. Tooth positions two and three in both jaws with teeth that are twice as long as those of the subsequent alveoli.
4. The 2<sup>nd</sup> and 3<sup>rd</sup> teeth are orientated cranio laterally and together with the rostral-most teeth form a narrow rosette due to a missing expansion of the tip of the rostrum.
5. Lateral margins of the rostrum gradually converge rostrally.
6. An estimated 24 and 20 tooth positions in the upper and the lower jaw respectively.
8. Inter alveolar space gradually increasing caudally, alveolar diameter about constant until tooth position 13.
7. Teeth between the eighth and thirteenth tooth positions in upper and lower jaw with an almost symmetrical interdigitation.
8. Height of the nasoantorbital fenestra approximately 22% that of its length and forming 24% of the total skull length.
9. Parietal with flat external face, dorsal margin of the short median occipital process is deflected with a triangular transversally convex dorsal face.
10. Thirteen trunk vertebrae.
11. Caudoventral margin of ischium concave.

*Barbosania gracilirostris* Elgin and Frey 2011a

**Included Material** - The only known specimen of this genus is MHNS/00/85 (Holotype).

**Diagnosis** - As for genus

### **2.1.3 Specimen Details**

**Collection number of the described specimen** - MHNS/00/85

**History and Locality Information** - The specimen originates from the NE of Brazil and was purchased by the Museum of Natural History Sintra. As such locality information is limited. That the specimen was secured in a blue/grey concretion indicates that it originated from the Romualdo Member (Albian, Lower Cretaceous), Chapada do Araripe, NE Brazil, and more specifically the Sierra de Maõsina.

### **2.1.4 Specimen Description**

As the specimen was published before the submission of this work readers are referred to Elgin and Frey (2011a) for a complete description and Figures 2.25 – 2.29 for documentation.

### **2.1.5 Additional Remarks**

Following the formal publication of *B. gracilirostris* in 2011 several conversations with other pterosaur workers brought to my attention that the diagnosis provided by Elgin and Frey (2011a) may be taken as a complete list of all characteristics that other specimens must possess before they might be considered synonymous, rather than regarding it as a differential diagnosis. Owing to the many similarities that this MHNS/00/85 shared with other taxa (specifically *Anhanguera fittoni*), and indeed the number of common characteristics that all ornithocheirids share, I had intended this diagnosis to describe features that in conjunction with one another might diagnose this species. Thus future specimens might be regarded as synonymous where only a handful of these characteristics included within the diagnosis are observed and no other more robust placement can be determined. The one exception to this remains Elgin and Frey's character 11, "Caudoventral margin of ischium concave," which is still recognised as apomorphic for this species.

The inherent differences in cranial configuration between specimens of *Barbosania* (and *Brasileodactylus*) and crested taxa that display greatly expanded rostral regions with large and robust teeth raise three immediate considerations of note which are further considered here: i) the validity of crestless taxa and how this feature relates to ontogeny; ii) the influence of these structures for cranial biomechanics/aerodynamics; iii) influence of skull shape with respects to prey capture.

**Crestlessness in ornithocheiroids** - The presence or absence of a cranial crest in pterosaurs can no longer be considered in such binary terms as the feature strongly influenced by ontogeny (Martill and Naish 2006). Thus where it may be absent in juvenile animals, the onset of maturity can produce rapid growth which is best demonstrated by the development of an elongated spar in *Nyctosaurus* (Bennett 2003b). Although the configuration in *Nyctosaurus* is now well known, the various configurations within the Ornithocheiridae and their relationships with ontogeny are substantially more difficult to decipher. Here specimens displaying skeletal features indicative of mature and sub-adult states both possess cranial crests (e.g. Kellner and Tomida 2000; Wellnhofer 1991b) leading a number of workers to regard crest shape as being largely unhelpful for taxonomic assessment (Fastnacht 2001; Veldmeijer 2006). As such the small number of specimens that lack this feature altogether may be considered taxonomically distinct (see Veldmeijer et al. 2009) and was one reason that Elgin and Frey (2011a) established a new genus to accommodate MHNS/00/85 rather than synonymise this with those specimens attributed to *Brasileodactylus* (Veldmeijer et al. 2009) and further relate these to crested forms known from the Araripe region of NE Brazil. The discovery of further specimens has done little to resolve this debate although specimens from China indicate that cranial crest are not always indicative of a mandibular crest (e.g. Lü et al. 2012), further complicating the situation. Thus while the practice of erecting genera or species on the basis of crestless taxa remains may at least remain partially controversial, the complete lack of a cranial or mandibular crest as a diagnostic feature (rather than crest shape itself) has not been discredited and to the author's knowledge no one has yet indicated that *B. gracilirostris* should be considered a junior synonym of another taxon.



The lack of a crest in *B. gracilirostris*, *Brasileodactylus araripensis*, and presumably juvenile taxa would have prohibited these individuals from using it as a keel to prevent or limit yawing torques as presented by Veldmeijer et al. (2007) and considered previously for species of *Coloborhynchus*. Regardless, while this implies various approaches to foraging within the Ornithocheiridae its effect must have been somewhat limited given the overall similarities in the ornithocheiroid skull and the absence of rostral crests in other long beaked/snouted pterosaurs. It therefore seems unlikely that the lack of a median rostral crest would have prohibited the animal from engaging in either surface capture activities, or snatching prey from just below the surface of the water. This is supported here by the presence of ribbed and closely interlocking teeth within *B. gracilirostris* (Figure 2.27 - 28) that would have permitted the animal to snatch slippery prey from the surface waters, although it is noted that the differences in interalveolar spacing, tooth size and thickness and the degree of the rostral expansion would clearly impose limits on the size and power of the potential prey species. In *B. gracilirostris* the narrow and gracile teeth, along with its relatively small size and lack of a robust rostral expansion, imply that it was restricted to a diet of small fish or other vertebrates when compared to *C. robustus*, which has larger and more robust teeth owing to its larger size and rostral expansion. Furthermore it might also be suggested that the lack of a median crest would permit the narrow and slender rostrum of *Barbosania gracilirostris* to have been operated with less muscular power than in *Anhanguera/Coloborhynchus*, in which the weight of the crest would have been added to that of the rostrum. The relative reduction in cervicooccipital musculature may perhaps explain the small supraoccipital process observed within *B. gracilirostris*. While inferring muscular power from surface area attachment alone can (and is) problematic, the similarity in skull morphology between these taxa suggests that such conclusions may be considered correct.

| <b>Element</b>                         | <b>length (mm)</b> | <b>Element</b>             | <b>length (mm)</b> |
|--|--------------------|----------------------------|--------------------|
| <b>Skull</b>                           |                    | <b>Long bones</b>          |                    |
| skull (occipital condyle - snout)      | 391                | humerus (right/left)       | 155/162            |
| NAOF                                   | 96*                | ulna (right/left)          | 223 / >111         |
| mandible (articulation to rostral tip) | 330                | carpus width (right)       | 58                 |
|  |                    | pteroideum (left)          | 129                |
| <b>Axial column</b>                    |                    | mc III                     | 137                |
| 9th cervical                           | 13                 | metacarpal IV (right/left) | 155 / 156          |
| notarium                               | 59                 | d4 p1 (right/left)         | >191.9 / >151.7    |
| body length                            | 209.5              | femur (right/left)         | 127 / 43*          |

Table 2. - *Barbosania gracilirostris*, MNHS/00/85, selected bone measurements. \* denotes an approximation or estimate value.

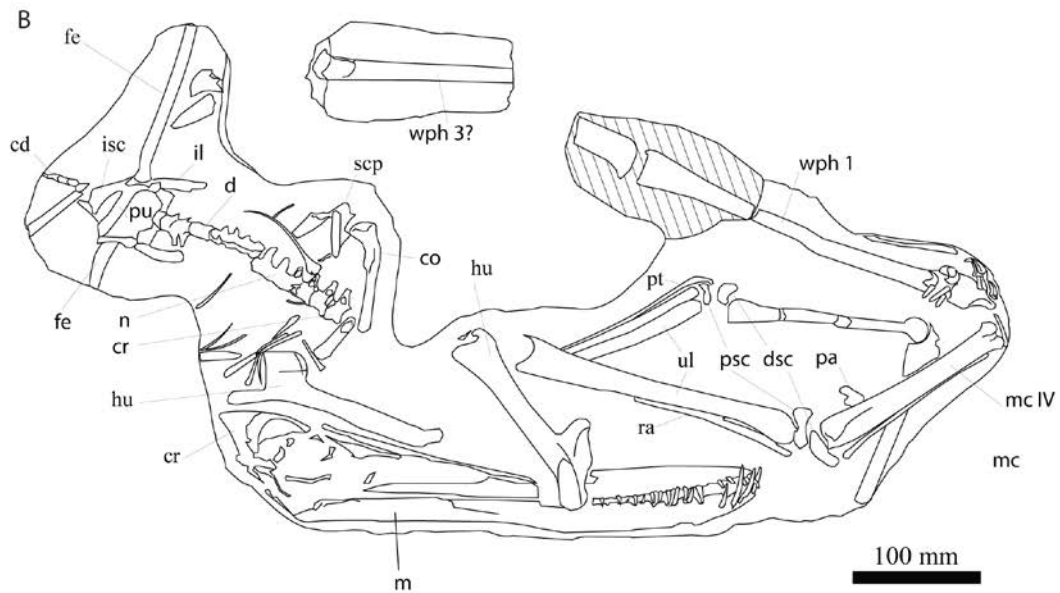


Figure 2.25. - *Barbosania gracilirostris* gen. et sp. nov. A, photograph and B, corresponding line tracing.

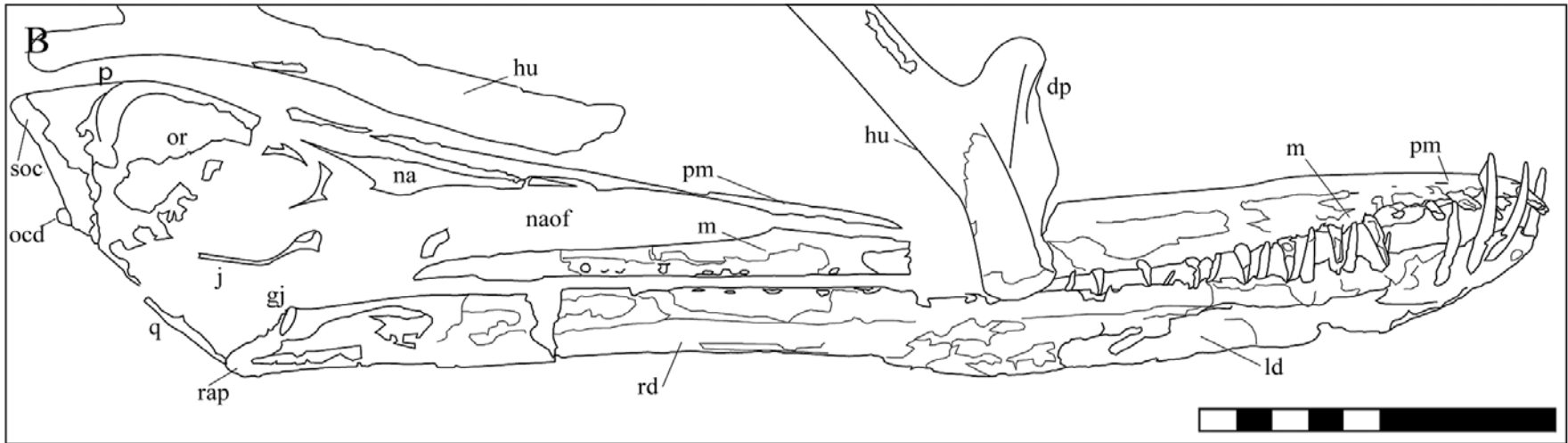
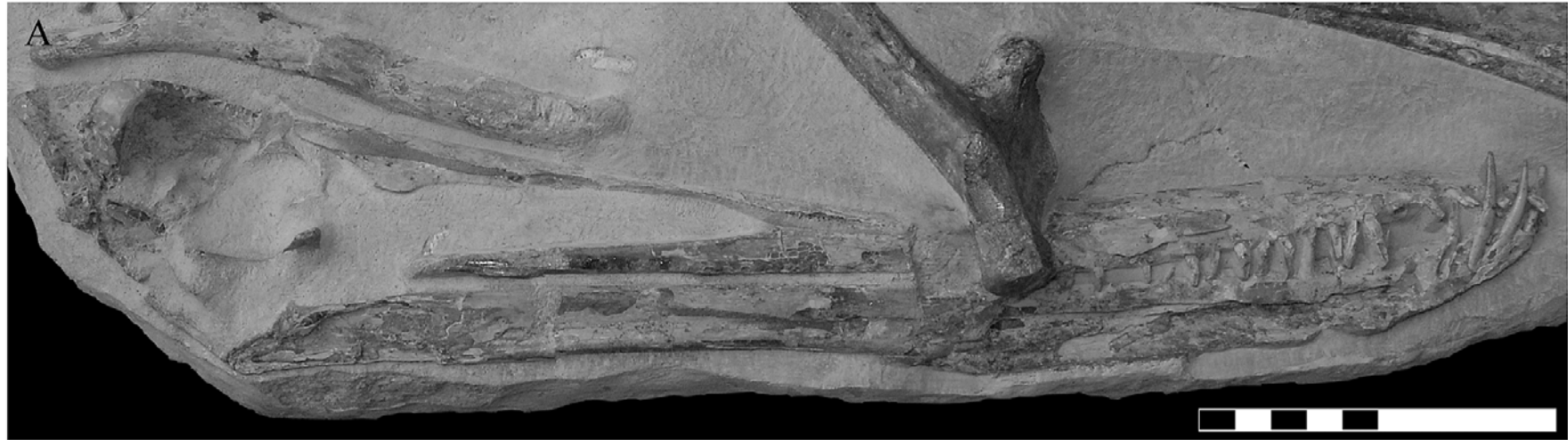


Figure 2.26 - *Barbosania gracilirostris* gen. et ep. nov. MNHS/00/85. Photograph (A) and corresponding line tracing (B).



Figure 2.27. A, *Barbosania gracilirostris* (MHNS/00/85). Photograph of the rostrum in left lateral view. B, close up of the rostrum showing the first few pairs of teeth. Small replacement teeth are visible growing behind the first tooth of the mandible and the third tooth of the upper jaw. In both pictures the skull is on top while the mandible is the lower of the two elements.



Figure 2.28. *Barbosania gracilirostris* (MHNS/00/85). A, B, photographs in various anterolateral views to illustrate the anterior-most pairs of teeth. Tooth order for the left hand side of the upper jaw is marked. C, close up of the anterior margin of the skull showing the newly developing mandibular teeth and an example of striations on the mature tooth.

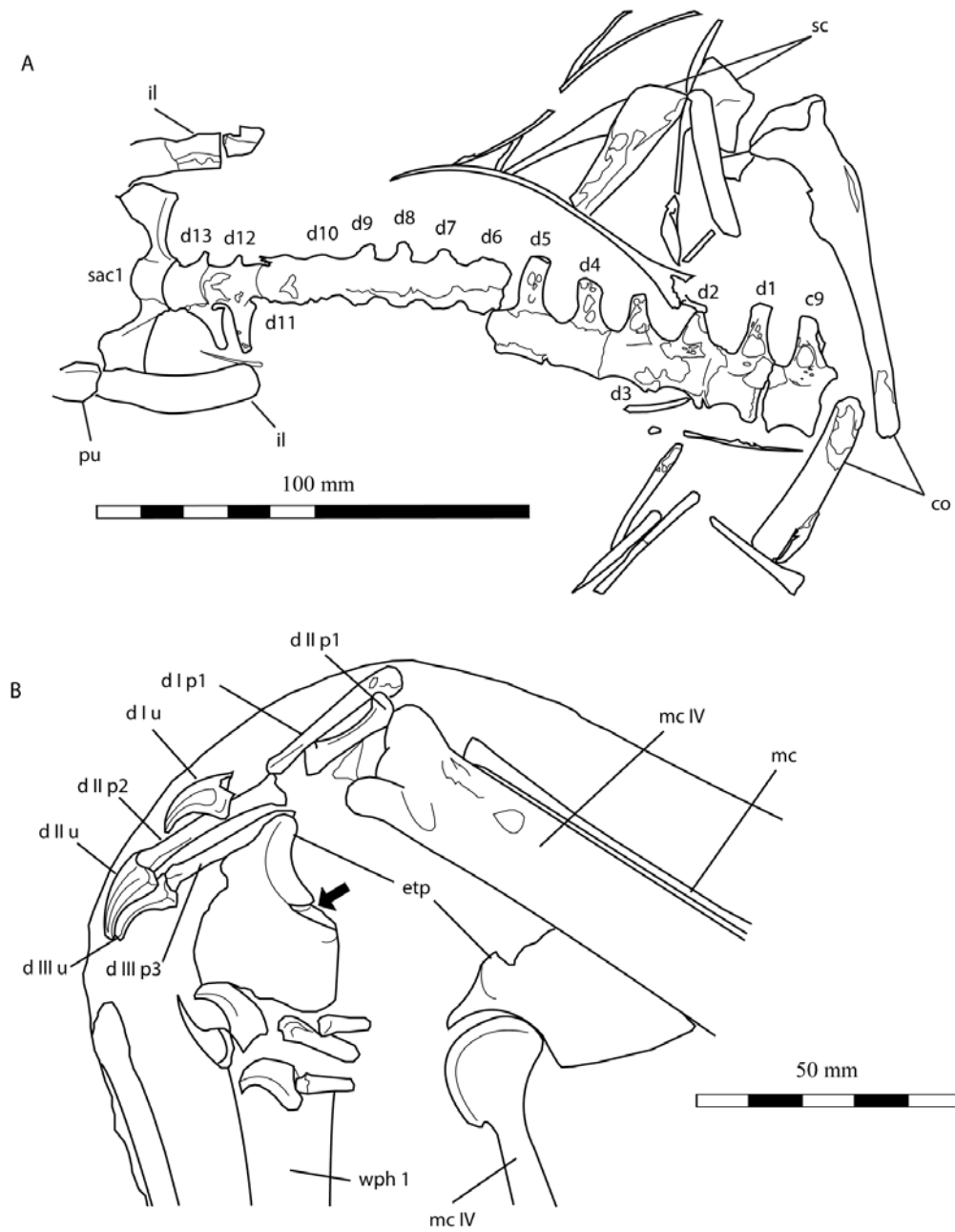


Figure 2.29. *Barbosania gracilirostris* (MNHS/00/85). Line tracings of the vertebral column and manus. A, vertebral column in its ventral aspect. B, wing metatarsophalangeal joint in its ventral aspect. Arrow denotes the position of the partially open suture.

## **2.2. The description of a new ornithocheirid specimen (SMNK PAL 3854)**

### **2.2.1 Introduction**

As indicated by the previous specimens, the remains of a number of very well preserved and largely complete ornithocheiroid pterosaurs are known from the Romualdo Member of NE Brazil, however, relatively few have been unearthed from the older Crato Member (Unwin and Martill 2007). Frey and Martill (1994) described one such specimen which demonstrated a number of similarities to a new specimen offered for sale to the SMNK, erecting it as a novel genus and species *Arthurdactylus conandoylei*. A second ornithocheirid fossil subsequently purchased, also lacking the head, and preserving a good portion of the body and limbs, but distinguished from *A. conandoylei* by slight difference in the biometrics of the long bones. The pes of this specimen has disarticulated, but the individual elements are well preserved, allowing the foot to be reconstructed. Comparisons with azhdarchoid material from the same region indicate that the ornithocheirid foot was very lightly built, suggesting that the latter animals spent significantly less time walking on the ground.

### **2.2.2 Systematic Palaeontology:**

Order Pterosauria Kaup 1834

Superfamily Ornithocheiroidea Seeley 1870

Family Ornithocheiridae Seeley 1870

ornithocheirid indet.

### **2.2.3 Specimen Details:**

**Collection number of the described specimen** - SMNK PAL 3854 (Figure 2.30 – 34)

**History & Locality Information** - The specimen is preserved on a pale slab of flat limestone and unlike those previously described specimens has been extensively crushed, although some three dimensional details remain. The specimen is indicative



of those known from the Nova Olinda Member of the Crato Formation (Aptian, Unwin and Martill 2007) but as it was purchased privately no further locality information is possible.

#### **2.2.4 Specimen Description**

The initial description of this specimen has now been accepted for publication and a full account of the descriptive palaeontology is given by Elgin and Frey (2012) attached at the end of this section.

| <b>Element</b>     | <b>mm</b> | <b>Element</b> | <b>mm</b> |
|--------------------|-----------|----------------|-----------|
| Cervical vertebrae |           | Humerus        |           |
| C5 length          | 37        | left           | 157       |
| C5 mid width       | 28        | right          | 160       |
| C6 length          | 33*       |                |           |
| C6 mid width       | -         | Ulna           |           |
| C7 length          | >25       | left           | 252       |
| C7 mid width       | -         | right          | 253       |
|                    |           |                |           |
| Caudal vertebrae   |           | Metacarpal IV  |           |
| 1                  | 10        | left           | 169       |
| 2                  | 11*       | right          | 169       |
| 3                  | 10.5      |                |           |
| 4                  | 12        | Wph 1          |           |
| 5                  | 12        | left           | 383       |
| 6                  | 11        | right          | 381       |
| 7                  | >6.9      |                |           |
| 8                  | 12        | Femur          |           |
| 9                  | 10        | left           | 161       |
| 10                 | 6.2       | right          | >150      |
| 11                 | >5        |                |           |
|                    |           | Tibia          |           |
| Scapula            | 73.5      | left           | >197      |
| Coracoid           | >61       | right          | 202       |

Table 3 – SMNK PAL 3854. Measurements of selected bone elements. All values are in mm, where \* denotes an approximate or estimated value.

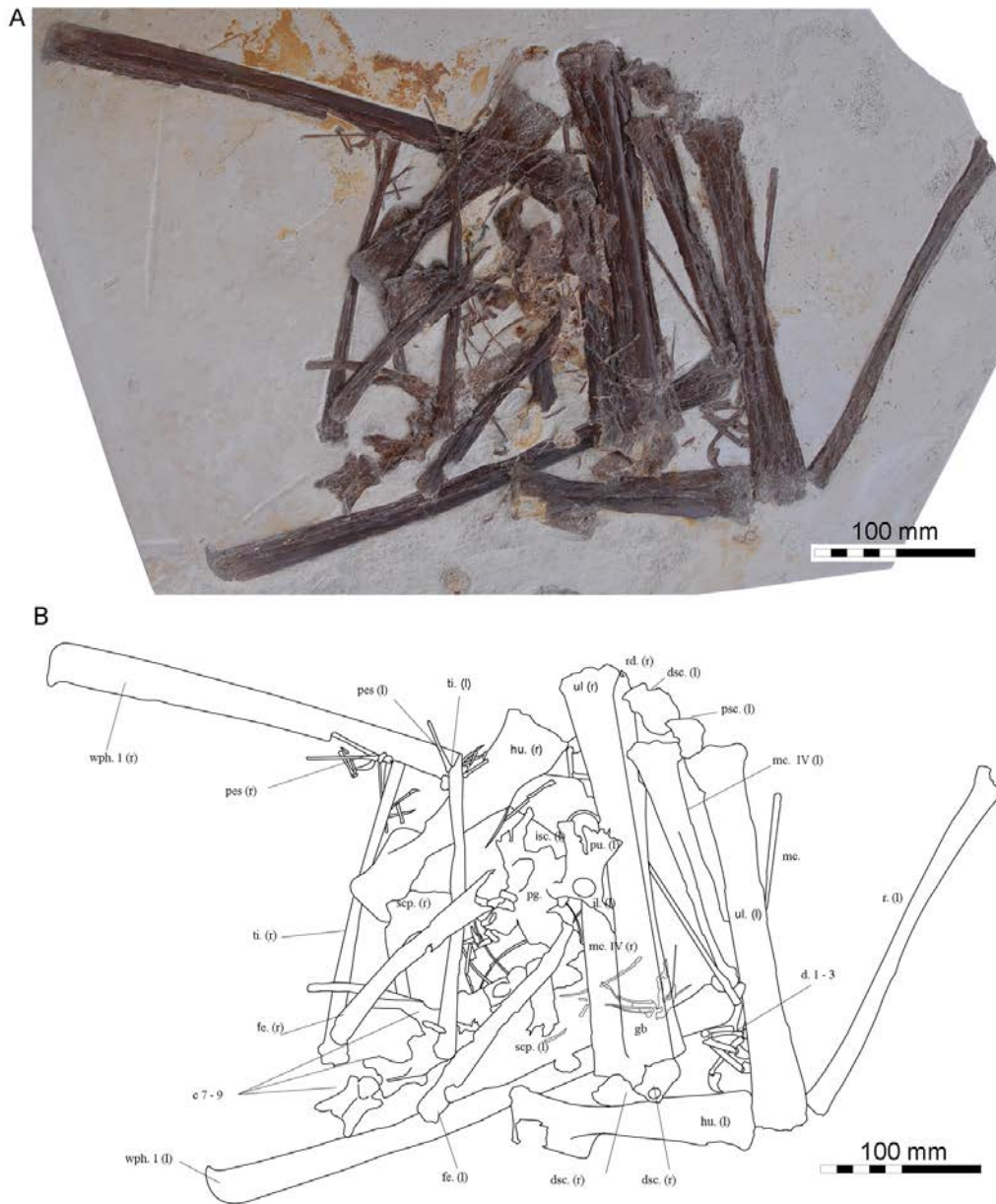


Figure 2.30. - ornithocheirid indet. SMNK PAL 3854. A, Photograph and B, corresponding line tracing.

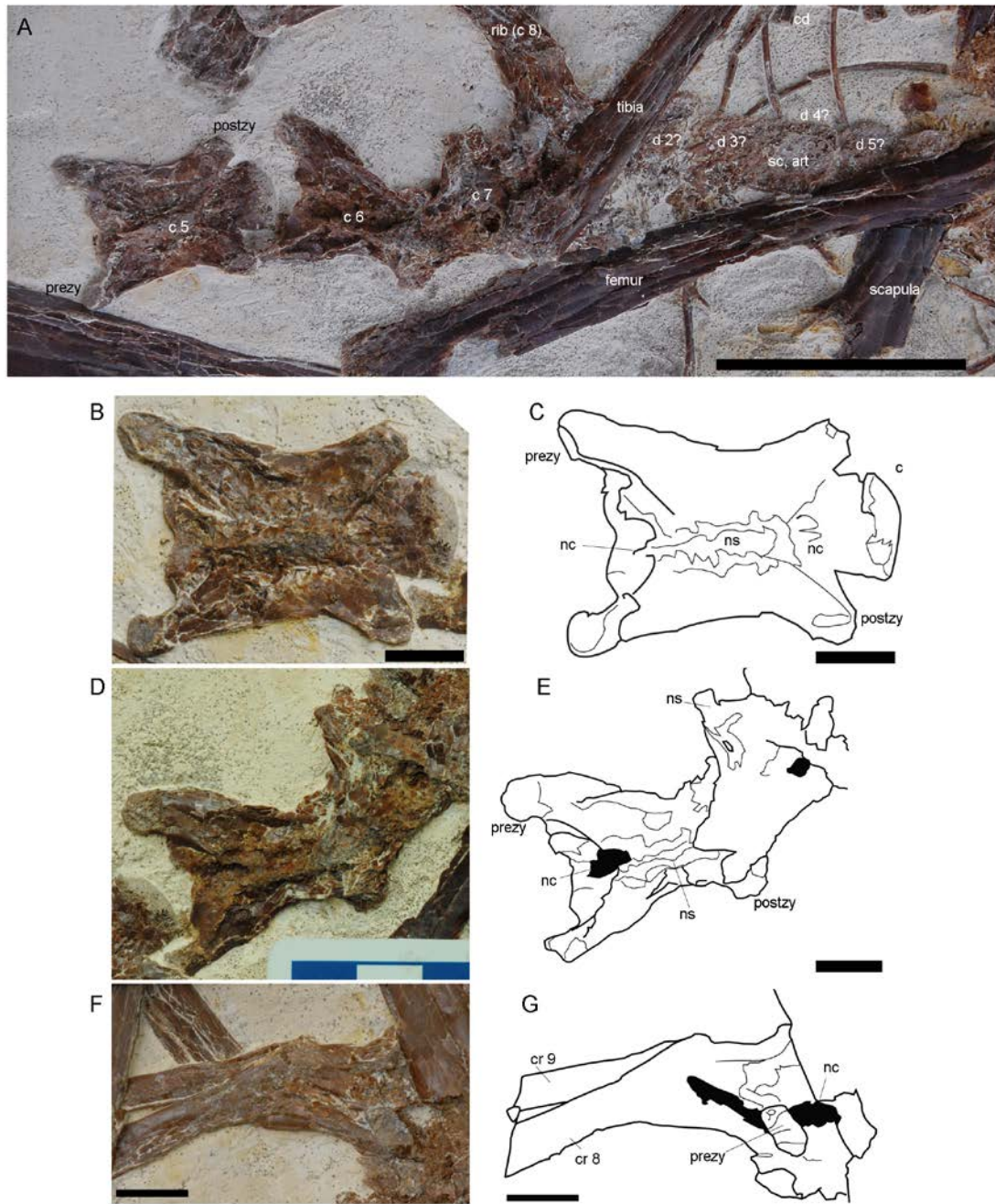


Figure 2.31. – ornithocheirid indet., SMNK PAL 3854. A, overview of the vertebral column centring on the cervicals and cranial dorsal vertebrae, forming a partial notarium. The caudal vertebrae are visible in the top right of the photograph. B-C, photograph and line tracing of the 7th cervical; D-E, 6th and 7th cervicals; F-G, 8th cervical and its associated rib overlying the right rib of the 9th cervical.



Figure 2.32 - A, Gastral basket of SMNK PAL 3854 and B, a close up of the left-most three ribs in A, and associated tissues.

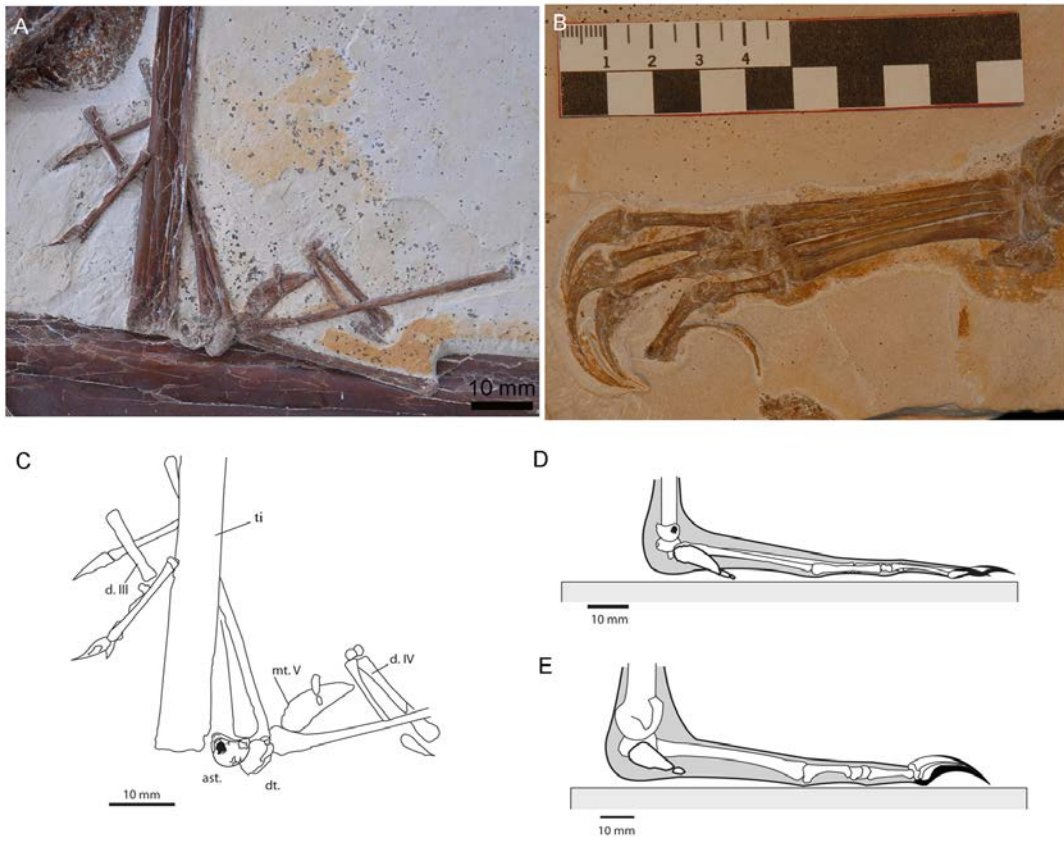


Figure 2.33 - Tibia, tarsals and pes. A, photograph of SMNK PAL 3854 and B, photograph of SMNK PAL 3830, illustrating the difference in pedal form. C, line tracing of SMNK PAL 3854 and reconstruction of the pes in both ornithocheirids (D, from SMNK PAL 3854) and azhdarchoids (E, from SMNK PAL 3830).

## Chapter 3

---

### DESCRIPTIVE PALAEOLOGY OF THE AZHDARCHOIDEA

### **3.0. Further examination of an indeterminate azhdarchoid specimen (SMNK PAL 3830)**

#### **3.0.1 Introduction**

The specimen SMNK PAL 3830 represents one of a number of partial azhdarchoids that are included within this work owing to a number of new and useful observations that such fossils bring to our understanding of the azhdarchoid postcranial skeleton and soft tissue structures. While Frey et al. (2003a) originally described this specimen as an azhdarchid, the bone ratios between the femur and tibia (0.69) and metatarsal and hind limb (0.11) are not unique to the Azhdarchoidea, and the fossil is instead regarded as an indeterminate member of the Azhdarchoidea (Unwin and Martill 2007). While Unwin and Martill (2007, p 499-502) erroneously noted a number of characteristics associated with the forelimb of this specimen (i.e. a wing metacarpal longer than the humerus; the proportions of the wing-finger phalanxes to the total digit length (46, 29, 19 and 7%); the ratio of the fore limb to the hind limb (2.93), this is corrected here as no antebrachial elements are preserved. Soft tissue remains included that of the brachiopatagium, preserving large/small scale folding patterns and coarse wrinkling along the trailing edge of the membrane, and well developed, keratinous claw sheaths (Frey et al. 2003a).

#### **3.0.2 Systematic Palaeontology**

Order Pterosauria Kaup 1834  
Superfamily Azhdarchoidea Unwin 2002  
Azhdarchoidea indet.

#### **3.0.3 Specimen Details**

**Collection number of the described specimen - SMNK PAL 3830 (Figure 3.1)**

**History & Locality Information** - The specimen is preserved on a pale slab of flat limestone indicative of the Nova Olinda Member of the Crato Formation (Frey et al. 2003a; Unwin and Martill 2007).

### **3.0.4 Specimen Remarks**

Frey et al. (2003a) originally described the specimen with particular emphasis on soft tissues surrounding the unguals of the pes and the fibrils present within the decayed remains of the brachiopatagium. The presence of the tissue traces extending to the ankle in this specimen formed part of the argument by Elgin et al. (2008) that the trailing edge of the brachiopatagium would have terminated against the soft tissues of the lower hind limb.

While Frey et al. (2003a) noted that fibrils associated with the decayed remains of the flight membrane occurred as fine striae up to 180 mm in length and approximately 0.1 mm in width, further examination provides a more precise range of values throughout various portions of the wing. The most distal fibrils, extending from the fourth metacarpal and considered part of the actinopatagium (Schaller 1984), are found to range in size from 0.037 – 0.121 mm in diameter (Figure 3.2), with individual fibrils being spaced typically 0.2 - 0.26 mm apart or, on average, ~3.9 fibres/mm. The more proximal fibrils are found close to the left leg and may thus be considered part of the tenopatagium. These are notably thicker than those more distal elements, ranging between 0.106 mm – 0.183 mm in width. Their chaotic distribution, however, makes it impossible to determine what their original spacing during life might have been *contra* to that of Frey et al. (2003a) who concluded that the fibrils became more densely packed proximally. Closer observation of these tight proximal bundles indicate that they fan out towards their proximal termini and were originally associated with a single strip of the patagia 70 mm in length that (unlike the rest of the wing) has undergone relatively little deformation. While one end of these fibrils appears to have remained embedded within the decaying tissue, the other was likely free to the current, resulting in the fibrils becoming increasingly entangled and twisted as the carcass of the animal floated before sinking.



Compared with other specimens for which fibril distribution is known, the figure of 3.9 fibrils/mm for SMNK PAL 3830 falls within the lower range known within the Pterosauria, where distributions of 3-8 per mm are observed in *Rhamphorhynchus* (Padian and Rayner 1993), and 4–7 fibrils per mm for *Jeholopterus* (Kellner et al. 2009), rising up to 9 per mm in the distal wing. A fibril thickness of ~ 0.1 mm measured in SMNK PAL 3830 is thicker than that known for *Rhamphorhynchus* (0.05 mm, Padian and Rayner 1993) but are comparable to those preserved in the proximal wing of *Jeholopterus* (Kellner et al. 2009). While fibril length is variable (4–8 mm in *Jeholopterus* versus < 180 mm here) the diameter of these elements is observed to remain more or less constant irrespective of the animals wingspan. While some overlapping of the fibres has occurred due to post-mortem movement the fibres here are situated within the same plane and therefore represent a single sheet rather than several overlying layers as noted for *Jeholopterus* (Kellner et al. 2009).

| <b>Element</b>           | <b>length (mm)</b> |
|--------------------------|--------------------|
| metacarpal IV (left)     | >172               |
| wph 1 (left)             | >243               |
|                          |                    |
| femur (right)            | 186                |
| tibiotarsus (right/left) | 274 / 273          |

Table 4. - Long bone measurements of SMNK PAL 3830.

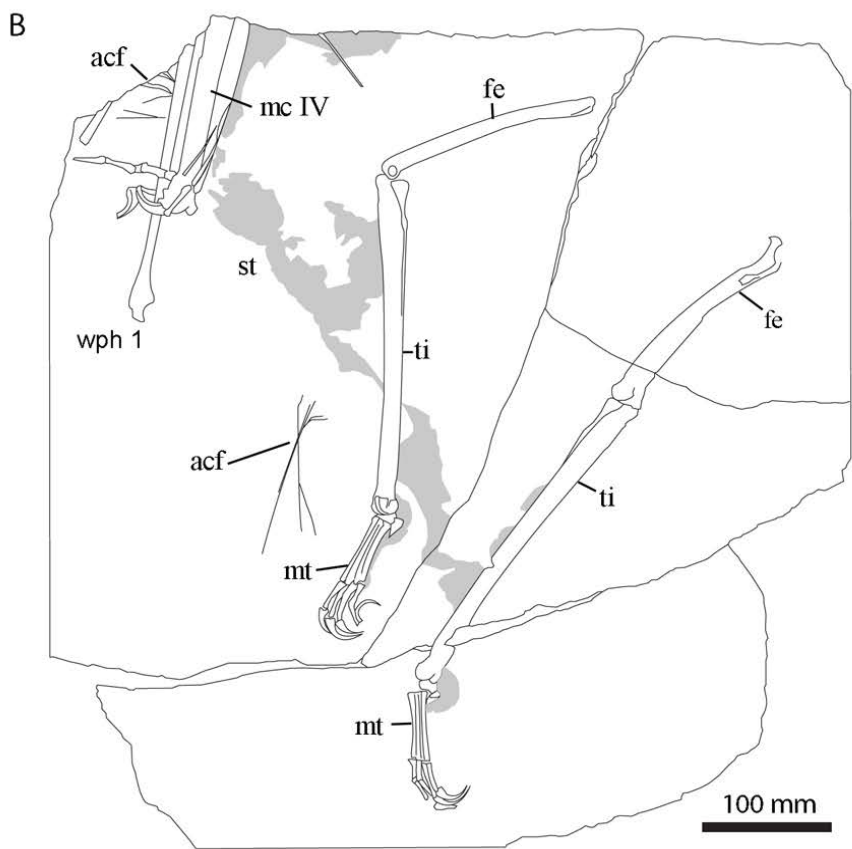


Figure 3.1. *Azhdarchoidea* indet. SMNK PAL 3830. A, photograph and B, corresponding line tracing.

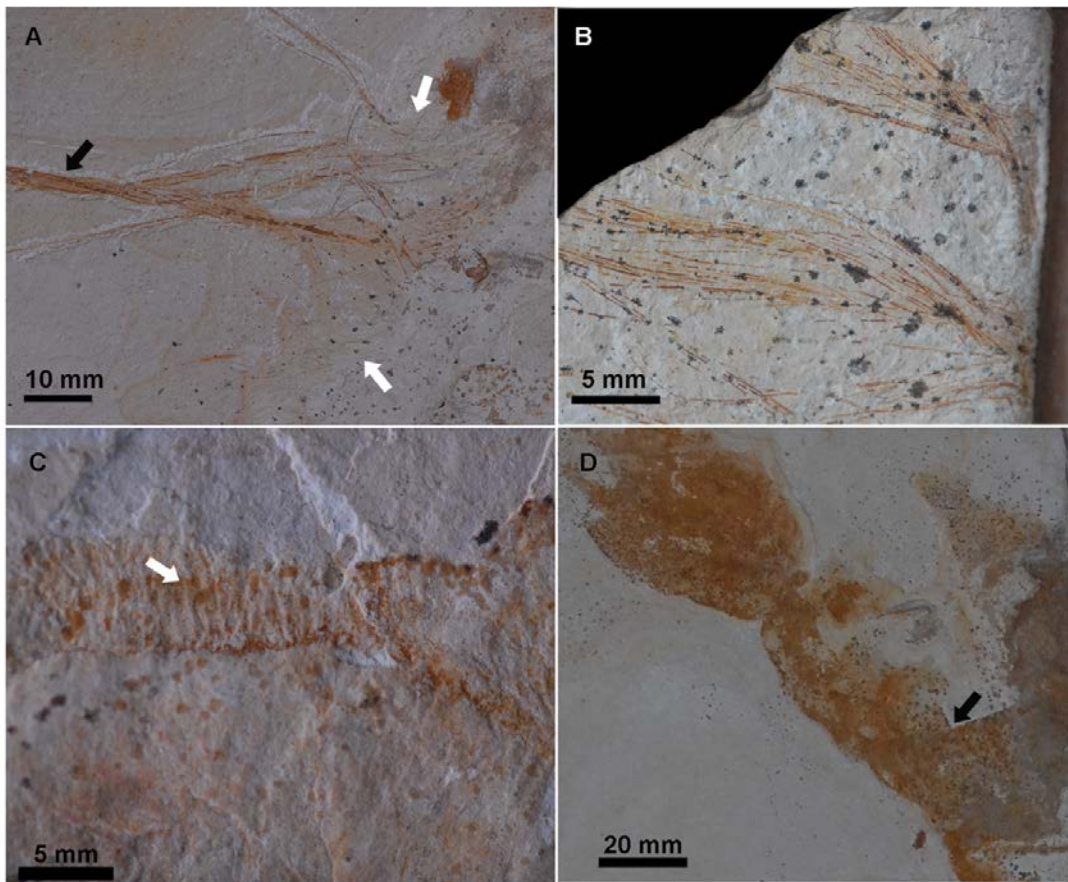


Figure 3.2. - Soft tissue features visible on the azhdarchoid specimen SMNK PAL 3830. A, actinofibrils loose from the main tissue trace. White arrows denote the preserved medial and lateral extent of the fibril sheet, elements of which intertwine distally to form a fibril bundle (black arrow). B, actinofibrils associated with the first wing finger phalanx; C, coarse series of wrinkles, interpreted to be part of the trailing edge of the brachiopatagium; D, remains of the left wing brachiopatagium. Arrow highlights the major fold in the trace.

## **3.1. Description of an indeterminate azhdarchoid (SMNK PAL 3900)**

### **3.1.1 Introduction**

Of the nine azhdarchoid specimens that preserve extensive postcranial remains and were recovered from the Nova Olinda Member of the Crato Formation, six preserve the complete (or near complete) fore and hind limbs in the absence of the torso (i.e. SMNK PAL 3830, 3900, 3855, 6409, MPSC R 868, MN 6527-V). Elgin et al. (2008) singled out one such specimen, SMNK PAL 3900, as an important example when considering the extent of the flight membrane, as the fossil preserves the corresponding fore and hind limbs, together with tissue attributed to the primary flight membrane, but lacks any elements of the torso or vertebral column. The absence of any distortion within the limestone matrix lead them to conclude that it was unlikely that the body, inflated by the gases of decay, drifted off, but rather the fore and hind limbs disarticulated from the carcass simultaneously and were held together by the wing membrane, that would have bound the limbs together.

While this specimen was also featured by Unwin and Martill (2007) during their cataloguing of the known Crato pterosaurs, no complete description was given and further examination indicates that the bones yield important information with regards to the azhdarchoid postcrania. As such it is described here with emphasis on unreported characteristics.

### **3.1.2 Systematic Palaeontology**

Order Pterosauria Kaup 1834  
Superfamily Azhdarchoidea Unwin 2002  
Azhdarchoidea indet.

### **3.1.3 Specimen Details**

**Collection number of the described specimen** - SMNK PAL 3900.

**History & Locality Information** - The specimen is preserved on a pale slab of flat limestone (Figure 3.3) indicative of the Nova Olinda Member of the Crato Formation (Frey et al. 2003a; Unwin and Martill 2007).

### **3.1.4 Specimen Description**

**Humerus** - The right humerus is observed in its ventral aspect, preserving a width of 15 mm about the mid-shaft of the bone that represents its narrowest point. The caudal tuberosity is broken and only the medial-most section remains, being sigmoidal in outline and merging with the humerus caput at almost a right angle. The base of the deltopectoral crest is 51.5 mm in width (i.e. 37 % the total humeral length), cranial to which the crest narrows rapidly due to the converging curvature of the medial and lateral margins. Both edges preserve a steep concave curvature that is steeper on the lateral margin than that of the medial margin. The medial margin forms a regular and continuous curve, merging with the cranial margin of the collum. Adjacent to the collum, between the deltopectoral crest and the posterior tuberosity, a large, oval pneumatic foramen, 11 by 7 mm in size, is present. The distal end of the humerus is 33 mm in width but the remains of the entepicondyle, trochlea and capitulum are too badly crushed to warrant a description.

**Radius & Ulna** - The right radius and ulna are long and narrow bones, whose individual lengths form a ratio of 1.3 with the humerus. A small oval depression on the distal articular surface of the right ulna is identified as the fovea that corresponds with the tubercle on the medial surface of the proximal syncarpal. The left ulna lies on the opposite side of the slab and is seen in its cranial aspect, where a prominent trochanter is observed on its proximal margin. A small fragment of bone preserved by the distal articulation surface of the bone, and accompanied by a more extensive impression in the sediment, is regarded as the left radius.

**Syncarpal** - The right proximal syncarpal is viewed in its craniodorsal aspect. The visible portion of the dorsal surface is very narrow but expands mediolaterally towards the cranial margin of the bone, the cranial face of which is blunt. The distal syncarpal block has rotated out of its natural position and the proximal articular surface, which is largely crushed, now overlies the caudal margin of the proximal syncarpal along with the distal-most portions of the radius and ulna. The more dorsal portion of this surface is concave. The dorsal surface of the distal syncarpal is sub-triangular in appearance and tapers in a cranial direction towards the preaxial carpal. The preaxial carpal is dominated by the development of a large fovea, partially occupied by a large, oval sesamoid, interpreted as the pisiform (Bennett 2008). The dorsal surface of the pisiform is smooth rather than marked by coarse striations.

On the left carpus two sesamoids, distinct from the pisiform described above, are observed overlying the cranial margin of the proximal syncarpal (Figure 3.4). The first of these is elongate and flat, the surface of which is marked by coarse striations. This articulates with and overlies the flat surface of the second sesamoid, which is itself marked by finer striations and displays a convex curvature on the opposing face. The distal syncarpal block has again moved free from its natural articulation and lies close by but exposed in its ventral aspect. The ventral surface is marked by a central concave depression within which a large pneumatic foramen penetrates the bone.

The first three metacarpalia are preserved close to the main shaft of the left wing metacarpal where a slender metacarpal (mc I) is observed and extends for a distance of >159 mm towards the distal syncarpal. The bone tapers dramatically from its distal termination, which is preserved as an impression of 2 mm in diameter, to the most proximal region of bone that is less than 0.5 mm in diameter. The second longest metacarpal (mc II) is at least 96 mm in length, where upon it makes contact with the first, and is lost from view, while the final metacarpal (mc III) is at least 51.8 mm before it terminates against mc II. Given the length of the first element it seems likely that mc I would have contacted, or terminated very close to the distal syncarpus.

**Metacarpal IV** - The fourth metacarpal of the right forelimb is preserved in craniodorsal view where the dorsal condyle is deflected dorsally against the long axis of the shaft in cranial view, although at what angle cannot be determined. The dorsal

surface of the condyle is concave and adjacent to the caudoproximal margin of the condyle there is a clear depression of the shaft that would have accommodated the posterior process of the first wing phalanx during flexion of the wing finger. The distal head along with the distal 37 mm of the shaft has broken off and been displaced from the main body, turning just short of 180° from its natural orientation.

**Phalanges** - The penultimate phalanges of the left fore limb are long, slender and slightly curved along the length of the shaft. Distally they expand to form a large condyle 11 mm in width that articulates with the ungual. The unguals are robust, strongly curved, and 32 mm in length. A deep sulcus is observed along the midline of the bone.

**Digit 4** - The right and left wing fingers are long and relatively slender with a uniform width of 12 - 13 mm. The caudal margin of the bone expands in a caudal direction at the distal edge of the bone, creating an expanded articular surface for the second phalanx. The distal articular surface is convex. The second wing finger phalanx of the right wing is slightly curved so that it would have been directed caudally during life while the third phalanx displays a slight curvature such that the bone is directed ventrally. The wing finger phalanges of the left wing are similar to those of the right but at least one phalanx, interpreted as the second (i.e. wph 2), is visible in its ventral aspect and displays a T-shaped profile in cross section.

**Femur** - The right femur is well preserved in its cranial aspect and measures 155 mm in length. The femoral caput is narrow, 18.5 mm in length, and offset 37° against the long axis of the shaft but expands to form a dome-shaped surface, 13 mm in width. The greater trochanter (e.g. Bennett 2001a, b) occupies the dorsolateral margin of the femur and is wide across its base, 8 mm, rising vertically 8 mm from the margin of the shaft so that its terminal point sits almost level with that of the caput. In cranial view the trochanter is observed as a prominent and robust sub-triangular feature. Below the greater trochanter the lesser trochanter (Bennett 2001a, b) has developed as a prominent ridge, extending for 9.5 mm close to the midline of the shaft. Approximately mid way along the shaft is a raised ridge that must have served as a muscle attachment point. The shaft of the bone itself curves laterally and the distal termination is 21 mm in width across epicondyles.

**Tibiotarsus** - The tibiae and fibulae are preserved in their natural articulation where the fibulae have fused with the tibiae at two locations, the first by the proximal articulation and the second located approximately 28 mm ventral to this. The distal portions of the fibulae are broken. The proximal tarsals have fully fused to the distal end of the shaft, forming a roller joint at the ankle and creating a tibiotarsus that is 234 mm in length and preserves a mid-shaft width of 12-13 mm. In lateral view the margins of the distal lateral condyle are raised above the rest creating a concave profile that merges with the main body of the shaft. Adjacent to the dorsal margin of the condyle a large depression has formed between the cranial margin of the condyle and the shaft. The intercondylar sulcus is visible but distorted.

**Tarsals** - The lateral distal tarsal is observed in its cranioventral aspect. In cranial view the bone is wedge shaped in appearance, tapering towards its medial margin. The ventral surface of the tarsal is smooth and pitted with a gentle convex profile. Towards the caudolateral portion of the bone and partially hidden by the overlying 4<sup>th</sup> metatarsal, is a depression regarded as the articular surface of the 5<sup>th</sup> metatarsal.

**Pes** - All five metatarsals of the right pes are preserved together but have moved out of a natural position with the tibiotarsus and now lie at around a 90° angle to the long axis of the shaft. The length of the five metatarsals are: 50 mm, 51 mm, 51 mm, 48 mm, 14 mm respectively, so that mt II = mt III > mt I > mt IV > mt V. The proximal articulation surface of metatarsal I is mediolaterally compressed while in mc III it is sub-triangular in profile. The proximal margin of the fourth metatarsal is greatly expanded and the lateral margin of the articular surface is concave. The shaft of the fourth metatarsal arches dorsally while the ventral surface for the distal shaft expands in a ventral direction, forming a process and a blunt articular surface. The fifth metatarsal is large, robust and sub-triangular in profile with a distinct concavity on its exposed surface. A single small (3.5 mm), sub-triangular phalanx is located in articulation with the fifth metatarsal. Three of the digits are preserved in natural articulation with their respective metatarsals however only two of these retain the unguals. The first phalanges of each digit are similar in morphology and narrow distally from a flat/slightly convex articular surface. The shaft arches dorsally and distally expands to form a roller-like articular surface



The condyles are splayed to form a Y-shape in dorsal view, the sulcus, which is wide and relatively deep, extending 3 mm onto the dorsal surface of the bone. Compared with the manual unguals those of the pes are narrow and display only a very mild curvature. The left pes is predominantly missing from the slab however its presence is confirmed by impressions of the metatarsals in the matrix and the terminal tips of two unguals adjacent to the right tibia.

**Tissue traces** - An extensive rusty coloured trace, clearly distinct from the general colouration of the slab and underlying many of the bony elements, is regarded as the remains of soft tissue, specifically that of the wing membrane. Although no structural features can be observed within this trace it is unlikely that the tissue could have belonged to any part of the animal other than the wing, being too extensive to have belonged to the soft tissue of fore or hind limbs and with no elements of the torso being preserved.

### 3.1.5 Additional Remarks

**Sesamoids of the carpus** - The carpal elements of azhdarchoid pterosaurs are associated with three distinct sesamoids. These are labelled A-C after Bennett (2001a) and are largely identical in form to those of observed within the pteranodontids, indicating that this configuration was widespread, if not universal, throughout the Pterodactyloidea. The first of these, element A, occupies its natural position within the V-shaped fovea of the preaxial metacarpal, the surface of this in SMNK PAL 3900 is striated for the attachment of tendons - acting as an anchorage for elongate muscles running distally along the wing spar and termination on the fourth metacarpal or phId4 (see Frey et al. 2006, Bennett 2007b, Prondvai & Hone 2009). The sesamoid Elements B and C are rarely observed in azhdarchoids and are paired together in what appears to be their natural state. Sesamoid B (Ses 1, Figure 3.4) is flat and forms an elongated oval body, the dorsal surface of which is marked by coarse striations orientated parallel to the long axis of the element. Sesamoid C (Ses 2, Figure 3.4) is a sub-circular element in dorsal or ventral view, one face of which is flat while the opposing face is generally convex. The flat face of sesamoid C makes contact with and overlies the striated face of element B, as was also noted in *Pteranodon* (YPM

2348). Although the natural position of elements B and C on the carpus during life is uncertain, the resting position of those in SMNK PAL 3900 overlies the cranial margin of the proximal syncarpal. The generally distal displacement of bones within the forearm of this specimen tentatively suggests that these elements were originally associated with the dorsal face of the proximal syncarpal.

| <b>Element</b>               | <b>length (mm)</b> |
|------------------------------|--------------------|
| humerus (right)              | 36                 |
| ulna (left/right)            | 178 / 177          |
| carpus                       | 30*                |
| metacarpal IV (left / right) | 183* / 170         |
| wph 1 (left/right)           | >274 / 296         |
| wph 2 (left/right)           | >95 / 185          |
| wph 3 (left/right)           | >128 / 121         |
| wph 4 (right)                | > 34               |
|                              |                    |
| femur (left/right)           | 151 / 157.5        |
| tibiotarsus (left/right)     | 230* / 234         |

Table 5. – Azhdarchoidea indet. SMNK PAL 3900. Selected long bone measurements. \* denotes an approximate or estimated value.

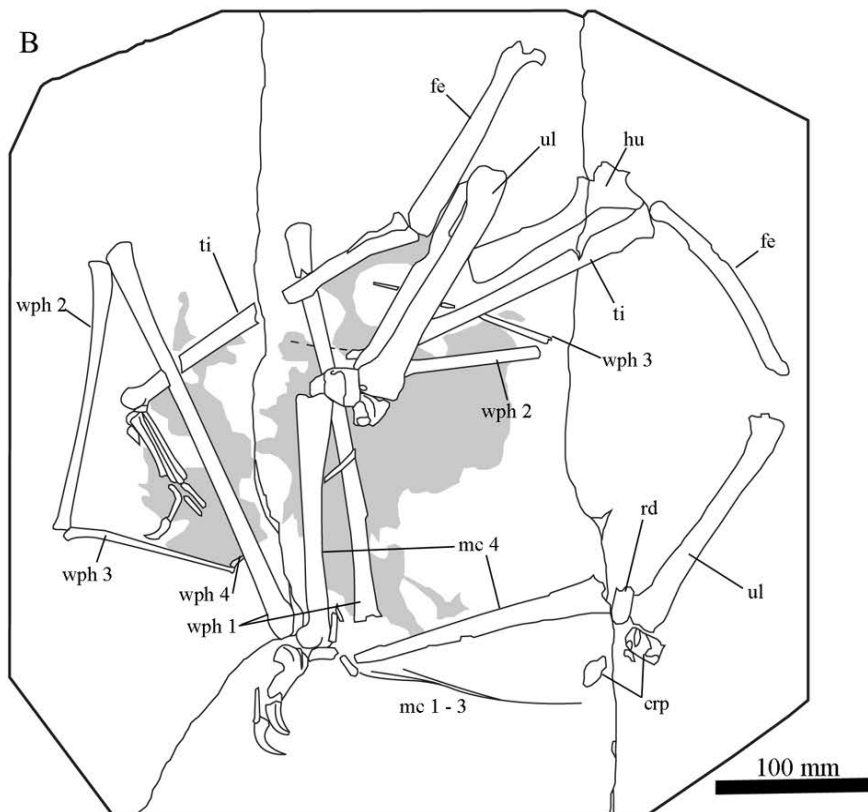


Figure 3.3. - *Azhdarchoidea* indet., SMNK PAL 3900. A, Photograph and B, corresponding line tracing. Dark grey area indicates the extent of the tissue trace.

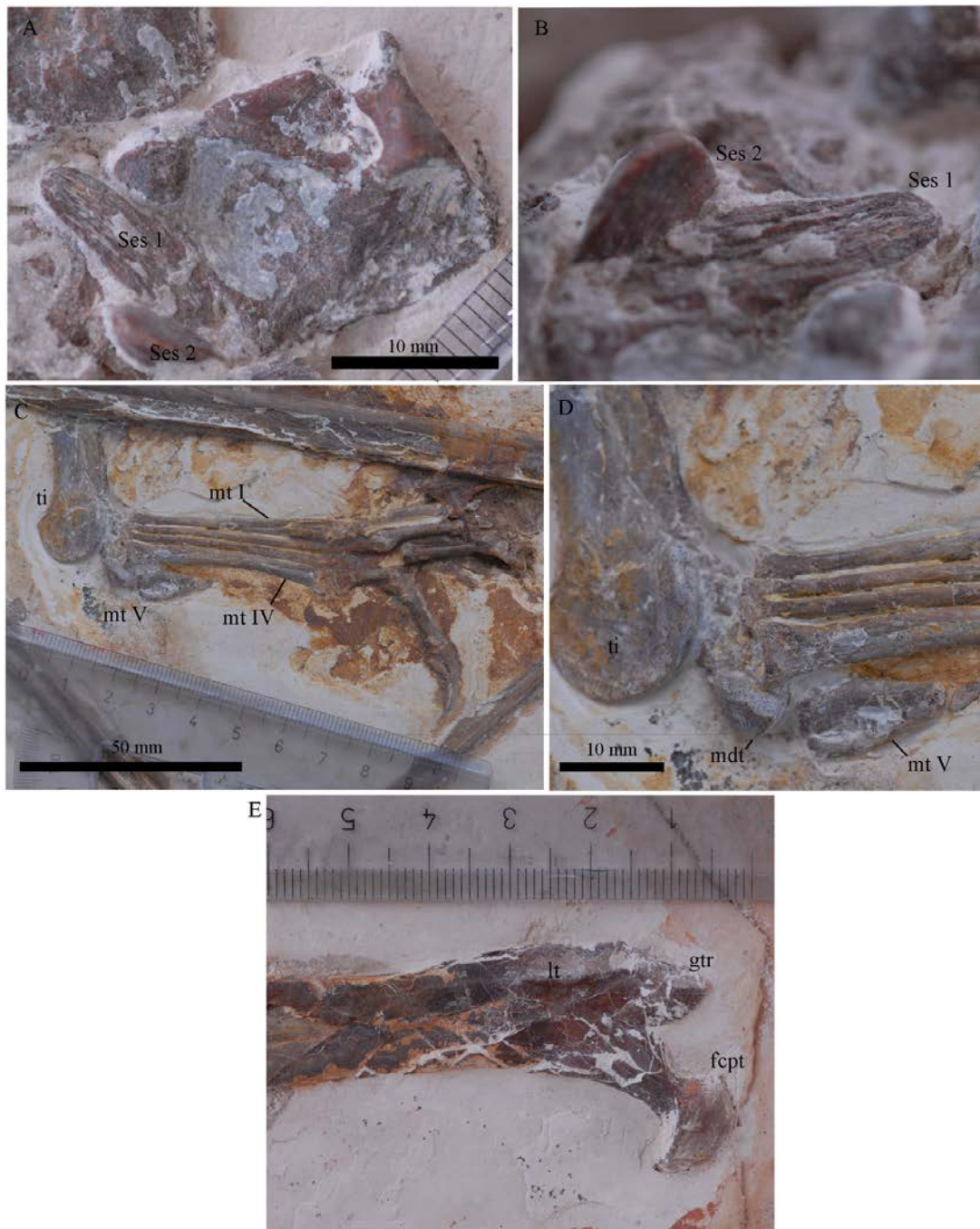


Figure 3.4. Features of interest on the indeterminate azhdarchoid SMNK PAL 3900. A, Left proximal syncarpus; B, close up of paired sesamoids; C, left pes; D, Close up of the left ankle; E, femoral collum and caput.

## **3.2. Description of an indeterminate azhdarchoid (SMNK PAL 3985)**

### **Introduction**

The extent of the pneumatic system in pterosaurs has been demonstrated in a variety of specimens, the number of elements incorporated into this system clearly increasing in more derived taxa (Claessens et al. 2009; Eck et al. 2011). Given that flight appears to have been the primary method of locomotion in these animals, the inferred weight reduction that this characteristic would have permitted is often thought to have been of great evolutionary significance – lowering the power cost of flapping flight and allowing pterosaurs to evolve to much larger sizes than would otherwise have been possible. In addition to this, pneumaticity impinges strongly on a variety of other factors, e.g. mass estimation (Wedel 2005; Witton 2008a, b; Henderson 2010), flight and locomotion dynamics (Habib 2008), physiology (Claessens et al. 2009) and histology (Steel 2008), meaning that mapping and understanding the extent of the pneumatic system greatly increases our knowledge of numerous aspects of pterosaurian palaeobiology.

Here a single juvenile specimen within the collection of the SMNK PAL 3985 shows a degree of damage that exposes the trabeculae orientations, and the extent of the pneumatic system which appears to penetrate into even very small elements early in ontogeny. The description and discussion of this specimen has now been accepted for publication and is detailed in Elgin and Hone (2013).

### **3.2.1 Systematic Palaeontology**

Order Pterosauria Kaup 1834  
Family Azhdarchoidea Unwin 2002  
Azhdarchoidea indet.

### **3.2.2 Specimen Details**

**Collection number of the described specimen - SMNK PAL 3985.**

**History & Locality Information** - Very little information is available for this specimen but the excellent preservation of the fossil within the concretion indicates that it originated from the Romualdo Member of NE Brazil (Albian).

### **3.2.3 Specimen Remarks**

Full details of this specimen are provided by Elgin and Hone (2013) which is attached at the end of this section (Figure 3.5).

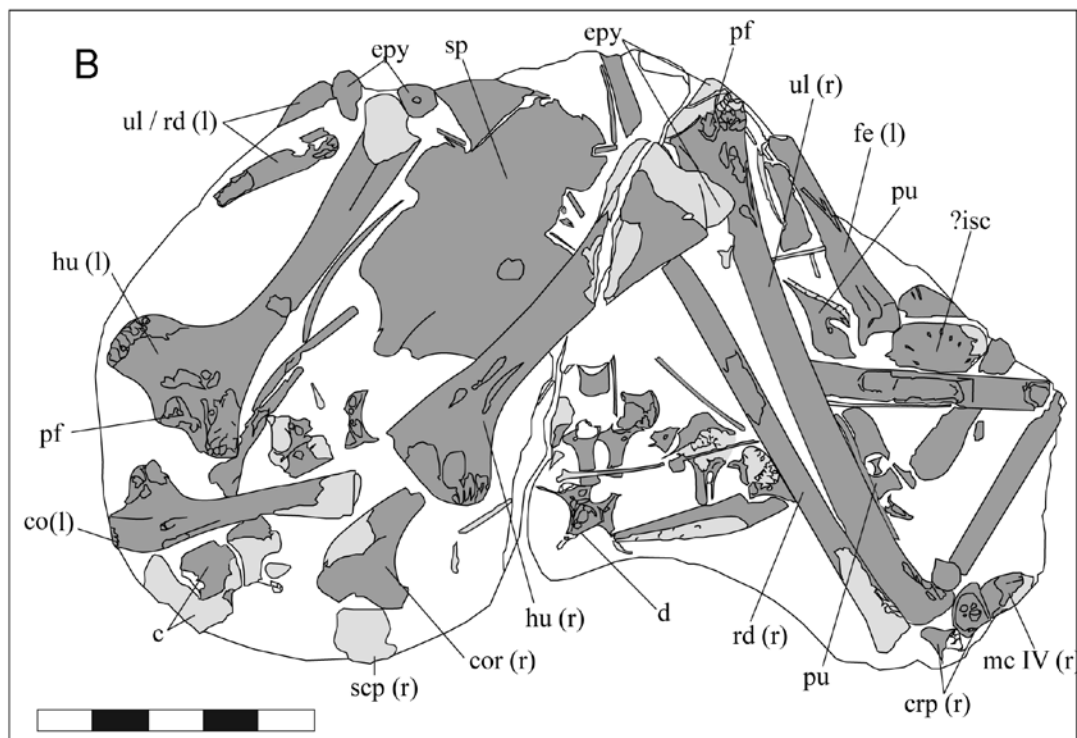
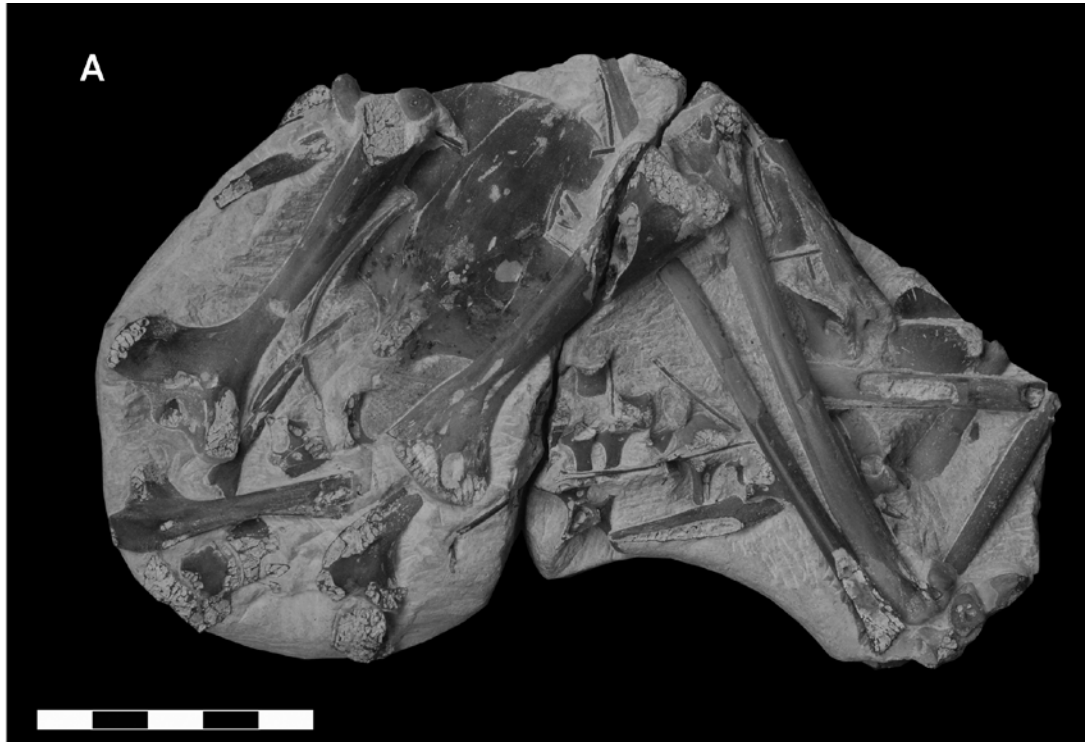


Figure 3.5. -. Indeterminate azhdarchoid SMNK PAL 3985. A, Photograph and B, corresponding line tracing. Scale bar = 50 mm.

### **3.3 The description of a new specimen of *Tapejara wellnhoferi* (SMNK PAL 3986)**

#### **3.3.1 Introduction**

*Tapejara wellnhoferi* represents one of the few azhdarchoids to be known from a combination of associated cranial and postcranial elements (Wellnhofer and Kellner 1991; Eck et al. 2011). Here a new specimen preserving a partial mandible, quadrate and some displaced elements of the postcranial skeleton including: the cervical vertebrae, antebrachial bones, first wing finger phalanges, and the pes, is found to be sufficiently similar to these other specimens to be assigned as *T. wellnhoferi*.

#### **3.3.2 Systematic Palaeontology**

Order Pterosauria Kaup 1834

Suborder Pterodactyloidea Plieninger 1901

Superfamily Azhdarchoidea Nesov 1984; *sensu* Unwin, 2003

Genus *Tapejara* Kellner 1989

**Diagnosis** (after Kellner 1989) - Toothless pterosaur with large sagittal crest on the anterior part of the skull extending backwards; very large nasopreorbital fenestra that occupies nearly half the skull in lateral view; rostrum inclined downwards.

*Tapejara wellnhoferi* Kellner 1989

**Included Material** - AMNH 24440; CD-R-080; SMNK PAL 1137; UOSG 12891; SMNK PAL 3986.

**Diagnosis** - Large and very high sagittal crest on the anterior part of the skull, extending backwards; rostrum very inclined downwards; absence of a mesial ridge on the palate; orbit situated below the level of the upper margin of the nasoantorbital fenestra.



### **3.3.3 Specimen Details**

**Collection number of the described specimen - SMNK PAL 3986**

**History & Locality Information** - The fossil is preserved on a split concretion that was purchased on behalf of the SMNK. The concretion originates from the Romualdo Member (Albian-?Cenomanian) of NE Brazil.

### **3.3.4 Specimen Description**

A full description of the specimen has now been accepted for publication and readers are referred to Elgin and Campos (2011) which is attached to the end of this section (Figure 3.6).

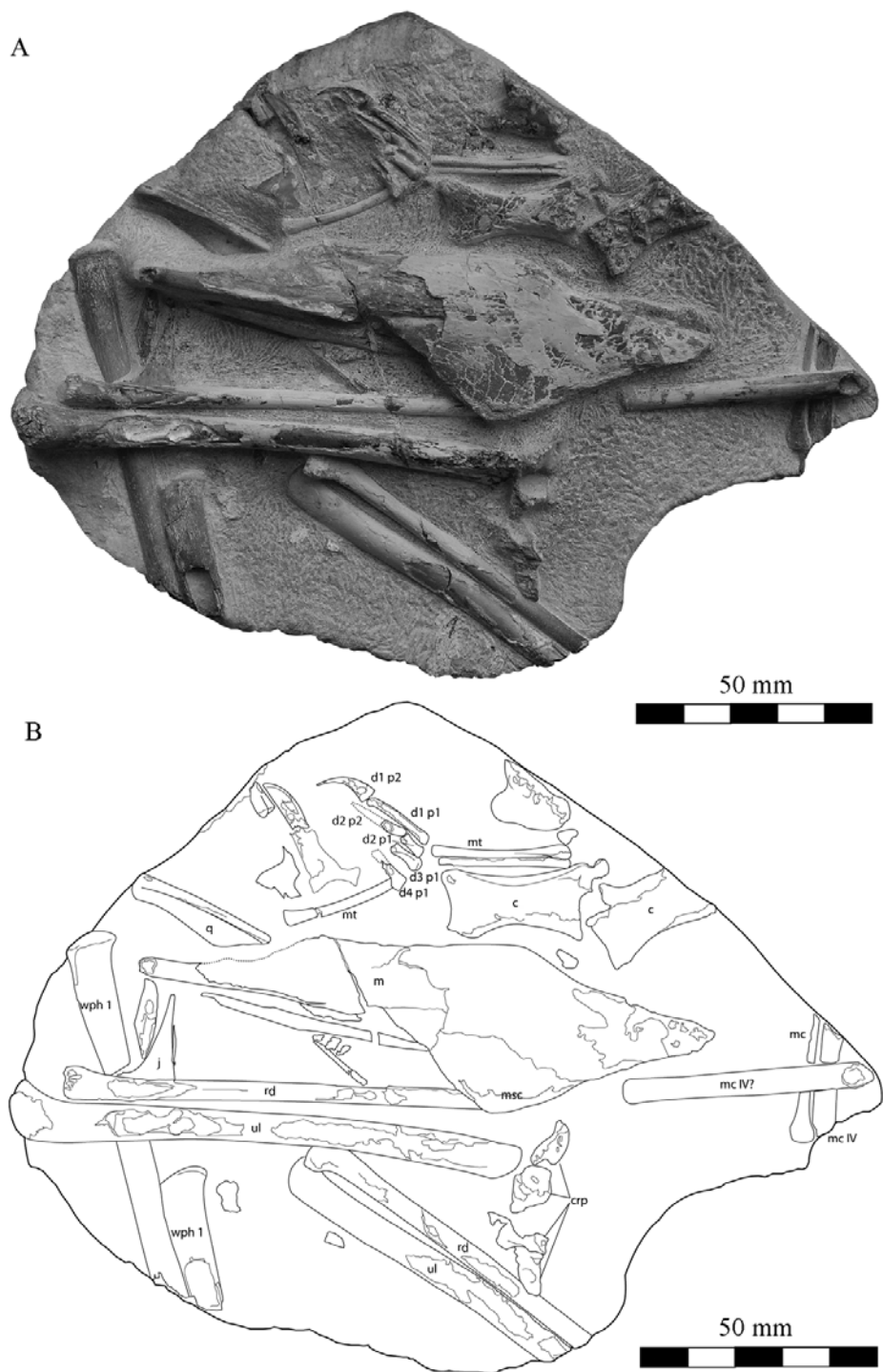


Figure 3.6. – *Tapejara wellnhoferi*, SMNK PAL 3986.

## **3.4 Description of an indeterminate azhdarchoid (SMNK PAL 6409)**

### **3.4.1 Introduction**

This specimen was included along with those described previously as evidence that the wing membrane extended between the fore and hind limbs during life by Elgin et al. 2011, who argued that a dark tissue trace, representing the brachiopatagium, bound the wing finger phalanges and the hind limb together as they settled. While Unwin and Martill (2007) have previously included this specimen within their catalogue of Crato pterosaurs, it lacked a full description and subsequent preparation exposed the medial distal tarsal, providing the rare opportunity to describe this bone in mature azhdarchoids.

### **3.4.2 Systematic Palaeontology**

Order Pterosauria Kaup 1834  
Superfamily Azhdarchoidea Unwin 2002  
Azhdarchoidea indet.

### **3.4.3 Specimen Details**

**Collection number of the described specimen** - SMNK PAL 6409 (Figure 3.7).

**History & Locality Information** - The specimen is preserved on a pale slab of flat limestone indicative of the Nova Olinda Member of the Crato Formation (Frey et al. 2003a; Unwin and Martill 2007).

### **3.4.4 Specimen Description**

**Sesamoids** - Two sesamoids, similar to those observed in SMNK PAL 3900 are found in association with each other and lie loose from the carpus. The first of these appears as an elongated oval, 18 mm by 6 mm, the dorsal surface of which is marked

by a number of striations orientated parallel to the long axis of the bone, while the second element is more rounded but lies on its side, partially overlapping the striated surface of the first sesamoid. These represent the sesamoids B and C (after Bennett 2001a). A single metacarpal is preserved as a thin rod of bone directed into the sediment and across the dorsal surface of the first wing finger phalanx.

**Manus** - The phalanges of the first three digits are slender and lack any noticeable curvature along the length of their shafts. A large excavation to accommodate the flexor muscle is observed on the ventral surface of the first phalanx of digit 1, immediately distal to the sulcus of the proximal condyles, while distally the phalanges terminate in an expanded roller joint. All three unguals share a common morphology where they are robust, slightly re-curved and preserve a large medial sulcus that runs almost the whole length of the bone, terminating just before the distal margin.

**Digit 4** - The individual phalanges of the left wing finger are visible in their ventral aspects. The proximal region of the first phalanx is comprised of dorsal and ventral positioned cotyles that are strongly concave to accept the distal condyles of the fourth metacarpal. The ventral cotyle is smaller than that of the dorsal and located slightly more distally, accommodating a set of condyles up to 19 mm in width. The larger dorsal cotyle expands the proximal region of the bone in a caudal direction, creating a process that rises over the dorsal surface of the fourth metacarpal during flexion of the wing finger. The cranial half of the articular surface is formed by the extensor tendon process that has mostly closed its suture with the phalanx but can still be distinguished from the main body by a small scar, visible across both the ventral and caudal surfaces of the bone. Immediately lateral to the ventral cotyle, between the main shaft of the phalanx and the caudal process, a large depression is interpreted to be the remains of a pneumatic foramen. The shaft of the phalanx is uniform in width and extends for a length of 308 mm, the distal surface of which is slightly convex. The second wing-finger phalanx has an expanded proximal surface that is only slightly concave in profile. The shaft is 206 mm in length and has developed a “T-shaped” profile in cross section, caused by a deep depression adjacent to the leading edge of the bone, followed immediately by a convex bulge near the caudal margin. The third phalanx is 127 mm in length and narrows distally with a gentle, caudally directed curvature. The fourth phalanx is only 46 mm in length and diminishes to minimum

width of 1 mm at the distal tip. A small oval scar, presumably for a ligament that would have bound the third and fourth phalanges together in life, is observed on the ventral surface adjacent to the proximal articulation. The shaft of the phalanx also preserves a caudally directed curve but to a much greater degree than that observed in the previous phalanges. The distal tip of the phalanx is blunt.

**Femur** - The left femur is preserved in caudal view where the collum is offset against the shaft at an angle of 32°. Immediately lateral to the base of the neck a pneumatic foramen, 9 mm in width, has developed in the tough between the collum and the greater trochanter. The greater trochanter forms as prominent sub-triangular protrusion by the lateral margin of femur, rising 6 mm dorsally from the shaft to sit level with the broken remains of the femoral head. An elevated ridge extends ventrally from the trochanter, merging with a raised section of bone that forms the dorsolateral margin of the shaft for a distance of no less than 11 mm. Another raised area of bone, smaller than that on the dorsolateral margin, occupies a position just ventral to the collum by the medial margin of the bone and is here regarded as the internal trochanter. The middle portion of the femoral shaft between these two trochanters is depressed and forms as a shallow trough. The shaft of the femur curves slightly laterally. The width of the bone across the remains of the condyles is measured at 24 mm.

**Tibiotarsus** - The left tibiotarsus lies level with the distal end of the femur but has rotated so that it is now observed in its medial aspect. The proximal articular surface is concave in profile and slightly expanded to accommodate the distal condyles of the femur. The shaft is initially wide, 17 mm, but tapers towards its distal margin. The fibula is missing from the slab suggesting that it had not yet fused to the tibia. The proximal tarsals have fully fused to the distal end of the tibia creating an expanded roller joint for the ankle, the medial condyle of which is marked by a depression on its medial face and preserves a width of 15.6 mm. The lateral condyle and the intercondylar sulcus are visible but heavily camouflaged by sediment cover. The complete length of the tibiotarsus is 253 mm.

**Distal tarsals** - The distal medial tarsal is observed in medial view occupying its natural position between the tibiotarsus and the metatarsals. The medial face is

broader than it is high and has a widely splayed, V-shaped appearance as a result of the cranial and caudal halves of the bone, which are clearly distinguished from one another. The cranial half forms a regular convex surface that acts as the articular region of the first metatarsals. The dorsal margin of the bone is directed in a craniodorsal direction and a small notch close to the cranial edge of the bone marks the beginning of the cranial tubercle. The caudoventral margin of this tubercle is slightly concave but merges with the larger convex surface of the cranial articulation. The cranial half of the bone tapers when seen from its cranial aspect where the craniodorsal portion is located medial to that of the ventral margin, creating a low lying region of bone in the central region of the tarsal. The dorsal margin of the caudal face of the tarsal is directed caudodorsally, i.e. perpendicular to that of the cranial half, creating a wide U-shaped articular surface for the distal condyles of the tibiotarsus. The ventral margin is strongly convex. The caudal half of the tarsal is generally convex and a shallow groove at least 6 mm in length originates at the caudodorsal margin, extending diagonally across the surface towards the central region of the tarsal. This is interpreted as the groove for the flexor tendon (after Bennett 2001). The cranial portion of this caudal half develops as a steeply sloping ramp that merges with the low lying region of the cranial half of the medial tarsal, forming a wide central depression that clearly distinguishes between the two halves of the bone.

**Metatarsals** - Only four metatarsals are visible and can be observed in their ventromedial aspect. Metatarsals II - IV show a similar morphology where the proximal articular surface is wide and sub-triangular in appearance but narrows to a thin (~ 29 mm by the mid shaft), dorsally arching shaft that terminates in a concave condyle formed by a ventral expansion of the bone. The fifth metatarsal is typical of derived pterodactyloids and is short, robust and sub-triangular in shape. The ventral surface is concave across its long axis while the proximal surface, which must have articulated with the distal tarsals, is slightly concave between its medial and lateral margins. The medial margin is generally convex while the lateral margin forms as low ridge. Distal to the fifth metatarsal a tiny sub-triangular phalanx occupies what would have been its natural position during life. The metatarsals are sub-equal in length and here the longest is metatarsal II (56 mm) > IV (54.5 mm) = III (54 mm) > V (17.5 mm).

**Pedal phalanges** - The penultimate phalanges of both the second and third digits are visible and retain a natural contact with their respective ungual. The unguals of the pes are sharp and strongly curved but are noticeably shorter and narrower than those of the manus. A deep sulcus runs along the centre of the bone.

**Tissue traces** - A large but irregular black trace covers much of the fossil, overlying the first three wing-finger phalanges, tibiotarsus, and parts of the pes. As both left fore and hind limbs sunk together in the absence of the torso this stain most likely represents the remains of the brachiopatagium although no actinofibrils or internal structures can be observed. The position and extent of the soft tissue trace prevents it from being attributed to the soft tissues of the fore and hind limbs. The state of preservation is unusual in that the membrane stain forms as a pocket a few millimetres in depth and can therefore be observed on several levels where the top most surface is no longer present. The upper surface of the trace is black and generally featureless although wrinkles similar to those observed in other membranes are can found on a small patch of sediment close to the mid shaft of the second wing finger phalanx. Within the membrane pocket the trace is again predominantly black and contains a number of minerals that fluoresce brightly under long wave ultra violet light (365nm); the surface layer itself does not fluoresce. In addition to this the internal region of the tissue is marked by a number of rod-like impressions where associated clusters form in a arc-like pattern of typically less than 45°, but up to 180°, and occasionally crosscut or overly their neighbouring structures. These are regarded as the products of mineral formation rather than part of the original tissue and latex peels have been taken for further analysis.

### **3.4.5 Additional Remarks**

**Distal Tarsals** - The distal tarsals are known in detail for only a limited number of specimens including the non-pterodactyloid *Dimorphodon* (Padian 1983), the pterodactyloids *Coloborhynchus* (Kellner & Tomida 2000), and *Pteranodon* (Bennett 2001a, b), and the azhdarchoids *Quetzalcoatlus* (see Bennett 2001a, b), and *Tapejara* (Kellner 2004b). Of the elements attributed to these azhdarchoids the former remains unpublished, while the latter belong to a juvenile animal, confidentially inferred by its

very small size and lack of skeletal fusion. The left distal tarsal of SMNK PAL 6409 is observed in its medial aspect, forming a widely splayed, V-shaped unit that is broader than it is high (Figure 3.8), the central portion of which is depressed and clearly divides the anterior and posterior sections of the bone. In medial view the morphology of the bone very closely resembles that described for *Pteranodon* (and presumably *Quetzalcoatlus*) by Bennett (2001a) where a pronounced notch along the anterodorsal margin of the bone marks the start of an anteriorly directed tubercle. A shallow sulcus, presumably for the *flexor digitorum* tendon (Bennett 2001a, b), is observed on the posteriodorsal section of the element and extends onto the posterior face of bone. The primary differences between the elements of *Pteranodon* and SMNK PAL 6409 are the absence of any foramina for the latter specimen.

In anterior view the lateral distal tarsal is wedge shaped. Bennett (2001a) noted a raised feature that extended onto the lateral tarsal for the articulation of the metatarsals, however, the anterior face of these bones is flat and smooth in both SMNK PAL 3030 and 3900, where anterior and distal faces of the bone meet at a right angle to one another. While the distal tarsals of MN 6532-V were only weakly triangular in shape relative to those of SMNK PAL 3830 this likely represent the relatively immaturity of the former specimen.

**Femur** - The presence of a large pneumatic foramen between the trochanter and collum in SMNK PAL 6409 appears to be widespread, if not universal within the Azhdarchoidea, having also been noted by Eck et al. (2011) for *Tapejara wellnhoferi*. The development of the lesser trochanter into a prominent, sub-triangular feature is largely diagnostic for azhdarchoids and points to a greater development of the abductor muscles (see Hutchison 2001), emphasising the increased role of terrestrial locomotion in these animals.



| Specimen    | Measurements (mm) |
|-------------|-------------------|
| wph 1       | 294               |
| wph 2       | 209               |
| wph 3       | 127               |
| wph 4       | 45                |
| femur       | 183               |
| tibiotarsus | 262               |

Table 6. – Long bone measurements of SMNK PAL 6409.

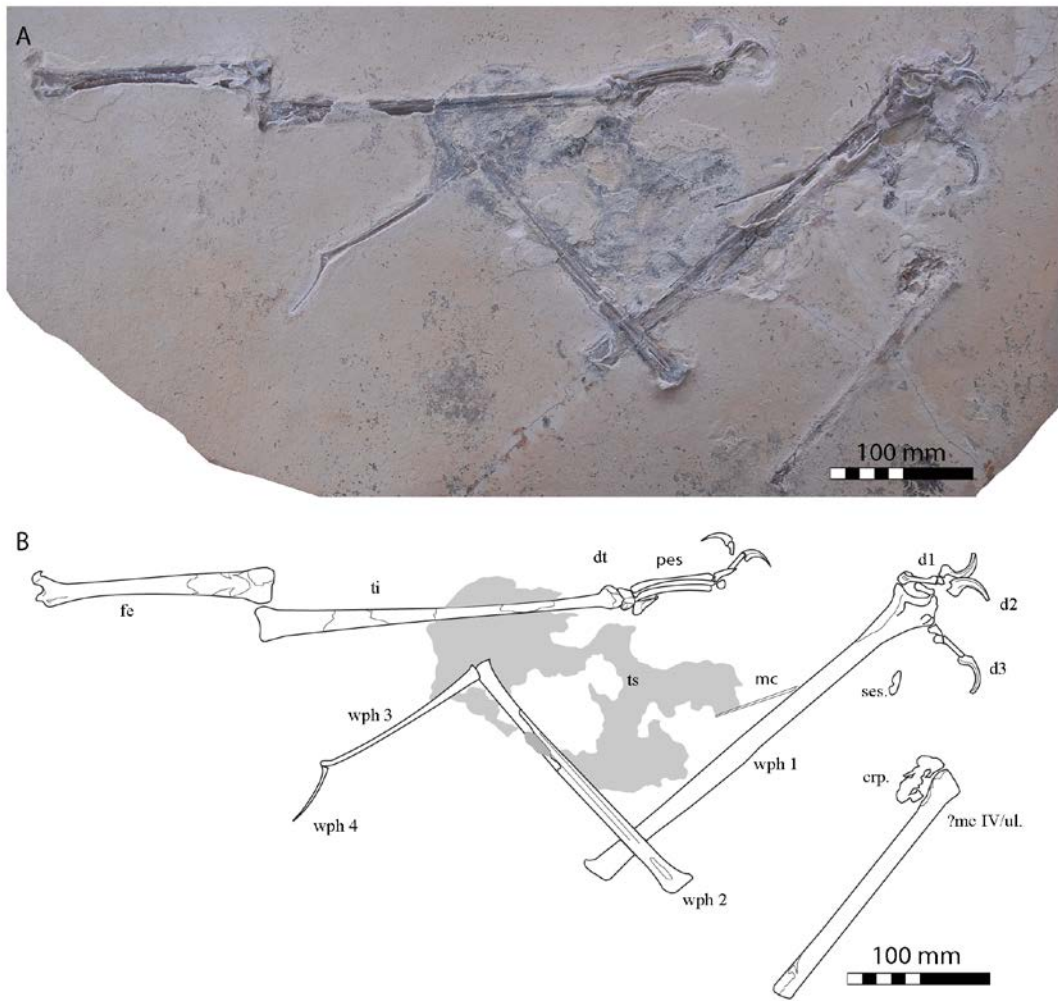


Figure 3.7. - Azhdarchoidea indet., SMNK PAL 6409. A, Photograph and B, corresponding line tracing.

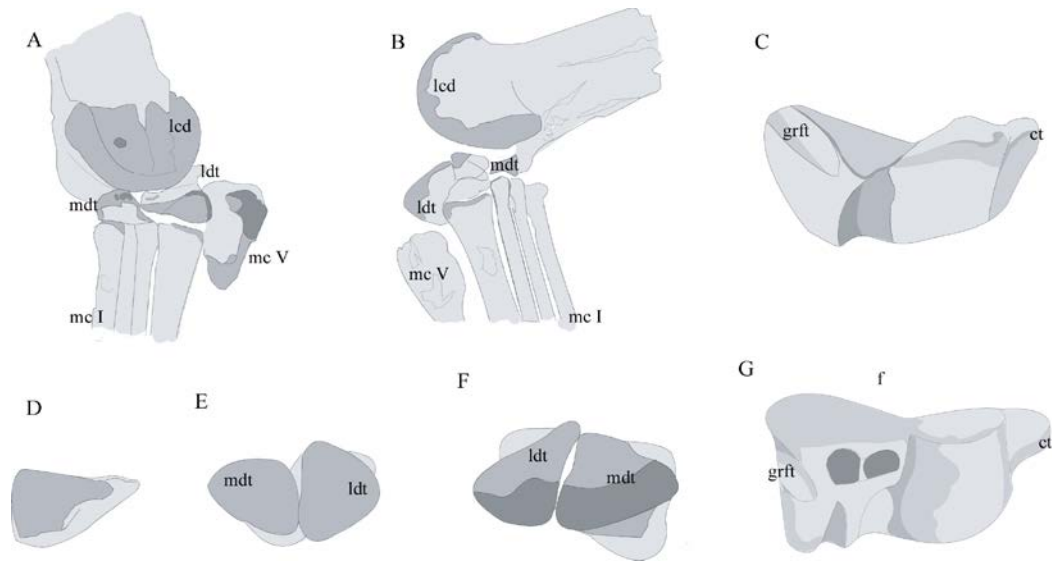


Figure 3.8. -. Ankle structure in the pterodactyloid pterosaurs. A, SMNK PAL 3830 left ankle region in cranial view; B, SMNK PAL 3900, right ankle in cranioventral view; C, SMNK PAL 6409, left medial distal tarsal in medial view; D, *Tapejara* sp. (MN 6532-V), distal tarsals in cranial view (adapted from Kellner 2004); E, *Pteranodon* (YPM 2462), distal tarsals in cranial view (adapted from Bennett 2001a); *Pteranodon* (YPM 2462), medial distal tarsal in medial view (adapted from Bennett 2001a).

### **3.5 The description of a novel genus and species *Microtuban altivolans* (SMNK PAL 6595).**

#### **3.5.1 Introduction**

Although pterosaurs achieved a global distribution throughout the Mesozoic (Barrett et al. 2008) the location of fossil finds are not evenly distributed, with the majority of those specimens known to science having been unearthed in specific localities of exceptional preservation in Western Europe (Wellnhofer 1970, 1975), Mid Western areas of the USA (Bennett 2001a, b), NE Brazil (Kellner and Tomida 2000; Unwin and Martill 2007), and the NE of China (Wang et al. 2005). As such, regions including Africa and the Middle East are particularly sparse with regards to pterosaur remains (Dalla Vecchia et al. 2001). Intermittent finds around the Cretaceous deposits of Lebanon and Israel indicate that, while pterosaurs were present, their remains remain relatively rare compared to other fossil *Lagerstätten*, despite many quarries in the former territory being exploited specifically for the commercial sale of fossil material.

This specimen was offered for sale to the SMNK from a local dealer in Lebanon and despite its crushed and broken state represents the most complete pterosaur known from the Arabian plate, preserving part of the cervical and dorsal vertebrae, pectoral girdle, and elements of the fore and hind limbs. A full description of the specimen has now been accepted for publication and readers are referred to Elgin and Frey (2011b).

#### **3.5.2 Systematic Palaeontology**

Order Pterosauria Kaup 1834

Super Family Pterodactyloidea Plieninger 1901

Family Azhdarchoidea Nesov 1984; *sensu* Unwin, 2003

Genus *Microtuban* Elgin and Frey 2011b

**Diagnosis** - An azhdarchoid pterosaur distinguishable by an unusually high ratio of the first and second wing-finger phalanges ( $wph\ 2/wph\ 1 = 0.85$ ) and a hyper-reduced fourth wing-finger phalanx, accounting for 1.1 % of the total wing-finger length.

**Included Material** - Only known specimen and holotype is SMNK PAL 6595.

*Microtuban altivolans* Elgin and Frey 2011b

**Diagnosis** - As for genus.

| Elements   | length (mm)  | Elements | length (mm) |
|------------|--------------|----------|-------------|
| cervical 7 | 23.6         | d1pI     | 12.5        |
| cervical 8 | 21.1         | d1u      | 11.0        |
| cervical 9 | ~ 9.0        | d2u      | 11.0        |
| dorsal 1   | ~10.0        | d3pI     | 17.0        |
|            |              | d3pII    | 3.0         |
| humerus    | 61.6 - 73.3* | d3pIII   | 10.5        |
| radius     | 92.0*        | d3u      | 11.0        |
| carpus     | 13.0         |          |             |
| pteroid    | >38.0        | wph I    | 135.0       |
| mc IV      | 122.0*       | wph II   | 114.5       |
| mc I?      | 50.0         | wph III  | 63.5        |
|            |              | wph IV   | 3.5         |

Table 7. - Bone measurements in SMNK PAL 6595. \* denotes an approximate or estimated value; mc, metacarpal; dp, digit and phalanx number; wph, wing-finger phalanx.

### **3.5.3 Specimen Details**

**Collection number of the described specimen** - SMNK PAL 6595 (Figures 3.9 – 10).

**History & Locality Information** - The specimen was purchased from a private collector from the Late Cretaceous limestone of Lebanon, surrounding the town of

Hjoûla. These deposits are regarded as part of the Sannine Formation, and have been dated as early Cenomanian.

#### **3.5.4 Specimen Description**

The specimen has been formally accepted for publication and a full description is given by Elgin and Frey (2011b) which is attached at the end of this section.

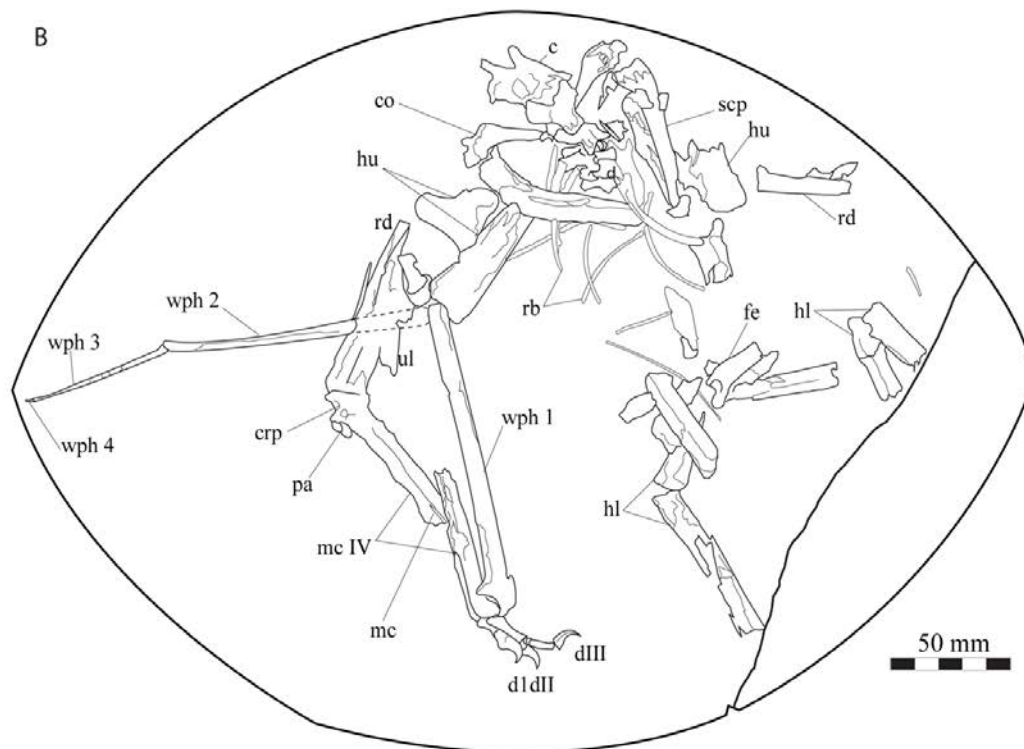


Figure 3.9. - *Microtuban altivolans*, SMNK PAL 6595. A, photograph; B, corresponding line drawing.

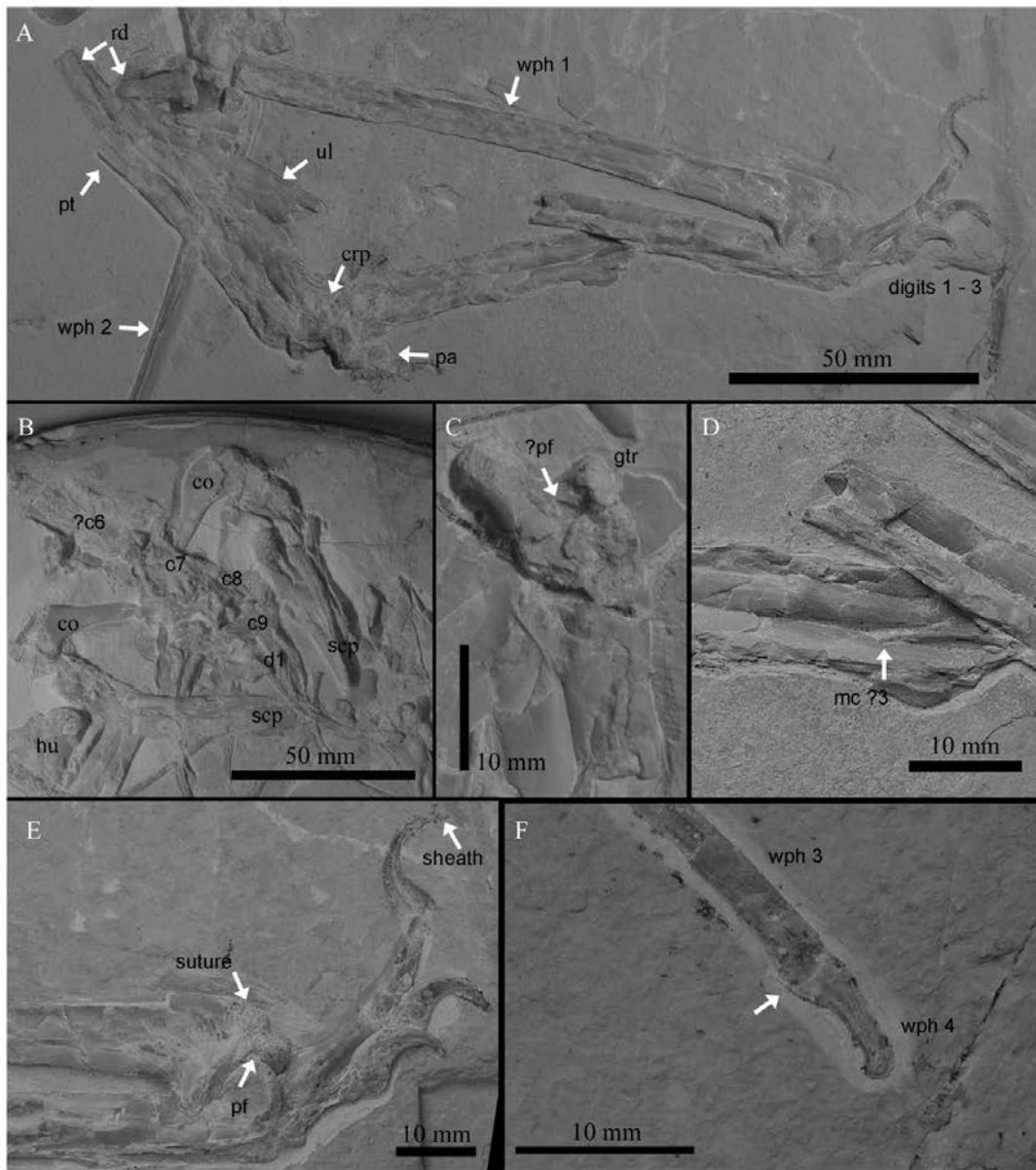


Figure 3.10. - Photographs of specific points of interest in SMNK PAL 6595. A, left forearm; B, pectoral girdle; C, right femur; D, middle shaft of metacarpal IV; E, metacarpophalangeal joint of the wing metacarpal and wing finger; F, wing finger phalanx IV.



## **3.6 The description of a new *Tupuxuara* –like azhdarchoid.**

### **3.6.1 Introduction**

Extensive postcranial remains attributed to azhdarchoids are rare and where they do occur are almost always fragmented and of little diagnostic worth – with the best examples of such specimens ending up in the hands of private collectors and disappear from scientific study (Unwin and Martill 2007). One such specimen, however, was acquired by the SMNK late into the writing of this thesis but its true value was unknown until a substantial portion of the concretions were prepared. At the time of writing the majority of the specimen has been exposed by the preparation staff at the museum, providing key bone ratios and warranting a preliminary description for the purpose of this work. Further preparation is required before the taxonomic placement of the specimen can be confidently stated.

### **3.6.2 Systematic Palaeontology**

Order Pterosauria Kaup 1834

Superfamily Azhdarchoidea Nesov 1984; *sensu* Unwin 2003

Family Thalassodromidae *sensu* Witton 2009

Genus cf. *Tupuxuara* Kellner and Campos 1988

**Diagnosis:** -Toothless pterosaur of medium size, possessing a large sagittal crests situated at the anterior part of the premaxilla that is extended backwards; presence of a medial ridge at the ventral part of the palate; first wing finger phalanx and metacarpal IV comparatively slender and long; proximal articulation of the first wing finger phalanx with two pneumatic foramina, one situated at the superior part of the articulation with the fourth metacarpal.

**Included Material** - *T. longicristatus*, MN 6591-V; *T. leonardii*, MCT 1495-R; SMNK PAL 4330; *T. deliradamus*, SMNK PAL 6410; KPMNH DL 84.

### **3.6.3 Specimen Details**

**Collection number of the described specimen** – NA. A collection number has not been assigned at the time of writing.

**History and Locality Information** - The specimen consisted of eight concretions that were purchased from a private dealer and were partly broken or damaged to expose the bones inside. These concretions were thus prepared almost from scratch in the laboratories of the SMNK and it was clear that all bones recovered belonged to a single azhdarchoid pterosaur. The provenance of the concretion was the Romualdo Member of the Chapada do Araripe, NE Brazil (Albian - ?Cenomanian) but no further information is possible.

### **3.6.4 Specimen Description**

The fossil is well preserved within a single large concretion that has been broken into eight primary segments. Although several sections of the fossil remain under preparation, a preliminary analysis is provided here owing to several features that are beneficial to the general theme of this thesis. A full account of the specimen is to be subsequently written following complete preparation. The skeleton represents the primary portion of the body fossil (Figures 3.11 - 12; Table 8) where a number of elements are broken along the margins of the concretion. The generally complete state of the fossil suggests that some sections, principally the distal wing metacarpal and first wing finger phalanx of the right wing, the shaft of the right tibia and pedal digits, and the wing finger phalanges of the left wing were all originally present. These are inferred to have been lost during the collection process or as a result of erosion. Damage to the fossil is light and restricted to the dorsal surface of the mandible, the central region of the sternal plate, and the caudal part of the pelvic girdle. Soft tissue is preserved as a dark grey / black trace that is restricted to the proximal portion of the forearm of the right wing and the left hand side of the thoracic vertebral series.

**Skull** – Only the posterior section of the cranium is preserved (Figure 3.13). The frontal and parietal bones have sutured to form a robust neurocranial block, where the division between the two bones is not clear – suggesting that these have fused

together. The rim of the orbit and the caudal margin of the parietal have been damaged with the loss of their compacta. The caudal margin of the parietal is strongly curved and indicates that a crest would have extended caudal to the preserved margin of the cranium. Only a small portion of the cranial crest is present as a thin sheet of bone positioned dorsal to the neurocranium (most likely an extension of the premaxilla). The lacrimal is complete and appears as a sub-triangular element where a single large circular fenestra occupies the centre of the bone. The lacrimal has separated from the neurocranium indicating that the two had not fused. The cranial margin of the lacrimal is regularly concave, the ventral branch of the bone is very slender. The jugal is situated directly ventral to the lacrimal and is a tri-radiate element that forms the cranio/caudoventral margins of the orbit and the caudoventral/ventral margins of the nasoantorbital fenestra. The dorsal branch of the bone that articulates with the lacrimal is slender and mostly straight, indicating that the caudal margin of the nasoantorbital fenestra would have been more straight than concave in lateral view. Both the left and right bars of the jugal are present, indicating that the skull collapsed upon itself. The cranially directed bar becomes very slender but its cranial termination is missing. Four segments of the right sclerotic ring are observed *in situ* within the cavity of the orbit. Beyond the caudal margin of the skull the left opisthotic bone is present. The dorsolateral margin of the bone is regularly concave while that of the ventrolateral margin is only slightly concave. The dorsal margin of the bones forms the ventral margin of the posterior temporal fenestra while the ventral margin is strongly concave and would have formed the dorsal margin of the posterior cranial fenestra.

**Mandible** – The mandible is elongate and tapers towards the cranial tip when observed in its lateral aspect, giving it a spear-like outline (Figure 3.14). No teeth or alveoli are present indicating that the animal was edentulous. In cross-section the mandible is typically sub-triangular with a transversely concave buccal margin. The distal portion of the left ramus is hidden by the overlying cranium but that of the right is exposed in its dorsomedial aspect. The fenestra meckeli separates the surangular from the angular immediately cranial to the articular. The caudal articulation of the surangular is concave and although the bone makes a firm contact with the articular the suture between these elements is open. The articulation for the quadrate forms as a deep furrow and is angled craniomedially.

**Vertebral column** – The vertebral column is preserved largely *in situ*. The atlas-axis complex is missing but the 3<sup>rd</sup> and 4<sup>th</sup> cervicals are preserved adjacent to the cranium, exposed in their right lateral aspects (Figure 3.13). Although sediment covers most of the neural spines no sutures are observed, indicating the centrum and neural spines have fully fused. The centrum of the 3<sup>rd</sup> cervical is pierced by two oval foramina. Two additional cervicals belonging to the mid-cervical series (likely the 6<sup>th</sup> and 7<sup>th</sup> cervicals) are observed in their left lateral aspects (Figure 3.14). Although largely hidden by sediment cover these bones are elongate with large prezygapophyses and high neural spines that extend the length of the vertebral body. A pneumatic foramen pierces the lateral flank of the vertebral body and the neurocentral sutures in both of these elements are fully closed. The 9<sup>th</sup> cervical is preserved in articulation with the remainder of the thoracic series and distinguished by its relatively large size and robust ribs, which are of a similar size to those of the first dorsal. The thoracic series is represented by at least 11 vertebrae, observed in their left ventrolateral aspects (Figures 3.15 - 16). The second vertebra is partially overlain by the sternal plate while the third is completely overlain, although its position is inferred by the presence of a loose rib. All thoracic vertebrae preserve a similar size and form, the corpora of which are sub-equal in length and width, and articulate with prominent, caudolaterally directed transverse processes. The ventral face of the first two transverse processes possess very large pneumatic foramina, which then appear to be absent in subsequent vertebrae until the 8<sup>th</sup> dorsal, where after these foramina have now become very small.

*Contra* to the state observed for the cervical series, the neurocentral sutures of the thoracic vertebrae are immature, where the vertebral body and neural arch of the cranial most elements have been slightly displaced. Although the caudal most elements also display an immature state, the vertebral body and neural arch form a tighter association with one another and the sutures are thinner – indicating an advanced state of fusion. Four sacrals are preserved in natural articulation with the thoracic series (Figure 3.18). The vertebral bodies are narrower than those of the thoracic series. The ribs of the first sacral vertebra are directed strongly caudolaterally, while in the remaining elements they are orientated laterally instead. The sutures of the sacral series are fully closed. Only a single caudal vertebra is preserved and has

been displaced from its natural position. It is sub-rectangular in shape, being approximately twice as long as it is wide, with a slightly splayed cranial margin.

**Pectoral girdle** – The coracoids are exposed in their ventral aspects but have disarticulated from the underlying scapulae, indicating that a scapulocoracoid has not formed (Figure 3.14). The coracoid body is expanded relative to the remainder of the element, with a concave dorsal margin forming the ventral portion of the glenoid fossa. Ventral to this a large, smooth and oval tubercle is situated just lateral to the onset of the shaft. The shaft itself is narrow and extends medially before expanding to form a forked articulation. The sternocoracoidal furca is widely splayed, the surface of which is smooth and convex. The saddle between the two forks of the furca is relatively shallow when compared to the ornithocheiroid configuration.

**Sternal plate** – The sternal plate is observed in its ventral aspect where it is almost rectangular in profile, being slightly longer than it is wide, and transversely concave (Figure 3.16). The lateral margins of the plate are crenulated for the articulation of the thoracic ribs, two of which are preserved along the right hand margin of the plate, while the caudal margin is convex. The cristospine is robust with a strongly concave caudoventral margin. The cranial section is broken and missing.

**Forelimb** – The bones of the forelimb are exposed primarily in their ventral or caudoventral aspects (Figures 3.15 – 17, 3.19). The humerus is a slender bone that displays an immature state as indicated by two large sesamoids, representing the trochlea and capitulum, which lie loose from the expanded distal articulation. The deltopectoral crest is unwarped and typical of that observed in other azhdarchoids, with sub-parallel medial/distal margins, and a large pneumatopore occupies the ventral face of the humerus between the deltopectoral crest and caudal process. The radius and ulna are slender and elongate, 1.26 times as long as the humerus. A single large sesamoid lies loose from the proximal articular face of the ulna. The elements of the proximal and distal carpus have disarticulated from one another but have not been displaced far. Within the right carpal region two elements of the proximal and distal are observed, displaying a series of complex profiles. The preaxial carpal is observed in its lateral view with an empty fovea, the large sesamoid that once occupied this being located close by. The pteroid lies adjacent to the radius and is an elongate

element, 58% the length of the ulna, with an expanded and concave articular surface. The shaft is narrow and tapers strongly towards its medial terminus. Just medial to the articular surface, the bone is strongly curved so the shaft would have been directed parallel to the radius/ulna. The wing metacarpal (mc IV) forms a ratio of 1.6 with the humerus and narrows distally from its proximal articulation. The distal articulation is created by the presence of a dorsal and ventrally located condyle. The preaxial metacarpals (i.e. mc I-III) are bulbous at their distal termini but taper strongly towards their proximal margins where they become exceedingly narrow (Figure 3.17). At least one of these metacarpals, here presumed to be the first (i.e. mc I), terminates against the distal carpals of the wrist. The wing finger phalanges are typical of other azhdarchoid pterosaurs where the length of the phalanges decreases distally with each successive element. The extensor tendon process is unfused from the proximal face of the first wing finger phalanx, while the shaft of this phalanx is pierced on its ventral face adjacent to the proximal articulation. The shaft of the phalanges themselves are straight, the proximal and distal regions of the bones have expanded to form the articular surfaces for their neighbouring elements.

**Pelvic girdle** – The elements of the pelvic girdle are unfused and have been slightly displaced from their natural positions (Figure 3.18). The ilium is a long, narrow and medially curving blade of bone that extends cranially and terminates level with the 10<sup>th</sup> thoracic vertebrae. Accounting for a slight displacement of the ilium it is likely that the cranial termination of bone lay lateral to the 9<sup>th</sup> thoracic vertebrae during life. The pubis forms as a mediolaterally compressed plate, thickest about its dorsal region that acts as the cranioventral portion of the acetabulum. The ventral margin is strongly, but irregularly, convex and a large foramen (obturator foramen) occupies part of the caudal margin. The ischium is badly damaged with the loss of much compacta and no osteological details are preserved.

**Hind limbs** – The semi-globular articular head of the femur is situated within the acetabulum with the femoral neck being offset against the shaft of the bone at an angle of 33° (Figures 3.18, 3.20). The femoral shaft is bowed slightly laterally and forms a ratio of 1.29 with that of the humerus. The tibia is badly damaged and missing much of its mid-shaft but makes a ratio of 1.73 with that of the humeral length and 1.34 with that of the femoral length. The proximal tarsals are loose from the distal

margin of the tibia and are semi-lunate in shape. The distal tarsals appear to be missing. The metatarsals are strongly bowed in a ventral direction (Figure 3.20).

**Soft tissue preservation** – Several patches of mineralized tissue are observed as a light/dark grey trace over a wide area of the fossil. The origin of two corresponding patches of tissue, located between the elbow regions and thoracic series on both arms is uncertain where no fibres or soft tissue structures are observed with the trace. As such it is not possible to confirm whether these traces represent the preserved remains of the wing membrane or that of the body tissues. A second trace also lacking internal features is regarded as being the preserved remains of the propatagium. This latter trace is located between the antebrachial bones of the right forearm and encompassing the proximal region of the pteroid; a state of preservation strikingly similar to that displayed by the Vienna *Pterodactylus*. A final trace of tissue, adjacent to the wing finger phalanges, is here regarded as part of the distal wing patagia due to the presence of zigzagged actinofibrils, identical to the pattern observed within *Jeholopterus* (Kellner et al. 2009).

### **3.6.5 Specimen Comments**

While a complete discussion of the taxonomic affinity of this specimen cannot be provided before preparation is complete, a sufficient amount has been exposed such that it would be amiss if this question was not considered here. It is confidently identified as an azhdarchoid pterosaur due to the relatively elongate metacarpal, femur and tibia (making respective ratios of 0.62, 0.78, and 0.58 with the humerus, see Unwin 2003). The outline of the “spear-like” mandible further distinguishes this specimen from the majority of specimens uncovered from the Araripe Basin of NE Brazil, where both *Tapejara* and *Tupandactylus* are characterised by a ventrally turned rostral tip and median sagittal crest (Wellnhofer and Kellner 1991; Kellner 2003, 2004a), while the ventral mandibular margin of *Thalassodromeus sethi* (Kellner and Campos 2002) turns dorsally close to the tip, creating a relatively blunt and robust rostral segment (Figure 3.21). Taxa with a similarly gracile and strongly tapered mandible from the NE of Brazil are therefore restricted to the genus *Tupuxuara* (i.e. *T. longicristatus*, *T. deliradamus*, and presumably also *T. leonardii*).

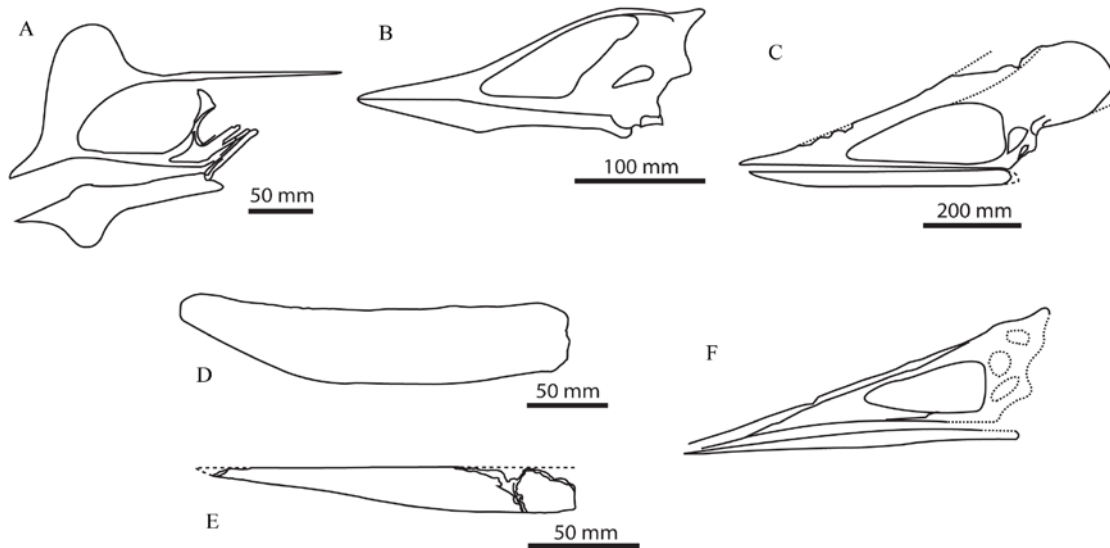


Figure 3.21 – Comparison of a variety of mandibles attributed to the Azhdarchoidea: A, *Tapejara wellnhoferi* (Iwaki specimen); B, *Shenzhoupterus chaoyangensis*; C, *Tupuxuara leonardii*; D, *Thalassodromeus sethi* (private specimen, Oberli Collection); E, cf. *Tupuxuara* (described specimen); F, *Jidapterus edentus*. Within the Early Cretaceous deposits of NE Brazil, only specimens attributed to the genus *Tupuxuara* are known to preserve a “spear-like” mandible.

A comparison with *T. leonardii* is not possible as the holotype preserves the cranial section of the skull which is not present here. The remaining two species, however, are well represented by two complete skulls (i.e. KPM NH DL 84 and IMCF 1052) and complemented by the presence of several additional specimens (i.e. CD-R-003, SMNK PAL 4330, SMNK PAL 6410). Witton (2009) reported that the major diagnostic difference between *T. deliradamus* and *T. longicristatus* was the angle of the quadrate to the jugal, this angle being higher in the former (i.e. 150° versus 130° respectively). At 161°, the angle between the jugal and quadrate of the described specimen is closest to that of *T. deliradamus* (Figure 3.22), albeit rather larger. Additionally, Witton (2009) argued that the caudal margin of the nasoantorbital fenestra was straighter in *T. deliradamus* relative to that of *T. longicristatus*, which is more concave. Although the skull of the described specimen has fragmented, the dorsal branch of the jugal that articulates with the lacrimal is almost straight (Figure 3.22), again suggesting a better relationship with *T. deliradamus*. The remaining diagnostic features of *T. deliradamus* are problematic for comparison as the nasoantorbital fenestra is incomplete but, reconstructing its dorsal margin based on the angle of the cranial margin of the lacrimal, the posterior margin of the nasoantorbital fenestra makes an angle of 134°, compared to 120° recorded by Witton



(2009) for *T. deliradamus* (SMNK PAL 6610). Thus the described specimen appears to be broadly similar to that of *Tupuxuara deliradamus* but it herein merely diagnosed to the level of the genus, for which a very robust affinity is proposed based on the form of the mandible. In spite of this the prefix cf. is added pending a formal publication of the specimen.

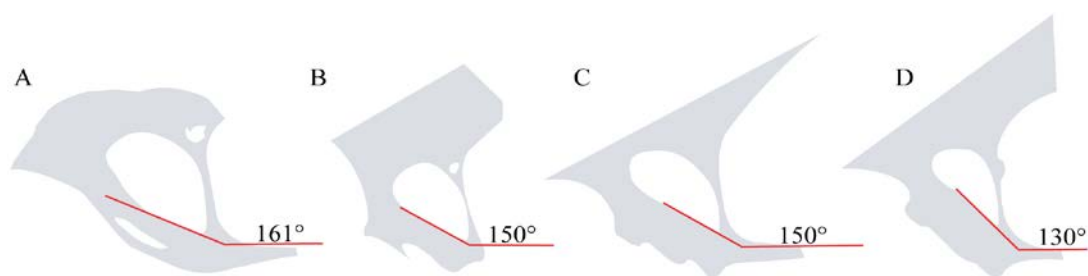


Figure 3.22. – Schematic comparison of *Tupuxuara* crania where: A, Described specimen; B, SMNK PAL 6410; C, KPMNH DL 84; D, SMNK PAL 4330. The reconstructed angle between the jugal and quadrate in the described specimen (A) exceeds that of both *T. deliradamus* (B-C) and *T. leonardii* (D). Figure adapted after Witton (2009).

**Morphometric maturity** - The specimen is morphologically immature using the criteria of Bennett (1993) as while the compacta and articular surfaces are well ossified, numerous elements are divided by sutures or lie loose. Although the order of suture closure has been covered within *Pteranodon* (Bennett 1993, 2001), and ornithocheirids (Kellner and Tomida 2000), little work has been done on the azhdarchoid skeleton (Eck et al. 2011). A crocodylian-like, caudal to cranial pattern of suture closure along the vertebral column, where the vertebral body fused with the neural arch and transverse processes was noted in pterosaurs by Kellner and Tomida (2000), however, unlike modern crocodiles they reported that the mid-cervicals (i.e. 3-7) fuse early in ontogeny, prior to those sutures of the thoracic series. The state of sutures within the described specimen, along with those preserved in SMNK PAL 1137 (Eck et al. 2011) confirm the observation of Kellner and Tomida (2000), where the caudal, sacral and mid cervical vertebrae have fully closed their neurocentral sutures while those of the thoracic series are still open (Figure 3.23). Within the thoracic series, however, the neurocentral sutures of the caudal most elements are less pronounced, with the central bodies and neural arches in tightly articulation, suggesting the onset of fusion. In contrast, the most cranial vertebrae are fully open

and the two elements are displaced, indicating that no fusion had occurred. The lack of fusion visible across the remainder of the skeleton indicates that the closure of the neurocentral sutures occurs relatively early in ontogeny, prior to the formation of the syncarpals, tibiotarsus and pelvic and pectoral girdles and indicates that this pattern of fusion can be broadly applied across the Pterodactyloidea.

Within *T. wellnhoferi* (SMNK PAL 1137) a similar condition to that of NSM-PV 19892 is observed where the atlas-axis complex is unfused, along with the 8<sup>th</sup> cervical, the body of which is missing, while the sutures of the middle cervicals are fully closed. The state of sutures within the thoracic series is variable with some preserving fully mature states while others are missing their vertebral bodies. As such the neurocentral sutures of pterodactyloids close relatively early in ontogeny, with the mid-cervicals, sacrals and caudals reaching their mature state prior to the closure of sutures in the appendicular skeleton. These observations thus support the conclusions of Kellner and Tomida (2000) but additionally indicate that the pattern of suture closure was largely unaltered even between distantly related taxonomic groups. Furthermore I add that closure of elements of the thoracic series occurs before that of the atlas-axis complex and the caudal-most cervical elements (i.e. 8 and 9).



Figure 3.23 - Thoracic column of cf. *Tupuxuara* (described herein) illustrating the sequence of closure of the neurocentral suture between the corpal body and the neural arch. The suture remains fully open in the more cranial elements while is closing in the more caudal elements, illustrating a caudal to cranial closure sequence. Cranial to caudal direction is from right to left.

| Right Element | Length (mm) | Left Element  | Length (mm) | Elements               | Length (mm) |
|---------------|-------------|---------------|-------------|------------------------|-------------|
| humerus       | 146         | humerus       | 149         | metatarsals            | 64          |
| ulna          | 183         | ulna          | 188         | Sacrals<br>(x4)        | 50          |
| radius        | 177         | radius        | 182         | Thoracic<br>vert. (x9) | 121         |
| pteroïd       | 107         | Metacarpal IV | 238         |                        |             |
| wph II        | 159         | wph I         | >271        |                        |             |
| wph III       | 111         | Mandible      | 471         |                        |             |
| femur         | 189         | PCRW          | 211*        |                        |             |
| Tibia         | 253         |               |             |                        |             |

Table 8. - cf. *Tupuxuara* Selected bone measurements. Where: PCRW, “praecaudale Rumpfwirbelsäule” (i.e. combined dorsal + sacral vertebrae length) after Wellnhofer (1970); wph, wing finger phalanx.

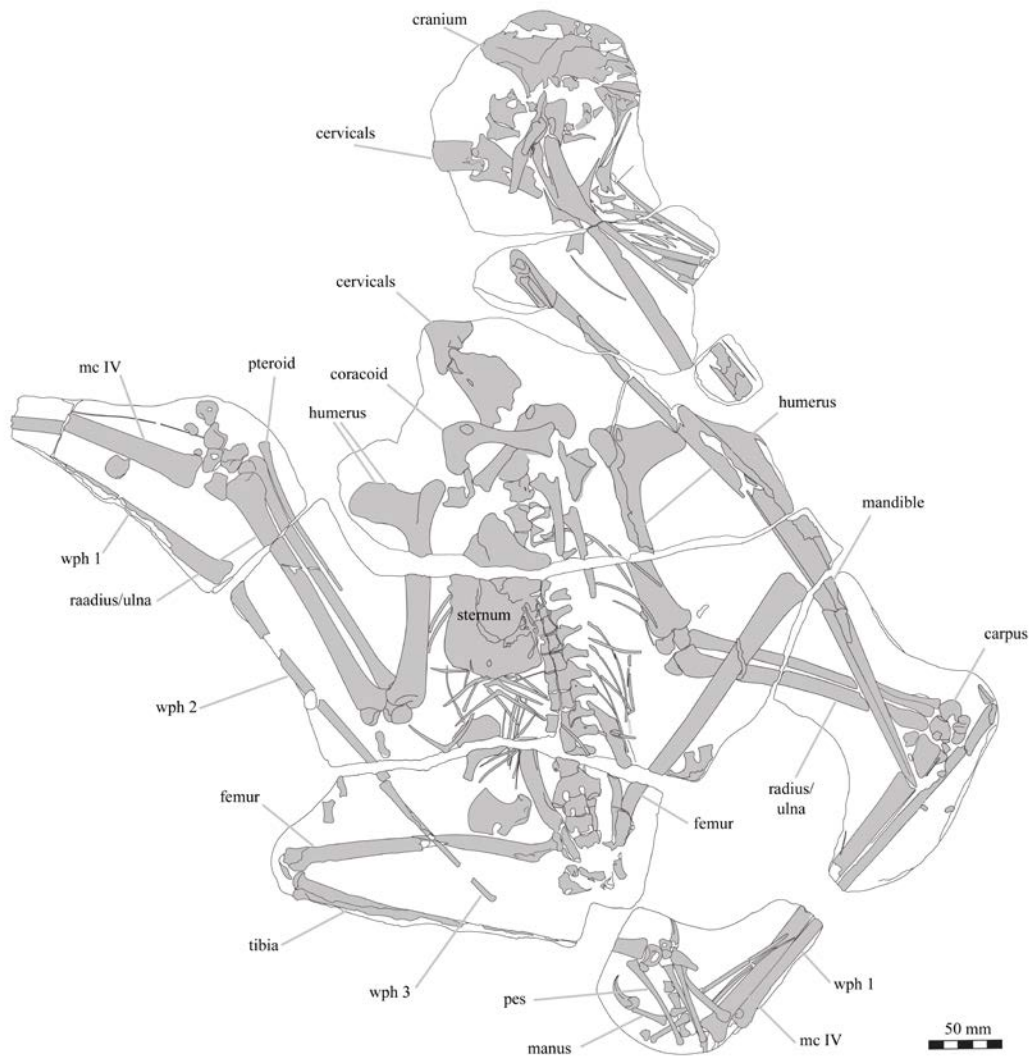


Figure 3.11. – cf. *Tupuxuara*. Line tracing with bone element shaded in grey. The largely complete nature of the specimen suggests that the absent sections of the skeleton (the middle cervicals and rostral portion of the skull) were lost as a result of poor collection.

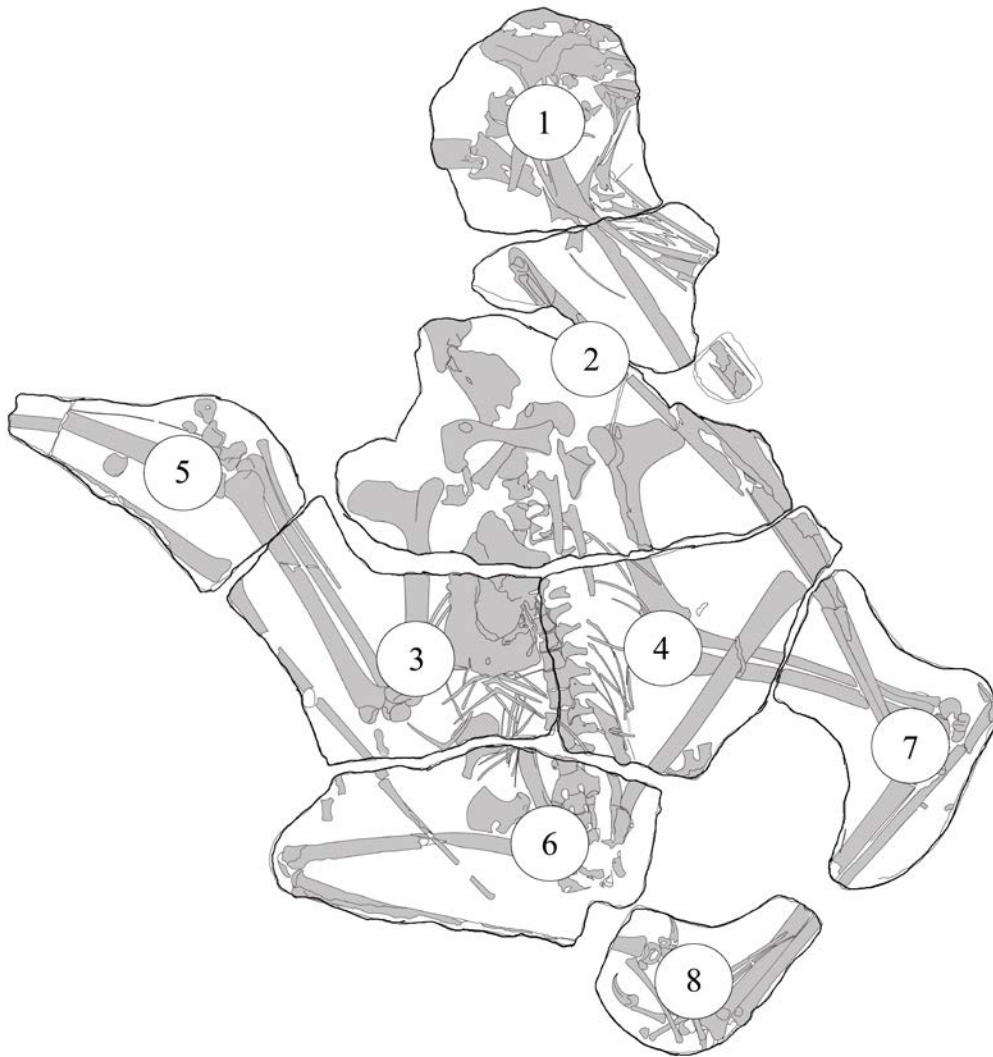


Figure 3.12 – cf. *Tupuxuara*. Major divisions of the concretion as referred to in the following figures.

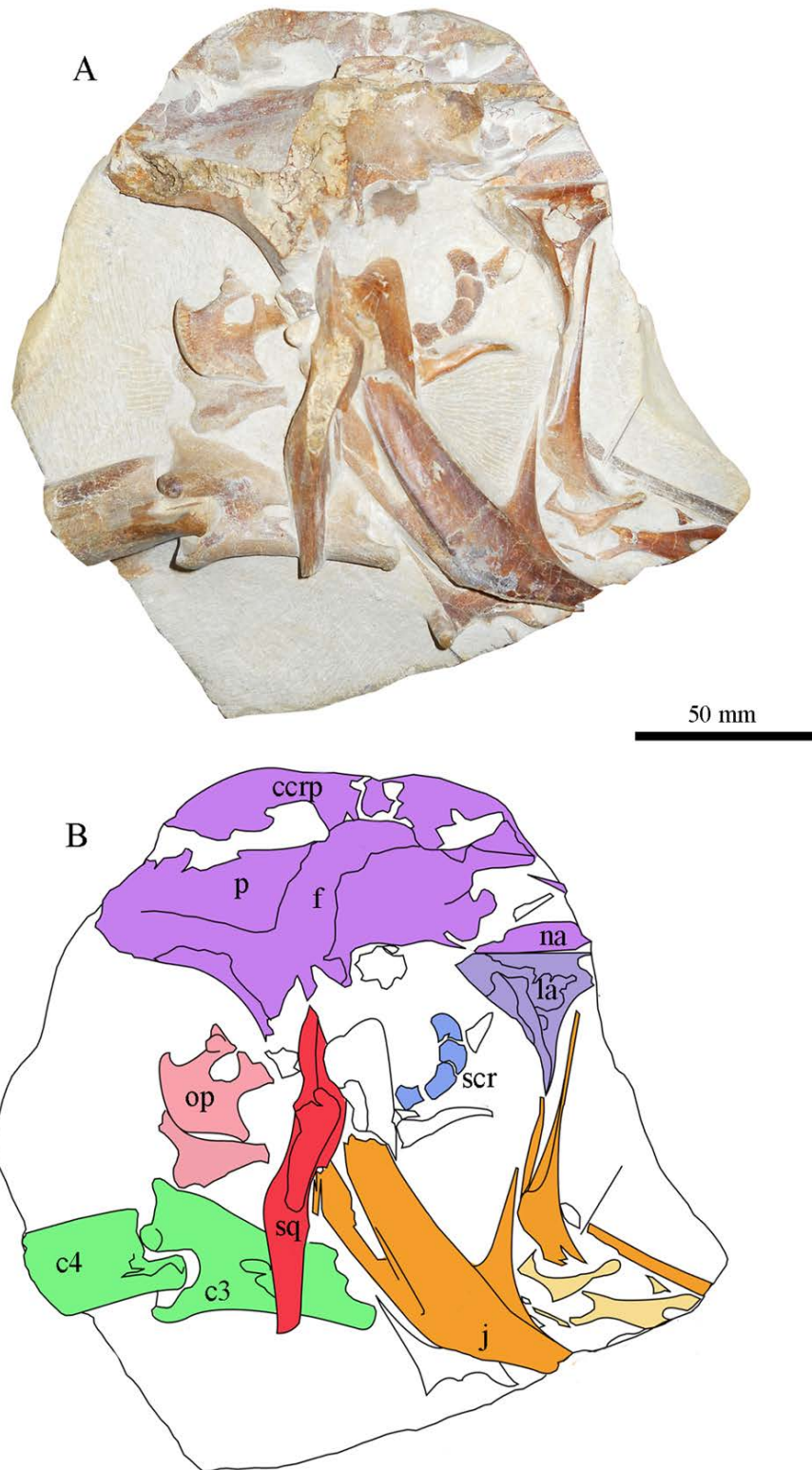


Figure 3.13. – cf. *Tupuxuara*. Concretion 1. A, Elements of the cranium, and B, corresponding line tracing.

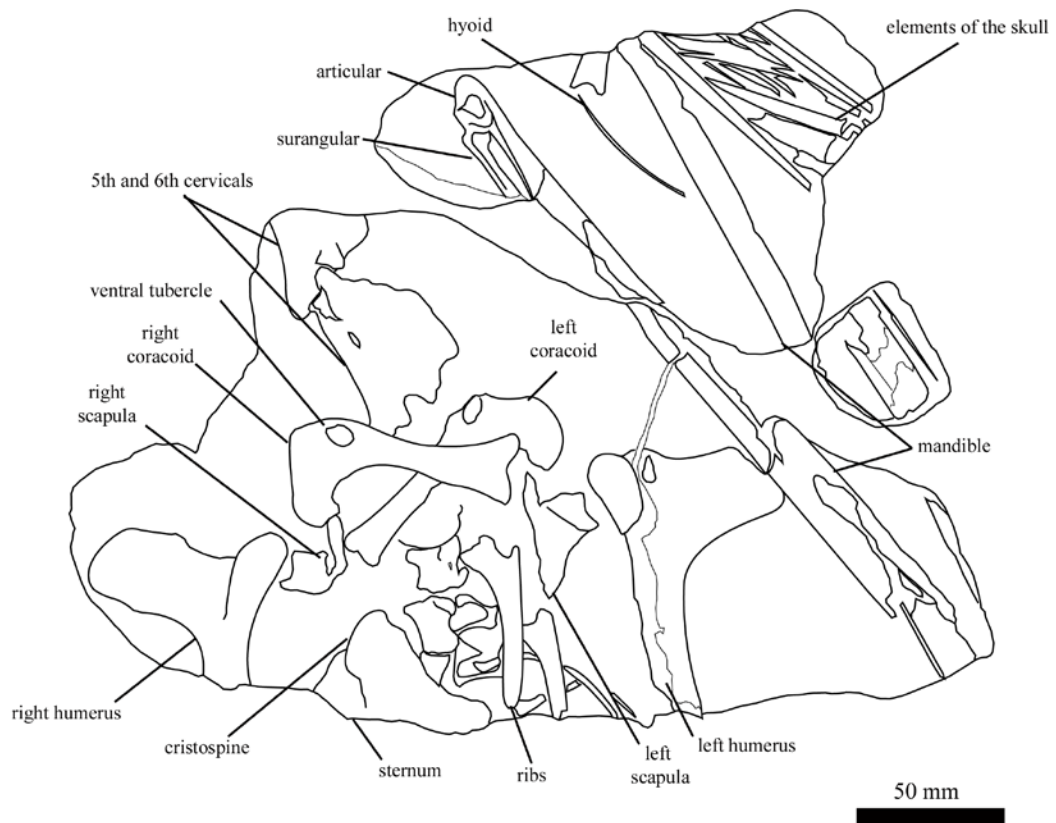


Figure 3.14. – cf. *Tupuxuara*. Concretion 2. Line tracing of the cranial section of the torso and middle portion of the mandible.

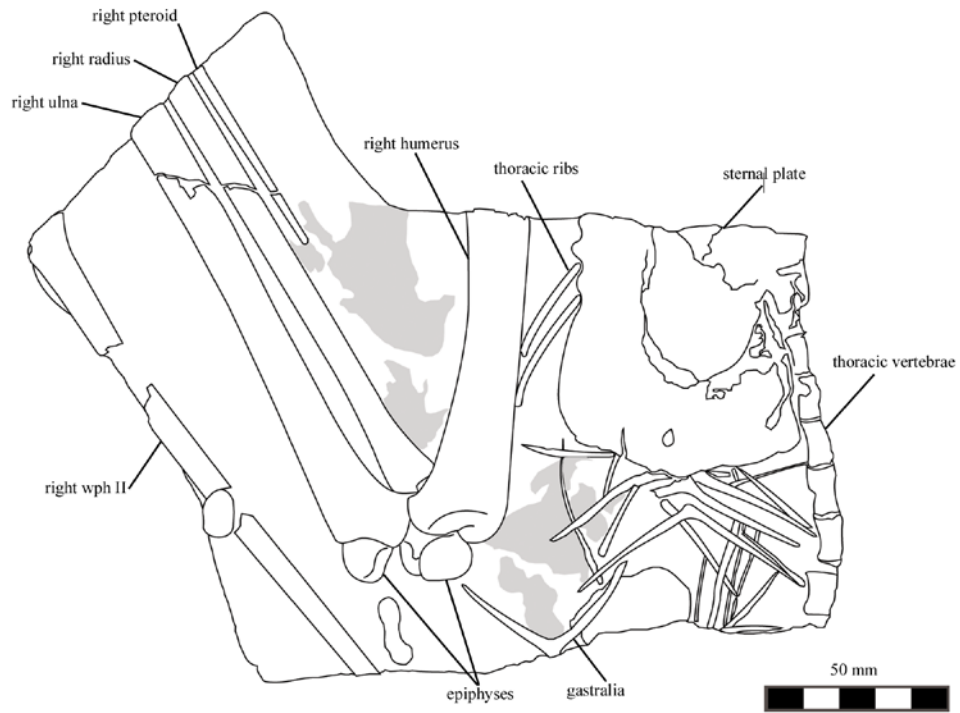


Figure 3.15. – cf. *Tupuxuara* . Concretion 3. Line tracing of the right half of the thoracic column. Grey shading indicates the preservation of soft tissue.

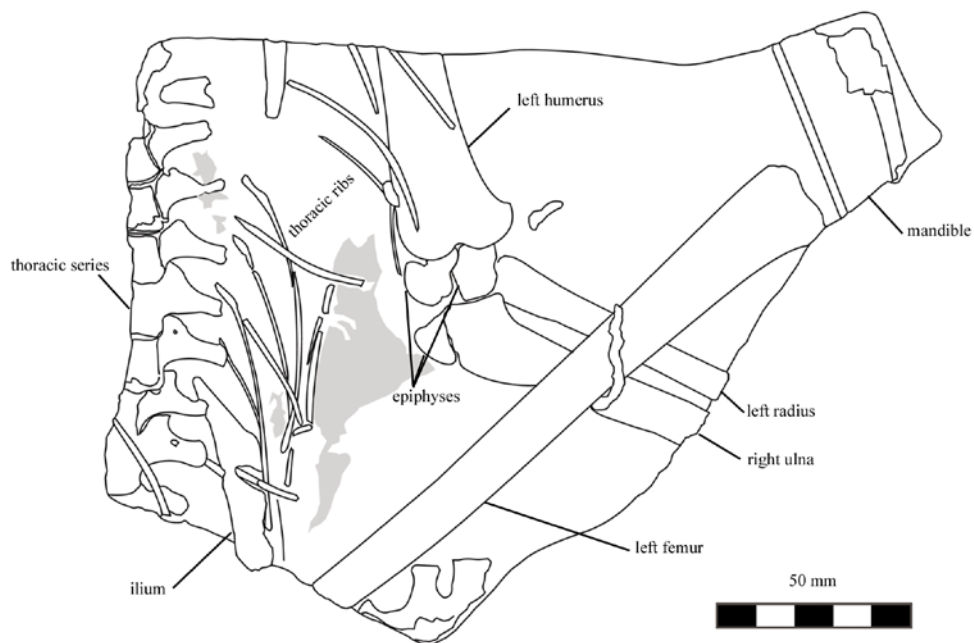


Figure 3.16 – cf. *Tupuxuara*. Concretion 4. Line tracing of the left half of the thoracic column. Grey shading indicates the preservation of soft tissue.



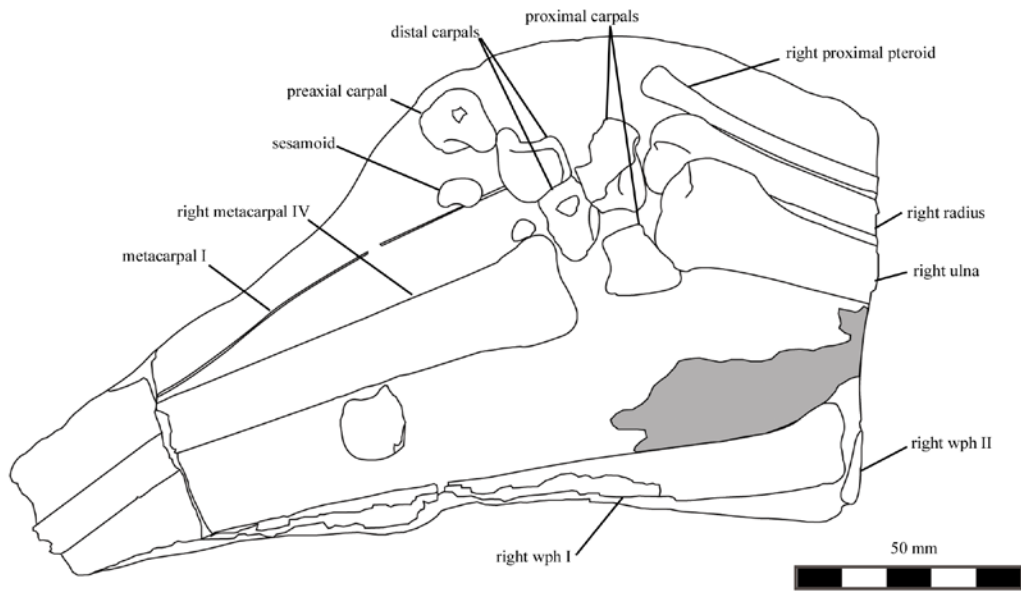


Figure 3.17 – cf. *Tupuxuara*. Concretion 5. Line tracing of concretion containing the right wrist. Grey shading indicates soft tissue preservation.

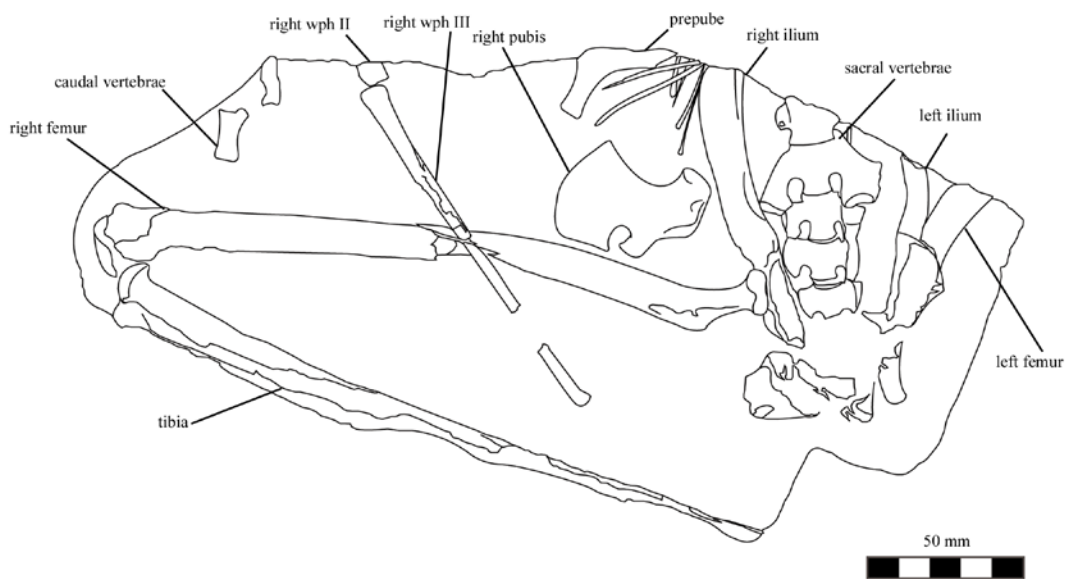


Figure 3.18. – cf. *Tupuxuara*. Concretion 6. Line tracing of the pelvic girdle and right hind limb.

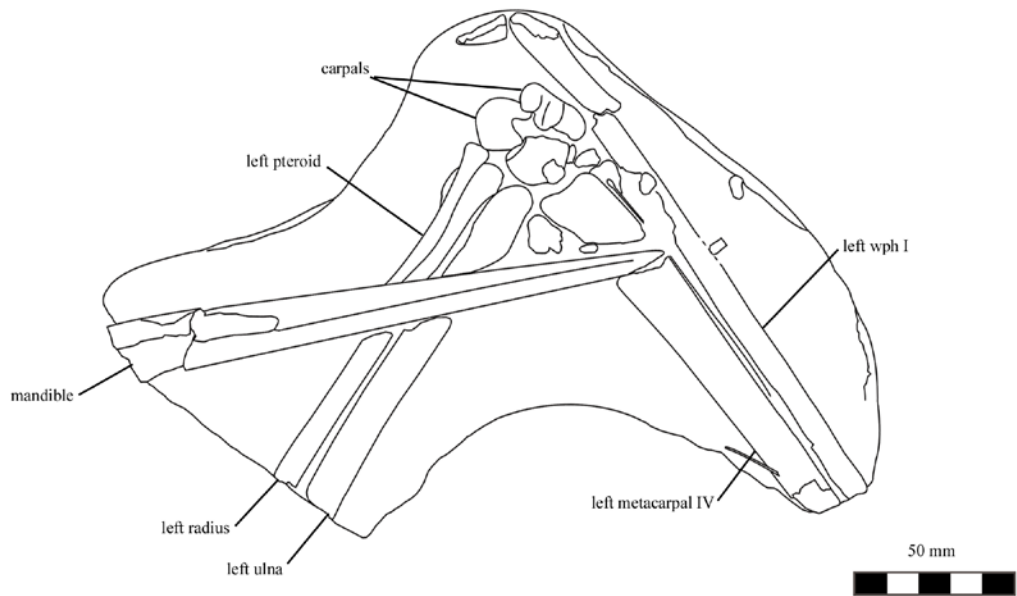


Figure 3.19. – cf. *Tupuxuara*. Concretion 7. Line tracing of the left wrist and mandible.

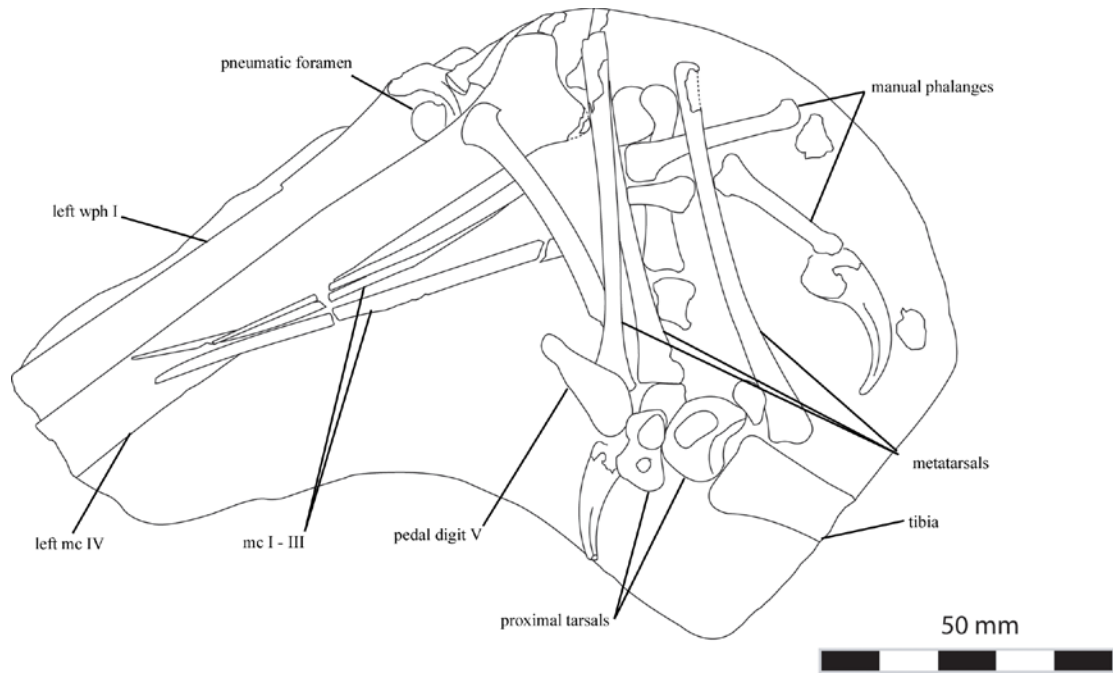


Figure 3.20. – cf. *Tupuxuara*. Concretion 8. Line tracing of the left manus and pes.

## Chapter 4

---

### PTEROSAURIAN JOINT MOBILITY

## **4.0 Comments and analysis of pterosaurian joint mobility.**

Within the context of this thesis a review of the pterosaurian joint mobility was deemed essential to set the limits for wing position, and its flexion/extension in both the mathematical and physical models developed in the next chapter. Although reconstructions of this type in extinct animals are problematic owing to the lack of soft tissue structures such as cartilage which can significantly alter the shape of a key articular surfaces, a sufficient number of well preserved and three dimensional specimens has allowed successive authors to propose a broad range of motions that can be generally applied within the Pterosauria. Herein, the range of motion determined through the manipulation of individual bones of SMNK PAL 1133, along with other material, is compared against works that have focused on this problem. A comparison and update of these values is subsequently provided with this stage regarded as a prerequisite for reconstructing pterosaurian wing beat cycles on which future work will focus.

### **4.1 Material and Methods**

Joint mobility in the specimen SMNK PAL 1133 was estimated through the manipulation of individual elements and the identification of bone locks between them. Long bones were directly manipulated with the assistance of a colleague, E. Prondvai, until physical contact of the bones prevented further movement (i.e. bone lock) or disarticulation occurred (i.e. > 50% of the surface was no longer in contact with the opposing element). Where movement occurs in only a single plane it was measured using a compass while the second person immobilised the skeletal elements. For more complex joints a camera or video camera was mounted on a tripod, and photographs and/or videos of the bones were taken at the maximum limits of motion. The footage was later analysed and angles were measured in Adobe Photoshop. Pre-existing casts of the bones of the forearm and distal wing spar were fixed together in natural articulation to observe the angles at maximum extension. The angles provided by the photographs and video footage of SMNK PAL 1133 can only be considered approximate values as no attempt was made to correct the angle based on the 3D position of the bone as was done by Wilkinson (2008).

## **4.2 Current limits of joint mobility in pterosaurs**

**Scapulocoracoid / Pectoral girdle-** No movement is possible between the scapula and coracoid as these elements fuse to create a unified scapulocoracoid later in ontogeny (Bennett 1993). This element in turn articulates with the sternum and vertebral column to create the pectoral girdle, four distinct configurations of which are observed among the Pterosauria (Figure 4.1). In addition to the relative position of the glenoid fossa in both “tapejarid” and “azhdarchid” configurations (see Frey et al. 2003b) these differ from the “ornithocheirid” models in a number of significant aspects. In the latter configuration the scapula is orientated more medially and typically braces itself against the neural spine of the fourth thoracic vertebra, where a shallow, oval concavity forms on the lateral faces of the neural spine to accommodate the medial surface of the scapula. This is contrasted with the remaining three configurations where the scapula is not firmly buttressed against the vertebral column and the scapular blade is orientated in a more craniolateral direction, forming a steep angle against the long axis of the vertebral column (~20-30°). The scapula in these taxa is more blade-like in appearance (being dorsally-ventrally compressed) and does not expand towards its medial edge as in ornithocheiroids.

Within the “ornithocheirid” configuration Wellnhofer (1991b) noted that some degree of flexion and extension of the pectoral girdle must have been possible and although Wilkinson (2008) subsequently considered the joint to be essentially immobile, he speculated that some degree of movement, in the order of 10°, may have been possible or the scapula would probably have fused to the notarium. This motion was more specifically defined by Bennett (2001b) who stated that the scapula could flex 15° from its “normal” position (i.e. 45-50° craniolaterally), with 20° of extension also being possible. In *Coloborhynchus robustus* (SMNK PAL 1133) the scapula is also directed craniolaterally but at an angle of 71° to the sagittal plane. Determining the degree of possible flexion and extension is problematic as much of the caudal and dorsal portion of the scapula articular end has been repaired with plaster. My own manipulations confirm that flexion is certainly possible because the scapula slides on the steeply slanted cranial portion of its articular surface while the surface caudal to this disarticulates from the notarium. From this I estimate that ~15° flexion was also

theoretically possible if the presence of soft tissue, mineralised tendons or sternal articulation did not restrict this in some way. As the caudal surface of the scapula is reconstructed I cannot estimate the degree of extension that may have been possible.

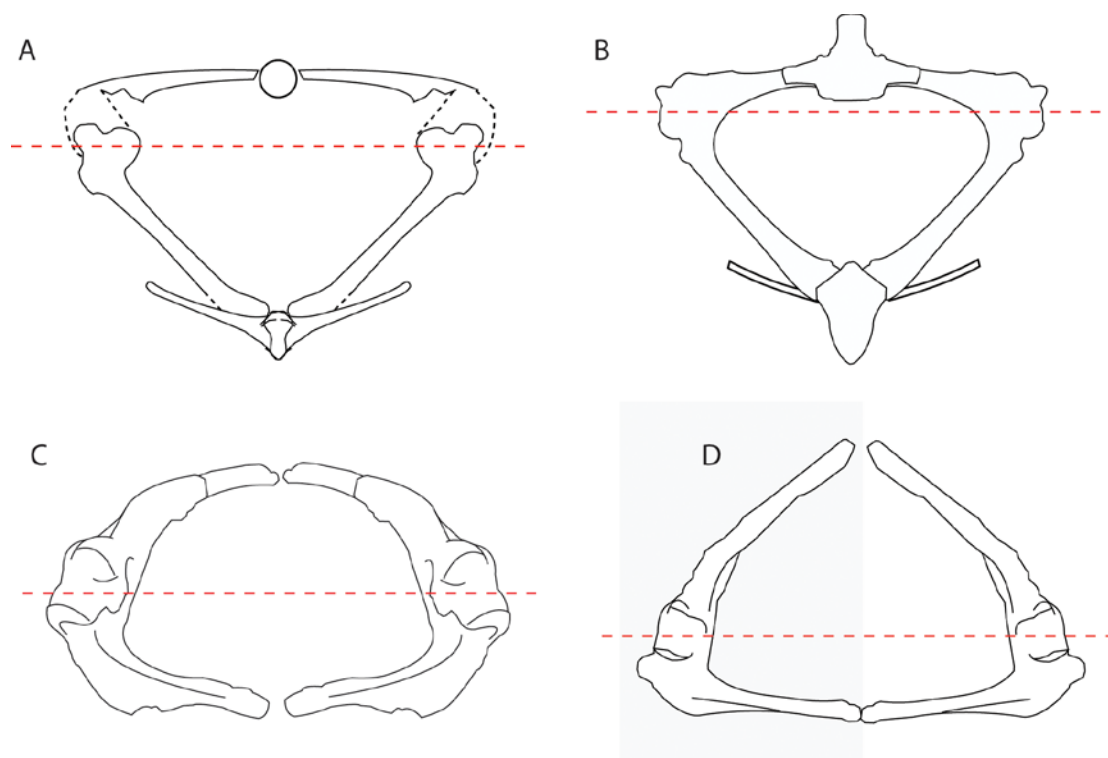


Figure 4.1. - Morphology of the scapulocoracoid. A, “Top wing” configuration of the non-pterodactyloids and basal pterodactyloids (e.g. *Dorygnathus*); B, “Top wing” configuration observed in ornithocheiroids (e.g. *Coloborhynchus*); C, “middle wing” configuration in derived azhdarchoids (e.g. *Quetzalcoatlus*); D, “bottom wing” configuration of the Tapejaridae (e.g. *Tapejara*). Dashed lines mark the position of the glenoid fossa and the level of the humerus.

The medial articulation of the coracoid attaches onto the cristospine of the sternum. The position of the articular surfaces and the angle at which the coracoids converge vary between pectoral configurations. The coracoids of the azhdarchid configuration lie almost horizontally, forming an angle of  $\sim 170^\circ$  between one another, with a small, medially located furca articulating with the lateral face of the cristospine. In the ornithocheirid construction, however, the coracoids form an angle of  $\sim 90^\circ$  and thus articulate onto the dorsolateral face of the cristospine. The articular surface itself is orientated transversely and has developed as a V-shaped incision as deep as it is wide. Wilkinson (2008) considered that any vertical movements between the coracoid and the sternum (i.e. elevation and depression) were regarded as unlikely because not only would this have caused disarticulation between the elements, but also because a high

degree of mobility would have been incompatible with it acting as a stable base for the humerus and pectoral adductors. There thus remains some controversy over the movements permitted between the sternocoracoid joint and the degree to which such movements (if any) can be applied between morphotypes.

**Shoulder joint** - The mobility of the shoulder represents one of the most complex joints of the pterosaurian skeleton owing to the dual role that the forelimb performed in both terrestrial and aerial locomotion. The position and extent of the saddle shaped glenoid fossa within each pectoral configuration have a pronounced effect on the range of motions available to the humerus.

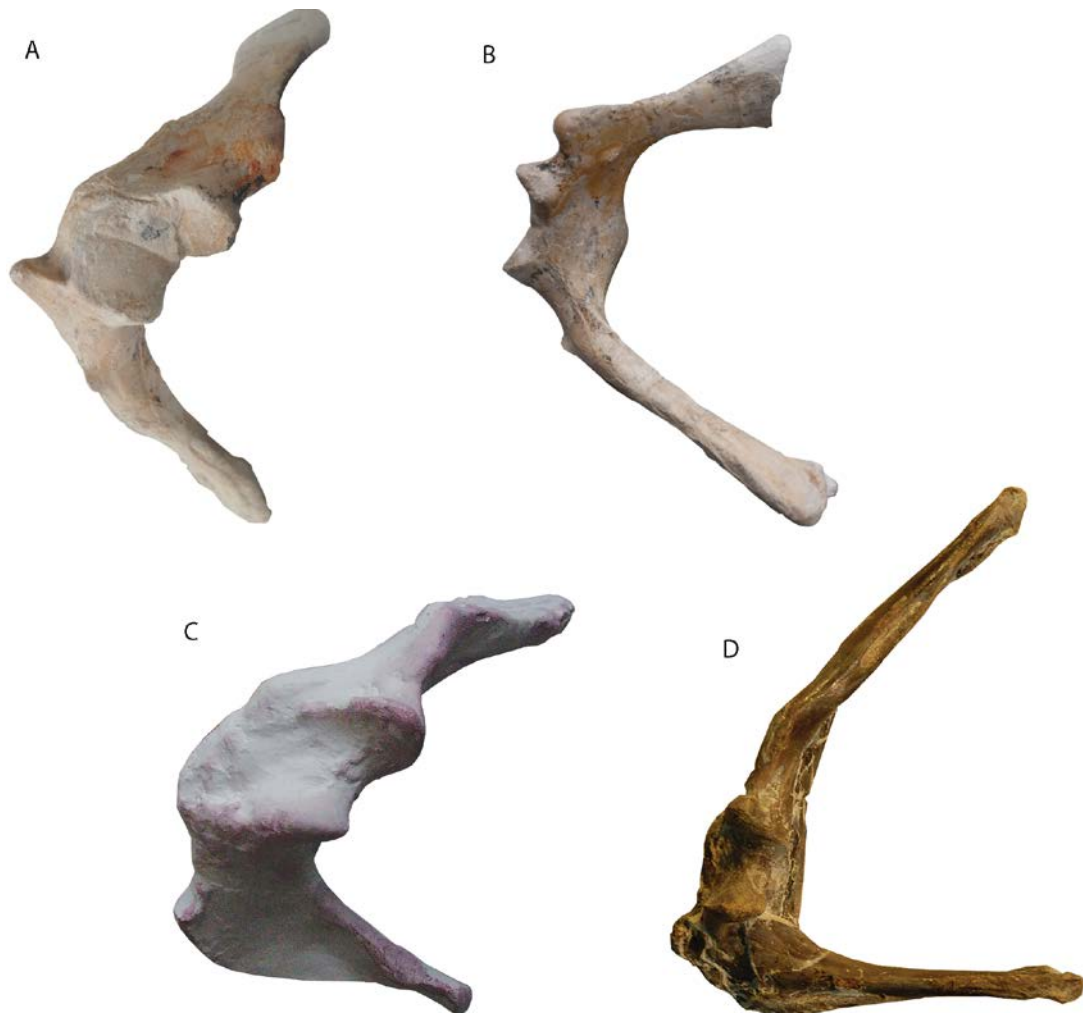


Figure 4.2. - Form of the glenoid fossa in ornithocheiroid and azhdarchoid pterosaurs. A – B, SMNK PAL 1133 in its lateral and caudal aspects. C, *Quetzalcoatlus* in lateral view; D, azhdarchoid indet., MN6685-V in caudal view. The glenoid fossa in

azhdarchoids is narrower than that of A – B in lateral view, with better defined dorsal and ventral ridges, and extends far onto the caudal face of the bone (i.e. D).

This is demonstrated within the “top decker” configuration, where the articular surface is restricted to the caudolateral side of the scapulocoracoid (Figure 4.2A) and does not extend onto the caudal surface to any noticeable degree (Figure 4.2B) but in the “middle” and “bottom” decker configurations the glenoid fossa extends and occupies much of the caudal aspect of the bone. Bramwell and Whitfield (1974) argued that *Pteranodon* (based on specimen BMNH 3378) could depress its humerus 25° below the horizontal while elevating it 70° during maximum upstroke, giving a total arc of 95°. In dorsal view they state that the humerus could be extended parallel to the transverse axis (i.e. = 0°) and flexed 65° behind this axis (i.e. caudolaterally). Although Bennett (2001b) generally agreed on this interpretation he differed on two points, that the humerus could be extended and flexed when depressed below the horizontal, and that it could also be flexed a little more than 65° against the transverse axis. Hazlehurst and Rayner (1992) proposed a radically different sort of movement based on the partial remains of *Santanadactylus*, stating that little to no elevation or depression was possible and that a rotational component was the major motion at this joint. I can indeed confirm that the shoulder joint of this specimen is difficult to manipulate without immediate disarticulation (pers. obs.) and although Wilkinson (2008) argued that the lack of movement available to this specimen may be due to its incompleteness, the humeral head and the glenoid fossa are well preserved. It is instead likely that cartilage and soft tissue allowed elevation and depression of the humerus during life as take off or large power strokes would be difficult without a significant range of vertical movement. In addition to this other specimens of ornithocheiroid taxa indicate that such vertical movement was possible.

Chatterjee and Templin (2004) argued for a vertical elevation of 60° by late upstroke in the specimen NSM-PV 19892 and a depression of as much as 65° below the horizontal plane, giving a total arc of 125°. The specimen, however, is morphologically immature and the glenoid fossa very smooth, which may have allowed more movement than was originally possible. Wilkinson (2008) subsequently estimated a cartilage thickness of 3 mm, i.e. ~7.5% the width of the humeral articular surface, for NSM-PV 19892. *Contra* to Wellnhofer (1991b), who gives the typical



gliding position of the humerus as being orientated 15-20° dorsal to the transverse plane and 15° caudally, Wilkinson (2008) instead interprets the shaft as lying along the horizontal plane and directed ~ 10° caudally. He further estimated the maximum range of elevation and depression of the humerus as ~70° and 25° respectively, giving a total arc of ~95°. Importantly the limit of depression is simple to determine as beyond this point the proximal portion of the humeral neck abuts against the ventral frill of the glenoid fossa, forming a bone lock. This is supported by my own observations of SMNK PAL 1133 which suggest that the humerus can be depressed between 45-50° ventral to the horizontal axis, while the maximum elevation that can be generated as the humerus is supinated is around 50°, giving a total arc of ~95-100° (Figure 4.3). This agrees perfectly with the results of Wilkinson (2008) as the arcs calculated here begin with the humerus elevated 20°, illustrated by Wellnhofer (1991b).

Despite the complexity involved with determining the degrees of freedom available to the shoulder joint it is reassuring that the majority of studies are in general agreement concerning the maximum elevation and depression of the humerus. Both myself and Wilkinson (2008) estimate an arc of 95°, along with Bramwell and Whitfield (1974) and Bennett (2001b), while other studies have reported similar values of 90° (Padian 1983) and 80° (Wellnhofer 1991b). Only the analysis of Chatterjee and Templin (2004) deviates from this consensus.

The cranial extension of the humerus has been found to have been extremely limited in pterosaurs as due to the caudoventral orientation of the glenoid fossa and its caudolateral positioning (Figure 4.4). Wellnhofer argued that the humerus could not be extended cranial of the transverse axis and retracted only 25° caudally to this, as the cranial portion of the humeral head would become disarticulated from the glenoid fossa with any additional movement. Bennett (2001b), however, countered this by noting that the humerus remains in contact with the caudal portion of the glenoid. Similar to Padian's (1983) suggestion that *Dimorphodon* could flex its humerus so that the long axis of the bone lies parallel with the vertebral column, Bennett's interpreted that the humerus of *Pteranodon* could be positioned to lie within 10° of the long axis, as a result of a >65° flexion of the humerus coupled with a 20° flexion of the shoulder girdle. Wilkinson (2008) noted an intermediate range of motions and

stated that from the close packed position (i.e.  $0^\circ$  elevation,  $10^\circ$  retraction from the transverse plane) the humerus could be protracted only  $10^\circ$ , thus lying parallel to the transverse axis and retracted by  $40^\circ$ , beyond which contact with the glenoid is lost. However, if the humerus was elevated and contact is mostly lost with the coracoidal portion of the glenoid then the humerus can roll freely, greatly increasing the measured range of protraction and retraction to  $30^\circ$  and  $50^\circ$  respectively.

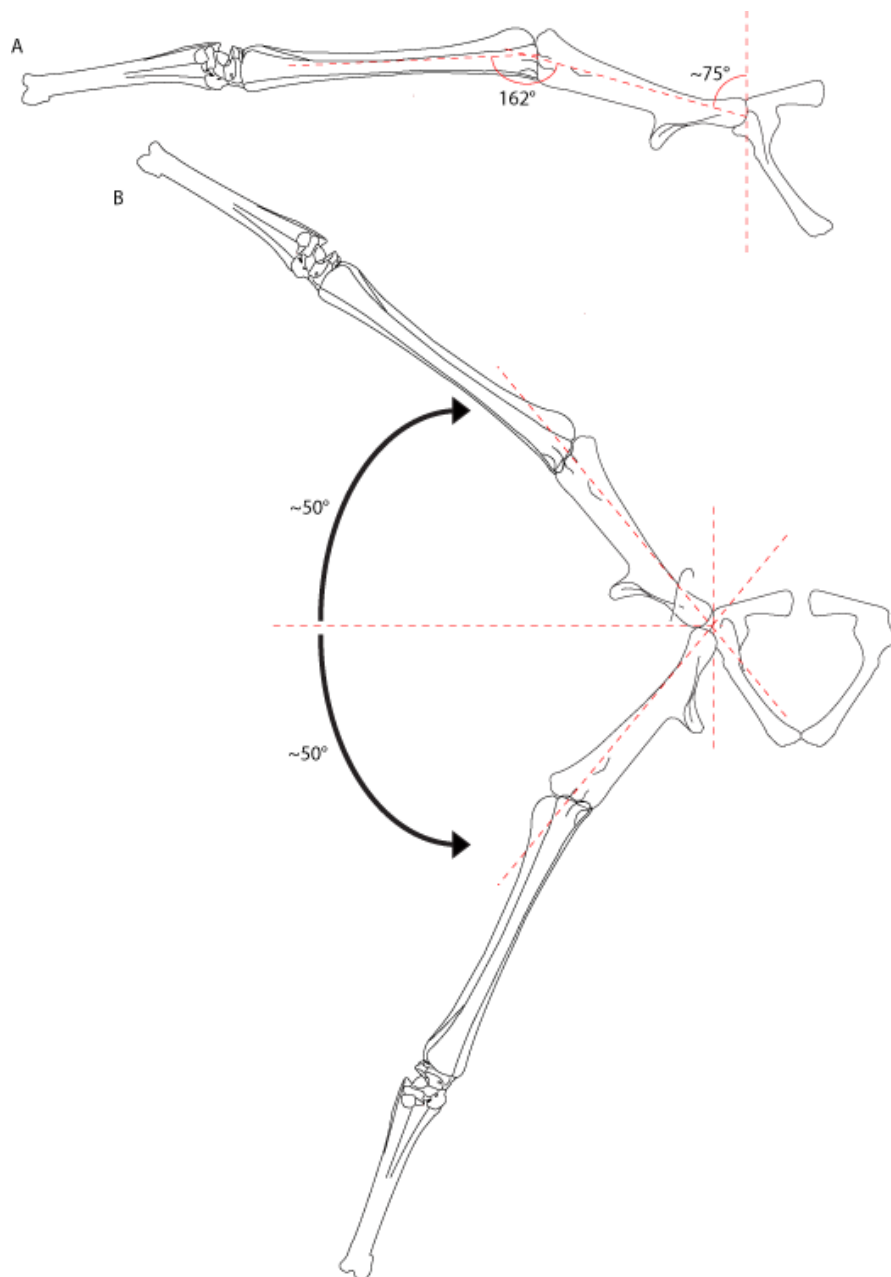


Figure 4.3 - Position of the forearm during gliding flight (A) and the maximum degrees of elevation and depression of the humerus in SMNK PAL 1133 (B). Dashed lines indicate the long axis of the humerus.

The kidney shaped articular surface of the humerus and the curvature of the glenoid fossa permit a large degree of rotation, where the humerus rotates about its long axis during terrestrial and aerial locomotion along with a pronation and supination of the fore arm. Hazlehurst and Rayner (1992) proposed that a 70° rotation of the humerus was possible in *Santanadactylus* and although their conclusion that rotation was the primary motion available at this joint is rejected, similar values have been reported from other workers. Chatterjee and Templin (2004) reported a rotation of ~ 85° in *Anhanguera* while Wilkinson (2008) proposed that the maximum range of supination and pronation was 50° and 30° respectively to give a total rotational component of 80°. My own workings on the joint suggest a smaller rotational arc of 62-63° between the maximum supination and pronation but a general consensus might be that the ornithocheirid construction supported a rotational component of between 70 – 80°. This same range of values was noted in extant birds (i.e. pigeons and starlings) by Poore et al. (1997).

The range of motions available to the azhdarchoid configurations must have been very similar given their common morphology and can be considered together. The position of the glenoid fossa in both of these configurations is located more ventrally than that observed in the ornithocheirid pectoral girdle but all morphotypes are united in the fact that the articular surface does not extend onto the cranial surface of the scapulocoracoid body. However, the glenoid fossa of the azhdarchoid configurations clearly extends onto caudomedial face of the scapulocoracoid and thusly allows for a far greater retraction of the humerus than was possible in ornithocheirid pterosaurs.

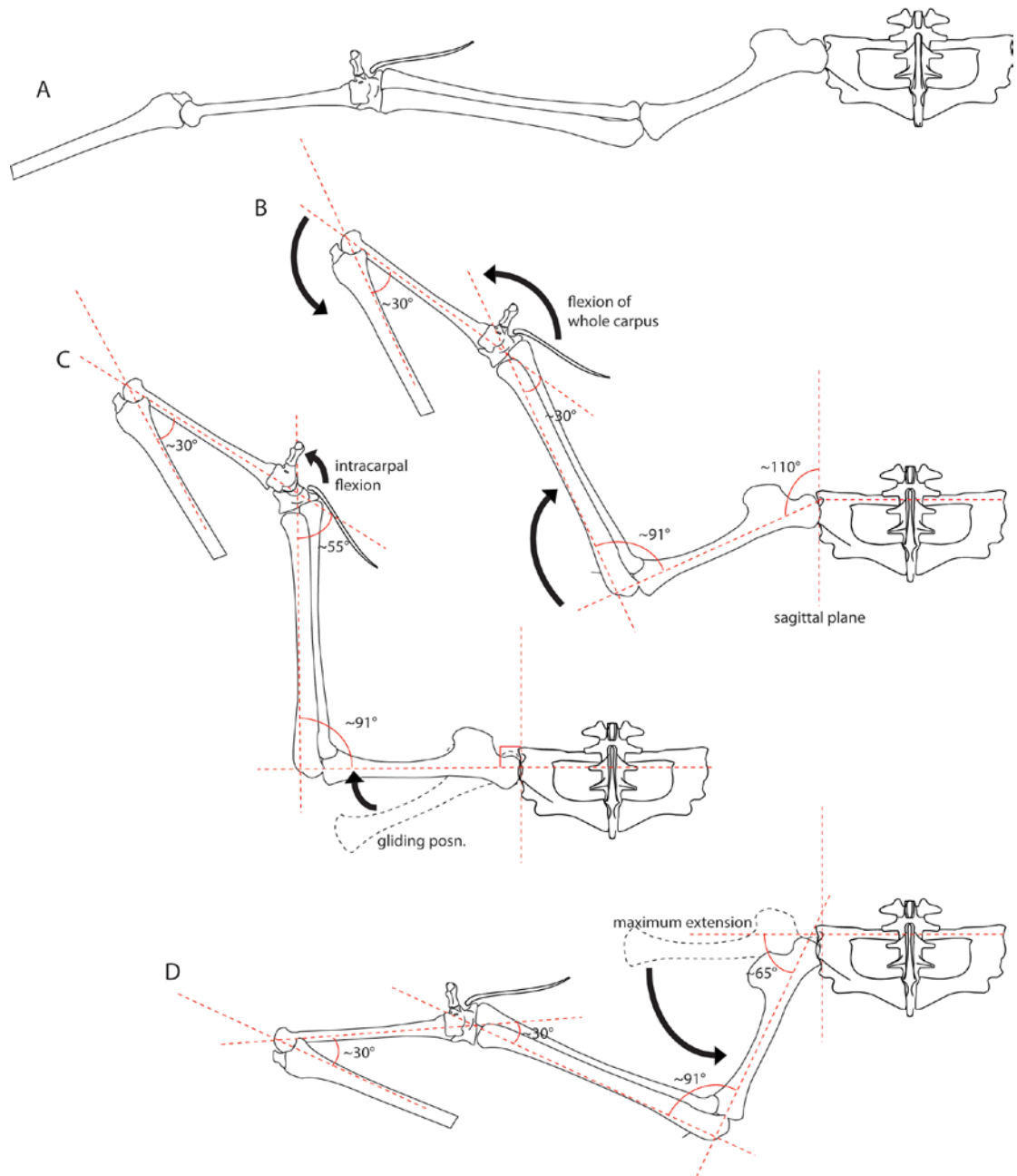


Figure 4.4 - Degrees of freedom in the forearm of SMNK PAL 1133 in dorsal view. A, hypothetical gliding position. B, flexion of major joints distal to the shoulder; C, maximum extension of the humerus; D, maximum flexion of the humerus and forearm.

Additionally a second humeral morphotype is recognised with respect to the position of the articular surface. Here the humeral neck is deflected dorsally at a greater angle to that of the ornithocheirid humerus (e.g.  $47^\circ$  in SMNK PAL 3856 versus  $22 - 25^\circ$  in SMNK PAL 1133) and the articular surface is more curved and orientated dorsomedially, directing the humeral shaft dorsally when placed in articulation with the scapulocoracoid, and allowing for a greater degree of elevation. This does not appear to be caused by a warping of the bone during taphonomy as the remainder of the humerus is in a good condition and an identical configuration is seen in *Quetzalcoatlus*, tapejarids, and more basal pterosaurs (e.g. *Dorygnathus*). Based on specimen TMM 41544 (*Quetzalcoatlus*) the humerus can be depressed to an angle of  $\sim 30-38^\circ$  below the transverse axis and elevated to  $\sim 65^\circ$  above it to give a total arc of between  $95 - 103^\circ$ . If the humerus is supinated, as would be expected during the upstroke of the wing, then it is difficult to determine the dorsal limit of elevation because the long axis of the shaft can reach a vertical position without disarticulation between the humeral head and the glenoid fossa. Rotation of the humerus when restricted to the caudolateral portion of the glenoid fossa is between  $56-68^\circ$ , although as my own observations for the ornithocheirid configuration were lower than those of previous workers the same may be expected of this as a result of the common methodology. As such the true rotational component may be slightly higher and more similar to that reported in ornithocheirid taxa.

The morphology of the humeral head and that of the glenoid fossa allow for a far greater vertical elevation of the humerus and a near complete retraction, allowing it to lie almost parallel with the axial column. If the articular surface of the humerus is placed flat against the glenoid fossa then the humeral shaft is directed dorsally at a very steep angle relative to the ornithocheirid condition. The morphology of the humeral head, combined with a more ventrally located glenoid fossa, allows the wings to be moved into a position more level with, or above, the centre of gravity, therefore making the pterosaur more stable during gliding flight. In such a way the azhdarchoids evolved a solution to a shoulder girdle that fulfils its dual roles in both terrestrial and aerial locomotion.

**Elbow joint** - Bennett defined the elbow as “a complex hinge that allows the radius and ulna to fold towards the humerus. There is no rotation of the ulna but the simple

convex-concave joint of the radius would permit it to rotate slightly on the humerus.” (Bennett 2001b, p119). At the position of maximum extension an angle of 150° between the humerus and radius/ulna remains fairly uncontroversial and is supported by numerous authors: Bennett (2000b, 150°); Bramwell and Whitfield (1974, 153°); Chatterjee and Templin (2004, 145°); Wellnhofer (1985, 150°); Wilkinson (2008, 160°). My own examinations of *C. robustus* (SMNK PAL 1133) indicate an angle of ~ 155°. In cranial view at the position of maximum extension Wellnhofer (1985) reported that the humerus and ulna of *Santanadactylus* met at an angle of 163°, while an angle of 162° is observed within *C. robustus* (Figure 4.5).

Although my interpretation of the position of the brachial and antebrachial bones at maximum extension is in general agreement with previous investigations, the available degree of flexion that can occur from this point remains extremely controversial. Several studies advocate only small degrees of flexion, in the order of 30 – 55°, between the bones (e.g. 30° for Hankin and Watson (1914); 40° for Wellnhofer (1985); 55° for Chatterjee and Templin (2004) while at the other extreme Unwin (1989) noted that the ulna in *Dimorphodon* could be folded tightly against the humerus, and Padian suggested that the elbow could close completely so that the ulna would lie parallel to the humerus. Bennett (2001b) also argued that a considerable degree of flexion was possible between the elements as the articular surface of the capitulum extends far on to the ventral surface of the humerus in three dimensionally preserved specimens (BMNH 1776, 8715; TMP 82-16-303) and faces proximally. He further suggested that Wellnhofer may have underestimated the degree of flexion due to *Santanadactylus* lacking its distal epiphyses and stated that *Pteranodon* could have flexed its elbow so that the ulna lay at 30° to the humerus, giving a closure arc of 120°. Wilkinson (2008) estimated a cartilage covering of the joint of 5 mm thickness (i.e. 6.5% the width of the distal humerus articular surface), and reported that an intermediate range of flexion of 90° was possible. Based on my own observations I can confirm that the size and position of the capitulum does indeed allow for a large degree of flexion. An alternative method for calculating the maximum degree of flexion is to slide the radius against the carpus, causing the carpus to flex until it no longer makes contact with the articular surface of the radius. The distance travelled by the radius thus allows the flexion of the elbow to be reconstructed. In *C. robustus* maximum flexion of the elbow is reached when the ulna lies at an angle of 89 - 73.5°

to the humerus and supports an intermediate closure arc of 66-76.5°. While this range of movement is not quite in agreement with that of Wilkinson (2008) it supports neither very large nor very small angles of maximum closure. Flexion of the elbow in all pterosaurs results in the ulna and radius being directed ventrally with respect to the long axis of the humerus and Bennett (2001b) reported that at maximum flexion an angle of 30° was present between the ulna and the humerus.

A single, privately held and three dimensional skeleton of *Dorygnathus* (Thermopolis specimen, pers.obs.) suggests that the elbow could be extended to 150°, as is also observed in pterodactyloid taxa, but could be flexed to an angle of 26° to give a total closure arc of 124°. This is well in excess of that found for most other pterosaurs with the exception of *Pteranodon* (Bennett 2001b). While it is simply possible that non pterodactyloid pterosaurs were better able to flex their elbows (e.g. *Dimorphodon*), the lack of any well defined condyles due to acid preparation almost certainly results in an overestimate of the motion available to the elbow. Maximum flexion of the elbow here is again coupled with a distal displacement of the radius (3.6% of the radius length) and flexion of the proximal syncarpal.

**Carpal joint** - There are five potential joints formed by the carpus: those of the radio-ulno-carpal, which is linked with the flexion of the elbow, the intersyncarpal joint, where the proximal and distal syncarpal blocks may slide against each other; the joint

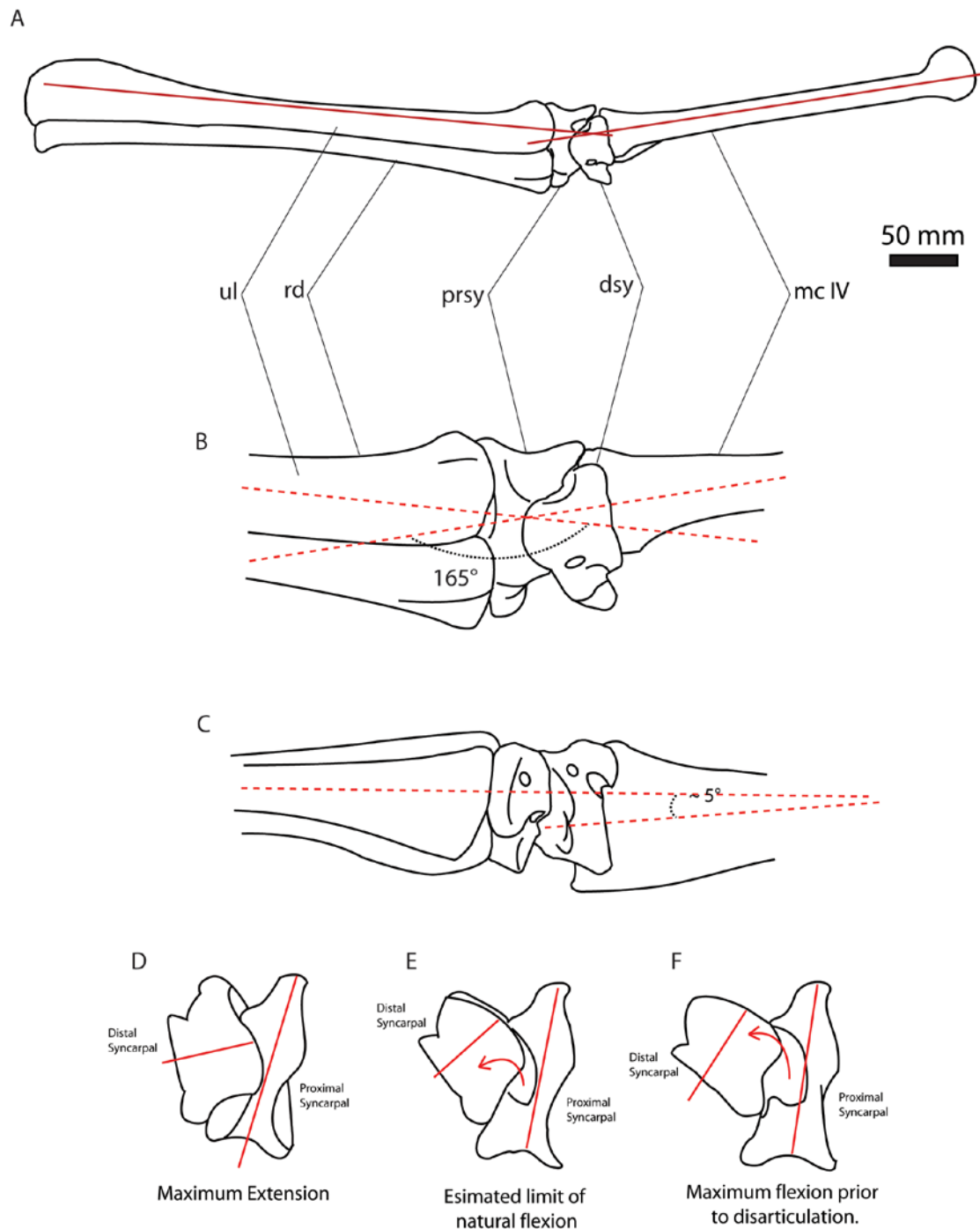


Figure 4.5. - Bone position and joint mobility of the carpus. Left carpus of SMNK PAL 1133 at maximum extension in dorsal (A-B) and cranial views (C). Left carpus in dorsal view at various degrees of flexion between the syncarpals of SMNK PAL 1134 (D-F). Abbreviations: ul, ulna; rd, radius; prsy, proximal syncarpal; dsy, distal syncarpal, metacarpal IV.



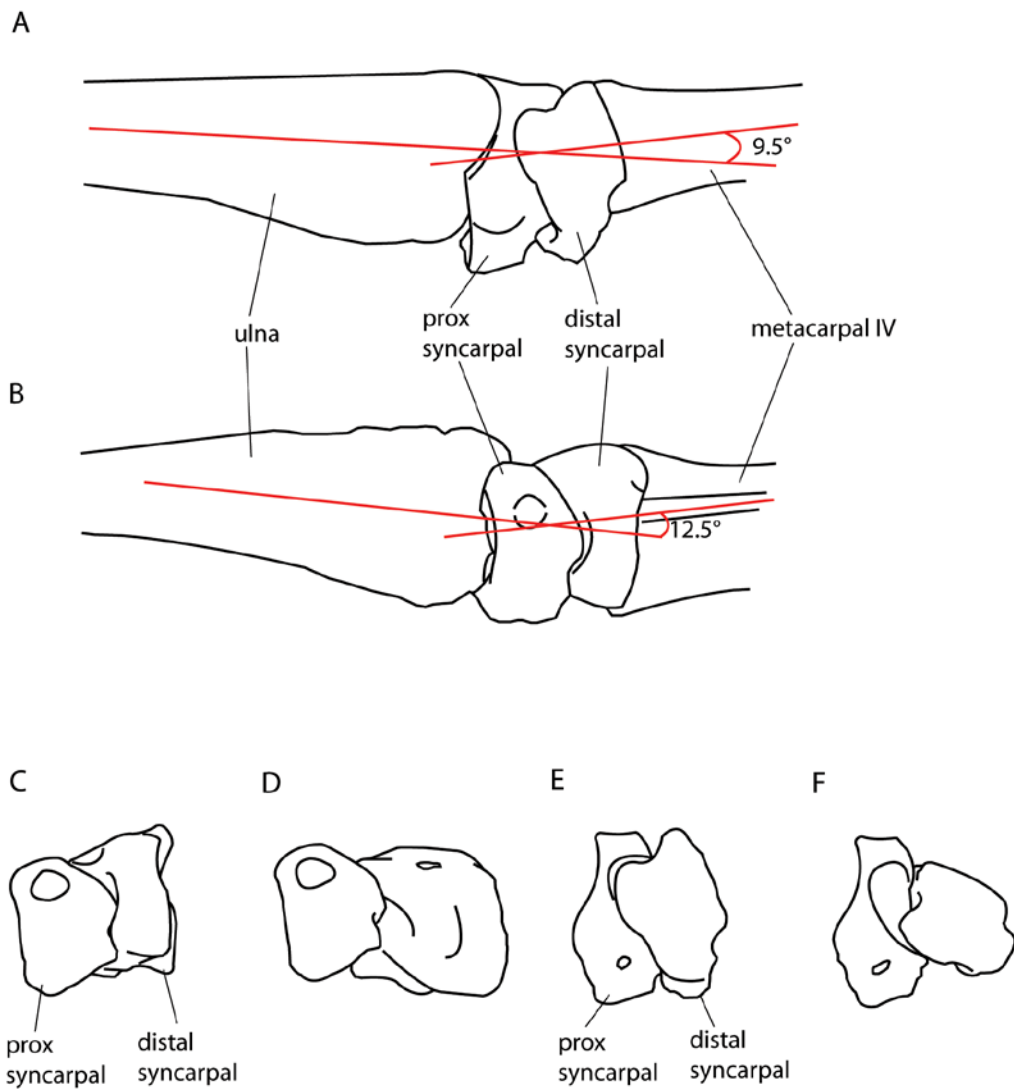


Figure 4.6. - The carpus region of *Quetzalcoatlus* sp. (TMM 42157-2, 42145-1) in maximum extension. A, dorsal view and B, cranial view. The maximum degrees of extension and flexion between the syncarpal blocks are illustrated in figures C - F where: C, maximum extension in cranial view; D, maximum extension in cranial view; E, maximum extension in dorsal view; F, maximum flexion in dorsal view. In dorsal view the maximum possible flexion before disarticulation occurs is  $\sim 32^\circ$ . This directs the distal syncarpal ventrally at an angle of  $29^\circ$ .

between the distal “cranial” carpal and the preaxial carpal, the pteroid and its articulation on the carpus; and the carpometacarpal joint. At maximum extension the angle between the radius/ulna and wing metacarpal is between  $165^\circ - 175^\circ$  (e.g. Wellnhofer 1985; Wilkinson 2008). In specimens of *Quetzalcoatlus* (TMM 42157-2,

42145-1) the angle between the ulna-syncarpals-Mc IV at maximum extension is 170.5° and 12.5° in cranial view, directing the distal wing dorsocaudally (Figure 4.6).

Although Bramwell and Whitfield (1974) suggested that the carpus might have been hyperextended to 17°, an examination of additional ornithocheirid materials (e.g. SMNK PAL 1135) provides no evidence suggest that this was correct. Indeed Wellnhofer (1985) argued against this and in *Santanadactylus* the joint was fully extended at 165°. Bennett (2001b) also disagreed that hyperextension between the syncarpals was possible but did not rule out any further extension (i.e. 165° – 180°). My own analysis of SMNK PAL 1133 suggests that the joint reached a maximum extension at 165° and concurs with the conclusions of Wellnhofer (1985). The first of the wrist joints, where the ulna and radius meet the carpus, has been well documented as flexion of the elbow will cause the radius to slide distally along the ulna, causing the carpus to extend ~30° caudally and ventrally. For SMNK PAL 1133 there is no deviation and flexion results in the carpus being directed caudally by between 27 - 31°, coupled with a ventral movement of 27°.

**Syncarpal mobility** - At maximum flexion with the ulna/radius orientated parallel to the transverse axis, the wing metacarpal is directed caudally by 35° and ventrally by 50°. The maximum range of angulation is about 25° between the two syncarpal blocks. During flexion the fourth metacarpal is retracted by 20° and depressed by 15°.

The intrasyncarpal joint is a sliding joint where the distal syncarpal may slide against the proximal one, the caudoventral motion resulting in the distal syncarpal being flexed and depressed slightly (Bennett 2001b). Bennett's (2001b) assessment is that the joint may be flexed ~25°, seconded by Wilkinson (2008), while Unwin (1988) noted a 30° movement in *Dimorphodon*. The mobility of this joint was not considered by Chatterjee and Templin (2004) while other authors suggest little to no movement was possible (Hankin and Watson 1974; Padian 1984; Wellnhofer 1985). I support the view that movement here was voluntary as the two carpals fit together, forming an excellent sliding surface, and the range of movement is simply too great for them not to have been utilised in this manner. Further to this if no movement between the two syncarpals were possible then it may be expected that the entire carpus would be reduced to a single functional unit through further fusion. The estimates of Bennett

(2001b), Unwin (1988) or Wilkinson (2008) are therefore more likely to be correct than conservative measurements. In my own examinations of fossil material the two syncarpal elements of *Anhanguera santanae* (AMNH 22555) do not fully disarticulate until a 38° movement has occurred, a similar degree of flexion, 36°, being observed in another ornithocheiroid (SMNK 1135 PAL). These are obviously extreme motions and I do not suggest that such a degree of flexion occurred during life due to the limitations imposed by soft tissues.

The preaxial carpal-distal syncarpal joint does not allow for a great deal of movement, however, in the absence of soft tissue it can be depressed, elevated and flexed medially and laterally (Wellnhofer 1985, 1991b) to move with the pull of the tendon that attached onto the pisiform located within the cranially located fovea (see Frey et al. 2006; Bennett 2007b).

The carpometacarpal joint allows rotational movement with the fourth metacarpal. Bramwell and Whitfield (1974) suggest that the metacarpals standard position was supinated as far caudally as possible and from here 15-20° of rotation was possible. This would move the metacarpal 5° forward and 8° downward. Bennett (2003c) describes an arthritic joint where grooves on the distal surface of the distal syncarpal mark out a 20° rotation. My own observations indicate that between 14 – 18° of rotation were possible. Bennett (2001b) further argued that the rotation of Mc IV from its normal position would result in a decrease in the angle of attack of the outer part of the wing and might be an important mechanism for controlling distal wing during flapping flight. In this scenario, any upward force acting on the outer part of the wing during down stroke might rotate Mc IV to decrease the angle of attack at an appropriate time. Pronation of the distal wing would certainly be important for changing the angle of attack and the creation of a twist between the root and tip.

Between the radio-ulno-carpal and intercarpal joints a large degree of flexion must have been possible and several specimens from the fossil record are interpreted as preserving the carpus at/close to its maximum extension. Bennett (2001b) illustrated one such specimen of *Pteranodon* (YPM 2425) in natural articulation with the Mc IV flexed at ~113° from the radius. Other fossils include: an example of *Gnathosaurus subulatus* that preserves an angle of 122° between the ulna and fourth metacarpal,

*Aurorazhdarcho* for which the left and right wrists make respective angles of 101° and 97° between the ulna and mc IV, and SMNK PAL 6595, for which an angle of 118° is noted. Assuming that a 20° flexion was possible between the two syncarpal blocks for *C. robustus*, the maximum possible angle of flexion between the ulna and metacarpal would have been ~115°.

In *Dorygnathus* the maximum flexion in the caudoventral plane is observed to be 31°, suggesting that a ~30° movement may be common amongst all pterosaur taxa. The intrasyncarpal joint permits substantially more flexion prior to any disarticulation, 70° caudally and 19° ventrally prior to disarticulation.

**Metacarpophalangeal joint** - The distal-most joint of consideration is that of the fourth metacarpophalangeal joint that acts as a hinge, allowing the distal wing to fold in the craniocaudal plane (Figure 4.7). During flexion the first wing finger phalanx undergoes a slight pronation (~20°, Wilkinson 2008) due to the caudodorsal orientation of the metacarpal condyles, allowing it to ride up over the caudodorsal surface of the wing metacarpal. In this way the animal could reduce the wing area when flying at high glide speeds and to protect the wings when moving on the ground. Bramwell and Whitfield (1974) suggested that at full extension the wph 1 formed an angle of 166° from the Mc IV and could be flexed in an arc of 136° so that the two bones formed an angle of 30°. Wellnhofer (1975) estimated a 140° flexion arc for *Rhamphorhynchus* and 130° arc for *Anhanguera*, while Chatterjee and Templin (2004) argued that the joint was fully extended at an angle of 165° and could be flexed to an angle of 35°, giving a total arc of 130°. Bennett (2001b) disagreed with Bramwell and Whitfield's (1974) interpretation and instead suggested that maximum extension in *Pteranodon* was ~175°. Flexion thus allowed the wph 1 to close to an angle of only 5° to that of the fourth metacarpal, giving a total closure arc of ~170°. Wilkinson (2008) stated that at maximum extension the first wing finger phalanx and the fourth metacarpal were parallel to each other and that a large range of flexion, 160°, was possible in SMNK PAL 1133. My own examinations of *C. robustus* indicate that there is no physical barrier to wph 1 being extended past 165° and while it is simple to move the bones into a hyper extended position whilst maintaining full articulation, maximum extension was almost certainly limited by soft tissue during life. Wilkinson (2008) also noted that even were the fourth metacarpal and wing finger phalanx to be

orientated parallel to one another then drag force acting on the spar during flight would have resulted in a small but unavoidable degree of flexion. In SMNK PAL 1133 the supination of the first wing finger phalanx during flexion causes it to ride over the posterodorsal surface of the fourth metacarpal, forming a bone lock when the elements make an angle of  $30^\circ$ . This bone lock is also observed in a smaller ornithocheirid (SMNK 1135 PAL), where a similar mobility of  $28^\circ$  is observed. The maximum possible flexion of the knuckle joint in ornithocheirid pterosaurs is therefore  $\sim 150^\circ$  if it is assumed that maximum extension of  $180^\circ$  was possible. The large range of extension proposed by Bennett (2001b) may be applicable only to *Pteranodon* but not to *C. robustus* or other ornithocheirids.

Hyperextension between the fourth metacarpal and first wing finger is possible in *Dorygnathus* where the wing finger can make an angle of up to  $184^\circ$  with the fourth metacarpal, although soft tissue would have prevented this and maximum extension is again likely to be  $180^\circ$ . Maximum flexion of wph 1 is not as great as in pterodactyloid taxa and reaches bone lock at  $56^\circ$ , giving a total closure arc of  $\sim 104^\circ$ .

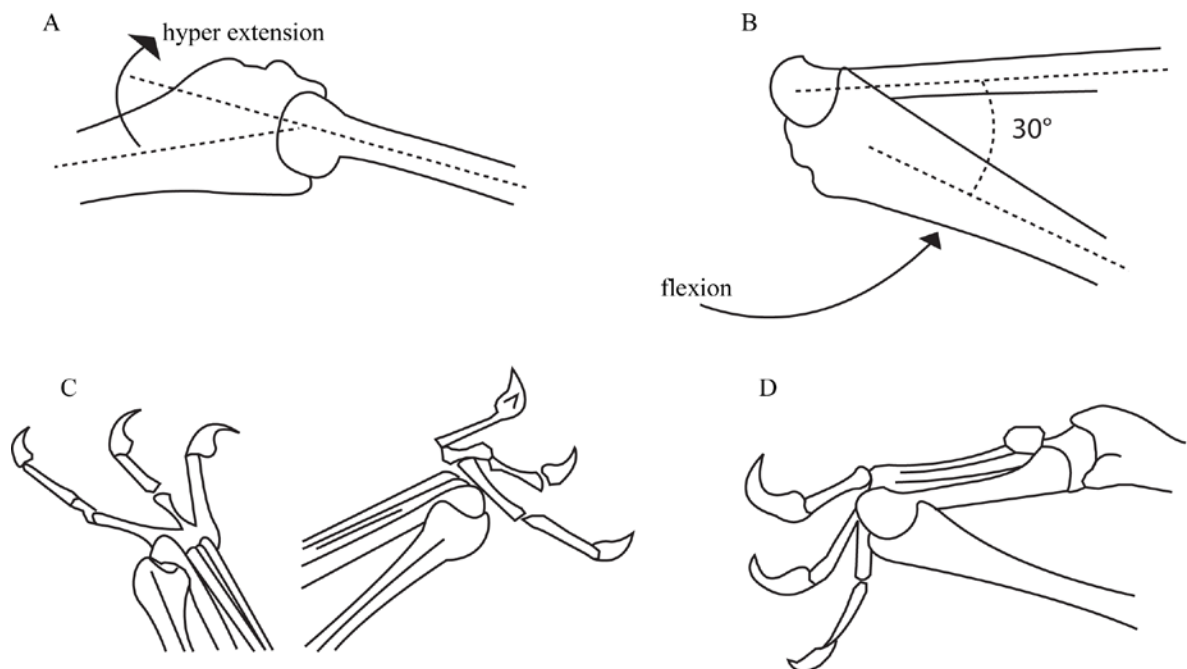


Figure 4.7. - A, maximum extension and B, maximum flexion in SMNK PAL 1133. Hyper-extension in A, as denoted by the arrow was likely prevented due to soft tissue. C – D, examples of wing flexion in well preserved fossil remains (*Pterodactylus* and *Rhamphorhynchus* respectively).

**Joints of the fourth digit** - The interphalangeal joints of digit IV, which form the distal portion of the wing, are generally agreed to have been incapable of voluntary movement owing to the lack of insertion points for flexor/extensor muscles (Bennett 2001a). The distal spar can therefore be considered as a single functional unit where any rotation or flexion/extension caused by drag forces would have been counteracted by soft tissue ligaments during life. The geometry of the wing spar, where it extends distally in a straight line or curves caudally is uncertain and conflicting evidence is observed from the fossil record. The wing phalanges of *Anurognathus* (Bennett 2007a) and *Jeholopterus* (Kellner et al. 2009) are preserved as being naturally flexed; a possible mechanism to help fold the wings out of harms way when on the ground. In contrast to this several specimens of *Pterodactylus* (e.g. BSP 1937 I 18A) have wing phalanges that are preserved as a single linear spar, while still more fossils (e.g. *Rhamphorhynchus*, JME SOS 4784; SMNK PAL 6595) preserve a slight caudally directed curvature. The fourth wing finger phalanx is thus known to curve caudally in some taxa e.g. *Pteranodon*, *Sinopterus*, but is straight in others. In cranial view the phalanges curve ventrally (Wilkinson 2008) when free from any aerodynamic loads. Two phalanges from a three dimensional specimen from the Romualdo Formation of Brazil (SMNK PAL 3845) consists of the first two wing finger phalanges that preserve a strong ventral curvature, where the wing was directed 163° ventrally from the transverse axis. Although the possibility does exist that these bones were bent by lithostatic pressure the majority of the curvature is present at the proximal and distal articulations which represent the thickest part of the bone, while the thinner shaft is undistorted.

**Hip joint** - The degrees of freedom available to the femur are very difficult to reconstruct because without soft tissue inference the femur can be moved freely within the acetabulum. From my manipulations of the bones, I estimate that the femoral shaft can be protracted 40°, and retracted 70°, cranial and ventral to the transverse axis. In cranial or caudal view it can also be elevated 20° and depressed 60° against the horizontal plane prior to the femoral head becoming disarticulated from the acetabulum (Figure 4.8).

**Knee joint** - The knee acts as a hinge where at the point of maximum extension the tibiotarsus and femur form an angle of  $175^\circ$ . The arc of flexion from this point is estimated at  $110^\circ$ .

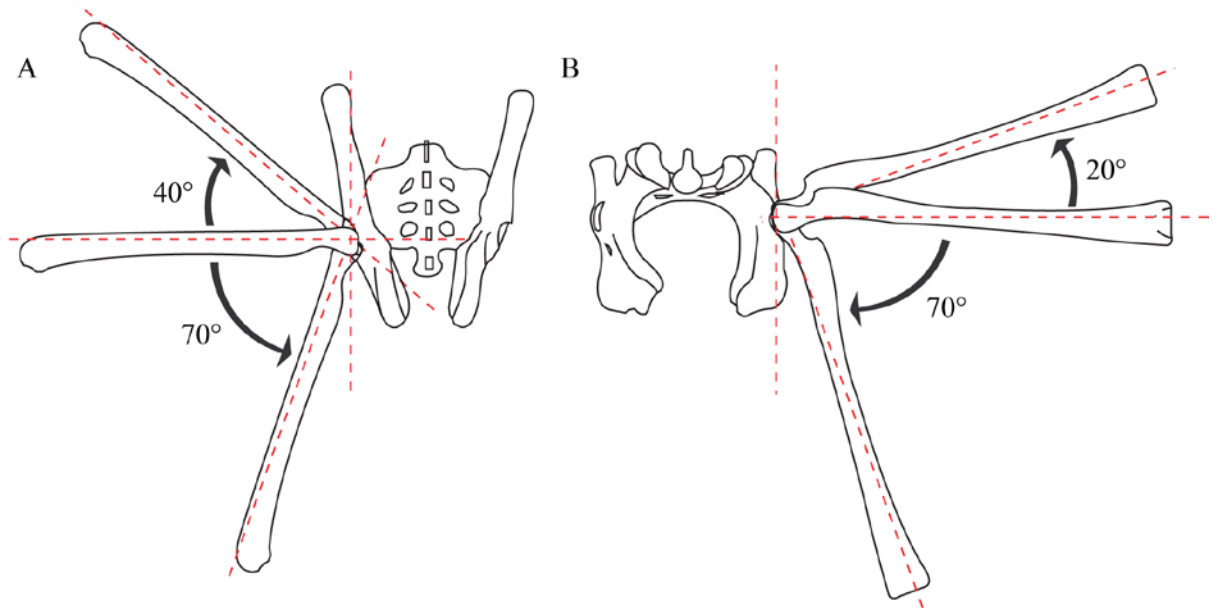


Figure 4.8. - Mobility of the femur of SMNK PAL 1133. A, maximum extension and flexion in dorsal view; B, maximum elevation and depression in cranial view.

### **4.3 Revised estimates of joint mobility**

Recent summaries of the joint mobility in ornithocheirids and *Pteranodon* were published by Wilkinson (2008) and Strang et al. (2009), and are summarised below in Table 9 (Figure 4.9). Despite the problems with reconstructing joint mobility in fossil taxa the majority of publications find a surprising degree of convergence for most pterosaurian joints, with the most controversial degrees of motion being the flexion of the elbow and the retraction of the humerus.

Based on a combination of previous studies and my own observations the following reconstructions are adopted here. The maximum humeral elevation and depression in ornithocheiroid taxa is  $\sim 50^\circ$  dorsal to the transverse axis and up to  $40\text{-}45^\circ$  ventral to this. In azhdarchoid taxa the humerus appears to have an increased vertical component, up to  $65^\circ$  against the transverse axis in a dorsal direction, but also has a reduced ventral component of only  $30\text{-}38^\circ$ . The rotational arcs of the humerus during

pronation and supination events are similar between ornithocheirid and azhdarchoid taxa, being 62-63° and 55.5 – 68°

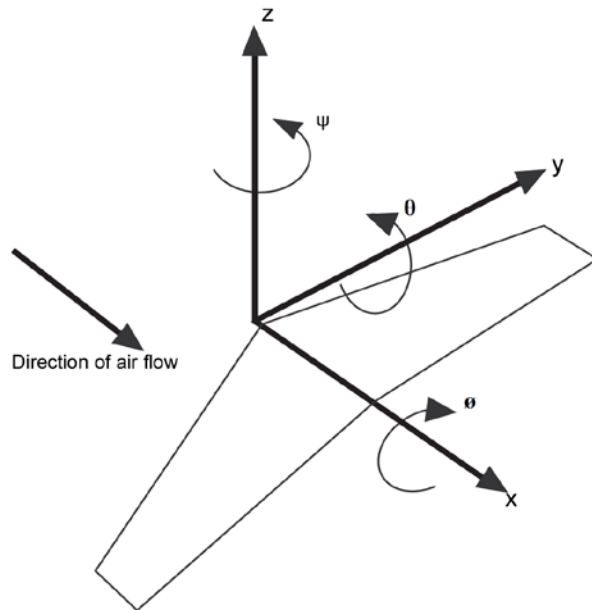


Figure 4.9. – Rotation of joints about the x, y and z-axes of the wing as described by Table 9. Figure adapted from Strang et al. (2009).

| Joint name                    | Shoulder    |              |           | Elbow        | Wrist   |          |           | Knuckle    |
|-------------------------------|-------------|--------------|-----------|--------------|---------|----------|-----------|------------|
|                               | $\phi$      | $\theta$     | $\psi$    | $\psi$       | $\phi$  | $\theta$ | $\psi$    | $\psi$     |
| Bramwell and Whitfield (1974) | [-25;70]    |              | [-65;0]   | [30;60]      |         | [-10;10] | [-45;17]  | [-150;-15] |
| Bennett (2001b)               | [-25;70]    | [-35;35]     | [-65;0]   | [30;150]     |         | [-10;10] | [-50;0]   | [-175;-5]  |
| Wellnhofer (1975)             | [-40;40]    |              | [-25;0]   | [30;70]      |         |          | [-45;-15] | [-150;-15] |
| Chatterjee and Templin (2004) | [-65;60]    | [-42.5;42.5] | [-70;-15] | [35;90]      |         |          | [-45;-15] | [-145;-15] |
| This study                    | [-45/50;50] |              |           | [25;91/96.5] | [-27;0] |          | [-42;-13] | [-151;-15] |

Table 9. - Pterosaur joint mobility given as Euler angles after Strang et al (2009).

respectively, but the larger value of ~70° presented in other studies for ornithocheirids may also be correct. During the upstroke, or with a pronounced supination of the bone, I interpret that the humerus of *C. robustus* can be flexed to lie at an angle of between 34 - 48° to the vertebral column although it is possible that extension of the shoulder girdle were it not constrained by soft tissue would further reduce this value. For



*Quetzalcoatlus* and other azhdarchoid pterosaurs the extension of the glenoid fossa onto the caudomedial surface of the scapulocoracoid allows the humerus to be supinated and directed steeply caudally to lie parallel with the long axis of the body.

The maximum angle for extension in elbow is 150° in all studied taxa and in cranial view I note a measurement of 162° for SMNK PAL 1133, a value that that is very similar to Wellnhofer's reconstruction of *Santanadactylus*. The humerus is interpreted here to have been directed ~ 18° dorsolaterally, rounded to a rough value of 20° at the natural gliding position, directing the ulna near parallel to the transverse axis. My own interpretation of the maximum flexion permitted at the elbow is intermediate between the lower estimates of a ~30 – 55° closure arc and Bennett's (2001b) argument that the ulna could flex to within 30° of the humerus. Having not personally examined the material of *Pteranodon* I will not comment on whether the value presented by Bennett is an overestimate of the joint folding or simply a taxonomic variation, but in *C. robustus* the ulna could not close much more than 89 - 74° against the humerus. As Wilkinson (2008) also supported a similar, but slightly higher, range of movements, i.e. 90° flexion arc, from examining the same material, I will therefore use an estimated closure arc of 66°- 90° for ornithocheiroid taxa.

Flexion of the carpus is uncontroversial and a complete flexion of the elbow is coupled with a ~30° caudal and ventral movement in both *C. robustus* and *Quetzalcoatlus*, suggesting that this motion is universally available in derived pterosaurs. The sliding motion between the two syncarpal blocks is impossible to determine but it was certainly below 36 - 38° in ornithocheiroids and 32° for *Quetzalcoatlus*, the points where disarticulation occurs. The maximum flexion that can occur across the carpus region thus seems to be fairly similar in most taxa, with the ulna and Mc IV forming an angle of between 113-122°. In maximum extension the two bones form at an angle of 165° in dorsal view and 175° in cranial view, directing the Mc IV both dorsally and caudally. For gliding flight the degree of movement available to the carpus is perhaps of lesser importance and would have been used far more extensively in both flapping flight and terrestrial locomotion.

Pro- or supination of the fourth metacarpal against the distal syncarpal was certainly possible and in *C. robustus* the range of motion appears similar to the 20° suggested by Bennett (2001b).

The maximum extension of wph 1 against the fourth metacarpal is here interpreted as being 180°, however, the typical gliding position used for the modelling process will instead be between 165-170°. Maximum flexion in ornithocheirid pterosaurs is taken to have occurred when the two bones form an angle ~ 28-30° as this represents a bone lock and no further movement is possible. Although these values differ from other taxa, specifically *Pteranodon* and *Quetzalcoatlus* where an almost complete flexion of the wing finger appears to have been possible (~5° from the Mc IV) this could simply be a case of interspecific variation or, in the case of *Quetzalcoatlus*, the warped nature of the cast.

The interphalangeal joints of the wing finger do not appear to have had any movement but could almost certainly flex slightly when under aerodynamic loads. For simplicity the wing finger in all models is reconstructed as a single, straight, un-jointed unit.

#### **4.4 Position and mobility of the pteroid**

The pteroid bone originates from the carpus and is incorporated into the leading edge of the propatagium. The origin, direction and, to a degree, function of the bone are however highly disputed. The bone was initially interpreted as the first digit by Goldfuss (1831), however, it has also subsequently been considered to be the product of a calcification of a tendon, as well as both a modified carpal or a neomorph. Unwin et al. (1996) performed the first histological analysis on a three dimensionally preserved pteroid and sesamoid from the pterosaur *C. robustus* (SMNK PAL 1133) and concluded that the pteroid was a true bone on account of it being both pneumatic and preserving multilayered cortical bone.

Marsh (1882) regarded the preaxial carpal and pteroid as being articulated together during life while Hankin (1912) was the first to illustrate a cranially directed pteroid, an idea continued by several subsequent authors (Frey and Reiß 1981; Frey and Martill 1994; Unwin et al. 1996; Wilkinson 2007; Wilkinson et al. 2005) who saw it as a means to support and control the propatagium while providing a high lift function during flight. This hypothesis, however, remained reliant on the assumption that the pteroid articulated within the open fovea of the preaxial carpal, a point disputed by Bennett (1991, 2001a,b, 2007b) who argued that a large sesamoid occupied this instead. The observations of Bennett (1991, 2001a,b, 2007b) are now supported by a number of specimens representing a wide diversity of pterosaur taxa, including those described herein, and as such the pteroid can no longer be considered to articulate in the fovea of the preaxial carpal, or have the ability to face or be directed cranially. Instead it is now universally supported that the pteroid was directed medially and formed part of the leading edge of the propatagium, following the original suggestion of Wagner (1858).

The articulation point on the wrist and the degrees of freedom available to the pteroid remain controversial, with opinions divided between placing the articular surface on the medial side of the preaxial carpal or elsewhere on the proximal syncarpal. Based on several specimens of *Pteranodon* Bennett (2007b) identified a bulbous ridge on the medial side of the preaxial carpal as the articular surface of the pteroid, suggesting that its absence in others was the result of ontogenetic immaturity. It is uncertain how

extensive this development is in other specimens as no robust development is viewed in the ornithocheirid SMNK PAL 1135, or the relatively mature SMNK PAL 1133 (Figure 4.10). The medial face of these are strongly concave and pitted with muscle scars or foramina, however, given the connection of a long tendon running across the sesamoid, many of these were likely to fix the preaxial carpal in place and prevent excessive medial and lateral displacements.

While Bennett (2007b) also argued that articulated specimens of *Eudimorphodon*, *Peteinosaurus*, *Rhamphorhynchus*, and *Pterodactylus* all preserve the pteroid with its articular end adjacent to the preaxial carpal this is disputed. In none of the photographs presented by Bennett (2007b) is this configuration preserved and instead a gap is observed between these two elements, where they have been pulled in opposite direction. This taphonomy is observed in a number of well preserved and articulated specimens (Figure 4.11). As such any connection between the pteroid and preaxial carpal was weak and that following the death of the animal the pteroid was displaced medially while the preaxial carpal was pulled distally.

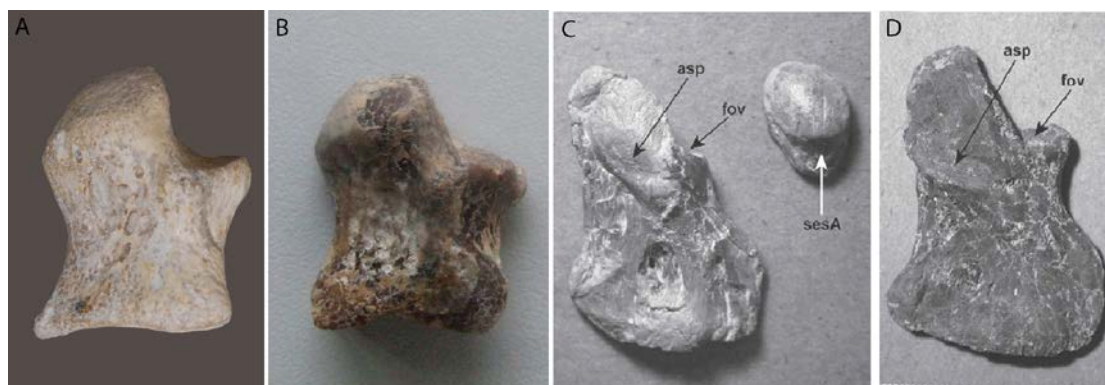


Figure 4.10. - Medial face of the preaxial carpal in A, SMNK PAL 1133; B, SMNK PAL 1135; C, KUV 2120; D, YPM 2414 (source: Bennett 2007b). Where: asp, articulation for the pteroid; ses, sesamoid; fov, fovea of the preaxial carpal.



Figure 4.11. - Relative positions of the pteroid and preaxial carpal indicating the post mortem displacement (also see figures of Bennett 2007b). Where: A-B, *Pterodactylus antiquus*; C, *Aurorazhdarcho* (Frey et al. 2011); D, ornithocheiroid indet (private collection, courtesy of Urs Oberli); E-F, *Changchengopterus*; G, *Darwinopterus modularis* (YH-2000); H, *Campylognathoides liasicus* (SMNHS 18875).

The tension acting on the preaxial carpal is dependant on the reconstruction of the length and function of tendon that anchors on the sesamoid. Three broad reconstructions (Figure 4.12) have been presented by Bennett (2001a, 2007b), Frey et al. (2006), and Prondvai and Hone (2009). In the configurations of Bennett (2001a, 2007b), the sesamoid of the preaxial carpal acts as an anchor point of the tendon of *M. extensor carpi ulnaris*, anchoring distally on the mid shaft of the fourth metacarpal, while the wing finger is extended via a tendon that runs from the humerus and across the cranial face of the carpus. In contrast to this Frey et al. (2006) and Prondvai and Hone (2009) proposed that the tendon passing across the sesamoid of the preaxial carpal anchored itself distally on the extensor process of the first wing-finger phalanx, and was responsible for extending the distal wing. Differences between the two latter configurations exist where in that of Frey et al. (2006) the tendon originates from *m. extensor digiti*, which anchors on the distal margin of the humerus, while that of Prondvai and Hone (2009) this is the *Ligamentum extensor digiti alae*, and originates from a more medial location on the humerus and the coracoid. A “hybrid” configuration was also provided by Prondvai and Hone (2009), where both the *Ligamentum extensor digiti alae* and the tendon of *m. extensor digiti* play a role in the extension the wing finger.

Regardless of whichever configuration is selected, the elbow, carpus and wing finger flex following the animal’s death, slackening the proximal portion of the wing-finger extensor tendon while tightening the portion distal to the carpus. The result of this is to pull the sesamoid, and with it the preaxial carpal, distally, accounting for the frequency by which this is observed within the fossil record. The configurations of Frey et al. (2006) and that of Prondvai and Hone (2009) would naturally result in a greater pull, due to their increased length, over that of Bennett (2007b).

In well preserved and articulated specimens the preaxial carpal remains adjacent to the distal syncarpal and is angled distally or pulled flat against the cranial face of the fourth metacarpal (Figure 4.11D), indicating that its displacement was restricted by additional muscles. In rarer cases it has been completely separated from the carpus and pulled distally along the shaft of the fourth metacarpal (e.g. MNHS/00/85).

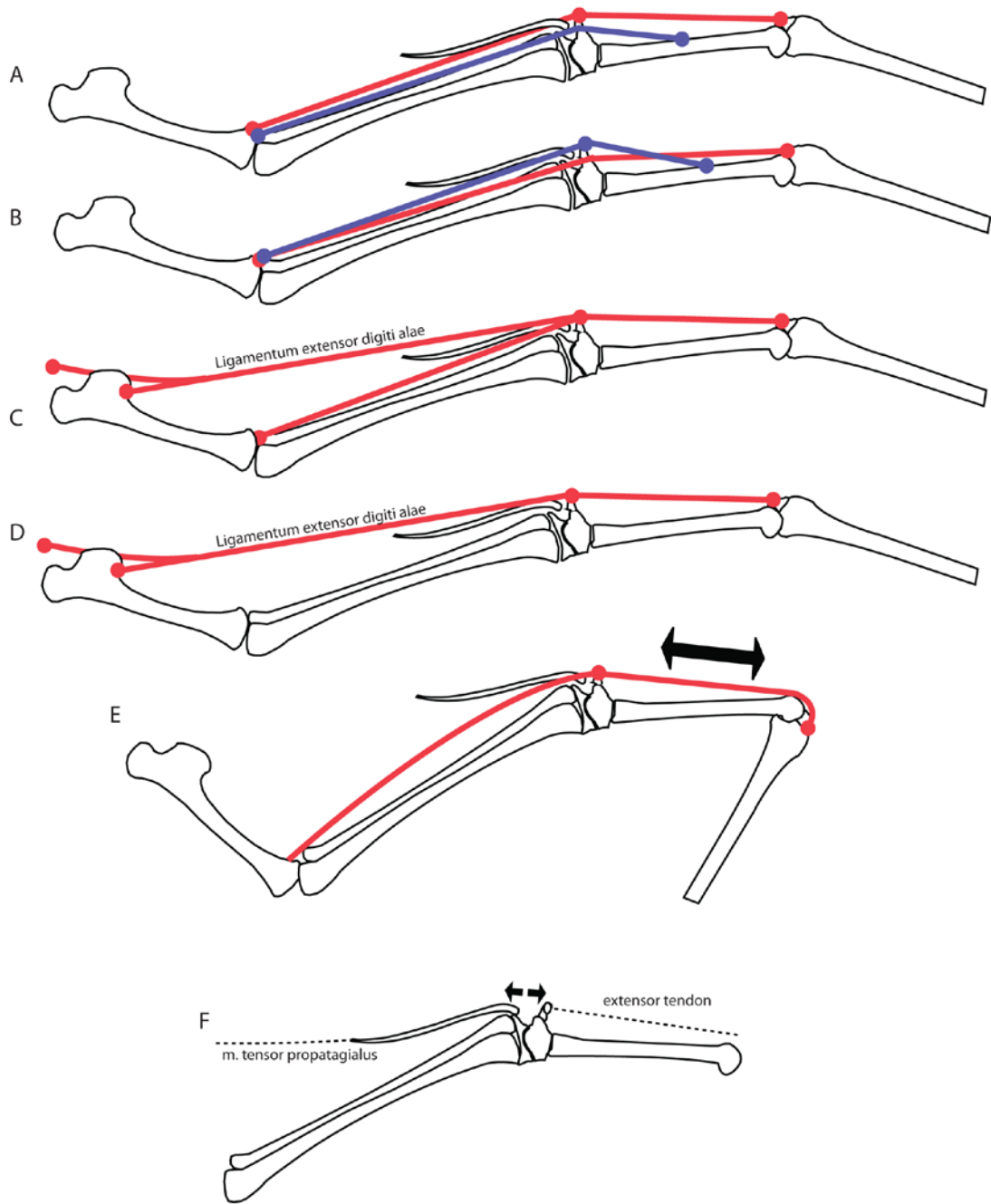


Figure 4.12. - Reconstructions of the primary extensor muscles and tendons of the wing finger in pterosaurs. Red lines indicate the extensor of the wing-finger while blue lines represent the extensor of the carpus and wing metacarpal. A, Frey et al. (2006); B, Bennett (2007b); C-D, Prondvai and Hone (2009). E, flexion of the elbow and wing finger after death leads to the preaxial carpal experiencing an increase in distal tension. The result of this is to pull the preaxial carpal distally while the pteroid remains either *in situ*, or is pull medially by the shrinking propatagium or *m. tensor propatagialis* (F).

In contrast to the *post mortem* actions of the preaxial carpal, the pteroid is not pulled distally except in very rare occasions (e.g. *Aurorazhdarcho*). Instead it is observed with its articular end between the proximal and distal syncarpals (e.g. MNHS/00/85), held in place by the tissue of the propatagium, or is instead drawn medially due to the tension of the proximal patagia and/or the pull of the *m. tensor propatagialis*, and lies adjacent to the proximal syncarpal or the ulna. In only one example do the preaxial carpal and the pteroid appear to have shared the same resting location (Wellnhofer 1991a). While this cannot be used to dismiss the reconstruction of Bennett (2007b) it indicates that the two elements were only loosely connected to one another and any connection was easily broken due the post mortem tension of the extensor tendon.

While I regard the articular position of the pteroid to be somewhat controversial and perhaps half formed by soft tissue or cartilage to explain the lack of a clear articular surface, the general conclusions on the mobility of the pteroid are widely supported and the bone must have been directed medially during life. The compressed articular surface indicates that the bone was restricted to a hinge-like motion, allowing it to extend the propatagium during flight and fold it against the proximal part of the forearm during terrestrial locomotion. If the motion available to the bone was restricted to a slight cranial and caudal extension/flexion, with no dorsal or ventral component, then the aerodynamic force alone would be responsible for cambering the patagia, the degree of which could be increased by a slight flexion of the pteroid. More likely, however, was that the pteroid was angled such that a slight dorsal and ventral component was generated when the bone was flexed or extended (i.e. Bennett 2007b). In this way the camber, and effect of the patagia, could be controlled by the animal.



## Chapter 5

---

### PTEROSAUR AERODYNAMICS

## **5.0 Introduction to the aerodynamics of biological fliers**

The study of flight within the animal kingdom is complicated by the variety of wing profiles and locomotory mechanisms observed in living animals, as well as the range of flow characteristics within which they operate. The primary study subjects in this field are naturally birds and bats, which are large enough in size that conventional aerodynamics are useful in estimating their performance. Furthermore carcasses or models can be readily utilised for wind tunnel experiments (Maybury et al. 2000; Maybury and Rayner 2001; Videler et al. 2004; Thomas 2010) and data can be subsequently coupled with field observations (Shamoun-Baranes et al. 2003). In rarer cases, and with significantly more trouble, live animals can be trained to fly within the working section of a wind tunnel (e.g. Pennycuick 1968, 1971; Pennycuick et al. 1996, 2000). The study of extinct flight, lacking many of the variables known or calculated in these ways must therefore borrow heavily from such studies (e.g. Chatterjee and Templin 2004, 2007); the result of which is that aerodynamic performance is often commented upon but relatively little data are provided.

As many palaeontologists who are interested in the aerial abilities of pterosaurs (or other extinct fliers) are unlikely to have a working knowledge of aerodynamics, a brief introduction to many of the basic concepts, terms, and equations encountered in subsequent chapters of this thesis is necessary. Several excellent texts that give a fuller account of aerodynamic theory of flight, along with its application to biological fliers, are recommended for those with a further interest in the subject (e.g. Pennycuick 1972; McNeill Alexander 2003; Shyy et al. 2008).

### **5.0.1 Aerodynamic forces**

In its simplest sense, an animal or aircraft that wishes to remain airborne while travelling in its desired direction is required to generate both lift and thrust forces. The former is necessary to counter the gravitational force pushing the animal downwards while the latter is required to overcome drag and produce forward momentum. Lift force generated by the wing is typically written in the form of:

$$\text{Eq.1.} \quad L = 0.5\rho Av^2 C_L$$

but is often replaced within the aerodynamic literature by a non-dimensional coefficient, allowing the performance and characteristics of various aerofoils to be compared irrespective of size. This lift coefficient, where force is non-dimensionalised with respect to the surface area of the wing, is subsequently written as:

$$\text{Eq.2.} \quad C_L = L / (0.5 \rho A v^2)$$

The production of lift itself can be understood via the principle of Bernoulli where (in simplified terms) any particle moving in the flow has three components of energy: kinetic, due to movement; gravitational, due to altitude; and pressure. If the flow is simplified to an inviscid state, by which we assume that viscosity is zero, then it follows that the individual particles will retain their energy indefinitely due to the lack of friction. In such a regime the components of energy can be expressed as:

$$\text{Eq.3.} \quad 0.5 \rho v^2 \delta V + \rho g h \delta V + p \delta V = \text{constant}$$

Here the left hand term ( $0.5 \rho v^2 \delta V$ ) refers to the kinetic energy of a particle, the middle term ( $\rho g h \delta V$ ) refers to the gravitational potential energy and  $p$  is the pressure energy ( $p \delta V$ ). The term  $\delta V$  refers to the volume of any given particle within the flow. When this inviscid flow reaches an aerofoil some of the fluid is directed up over the top surface, resulting in an increase in velocity, while some is deflected downwards, slowing in its velocity instead (Figure 5.1A). For equation 3 the change in gravitational energy will be negligible as both gravity and altitude will remain more or less constant over the surface of the aerofoil. As  $0.5 \rho v^2 \delta V + p \delta V$  must equal to a constant, it therefore follows that an increase in velocity corresponds to a decrease in pressure energy and vice versa. The difference in flow velocity over the top and bottom surfaces of the aerofoil results in the development of a pressure differential and in turn generates a lift force acting normal to the top surface of the wing (Figure 5.1B).

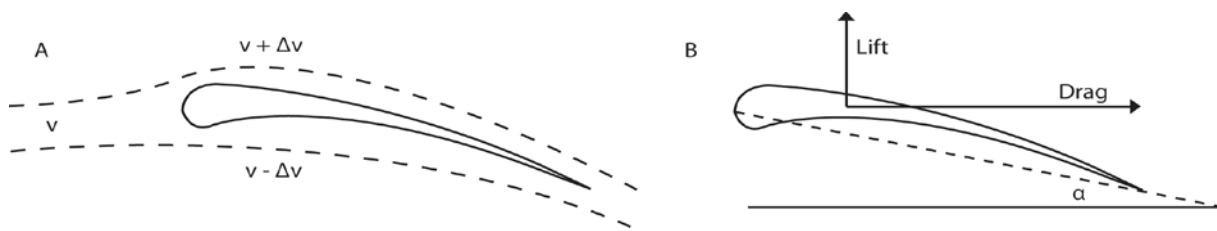


Figure 5.1. - A, flow increases in velocity ( $v$ ) as it travels over the dorsal side of the wing profile relative to the flow on the ventral surface (A). The resulting pressure differential causes lift to be directed normal to the wings surface (B) (adapted from McNeill Alexander 2003).

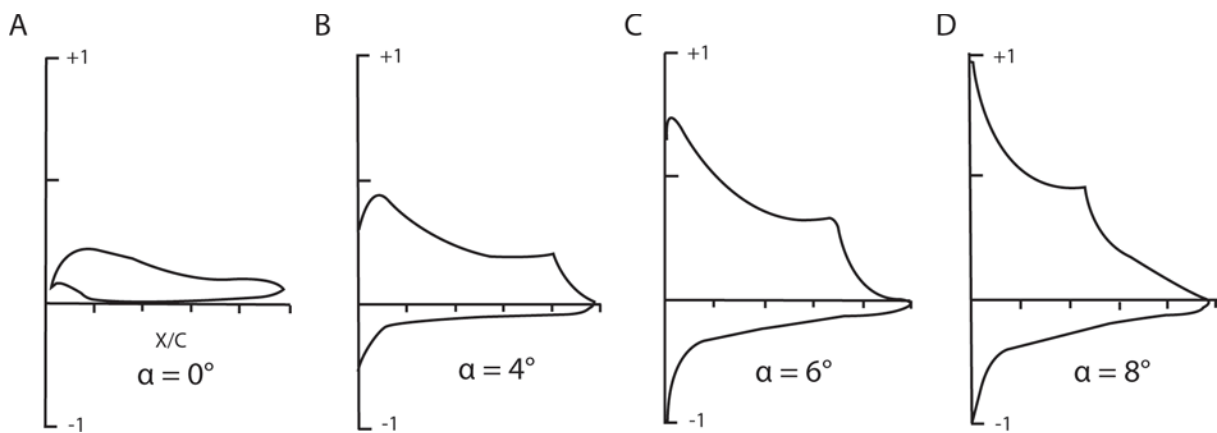


Figure 5.2. – Example of a pressure distribution over the surface of the Clark Y wing section at increasing angles of attack ( $\alpha$ , Marchman and Werme 1984). The upper and lower lines denote the differences in pressure between the upper and lower surfaces of the aerofoil, indicating in this example, an increase in pressure distribution (and subsequently greater lift) with higher angles of attack.

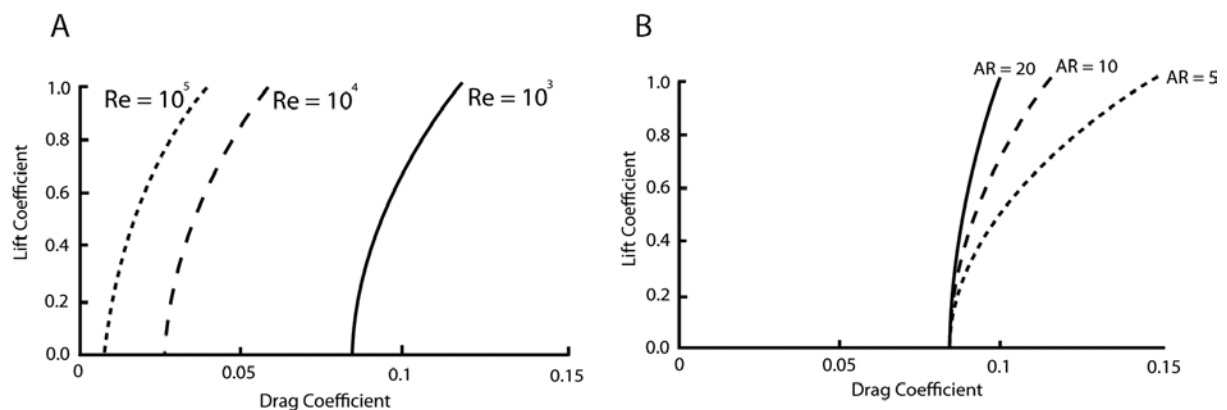


Figure 5.3. - A, Effects of the Reynolds number (A) and aspect ratio on coefficients of lift and drag (source: McNeill Alexander 2003).

The magnitude of lift generated is dependant on the magnitude of the pressure differential between the upper and lower surfaces of the wing and is therefore heavily influenced by the shape, aspect ratio, angle of attack, and camber of the aerofoil in question (Figure 5.2). Higher degrees of wing camber typically increase the velocity of the flow directed upwards and produce higher values of lift due to the development of larger pressure differentials. In contrast flat plates make the poorest wing sections as the pressure difference on the upper and lower surfaces of the wing is small. The performance of wings is also greatly influenced by the Reynolds number at which the animal operates (Figure 5.3A). This is a numerical value defined as the ratio of viscous to inertial forces and defines the flow regime, where below a critical transition point of  $\sim 10^6$  the flow is said to be laminar, while values in excess of this indicate turbulent conditions. Biological fliers such as birds and bats operate completely within laminar flow regimes, defined by Reynolds numbers in the range of  $10^4 - 10^5$ , while insects fly at very low Reynolds numbers where viscous forces dominate.

At Reynolds numbers below  $10^6$  the laminar flow is susceptible to separation from the aerofoil and may give rise to a wide range of wing behaviour, meaning that the evolution of the wing configuration is largely influenced by the Reynolds numbers within which they must operate. At Reynolds numbers of  $>168,000$  aero foils with a cambered section represent the most efficient wing form, while at lower values of  $\sim 42,000$ , very thin cambered plates are found to be superior. Given their range of size, pterosaurs are firmly situated within a flow regime defined by Reynolds numbers of  $10^4-10^5$  and would have benefited greatly from the development of a cambered wing section, with very large azhdarchids, upon attaining their adult size appearing to be the only biological fliers to have crossed the turbulent transition ( $Re > 10^6$ ).

As previously noted the production of lift can be increased through changing the angle of attack at which the flight surface meets the flow. Steeper positive angles direct the flow upwards at a faster velocity which results in a greater pressure differential (Figure 5.2). However, beyond a certain angle of attack unique for each wing section, the flow lacks the necessary energy to remain attached to the surface of the wing causing the pressure differential to break down. At this point lift production decreases and the aircraft begins to stall. On a graphic plot, the point of stall is taken to be the point where lift force plateaus or rapidly declines (Figure 5.4A).

In addition to its angle, the aspect ratio of an aerofoil also has an effect on lift production, where wings with a high aspect ratio generate both a steeper lift gradient and higher maximum values of lift, but reach their stall point at a lower angle of attack relative to low aspect ratio wings (Figure 5.4B).

Using the principle of Bernoulli it is possible to roughly determine the lift force if the velocity at which the flow is directed upwards is known, however, lift is instead more commonly calculated from wind tunnel experiments or computer programmes for a given aerofoil. Within aerodynamic literature, specifically that dealing with biological fliers and where no wind tunnel data is available, lift is often taken to be equal to the mass of the animal multiplied by the gravitational acceleration, where this represents the minimum upwards force required to keep the animal airborne at a constant altitude. Experiments on biological and manmade aircraft indicate that the coefficient of lift is typically a maximum of 1.5 for a cambered wing, with values in the range of 1.2 – 1.5 also being considered appropriate (McNeill Alexander 2003).

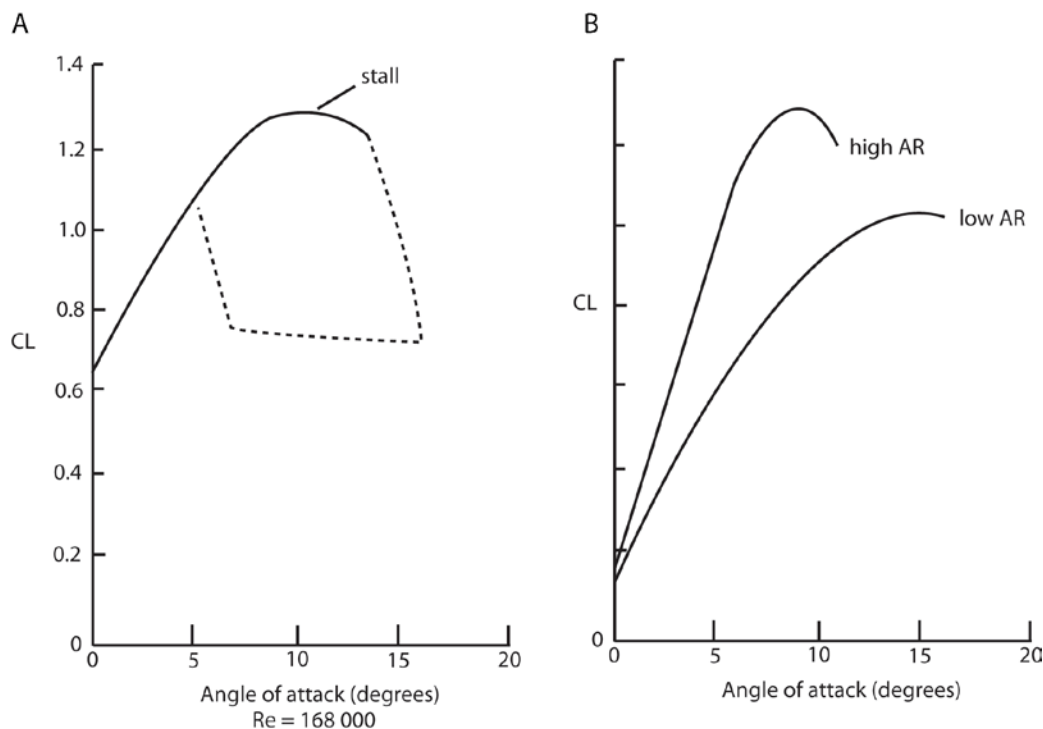


Figure 5.4. - The effect of angle of attack on lift production and the onset of stall (A). The dotted line indicates the inferred effect of the angle of attack on lift production post stall. B, Hypothetical example of the aspect ratio effect on lift generation and stall.

Unlike lift, the second principal force acting on the animal, drag, is an aerodynamic penalty that impairs flight performance and resists the inertial motion of an object through a viscous substance. Drag and its non-dimensional coefficient are respectively written as:

$$\text{Eq.4.} \quad F_{\text{drag}} = 0.5\rho Av^2 CD$$

$$\text{Eq.5.} \quad CD = F_{\text{drag}} / (0.5 \rho Av^2)$$

When comparing different aerodynamic studies it is important to ensure the reference area used to non-dimensionalise the coefficient is constant. While this is usually the surface area of the wing it can also be written as the wetted surface area or projected frontal area (when considering the body or fuselage) depending on the component of drag being studied.

Drag, or more correctly total drag ( $D_{\text{total}}$ ), is comprised of three major components: lift induced drag ( $D_i$ ), profile drag ( $D_{\text{pro}}$ ), and parasite drag ( $D_{\text{par}}$ ), where:

$$\text{Eq.6.} \quad D_{\text{total}} = D_i + D_{\text{par}} + D_{\text{pro}}$$

As with lift the coefficient form of drag represents a non-dimensional value with respect to a specific reference area where:

$$\text{Eq.7.} \quad CD_i = D_i / (0.5 \rho Av^2)$$

$$\text{Eq.8.} \quad CD_{\text{pro}} = D_{\text{pro}} / (0.5 \rho Av^2)$$

$$\text{Eq.9.} \quad CD_{\text{par}} = D_{\text{par}} / (0.5 \rho Av^2)$$

The first of these components, lift induced drag is proportional to the square of the airflow and is, as its name suggests, a by-product of lift that varies in magnitude along the wing, becoming stronger towards the wing tips. The effects decrease as both velocity and aspect ratio increase. Span-wise flow resulting from the pressure differential build up on the top and bottom sides of the wing gives rise to shedding vortices at the wing tips as it attempts to equalise, creating a downwash and directing the lift vector in a more caudal direction. Kinetic energy is imparted to these vortices at a rate of  $2L^2/\pi vb^2$  and, where work is force multiplied distance, is multiplied by velocity to give:

$$\text{Eq.10.} \quad D_i = 2L^2/\pi v^2 A^2$$

While an elliptical distribution of the load can be achieved by the development of an elliptical wing section, whereby lift at the wing tips is reduced to almost zero and all parts of the wing experience the same downwash, this is not common, and instead flow is directed over the aerofoil at the different velocities. The result of this is that the induced drag component will be higher than that calculated from Equation 10 and to compensate an additional term,  $k_{\text{induced}}$ , is added to the equation; representing the deviation of lift over the wing section from that of a perfect elliptical pattern. Spedding and McArthur (2010) demonstrated several problems with this term and its application within the aeronautical literature, particularly when applied to biological fliers. Here the term  $k$  is typically a little over 1 when representing the span efficiency and a little under 1 when written inversely as a “power inducted correction factor” (i.e. “ $e$ ”). In biological literature  $k$  is often given an assumed value of 1.1 – 1.2 and  $e = \sim 0.9$ , with no further discussion. When the calculation applies to a wing of finite length further modification of Equation 10 may incorporate the aspect ratio (i.e.  $AR = b^2/A$ ) and the equation is now written as:

$$\text{Eq. 11.} \quad D_i = 2 k_{\text{induced}} L^2 / \pi v^2 A * AR$$

Or in its non-dimensional form as:

$$\text{Eq. 12.} \quad D_i = CL^2 / \pi AR (1 + \delta)$$

where:  $e = 1/(1 + \delta)$ , with  $\delta$  representing the deviation from a perfect elliptical loading state (i.e. 1). Often this appears in the literature as:

$$\text{Eq. 13.} \quad D_i = CL^2 / \pi A R e$$

In all of these equations the term “ $e$ ” accounts only for the departure from a perfect state of elliptical loading with no consideration of the variations of  $CL$  with  $CD$ . To account for the change of lift to drag ratio with angle of attack,  $e$  must be ideally altered to the form:

$$\text{Eq. 14.} \quad e = 1/(1 + \delta + k\pi AR)$$



Unlike lift induced drag that forms a part of total drag only when lift is produced, the remaining components of drag are proportional to the square of velocity and are present even in the absence of lift. The second component, profile drag, is taken as the sum of friction drag acting on the surface of the wing, along with drag created by the differences in pressure up and down wind of object immersed into the flow (typically the leading edge of the wing spar). The friction drag acts on the total surface area of the aerofoil and for an object moving at a velocity of  $v$ , Reynolds number of  $Re$ , fluid density of  $\rho$ , and total area of  $A_{total}$  then the drag can be written as:

$$\text{Eq.15.} \quad D_{\text{friction}} = 0.5 \rho A_{\text{total}} v^2 (1.33 Re^{-0.5}) \text{ and}$$

$$\text{Eq.16.} \quad D_{\text{friction}} = 0.5 \rho A_{\text{total}} v^2 (0.074 Re^{-0.2})$$

for high and low Reynolds numbers respectively (Prandtl and Tietjens 1957). The final form of drag, the parasite drag, applies only to the remainder of the body not associated with the production of lift, the head, neck, body and legs of biological animals or the fuselage of aircraft. As such the total drag acting on the wing can be calculated by combining Equations 11 and 15 so that:

$$\text{Eq.17.} \quad D_{\text{wing}} = 0.5 \rho A_{\text{total}} v^2 (1.33 Re^{-0.5}) + 2 k_{\text{induced}} L^2 / \pi v^2 A^* AR$$

To account for the small amount of pressure drag that must be present the left hand term for skin friction is rewritten as the profile drag coefficient along with a profile drag factor  $K_{\text{profile}}$  where:

$$\text{Eq.18.} \quad D_{\text{wing}} = 0.5 \rho A_{\text{total}} v^2 (2.7 k_{\text{profile}} Re^{-0.5}) + 2 k_{\text{induced}} L^2 / \pi v^2 A^* AR$$

Rearrangement and conversion to present the terms in their non-dimensional form allows the coefficient of drag acting on the wing to be written as:

$$\text{Eq.19.} \quad CD_{\text{wing}} = 2.7 k_{\text{profile}} Re^{-0.5} + k_{\text{induced}} CL^2 / \pi AR \text{ (McNeill Alexander 2003)}$$

If the parasite drag is known based on the frontal surface area of the body or fuselage can be added to equation 19 or in its coefficient form to equation 14 to give the total drag acting on

the wing. Note that all of these formulae account only for the deviation of the load from an elliptical state where  $e = 1/(\delta + 1)$ .

### **5.0.2 Gliding flight**

Gliding represents a simple form of aerial locomotion where the animal does not expend any energy in the form of wing beats to overcome drag and frictional forces, instead converting potential energy into kinetic energy by sacrificing altitude. As vertical height must always be lost, the direction of flight makes an angle to the horizontal of  $\alpha^\circ$  (Figure 5.5), the value of which ranges between only a few degrees for the most efficient gliding birds, and up to  $90^\circ$  where the animal is described as parachuting. During a glide the lift and drag forces acting on the wing can be defined as:

$$\text{Eq.20.} \quad D = \sin\alpha Mg$$

$$\text{Eq.21.} \quad L = \cos\alpha Mg$$

For very small angles of attack,  $\cos\alpha$  approaches 1.0, effectively reducing Equation 21 to  $L = Mg$ .

Based on Equation 1 (i.e.  $L \text{ or } mg = 0.5\rho v^2 SA$ ) it can be seen that as flight velocity decreases more lift is required to keep the aircraft airborne. During a glide the wings are assumed to be stationary, although this is not necessarily true for biological fliers that can bank their wings to provide stability or fine directional controls, particularly during gusty conditions. For the sake of simplicity, however, a rigid wing is often adopted. If it is assumed that the animal performs a straight glide then thrust must be generated from a loss of altitude, allowing the vertical sinking velocity to be calculated as:

$$\text{Eq.22.} \quad V_s = V_s \alpha = DV/Mg$$

Here the wing has a single coefficient of lift and drag at any given angle of attack. When plotted over a range of angles of attack this produces a C-shaped a polar plot of  $C_D$  and  $C_L$  (Figure 5.6) from which the horizontal velocity and corresponding vertical sinking velocity are respectively calculated by:

$$\text{Eq.23.} \quad V = \sqrt{2Mg/CL\rho A}$$

$$\text{Eq.24.} \quad V_s = (CD/CL)V = \sqrt{((2Mg*CD^2)/(\rho ACL^3))} = -V*ATAN(1/(L/D))$$

The resulting gliding polars shows the flight characteristics of a particular wing, where vertical sink increases rapidly at both slow and fast horizontal velocities, giving a relatively narrow range of desirable flight speeds. The highest point of the gliding curve is termed the minimum sink velocity ( $V_{ms}$ ) and represents the optimal horizontal velocity to stay airborne for the longest possible period where vertical sink is minimised. A second point, termed the maximum range velocity ( $V_{mr}$ ), occurs at the tangent to the glide polar and represents the optimal velocity to travel the greatest distance for any given loss in altitude. In the illustrated example of Figure 5.6 the horizontal velocities of the petrel and the vulture adapted from Tucker and Parrott (1970) are approximately 8 and 14 ms respectively at the point of minimum sink, indicating the target velocity to maximise their time in the air. At the maximum range speeds the flight velocities of the two birds have increased to approximately 11.5 and 15 ms respectively, the desired velocities to travel as far as possible without expending any energy in the form of flapping. The difference between the maximum range and minimum sink speeds in aircraft, biological or otherwise, are not constant, demonstrated in this scenario the vulture, where  $V_{ms}$  and  $V_{mr}$  are close together, suggesting that the animal would have actively sought a very narrow range of flight speeds. The petrel on the other hand has a larger difference between these two velocities and would experience a range of flight velocities depending on the immediate intentions of the bird. At the point of minimum sink the gliding ratio is at its maximum and can be written as:

$$\text{Eq.25.} \quad \mathcal{E}_{\max} = v(\min V_s)/(\min v V_s)$$

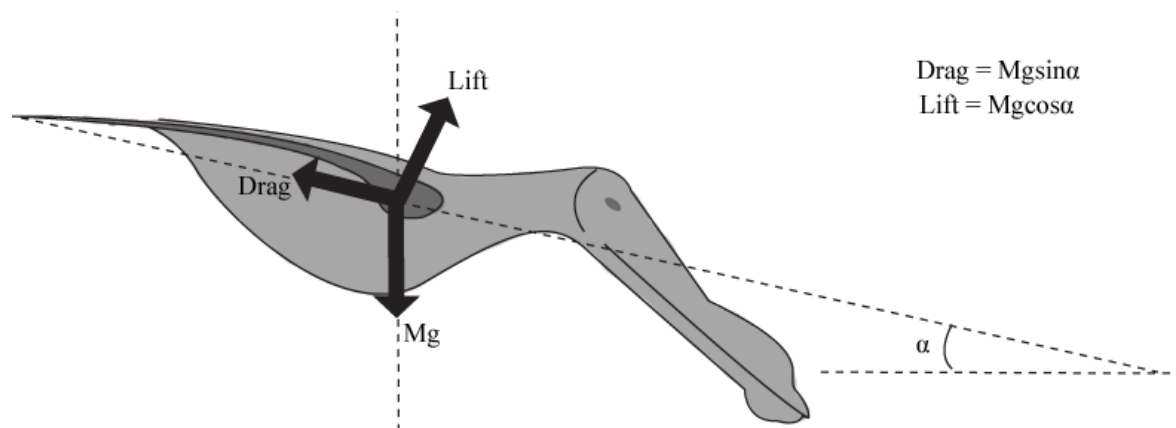


Figure 5.5. - Forces acting on a pterosaur during gliding flight where: M, body mass (kg); g, gravitational acceleration (9.8 ms);  $\alpha$ , angle of attack.

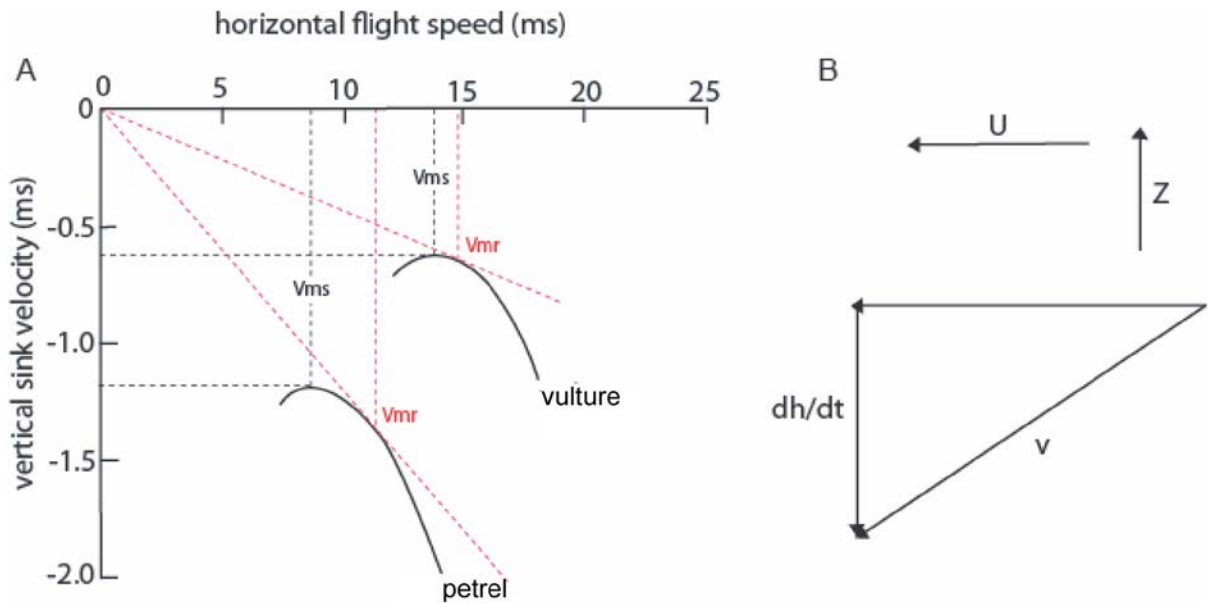


Figure 5.6. - A, Gliding polar of two biological fliers, adapted from Tucker and Parrott (1970). For a single wing configuration the horizontal and vertical velocities can be defined by the curves above, increasing rapidly at both fast and slow flight speeds. The top of the curve represents the minimum sinking speed ( $V_{ms}$ ). A tangent to the curve represents the point where L:D is maxed and is referred to as the maximum range speed ( $V_{mr}$ ). B, Velocity vector diagrams showing the relationship between glide angle and rate of change of altitude ( $dh/dt$ ).  $U$  and  $Z$  represent the horizontal and vertical velocity vectors respectively. Adapted from Tucker and Parrott (1970).

The shape of CL/CD polar is highly dependant on the aspect ratio of the wing in question where typically, higher aspect ratio wings generate higher values of CL at lower values of CD. The relationships between wing load, aspect ratio and gliding performance is illustrated in Figure 5.7 where, despite a constant aspect ratio, a high wing load is associated with higher velocities of minimum sink, maximum range and vertical sink velocities. Further increasing aspect ratio, but keeping wing load constant, again also leads to faster flight velocities but is coupled with a reduction in vertical sink. Aircraft with higher wing loads are therefore associated with smaller glide angles.

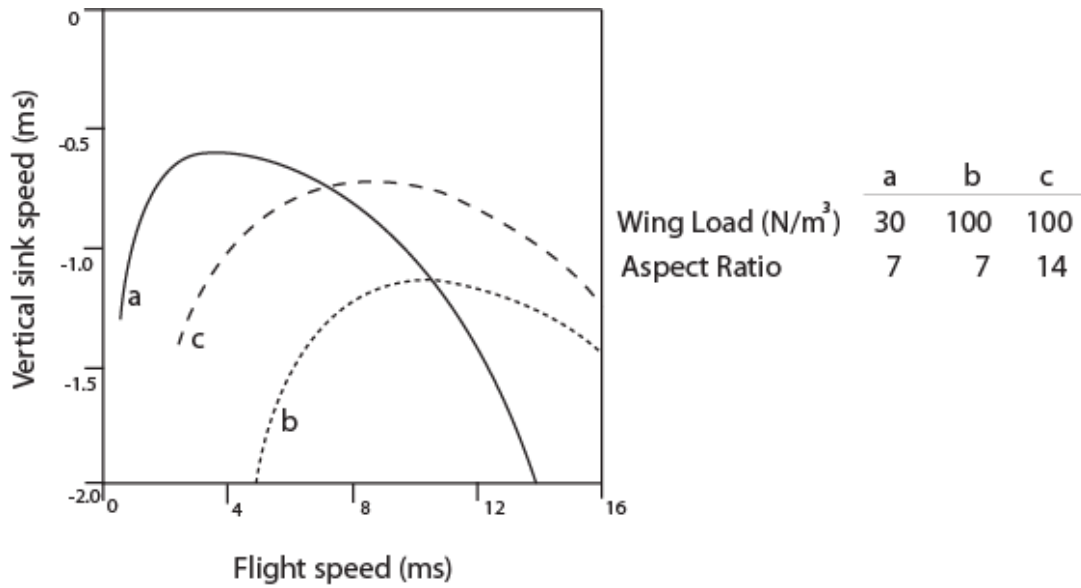


Figure 5.7. - Relationship of wing load and aspect ratio with gliding performance (source: McNeill Alexander 2003).

### 5.0.3 Circling performance

The equations covered by the section above apply only to a pterosaur during a straight glide, however, to initiate a turn the animal is required to bank both its wings, resulting in the lift force being directed at an angle of  $\Phi^\circ$  to the vertical (Figure 5.8). As a result of this, horizontal and vertical velocities increase as the aircraft accelerates into a turn and may be described by:

$$\text{Eq.26.} \quad V_t = V/(\cos\Phi)^{0.5}$$

$$\text{Eq.27.} \quad V_{st} = V_s/(\cos\Phi^3)^{0.5}$$

As such the length of the radius defining the turn is given by the equation:

$$\text{Eq.28.} \quad r = (Mg/A) * (2/(\rho g C L \sin\Phi)) = 2M/\rho A C L \sin\Phi$$

Estimating circling performance in this manner is useful for a comparison of the circling performance of extinct pterosaurs with extant biological fliers (Figure 5.9). Increasing the banking angle results in progressively tighter circling radius given by Equation 28 but at the expense of a further increase in both  $V_t$  and  $V_{st}$ . The term circling envelope is used to describe the radius of a turn relating to the minimum sinking speed.

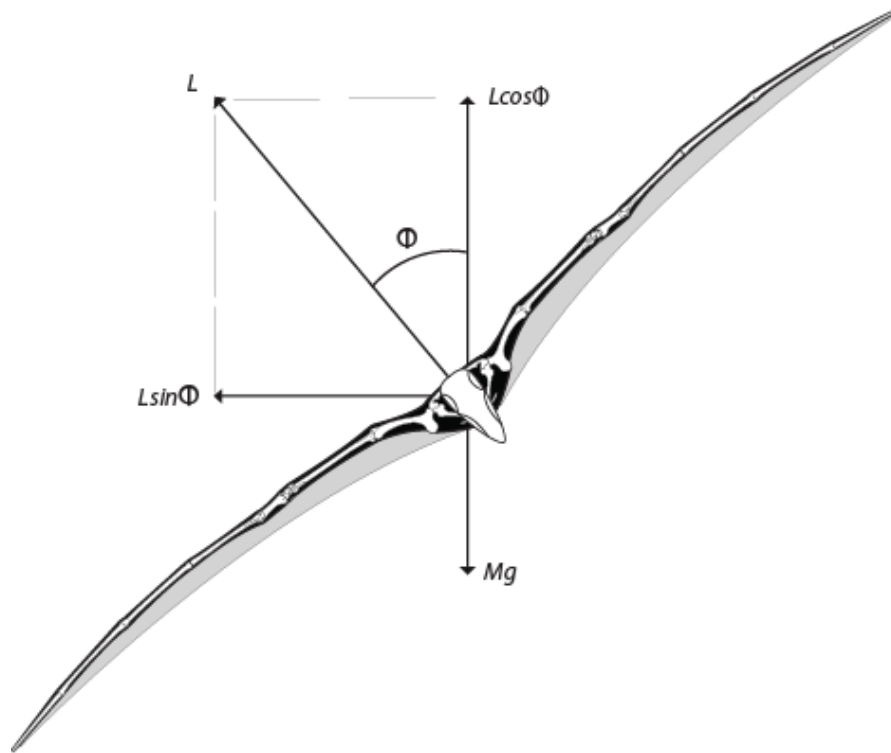


Figure 5.8. - Forces acting on a pterosaur during a banking manoeuvre where:  $M$ , body mass (kg);  $g$ , gravitational acceleration (i.e. 9.8 ms);  $L$ , lift (N);  $\Phi$ , banking angle.

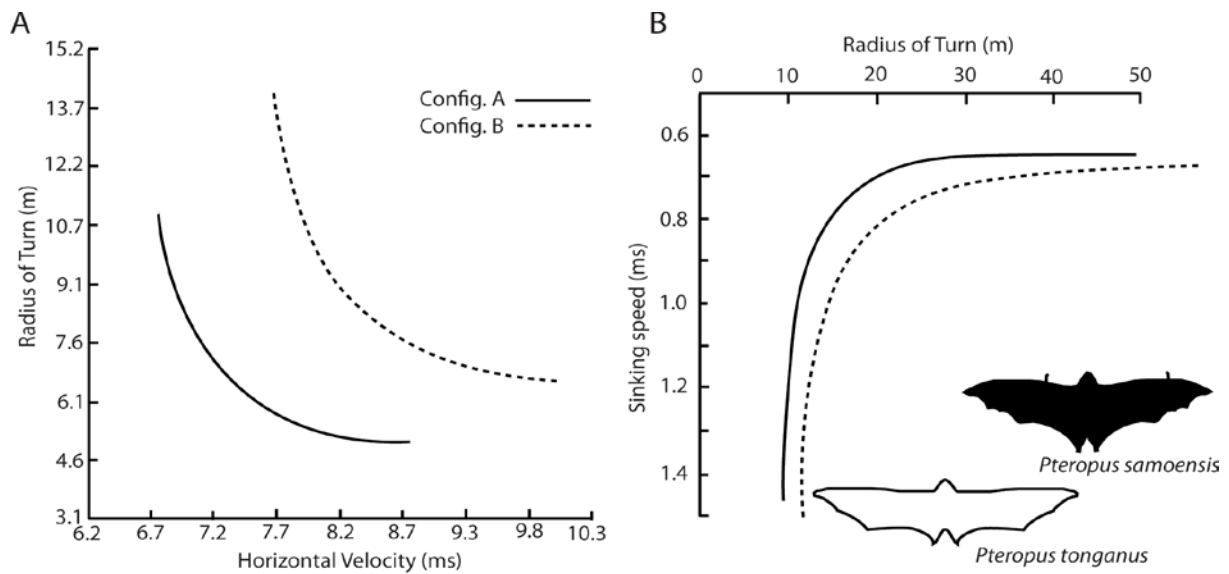


Figure 5.9. Circling curves produced for (A) configurations of *Pteranodon* (Bramwell 1971) and (B) as an extant example, the bats of the genus *Pteropus* (Norberg et al. 2000).

## **5.1 Introduction to pterosaur aerodynamics and methodologies**

A combination of powered flight and gliding appears to have been the primary methods of locomotion favoured by pterosaurs, given the presence of fully developed wings within even the most primitive taxa (Sharov 1971; Wild 1984; Wild 1994; Bakhurina and Unwin 2003). Flightless ness is unknown for this clade and even within certain ctenochasmatids and the Azhdarchoidea, where terrestrial locomotion is inferred to have been more widespread, and there is no evidence that the wing diminished in any way; except for a reduction of the terminal wing finger phalanx (Kellner and Langston 1996; Elgin and Frey 2012). This latter point, however, likely has more to do with reducing the aspect ratio for aerodynamic purposes.

As the first and largest volant vertebrates it is perhaps unsurprising that pterosaurian flight has been subject to investigation by numerous authors over the last century, who reconstructed flight characteristics from comparisons with gliding aircraft (Bramwell and Whitfield 1974; Brower 1980, 1982, 1983), or mathematical theory derived from related aerodynamical studies (Bramwell 1971; Bramwell and Whitfield 1970; Chatterjee and Templin 2004). Although certain criteria necessary for accurate estimates of performance are impossible to retrieve for extinct animals, these including both wing camber and membrane aeroelasticity, sufficiently useful estimates may still be produced where three important variables are known: i) reconstruction of the skeletal configuration, ii) shape and surface area of the flight surfaces, and iii) accurate estimation of mass. As such a consensus has been established over the years whereby pterosaurs are portrayed as relatively slow and highly manoeuvrable fliers (e.g. Langly 1902; Williston 1911; Hankin and Watson 1914; Bramwell 1971; Bramwell and Whitfield 1970; 1974; Heptonstall 1971; Stein 1975; Brower 1980, 1982, 1983; Hazlehurst and Rayner 1992; Chatterjee and Templin 2004; Wilkinson 2007, 2008), often able to out perform extant birds with respect the circling ability and returning high ratios of lift:drag, resulting is superb gliding ratio.

While a reconstruction of the gliding position remains relatively uncontroversial given the degree of study focused on pterosaurian anatomy (see Chapter 4), the remaining

two required variables, i.e. wing shape and mass, are more uncertain; small changes to which have the potential to significantly alter final estimations of aerial performance. Given recent controversies over both mass estimation and wing profile a brief reassessment of the aerodynamic ability of the Pterosauria is required. Moving on from pterosaurian anatomy this section of the thesis aims to investigate the flight/gliding dynamics of a variety of taxa through a range of experimental and mathematical methods, and altering critical variables within the flight equations to address output sensitivity.

## **5.2 Methodologies**

### **5.2.1 Skeletal Reconstruction**

A reconstruction of the pterosaurian skeleton during gliding flight was obtained from a combination of Wellnhofer (1985) and personal studies of the joint mechanics of three dimensional fossil material where the humerus is angled  $20^\circ$  dorsally and  $15^\circ$  caudally. This forms an angle of  $162^\circ$  with the ulna in cranial view and directs the latter bone more or less perpendicular to the axis of the body. In dorsal view the ulna meets the humerus to form an angle of  $155^\circ$  and directs the ulna in a craniolateral direction, providing sufficient space medially for the propatagium to develop as a useful flight surface. The angle between the ulna and fourth metacarpal in this position, joined by the syncarpus, is approximately  $150^\circ$  in dorsal view, projecting the metacarpals almost directly laterally. The phalanges of the wing finger itself (i.e. digit 4) are estimated to have made an angle of approximately  $165^\circ$  with the fourth metacarpal during passive gliding. The position occupied by the hind limbs is harder to interpret owing to the large degree of movement available to the femur and uncertainty over angle of the tibia, which would have had an active role in tensioning the proximal section of the brachiopatagium. Herein the femur was directed caudally at an intermediate value of  $45^\circ$  in dorsal view, and made an angle of  $130^\circ$  with the tibia, which was orientated directed craniocaudally.



### **5.2.2 Wing Reconstruction**

The shape and extent of the primary flight membrane in pterosaurs, the brachiopatagium is herein taken to run from the tip of the distal most wing finger phalanx, with the trailing edge terminating level with the ankle or lower tibia after Elgin et al. (2011, Figure 5.10). The resulting configuration, supported by exceptionally preserved fossil specimens, is therefore more similar to the traditional broad/ankle chord model (Bakhurina and Unwin 2003; Unwin and Bakhurina 1994, 1995; Kellner et al. 2009) and as such *contra* to a the narrow chord model, popularised during the 1980s and 1990s (Brower 1980, 1982, 1983; Padian 1983, 1985, 1987; Padian and Rayner 1993; Peters 2001). While a number of aerodynamic studies have utilised a wing whose trailing edge terminates medially level with the torso or hip (Brower 1980, 1982, 1983; Chatterjee and Templin 2004; also see Dyke et al. 2006) this configuration is reliant on membranes that has severely contracted *post mortum*, is *contra* to membranes preserved in exceptional specimens (e.g. *Anurognathus ammoni*, *Beipiaopterus chenianus*, *Eosipterus yangi*, *Eudimorphodon ranzii*, *Jeholopterus ningchangensis*, *Rhamphorhynchus muensteri*, *Sordes pilosus*), and contradicted by the observation that paired fore- and hind limbs often settle together due to a membranous connection (Frey et al. 2003a; Unwin and Martill 2007); also demonstrated previously in Chapter 3. As such a “narrow” chord model is rejected herein. Following Elgin et al. (2011) an ankle wing configuration must have evolved very early on in the lineage and was never fundamentally altered throughout their subsequent evolutionary history. Alterations in hind limb/forelimb lengths provided the driving mechanism whereby the shape of the main wing was altered (Witton 2008a; Elgin et al. 2011).

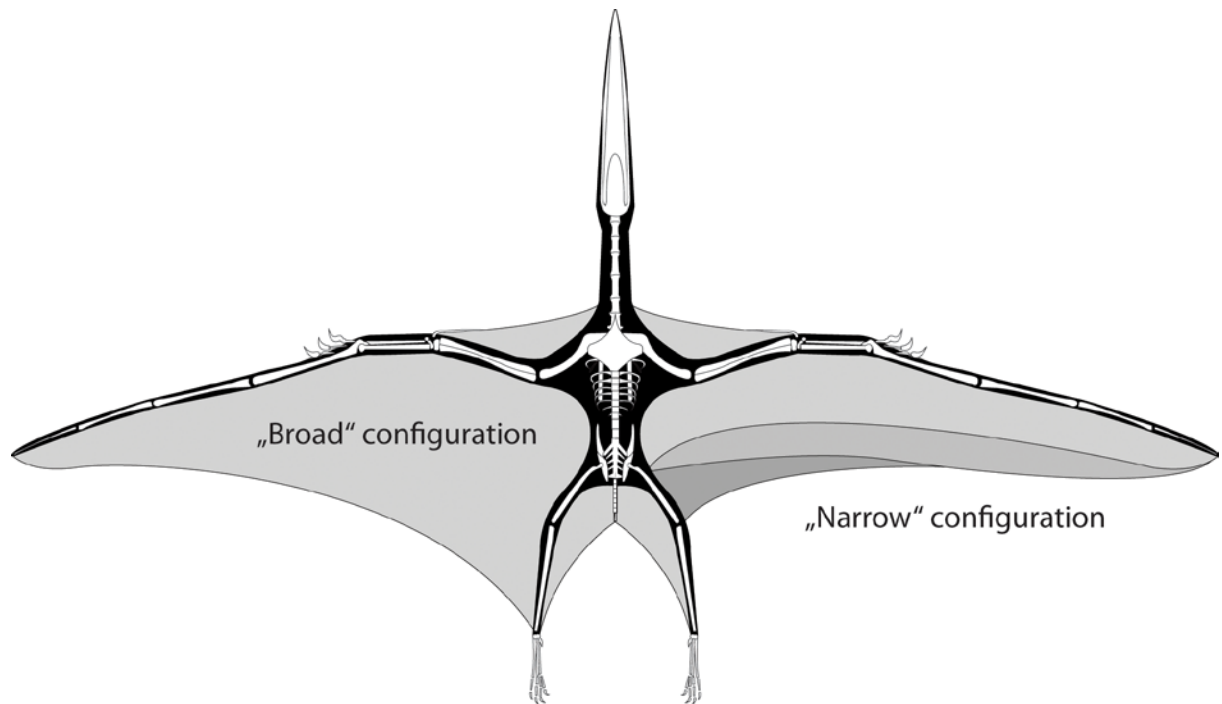


Figure 5.10 – Contrasting extent of the main wing membrane in pterosaurs. The broader, ankle chord (i.e. “bat-like”) configuration is illustrated left while the three narrow, body/hip (i.e. “bird-like”) configurations are shown to the right.

### **5.2.3 Mass Relationships**

As with wing shape, estimations of pterosaurian mass have been reappraised in recent years, with several authors contesting the long established consensus that pterosaurs enjoyed an ultra lightweight frame (e.g. Prondvai et al. 2008; Witton 2008a, b); a result synonymous with the use of volumetric study models. As such, where previous mass estimations for the Cretaceous pterodactyloid *Pteranodon* were as low as 14.94 kg (Brower 1983) - 16.6 kg (Bramwell and Whitfield 1974; Chatterjee and Templin 2004), with upper estimates of 22.7 kg (Heptonstall 1971), 23.8 kg (Bramwell and Whitfield 1974), and 27.8 kg (Kripp 1943), results returned by scaling relationships indicated a significant increase in mass. This divergence is highlighted by using the giant azhdarchid *Quetzalcoatlus* as an example, where more traditional estimates of ~70 kg (Chatterjee and Templin 2004) are contrasted against much heavier values of 250 kg (Witton 2008a, b). While Henderson (2010) subsequently presented a model predicting that large azhdarchids could reach a mass of 544 kg this was contested by Witton and Habib (2010).

Divergence in methodology and total mass estimation mean that any mathematic assessment of pterosaurian biomechanical or aerodynamic performance must accommodate two very different final estimates. Herein, both of these estimates are adopted to give a wide range of characteristics that may be subsequently compared. These values will be casually referred to as “light” or “heavy” mass estimations, respectively following results presented Chatterjee and Templin (2004) and Witton (2008a, b); accepting that these represent only two of many divergent examples of mass estimation, and are calculated as follows:

**“Light” mass estimation:**

Eq. 30.  $M_{bm} = 0.1863b^{2.4767}$  (Chatterjee and Templin 2004)

**“Heavy” mass estimation:**

Eq. 31.  $M_{bm} = 0.681b^{2.807}$  (non-pterodactyls, Witton 2008a, b)

Eq. 32.  $M_{bm} = 0.519b^{2.55}$  (pterodactyls, Witton 2008a, b)

#### **5.2.4 Theoretical Modelling**

Theoretical modelling was conducted through the alteration of individual variables in a variety of stimulatory and / or mathematical software. Data on variables such as mass and wing shape was sourced from the published literature or based on templates created from fossil material as described previously. Such templates were made by photographing pterosaur specimens and scaling/arranging the bony elements into the appropriate flight position with Adobe Illustrator. Where wing area was required, the template was imported into Adobe Photoshop and the percentage of total pixels occupied by the template were calculated, allowing a direct calculation of wing area. For simplicity the total wing area and span is here taken to include the strip of the body that lies medial to the brachiopatagium.

### **5.2.5 Computer based modelling**

Computer based modelling was achieved through the use of the freeware program “TORNADO,” along with a CFD analysis in association with the DLR and KIT. Coordinates along the leading and trailing edges of the wing templates were calculated in Microsoft Excel, and the resulting geometric models were imported into TORNADO (Figure 5.11). As the exact centre of gravity in pterosaurs is uncertain this was positioned on the body segment in line with the quarter chord. Instructions on the use of the programme, developed as a collaboration between the Royal Institute of Technology (KTH), Stockholm, Sweden, the University of Bristol, UK, and the University of Linköping, can be found at <http://www.redhammer.se/tornado/>.

For the CFD study, the template was created using the skeleton of *Coloborhynchus robustus* (SMNK PAL 1133), described earlier in this thesis. Photographs of bony elements were taken from several aspects, and digitally scaled and repositioned with Adobe CS 3 to produce a working template. This template was sectioned along its sagittal and transverse planes and the relative coordinates were calculated in Adobe Illustrator, the section geometry being subsequently reduced to a series of best fit curves. The cross section of the wing bones at key points along the spar was determined from the actual bones. Sections of the model were visualised using the in-house program MoDGen (courtesy of the DLR, Göttingen) and minor modifications of the geometry were subsequently made using the graphics program RHINOCEROS at KIT (Figure 5.12). The body sectioning proved too problematic for ModGens and was reconstructed directly from the 2D cross-section in RHINOCEROS. Rescaling of the wing section, along with minor modifications to remove inconsistencies and alter the wing tips were performed in RHINOCEROS by S. Rück (KIT) under the supervision of the author.

### **5.2.6 Calibration and operation of the wind tunnel**

All physical model experiments were conducted within an open section wind tunnel housed in the Karlsruhe Institute of Technology. The tunnel section was approximately 2 m in width allowing for the mounting of models up to 1.5 m in span (Figure 5.13). Although larger models could be accommodated, this limitation

ensured that all parts of the model remained permanently situated within the main body of the flow.

A new measuring balance, FTS-Gamma SI-65-5 ([www.schunk.com](http://www.schunk.com)), was purchased specifically for this project and was both installed and calibrated by an engineering student at KIT. The balance was capable of recording up to 65 N of force in the x- and y- axes (drag and side force), 200 N in the z-axis (Lift) and was accurate to 1/40<sup>th</sup> and 1/20<sup>th</sup> of a Newton respectively.

While the initial testing and calibration of the device was the responsibility of the KIT, subsequent tests were conducted by the author. Sampling runs taken from three of the fixed wing models (i.e. representing the genera *Aurorazhdarcho*, *Coloborhynchus*, *Sinopterus*, Figure 5.14) at  $\alpha = 0^\circ$  and a velocity of 10 ms indicated that all force and torque data was normally distributed. At higher velocities the wing spar of the models began to flutter and further sampling runs were arranged to ensure that no data spikes or skewing occurred. At the maximum recorded flight speed of 20 ms the force and torque data remained normally distributed, indicating that no data spikes or skewing existed, although the range of recorded values was greatly increased (Figure 5.14; Table 10).

### **5.2.7 Set up of the mounting bracket**

Models were mounting onto a custom built bracket, 1.47 m in height, and positioned in the centre of the working section of the tunnel. The base of the mounting strut consisted of a solid base onto which the measuring balance and narrow mounting strut were fixed. The vertical mounting strut of the model was fixed onto this with a bolt but could otherwise be freely rotated in the vertical plane, allowing the pitch (i.e. angle of attack) of the model to be controlled (Figure 5.15A). No mechanism existed for determining the angle and prior to each experimental run the position of the mounting strut was measured with a protractor and photographed from a standardised position. For the cranium models a new L-shaped bracket was created. The strut of the model was positioned on the top surface of this bracket and could be freely rotated in the horizontal plane, thereby allowing the head to be yawed (Figure 5.15B).

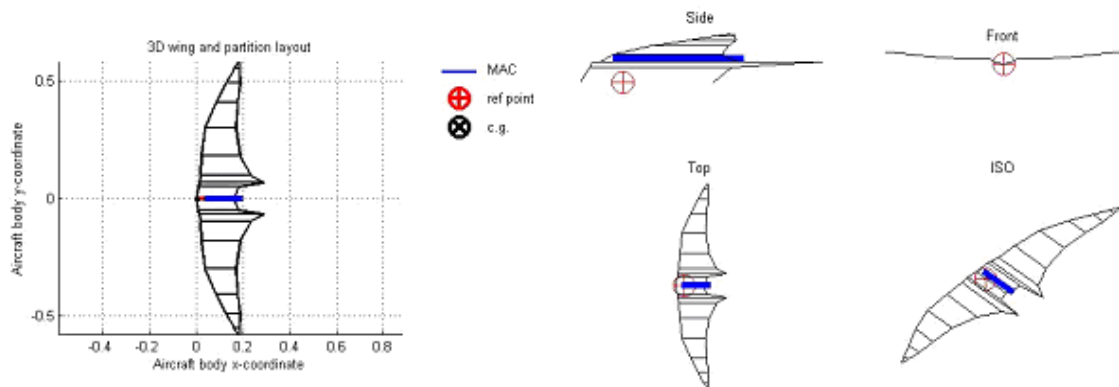
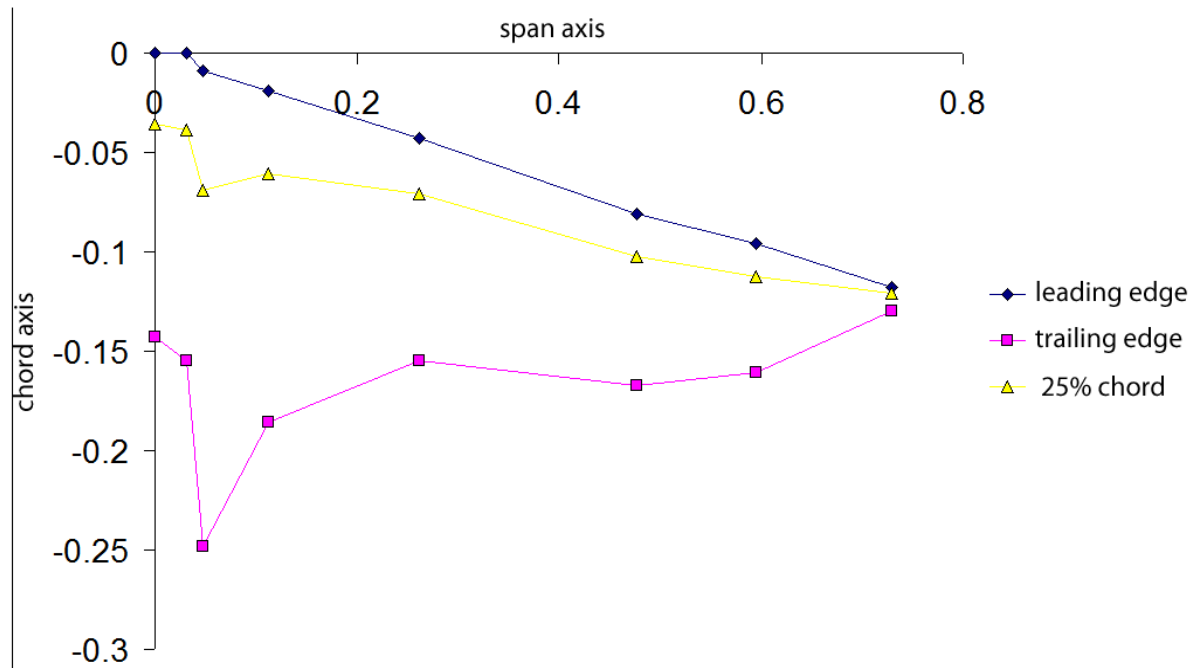


Figure 5.11. - Flat plate, geometrical model of the pterosaur *Sinopterus dongi* with the long axis of the body centred on y-axis (top). Lift producing surfaces of the wing are typically divided into 9 segments to calculate theoretical lift/drag (bottom), although slight variation to this number was needed for some taxa to more accurately define the wing shape.

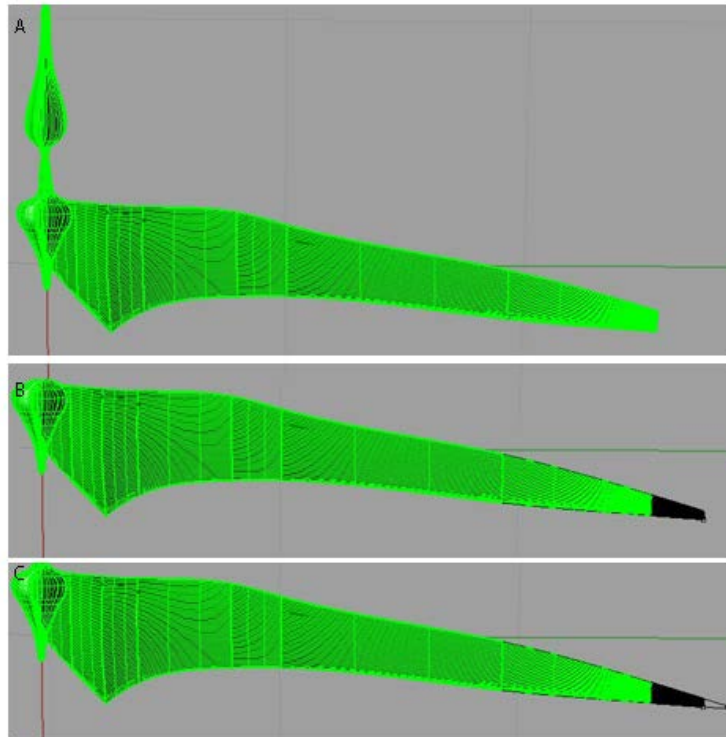


Figure 5.12. - Example of the model template in RHINOCEROS showing modifications of the wing geometry where the distal tip (shown in black) is narrowed (A – C).

| Taxon                 | Drag (N)        | Side force (N)   | Lift (N)        | Roll (Nm)         | Pitch (Nm)       | Yaw (Nm)          |
|-----------------------|-----------------|------------------|-----------------|-------------------|------------------|-------------------|
| <i>Aurorazhdarcho</i> |                 |                  |                 |                   |                  |                   |
| 10ms                  | 0.50 (0.258)    | -0.20 (0.374)    | 2.95<br>(0.345) | 0.005<br>(0.087)  | 0.125<br>(0.058) | -0.02<br>(0.014)  |
| 20 ms                 | 2.20<br>(0.663) | -0.45<br>(0.923) | 7.80<br>(1.299) | -0.01<br>(0.222)  | 0.47<br>(0.127)  | -0.01<br>(0.043)  |
| <i>Coloborhynchus</i> |                 |                  |                 |                   |                  |                   |
| 10 ms                 | 2.20<br>(0.374) | -0.05<br>(1.559) | 9.65<br>(1.616) | 0.017<br>(0.979)  | 0.265<br>(0.167) | 0.0085<br>(0.254) |
| 20 ms                 | 6.90<br>(1.356) | 0.4<br>(3.839)   | 29.3<br>(4.590) | -0.96<br>(1.908)  | 0.705<br>(0.462) | 0.24<br>(0.990)   |
| <i>Sinopterus</i>     |                 |                  |                 |                   |                  |                   |
| 10 ms                 | 1.35<br>(0.345) | -0.05<br>(0.808) | 9.1<br>(1.299)  | 0.0095<br>(0.450) | 0.145<br>(0.081) | 0.03<br>(0.084)   |
| 20 ms                 | 5.00<br>(1.544) | -0.20<br>(3.204) | 25.5<br>(3.955) | 0.135<br>(1.253)  | 0.515<br>(0.358) | 0.21<br>(0.251)   |

Table 10. - Mean force values for selected models, where the angle of attack is zero. Figures in brackets indicate one standard deviation from the mean.

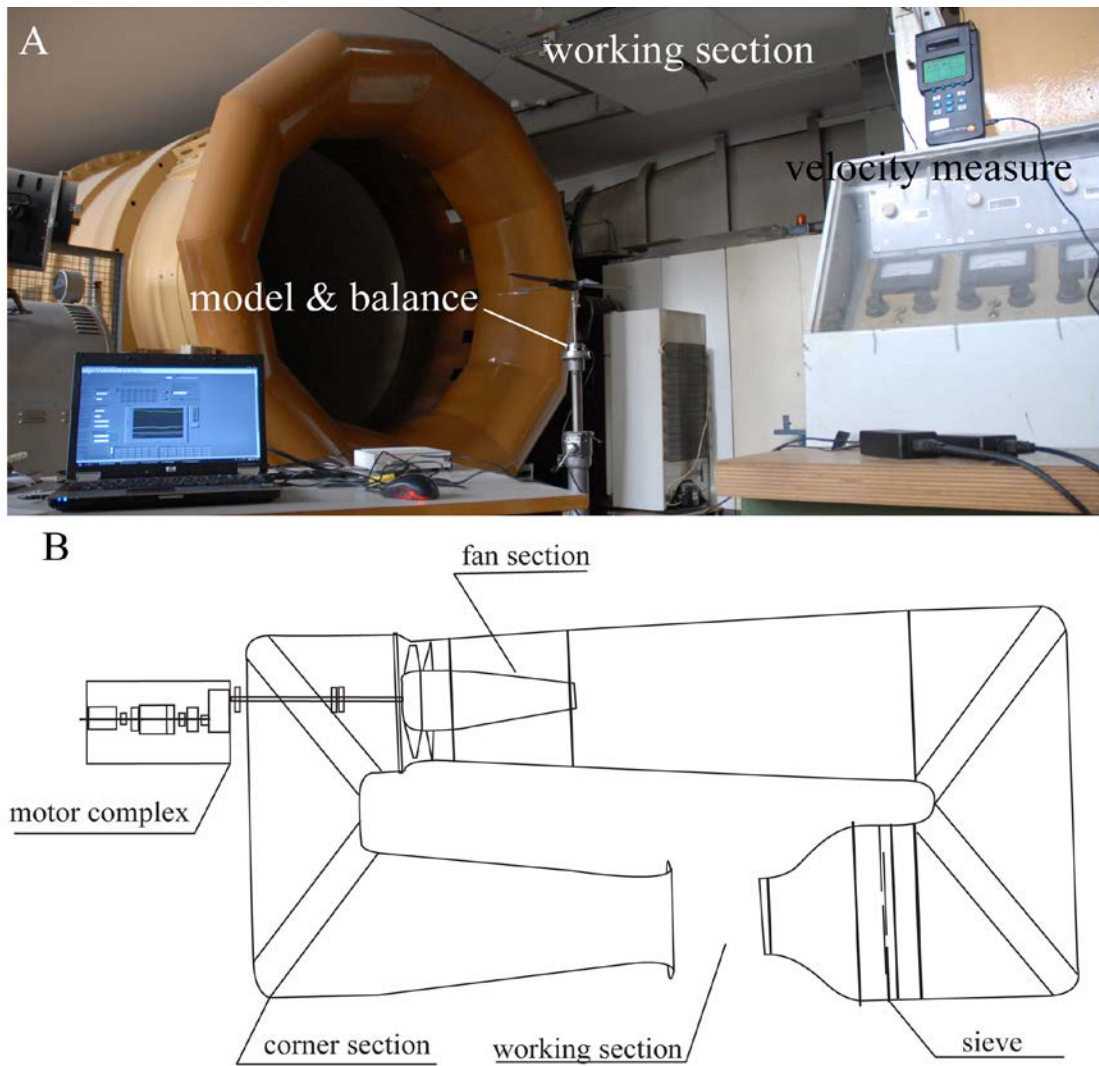


Figure 5.13. - A, Model mounted in the working section of the wind tunnel at the Karlsruhe Institute of Technology (KIT) along with the schematic of the machine (B). Direction of flow is clockwise (from right to left in both pictures).



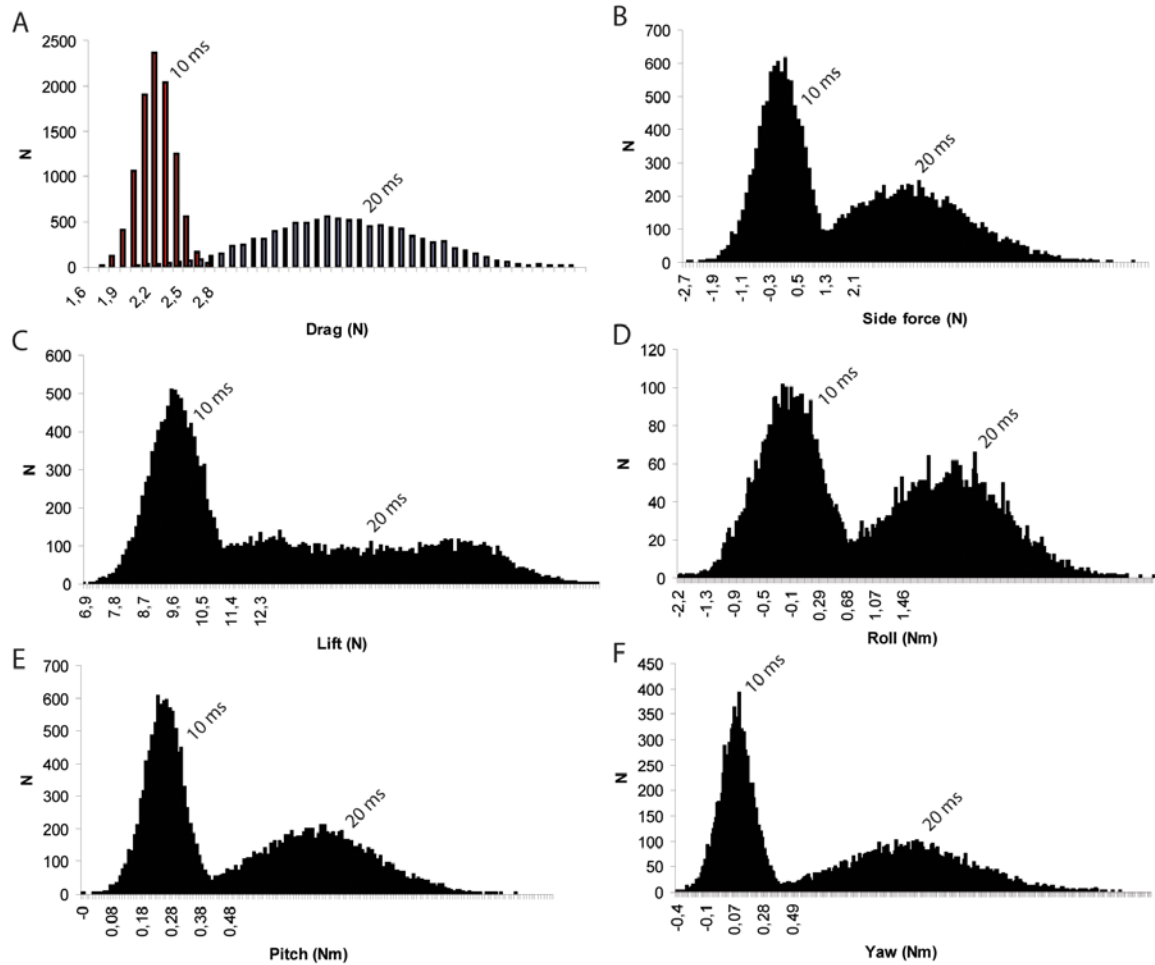


Figure 5.14. - Force distribution during calibration tests of the *Coloborhynchus* model at 10 and 20 ms. Data remains normally distributed at faster flight velocities although the standard deviation increases as a result of higher degrees of scatter.

### 5.2.8 Set up of the velocity control

The flow velocity was manually adjusted via a dial linked to the fan control but velocity readings were taken by a measuring device (testo 350 –M/XL – testo 454) mounted upwind from the model. In the rare occasions when this device was not available the flow velocity could be calculated from:

$$\text{Eq. 33.} \quad v_{\infty} [\text{ms}] = \sqrt{16.6 \cdot \rho [\text{mmWS}]}$$

where  $v$  = velocity (metres per second) and  $\rho$  = dynamic pressure (mm of water).

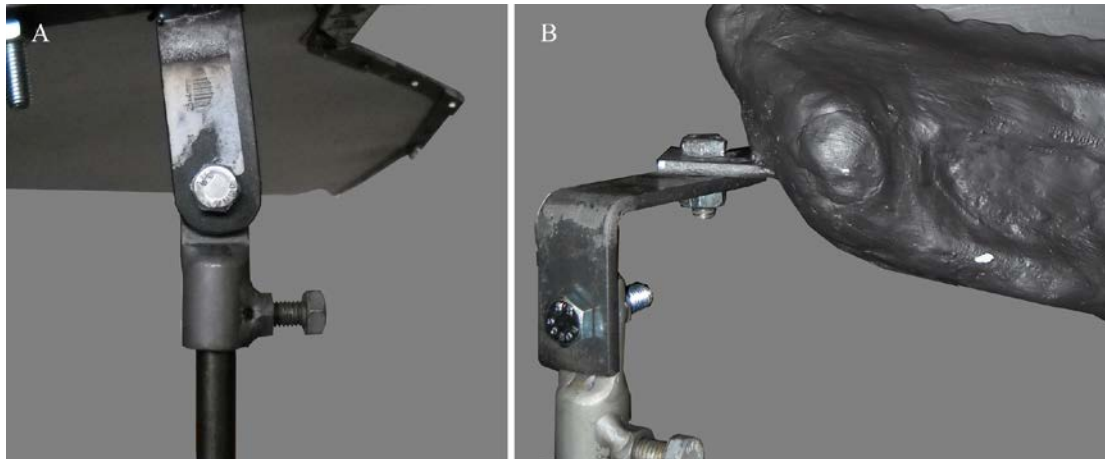


Figure 5.15. - Mounting brackets of (A) the flight models, allowing pitch; and (B), cranial models, allowing pitch and yaw movements.

Neither of these steps required any further work or calibration on the part of the author. After the flight models were fixed into the working section the measuring balance was “zeroed,” by means of a calibration, to compensate for the addition of this new weight. This step was repeated every time the angle of attack was altered due to the new position and weight distribution of the model. A single calibration run was taken with a flow velocity of zero (i.e. fan off), the results of which were subtracted from all subsequent runs at that angle of attack.

| Measurement   | Height (cm) |
|---|-------------|
| Floor to the base of the balance.   | 116.2       |
| Base of the balance to the articular joint of the model                     | 26.4        |
| Diameter of the mounting strut  | 0.12        |
| Height of the wing above the articular joint (for isolated wing model only) | 6           |
|   |             |
| Total height of the mounting strut  | 148.6       |

Table 11. - Measurements of the mounting strut housing the measuring balance.

Data readings were recorded for flow velocities between 4 ms up to 20 ms, increasing in 1 ms increments. Higher velocities were produced only when it was necessary to simulate higher Reynold number regimes. At each sample velocity the force and torque data were recorded for 100 seconds at a sampling rate of 10 readings per second by the program LABview. Multiple angles of attack were recorded for each individual model. Where it was not possible to complete all experiments within a single day, the angle of attack was reset to 0° the following day and the data compared to ensure that no significant variations between data sets existed.

Control of the flow velocity had to be manually achieved, inevitably introducing a small degree of inaccuracy into the experiments. This was a result of fluctuations in the flow velocity caused by the intermittent speeding up and slowing down of the fan motor. To make the reading as accurate as possible the velocity measurements were desirably kept to within  $\pm 0.1$  ms of the target velocity and typically never exceeded  $\pm 0.2$  ms. The high sample rate and long period of recording (i.e. 100) are here considered to be sufficient to smooth out temporary changes in flow velocity.

### **5.2.9 Construction of fixed wing models**

Fixed wing models used within the wind tunnel were cut from a plywood base with individual wooden rods cut to fit the corresponding elements of the forearm (Figure 5.16). These elements were orientated in their theoretical flight position with the wing finger at maximum extension. The major joints were strengthened by a combination of aluminium strips and epoxy putty. The wing membrane was cut from a single sheet of PVC that was glued onto the wing spar and body template, creating a small to moderate camber. The body was cut from blocks of polystyrene foam and gaps or irregularities were filled or smoothed over with epoxy putty. All construction took place within the preparation lab of the SMNK under the supervision of Rene Kastner.

### **5.2.10 Construction of body casts**

A latex mould of the model representing the genus *Aurorazhdarcho* (Frey et al. 2011) was created at the SMNK. The mould was filled with a soft foamy resin, creating a

replica of the original model. The surface was later coated with a harder resin for protection. Following the casting process the mounting strut was added by removing a small part of the ventral surface and excavating a section of the torso. The mounting strut was tightly fitted into this excavation and further secured with hard drying epoxy resin.

### **5.2.11 Construction of cranial models**

Models representing the crania of selected taxa were built from a variety of material (Figure 5.17). That of *Nyctosaurus* was created from a template based on specimens KJ 1 and 2 (Bennett 2003b), where the midline of the model was constructed from aluminium and filled out with epoxy putty to an appropriate bulk. The vertically orientated portion of crest was formed by a length of laterally compressed aluminium tubing fixed to the skull. The horizontal bar was also created by flattening a length of aluminium tubing and fixing it to the vertical bar at the correct position. This, however, was modelled on KJ1, the horizontal bar of which is incomplete when compared to KJ2 and is thus smaller than it should otherwise be. Nonetheless this is unlikely to significantly influence the results presented later. A mounting strut was fixed about the position of the occipital condyle and extended caudally behind the skull. A resin cast of the cranium of a specimen of *Anhanguera* from the collection of Urs Oberli was adapted by reconstructing a mandible of the same length and width and gluing it into position. The occipital region was excavated and the horizontally orientated mounting strut was fixed into position with epoxy. The remaining three specimens, *Tupandactylus navigans*, *Tupandactylus imperator*, and *Quetzalcoatlus* sp. were respectively created from templates of the fossil specimens: SMNK PAL 2343/2344 (Frey et al. 2003c), SMNK PAL 2839 (Frey et al. 2003c), TMM 41961 (Kellner and Langston 1996). An aluminium sheet acted as the vertical base, forming the midline of these models, while the remainder of the crania were sculpted from a single block of foam. The lateral extent of the skull in these specimens is unknown and so it was estimated from personal examination of the material or photographs. The mounting strut was positioned horizontally, level with position of the occipital condyle. The effects of Reynolds numbers on the data was tested on *Nyctosaurus* where the tunnel velocity was increased up to 25 ms to see if the data deviated significantly from the predicted curves. As no significant change was apparent

between these datasets, regression lines or curves from the recorded data can be used to investigate the forces and torques at high velocities.

| <b>Models</b>                   | <b>Lateral surface area (m<sup>2</sup>)</b> | <b>Reference chord (m)<sup>+</sup></b> |
|---------------------------------|---|--|
| <i>Anhanguera</i>               | 0.04342                                     | 0.496                                  |
| <i>Nyctosaurus</i>              | 0.020073                                    | 0.206                                  |
| <i>Quetzalcoatlus</i>           | 0.030699                                    | 0.495                                  |
| <i>Tupandactylus navigans</i> * | 0.037376                                    | 0.175                                  |
| <i>Taupandactylus imperator</i> | 0.060602                                    | 0.176                                  |

Table 12. - Characteristics of the various cranial models. Where: \* = half life size; + = ref chord taken to be the distance from the tip of the rostrum to the occipital condyle.

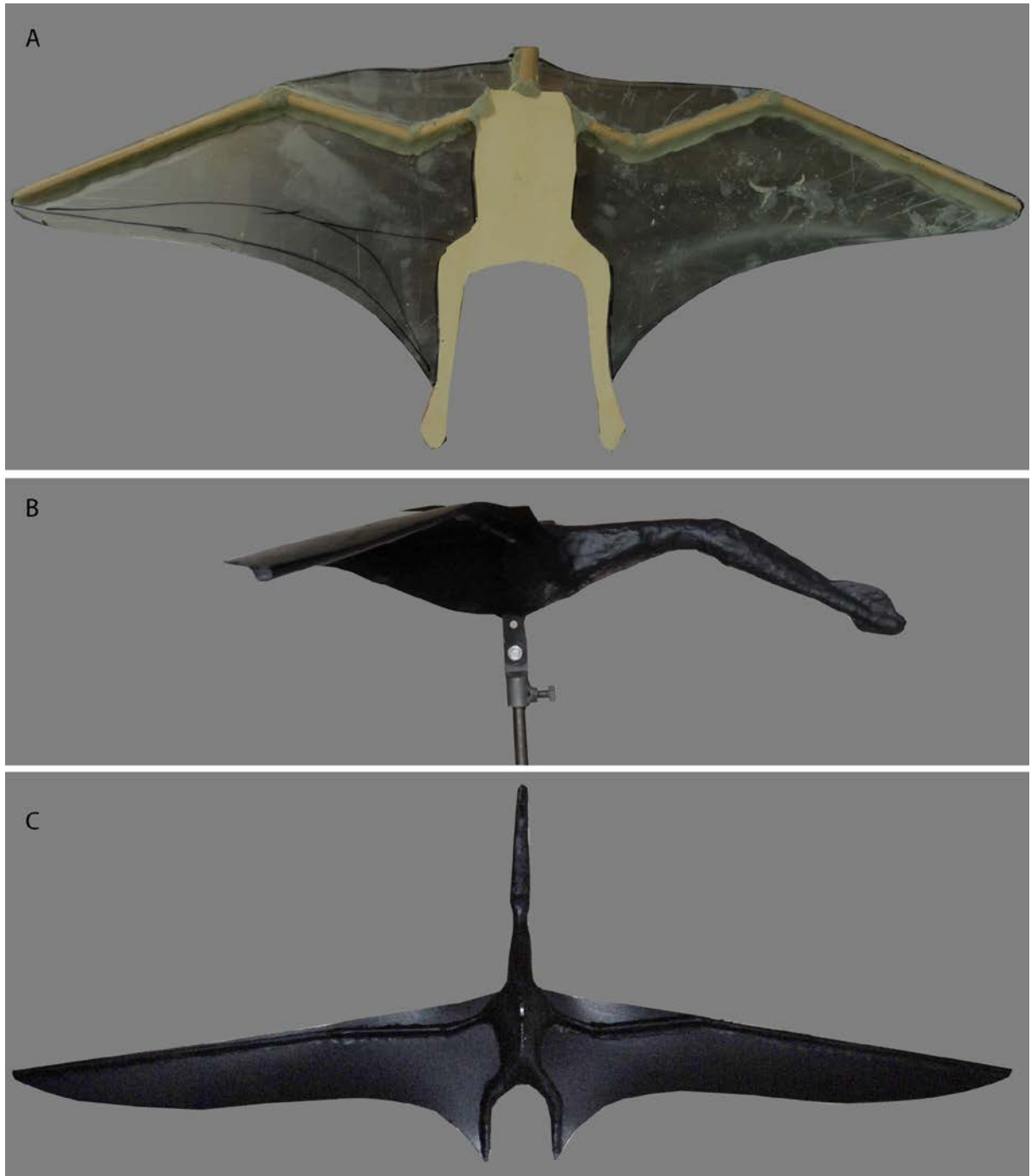


Figure 5.16. - Fixed wing models, construction and complete model. A, body template cut from a single strip of plywood along with the naked wing spar in the *Anurognathus* configuration; B, *Coloborhynchus* model at 1/4 life scale, mounted in the working section and seen in lateral view; C, *Coloborhynchus* as viewed from upwind.

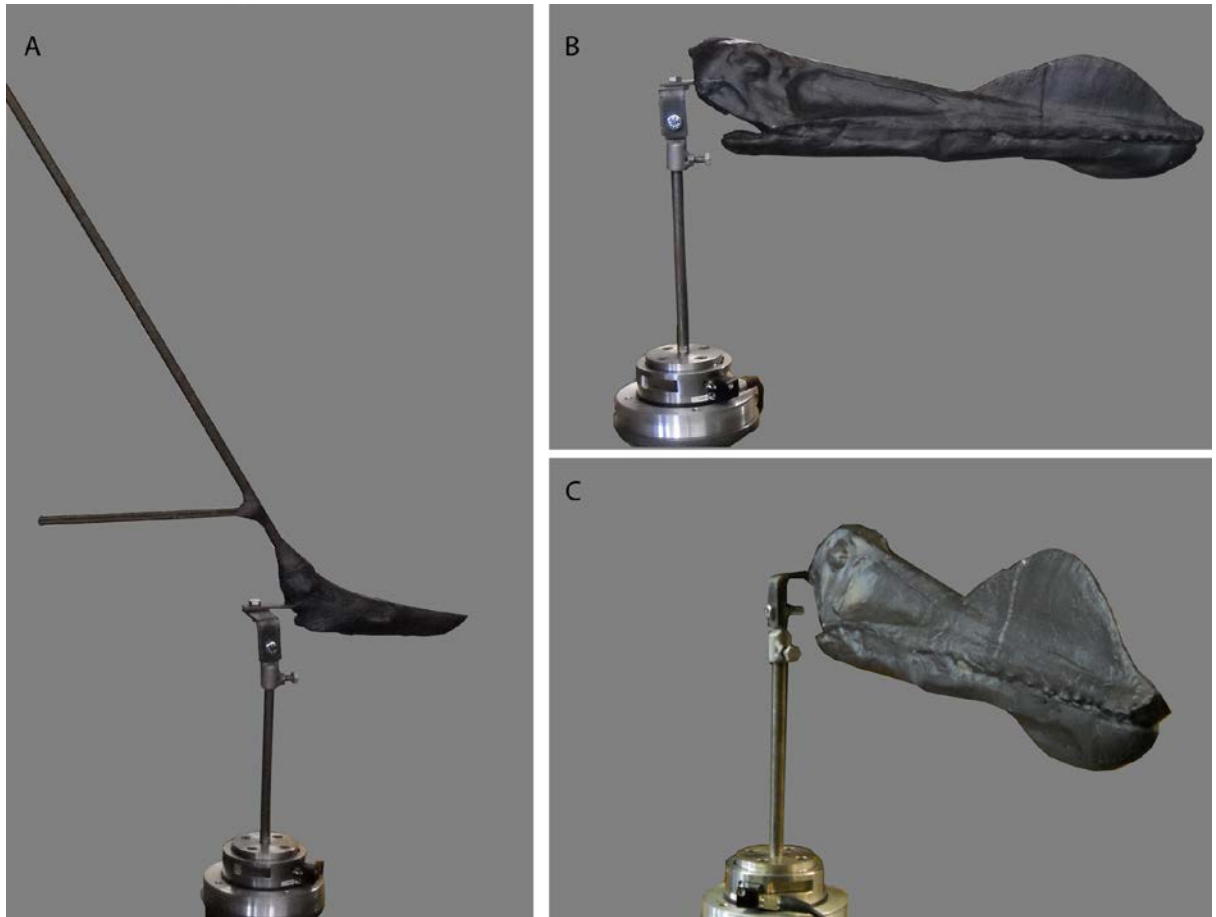


Figure 5.17. - Cranial models mounted in the wind tunnel at KIT. A, *Nyctosaurus* in lateral view; B, *Anhanguera* in lateral view; C, *Anhanguera* in craniolateral view.

## **5.3 Wind tunnel experiments**

### **5.3.1 Aerodynamics of the pterosaurian body**

As noted previously, estimates of body drag can vary greatly within the aerodynamic literature depending on the study taxon. While low coefficients are reported for a number of birds, e.g. 0.0132 and  $< 0.01$  for an albatross (Tucker and Parrott 1970; Pennycuick et al. 1988), 0.11 for a peregrine (Tucker 2000), and 0.12 for a red-tailed hawk (Tucker 2000), estimates for passerines are significantly higher at an average value of 0.37 (Hendenström and Liecti 2001). Experiments on dead animals or models also yield variable coefficients in the range of 0.14 – 0.4 (e.g. Pennycuick et al 1988; Tucker 1990), however, the interaction of the body elements during life is important as illustrated by the peregrine falcon (*Falco peregrinus*), where the drag coefficient is reduced from 0.24 on a wingless carcass to 0.14 on a smooth model (Tucker 2000).

Here, the body cast of *Aurorazhdarcho* (Frey et al. 2011) showed a very low parasite drag coefficient when orientated directly into the flow (Figure 5.18). The slightly negative value observed at flow velocity of 5 ms (i.e.  $Re = 32\,124$ ) is attributed to the very low force values recorded by the balance prior to the calibration equation being applied. At low angles of attack the gradient for all three recorded Reynolds number profiles is similar, but beyond an angle of  $6^\circ$ ,  $CD_{par}$  increases dramatically at very slow flight speeds. At faster flight speeds the effect of Reynolds number on  $CD_{par}$  is less pronounced, with little difference being observed between the profiles at 10 and 15 ms ( $Re = 64\,248$  and  $98\,372$  respectively). With the exception of take off and landing, dramatic pitching of the body is not expected during flight, suggesting that angles of attack less than  $\sim 10^\circ$  might be appropriate for determining the  $CD_{par}$  of a gliding pterosaur. As such an average  $CD_{par}$  of 0.033 ( $Re = 64\,248$ ) and 0.027 ( $Re = 96\,372$ ) at  $\alpha = 10^\circ$  likely represent the maximum values of this coefficient during gliding flight. These values are lower still if the animal pitched its body forward, where  $CD_{par}$  of 0.016 ( $Re = 64\,248$ ) and 0.013 are recorded instead ( $Re = 96\,372$ ). Results for *Aurorazhdarcho* are lower than many of those noted for birds above which is likely, in part, attributed to the smooth surface of the model. As long as the body is not pitched more than  $5 - 10^\circ$  from a horizontal orientation, particularly if it slopes forwards,



values are similar to those reported by Brower (i.e. 0.013 – 0.02) for the larger pterodactyls *Pteranodon* and *Nyctosaurus*. Values of 0.005 adopted for *Pteranodon* by Bramwell and Whitfield (1974), while although anomalously low when compared to other studies, are supported here only where the body is pitched no more than a couple of degrees from a horizontal position. Given the sharp decline in  $CD_{par}$  as the angle of pitch is lessened it is not possible to give an average value to be assigned to this taxon, however, values of between 0.01 – 0.016 seem appropriate for this taxon, accounting for a sufficient degree of movement of the body.

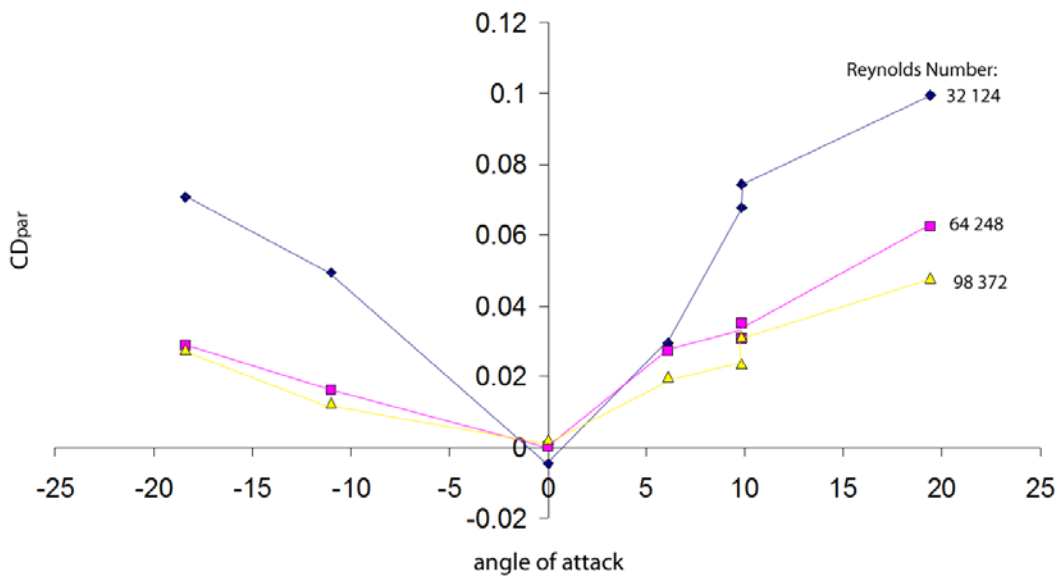


Figure 5.18. - Coefficient of parasite drag against angle of attack for a body cast of the pterosaur *Aurorazhdarcho* at selected Reynolds numbers.

### **5.3.2 Aerodynamics of cranial models**

Models of each study examples (Table 13; Figure 5.19) were fixed at 0° pitch while the yaw was altered between 0-60° in 20° increments to give a total of four distinct experimental setups. The flow velocity in the wind tunnel ranged from 4-20 ms for each of these positions where the situation permitted. In some situations it was not possible to determine the maximum yaw position as the torque at higher angles was too great for the balance, causing the model to loosen its connection to the mounting strut and immediately bringing the experiment to a halt. In other cases the higher flow velocities were problematic where vibrations developed and threatened to damage the model.

During one run an unexpected acceleration of the fan and the resulting gust caused the large crested model of *T. imperator* to tear off the mounting bracket and break in two. As a result of this, data for this model is only available for a single angle of attack and for a limited range of velocities.

| Models                          | Lateral surface area (m <sup>2</sup> ) | Reference chord (m) <sup>+</sup> |
|---------------------------------|--|----------------------------------|
| <i>Anhanguera</i>               | 0.043420                               | 0.496                            |
| <i>Nyctosaurus</i>              | 0.020073                               | 0.206                            |
| <i>Quetzalcoatlus</i>           | 0.030699                               | 0.495                            |
| <i>Tupandactylus navigans</i> * | 0.037376                               | 0.175                            |
| <i>Tupandactylus imperator</i>  | 0.060602                               | 0.176                            |

Table 13. - Characteristics of the various cranial models. Where: \* = half life size; + = ref chord taken to be the distance from the tip of the rostrum to the occipital condyle.

Force and torque coefficients acting on the remaining models at a flow velocity of 10 ms are summarised below (Table 14, Figure 5.20), all of which produce a large increase in the coefficient of drag as the head is yawed to the side. The CD of *Quetzalcoatlus* for example, increases 21.25 times over a range of 60°, for *Nyctosaurus* this is 7.61, and *Anhanguera* it was 9.67 but over a narrower range of 0-40°. Notably, although CD is typically very low when the head is orientated directly into the wind due to the stream lined form of the skull, the lowest CD recorded for *Nyctosaurus* is relatively high at 0.13, compared to the values of <0.06 observed in other models. This appears to be a direct consequence of the long vertically orientated strut that forms the leading edge of the crest. Although the strut itself is streamlined, being blade-like in cross section, its position and length nonetheless contribute substantially to drag production.

Two models with vertically orientated crests, *Nyctosaurus* and *T. navigans*, show similar patterns of roll and pitch coefficients. In the former (i.e. roll) the slope gradient increases sharply between 0° and 20°, and plateaus beyond 20°, while pitch increases linearly all the way up to a yaw position of 60° where:

Eq. 34.  $C_{pitch} = 0.0301\alpha + 0.3572$  (*Nyctosaurus*)

Eq. 35.  $C_{pitch} = 0.0247\alpha - 0.0045$  (*T. navigans*)

By contrast the roll coefficients of *Anhanguera* and *Quetzalcoatlus* reach only about 40% that of *T. navigans* at yawing angles of 40° and 60°. *Tupandactylus navigans* and *Nyctosaurus* also share an almost identical pattern of side force coefficient, which mirrors that of roll by increasing rapidly between 0° and 20° and decreasing slightly thereafter. *Quetzalcoatlus* records a coefficient ~55% that of *T. navigans* at a yaw position of 20°, but is comparable to both this and *Nyctosaurus* at higher angles of yaw. The coefficient in *Anhanguera* is very low compared to all other models. All models have a sufficiently distinct coefficient of yaw regardless of their similarities of their similarities in previous graphs.

### ***Anhanguera* sp.**

Drag remains relatively low at slower speeds (e.g. 0.15 N at 10 ms) but increases with velocity to reach 0.76 N at a flow of 20 ms. Yawing the head 20° essentially doubles the drag acting on the skull (i.e. 0.38 N at 10ms and 1.84 N at 20 ms) while by the time the head is yawed 40°, drag has increased by approximately 10 times the original amount (e.g. 1.56 N at 10 ms and ~4.84 N at 20 ms). It was not possible to test this model at a greater yaw position as the resulting torque caused the head and bracket to swing around 180°, immediately halting the experiment. Both side force and yaw torque increase rapidly with a turn of the head. At 10 ms these are recorded as being 0.04 N and 0.0005 Nm respectively, but increase to 1.05 N and 0.43 Nm at a 20° yaw and 2.45 N and 1.14 Nm by 40°. Increasing the velocity to 20 ms at a yaw position of 0° returns values of 0.19 N and 0.0017 Nm for side force and yaw torque respectively. By a yaw angle of 20° this has increased to 5.2 N and 2.13 Nm and by 40° yaw it has further increased to ~ 9.99 N and 4.63 Nm.

### ***Nyctosaurus gracilis***

Drag on the head increases from its starting value of 0.18 N at 10 ms (0°  $\alpha$ ) to 0.44 N after a 20° turn of the head, corresponding to a force increase of 2.44 times, 0.78 N at 40° (i.e., x4.31 increase) and 1.25 N by 60° (i.e., x6.94 increase). At 20 ms the drag is recorded as being 0.63 N (0°  $\alpha$ ), increasing to 1.8 N at 20° yaw, 3.79 N at 40° yaw, and 5.55 N at 60° yaw. The largest torque acting on the model is pitch, followed closely by

roll, and is substantially larger than the yaw torque. At 0° yaw position and 10 ms the values for roll and pitch are 0.06 Nm and 0.09 Nm respectively, increasing to 0.26 Nm and 0.36 Nm at 20 ms. Roll torque increases by 4.37 times by 20° yaw, and levels off thereafter, while pitching torque increases by 2.76 times by 20° yaw, 4.32 times by 40° yaw, and 6.14 times at 60° yaw.

### ***Tupandactylus navigans***

This model was constructed at ½ life size and so it is more useful to scale the recorded forces and torques up to the animals natural size. In this way a drag force of 0.65 N is expected at 10 ms and 2.57 N at 20 ms when the head is orientated directly into the flow. By a yaw angle of 20°, drag has increased 4.69 times to 3.04 N at a velocity of 10 ms, and 12.09 N at 20 ms. By 40° yaw the drag has further increased to 6.76 N (10 ms) and 27.48 N (20 ms), and by 60° yaw drag stands at 7.64 N (V = 10 ms) and 37.17 N (V = 20 ms). The most dominant torque acting on the crest of *T. navigans* is roll, which increases from 0.69 Nm at 10 ms, to 4.86 Nm at 20° yaw before levelling out (5.09 Nm at 40° yaw) and subsequently decreasing at higher angles of yaw (i.e. 3.54 Nm at 60° yaw). At higher angles of yaw pitching torque becomes dominant (e.g. 4.79 Nm at 60° yaw). Were *T. navigans* to fly at a very fast velocity (e.g. 20 ms) then the forces acting on the crania become quite substantial when combined with a simple turn of the head. At a flight velocity of 20 ms and a yaw angle of 0°, the roll, pitch and yaw torques stand at 2.76 Nm, 2.54 Nm, and 1.4 Nm respectively. Increasing the yaw of the head to 20° subsequently increases these to 19.8 Nm, 6.13 Nm, and 7.89 Nm respectively, while a 40° turn predicts values of 21.19 Nm, 16.26 Nm, and 11.23 Nm respectively.

### ***Quetzalcoatlus northropi***

At a velocity of only 10 ms this model produces a drag force of 0.0956 N when the skull is orientated into the flow, steadily rising to 1.62 N after a 60° turn of the head; making the forces acting on this model, relative to others, rather low. Side force at 0° yaw (10 ms) is 0.0617, increasing up to 1.0035 at an angle of attack of 60°, while roll, pitch and yaw torques start at 0.0132 Nm, 0.0257 Nm, 0.0157 Nm respectively (0°, 10 ms) and increase to 0.4108 Nm, 0.3160 Nm, and 0.5039 Nm following the maximum yaw of the head. If the forces are scaled up to an adult sized *Quetzalcoatlus* from the

relationship  $D = CDpv^2A$  where the reference length is now 1.98 m, then the drag acting on the skull at 10 ms and 20 ms with zero yaw is estimated to have been only 1.24 N and 4.97 N respectively. This would have increased to 21.14 N and 84.56 N respectively following a 60° turn of the head if Reynolds Numbers did not significantly alter the results. Given the large size of the adult animal and its position with a turbulent flow regime (i.e. above the critical transition of  $Re = 10^6$ ) the accuracy of this calculation is uncertain.

| Taxon               | Force Coefficients |        |            |        |        |        |
|---------------------|--------------------|--------|------------|--------|--------|--------|
| angle of attack     | Coeff.             | Coeff. | Coeff.     | Coeff. | Coeff. | Coeff. |
| <i>Q. northropi</i> | Drag               | Lift   | Side force | Roll   | Pitch  | Yaw    |
| 0°                  | 0.05               | 0.14   | -0.03      | 0.01   | 0.01   | 0.02   |
| 20°                 | 0.14               | 0.01   | -0.35      | 0.20   | 0.02   | 0.15   |
| 40°                 | 0.5                | -0.22  | -0.68      | 0.46   | 0.07   | 0.41   |
| 60°                 | 0.86               | -0.22  | -0.53      | 0.44   | 0.17   | 0.54   |

| <i>N. gracilis</i> | Coeff. | Coeff. | Coeff.     | Coeff. | Coeff. | Coeff. |
|--------------------|--------|--------|------------|--------|--------|--------|
|                    | Drag   | Lift   | Side force | Roll   | Pitch  | Yaw    |
| 0°                 | 0.15   | 0.03   | -0.1       | 0.26   | 0.35   | 0.05   |
| 20°                | 0.37   | 0.05   | -0.66      | 1.13   | 0.98   | 0.13   |
| 40°                | 0.63   | 0.02   | -0.65      | 1.14   | 1.53   | 0.22   |
| 60°                | 1.01   | 0.09   | -0.57      | 1.04   | 2.17   | 0.26   |

| <i>T. navigans</i> | Coeff. | Coeff. | Coeff.     | Coeff. | Coeff. | Coeff. |
|--------------------|--------|--------|------------|--------|--------|--------|
|                    | Drag   | Lift   | Side force | Roll   | Pitch  | Yaw    |
| 0°                 | 0.05   | 0.05   | -0.03      | 0.08   | 0.06   | 0.04   |
| 20°                | 0.27   | -0.06  | -0.63      | 1.25   | 0.40   | 0.52   |
| 40°                | 0.58   | -0.10  | -0.59      | 1.27   | 0.98   | 0.68   |
| 60°                | 0.84   | -0.12  | -0.49      | 1.11   | 1.51   | 0.83   |

| <i>Anhanguera</i> | Coeff. | Coeff. | Coeff.     | Coeff. | Coeff. | Coeff. |
|-------------------|--------|--------|------------|--------|--------|--------|
|                   | Drag   | Lift   | Side force | Roll   | Pitch  | Yaw    |
| 0°                | 0.06   | -0.02  | 0.00       | 0.01   | 0.01   | 0.00   |
| 20°               | 0.14   | -0.39  | -0.04      | 0.19   | 0.01   | 0.32   |
| 40°               | 0.58   | -0.92  | -0.17      | 0.44   | 0.09   | 0.86   |

Table 14. - Force and torque coefficients for four pterosaur crania: *Anhanguera*, *Nyctosaurus gracilis*, *T. navigans*, *Quetzalcoatlus*, at a variety of yaw positions. A flow velocity of 10 ms was used for these calculations.

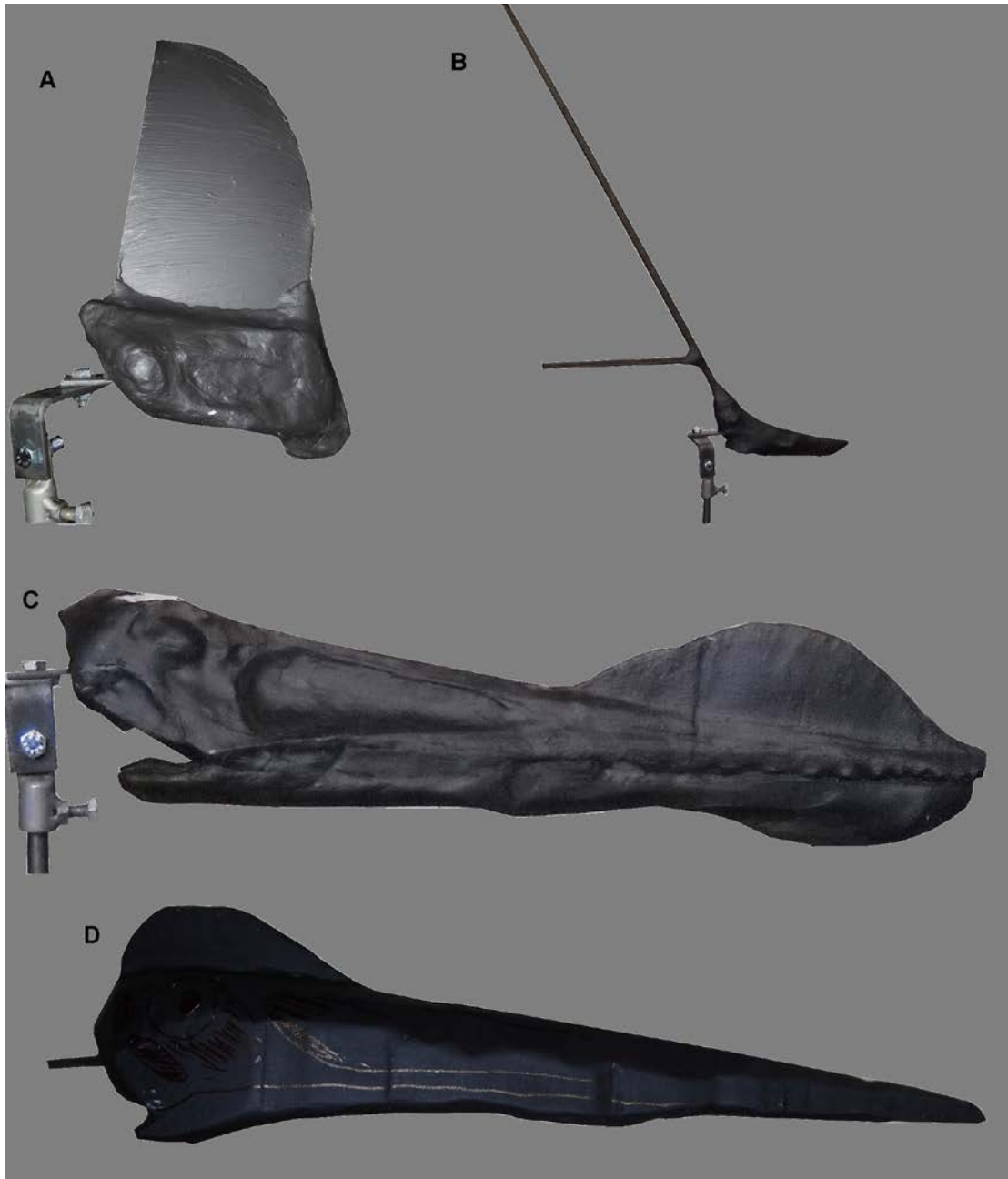


Figure 5.19 - Photographs of the cranial models of A, *Tupandactylus navigans*; B, *Nyctosaurus gracilis*; C, *Anhanguera* sp.; D, *Quetzalcoatlus northropi*.

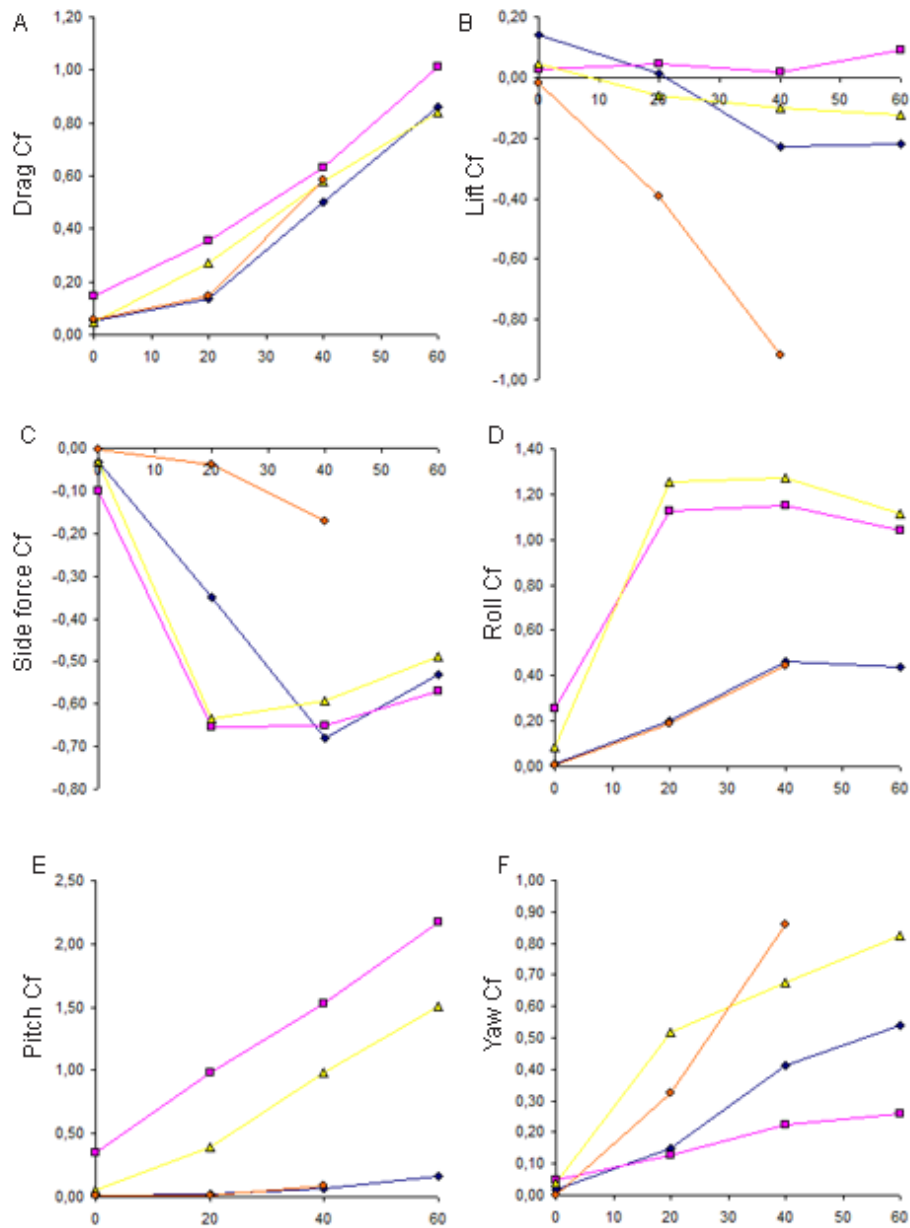


Figure 5.20. - Plots of the force and torque coefficients against the angle of attack in various head crest models where: pink squares, *Nyctosaurus gracilis*; yellow triangles, *Tupandactylus navigans*; blue circles, *Quetzalcoatlus northropi*; orange diamonds, *Anhanguera sp.*

### 5.3.3 Parasite drag and torque in relation to wing surface area.

Where wing surface area can be calculated it is useful to determine what composition of the animals total parasite drag or torques are a direct result of the head and crest.

The wing surface areas of the selected taxa were calculated from scaling mostly complete fossil specimens to the size of the test model and reconstructing the wing membrane to the ankle as has been argued for previously. For *Nyctosaurus* this is based on specimens KJ1 and KJ2 (Bennett 2003a), *Quetzalcoatlus* is based on the model of TTU P10390 (Chatterjee and Templin 2004), and *Anhanguera* is based on NSM-PV 19892 (Kellner and Tomida 2000). As no good model was available for *T. navigans* at the time of writing, no data is presented. Based on these reconstructions the total surface areas for *Anhanguera*, *Nyctosaurus*, and *Quetzalcoatlus* are 1.046 m<sup>2</sup>, 0.129 m<sup>2</sup>, and 1.357 m<sup>2</sup> respectively, the results of which are illustrated in Table 15 below.

| <b>Yaw angle</b>        | <b>0°</b>    | <b>0°</b>    | <b>20°</b>   | <b>20°</b>   | <b>40°</b>   | <b>40°</b>   | <b>60°</b>   | <b>60°</b>   |
|-------------------------|--------------|--------------|--------------|--------------|--------------|--------------|--------------|--------------|
| <b>Velocity (right)</b> | <b>10 ms</b> | <b>15 ms</b> | <b>10 ms</b> | <b>15 ms</b> | <b>10 ms</b> | <b>15 ms</b> | <b>10 ms</b> | <b>15 ms</b> |
| <b>Taxon (down)</b>     |              |              |              |              |              |              |              |              |
| <i>Anhanguera</i>       | 0.002        | 0.003        | 0.006        | 0.007        | 0.024        | 0.024        | x            | x            |
| <i>Nyctosaurus</i>      | 0.02         | 0.02         | 0.06         | 0.06         | 0.1          | 0.12         | 0.16         | 0.16         |
| <i>Quetzalcoatlus</i>   | 0.001        | x            | 0.003        | x            | 0.01         | x            | 0.02         | x            |

Table 15. - Coefficients of drag for three of the study taxa at a variety of velocities and angles of yaw. Results are non-dimensionalised by the surface area of the wing.

### 5.3.4 Discussion

The parasite drag used for the sum of the body and head in previous studies ranges from 0.005 (*Pteranodon*, Bramwell and Whitfield 1974) to 0.01254 / 0.01958 (*Pteranodon* / *Nyctosaurus*, Brower 1983), producing a rather large disparity between these analyses. If the results of the head crest modelled for this analysis are representative, then at an angle of attack and a flight speed of 0° and 10 ms respectively, the head therefore accounts for 25-40% of the total parasite drag based on Bramwell and Whitfield but only 13-16% based on that of Brower.

At higher angles of attack the coefficient of drag produced by the study models can exceed that of body and indicate the extent to which yawing the head can increase the total parasite drag of the animal. For example, the cranial model of *Anhanguera* at an



angle of attack of 40° generates a coefficient of drag of 0.024, i.e. 191% (Brower 1983) or 480% (Bramwell and Whitfield 1974) the  $CD_{par}$  attributed to the body alone.

Drag coefficients in *Nyctosaurus* (in addition to side force, roll and pitch) are unusually high when compared to the other models despite the similarities in size and smoothness/material composition. As such they are regarded as a direct result of the cranial crest. Despite being built out of compressed and relatively rigid aluminium tubing, the crest fluttered when placed in even very light velocities and must account for the increased drag force recorded for this model. Given the long length of the crest in life and its narrow, blade-like cross section, it seems probable that flutter would have been unavoidable during flight, although I acknowledge that the structural properties of bone and aluminium are certain to differ. Unfortunately, it was not possible here to separate the force components generated by that of the model from those caused by flutter. The increase these forces and torques are certainly an undesirable consequence of the crest and would have only acted to destabilise the head or reduce the performance of the aircraft.

For those pterosaurs that have a vertically orientated crest, *Nyctosaurus*, *T. navigans* (and likely taxa such as *P. sternbergi*), roll and pitch coefficients become increasingly important, the former reaching its maximum value after only a 20° yaw of the head. The rapid increase in roll coefficient partially explains the development of the tight contact between the pre- and postzygapophyses of the cervical vertebrae (Bennett 2001a), which resist torque induced rolling motions between vertebrae.

While several authors have argued in favour of a potential aerodynamic function of the cranial crest in pterosaurs, the diversity of forms between closely related taxa, allometric growth (Tomkins et al. 2010), ontogenetic variability (Martill and Naish 2006), and different sizes between putative male and female specimens (Bennett 1992, 2001a, b) together make a strong argument that the feature evolved primarily as a sexual display. The potential aerodynamic functions, however, are problematic to disprove numerically as a crest of any shape, size and position will influence the aerodynamics of the skull, regardless of their evolutionary function. Here the only thing that can be done is to examine each taxa individually and comment on the effectiveness

of the structure relative to other controls the animal had at its disposal, and whether the animal was likely to utilise them.

The first such argument concerns the head and crest being deployed as a air brake (Stein 1975) and while the crest does indeed produce additional drag as it is yawed to the side (see above), it is difficult to envisage a scenario in which a pterosaur would use its head and crest to slow its forward velocity (Elgin et al. 2008). As noted by Bennett (1992) the maximum drag would be produced if the head was turned perpendicular to the direction for travel but this would severely limit the animals depth perception and visibility of incoming obstacles, particularly during landing which would be the only time such a large increase in drag would be desired. Pterosaurs instead could have adopted several methods to slow their flight when necessary, including twisting the wings and lowering the hind limbs to produce drag from the combined surface area of the legs and uropatagium. Based on the estimated wing surface area the drag generated by the head and crest is low and remains lower than  $<0.03$  even after a  $60^\circ$  turn of the head and flat plate models indicate that the wings were undoubtedly better suited for drag generation. For *Anhanguera* the head yawed to an angle of  $20^\circ$  generates a drag coefficient equal to the lift induced drag of a wing pitched by  $6^\circ$ , while a  $40^\circ$  yaw is equivalent to a pitch of  $10^\circ$ . Likewise for *Quetzalcoatlus* a  $20^\circ$  yaw of the head generates as much drag as the lift induced component of a wing pitch to  $3-4^\circ$ , while a  $40^\circ$  yaw is equivalent to a wing pitch of  $8^\circ$ . Small adjustments of the wing could therefore easily generate drag equal to the head crests when they were turned at low angles. These examples are simplistic as they of course ignore profile drag, which itself can be an order of magnitude higher than that of lift induced drag, but still illustrate the futility of suggesting that the cranial crest may have acted as an airbrake or a means to generate additional drag. As such while in practice a small turn of the head would have lead to an increase in parasite drag and contributing to the total drag of the animal, there is no reason to suppose that this was commonly used by the animals during life.

The idea that the crest acted as counterbalance has been discussed by Elgin et al. (2008) for *Pteranodon*, but here the selection of models cannot add much to this discussion as only in *Nyctosaurus* does the crest extend caudally beyond the occipital condyle. Without a caudally situated crest the counterbalance is impossible as aerodynamic forces will only push the head further in the direction of yaw. Although Xing et al.

(2009) reconstructed *Nyctosaurus* with a large sail-like crest, this reconstruction is hypothetical and unsupported by the original description of the fossil material (Bennett 2003b). At all points of yaw in this study the aerodynamic centre of pressure, calculated by  $r = T/(F\sin\theta)$ , where  $r$  is the centre of pressure,  $T$  is torque,  $F$  is the side force and  $\theta$  is the angle of yaw, is forward of the occipital condyle and the crest does not act as a counterbalance.

A further potential role of the crest is to act as a forward rudder. Rudders do not initiate a turn in aircraft, which is instead caused by the banking of the wings, but rather assist in keeping the nose of the aircraft pointing into the direction of the turn. To maximise their effectiveness such features are located as far as possible from the aircraft's centre of gravity, which in pterosaurs is estimated to be just caudal to the glenoid fossa of the shoulder girdle (Bramwell and Whitfield 1974). As such, features attributed as rudders are found precisely where we would expect them in pterosaurs, the terminal end of the caudal series in non-pterodactyloid individuals and the head of the short tailed pterodactyloids. The magnitude of the side forces and yawing torques acting on the head crests have been presented and would certainly allowed a rudder effect to occur, however, it should be noted that only a limited number of non-pterodactyloids have been confirmed to develop a caudal vane (e.g. *Pterorhynchus*, *Rhamphorhynchus*, *Sordes*) while other long tailed non-pterodactyloid specimens instead develop a cranial crest (e.g. *Eudimorphodon*, *Raeticodactylus* (Stecher 2008), *Darwinopterus* (Lü et al. 2009). Additionally as no extant biological flier has developed an additional feature to act as a rudder there is no good reason to suppose that pterosaurs required one also.

### **5.3.3 Aerodynamics of fixed wing models**

A total of four models with fixed and immobile wings were constructed for the series of wind tunnel experiments. The taxa: *Coloborhynchus robustus* (SMNK PAL 1133, this study), *Sinopterus dongi* (Wang and Zhou 2003; private specimen *pers. obs*), and *Aurorazhdarcho micronyx* (Frey et al. 2011; Bennett 2013) were selected to provide a good cross section throughout the Pterodactyloidea with regards to mass and wing shape. Due to its small size, good preservation, and unusual wing profile the anurognathid *Anurognathus ammoni* (Bennett 2007a) was also constructed to provide comparative data for the more basal members of the lineage. As with the cranial crest each model was

mounted on the bracket inside the working section of the wind tunnel (see Section 5.2) and subjected to flow velocities of between 4 and 20 ms. As yaw and rolling moments of the model were not permitted due to the makeup of the mounting bracket pitch was the only variable that could be actively changed with each iteration of the experiment. Vital characteristics for each of these models are located in Table 16.

**Anurognathus** -The onset of stall in *Anurognathus* is relatively well marked at  $13^\circ$  followed by a slow decline of lift at higher angles of attack (Figure 5.21). As such  $CL_{max}$  of 1.16, occurs at this point at a Reynolds number of 34 250 and decreases in magnitude as Reynolds number increases further (i.e. 1.04 at  $Re = 68\ 500$ , and 0.89 at  $Re = 102\ 750$ ). The gradient of the lift slope is calculated as 0.0611 while the point of zero lift (i.e. where the slope intersects the x-axis) occurs at an angle of attack of  $-5.6^\circ$ . Consequently the angle of attack may be modified by  $5.6^\circ$  to determine the point where the slope crosses the y-axis at zero.

The highest measured ratio of L/D from this model was only 5.48 at a Reynolds number of 34 250 (Figure 5.22). Based on the polar curve this also coincided with the lowest measured value of the total drag coefficient (i.e.  $CD = 0.087$ ) at a lift coefficient of 0.48. As such total drag remains relatively high and predicts fast sinking speeds where at a Reynolds number of 68500 the horizontal velocity at the point of minimum sink is 6.72 ms and vertical sinking velocity is -1.66 ms for a heavy mass individual (i.e. 1.44 N). At maximum range speed the horizontal velocity is 7.68 ms and vertical sink - 1.72 ms. For a light mass individual (0.54 N) the horizontal velocity at the point of minimum sink is reduced to 4.12 ms and a vertical sink of -1.01 ms while the maximum range speed is 4.71 ms ( $V_s = -1.01$  ms).

The turning performance between heavy and light mass estimates are pronounced where the heavier mass configuration ( $M = 1.44$  N) has a turning radius of 26.5 m at the point of minimum sink,  $V_{st} = -1.7$  ms and a horizontal velocity of 6.77 ms. This decreases to 13.5 m at a banking angle of  $20^\circ$  ( $V_t = 6.93$  ms,  $V_{st} = -1.82$  ms) and 9.2 m at a banking angle of  $30^\circ$  ( $V_t = 7.22$ ms,  $V_{st} = -2.05$  ms). In contrast to this a light mass configuration ( $M = 0.54$  N) has a turning radius of only 10 m at the point of minimum sink ( $V_t = 4.15$  ms,  $V_{st} = -1.04$  ms), decreasing to 5 m at a  $20^\circ$  bank ( $V_t = 4.25$  ms,  $V_{st} = -1.11$  ms) and only 3.5 m at  $30^\circ$  ( $V_t = 4.42$  ms,  $V_{st} = -1.26$  ms).

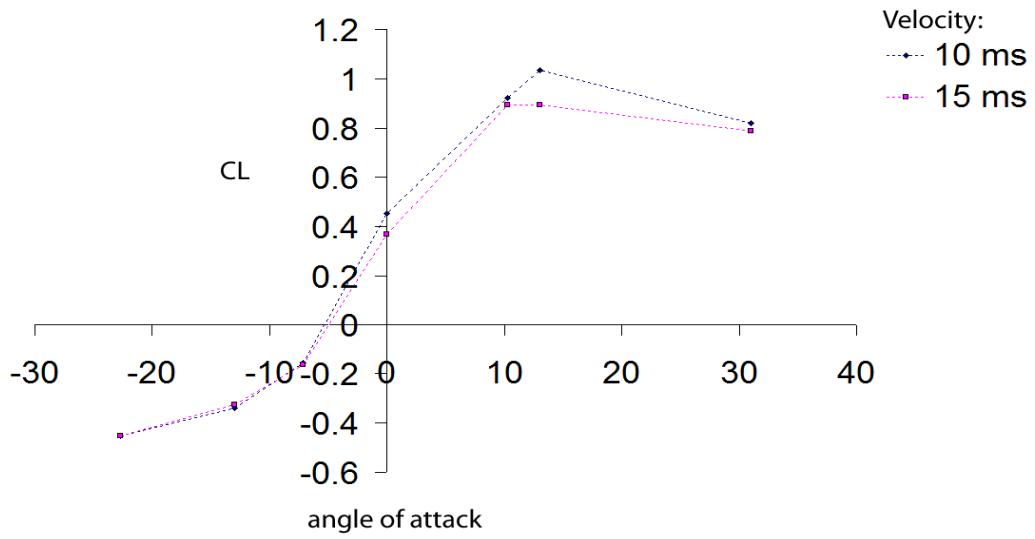


Figure 5.21. - Plot of the coefficient of lift versus angle of attack for *Anurognathus* at selected flight velocities.

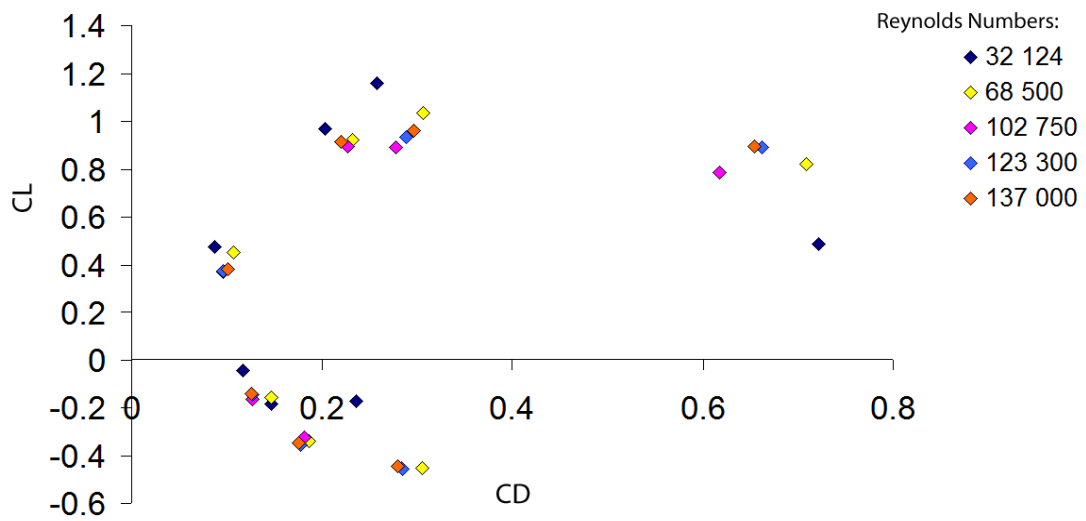


Figure 5.22. - Polar curve for *Anurognathus* across several Reynold numbers.

| Taxon                                      | Total span (b) | b <sup>2</sup> | Surface area (m <sup>2</sup> ) | Wetted surface area (m <sup>2</sup> ) | Aspect ratio | Mean aerodynamic chord (m) | Mass (kg) | Mass (N) | Wing load (N/m <sup>2</sup> ) |
|--|----------------|----------------|--------------------------------|---------------------------------------|--------------|----------------------------|-----------|----------|-------------------------------|
| <i>Anurognathus ammoni</i> - model         | 0.61           | 0.3721         | 0.061                          | 0.1525                                | 6.1          | 0.1                        | 0.15      | 1.44     | 23.66                         |
| <i>Anurognathus ammoni</i> - life size     | 0.31           | 0.093          | 0.0305                         | 0.0763                                | 6.1          | 0.5                        | 0.03      | 0.25     | 8.20                          |
| <i>Aurorazhdarcho micronyx</i> - life size | 0.59           | 0.3463         | 0.114                          | 0.2851                                | 12.1         | 0.09                       | 0.79      | 7.71     | 67.65                         |
| <i>Coloborhynchus robustus</i> – life size | 5.83           | 33.9889        | 5.2594                         | 13.148                                | 12.9         | 0.35                       | 46.52     | 456.34   | 173.53                        |
| <i>Coloborhynchus robustus</i> - model     | 1.46           | 2.1316         | 0.3287                         | 0.8218                                | 12.9         | 0.09                       | 1.36      | 13.31    | 80.96                         |
| <i>Sinopterus dongi</i> – life size        | 1.21           | 1.4641         | 0.176                          | 0.44                                  | 8.3          | 0.13                       | 0.84      | 8.28     | 47.04                         |

Table 16. – Characteristics of the fixed wing flight models and their life sized counterparts. Mass is calculated after Witton (2008a, b).

*Aurorazhdarcho* - Stall in this model occurs at an angle of attack of  $13^\circ$  (Figure 5.23). A maximum CL of 1.86 is recorded at a velocity of 5 ms while the maximum CL's prior to stall at other selected flight speeds are 1.24 (10 ms); 1.17 (15 ms); and 1.24 (20 ms). For each of these three flight velocities, corresponding to Reynolds number of 32 124 (5 ms), 64 248 (10 ms), 96 372 (15 ms), the angle of attack at which CL = 0 are  $-1.76^\circ$ ,  $-4.69^\circ$  and  $-5.24^\circ$  respectively. The maximum value of CL recorded for this model at the proposed onset of stall (and a Reynolds number of 32 124 was 1.51, decreasing to 1.24 at a Reynolds number of 64 248 and 1.17 at Re = 96 372.

Based on the polar curve of Figure 5.24, the maximum ratio of L/D is 6.3, however, at  $\alpha = 0^\circ$  and flight velocities of 6 and 7 ms, low values of drag correspond to a large jump in L/D ratios of 18.7 to 9.1 respectively. With the exception of these points the L/D curve closely matches the theoretical predictions if a K value of 5.0 is used which, as with the other fixed wing models examined here, is substantially lower than that attributed to other biological fliers.

The polar curve indicates that at a Reynolds number of 64 248 the  $CD_{min}$  is 0.111 and therefore a higher than expected sinking velocity is produced by the gliding polar. After adopting a heavy mass estimate for this animal the polar data itself returns a  $V_{ms}$  of -1.83 ms at a horizontal velocity of 10.3 ms, while a light mass animal would have had a  $V_{ms}$  of only -1.09 ms at a velocity of 6.1 ms. The presence of some data points with higher than expected  $V_{ms}$ , resulting from the combination of data collected over several days, makes it relatively difficult to fit the data to a quadratic curve. Quadratic curves based on the data presented in Figure 5.24 predict slightly larger values of  $V_{ms}$  than the polar data itself, i.e. -2.1 ms at  $V = 8$  ms, and -2.17 ms at  $V = 11$  ms. At the higher Reynolds number of 96 372 the data distribution appears to be slightly better and quadratic equations calculate the  $V_{ms}$  to be either -2.26 ms at  $V = 12$  ms (selected data points) or -2.5 ms at  $V = 2.5$  ms. The best glide ratio calculated from the glide polar is only 5.6.

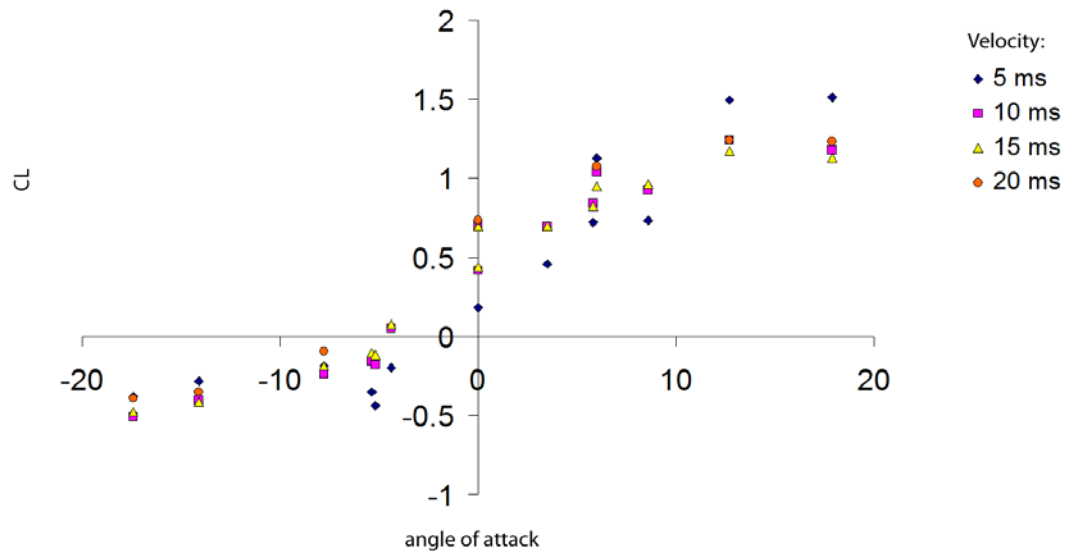


Figure 5.23 - Plot of the coefficient of lift versus angle of attack for *Aurorazhdarcho* at selected flight velocities.

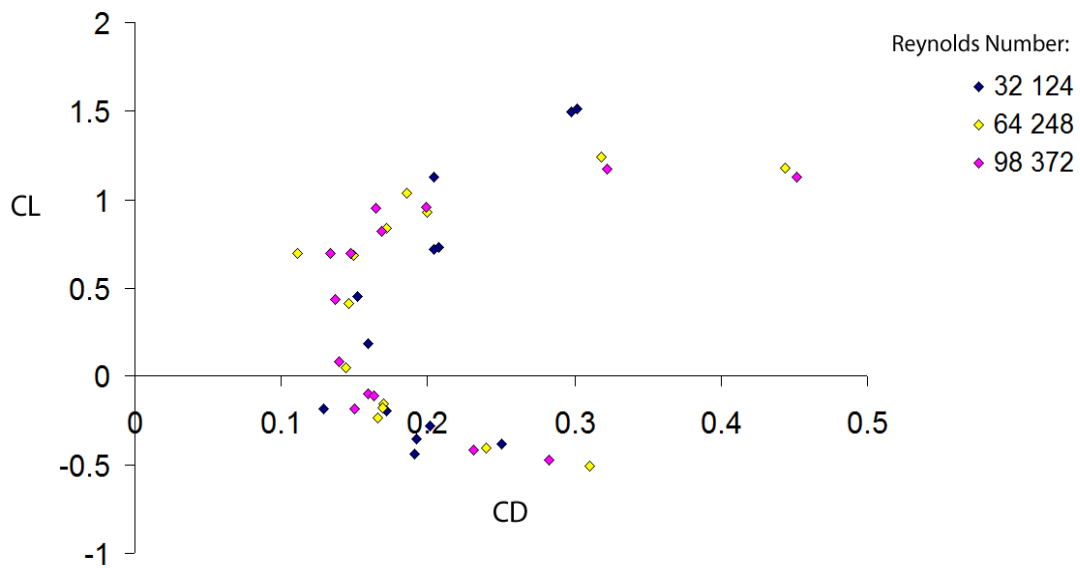


Figure 5.24 - Polar curve plot of *Aurorazhdarcho* across four Reynolds number regimes.

Data for the circling performance derived from the polar curve indicates that the turning radius decreases rapidly with increasing bank angle. This occurs at a cost of increased  $V_{ts}$ , the minimum turning radius occurring at a  $V_{ts}$  marginally higher than the minimum calculated  $V_{ms}$ . At a banking angle of only  $10^\circ$  the turning radius would have been 52.07 m; the turning radius halving in size at  $20^\circ$  (26.43 m) and  $30^\circ$  (18.08



m). Beyond this point the turning radius plateaus, decreasing from 18.08 m at a 30° bank to 9.18 m at 80°. For a light mass animal the turning radius is substantially lower, 18.44 at a banking angle of 10° and decreasing down to 3.25 m if the animal was to bank sharply to an angle of 80° (i.e. only 35.4% the radius of the heavy mass animal).

***Coloborhynchus*** - The model of *Coloborhynchus* represents an animal one quarter the size of specimen SMNK PAL 1133. The results can thus either be taken at face value to represent a juvenile/sub adult (assuming isometric scaling) or can be scaled up to the correct adult size. The Reynolds numbers of an adult individual range from 154 125 at a velocity of 5 ms, up to 616 500 at 20 ms; well below the turbulent transition of  $\sim 10^6$ . Nondimensional coefficients remain constant regardless of the desired size of the animal providing the same geometry is used and all given force coefficients are equally applicable to both the model and a life sized *Coloborhynchus*.

The CL/ $\alpha$  plot shows a slight reflex between an angle of attack of 6 - 7.3° and plateaus beyond this point, indicating the onset of stall (Figure 5.25). No decrease in the lift coefficient is noted, even at high angles of attack, indicating that the flow remained attached to the wing at all points during this experiment. The largest CL value recorded for this model was 1.22 (measured at 4 ms,  $\alpha = 6^\circ$  and  $19.4^\circ$ ). At the proposed onset of stall, i.e.  $6^\circ$ , the CL<sub>max</sub> at each Reynolds number was 1.14 (Re = 30 140), 1.06 (Re = 60 280), 0.99 (Re = 90 420), 1.05 (Re = 108 544). The angle of attack where CL = 0 is calculated as  $-9.27^\circ$  from the regression  $y = 0.0765 \alpha + 0.7095$ .

From the polar curve the CD<sub>min</sub> is 0.1 at a Reynolds number of 30 140, and corresponds to a CL value of 0.25 (Figure 5.26). Increasing the Reynolds number increases the CD<sub>min</sub> to a small degree, e.g. 0.12 at Re = 60 280. Subsequent increases in the Reynolds number increase the CD<sub>min</sub> to 0.11 (i.e. Re = 90 420, 108 544), indicating that CD<sub>min</sub> is not greatly influenced by Reynolds number over the measured range. The only other slight difference resulting from the increase in Reynolds number is that the top most curve of the C-shaped polar decreased in magnitude, following a reduction in CL.

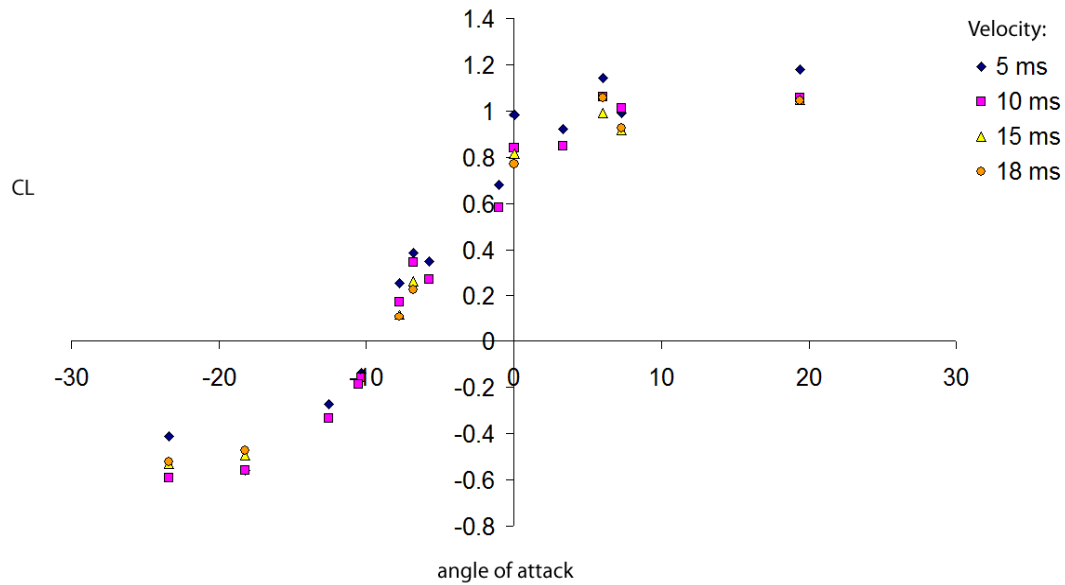


Figure 5.25 - Plot of the coefficient of lift versus angle of attack for *Coloborhynchus* at selected flight velocities.

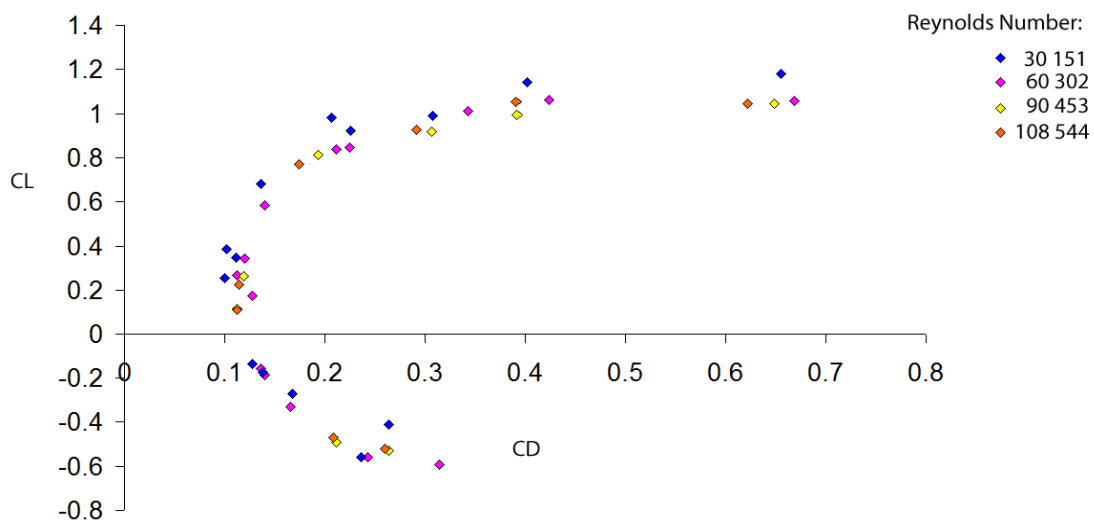


Figure 5.26 - Polar curve of lift and drag coefficients for *Coloborhynchus* across Reynolds numbers.

The  $L/D_{\max}$  for each Reynolds number regime is unusually low, ranging from a high of 4.74 at  $Re = 30\ 140$  to 4.17 at  $Re = 60\ 280$ . As a result, the gliding profile of *Coloborhynchus* is suspect ( $\epsilon = 4.06$ ), with a  $V_{ms}$  of  $-3.09$  ms occurring at a horizontal velocity of  $12.53$  ms for a heavy mass animal. A lighter mass animal has a  $V_{ms}$  of  $-1.83$  ms at a horizontal velocity of  $7.41$  ms, i.e. 59.1% that of the heavy mass estimate.

The turning radius decreases rapidly with increasing bank angle but in all cases it is associated with a very large  $V_{st}$ . For a heavy mass animal the turning radius is 73.07 m at a bank angle of only  $10^\circ$ , decreasing to 37.1 m for a banking angle of  $20^\circ$  and  $25.38^\circ$  by  $30^\circ$ . The turning radii for a light mass animal are exactly 35% of those given by the heavy mass estimation, i.e. 25.6 m at a bank angle of  $10^\circ$ .

***Sinopterus*** - The onset of stall appears to occur at around  $\alpha = 5.9^\circ$  (Figure 5.27) and is accompanied by a long flat stall profile in which no obvious decrease in lift coefficient is observed; as already noted in *Coloborhynchus*. The maximum CL recorded during the course of these experiments was 1.07, with the CL at the proposed onset of stall for each tested Reynolds number regime being 0.95 ( $Re = 44\ 525$ ), 0.88 ( $Re = 89\ 050$ ), 0.88 ( $Re = 133\ 575$  and  $178\ 100$ ). The angle of attack where  $CL = 0$  is  $-7.17^\circ$ , given by the regression line  $y = 0.0682x + 0.4893$ .

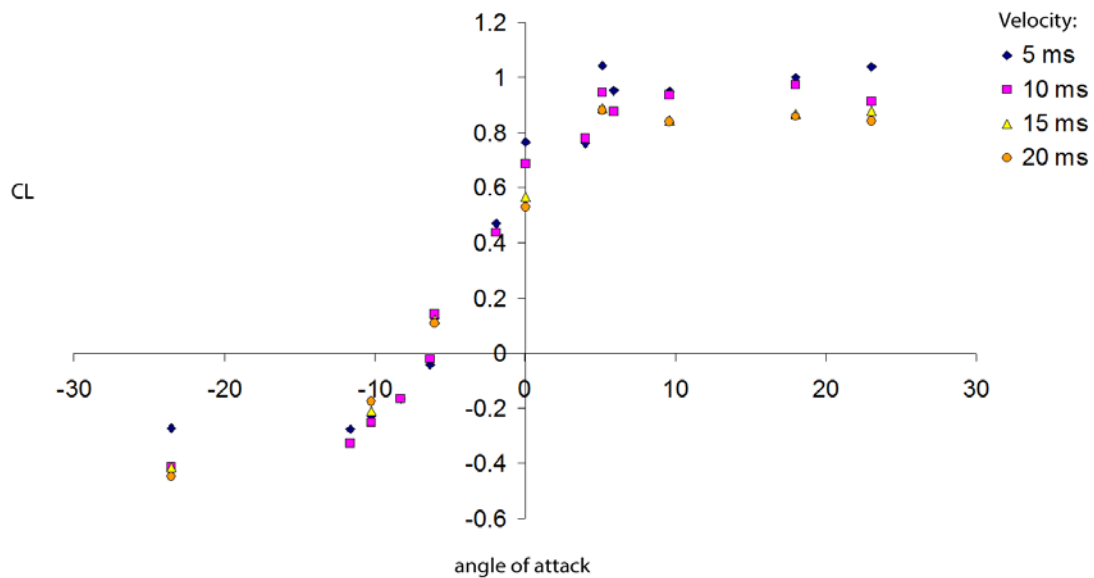


Figure 5.27 - Plot of the coefficient of lift versus angle of attack for *Sinopterus* at a variety of flight velocities.

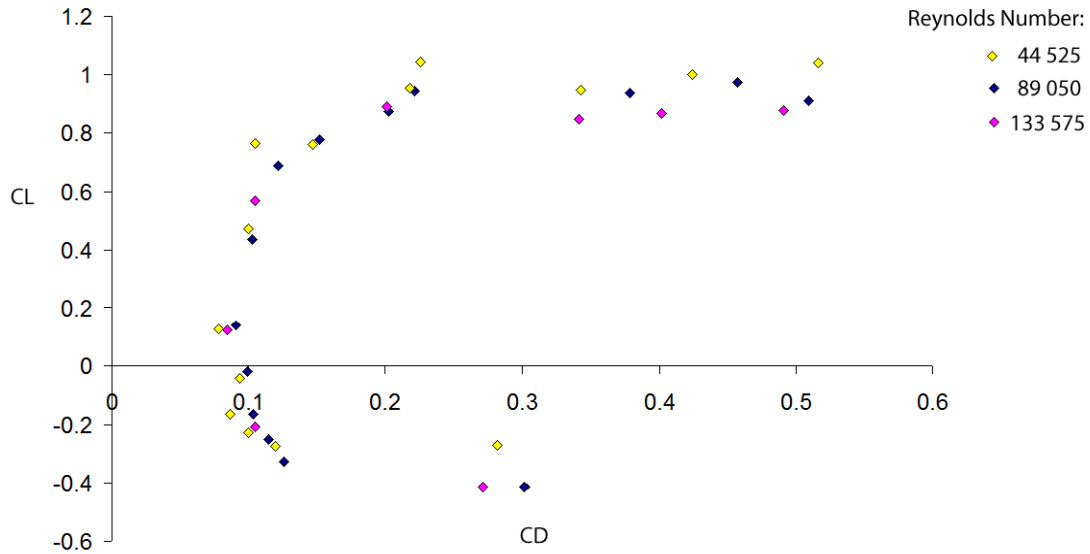


Figure 5.28 - Polar curve of lift and drag coefficients for the model *Sinopterus* across a variety of Reynolds number.

The polar plot of lift and drag coefficients records a  $CD_{min}$  of 0.078 at a Reynolds number of 44 525 (Figure 5.28). As with other models the  $CD_{min}$  does not appear to be influenced by changing Reynolds number over the recorded range, initially increasing to 0.091 by  $Re = 89\ 050$  and subsequently decreasing to 0.084 at  $Re = 133\ 575$  and 178 100. As is also observed in *Coloborhynchus* the  $CL$  is reduced at higher values of  $CD$  as Reynolds number increases.

The  $L/D_{max}$  derived from the polar curves is 7.31 (down from a maximum of 7.7 recorded at  $0^\circ$  and a flight velocity of 4 ms). At higher Reynolds numbers this value is slightly lower i.e. 5.422 ( $Re = 133\ 575$ ), 5.376 ( $Re = 178\ 100$ ). As noted in other fixed wing models the low  $L/D$  ratios result in a poorer than expected gliding performance ( $\epsilon_{max} = 5.71$ ) where the minimum sink speed for a heavy mass animal is calculated as -1.84 ms, corresponding to a horizontal flight velocity of 10.54 ms. A light mass model has a  $V_{ms}$  of -1.1 ms at a horizontal velocity of 6.27 ms, i.e. 59.5% that of the heavy mass animal.

Using a heavy mass estimate the turning radius is 47.47 m at a bank angle of only  $10^\circ$ , decreasing to 24.10 m for a banking angle of  $20^\circ$  and 16.02° by  $30^\circ$ . The turning radii for a light mass animal are 35.4% those given by the heavy mass estimation, i.e. 16.35 m ( $10^\circ$ ), 8.3 m ( $20^\circ$ ), 5.68 m ( $30^\circ$ ).

### 5.3.4 Discussion

All the studied models show the expected linear increase of lift with angle of attack prior to stall, however, despite differences in wing profile and aspect ratios there is little to distinguish between the  $CL/\alpha$  gradient of the individual models; where *Anurognathus* = 0.0611, *Aurorazhdarcho* = 0.0845, *Coloborhynchus* = 0.0765, *Sinopterus* = 0.0682 (Figure 5.29). While the lift coefficients fall within the low end of those known for biological fliers, the lift slope gradients are only around half as large as those calculated for *Rhamphorhynchus* (0.11) by Klaus (2008). *Coloborhynchus* and *Aurorazhdarcho* produce the steepest lift gradients as a result of their higher aspect ratio wings although these are not as distinct from the other models as might have been expected. The onset of stall in all models is confusing and is identified by a plateau in the  $CL/\alpha$  curve suggesting that the flow remained attached to the wings for a large range of  $\alpha$  after the stall point had been passed. Although higher aspect ratio wings should be expected to stall first the indistinct range of lift slope gradients reported above suggested that a typical stall profile was unlikely to have been produced. The onset of stall occurs first in *Sinopterus*, which has an aspect ratio of 8.32, at an angle of attack of  $13^\circ$ , followed by *Anurognathus* ( $15.8-18.6^\circ$ , AR = 6.1), *Coloborhynchus* ( $15.3 - 16.5^\circ$ , AR = 13), and finally *Aurorazhdarcho* at  $\alpha = 17.4^\circ$  (AR = 14.84). Note that each of these angles have been modified where  $\alpha = 0^\circ$  is taken as the position where  $CL = 0$ , i.e. the point where no lift occurs. The maximum lift coefficients recorded from these studies (Table 17) are slightly lower than those known from similarly thin airfoils e.g. Eiffel 13 ( $CL_{max} = 1.2$ ), Göttingen 265 (1.6), Göttingen 464 (1.6), Göttingen 400 (1.1), suggesting that the models are likely to slightly underestimate the amount of lift generated by the pterosaurian wing.

| <b>Taxon</b>          | <b><math>CL_{max}</math></b> |
|-----------------------|------------------------------|
| <i>Anurognathus</i>   | 1.03                         |
| <i>Aurorazhdarcho</i> | 1.51                         |
| <i>Coloborhynchus</i> | 1.14                         |
| <i>Sinopterus</i>     | 0.95                         |

Table 17. -  $CL_{max}$  for the study taxa taken from the onset of stall.

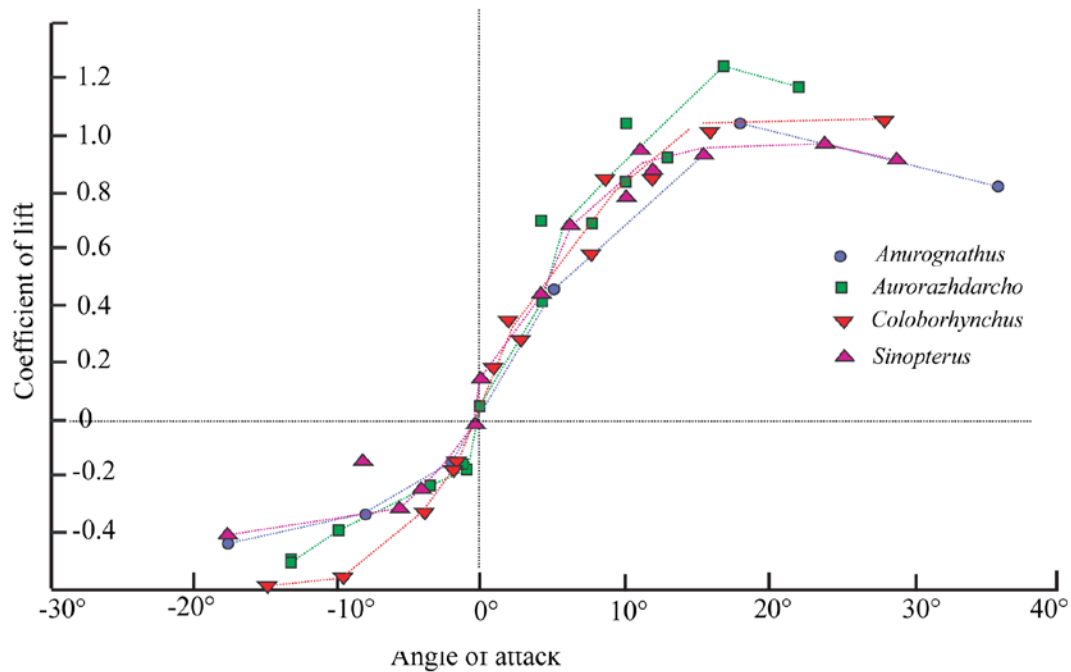


Figure 5.29. - Comparison of the CL and angle of attack for each of the four study taxa.

The lift data described above is lower than expected and at all times is coupled with abnormally high values of  $CD_{total}$ , which reach a minimum of about 0.1 for all models. As a result of the low lift slope gradient, combined with a very high  $CD_{total}$ , a low range of L/D ratio is observed, and in turn produces high values of  $V_{ms}$  even when light mass estimates are substituted into the equations (see Table 18). The values of  $V_{ms}$  illustrated below exceed those calculated for the majority extant birds and bats when a heavy mass estimation is used (e.g. Pennycuick 1968, 1971; Tucker and Parrott 1970; Norberg et al. 2000). As such the polar plots for the model pterosaurs are intermediate between those known from most other biological fliers and those with substantially poorer glide ratios e.g. poor performance gliders ( $V_{ms} = 2.32$  ms, McMasters 1794), *Columba livia* ( $V_{ms} = 2.67$  ms, Pennycuick 1968; McMasters 1974). Using a light mass estimation the values remain high but are comparable to those given to some birds and bats, i.e. *Coragyps atratus*, Black vulture ( $V_{ms} = 1.1$  ms, Tucker and Parrott 1970); *Fulmarus glacialis*, Fulmar petrel ( $V_{ms} = 1.24$  ms, Pennycuick 1960); *Rousettus aegyptiacus*, Dog-faced bat (1.17 ms, Pennycuick 1971).

Despite the problematic values of  $V_{ms}$  the horizontal velocity is not derived from the L/D ratio, instead being primarily a product of mass and lift coefficient:

Eq. 36. 
$$V_{ms} = \sqrt{(2Mg)/(\rho CLS)}$$

As such the horizontal velocity is likely to be close to the true value although the slightly lower than expected maximums as noted above lead me to believe that the CL of the pterosaurian wing would have been slightly higher, leading to a slight decrease in horizontal velocity.

| Taxon                 | L/D  | Heavy Mass |                           | Light Mass |                           |
|-----------------------|------|------------|---------------------------|------------|---------------------------|
|                       |      | V (ms)     | V <sub>minsink</sub> (ms) | V (ms)     | V <sub>minsink</sub> (ms) |
| <i>Anurognathus</i>   | 9.97 | 5.65       | -1.39                     | 3.50       | -0.86                     |
| <i>Aurorazhdarcho</i> | 5.58 | 10.30      | -1.83                     | 6.13       | -1.09                     |
| <i>Coloborhynchus</i> | 3.98 | 12.53      | -3.09                     | 7.41       | -1.83                     |
| <i>Sinopterus</i>     | 5.65 | 10.54      | -1.85                     | 6.27       | -1.10                     |

Table 18. - Minimum sinking velocity ( $V_{minsink}$ ) for each of the studied pterosaur taxa along with their corresponding horizontal flight speed and L/D ratio.

An attempt to understand the unusually high values of  $CD_{total}$  was made using the fixed wing, and body cast models of *Aurorazhdarcho* and comparing these against estimates from flat plate models (see subsequent sections). Flat plate models for a range of velocities (4-20 ms,  $Re = 38\ 548 - 128\ 496$ ) suggest a  $CD_{par}$  of between 0.015 – 0.02. While the body model by itself approaches a  $CD_{par}$  of close to zero when the body is oriented parallel to the flow the complete model, when orientated in the same way, returns a  $CD_{total}$  of 0.11 ( $Re = 64\ 248$ ), indicating that a significant portion of the total drag is due to the configuration of the wings, and the interaction of flow between the wings and body. This is further supported by the relatively low values of CL returned from all of the study models (Table 17), coupled with high values of drag which suggests that the curved wing profile and leading edge are unrepresentative of the living animals. A further breakdown of the individual components of drag however is not possible at this point in time but it indicates that

further investigation is required the exact problem with the wing configuration of these models. In an attempt to do this, a further experiment was devised using more complex jointed models onto which membranous flight surfaces of different aero elastic properties could be attached. Although a study into pterosaurian joint mechanics and several working models were completed, experiment were limited due to a lack of cooperation with supporting institutions, and eventually abandoned due to time constraints. As such wind tunnel modelling of the full model models is not satisfactorily resolved and results of the latter experiments are presented as part of the Appendix rather than within this chapter.

### **5.3.5 Summary of experimental results**

The body drag component for the small pterodactylid *Aurorazhdarcho micronyx* (Frey et al. 2011) is found to closely approach zero at very low angles of attack, and as such most closely resembles values of 0.005, proposed by Bramwell and Whitfield (1974) for *Pteranodon*. Accounting for a small degree of forward pitch that would have inevitably occurred during gliding flight,  $CD_{par}$  is found to have reached a maximum of 0.013 – 0.016 in this taxon, supporting those coefficients presented by some workers such as Brower (1982), who proposed figures of 0.013 and 0.02 for *Pteranodon* and *Nyctosaurus* respectively, Tucker and Parrott (1970) and Pennycuick et al. (1988) who respectively supported figures of 0.0132 and  $< 0.01$  for an albatross. Only at high angles of pitch,  $> 10^\circ$ , do  $CD_{par}$  values approach those proposed for several other extant birds (e.g. Pennycuick 1988; Tucker 2000; Hendenström and Liecti 2001) and a range of unpolished models or carcasses (Pennycuick 1988; Tucker 2000). In contrast to this a significant higher figure of 0.02-0.022 is recorded for the much larger model of *Coloborhynchus robustus*, although this figure is likely the result of a relatively deep sternum and a large crested skull.

Yawing moments of the head in all study taxa lead to a significant increase in drag, which can exceed that of the total  $CD_{par}$  in a horizontal orientation (with the head increasing the parasite drag of the animal by 20 – 91% through a  $40^\circ$  turn), but still remains minor compared to that generated by the wings; suggesting that, in addition to biological/behavioural arguments (e.g. Bennett 1993), its use as an air brake cannot be supported. Further aerodynamically useful functions such as a counterbalance are



also dismissed as the aerodynamic centre of pressure in all studied forms lies cranial to the occipital condyle during yaw, indicating that yaw can only act to destabilise the head. The only studies supporting this function rely on incorrect or hypothetical (and unproven) cranial reconstructions of the pterodactyloid *Nyctosaurus* (Xing et al. 2009). My own cranial models of *Nyctosaurus* indicate that the presence of the highly elongate crest contribute significantly to rolling torques and produced a  $CD_{par}$  that equalled the entire body model of *C. robustus* (i.e. 0.02), rising up to 0.16 following a  $60^\circ$  yaw of the head.

With regards to the fixed wing models the configuration and make up of the wings gives very poor aerodynamic results and making any firm conclusions from this series of experiments suspect. The high drag to lift ratios mean that the information presented above must represent the “worst” performance available to each taxon and vertical sinking velocity would be markedly reduced for the actual animal itself. As such the subsequent sections focusing on mathematical and theoretical simulations are regarded as being more representative.

## **5.4 Theoretical simulations**

### **5.4.1 Flat plate theoretical performance**

Independent of the wind tunnel data covered in the previous section, lift acting over the total surface of the wing may be taken as being equal to that of the animal's mass times the gravitational acceleration (i.e. 9.81 ms), representing the minimum force required to support the animal in horizontal flight. Alternately a maximum lift coefficient of 1.2 – 1.4, which appears appropriate for bird-like wing sections and is slightly larger than the  $CL_{max}$  recorded for the fixed wing wind tunnel models, can be adopted for a pterosaurian configurations.

An additional method of calculating the forces acting on a wing section is to determine the parasitic drag through the calculation of the “equivalent parasitic area” (Perkins and Hage 1950). Here the steps laid out in Tucker and Parrott (1970) are followed where the area can be “thought as the wetted area of a hypothetical object with the same parasite drag as the total aircraft, but with a parasitic drag coefficient ( $CD_{par}$ ), arbitrarily assigned to 1.0,” and the relationship written as:

$$\text{Eq. 37.} \quad 0.5\rho CD_{par1} * f * v^2 = 0.5\rho CD_{par2} * S_w * v^2$$

Here  $CD_{par1}$  is equal to the parasitic drag coefficient of the hypothetical object (i.e. = 1.0),  $CD_{par2}$  is the parasitic drag coefficient of the pterosaur in question, while  $S_w$  is its wetted surface area.

Modification of Eq. 37 is advantageous whereby it allows a comparison of aircraft at a wide range of Reynolds numbers, with  $CD_{par}$  being given as the parasitic drag coefficient of a thin, flat plate, orientated parallel to the wind flow and with a turbulent boundary layer rather ( $C_f$ ). Here the turbulent boundary layer is calculated as a function of Reynolds number, where:

$$\text{Eq. 38.} \quad C_f = 0.455(\log_{10} Re)^{-2.58}$$

This is substituted in place of  $CD_{par1}$  in Equation 37 which, after cancellations and rearrangements, gives:

Eq. 39.  $S_w CD_{par}/C_f = K S_w = f,$

where  $f$  is now the wetted area of the flat plate with the same drag as the aircraft in question and  $K$  is the ratio of the parasitic drag coefficient of the aircraft to that of the plate at an appropriate  $Re$  number.  $K$  values that have been obtained for other aircraft are shown in Table 19 Very low values of  $K$  appear to be reserved for engineered aircraft while a range of values are observed for the full range of biological fliers.

| Aircraft         | K   |
|------------------|-----|
| Falcon           | 2.4 |
| Vulture          | 2.2 |
| Gull             | 3.5 |
| Fulmar           | 4.1 |
| Pigeon           | 4.3 |
| Astro-mite model | 1.8 |
| SHK sailplane    | 0.7 |

Table 19. -  $K$ -values for various birds and man-made aircraft (Tucker and Parrott 1970).

Tucker and Parrott (1970) used a  $K$  value of 2.2 in their study of falcon flight as it was the lowest value noted for birds that they considered accurate (*contra* Raspert 1950, 1960). As  $K$  remains an unknown variable for pterosaurs a range of numbers were adopted herein. The effect of  $K$  on the predicted lift to drag ratio is illustrated in Figure 5.30 where for *Coloborhynchus*, at velocities in excess of 10 ms, the  $L/D$  ratios diverge and are highly dependant on  $K$ . At velocities below 10 ms, however, the effect appears to be negligible.

Following the selection of a satisfactory value of  $K$ , several additional variables are required to calculate theoretical drag, these being: weight, wing span, surface area, wetted surface area, chord and an appropriate air speed. The wing span is determined from fossil evidence or bone element regressions whilst surface area and chord are

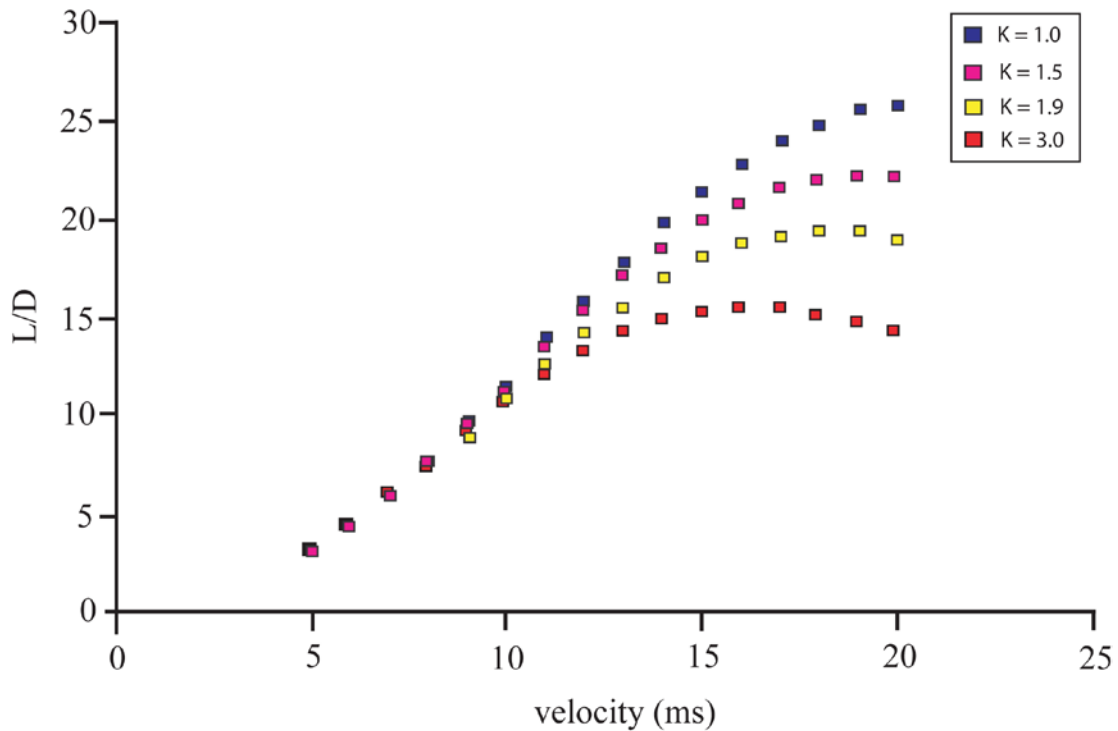


Figure 5.30. - Theoretical L/D performance for various values of K in the pterosaur *Coloborhynchus*.

taken to from an ankle-chord wing. The wetted surface area is here defined as 2.5 times the total surface area.

Selecting a small *Coloborhynchus* as a case example, these variables are measured or reconstructed as: mass (M) = 13.29N, span (b) = 1.46 m, surface area (S) = 0.16 m<sup>2</sup>, wetted surface area (S<sub>w</sub>) = 0.41 m<sup>2</sup>, chord (c) = 0.09 m, and velocity (V) = 10 ms. If lift is equal the mass of the animal times the gravitational acceleration (i.e. 13.29 N), then the induced drag is 0.47 N. The parasitic drag, calculated from  $CD_{par} = K \cdot Cf$  and including drag attributed to the wetted surface area of the wing, is substantially higher at 5.14 N. Total drag can thus be defined as the sum of the calculated induced drag and the parasite drag, written as:

$$\text{Eq. 40.} \quad D = (2L^2)/(\pi\rho(MVb)^2) + (\rho CD_{par}S_w v^2)/2$$

An estimation of the L/D ratio in an aircraft, knowing only the air speed, K, wing area, wing span and body mass, is subsequently written as:

Eq. 41. 
$$L/D = 1.67W(Vb)^2/W^2 + 2.48 * C_{D_{par}} * S * b^2 V^4$$

As induced drag is high at low speeds and decreases with increasing velocity, while parasitic drag is high at fast speeds, a U-shaped curve is produced to show that total drag is high at both fast and slow speeds. The lowest point of the curve, lying somewhere between the fast and slow maximums, represents the velocity at which drag is minimised and may be calculated by setting the derivative of total drag, with respect to velocity, to zero.

Eq. 42. 
$$V = (4L^2/\pi C_{D_{par}} * S w * (\rho M b)^2)^{0.25}$$

By using this method, and assuming a K value of 2.2, the horizontal velocity at which drag is minimised in *Coloborhynchus* would have been 10.34 ms. Calculations for a range of taxa across the Pterosauria for which the above steps were subsequently repeated are illustrated in Table 20, however, any alterations to either K or the span efficiency (here set as 0.9), will have a marked effect on the presented results. Where possible specimens similar to those selected for wind tunnel experiments were used, however, *Sinopterus dongi* was substituted for *T. navigans*, as no good postcranial remains were known for this specimen prior to Eck et al. (2011).

The lift to drag ratios of the pterosaurian configurations calculated here are noteworthy in that almost all ratios exceed those calculated for birds (Table 21). *Coloborhynchus* with its large glider-like wings has the highest L/D prediction of 18, occurring at a horizontal speed of 18 ms (heavy mass after Witton 2008a, b), and compares well with that of a wandering albatross (*Diomedea exulans*) whose own estimated L/D<sub>max</sub> is around 20. The velocity at which minimum drag occurs is calculated as 15.7 ms. The lowest L/D<sub>max</sub> found among the study taxa belongs to that of *Anurognathus* with a value of 8.4 and corresponds to a flight speed of only 5 ms. Table 22 presents the results of these calculations in full.

| <b>Taxon</b>                         | <b>L/D<sub>max</sub></b> | <b>Velocity (L/D<sub>max</sub>)</b> | <b>Velocity (CD<sub>min</sub>)</b> |
|--------------------------------------|--------------------------|-------------------------------------|------------------------------------|
| <i>Anurognathus</i>                  | 8.4                      | 5 ms                                | 5.00 ms                            |
| <i>Aurorazhdarcho</i>                | 14.24                    | 10 ms                               | 9.21 ms                            |
| <i>Coloborhynchus</i><br>(1/4 scale) | 14.85                    | 11 ms                               | 9.89 ms                            |
| <i>Coloborhynchus</i>                | 18.07                    | 18 ms                               | 15.70 ms                           |
| <i>Rhamphorhynchus</i>               | 13.39                    | 7 ms                                | 6.48 ms                            |
| <i>Sinopterus</i>                    | 11.89                    | 9 ms                                | 8.39 ms                            |

Table 20. - Theoretical L/D max for several pterosaur taxa taken from a flat plate model and the velocity at which it occurred.  $K = 2.2$ ,  $M^2 = 0.9$ . Mass estimates Witton (2008a, b).

| <b>Aircraft</b> | <b>L/D</b> |
|-----------------|------------|
| Fulmar          | 8.3        |
| Gull            | 8.7        |
| Falcon          | 10         |
| model aircraft  | 10         |
| Black vulture   | 11.6       |

Table 21. - Lift/drag ratios for selected man-made and biological fliers.

*Sinopterus*

| Velocity (ms) | Re number | CD <sub>i</sub> | CD <sub>par</sub> | V (ms) CD <sub>min</sub> | L/D   |
|---------------|-----------|-----------------|-------------------|--------------------------|-------|
| 4             | 35 620    | 0.9622          | 0.0201            | 8.39                     | 4.51  |
| 5             | 44 525    | 0.3941          | 0.0190            | 8.51                     | 6.65  |
| 6             | 53 430    | 0.1901          | 0.0182            | 8.60                     | 8.72  |
| 7             | 62 335    | 0.1026          | 0.0175            | 8.68                     | 10.39 |
| 8             | 71 240    | 0.0601          | 0.0170            | 8.75                     | 11.46 |
| 9             | 80 145    | 0.0375          | 0.0166            | 8.81                     | 11.89 |
| 10            | 89 050    | 0.0246          | 0.0162            | 8.86                     | 11.78 |
| 11            | 97 955    | 0.0168          | 0.0158            | 8.91                     | 11.31 |
| 12            | 106 860   | 0.0119          | 0.0155            | 8.95                     | 10.63 |
| 13            | 115 765   | 0.0086          | 0.0152            | 8.99                     | 9.87  |
| 14            | 124 670   | 0.0064          | 0.0150            | 9.03                     | 9.09  |
| 15            | 133 575   | 0.0049          | 0.0148            | 9.06                     | 8.34  |
| 16            | 142 480   | 0.0038          | 0.0146            | 9.09                     | 7.64  |
| 17            | 151 385   | 0.0029          | 0.0144            | 9.12                     | 7.00  |
| 18            | 160 290   | 0.0023          | 0.0142            | 9.15                     | 6.43  |
| 19            | 169 195   | 0.0019          | 0.0140            | 9.18                     | 5.91  |
| 20            | 178 100   | 0.0015          | 0.0139            | 9.20                     | 5.44  |

*Coloborhynchus - life size*

| Velocity (ms) | RE number | CD <sub>i</sub> | CD <sub>par</sub> | V (ms) CD <sub>min</sub> | L/D   |
|---------------|-----------|-----------------|-------------------|--------------------------|-------|
| 5             | 154125    | 3.4461          | 0.0143            | 15.70                    | 3.08  |
| 6             | 184950    | 1.6619          | 0.0138            | 15.86                    | 4.40  |
| 7             | 215775    | 0.8970          | 0.0133            | 15.99                    | 5.90  |
| 8             | 246600    | 0.5258          | 0.0130            | 16.10                    | 7.54  |
| 9             | 277425    | 0.3283          | 0.0126            | 16.20                    | 9.27  |
| 10            | 308250    | 0.2154          | 0.0124            | 16.29                    | 11.00 |
| 11            | 339075    | 0.1471          | 0.0121            | 16.37                    | 12.66 |
| 12            | 369900    | 0.1039          | 0.0119            | 16.44                    | 14.19 |
| 13            | 400725    | 0.0754          | 0.0117            | 16.50                    | 15.50 |
| 14            | 431550    | 0.0561          | 0.0116            | 16.56                    | 16.56 |
| 15            | 462375    | 0.0425          | 0.0114            | 16.62                    | 17.34 |
| 16            | 493200    | 0.0329          | 0.0113            | 16.67                    | 17.83 |
| 17            | 524025    | 0.0258          | 0.0111            | 16.72                    | 18.07 |
| 18            | 554850    | 0.0205          | 0.0110            | 16.77                    | 18.07 |
| 19            | 585675    | 0.0165          | 0.0109            | 16.82                    | 17.88 |
| 20            | 616500    | 0.0135          | 0.0108            | 16.86                    | 17.53 |

*Coloborhynchus* - 1/4 scale

| Velocity (ms) | RE number | CD <sub>i</sub> | CD <sub>par</sub> | V (ms) CD <sub>min</sub> | L/D   |
|---------------|-----------|-----------------|-------------------|--------------------------|-------|
| 5             | 37675     | 0.7514          | 0.0198            | 9.89                     | 6.31  |
| 6             | 45210     | 0.3624          | 0.0189            | 10.00                    | 8.60  |
| 7             | 52745     | 0.1956          | 0.0182            | 10.09                    | 10.80 |
| 8             | 60280     | 0.1147          | 0.0177            | 10.17                    | 12.64 |
| 9             | 67815     | 0.0716          | 0.0172            | 10.24                    | 13.95 |
| 10            | 75350     | 0.0470          | 0.0168            | 10.30                    | 14.67 |
| 11            | 82885     | 0.0321          | 0.0164            | 10.36                    | 14.85 |
| 12            | 90420     | 0.0226          | 0.0161            | 10.41                    | 14.60 |
| 13            | 97955     | 0.0164          | 0.0158            | 10.46                    | 14.05 |
| 14            | 105490    | 0.0122          | 0.0156            | 10.50                    | 13.33 |
| 15            | 113025    | 0.0093          | 0.0153            | 10.54                    | 12.52 |
| 16            | 120560    | 0.0072          | 0.0151            | 10.58                    | 11.69 |
| 17            | 128095    | 0.0056          | 0.0149            | 10.61                    | 10.87 |
| 18            | 135630    | 0.0045          | 0.0147            | 10.65                    | 10.09 |
| 19            | 143165    | 0.0036          | 0.0145            | 10.68                    | 9.37  |
| 20            | 150700    | 0.0029          | 0.0144            | 10.71                    | 8.70  |

*Anurognathus*

| Velocity (ms) | Re number | CD <sub>i</sub> | CD <sub>par</sub> | V (ms) CD <sub>min</sub> | L/D  |
|---------------|-----------|-----------------|-------------------|--------------------------|------|
| 4             | 13700     | 15.4955         | 0.0257            | 5.00                     | 7.30 |
| 5             | 17125     | 6.3470          | 0.0242            | 5.07                     | 8.40 |
| 6             | 20550     | 3.0608          | 0.0231            | 5.13                     | 8.31 |
| 7             | 23975     | 1.6522          | 0.0222            | 5.19                     | 7.57 |
| 8             | 27400     | 0.9685          | 0.0214            | 5.23                     | 6.63 |
| 9             | 30825     | 0.6046          | 0.0208            | 5.27                     | 5.74 |
| 10            | 34250     | 0.3967          | 0.0203            | 5.30                     | 4.95 |
| 11            | 37675     | 0.2709          | 0.0198            | 5.33                     | 4.29 |
| 12            | 41100     | 0.1913          | 0.0194            | 5.36                     | 3.74 |
| 13            | 44525     | 0.1389          | 0.0190            | 5.39                     | 3.29 |
| 14            | 47950     | 0.1033          | 0.0187            | 5.41                     | 2.91 |
| 15            | 51375     | 0.0784          | 0.0184            | 5.44                     | 2.59 |
| 16            | 54800     | 0.0605          | 0.0181            | 5.46                     | 2.32 |
| 17            | 58225     | 0.0475          | 0.0178            | 5.48                     | 2.09 |
| 18            | 61650     | 0.0378          | 0.0176            | 5.49                     | 1.89 |
| 19            | 65075     | 0.0304          | 0.0174            | 5.51                     | 1.72 |
| 20            | 68500     | 0.0248          | 0.0172            | 5.53                     | 1.58 |



*Aurorazhdarcho*

| Velocity (ms) | Re number | CD <sub>i</sub> | CD <sub>par</sub> | V (ms) CD <sub>min</sub> | L/D   |
|---------------|-----------|-----------------|-------------------|--------------------------|-------|
| 6             | 38549     | 0.2692          | 0.0197            | 9.21                     | 9.30  |
| 7             | 44974     | 0.1453          | 0.0190            | 9.29                     | 11.40 |
| 8             | 51399     | 0.0852          | 0.0184            | 9.37                     | 12.99 |
| 9             | 57823     | 0.0532          | 0.0179            | 9.43                     | 13.93 |
| 10            | 64248     | 0.0349          | 0.0174            | 9.49                     | 14.24 |
| 11            | 70673     | 0.0238          | 0.0170            | 9.54                     | 14.04 |
| 12            | 77098     | 0.0168          | 0.0167            | 9.59                     | 13.50 |
| 13            | 83523     | 0.0122          | 0.0164            | 9.64                     | 12.75 |
| 14            | 89948     | 0.0091          | 0.0161            | 9.68                     | 11.91 |
| 15            | 96372     | 0.0069          | 0.0159            | 9.71                     | 11.05 |
| 16            | 102797    | 0.0053          | 0.0156            | 9.75                     | 10.22 |
| 17            | 109222    | 0.0042          | 0.0154            | 9.78                     | 9.43  |
| 18            | 115647    | 0.0033          | 0.0152            | 9.81                     | 8.70  |
| 19            | 122072    | 0.0027          | 0.0151            | 9.84                     | 8.04  |
| 20            | 128497    | 0.0022          | 0.0149            | 9.87                     | 7.43  |

*Rhamphorhynchus*

| Velocity (ms) | Re number | CD <sub>i</sub> | CD <sub>par</sub> | V (ms) CD <sub>min</sub> | L/D   |
|---------------|-----------|-----------------|-------------------|--------------------------|-------|
| 5             | 27058     | 0.1503          | 0.0215            | 6.48                     | 10.92 |
| 6             | 32469     | 0.0725          | 0.0205            | 6.55                     | 12.76 |
| 7             | 37881     | 0.0391          | 0.0198            | 6.62                     | 13.39 |
| 8             | 43292     | 0.0229          | 0.0191            | 6.67                     | 13.05 |
| 9             | 48704     | 0.0143          | 0.0186            | 6.72                     | 12.15 |
| 10            | 54115     | 0.0094          | 0.0181            | 6.76                     | 11.04 |
| 11            | 59527     | 0.0064          | 0.0177            | 6.80                     | 9.91  |
| 12            | 64938     | 0.0045          | 0.0174            | 6.83                     | 8.85  |
| 13            | 70350     | 0.0033          | 0.0171            | 6.87                     | 7.91  |
| 14            | 75761     | 0.0024          | 0.0168            | 6.89                     | 7.08  |
| 15            | 81173     | 0.0019          | 0.0165            | 6.92                     | 6.35  |
| 16            | 86584     | 0.0014          | 0.0163            | 6.95                     | 5.73  |
| 17            | 91996     | 0.0011          | 0.0160            | 6.97                     | 5.19  |
| 18            | 97407     | 0.0009          | 0.0158            | 6.99                     | 4.71  |
| 19            | 102819    | 0.0007          | 0.0156            | 7.02                     | 4.30  |
| 20            | 108230    | 0.0006          | 0.0155            | 7.04                     | 3.94  |

Table 22. - Theoretical values of CD<sub>par</sub>, CD<sub>i</sub> based on the flat plate model for each of the study taxa. The velocity at the CD<sub>min</sub> and L/D ratios are calculated from this data.

#### **5.4.2 Performance estimates of TORNADO models**

Following the steps laid out within section 5.2 the geometric models of six taxa were loaded into the programme TORNADO and pitched in 1° increments, through an angle of attack of -5° to 20°. The force outputs were subsequently calculated and the sum of the lift induced and skin friction drag coefficients are illustrated in Figure 5.31.

Here, recorded values of CD approach close to zero on the left hand side of the curve as the simulation considers neither the parasite drag of the body nor the drag resulting from wing spar, both of which have been calculated separately. Although this study focuses on pterodactyls, the non-pterodactyl *Dorygnathus banthensis* was included for the ability to present a comparison between the major divisions of the Pterosauria.

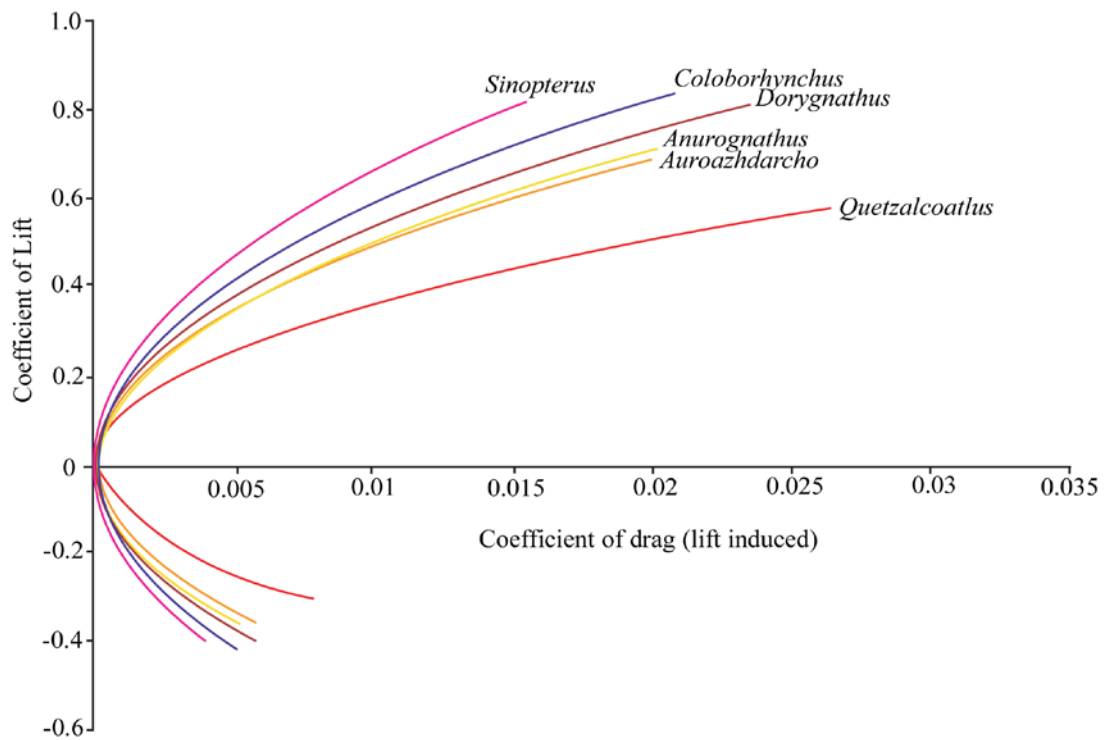


Figure 5.31. - TORNADO output of lift coefficient against the induced drag coefficient in six pterosaur taxa.

The parasite drag coefficient is unknown but was varied between the reported values of 0.005 and 0.02 inline with data collected for the body model simulation of *Aurorazhdarcho*, and supported by previous studies (e.g. Bramwell and Whitfield 1974; Brower 1982). Profile drag coefficient was adopted from Tucker (1988), whose experiments on birds suggested a relationship of  $CD_{pro} = 0.035 - 0.078CL + 0.08CL^2$ , and that of Klaus (2008), where  $CD_{pro} = 0.085 - 0.084CL + 0.0325CL^2$ . Altering these variables produced a range of aerodynamic values and polar curves which encompass the likely performance range for each geometric shape (Tables 23 and 24). Increasing the parasite drag of the body for example leads to an increase in sinking velocity along with a reduction of the horizontal flight speed and L/D ratio. With regards to

circling performance the turning radii became tighter at the expense of increased vertical sink and lower  $V_t$ .

The alteration of mass estimates between those light weight volumetric values (e.g. Chatterjee and Templin 2004) and more recent heavy mass estimates (i.e. Witton 2008a, b) had an expectedly profound effect on the gliding performance of all pterosaur geometries.

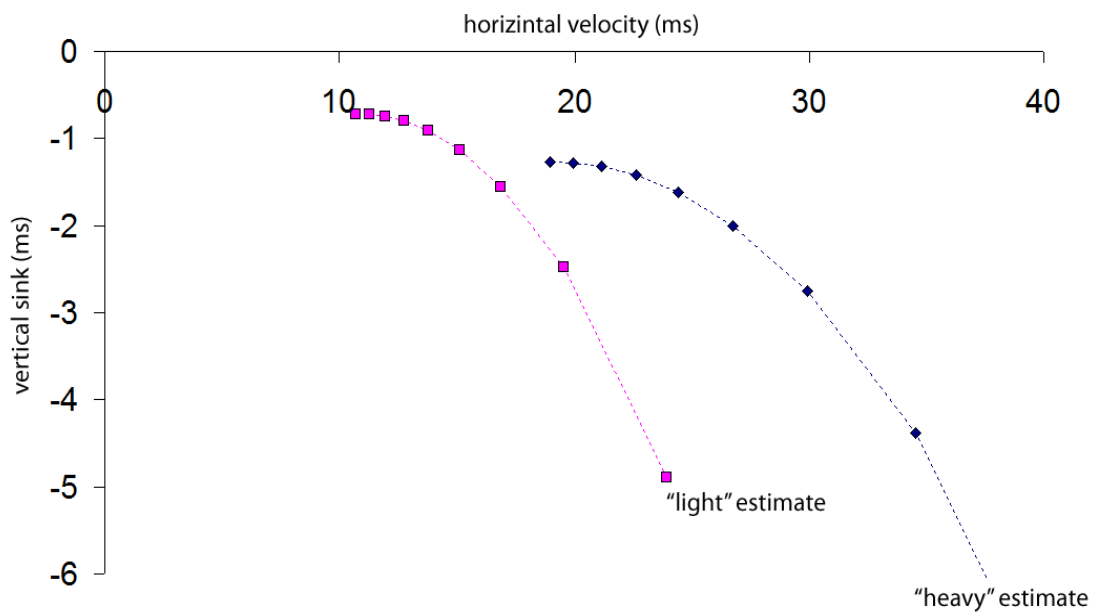


Figure 5.32. - Variation in gliding performance as an effect of mass in *Coloborhynchus*,  $CD_{par} = 0.01$ .

As illustrated by Figure 5.32 the tangent to the polar curve remains unchanged regardless of mass (being instead mostly influenced by the geometry of the wing), however, the curve is instead displaced along the line representing the glide angle; moving right for an increase in mass (correlating to both an increase in both horizontal velocity and vertical sink speed) and left for lighter estimates. Here a heavy mass estimate for *Coloborhynchus* at the point of minimum sink gives the animal a horizontal velocity of 18.93 ms and a vertical sinking speed of 1.28 ms. Employing a lighter mass estimate of 137.2 N (rather than 455.9 N, i.e. 30% the original value) reduces the minimum sinking speed to a horizontal component of 10.38 ms (i.e. 55% that of the heavier mass estimate), and the vertical sink speed to 0.7 ms. For *Quetzalcoatlus* ( $CD_{par} = 0.01$ ) a heavy mass of 2450 N returns a minimum sink speed

of 17.58 ms, coupled with a vertical sink speed of 1.75 ms, while a mass of only 686 N (i.e. 28% the original value) gives values of 9.30 ms and 0.92 ms respectively (i.e. 53% that of the heavier estimate). For both examples the glide angle remains constant between varying estimates and is only altered by a change to either geometry or  $CD_{par}$ . Polar glide curves for the remainder of the models are illustrated in Figures 5.33 – 5.44 with a summary of the data presented in Tables 23 and 24 for a variety of variables.

| <b>CD<sub>par</sub></b> | <b>0.005</b> | <b>0.01</b>              | <b>0.02</b> | <b>0.005</b> | <b>0.01</b>   | <b>0.02</b> | <b>0.005</b> | <b>0.01</b>    | <b>0.02</b> | <b>0.005</b> | <b>0.01</b>   | <b>0.02</b> | <b>0.005</b> | <b>0.01</b>    | <b>0.02</b> |
|-------------------------|--------------|--------------------------|-------------|--------------|---------------|-------------|--------------|----------------|-------------|--------------|---------------|-------------|--------------|----------------|-------------|
| <b>Taxon/Variable</b>   |              | <b>L/D<sub>max</sub></b> |             |              | <b>V (ms)</b> |             |              | <b>Vs (ms)</b> |             |              | <b>V (mr)</b> |             |              | <b>Vs (mr)</b> |             |
| <i>Anurognathus</i>     | 16.56        | 14.52                    | 11.85       | 8.84         | 5.83          | 5.84        | -0.37        | -0.41          | -0.49       | 6.53         | 6.16          | 5.84        | -0.39        | -0.42          | -0.49       |
| <i>Aurorazhdarcho</i>   | 15.85        | 13.96                    | 11.84       | 9.05         | 8.63          | 8.63        | -0.61        | -0.67          | -0.83       | 10.11        | 10.11         | 10.81       | -0.64        | -0.72          | -0.91       |
| <i>Coloborhynchus</i>   | 18.40        | 16.01                    | 12.94       | 19.95        | 21.16         | 18.13       | -1.15        | -1.32          | -1.49       | 22.6         | 21.16         | 21.16       | -1.23        | -1.32          | -1.63       |
| <i>Dorygnathus</i>      | 17.20        | 15.07                    | 12.23       | 14.51        | 15.39         | 13.13       | -0.89        | -1.02          | -1.14       | 16.46        | 15.39         | 14.51       | -0.96        | -1.02          | -1.18       |
| <i>Sinopterus</i>       | 19.63        | 16.86                    | 13.70       | 10.63        | 10.09         | 9.22        | -0.56        | -0.62          | -0.73       | 11.28        | 11.28         | 10.63       | -0.57        | -0.66          | -0.78       |
| <i>Quetzalcoatlus</i>   | 12.01        | 10.73                    | 8.99        | 17.92        | 17.08         | 15.71       | -1.57        | -1.70          | -1.92       | 20.05        | 20.04         | 18.89       | -1.67        | -1.86          | -2.09       |

| <b>CD<sub>par</sub></b> | <b>0.005</b> | <b>0.01</b>              | <b>0.02</b> | <b>0.005</b> | <b>0.01</b>   | <b>0.02</b> | <b>0.005</b> | <b>0.01</b>    | <b>0.02</b> | <b>0.005</b> | <b>0.01</b>   | <b>0.02</b> | <b>0.005</b> | <b>0.01</b>    | <b>0.02</b> |
|-------------------------|--------------|--------------------------|-------------|--------------|---------------|-------------|--------------|----------------|-------------|--------------|---------------|-------------|--------------|----------------|-------------|
| <b>Taxon/Variable</b>   |              | <b>L/D<sub>max</sub></b> |             |              | <b>V (ms)</b> |             |              | <b>Vs (ms)</b> |             |              | <b>V (mr)</b> |             |              | <b>Vs (mr)</b> |             |
| <i>Anurognathus</i>     | 16.56        | 14.52                    | 11.85       | 3.65         | 3.65          | 3.65        | -0.23        | -0.26          | -0.31       | 4.09         | 3.85          | 3.65        | -0.25        | -0.26          | -0.31       |
| <i>Aurorazhdarcho</i>   | 15.85        | 13.96                    | 11.84       | 5.40         | 5.15          | 5.15        | -0.36        | -0.40          | -0.49       | 6.04         | 6.04          | 6.46        | -0.38        | -0.43          | -0.54       |
| <i>Coloborhynchus</i>   | 18.40        | 16.01                    | 12.94       | 11.28        | 11.96         | 10.25       | -0.65        | -0.75          | -0.84       | 12.79        | 11.96         | 11.96       | -0.69        | -0.75          | -0.92       |
| <i>Dorygnathus</i>      | 17.20        | 15.07                    | 12.23       | 6.63         | 7.55          | 6.44        | -0.41        | -0.50          | -0.56       | 7.52         | 7.55          | 7.12        | -0.43        | -0.50          | -0.58       |
| <i>Sinopterus</i>       | 19.63        | 16.86                    | 13.70       | 6.34         | 6.01          | 5.49        | -0.33        | -0.37          | -0.43       | 6.72         | 6.72          | 6.33        | -0.34        | -0.39          | -0.46       |
| <i>Quetzalcoatlus</i>   | 12.01        | 10.73                    | 8.99        | 9.83         | 9.37          | 8.62        | -0.86        | -0.93          | -1.05       | 11.00        | 10.99         | 10.37       | -0.91        | -1.02          | -1.15       |

Table 23. – Horizontal velocity and minimum sink velocity for selected pterosaurs at minimum sink and maximum range speeds. The coefficient of parasite drag is altered from 0.005 – 0.02. Heavy mass estimates (top); light mass estimates (bottom). CD<sub>pro</sub> taken after Tucker (1988).

| <b>Taxon/Variable</b> | <b>Bank</b> | <b>Vt</b> | <b>Vst</b> | <b>radius</b> | <b>Vt</b> | <b>Vst</b> | <b>radius</b> |
|-----------------------|-------------|-----------|------------|---------------|-----------|------------|---------------|
| <i>Anurognathus</i>   | 10°         | 5.88      | -0.42      | 20.04         | 2.30      | -0.16      | 7.85          |
|                       | 20°         | 6.02      | -0.45      | 10.17         | 2.36      | -0.18      | 3.98          |
|                       | 30°         | 6.27      | -0.51      | 6.96          | 2.45      | -0.20      | 2.72          |
|                       | 40°         | 6.67      | -0.61      | 5.41          | 2.61      | -0.24      | 2.12          |
|                       | 50°         | 7.28      | -0.80      | 4.54          | 2.85      | -0.31      | 1.78          |
|                       | 60°         | 8.26      | -1.16      | 4.02          | 3.23      | -0.45      | 1.57          |
|                       |             |           |            |               |           |            |               |
| <i>Aurorazhdarcho</i> | 10°         | 8.69      | -0.69      | 43.73         | 4.71      | -0.37      | 15.60         |
|                       | 20°         | 8.90      | -0.74      | 22.20         | 4.82      | -0.40      | 7.92          |
|                       | 30°         | 9.27      | -0.83      | 15.19         | 5.02      | -0.45      | 5.42          |
|                       | 40°         | 9.86      | -1.00      | 11.81         | 5.33      | -0.54      | 4.21          |
|                       | 50°         | 10.76     | -1.30      | 9.91          | 5.82      | -0.70      | 3.54          |
|                       | 60°         | 12.20     | -1.90      | 8.77          | 6.60      | -1.03      | 3.13          |
|                       |             |           |            |               |           |            |               |
| <i>Coloborhynchus</i> | 10°         | 19.08     | -1.31      | 210.65        | 10.47     | -0.72      | 67.35         |
|                       | 20°         | 19.53     | -1.4       | 106.95        | 10.71     | -0.77      | 34.20         |
|                       | 30°         | 20.35     | -1.58      | 73.16         | 11.16     | -0.87      | 23.39         |
|                       | 40°         | 21.63     | -1.9       | 56.91         | 11.87     | -1.04      | 18.20         |
|                       | 50°         | 23.62     | -2.48      | 47.75         | 12.95     | -1.36      | 15.27         |
|                       | 60°         | 26.78     | -3.61      | 42.24         | 14.69     | -1.98      | 13.50         |
|                       |             |           |            |               |           |            |               |
| <i>Dorygnathus</i>    | 10°         | 13.87     | -1.00      | 111.39        | 6.80      | -0.49      | 26.80         |
|                       | 20°         | 14.20     | -1.07      | 56.55         | 6.97      | -0.53      | 13.60         |
|                       | 30°         | 14.79     | -1.21      | 38.69         | 7.26      | -0.60      | 9.31          |
|                       | 40°         | 15.73     | -1.46      | 30.09         | 7.72      | -0.72      | 7.24          |
|                       | 50°         | 17.17     | -1.90      | 25.25         | 8.42      | -0.93      | 6.07          |
|                       | 60°         | 19.47     | -2.77      | 22.34         | 9.55      | -1.36      | 5.37          |
|                       |             |           |            |               |           |            |               |
| <i>Sinopterus</i>     | 10°         | 10.17     | -0.63      | 59.83         | 6.05      | -0.38      | 21.23         |
|                       | 20°         | 10.41     | -0.68      | 30.38         | 6.19      | -0.41      | 10.78         |
|                       | 30°         | 10.84     | -0.77      | 20.78         | 6.45      | -0.46      | 7.37          |
|                       | 40°         | 11.53     | -0.93      | 16.16         | 6.86      | -0.55      | 5.74          |
|                       | 50°         | 12.59     | -1.20      | 13.56         | 7.49      | -0.72      | 4.81          |
|                       | 60°         | 14.27     | -1.75      | 12.00         | 8.49      | -1.04      | 4.26          |

cont.....

| <b>Taxon/Variable</b> | <b>Bank</b> | <b>V<sub>t</sub></b> | <b>V<sub>st</sub></b> | <b>radius</b> | <b>V<sub>t</sub></b> | <b>V<sub>st</sub></b> | <b>radius</b> |
|-----------------------|-------------|----------------------|-----------------------|---------------|----------------------|-----------------------|---------------|
| <i>Quetzalcoatlus</i> | 10°         | 17.21                | -1.74                 | 171.42        | 9.11                 | -0.92                 | 51.61         |
|                       | 20°         | 17.62                | -1.86                 | 87.04         | 9.32                 | -0.99                 | 26.20         |
|                       | 30°         | 18.35                | -2.11                 | 59.54         | 9.71                 | -1.11                 | 17.92         |
|                       | 40°         | 19.51                | -2.53                 | 46.31         | 10.33                | -1.34                 | 13.94         |
|                       | 50°         | 21.30                | -3.29                 | 38.86         | 11.27                | 1.74                  | 11.70         |
|                       | 60°         | 24.15                | -4.80                 | 34.37         | 12.78                | -2.54                 | 10.34         |

Table 24. - Circling performance in selected pterosaurs at various angles of bank. Left hand values derived from heavy mass pterosaurs (Witton 2008a, b), right hand values represent light mass estimates (Chatterjee and Templin 2004).

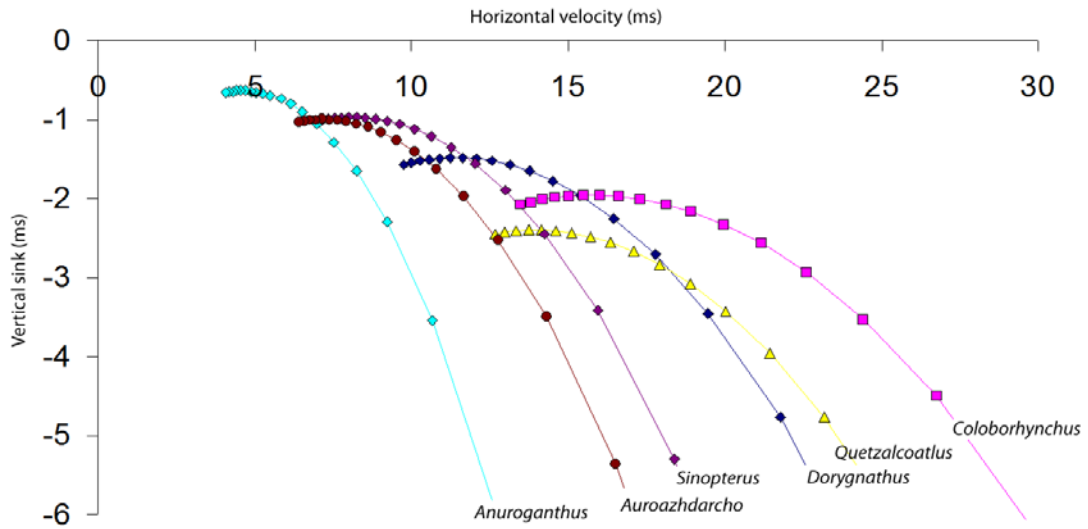


Figure 5.33. - Gliding curves for the geometric models of selected pterosaurs. The coefficient of parasite drag is reconstructed after Bramwell and Whitfield where,  $CD_{par} = 0.005$ , while mass is estimated after Witton (2008a, b).

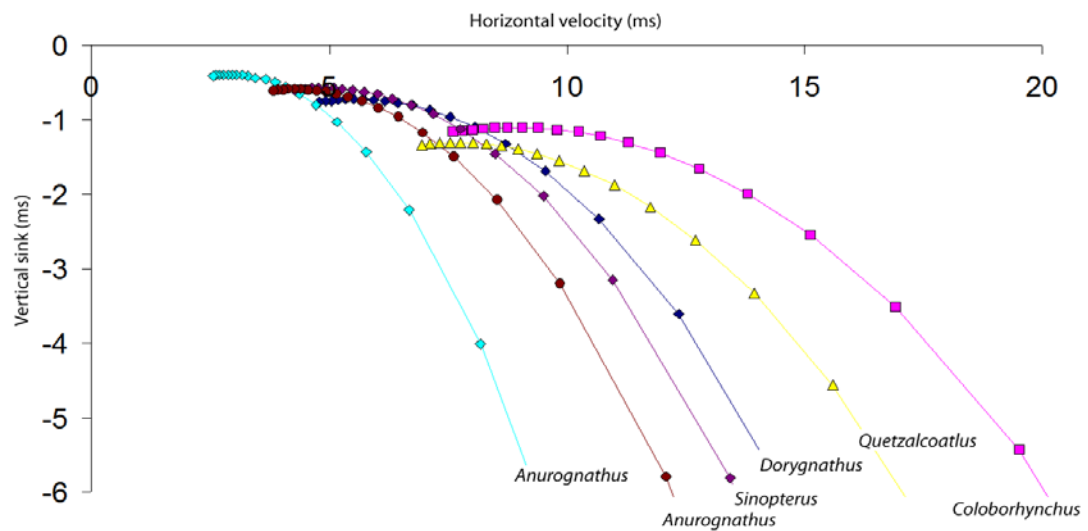


Figure 5.34 - Gliding curves for the geometric models of selected pterosaurs. The coefficient of parasite drag is reconstructed after Bramwell and Whitfield (1974) where,  $CD_{par} = 0.005$ , while mass is estimated after Chatterjee and Templin (2004).



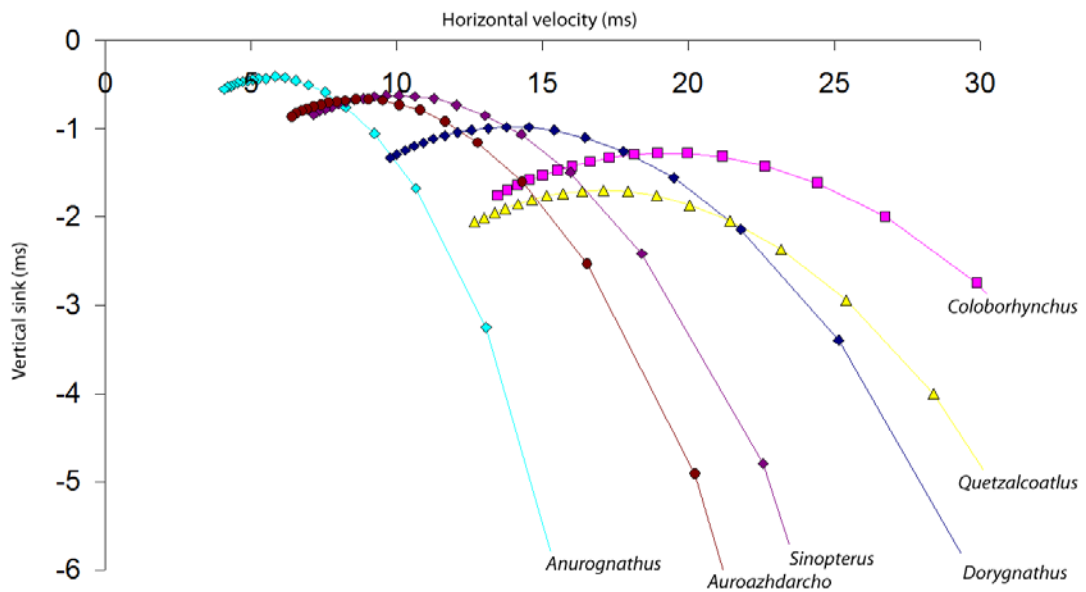


Figure 5.35. - Gliding curves for the geometric models of selected pterosaurs. The coefficient of parasite drag is set to 0.01, while mass is estimated after Witton (2008a, b).

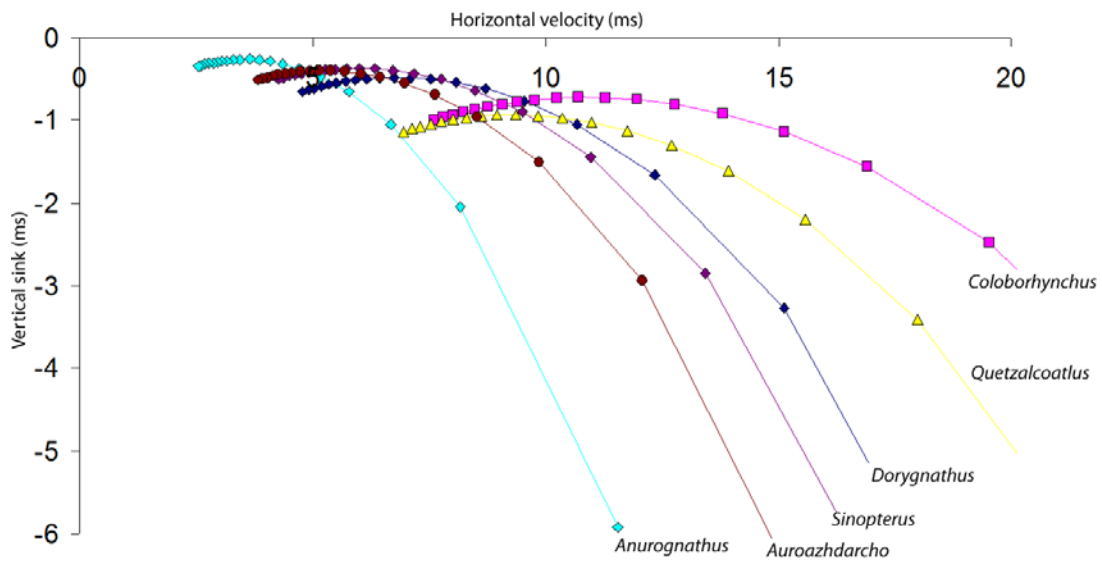


Figure 5.36. - Gliding curves for the geometric models of selected pterosaurs. The coefficient of parasite drag is set to 0.01, while mass is estimated after Chatterjee and Templin (2004).

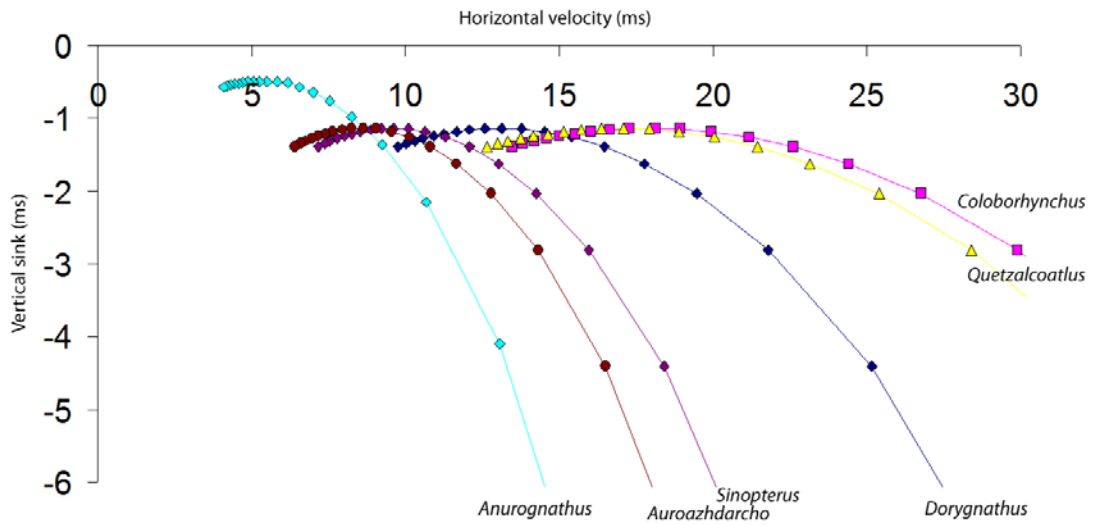


Figure 5.37 - Gliding curves for the geometric models of selected pterosaurs. The coefficient of parasite drag is set to 0.02, while mass is estimated after Witton (2008a, b).

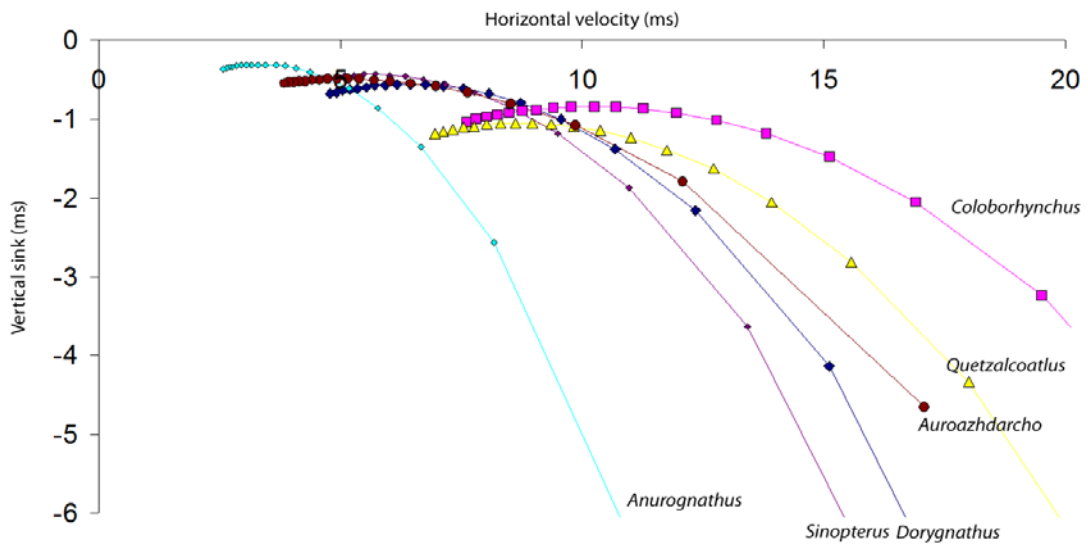


Figure 5.38. - Gliding curves for the geometric models of selected pterosaurs. The coefficient of parasite drag is set to 0.02, while mass is estimated after Chatterjee and Templin (2004).

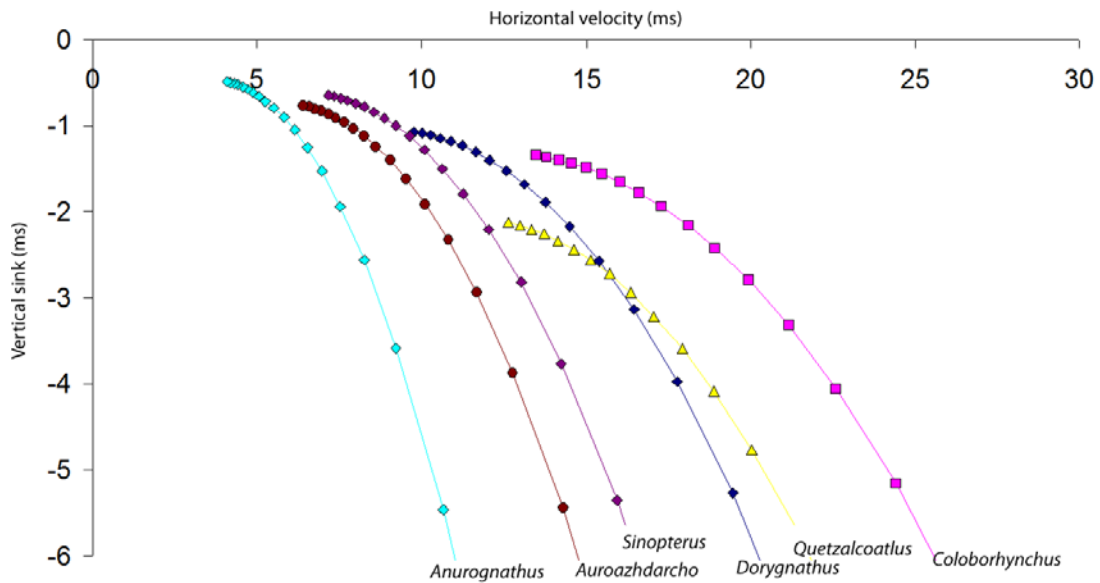


Figure 5.39. - Gliding curves for the geometric models of selected pterosaurs. The coefficient of parasite drag is reconstructed after Bramwell and Whitfield (1974) where,  $CD_{par} = 0.005$ , while mass is estimated after Witton (2008a, b).  $CD_{pro}$  is derived from the equations of Klaus (2008) based on the high aspect wings of *Rhamphorhynchus*.

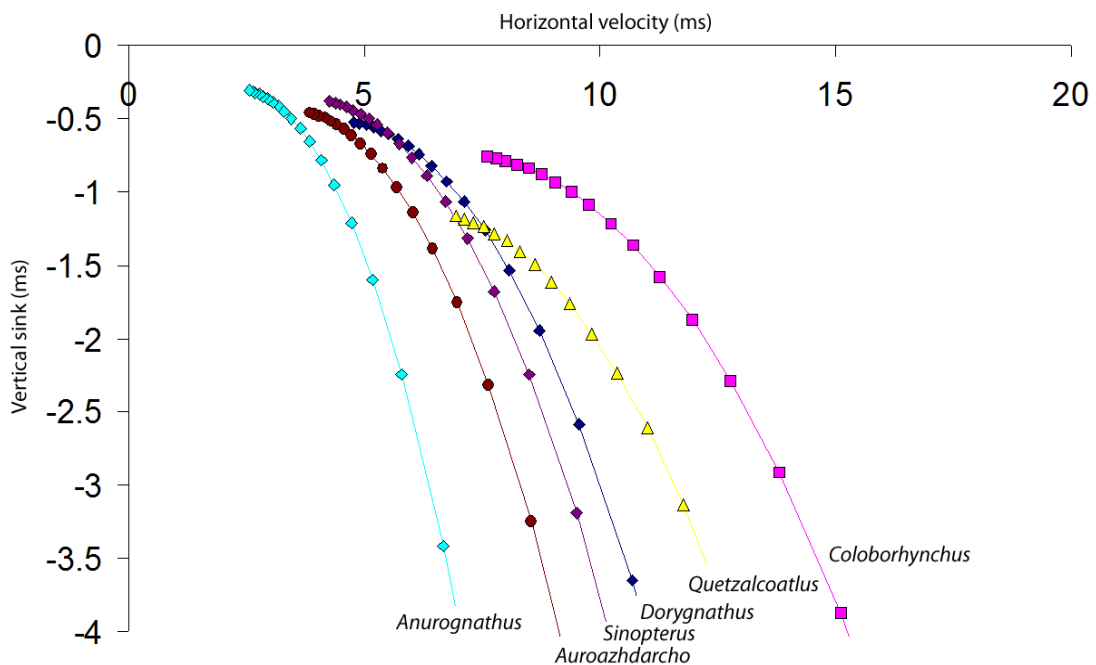


Figure 5.40. - Gliding curves for the geometric models of selected pterosaurs. The coefficient of parasite drag is reconstructed after Bramwell and Whitfield (1974) where,  $CD_{par} = 0.005$ , while mass is estimated after Chatterjee and Templin (2004).  $CD_{pro}$  is derived from the equations of Klaus (2008) based on the high aspect wings of *Rhamphorhynchus*.

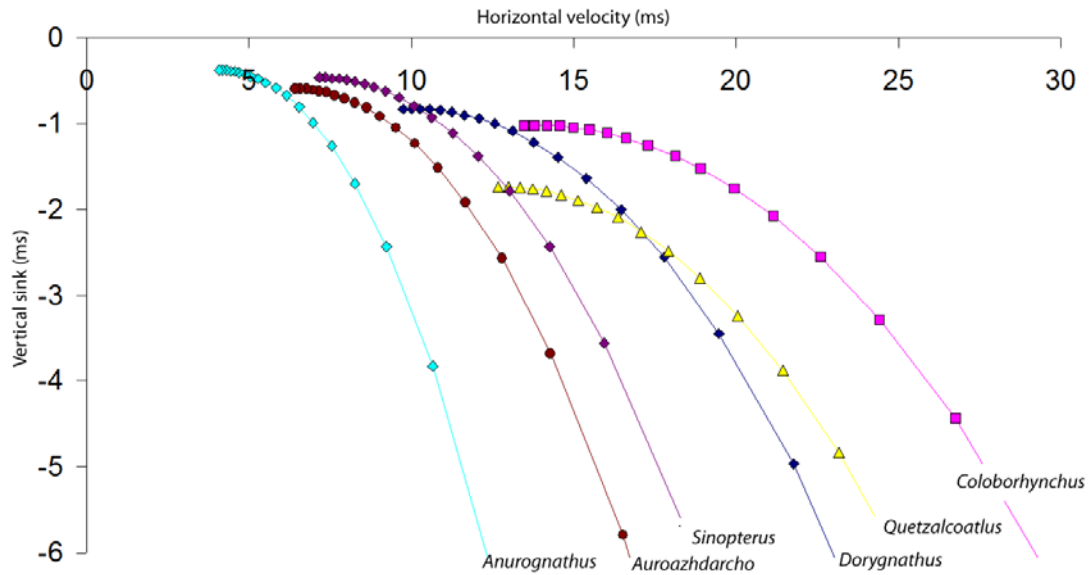


Figure 5.41. - Gliding curves for the geometric models of selected pterosaurs. The coefficient of parasite drag is set to 0.01, while mass is estimated after Witton (2008a, b).  $CD_{pro}$  is derived from the equations of Klaus (2008) based on the high aspect wings of *Rhamphorhynchus*.

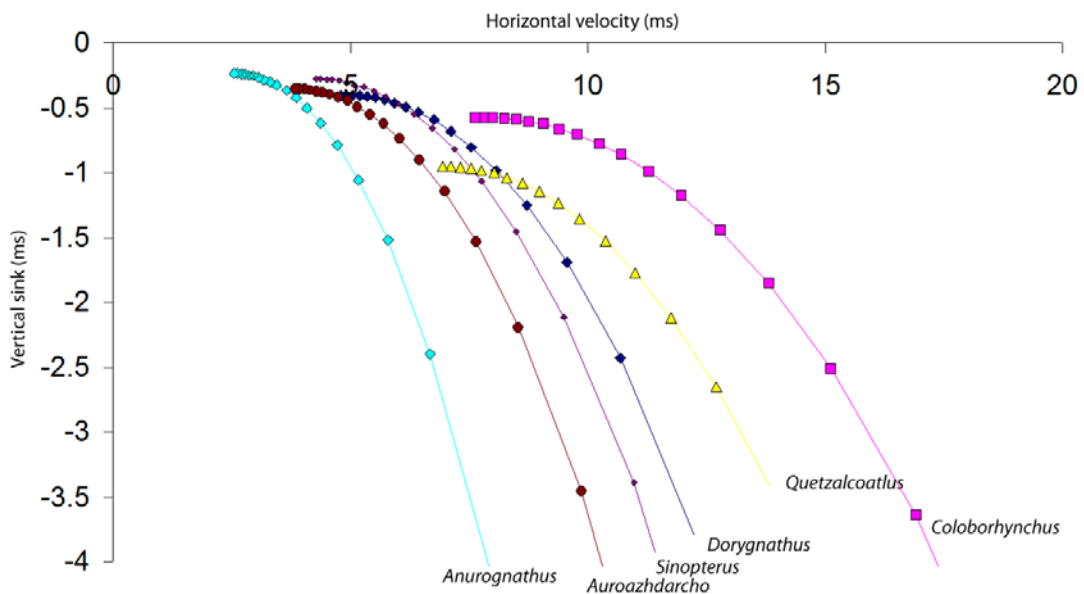


Figure 5.42. - Gliding curves for the geometric models of selected pterosaurs. The coefficient of parasite drag is set to 0.01, while mass is estimated after Chatterjee and Templin (2004).  $CD_{pro}$  is derived from the equations of Klaus (2008) based on the high aspect wings of *Rhamphorhynchus*.

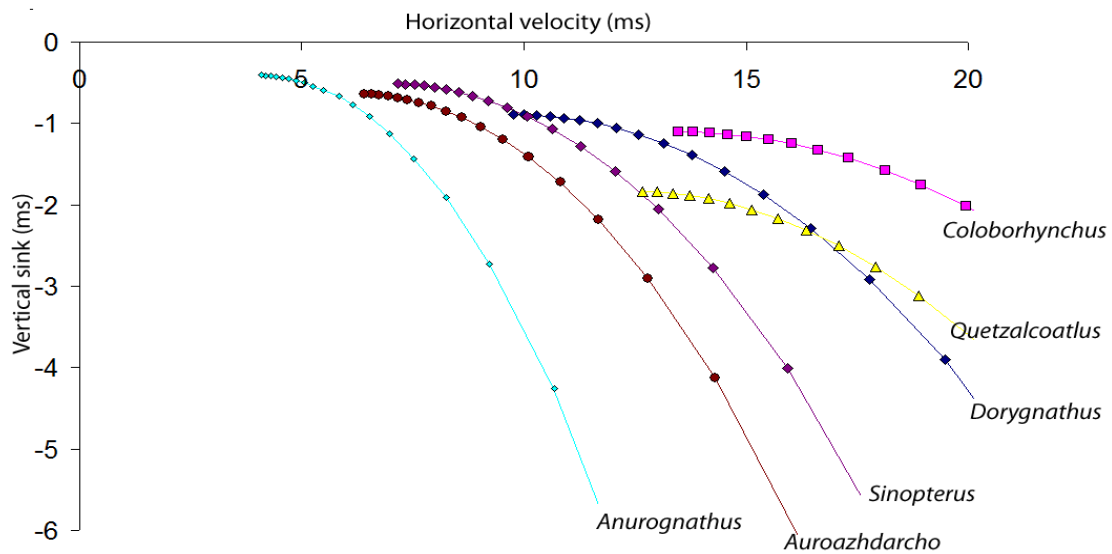


Figure 5.43. - Gliding curves for the geometric models of selected pterosaurs. The coefficient of parasite drag is set to 0.02, while mass is estimated after Witton (2008a, b).  $CD_{pro}$  is derived from the equations of Klaus (2008) based on the high aspect wings of *Rhamphorhynchus*.

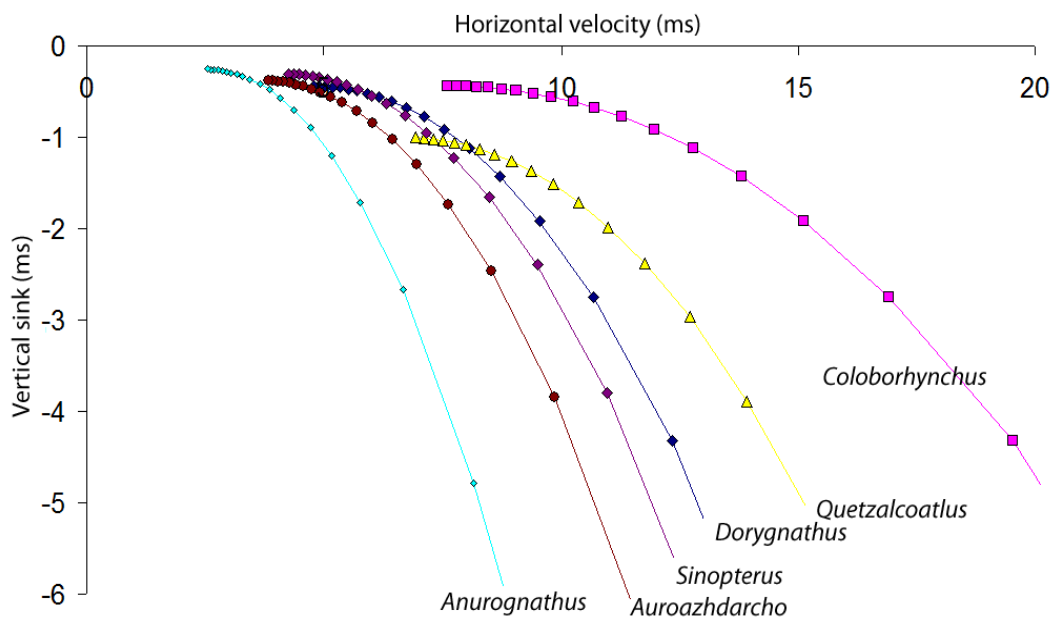


Figure 5.44. - Gliding curves for the geometric models of selected pterosaurs. The coefficient of parasite drag is set to 0.02, while mass is estimated after Chatterjee and Templin (2004).  $CD_{pro}$  is derived from the equations of Klaus (2008) based on the high aspect wings of *Rhamphorhynchus*.

| <b>Taxon</b>          | <b>gradient of<br/>tangent to polar</b> | <b>Vertical/Horizontal<br/>ratio</b> |
|-----------------------|---|--------------------------------------|
| CD = 0.005            |   |                                      |
| <i>Anurognathus</i>   | -0.06                                   | 1:16.7                               |
| <i>Aurorazhdarcho</i> | -0.06                                   | 1:15.8                               |
| <i>Coloborhynchus</i> | -0.05                                   | 1:18.4                               |
| <i>Dorygnathus</i>    | -0.06                                   | 1:17.1                               |
| <i>Sinopterus</i>     | -0.05                                   | 1:19.8                               |
| <i>Quetzalcoatlus</i> | -0.08                                   | 1:12.0                               |
| CD = 0.01             |   |                                      |
| <i>Anurognathus</i>   | -0.07                                   | 1:14.7                               |
| <i>Aurorazhdarcho</i> | -0.07                                   | 1:14.0                               |
| <i>Coloborhynchus</i> | -0.06                                   | 1:16.0                               |
| <i>Dorygnathus</i>    | -0.07                                   | 1:15.1                               |
| <i>Sinopterus</i>     | -0.06                                   | 1:17.1                               |
| <i>Quetzalcoatlus</i> | -0.09                                   | 1:10.8                               |

Table 25. - Gradient of the tangent to the gliding polar and the effect of varying the parasite drag coefficient on potential glide distance.

### **5.4.3 Estimates from previous studies**

Klaus (2008) used a geometric model of *Rhamphorhynchus* to run several simulations on pterosaur flight dynamics, trimming the wings to their optimal configuration during flight. The two components of drag calculated from this study (induced and parasite) follow the quadratic curves:

$$\text{Eq. 42} \quad CD_{\text{par}} = 0.0325CL^2 - 0.084CL + 0.085$$

$$\text{Eq. 43} \quad CD_i = 0.0250CL^2$$

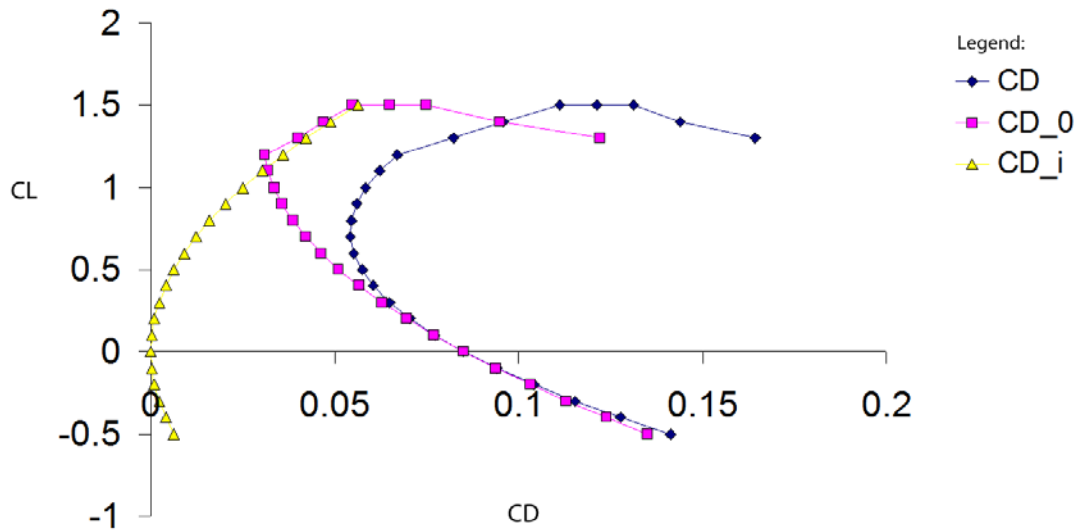


Figure 5.45. - Theoretical drag coefficients based on the above wing profile. Where  $CD$  = total drag;  $CD_0$  = parasite drag (skin friction + pressure);  $CD_i$  = lift-induced drag.

As *Coloborhynchus* also shares a similar high aspect ratio configuration, these were adopted here (Figure 5.45) where the sum of the curves gives the total drag polar and was used to recover the  $L/D$  ratio for a given coefficient of lift. The glide polar can subsequently be plotted from this by determining the  $V_s$  for any given  $CL$ :

$$\text{Eq. 44} \quad V_s = -V \cdot \text{ATAN}(1/(L/D))$$

or

$$\text{Eq. 45} \quad V_s = \sqrt{(2L \cdot CD^2) / (\rho \cdot SA \cdot CL^3)}$$

As with the previous section, Figure 5.46 also illustrates the effect of using different weight estimates for a single geometry. Here an increase in mass from a 4.12 N juvenile animal to a 13.24 N juvenile leads to the horizontal velocity at the point of minimum sink increased from 6.02 ms to 10.8 ms. Likewise in adult specimens (i.e. SMNK PAL 1133) the velocities are 8.65 ms ( $V_s = -0.48$ ) for a light mass estimate and 15.37 ms (15.37 ms) for a heavy mass estimate, giving the tangent to the polar a gradient of -0.05578.

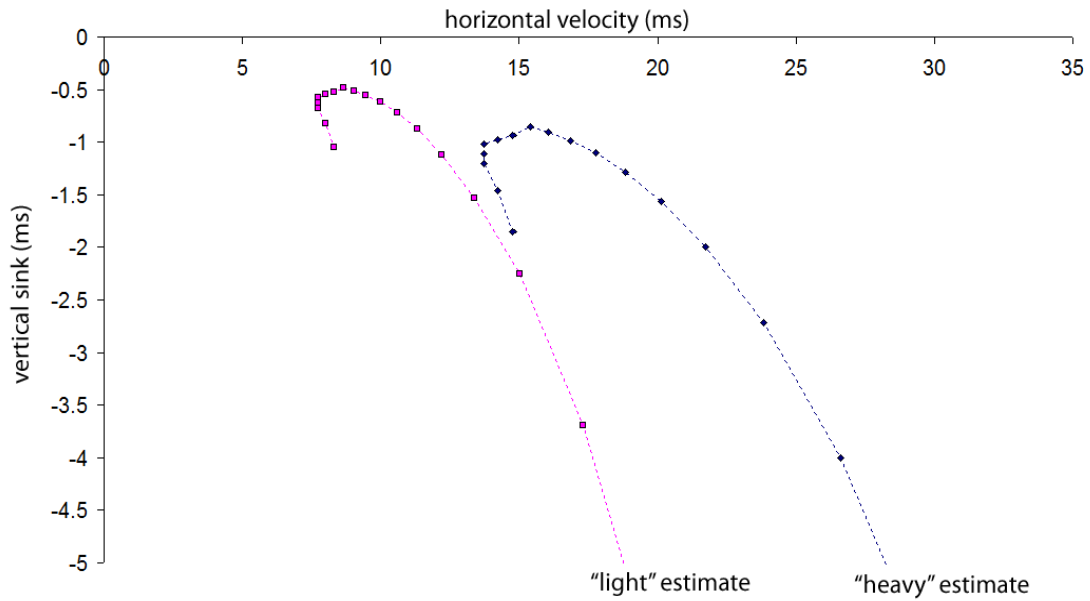


Figure 5.46. - Glide polar of *Coloborhynchus*. The two curves represent an animal of the same shape and area but different mass, where the red line represents an animal weighing 4.12 N and the yellow 13.24 N.

Bramwell and Whitfield (1974) calculated the performance of *Pteranodon* by taking the polar data from a Göttingen 417A glider wing for three Reynolds numbers and adopting a  $CD_{par} = 0.005$ . Although Bramwell and Whitfield originally applied this data to a large *Pteranodon*, it is equally applicable assign this data to any large pterosaur with a similar aspect ratio and wing geometry. Applying this data directly to an almost complete specimen of *Coloborhynchus* (SMNK PAL 1133) gives three size classes based on the Reynolds number; a 6.44 m adult ( $Re = 420\ 000$ ); a 2.58 m sub adult ( $Re = 168\ 000$ ) and a 0.64 m juvenile ( $Re = 42\ 000$ ), covering the full developmental range of this taxon (Table 26).

| Reynolds number | b (m) | Mass_h (N) | V_ms (ms) | V_h (ms) | Mass_l (N) | V_ms (ms) | V_h (ms) |
|-----------------|-------|------------|-----------|----------|------------|-----------|----------|
| 420 000         | 6.44  | 587.6      | -1.2      | 17.47    | 184        | -0.67     | 9.79     |
| 168 000         | 2.58  | 57         | -1.78     | 14.37    | 19.1       | -1.03     | 8.32     |
| 42 000          | 0.64  | 1.63       | -1.44     | 9.16     | 0.6        | 0.88      | 5.58     |

Table 26. - Minimum sinking speed and horizontal flight velocity for a light mass and heavy mass *Coloborhynchus* (SMNK PAL 1133) based on the Göttingen 417a glider wing.



As a consequence of their mass, the heavier juvenile configuration now records a minimum sink velocity occurring at approximately the same velocity experienced by a “light weight” adult (i.e. 9.16 ms versus 9.79 ms). The minimum sink velocity of a heavier adult form is calculated as 17.5 ms, 1.78 times that of the lighter model.

A further study that can be readily altered is that of Brower (1982), who selected a specimen of *Pteranodon* with a wing span of 6.95 m and is roughly equivalent to the maximum size attained by this species (Bennett 2001b). Here I have applied Brower’s data to the almost complete specimen of YPM 2493 that has a wing span of 5.43 m and would have weighted either 12.3 kg (120.6 N) or 38.7 kg (379.4 N) depending on the preferred method of estimation. Figure 5.47 illustrates that the heavier model had a  $V_{ms}$  of -0.81 ms, which occurs at a horizontal velocity of 15.2 ms, and a maximum range speed that was very similar. In contrast a light mass animal would have shown a  $V_{ms}$  of -0.51 ms, occurred at a forward velocity of 9.46 ms. Increasing the mass of the animal by a factor of 2.58 is thus correlated with an increase of 1.61 in both flight speed and minimum sink speed.

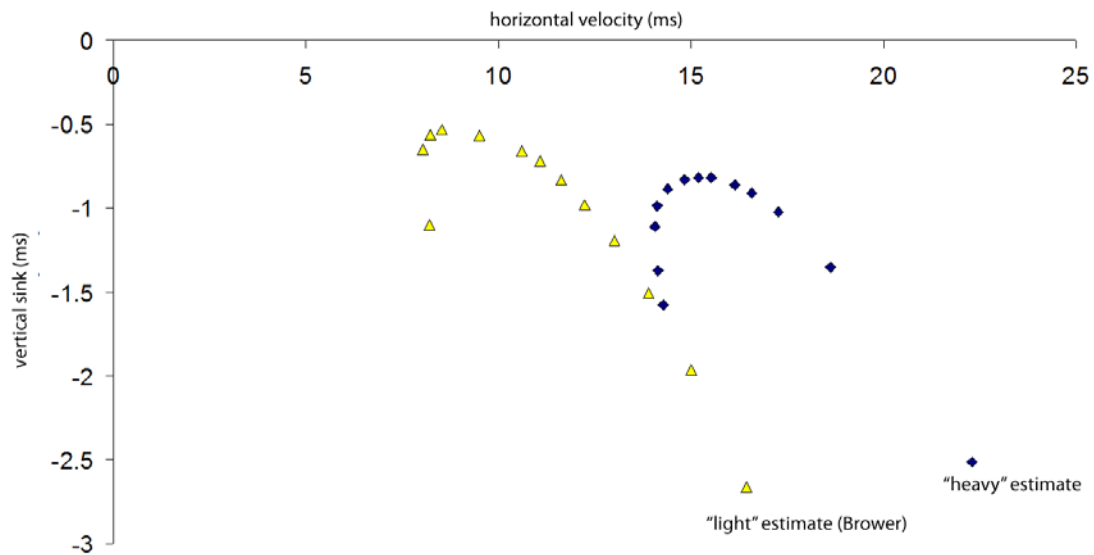


Figure 5.47. - Polar gliding curves of heavy and light mass variants of *Pteranodon* YPM 2493 after Brower (1982). Light and heavy mass estimates are 14.94 kg (146.4 N) and 38.7 kg (379.2 N) respectively.

#### 5.4.4 CFD simulation of *Coloborhynchus robustus*

A model of *C. robustus* derived from the skeleton of SMNK PAL 1133 was used to form the basis of a commutative fluid dynamics (CFD) analysis (Figures 5.48-50). Owing to the limited amount of time available to the author and workers at the KIT only three angles of attack ( $0^\circ$ ,  $3^\circ$  and  $6^\circ$ ) were sampled, however, this was judged to be a sufficient range to cover the of pro- and supination of the wing prior to stall.

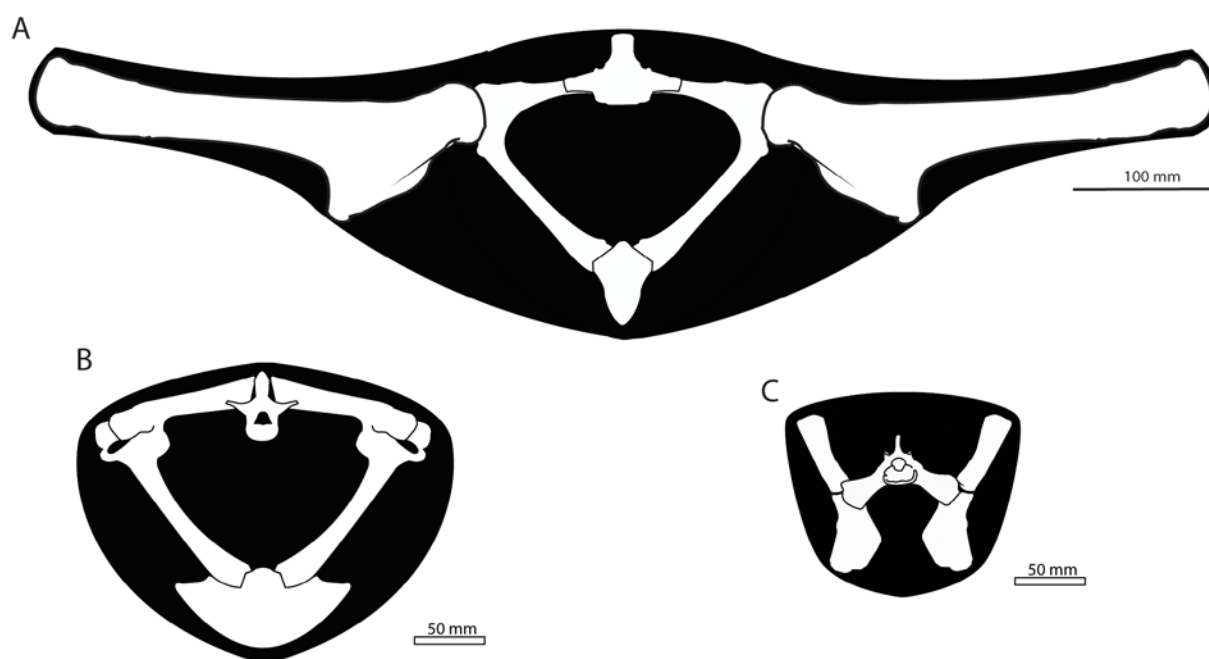


Figure 5.48. - Body templates of *Coloborhynchus robustus* (SMNK PAL 1133). A, pectoral girdle and humeri in cranial view (A); pectoral girdle in its caudal aspect (B); and pelvic girdle in cranial view (C). The hypothetical extent of the soft tissue is shown in black.

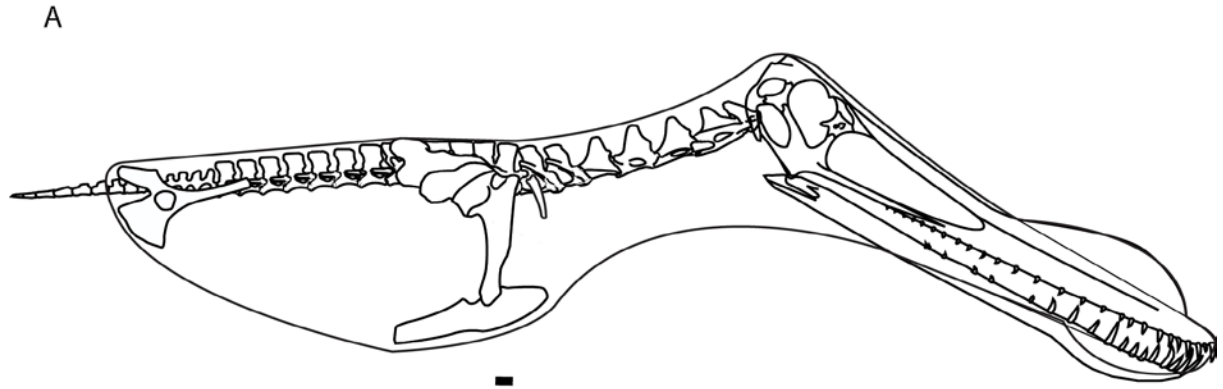


Figure 5.49. - Body template of *Coloborhynchus robustus* (SMNK PAL 1133) in right lateral view.

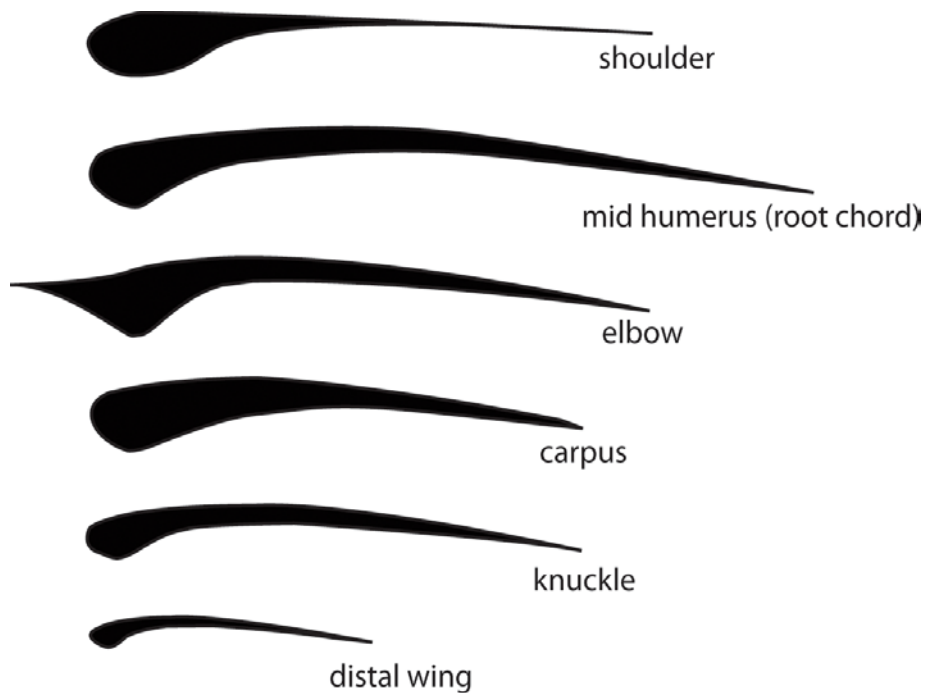


Figure 5.50. - Cross section of the wing spar and membrane of *Coloborhynchus robustus* (SMNK PAL 1133).

The forces acting on the model are summarised in Table 27. No sudden stall was observed at higher angles of attack and instead CL continued to increase at 0.1 for each degree of pitch, giving a lift coefficient of 0.52, 0.8 and 1.1 at angles of  $0^\circ$ ,  $3^\circ$  and  $6^\circ$  respectively. As such the maximum recorded lift force occurs at an angle of attack of  $6^\circ$  and reached 86 N in magnitude. The lift slope can be subsequently

defined by the equation  $CL = 0.09 \alpha + 0.5233$ . Unlike lift the drag force coefficient acting on the body, i.e. parasite drag ( $CD_{par}$ ), remains stable, increasing from 0.02 to 0.022 at higher angles of attack and constituting 24% and 42% of the total drag at  $\alpha = 0^\circ$  and  $3^\circ$  respectively. For the lower angles of attack, i.e.  $0^\circ$  and  $3^\circ$ , the respective L/D ratio is calculated as 6.13 (corresponding to a  $V = 23.4$  ms and  $V_s$  of  $-2.43$  ms) and 15.4 ( $V = 18.8$  ms,  $V_s = -0.97$  ms).

At an angle of attack of  $6^\circ$  the drag acting on the wing is negative and is clearly problematic for the extrapolation of forces at higher values of  $\alpha$ . The reason for the incorporation of negative drag into this simulation is uncertain as the remainder of the results appear to be uncontroversial, suggesting that this cannot be attributed to an unknown error in the mathematic model. At the same time, however, the wing section profile does not indicate why thrust should be produced.

| Angle of Attack | Forces | Force Values (N) |      |       | Coefficient |       |        |
|-----------------|--------|------------------|------|-------|-------------|-------|--------|
|                 |        | Wing             | Body | Total | Wing        | Body  | Total  |
| $0^\circ$       | Lift   | 41.61            | 0.01 | 41.62 | 0.514       | 0.000 | 0.515  |
|                 | Drag   | 5.21             | 1.58 | 6.79  | 0.064       | 0.020 | 0.084  |
|                 | Shear  | 0.69             | 1.98 | 2.68  | 0.009       | 0.024 | 0.033  |
| $3^\circ$       | Lift   | 63.75            | 0.94 | 64.69 | 0.788       | 0.012 | 0.800  |
|                 | Drag   | 2.43             | 1.76 | 4.19  | 0.030       | 0.022 | 0.052  |
|                 | Shear  | 0.03             | 1.98 | 2.00  | 0.000       | 0.024 | 0.025  |
| $6^\circ$       | Lift   | 86.00            | 0.02 | 86.02 | 1.063       | 0.000 | 1.064  |
|                 | Drag   | -1.94            | 1.74 | -0.2  | -0.024      | 0.022 | -0.002 |
|                 | Shear  | 2.75             | 2.12 | 4.87  | 0.034       | 0.026 | 0.060  |

Table 27. - Force values and their corresponding coefficients derived from the CFD simulation of *Coloborhynchus robustus* (SMNK PAL 1133).

The distribution of pressure coefficients contours over the model indicates that the highest forces are concentrated on the caudoventral section of the neck, the shoulders, the ventral surface of the propatagium and proximal section of the forelimb (Figure 5.51). A further area of high pressure, marked out by wedge shaped section of the flight membrane immediately caudal to the fourth metacarpal, is due to the downward deflection of the flow over the most cambered section of the aerofoil.

The distribution of pressure coefficients are further illustrated through span-wise sections of the wing (Figures 5.52 - 53) where the relatively bulky leading edge strut,

formed by the tissue of the forelimb, deflects the flow both up and down around the wing at a relatively similar velocity, leading to similar pressure conditions on top and bottom surfaces of the wing. This effect is minimised lateral to the wrist where the bone and tissue components of the wing become substantially smaller. Pressure coefficients are again highest where the flow first makes contact with the wing.

The velocity component over the span-wise sections of the wing is illustrated in Figure 5.54 where a large wake of slow moving air forms behind the body as a result of the deep sternum. A similar consequence is noted on the wing spar slow moving air forms behind the bulky leading edge.

Continuing from previous observations, if the drag coefficient from the *Anhanguera* cranial model can be directly applied to that *Coloborhynchus*, something that appears likely given the geometric similarities between skulls, then the head is subsequently responsible for 15% of the total parasite drag coefficient, where total parasite drag is 0.02.

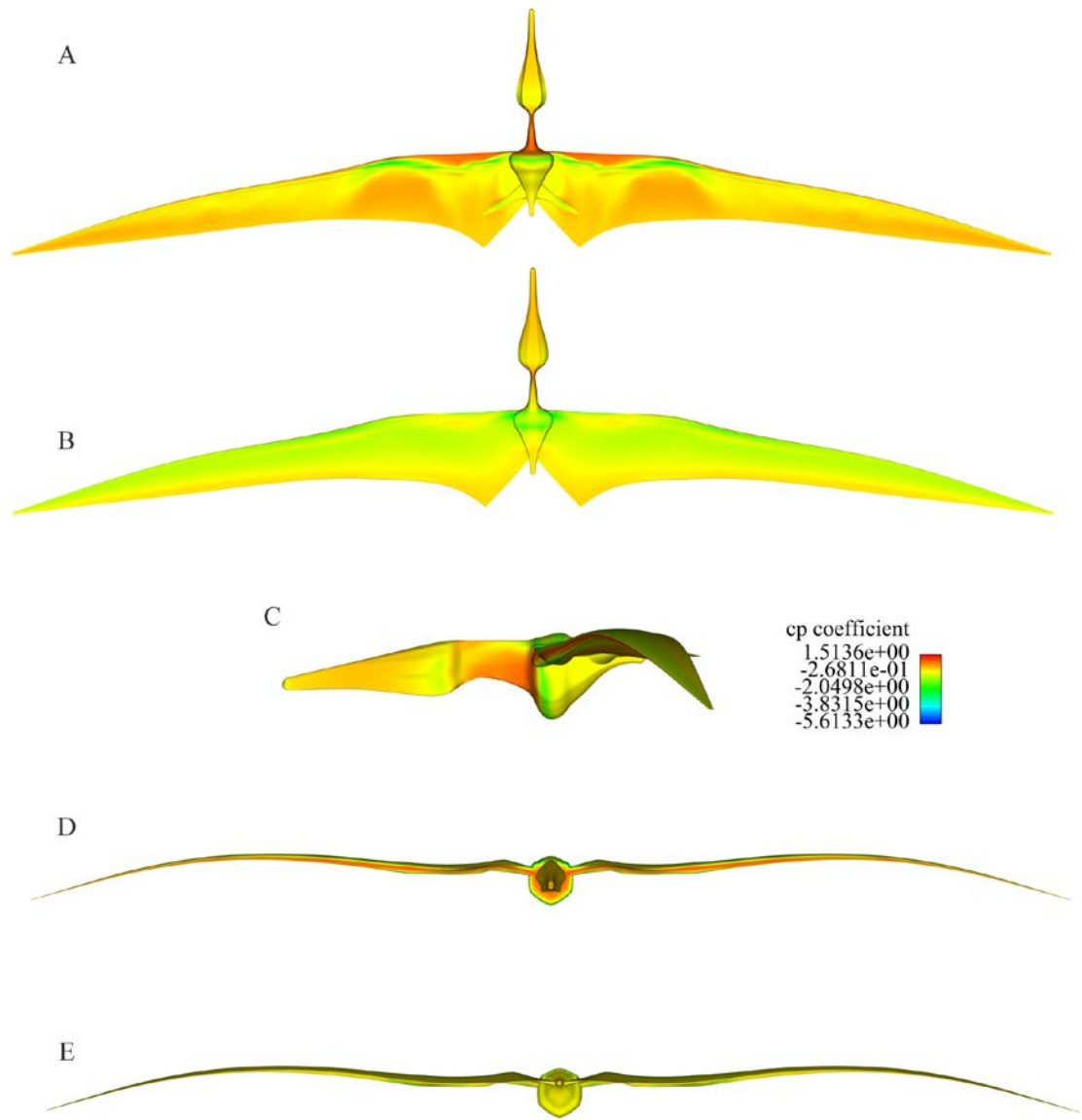


Figure 5.51. - Pressure coefficients and their distribution over the *Coloborhynchus* geometry in A, ventral, B, dorsal, C, right lateral, D, cranial; E, caudal; F, craniolateral; G, ventrolateral; H, caudolateral; I, craniodorsal; J, cranioventral aspects. (continued over page).

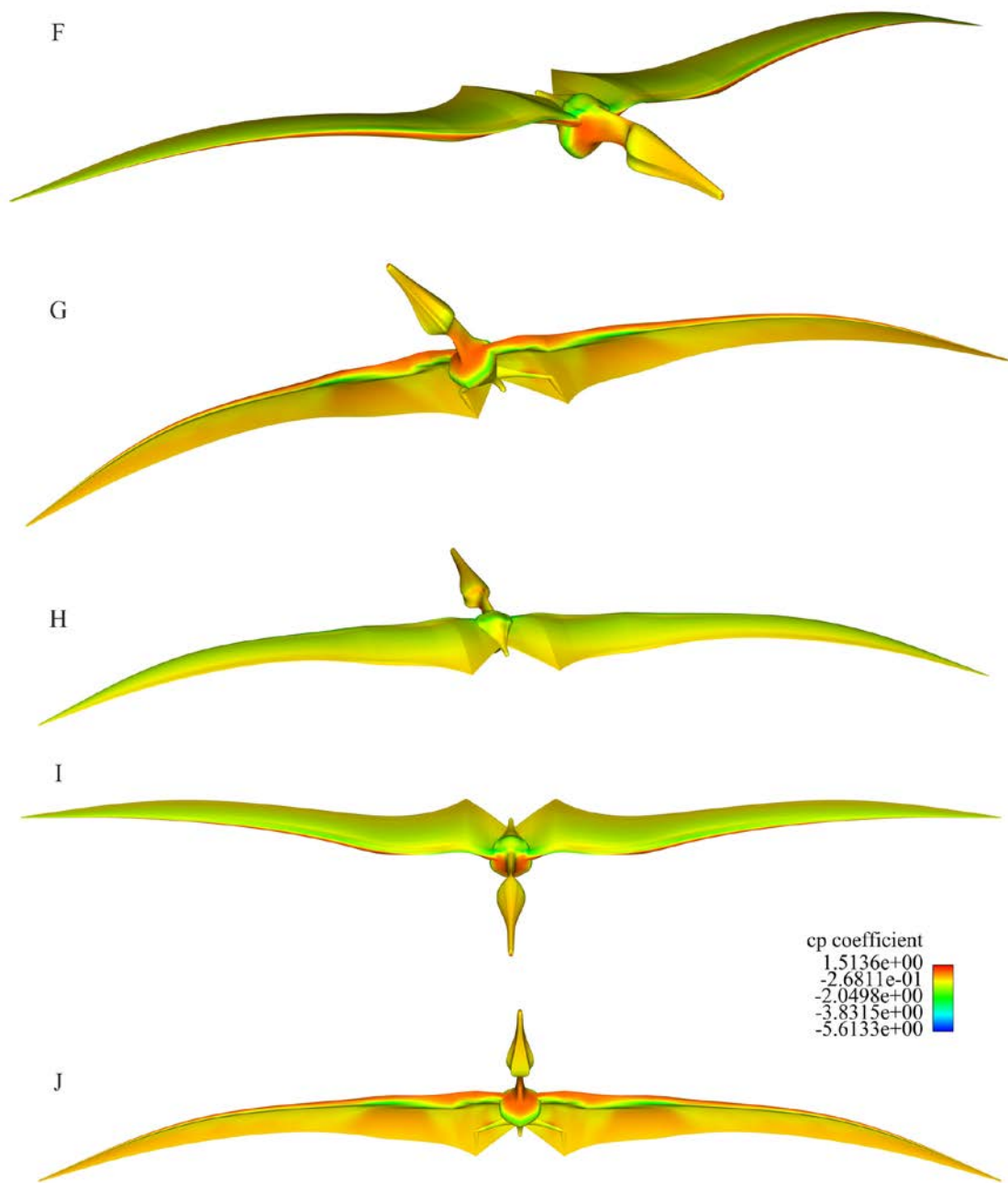


Figure 5.51 - continued from the previous page.

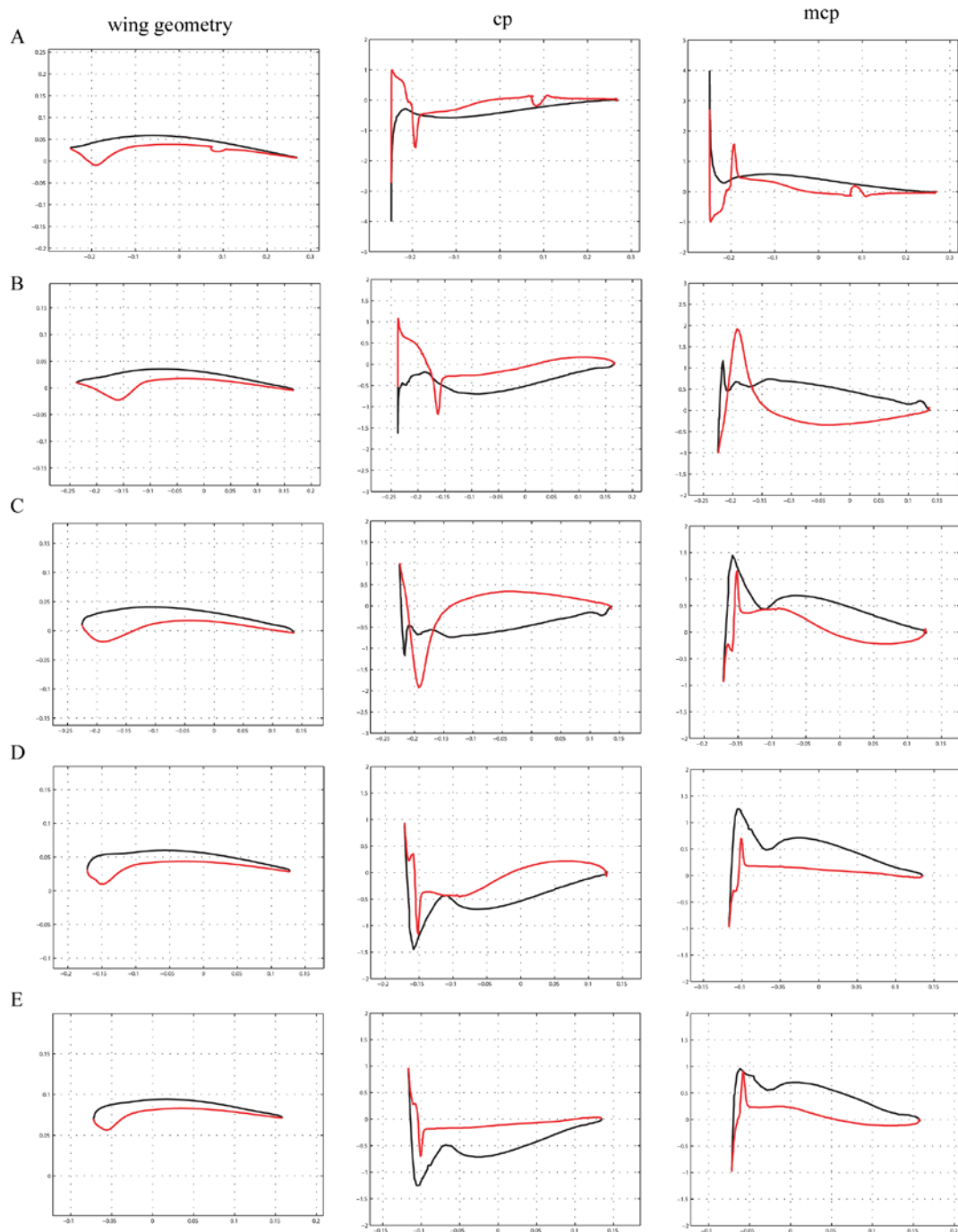


Figure 5.52. – Wing geometry and pressure distribution over the surface of the wing, where the upper surface is shown in black while the lower surface is shown in red. Geometry sections are span wise, moving laterally towards the tip in 0.25 m intervals, with A representing the section of the wing 0.25 m lateral to the median sagittal plane of the body. Section J represents the wing just medial to the tip, 2.75 m from the midline of the body. The spiking on the pressure profiles is caused by the thick leading edge spar (i.e. tissue of the forearm) whereby the flow is deflected up and down at relatively similar rates. This effect is particularly strong in medial sections of the wing (A-D) but becomes much less pronounced in more lateral sections as the forearm becomes thinner in section (E-J). Continued overleaf.



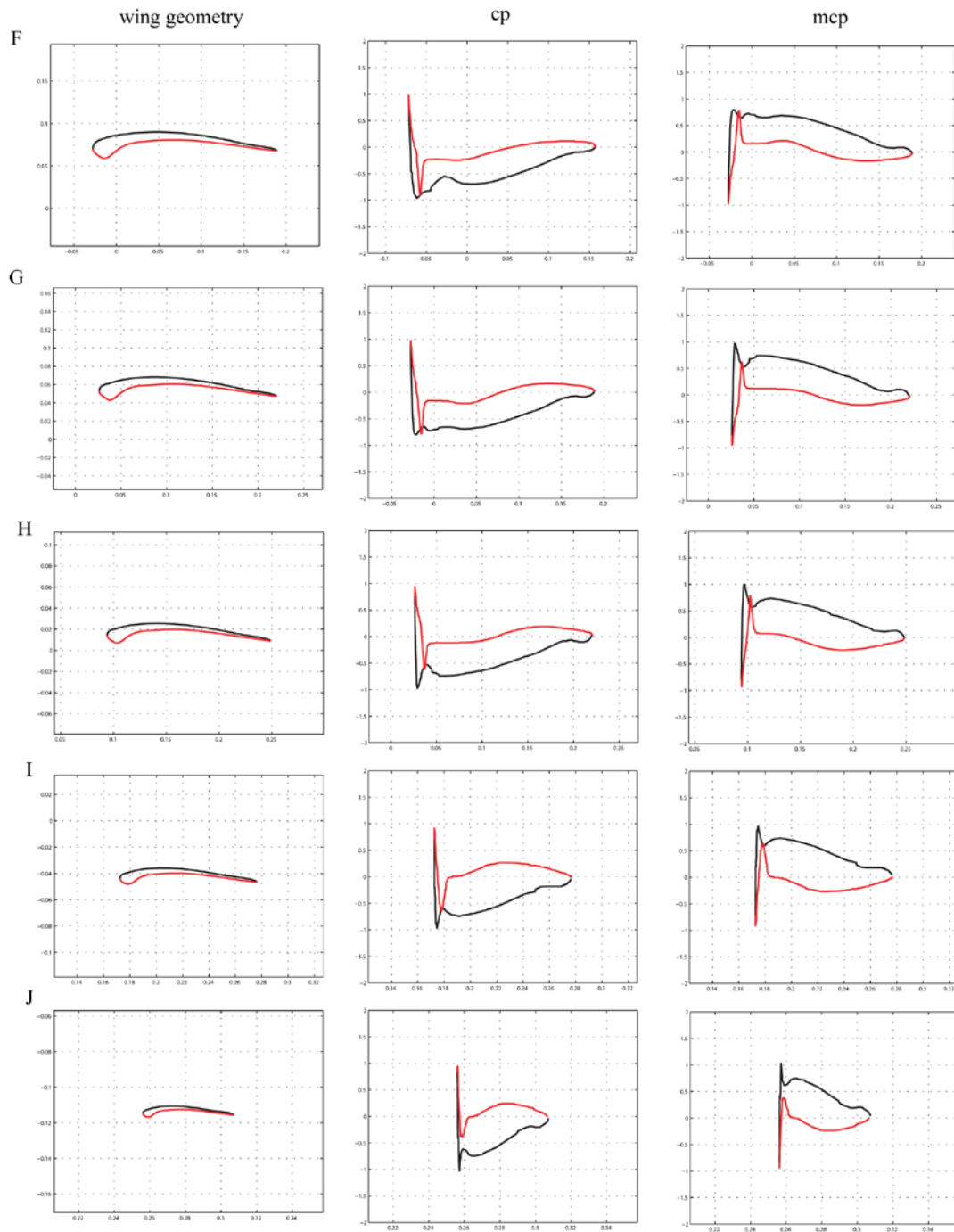


Figure 5.52. – continued from previous page.

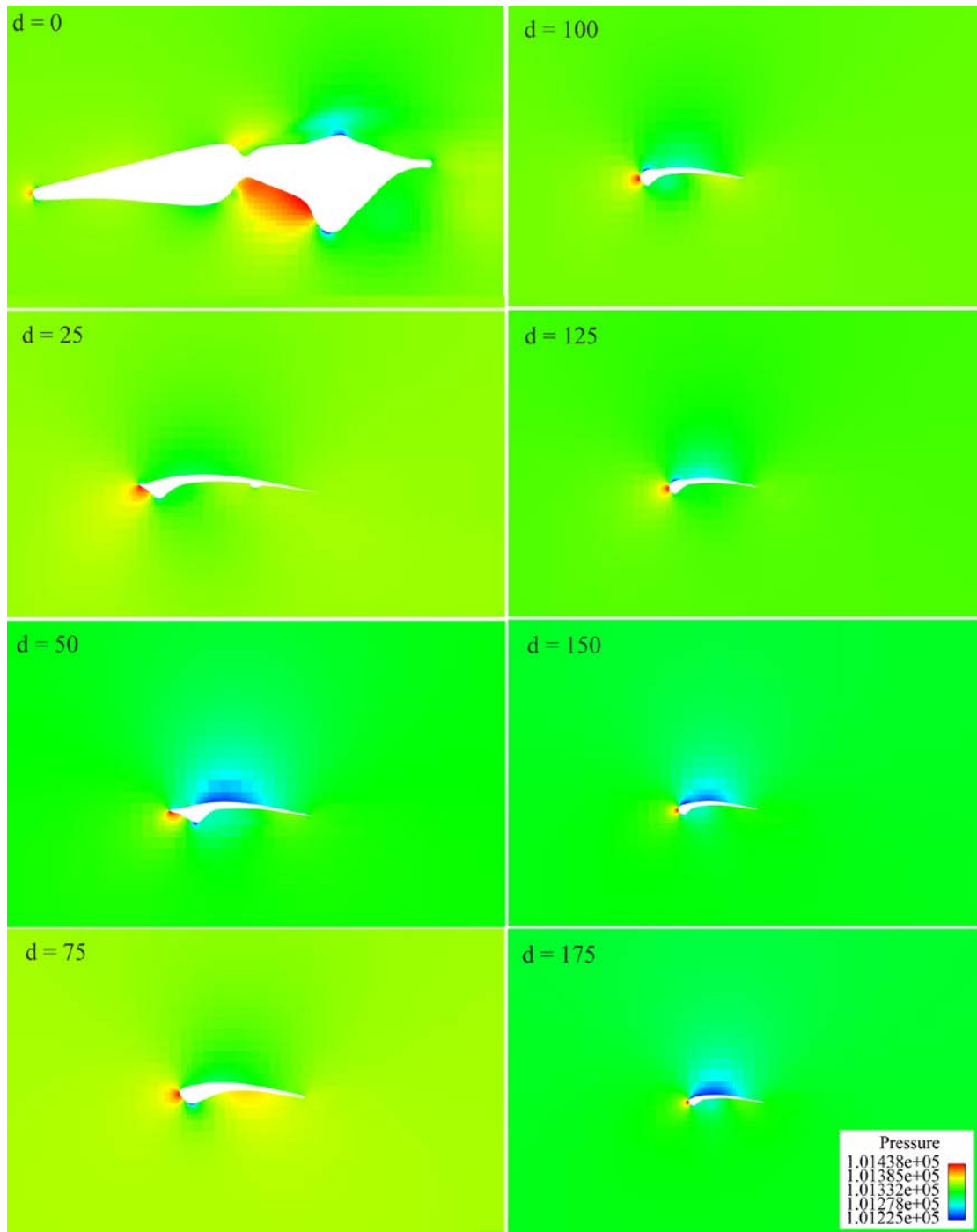


Figure 5.53. - Pressure distribution across span-wise sections of the body and wing. The  $d$ -value represents the distance from the midline in mm. Pressure is concentrated at the leading points of the head, body and wing sections, particularly across the propatagial region. White shapes indicate the model sections. Figure continued over the page.

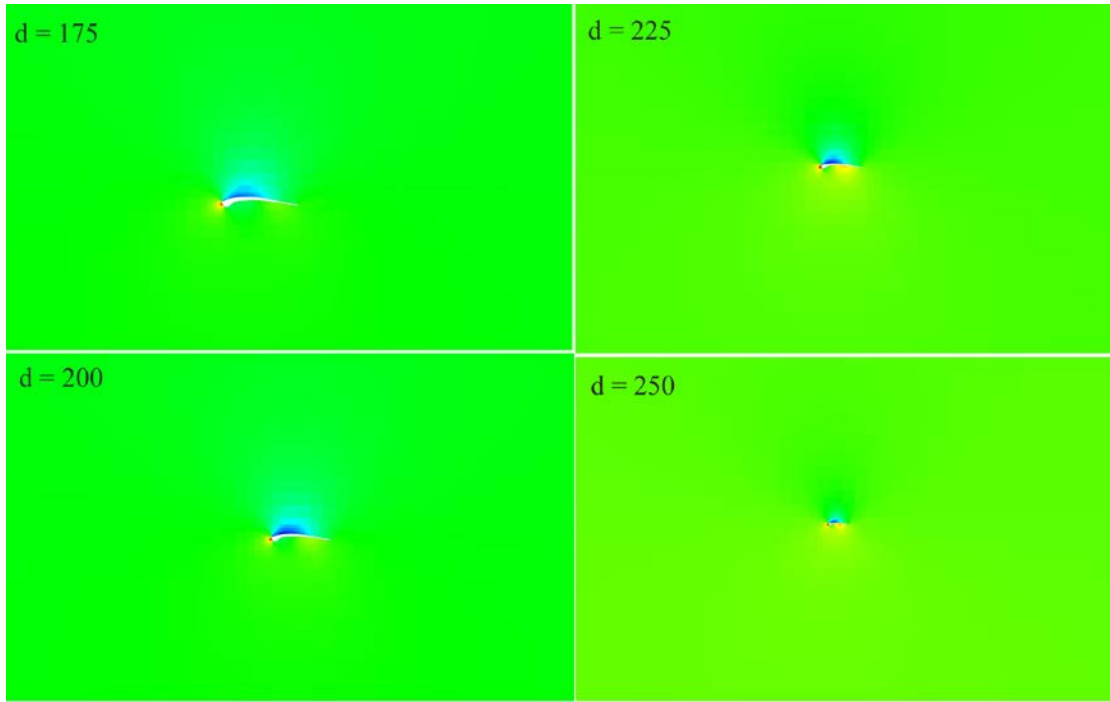


Figure 5.53 - continued from the previous page.

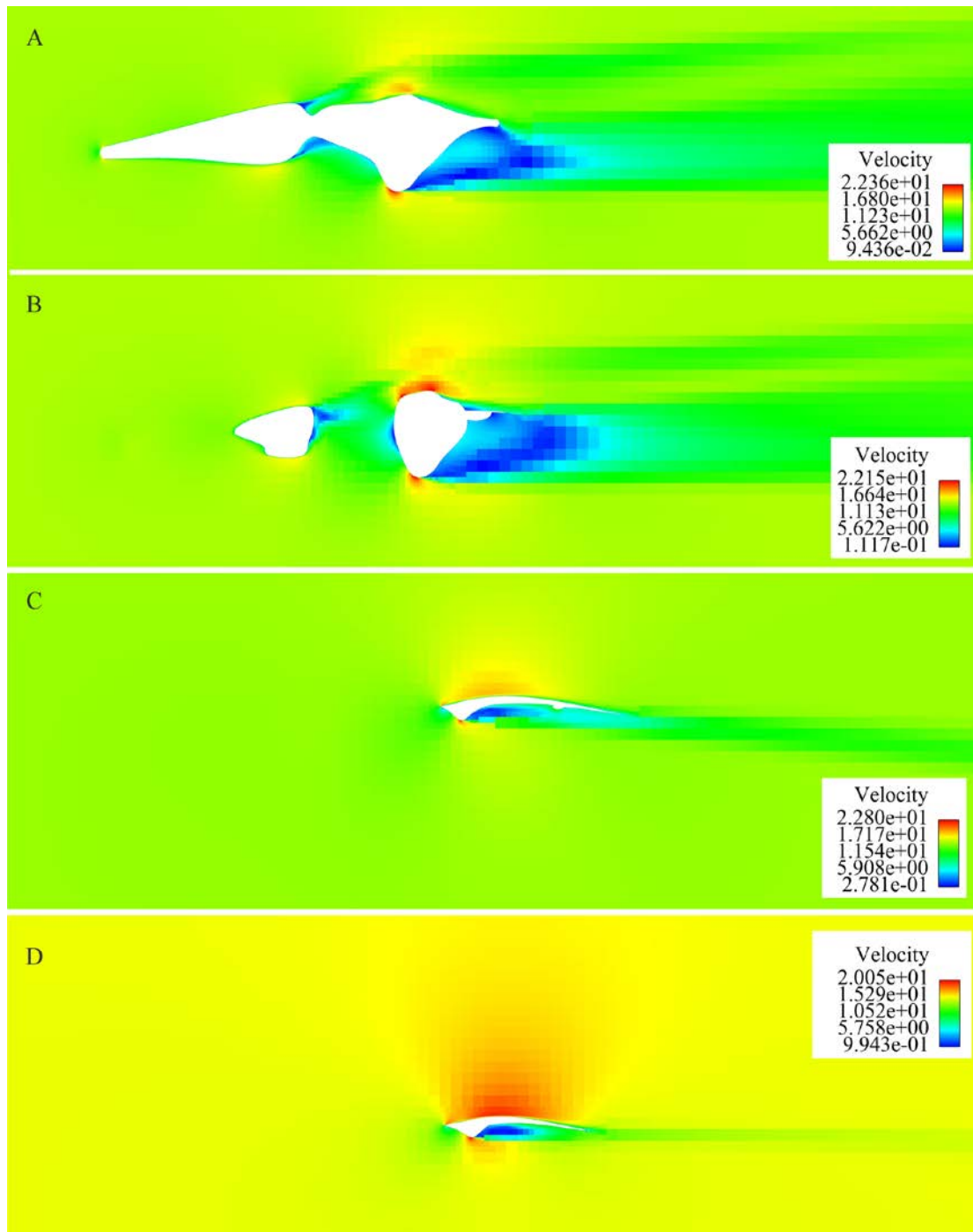


Figure 5.54. - Velocity profiles across span wise sections of the body and wing where: A, midline of torso, B, proximal torso section; C, proximal wing section; D, mid-wing section. The caudoventral regions of body produce large bodies of slow moving air, leading to formation of a large proximal wake.

#### **5.4.5 Summary of theoretical data**

While both the “flat plate” examples and the tornado geometries ignore or require addition input to determine the profile drag of the wing spar, they are useful due to

their simplicity, allowing several taxa to be examined rapidly. Several differences, however, are apparent between these methodologies, where in all cases the  $L/D_{\max}$  of the TORNADO geometries exceeds those of the flat plate models. Although some of values are relatively close matches (e.g. *Coloborhynchus* 18.4 versus 18.1 for the TORNADO and flat plate models respectively) two of the TORNADO geometries, *Anurognathus* and *Sinopterus*, are calculated to have  $L/D_{\max}$  ratios that greatly exceed those of the flat plate models, i.e. 16.56 versus 8.4 for *Anurognathus* and 19.63 versus 11.9 for *Sinopterus*, and appear as a consequence of low values of lift. In all examples the maximum range velocities of the TORNADO geometries are up to 31% higher than those of comparable flat plate models (e.g. 18 ms versus 22.6 ms for *Coloborhynchus*; 5 ms vs 6.53 ms for *Anurognathus*; 9 ms vs 11.28 ms for *Sinopterus*).

The body drag coefficient of 0.005 used for *Pteranodon* by Bramwell and Whitfield (1974) is here regarded as being unusually low and is *contra* to the values calculated using the CFD analysis where values of 0.02 for *Coloborhynchus* are more supportive of those proposed by Brower (1982).

The general conclusions of the theoretical studies vary depending on the preferred method of mass estimation. Low mass estimates produce slow speed fliers with low vertical sinking velocities and very good circling performances. By contrast the heavier mass estimates result in substantially faster flight speeds, corresponding to greater vertical sink speeds and larger circling radii.

The uncertainties over of the true values of  $CD_{\text{par}}$  and  $CD_{\text{pro}}$ , however, are manifested in the output of the TORNADO based models, the results being largely dependant on these variables. As the  $CD_{\text{pro}}$  is influenced by both wing profile and Reynolds number its direct application from one study to another is problematic but necessary where no other data is known. This is clearly illustrated by the quadratic equations of three authors focusing on biological flight where despite them having been conducted in similar flow regimes, they return very different results (Figures 5.55 - 56).

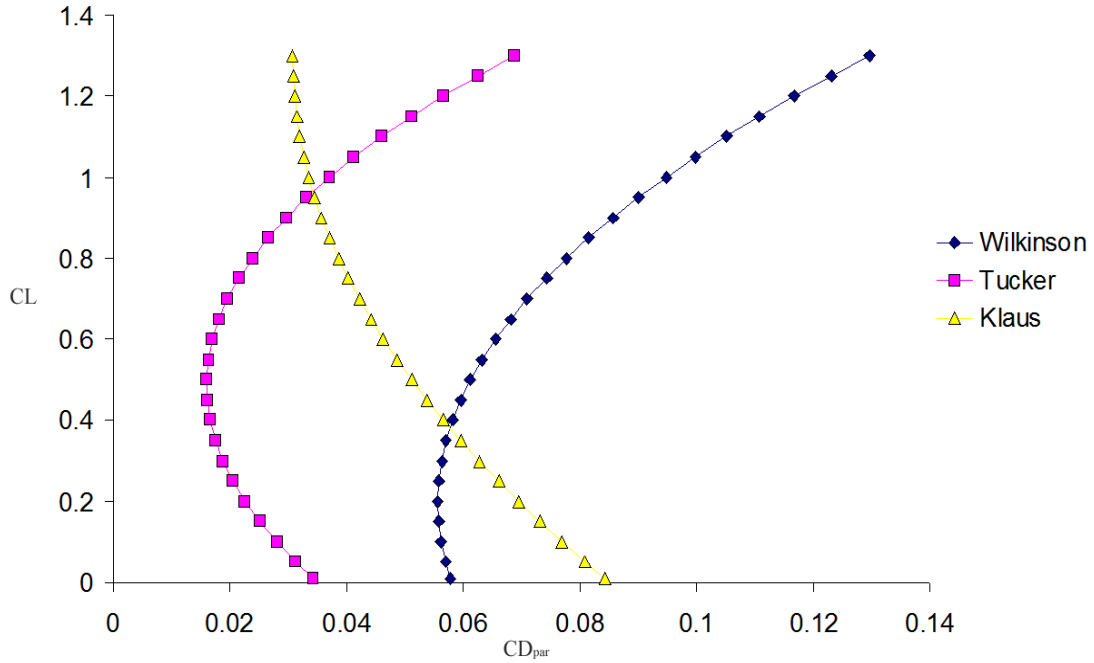


Figure 5.55. - Quadratic equations developed for the calculation of  $CD_{PRO}$  in biological fliers where:  $CD_{pro} = 0.0608CL^2 - 0.024CL + 0.058$  ( $Re = 10^5$ , Wilkinson et al. 2005);  $CD_{pro} = 0.08CL^2 - 0.078CL + 0.035$  ( $Re = 1.2 \cdot 10^5$ , Tucker 1988);  $CD_{pro} = 0.0325CL^2 - 0.084 + 0.085$  ( $Re = 52\ 850$ , Klaus 2008).

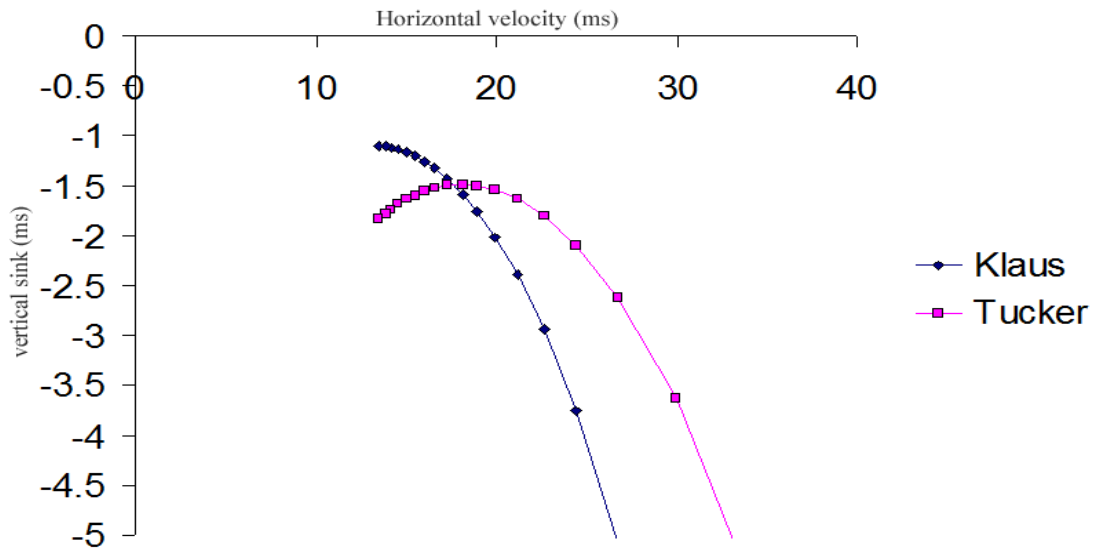


Figure 5.56. - Comparison of the theoretical gliding performances in the ornithocheiroid *Coloborhynchus* (SMNK PAL 1133) where  $CD_{pro}$  is calculated from the equations of Tucker (1988) and Klaus (2008).

Comparing the  $CD_{pro}$  of Tucker and Klaus for a model of *Coloborhynchus* the  $CD_{pro}$  of Klaus is higher than that of Tucker at low values of  $CL$  ( $< 0.95$ ) and lower at higher values of  $CL$ . In addition to this the  $L/D_{max}$  of Klaus is lower at 15.3 compared with

18.4. Such differences can be readily visualised in the form of a polar gliding curve, as given for *Coloborhynchus* in Figure 5.56, where the minimum sinking velocities are -0.98 ms compared with -1.5 ms, while the horizontal velocity is substantially lower at 14.2 ms compared to 20 ms. The maximum range speed is 16 ms ( $V_s = -1.04$  ms) down from a value of 22.6 ms. The characteristics of the wing profile are therefore very important to reconstruct as accurately as possible. While this statement should be obvious for any aerodynamic study it highlights the difficulty with reconstructing even simple gliding performance in an extinct animal for which no good cross sectional data of the wing exists. As such approximations or estimates, even when based on previous studies or other biological fliers, must be treated with caution and can be expected to give no more than a general impression of flight performance in pterosaurs.

## **5.5 Chapter Summary**

A comparison of theoretical with experimental data is complicated owing to the poor ratios of lift to drag exhibited by the fixed wing models. However, an overview of the generalised flight characteristics of the Pterodactyloidea is still possible.

Where low estimates of mass were used the results are comparable to older studies, where pterosaurs adopted a very slow horizontal speed during gliding flight (i.e. 3.85 – 11.96 ms), coupled with very low rates of vertical sink and superb circling radii. Superb circling performances are reflected in even medium and large taxa such as *Coloborhynchus* and *Quetzalcoatlus*, for which a shallow bank of only  $10^\circ$  returns radii of 67.35 m and 51.61 m respectively. For smaller animals such as the azhdarchoid *Sinopterus*, this is reduced to only 21.23 m at a  $10^\circ$  bank and can be as tight as 4.26 m by adopting a banking angle of  $60^\circ$ .

Substituting heavier masses into the flight formulae and bringing wing loads to a comparable state with extant birds (Witton 2008a, b) leads to an increase in horizontal flight speed, vertical sinking velocity, and circling radii, but preserves the original glide angle. Despite the increase in velocity, the Pterosauria still cover a substantial range of flight speeds where the tiny anurognathids (e.g. *Anurognathus*) retain a

horizontal velocity  $< 6$  ms, the very slow gliding speeds of anurognathids resulting in exceedingly tight circling radii (typically  $< 10$  m) that undoubtedly would have assisted the animals to fulfil their niche as aerial insectivores. Larger gliding forms such as *Coloborhynchus* and *Quetzalcoatlus* occupy the upper range of the scale where the best horizontal velocities are calculated as being between 15 – 18 ms, despite the former taxon being around half the size of the latter where the substantial increase in mass of the *Quetzalcoatlus* was offset by the increase in hind limb length and subsequently larger wing area. Given the problems associated with flapping flight at large sizes (see Sato et al. 2009), the increase in hind limb length was likely essential for this animal to have adopted gliding flight within a safe range of flight velocities. The faster glide speeds of larger pterodactyloids as a result of their mass indicates shorter travelling times and a faster paced mode of life, where the capture of prey on the wing now takes place at velocities up to twice those suggested by light mass studies. The faster pace of prey capture and gliding flight is consistent with the enlarged flocculus, optical lobes, and semicircular canals reported from endocasts of the pterosaurian brain cavity (Eck et al. 2011). While landing, particularly in large heavy azhdarchids, might be considered more dangerous owing to the increased minimum useful speed, pterosaurs would still have been able to pitch rapidly just prior to landing, suddenly increasing drag and slowing the animal to a safe velocity. As quadrupeds, pterosaurs also would have had an advantage over fast extant fliers where immediately after touchdown they could fall forward onto their forelimbs (Mazin et al. 2009) and absorb some the impact rather than collapsing onto their bellies as observed in albatross.

Determining usable values of body (parasite) and profile drag coefficients are problematic and the resolution of these is suggested as a primary goal of any future research. While that calculated for birds by Tucker (1988), and used extensively here may perhaps be useful for many pterosaurian taxa, it is certainly not universally applicable as suggested by the CFD body drag of *Coloborhynchus*. Coefficients of this latter taxon instead indicate a better association with the equations of Klaus (2008) for the non-pterodactyloid *Rhamphorhynchus*. This largely accounts for the discrepancy between horizontal velocities at maximum range, where speeds of 15 ms are returned following Klaus (2008) while 21 ms are noted after Tucker (1988). Taking the  $CD_{par}$  of 0.02 returned by the CFD analysis *C. robustus* indicates that



during life the adult animal experienced flight velocities of between 15 ms (based on Klaus 2008) – 18 ms (based on Tornado and flat plate models) at the point of maximum range, with a gliding gradient between 12 – 13. While the maximum range velocity of *C. robustus* remains relatively constant between methodologies, some disparity occurs between the maximum ratios of L/D, where the Tornado geometric models produced relatively low ratios of L/D, 12.9 – 16 when compared to both flat plate simulations (L/D = 18) and more sophisticated models such as that of Klaus (2008; L/D = 17.91) and my own CFD model (L/D > 26.3). As such the former geometries are likely to produce a slight underestimate of true performance of high aspect ratio configurations such as that displayed by *Coloborhynchus*. The very low values of L/D produced by the corresponding model mounted within a wind tunnel, where  $L/D_{\max} < 5$ , indicates that some component of the model resulted in up to 4 times as much drag than should have otherwise been expected.

While these flight models did not produce the desired results, wind tunnel experiments on the body of *Aurorazhdarcho* suggest that  $CD_{\text{par}}$  for this animal should remain below 0.015 at low angles of pitch, while for *C. robustus* a steady result of 0.02 appears more appropriate. Head crest models do not support an aerodynamic function for the cranial crest but do provide an abundance of data on their effects on  $CD_{\text{par}}$  as they are yawed. While the majority of the head models display very low coefficients of drag, only leading to sudden increases in force and torque when yawed, the elongate crest of *Nyctosaurus* is in fact aerodynamically undesirable even when directed parallel to the flow; the drag coefficient being up to 10 times higher than that of the ornithocheirid *Anhanguera*.

## Concluding Statement

As introduced in Chapter 1 this thesis has dealt with two distinct primary aims, these being the description of ornithocheiroid and azhdarchoid pterosaurs housed within the State Museum of Natural History Karlsruhe, and the aerodynamic characteristics of several pterodactyloid and non-pterodactyloid taxa.

To relate these diverse aims, the first section of the dissertation focused on the descriptive palaeontology and utilised my understanding of the pterosaurian *bauplan* through the anatomical characteristics, wing structure and extent, and joint mobility to create the subsequently used aerodynamic models. As such the detailed study of the largely complete ornithocheiroid SMNK PAL 1133 yielded not only a new specimen attributable to the established species *Coloborhynchus robustus*, but also allowed for the creation of the model template for the physical, theoretical and CFD aerodynamic simulations. Likewise the description of a new azhdarchoid *Microtuban altivolans* (Elgin and Frey 2011b) and further study of a new specimen of cf. *Tupuxuara* influenced the azhdarchoid flight models, here typified by *Sinopterus* due to the number of well preserved specimen available to study. While both *Tapejara wellnhoferi* (Eck et al. 2011) and / or cf. *Tupuxuara* (this study) would have made fine reference specimens, good examples of these did not become available until a late point of this thesis. A number of non-pterodactyloid taxa were included in the theoretical section of Chapter 5 (in addition to a single model of *Rhamphorhynchus* for which a fixed wing model was also constructed) due to the cooperation with E. Prondvai who was primarily fixated on the more basal pterosaur species. While funding for a follow on to this project was not forthcoming, the data from these specimens are retained for comparative purposes despite the focus of this dissertation being on pterodactyloids.

The “narrow wing” pterosaur configuration was confidently discarded after Elgin et al. (2011) reconstruct all subsequent aerodynamic models according to a configuration where the trailing edge of the brachiopatagium terminates against the soft tissue of the hind limb. This was based partially on a number of azhdarchoid remains within the SMNK where fore and hind limbs from the same side of the body had separated

together in union, minus elements of the torso, and as such the inclusion of these fossils within the overall description was deemed necessary.

A number of goals proposed at the onset of this project were never, or only partially realised, where the full extent of the joint mobility outlined in Chapter 4 was incorporated into prototype models for which only limited testing was possible before the premature termination of project funding. As such the section on joint mobility was retained to justify the configurations used for the gliding flight simulations. Additionally it adding extra information on the mobility observed within the Ornithocheiroidea and more rarely reported estimations from the Azhdarchoidea, where the range of motion when the humerus is raised or flexed appears to be greater. The flexible wing model data is not presented within the main body of Chapter 5 but is instead available through the appendix. Likewise reconstruction of a membranous wing for the physical wind tunnel models using the data obtained from *Tupuxuara*, SMNK PAL 3830, and Kellner et al. (2009), Elgin et al. (2011), was never adequately constructed by collaborators.

With regards to the aims proposed at the onset of the thesis all were effectively completed where descriptions of the SMNK fossils erects two holotypes (Elgin and Frey 2011a, b), a new exceptional specimen of an established taxon (*Coloborhynchus robustus*), the most complete specimen of *Tupuxuara* known to science, and a variety of rare ornithocheiroid and azhdarchoid pterosaurs (Elgin and Campos 2011; Elgin and Frey 2012; Elgin and Hone 2013). The palaeontological significance of these specimens is noted, where new observations on the ontogeny / maturity (Elgin and Frey 2008; this work) and crestlessness in ornithocheiroids (Elgin and Frey 2011a), taphonomy (Elgin et al. 2011), pedal / ankle structure (Elgin and Frey 2011c; this work), pneumaticity (Elgin and Hone 2013), soft tissue (Elgin et al. 2011; this work); the pelvic symphysis (this work), and presence of traits with broader taxonomic implications (e.g. wing finger phalanges, Elgin and Frey 2011b; metacarpalia, this work). A reassessment of the joint mechanics, as noted above, is included where much support is found for an intermediate range of motions within the Ornithocheiroidea. The morphometric data derived from the descriptive section of this thesis, while useful for reconstructing missing elements, was not regarded as forming a significant section of the thesis (it was not used extensively for the generation of the

subsequent aerodynamic models) and so while not included in the main body of text can also be found within the appendix at the end of this dissertation.

With the completion of all palaeontological aims the mathematical and physical models were construction based on the combined data derived from these descriptions. A comparison of the various models, while an important aim, is complicated by the poor lift:drag results generated from the fixed wing models which is regarded as not representative of the real animals. As such this aim is only partially completed as while the experimental data is not usable, the theoretical and CFD simulations appear to be a much better representation of what would be expected from such animals during gliding flight and should be used in place of the physical models. Despite this setback the cranial and body models performed well and go a long way to quantifying the individual sections of the pterosaurian body with regards to their aerodynamics. It is hoped that this information can be effectively incorporated into any future studies on the aerodynamics of this enigmatic groups.

## References

- Abdel-Rahman, A.-F.M., and Nader, F.H. 2002. Characterization of the Lebanese Jurassic-Cretaceous carbonate stratigraphic sequence: a geochemical approach. *Geological Journal*, 37, 69-91.
- Anderson, J.D. Jr. 2007. Fundamentals of Aerodynamics. 4th Ed. McGraw-Hill Education, 1008pp.
- Andres, B. and Ji, Q. 2008. A new pterosaur from the Liaoning Province of China, the phylogeny of the Pterodactyloidea, and convergence in their cervical vertebrae. *Palaeontology* 51: 453-469.
- Andres, B., Clark, J.M., and Xing, X. 2010. A new rhamphorhynchid pterosaur from the Upper Jurassic of Xinjiang, China, and the phylogenetic relationships of basal pterosaurs. *Journal of Vertebrate Paleontology* 30, 163-187.
- Arambourg, C. 1954. Sur la présence d'un Ptérosaurien gigantesque dans les phosphates de Joranie. *Comptes Rendus de l'Académie des Sciences de Paris* 238: 133-4.
- Bakhurina, N.N. and Unwin, D.M. 2003. Reconstructing the flight apparatus of *Eudimorphodon*. *Rivista del Museo Civico di Scienze Naturali "Enrico Caffi"* 22: 5-8.
- Barrett, P.M., Butler, R., Edwards, N.P., and Milner, A.R. 2008. Pterosaur distribution in time and space: an atlas. 61-107. In: E., Buffetaut and J.-M., Mazin (eds) 2003. *Evolution and Palaeobiology of Pterosaurs*. Geological Society, London, Special Publications 217: 247pp.
- Bennett, S.C. 1989. A pteranodontid pterosaur from the Early Cretaceous of Peru, with comments on the relationships of Cretaceous pterosaurs.
- Bennett, S.C. 1990. A pterodactyloid pterosaur pelvis from the Santana Formation of Brazil: Implications for terrestrial locomotion. *Journal of Vertebrate Paleontology* 10: 80-85.
- Bennett, S.C. 1992. Sexual dimorphism of *Pteranodon* and other pterosaurs, with comments on cranial crests. *Journal of Vertebrate Paleontology* 12: 422-434.
- Bennett, S.C. 1993. The ontogeny of *Pteranodon* and other pterosaurs. *Palaeobiology* 19: 92-106.
- Bennett, S.C. 1994. Taxonomy and systematics of the Late Cretaceous pterosaur *Pteranodon* (Pterosauria, Pterodactyloidea). *Occasional papers of the Natural History Museum, The University of Kansas* 169: 1-70.
- Bennett, S.C. 1995. A Statistical study of *Rhamphorhynchus* from the Solnhofen Limestone of Germany: Year-classes of a single large species. *Journal of Palaeontology* 69: 569-580.
- Bennett, S.C. 1996. Year-classes of pterosaurs from the Solnhofen limestone of Germany: taxonomy and systematic implications. *Journal of Vertebrate Paleontology* 16: 432-444.
- Bennett, S.C. 2001a. The osteology and functional morphology of the Late Cretaceous pterosaur *Pteranodon*, Part 1. General description of osteology. *Palaeontographica, A* 260: 1-112.
- Bennett, S.C. 2001b. The osteology and functional morphology of the Late Cretaceous pterosaur *Pteranodon*, Part 2. Size and functional morphology. *Palaeontographica, A* 260: 113-153.
- Bennett, S.C. 2003a. Morphological evolution of the pectoral girdle of pterosaurs: myology and function. 191-215. In: E., Buffetaut and J.-M., Mazin (eds) 2003. *Evolution and Palaeobiology of Pterosaurs*. Geological Society, London, Special Publications 217: 247pp.
- Bennett, S.C. 2003b. New crested specimens of the Late Cretaceous pterosaur *Nyctosaurus*. *Paläontologische Zeitschrift* 77: 61-75.
- Bennett, S.C. 2003c. A survey of pathologies of large pterodactyloid pterosaurs. *Palaeontology* 46, 185-198.
- Bennett, S.C. 2005. Pterosaur science or pterosaur fantasy? *Prehistoric Times* 70: 21-23, 40-41.
- Bennett, S.C. 2007a. A second specimen of the pterosaur *Anurognathus ammoni*. *Paläontologische Zeitschrift* 81: 376-398.
- Bennett, S.C. 2007b. Articulation and function of the pteroid bone in pterosaurs. *Journal of Vertebrate Paleontology* 27: 881-891.
- Bennett, S.C. 2008. Morphological evolution of the forelimb of pterosaurs: myology and function. 127-141. In: E., Buffetaut and J.-M., Mazin (eds) 2003. *Evolution and Palaeobiology of Pterosaurs*. Geological Society, London, Special Publications 217: 247pp.
- Benton, M.J. 1999. *Scleromochlus taylori* and the origin of dinosaurs and pterosaurs. *Philosophical Transactions of the Royal Society of London* B354: 1423-1446.
- Bramwell, C.D. 1971. Aerodynamics of *Pteranodon*. *Biological Journal of the Linnean Society* 3: 313-328.

- Bramwell, C.D. and Whitfield, G.R. 1970. Flying speed of the largest aerial vertebrate. *Nature* 225: 660-661.
- Bramwell, C.D. and Whitfield, G.R. 1974. Biomechanics of *Pteranodon*. *Philosophical Transactions of the Royal Society, London, B* 267: 503-581.
- Brochu, C.A. 1995. Heterochrony in the crocodylian scapulocoracoid. *Journal of Herpetology* 29: 464-468.
- Brochu, C.A. 1996. Closure of the neurocentral sutures during crocodylian ontogeny: implications for maturity assessment in fossil archosaurs. *Journal of Vertebrate Paleontology* 16: 49-62.
- Brower, J.C. 1980. Pterosaurs: How they flew? *EPISODES* 4: 21-24.
- Brower, J.C. 1982. The aerodynamics of an ancient flying reptile. *Syracuse Scholar*: 45-57. Syracuse, NY.
- Brower, J.C. 1983. The aerodynamics of *Pteranodon* and *Nyctosaurus*, two large pterosaurs from the Upper Cretaceous of Kansas. *Journal of Vertebrate Paleontology* 3: 84-124.
- Brower, J.C. and Venus, J. 1981. Allometry in pterosaurs. *University of Kansas Paleontological Contributions* 105: 1-32.
- Brown, B. 1943. Flying reptiles. *Natural History* 52: 104-111.
- Barrett, P.M., Butler, R.J., Edwards, N.P., Milner, A.R. 2008. Pterosaur distribution in time and space: an atlas. *Zitteliana* B28: 61-107.
- Campos, D.A. and Kellner, A.W.A. 1997. Short note on the first occurrence of Tapejaridae in the Crato Member (Aptian), Santana Formation, Araripe Basin, Northeast Brazil. *Anais da Academia Brasileira de Ciências* 69: 83-87.
- Chatterjee, S. 2009. The sailing performance of the crested pterodactyloid *Tapejara* from the Early Cretaceous of Brazil. Portland GSA Annual Meeting.
- Chatterjee, S. and Templin, R.J. 2004. Posture, locomotion, and paleoecology of pterosaurs, *Geological Society of America, Special Paper* 376: 1-64.
- Chatterjee, S., and Templin, R.J. 2007. Biplane wing planform and flight performance of the feathered dinosaur *Microraptor gui*. *PNAS* 104: 1576-1580.
- Chatterjee, S., and Templin, R.J. 2012. The flight dynamics of *Tapejara*, a pterosaur from the Early Cretaceous of Brazil with a large cranial crest. *Acta Geologica Sinica-English*, doi: 10.1111/1755-6724. 12007.
- Chiappe, L.M., Codorniu, L., Grellett-Tinner, G., and Rivarola, D. 2004. Argentinian unhatched pterosaur fossil. *Nature* 432: 571-572.
- Claessens, L.P.A., O'Conner, P.M., and Unwin, U.M. 2009. Respiratory Evolution Facilitated the Origin of Pterosaur Flight and Aerial Gigantism. *PLOS ONE* 4: doi:10.1371/journal.pone.0004497.
- Clark J.M., Hopson, J.A., Hernández R., Fastovsky D.E., Montellano, M. 1998. Foot posture in a primitive pterosaur. *Nature* 39: 886-889.
- Codorniu, L., Chiappe, L.M., and Cid, F.D. 2013. First occurrence of stomach stones in pterosaurs. *Journal of Vertebrate Paleontology* 33: 647-654.
- Collini, C. 1784. Sur quelques Zoolithes du Cabinet d'Historie naturelle de S.A.S.E Palatine et du Bavière, à Mannheim. *Acta Academiae TheodoroPalatinae, Mannheim, Pars Physica* 5: 58-103.
- Cuvier, G. 1801. Reptile volant. Extrait d'un ouvrage sur les espèces de quadrupèdes don't on a trouvé les ossemens dans l'intérieur de la terre. *Journal de Physique, de Chimie et d'Histoire Naturelle* 52: 253-267.
- Cuvier, G. 1809. Mémoire sur le squelette fossile d'un Reptil volant des environs d'Aichstedt, que quelques naturalistes ont pris pour un olseau, et donc nous formons un genre de Sauriens sous le nom de Ptero-Dactyle. *Annales du Musée d'Histoire Naturelle Paris* 13: 424.
- Dalla Vecchia, F. 1997. New observations on the osteology and taxonomic status of *Preondactylus buffarini* Wild 1984 (Reptilia, Pterosauria). *Bollettino della Società Paleontologica Italiana* 36: 355-366.
- Dalla Vecchia, F.M. 2003. New morphological observation on Triassic pterosaurs. 23-44. In: E., Buffetaut and J-M., Mazin (eds) 2003. *Evolution and Palaeobiology of Pterosaurs*. Geological Society, London, Special Publications 217: 247pp.
- Dalla Vecchia, F.M., Arduini, P., and Kellner, A.W.A. 2001. The first pterosaur from the Cenomanian (Late Cretaceous) *Lagerstätten* of Lebanon. *Cretaceous Research* 22: 219-225.
- Davis, P.G., and Briggs, D.E.G. 1998. The impact of decay and disarticulation on the preservation of fossil birds. *PALAIOS* 13: 3-13.
- Dyke, G.J., Nudds, R.L. and Rayner, J.M. 2006. Limb disparity and wing shape in pterosaurs. *Journal of Evolutionary Biology* 19: 1339-1342.

- Döderlein, L. 1923. *Anurognathus ammoni*, ein neuer Flöugsaurier. *Sitzungsberichte der Bayerischen Akademie Wissenschaften, math. –naturwiss. Klasse.* 117-164.
- Eck, K. 2008. Die Osteologie von *Tapejara wellnhoferi* Kellner, 1989 aus der Santana Formation des Araripe Beckens (NO-Brasilien). University of Heidelberg, Unpublished diploma thesis.
- Eck, K., Elgin, R.A., and Frey, E. 2011 On the osteology of *Tapejara wellnhoferi* Kellner 1989 and the first occurrence of a multiple specimen assemblage from the Santana Formation, Araripe Basin, NE-Brazil. *Swiss Journal of Palaeontology*. doi:10.1007/s13358-011-0024-5
- Elgin, R.A. and Frey, E. 2008. You show me your sutures and I'll tell you your age: Age traces in a young *Anhanguera* skeleton. EAVP Abstracts 2008, Slovakia.
- Elgin, R.A. and Campos, H.B.N. 2011. A new specimen of the azhdarchoid pterosaur *Tapejara wellnhoferi*. *Historical Biology*. doi: 10.1080/08912963.2011.613467.
- Elgin, R.A., and Frey, E. 2011a. A new ornithocheirid *Barbosania gracilirostris* gen. et. sp. nov. (Pterosauria, Pterodactyloidea) from the Santana Formation (Cretaceous) of NE Brazil. *Swiss Journal of Palaeontology*, doi: 10.1007/s13358-011-0017-4.
- Elgin, R.A., and Frey, E. 2011b. A new azhdarchoid pterosaur from the Cenomanian (Late Cretaceous) of Lebanon. *Swiss Journal of Geosciences*, doi: 10.1007/s00015-011-0081-1.
- Elgin, R.A., and Frey, E. 2012. A nearly complete ornithocheirid pterosaur from the Crato Formation (Aptian, Early Cretaceous) of NE Brazil. *Acta Palaeontologica Polonica*, doi: 10.4202/app.2010.0079.
- Elgin, R.A. and Hone D.W.E. 2013. Pneumatization of an immature azhdarchoid pterosaur. *Cretaceous Research* 45: 16-24.
- Elgin, R.A., Grau, C.A., Palmer, C., Hone, D.W.E., Greenwell, D., and Benton, M.J. 2008. Aerodynamic characteristics of the cranial crest in *Pteranodon*. *Zitteliana B28*: 167-174.
- Elgin R.A., Hone, D.W.E., and Frey, E. 2011. The extent of the pterosaur flight membrane. *Acta Palaeontologica Polonica*, 56: 99-111.
- Fastnacht, M. 2001. First record of *Coloborhynchus* (Pterosauria) from the Santana Formation (Lower Cretaceous) of the Chapada do Araripe, Brazil. *Paläontologische Zeitschrift* 75: 23–26.
- Fastnacht M. 2008. Tooth replacement pattern of *Coloborhynchus robustus* (Pterosauria) from the Lower Cretaceous of Brazil. *Journal of Morphology* 269: 332-348.
- Fastnacht, M., Hess, N., Frey, E., and Weiser, H-P. 2002. Finite element analysis in vertebrate palaeontology. *Senckenbergiana lethaea* 82: 195-206.
- Frey, E., and Reiß, J. 1981. A new reconstruction of the pterosaur wing. *Neues Jahrbuch für Geologie und Paläontologie Abhandlungen* 161: 1-27.
- Frey, E. and Martill, D.M. 1994. A new pterosaur from the Crato Formation (Lower Cretaceous, Aptian) of Brazil. *Neues Jahrbuch für Geologie und Paläontologie Abhandlungen* 194: 379-412.
- Frey, E., and Martill, D.M. 1996. A reappraisal of *Arambourgiania* (Pterosauria, Pterodactyloidea): One of the world's largest flying animals. *Neues Jahrbuch für Geologie und Paläontologie Abhandlungen* 199: 221-247.
- Frey, E. and Martill, D.M. 1998. Soft tissue preservation in a specimen of *Pterodactylus kochi* (Wagner) from the Upper Jurassic of Germany. *Neues Jahrbuch für Geologie und Paläontologie Abhandlungen* 210: 421-441.
- Frey, E., Tischlinger, H., Buchy, M-C. and Martill, D.M. 2003a. New specimens of Pterosauria (Reptilia) with soft parts with implications for pterosaurian anatomy and locomotion. 233-266. In: E., Buffetaut, and J-M., Mazin, (eds). *Evolution and Palaeobiology of Pterosaurs*. Geological Society, London, Special Publications 217: 247pp.
- Frey, E., Buchy, M-C., and Martill, D.M. 2003b. Middle- and Bottom-decker Cretaceous pterosaurs: unique designs in active flying vertebrates. 267-274. In: E., Buffetaut, and J-M., Mazin, (eds). *Evolution and Palaeobiology of Pterosaurs*. Geological Society, London, Special Publications 217: 247pp.
- Frey, E., Martill, D.M., and Buchy, M-C. 2003c. A new species of tapejarid pterosaur with soft-tissue head crest. 65-72. In: E., Buffetaut, and J-M., Mazin, (eds). *Evolution and Palaeobiology of Pterosaurs*. Geological Society, London, Special Publications 217: 247pp.
- Frey, E., Buchy, M-C., Stinnesbeck, W., González González, A., and Stefano, A. 2006. *Muzquizopteryx coahuilensis* n.g., n. sp. a nyctosaurid pterosaur with soft tissue preservation from the Coniacian (Late Cretaceous) of northeast Mexico (Coahuila). *ORYCTOS* 6: 19-40.
- Frey, E., Meyer, C.A., and Tischlinger, H. 2011. The oldest azhdarchoid pterosaur from the Late Jurassic Solnhofen Limestone (Early Tithonian) of Southern Germany. *Swiss Journal of Geosciences*, 104: 35-55.

- Gauthier, J.A. 1986. Saurischian monophyly and the origin of birds. *Memoirs of the Californian Academy of Science* 8: 1-55.
- Goldfuss, A.1831. Beiträge zur Kenntnis verschiedener Reptilien der Vorwelt. *Nova Acta Academiae Leopoldinae* 15: 61-128.
- Habib, M.B. 2008. Comparative evidence for quadrupedal launch in pterosaurs. *Zitteliana* B28: 159-166.
- Hankin, E.H. 1912. The development of animal flight. *Aeronautical Journal* 70: 24-40.
- Hankin, E.H. and Watson, D.S.M. 1914. On the flight of Pterodactyls. *The Aeronautical Journal* 18: 324-335.
- Hazlehurst, G.A. 1991. The morphometric and flight characteristics of the Pterosauria. University of Bristol. Unpublished PhD thesis, 274pp.
- Hazlehurst, G.A. and Rayner, J.M.V. 1992. Flight characteristics of Triassic and Jurassic Pterosauria: an appraisal based on wing shape. *Paleobiology* 18: 447-463.
- Heptonstall, W.B. 1971. An analysis of the flight of the Cretaceous pterodactyl *Pteranodon ingens* (Marsh). *Scottish Journal of Geology* 7: 61-78.
- Hendenström A., and Liechti F. Estimates of Body Drag Coefficient on the Basis of Dives in Passerine Birds. *Journal of Experimental Biology* 204: 1167-1175.
- Henderson, D.M. 2010. Pterosaur body mass estimates from three-dimensional mathematical slicing. *Journal of Vertebrate Paleontology* 30: 768-785. doi: 10.1080/02724631003758334.
- Hone, D.W.E., and Benton, M.J. 2007. Cope's Rule in the Pterosauria, and differing perceptions of Cope's Rule at different taxonomic levels. *Journal of Evolutionary Biology*: doi:10.1111/j.1420-9101.2006.01284.x
- Hone, D.W.E., Naish, D., and Cuthill, I.C. 2011. Does mutual sexual selection explain the evolution of head crests in pterosaurs and dinosaurs? *Lethaia* 45: 139-156.
- Hutchinson, J. 2001. The evolution of femoral osteology and soft tissues on the line to extant birds (Neornithes). *Zool J Linn Soc* 131:169–197
- Irmis, R. B., Parker, W. G., Nesbitt, S. J. and Liu, J. 2007 Early ornithischian dinosaurs: the Triassic record. *Historical Biology* 19, 3–22. (doi:10.1080/08912960600719988)
- Ji, S-A. and Ji, Q. 1997. Discovery of a new pterosaur from western Liaoning, China. *Acta Geologica Sinica* 71: 1-6.
- Ji, Q., Ji, S-A., Cheng, Y-N., You, H-L., and Lü, C-X. 2004. Pterosaur egg with a leathery shell. *Nature* 432: 572.
- Jouve, S. 2004. Description of the skull of a *Ctenochasma* (Pterosauria) from the latest Jurassic of eastern France, with a taxonomic revision of European Tithonian Pterodactyloidea. *Journal of Vertebrate Paleontology* 24: 542-554.
- Kaup, J. 1834. An examination in compliance with the division of mammals into 6 tribes and amphibians into 6 Orders. *Isis* 3: 311-315.
- Kellner, A.W.A. 1989. A new edentate pterosaur of the Lower Cretaceous from the Araripe Basin, Northeast Brazil. *Anais da Academia Brasileira de Ciências* 61: 439-446.
- Kellner, A.W.A. 1995. The relationships of the Tapejaridae (Pterodactyloidea) with comments on pterosaur phylogeny. *Sixth Symposium on Mesozoic Terrestrial Ecosystems and Biota, Short Papers*: 73-77.
- Kellner, A.W.A. 1996a. Description of new material of Tapejaridae and Anhangueridae (Pterosauria, Pterodactyloidea) and discussion of pterosaur phylogeny. Unpublished PhD thesis. Columbia University, 364pp.
- Kellner, A.W.A. 1996b. Description of the Braincase of two Early Cretaceous pterosaurs (Pterodactyloidea) from Brazil. *American Museum Novitates* 3175: 34pp.
- Kellner, A.W.A. 2003. Pterosaur phylogeny and comments on the evolutionary history of the group. 105-137. In: E., Buffetaut, and J-M., Mazin, (eds) 2003. *Evolution and Palaeobiology of Pterosaurs. Geological Society, London, Special Publications* 217: 247pp.
- Kellner, A.W.A. 2004a. New information on the Tapejaridae (Pterosauria, Pterodactyloidea) and discussion of the relationships of this clade. *Ameghiniana* 41: 521-534.
- Kellner, A.W.A. 2004b. The Ankle Structure of Two Pterodactyloid Pterosaurs from the Santana Formation (Lower Cretaceous), Brazil. *Bulletin American Museum of Natural History*. 285: 25-35.
- Kellner, A.W.A., and Langston Jr., W. 1996. Cranial remains of *Quetzalcoatlus* (Pterosauria, Azhdarchidae) from Late Cretaceous sediments of Big Bend National Park, Texas. *Journal of Vertebrate Paleontology* 16: 222-231.
- Kellner, A.W.A. and Tomida, Y. 2000. Description of a new species of Anhangueridae (Pterodactyloidea) with comments on the pterosaur fauna from the Santana Formation (Aptian – Albian), northeastern Brazil. *National Science Museum Monographs, Tokyo* 17: 138pp.



- Kellner A.W.A., and Campos D.A. 2002. The function of the cranial crest and jaws of a unique pterosaur from the Early Cretaceous of Brazil. *Science* 297: 389-392.
- Kellner, A.W.A., Wang, X., Tischlinger, H., Campos, D.A., Hone, D., and Meng, X. 2009. The soft tissue of *Jeholopterus* (Pterosauria, Anurognathidae, Batrachognathinae) and the structure of the pterosaur wing membrane. *Proceedings of the Royal Society B*: doi:10.1098/rspb.2009.0846.
- Kellner, A.W.A., Campos, D., Sayão, J., Saraiva, A.A.F., Rodrigues, T., Oliveira, G., Cruz, L.A., Costa, F., Silva, H.P., and Ferreira, J.S. 2013. The largest flying reptile from Gondwana: a new specimen of *Tropeognathus* cf. *T. mesembrinus* Wellnhofer 1987 (Pterodactyloidea, Anhangueridae) and other large pterosaurs from the Romualdo Formation, Lower Cretaceous, Brazil. *Anais da Academia Brasileira de Ciências* 85: 113-135.
- Klaus, M. 2008. Multi-body simulation of a pterosaur: Insights on flight mechanics and aerodynamics. Deutsches Zentrum für Luft- und Raumfahrt, DLR IB 232-2008 J 10. Unpublished Diploma Thesis.
- Kripp, D. 1943. Ein Lebensbild von *Pteranodon ingens* auf flugtechnischer Grundlage. *Luftwissen* 8:217-246.
- Lawson, D.A. 1975. Pterosaur from the Latest Cretaceous of West Texas: Discovery of the Largest Flying Creature. *Science* 185: 947-948.
- Lee, Y-N. 1994. The Early Cretaceous pterodactyloid pterosaur *Coloborhynchus* from North America. *Palaeontology* 37: 755-763.
- Lockley, M.G., Harris, J.D., and Mitchell, L. 2008. A global overview of pterosaur ichnology: track site distribution in space and time. *Zitteliana* B28: 185-198.
- Lü, J-C. 2003. A new pterosaur: *Beipiaopterus chenianus*, gen. et sp. nov. (Reptilia: Pterosauria) from the Western Liaoning Province of China. *Memoir of the Fukui Prefectural Dinosaur Museum* 2: 153 - 160.
- Lü, J-C., and Ji, Q. 2006. Preliminary results of a phylogenetic analysis of the pterosaurs from western Liaoning and surrounding areas. *Journal of Paleontological Society of Korea* 22: 239-261.
- Lü, J-C. Gao, C., Meng, Q., Liu, J., and Ji, Q. 2006a. On the Systematic Position of *Eosipterus yangi* Ji et Ji 1997 among Pterodactyloids. *Acta Geologica Sinica* 80: 643-646.
- Lü, J-C., Jin, X., Unwin, D.M., Zhao, L., Azuma, Y., and Ji, Q. 2006b. A New Species of *Huaxiaopterus* (Pterosauria: Pterodactyloidea) from the Lower Cretaceous of Western Liaoning, China with Comments on the Systematics of Tapejarid Pterosaurs. *Acta Geologica Sinica* 80: 315-326.
- Lü, J., Unwin, D.M., Xu, L., Zhang, X. 2008. A new azhdarchoid pterosaur from the Lower Cretaceous of China and its implications for pterosaur phylogeny and evolution. *Naturwissenschaften* 95: 891 - 897
- Lü, J-C., Unwin, D.M., Jin, X., Liu, Y., and Ji, Q. 2009. Evidence for modular evolution in a long-tailed pterosaur with a pterodactyloid skull. *Proceedings of the Royal Society B*: doi 10.1098/rspb.2009.1603.
- Lü, J-C., Pu, H., Xu, L., Wu, Y., and Wei, X. 2012. Largest toothed pterosaur skull from the Early Cretaceous Yixian Formation of Western Liaoning, China, with comments on the Family Boreopteridae. *Acta Geologica Sinica* 86, 287-293.
- Marchman, J.F., and Werme, T.D. 1984. Clark-Y airfoil performance at low Reynolds numbers. AIAA 22<sup>nd</sup> Aerospace Sciences Meeting, Reno, Nevada, USA. AIAA-84-0052.
- Martill, D.M. 2007. The age of the Cretaceous Santana Fossil Konservat Lagerstätte of north-east Brazil: a historical review and an appraisal of the biochronostratigraphic utility of its palaeobiota. *Cretaceous Research* 28: 895-920.
- Martill, D.M., and Naish, D. 2006. Cranial crest development in the azhdarchid pterosaur *Tupuxuara*, with a review of the genus and tapejarid monophyly. *Palaeontology* 49: 925-941.
- Maybury, W.J., and Rayner, J.M.V. 2001. The avian tail reduces body parasite drag by controlling flow separation and vortex shedding. *Proceedings of the Royal Society of London, B* 268: 1405-1410.
- Maybury, W.J., Rayner, J.M.V., and Couldrick, L.B. 2000. Lift generation by the avian tail. *Proceedings of the Royal Society of London, B* 268: 1443-1448.
- Mazin, J-M., Billon-Bruyat, J-P., and Padian, K. 2009. First record of a pterosaur landing trackway. *Proceedings of the Royal Society B*: doi 10.1098/rspb.2009.1161
- McNeill Alexander, R. 2003. Principles of animal locomotion. Princeton University Press. 371 pp.
- Naish, D., Simpson, M., and Dyke, G. 2013. A new small-bodied azhdarchoid pterosaur from the Lower Cretaceous of England and its implications for pterosaur anatomy, diversity and phylogeny. *PLoS ONE* 8, doi: e58451. doi:10.1371/journal.pone.0058451.
- Nesov, L.A. 1984. Upper Cretaceous pterosaurs and birds from Central Asia. *Paleont. Zhur.* 1: 47-57.

- Norberg, U.M.L., Brooke, A.P., and Trewshella, W.J. 2000. Soaring and non-soaring bats of the family Peropodidae (Flying foxes, *Pteropus* spp.): Wing morphology and flight performance. *The Journal of Experimental Biology* 203: 651-664.
- Oliver, J.S., and Graham, R.W. 1994. A catastrophic kill of ice-trapped coots: time-averaged versus scavenger-specific disarticulation patterns. *Paleobiology* 20: 229-244.
- Owen, R. 1851. Monograph on the Fossil Reptilia of the Cretaceous Formations. *Monographs of the Palaeontological Society* 1: 80-104.
- Owen, R. 1859a. On the remains of new and gigantic species of pterodactyle (*Pter. fittoni* and *Pter. sedgwickii*) from the Upper Greensand near Cambridge. *Reports of the British Association for the Advancement of Science* 28: 98-103.
- Owen, R. 1859b. Supplement (No. I) to the monograph on the fossil Reptilia of the Cretaceous Formations. *Monographs of the Palaeontological Society*: 1-19.
- Owen, R. 1860a. On the orders of fossil and recent Reptilia and their distribution in time. *Reports of the British Association for the Advancement of Science* 29: 153-166.
- Owen, R. 1860b. On the vertebral characters of the order Pterosauria, as exemplified in the genus *Pterodactylus* (Cuvier) and *Dimorphodon* (Owen). *Philosophical Transactions of the Royal Society of London* 149: 161-169.
- Owen, R. 1861. Supplement (No. III) to the Monograph on the Fossil Reptilia of the Cretaceous Formations. *Monographs of the Palaeontological Society*: 1-19.
- Owen, R. 1874. A monograph on the fossil Reptilia of the Mesozoic Formations. *Monographs of the Palaeontological Society*: 1-14.
- Padian, K. 1983. Osteology and functional morphology of *Dimorphodon macronyx* (Buckland) (Pterosauria: Rhamphorhynchoidea) based on new material in the Yale Peabody Museum. ???
- Padian, K. 1984. The origin of pterosaurs. 163-168. In: Reif, E.W. and Westphal, F. (eds) *Symposium on Mesozoic Terrestrial Ecosystems: Short papers. Third Attempto. Tubingen, Germany.*
- Padian, K. 2008. Were pterosaurs ancestors bipedal or quadrupedal?: Morphometric, functional, and phylogenetic considerations. *Zitteliana* B28: 21-33.
- Padian, K. and Rayner, J.M.V. 1993. The wings of pterosaurs. *American Journal of Science* 293-A: 91-166.
- Palmer, N. 2000. Ministerial Advisory Panel on Illicit Trade. Report for the Department for Culture, Media, and Sport. 76pp.
- Pennycuik, C.J. 1960. Gliding flight of the fulmar petrel. *Journal of Experimental Biology* 37: 330-338.
- Pennycuik, C.J. 1968. A wind tunnel study of gliding flight in the pigeon *Columba livia*. *Journal of Experimental Biology* 49: 509-526.
- Pennycuik, C.J. 1971. Gliding flight of the white-backed vulture *Gys africanus*. *Journal of Experimental Biology* 55: 13-38.
- Pennycuik, C.J. 1972. Animal flight. *Studies in Biology no. 33. Hodder Arnold.*
- Pennycuik, C.J. 1986. Mechanical constraints on the evolution of flight. *Memoirs of the Californian Academy of Science* 8: 83-98.
- Pennycuik, C.J., Klaassen, M., Kvist, A., and Lindström, A. 1996. Wingbeat frequency and the body drag anomaly: Wind-tunnel observations on a thrush nightingale (*Luscinia luscinia*) and a teal (*Anas crecca*). *The Journal of Experimental Biology* 199: 2757-2765.
- Pennycuik, C.J., Henderström, A., and Rosén, M. 2000. Horizontal flight of a swallow (*Hirundo rustica*) observed in a wind tunnel, with a new method for directly measuring mechanical power. *The Journal of Experimental Biology* 203: 1755-1765.
- Perkins, C.D. and Hage, R.E. 1950. Airplane performance stability and control. *New York: Wiley and Sons.*
- Peters, D. 2000. A re-examination of four prolacertiforms with implications for pterosaur phylogenesis. *Rivista Italiana di Paleontologia e Stratigrafia* 105: 293-336.
- Peters, D. 2001. Wing shape in pterosaurs. *Nature* 374: 315-316.
- Plieninger, F. 1901. Beiträge zur Kenntnis der Flugsaurier. *Palaeontographica* 53: 209-313. [In German].
- Poore, S.O., Sanchez-Halman, A., Goslow Jr, G.E. 1997. Wing upstroke and evolution of flapping flight. *Nature* 387: 799-802.
- Prondvai, E., Tanács, and Frey, E. 2008. Mass estimate of pterosaurs: A case study on Rhamphorhynchus and the problems of finding the best method. *6<sup>th</sup> Meeting of the EAVP, Abstracts*.80-81.

- Prondvai, E. and Hone, D.W.E. 2009. New models for the wing extension in pterosaurs. *Historical Biology*: doi: 10.1080/08912960902859334.
- Rodrigues, T., and Kellner A.W.A. 2013. Taxonomic review of the *Ornithocheirus* complex (Pterosauria) from the Cretaceous of England.
- Schaller, D. 1985. Wing evolution. In: Hecht, M. K., Ostrom, J. H., Viohl, G. and Wellnhofer, P, (eds). *The Beginnings of Birds. Proceedings of the International Archaeopteryx Conference, Eichstätt, 1985*. Freunde des Jura-Museums, Eichst-itr, 333-348.
- Seeley, H.G. 1864a. On pterodactyls, and on a new species of *Pterodactylus machaerorhynchus*. *Proceedings of the Cambridge Philosophical Society*: 228.
- Seeley, H.G. 1864b. On the Osteology and classification of pterodactyls, Part II, with descriptions of the new species *P. hopkinsi* and *P. oweni*. *Proceedings of the Cambridge Philosophical Society*: 228.
- Seeley, H.G. 1864c. On Saurornia and the classification of *Pterodactyles*, Part III. *Proceedings of the Cambridge Philosophical Society*: 228.
- Seeley, H.G. 1865a. On the literature of English pterodactyls. *Annals and Magazine of Natural History* 3: 148-153.
- Seeley, H.G. 1865b. On the pterodactyle as evidence of a new subclass of Vertebra (Saurornia). Report of the British Association for the Advancement of Science: 34: 69.
- Seeley, H.G. 1866. An epitome of the evidence that pterodactyls are not reptiles, but a new subclass of vertebrate animals aligned to birds (Saurornia). *Annals and Magazine of Natural History* 3: 321-331.
- Seeley, H.G. 1869a. Index to the fossil remains of Aves, Ornithosauria and reptilian, from the secondary system of strata arranged in the Woodwardian Museum of the University of Cambridge. XXIII + 143 pp., Deighton, Bell and Co., Cambridge.
- Seeley, H.G. 1869b. On the bird-like characters of the brain and metatarsus in the *Pterodactylus* from the Cambridge Greensand. *Proceedings of the Cambridge Philosophical Society*: 129-130.
- Seeley, H.G. 1870. The Ornithosauria: an elemental study in the bones of pterodactyls, made from fossil remains found in the Cambridge Upper Greensand, and arranged in the Woodwardian Museum of the University of Cambridge, XXIII + 143 pp., Deighton, Bell and Co., Cambridge.
- Seeley, H.G. 1881. On evidence of two ornithosaurians referable to the genus *Ornithocheirus*, from the Upper Greensand of Cambridge, preserved in the collections of W. Reed, Esq., F.G.S. *Geological Magazine* 8: 13-20.
- Seeley, H.G. 1891a. The ornithosaurian pelvis. *Annals and Magazine of Natural History* 6: 237-255.
- Seeley, H.G. 1891 b. On the shoulder girdle in Cretaceous Ornithosauria. *Annals and Magazine of Natural History* 6: 438-445.
- Seeley, H.G. 1901. *Dragons of the Air: an account of Extinct Flying Reptiles*. Methuen. 239pp.
- Sereno, P.C. 1991. Basal Archosaurs: Phylogenetic relationships and functional implications. *Journal of Vertebrate Paleontology* 11: 1-53. Supplement to volume 4.
- Shamoun-Baranes, J., Leshem, Y., Yom-Tov, Y., and Liechti, O. 2003. Differential use of thermal convection by soaring birds over central Israel. *The Condor* 105: 208-218.
- Sharov, A.G. 1971. (New flying reptiles from the Mesozoic of Kazakhstan and Kirgizia) (In Russian). *Trudy Akademii Nauk SSSR, Palaeontologicheskii Institut* 130: 104-113.
- Shyy, W., Lian, Y., Tang, J., Viieru, D., and Liu, H. 2008. *Aerodynamics of low Reynolds number flyers*. Cambridge University Press, New York, USA. 177 pp.
- Sömmerring, S.T. von. 1812. Über einen *Ornithocephalus*. *Denkschriften der Kniglichen Bayerischen Akademie der Wissenschaften, math -phys Classe* 3: 89-158.
- Spedding, G.R., and McArthur, J. 2010. Span efficiencies of wings at low Reynolds numbers. *Journal of Aircraft* 47: 120-128.
- Stecher, R. 2008. A new Triassic pterosaur from Switzerland (Central Austroalpine, Grisons), *Raeticodactylus filisurenensis* gen. et sp. nov. *Swiss Journal of Geosciences* doi:10.1007/s00015-008-1252-6.
- Steel, L. 2008. The palaeohistology of pterosaur bone: an overview. *Zitteliana* B28: 109-125.
- Stein, R.S. 1975. Dynamic analysis of *Pteranodon ingens*: a reptilian adaptation to flight. *Journal of Paleontology* 49: 534-548.
- Strang, K.A., Kroo, I., Gerritsen, M., and Delp, S. 2009. Efficient flight of pterosaurs – an unsteady aerodynamic approach. 47<sup>th</sup> AIAA Aerospace Sciences Meeting, Orlando, Florida. AIAA 2009-1301. 37 pp.

- Taquet, P., and Padian, K. 2004. The earliest known restoration of a pterosaur and the philosophical origins of Cuvier's *Ossemen Fossiles*. *Comptes Rendus Palevol* 3: 157-175.
- Tchernov, E., Polcyn, M. J. and Jacobs, L. L. 1996. Snakes with legs: the Cenomanian fauna of 'Ein Yabrud, Israel. *Journal of Vertebrate Paleontology* 16: (Supplement to No. 3), Abstracts, 68A.
- Thomas, A.L.R. 2010. On the aerodynamics of bird's tails. *Philosophical Transactions: Biological Sciences* 340: 361-380.
- Tischlinger, H. and Frey, E. 2002. Ein *Rhamphorhynchus* (Pterosauria, Reptlia) ungewöhnlicher Flughauterhaltung aus dem Solnhofener Plattenkalk. *Archaeopteryx* 20: 1-20.
- Tomkins, J.L., LeBas, N.R., Witton, M.P., Martill, D.M., and Humphries, S. 2010. Positive allometry and the prehistory of sexual selection. *The American Naturalist* 176: doi:10.1086/653001.
- Tucker, V.A. 1988. Gliding flight: speed and acceleration of ideal falcons during diving and pulling out. *Journal of Experimental Biology* 201: 403-414.
- Tucker, V.A. 1990. Body drag, feather drag and interference drag of the mounting strut in a peregrine falcon, *Falco peregrinus*. *Journal of Experimental Biology* 149: 449-468.
- Tucker, V.A. 2000. Gliding Flight: Drag and Torque of a Hawk and a Falcon with straight and turned heads, and a lower value for the parasite drag coefficient. *The journal of Experimental Biology* 203: 3733-3744.
- Tucker, V.A., and Parrott, G.C. 1970. Aerodynamics of gliding flight in a falcon and other birds. *Journal of Experimental Biology* 52: 345-367.
- Unwin, D.M. 1987. Pterosaur extinction: nature and causes. *Mém. Soc. Géol. France* 150: 105-111.
- Unwin, D.M. 1988. New remains of the pterosaur *Dimorphodon* (Pterosauria: Rhamphorhynchoidea) and the terrestrial ability of early pterosaurs. *Modern Geology*, **13**: 57-68.
- Unwin, D.M. 1989. A predictive method for the identification of vertebrate ichnites and its application to pterosaur tracks. In: Gillette, D. M. and Lockley, M. (eds), *Dinosaur tracks and traces*, pp 259-274, Cambridge University Press, Cambridge.
- Unwin, D.M. 1992. The phylogeny of the Pterosauria. *Journal of Vertebrate Palaeontology* 12 (supplement): 57A.
- Unwin, D. M. 1995. Preliminary results of a phylogenetic analysis of the Pterosauria (Diapsida: Archosauria). 69-72. In: Sun, A. and Wang Y. (eds) *Sixth Symposium on Mesozoic Terrestrial Ecosystems and Biota. Short Papers*.
- Unwin, D.M. 2001. Pterosaur Locomotion. 417-420. In: Briggs, D.E.G. and Crowther, P.R. (Eds.) *Paleobiology II*. Wiley-Blackwell, 600 pp.
- Unwin, D.M. 2001. An overview of the pterosaur assemblage from the Cambridge Greensand (Cretaceous) of Eastern England. *Mitt. Mus. Nat'kd Berl. Geowiss. Reihe. . 4*: 189-221.
- Unwin D.M. 2002. Pterosauria (Pterosaurs). In: *Encyclopedia of Life Sciences* 15: 700-702. London. Nature Publishing Group.
- Unwin, D.M. 2003. On the phylogeny and evolutionary history of pterosaurs. 139-190. In: E., Buffetaut and J-M., Mazin (eds) 2003. *Evolution and Palaeobiology of Pterosaurs*. Geological Society, London, *Special Publications* 217: 247pp
- Unwin, D.M. 2005. *The Pterosaurs from Deep Time*. Pi Press, New York, 347pp.
- Unwin, D.M., and Bakhurina, N.N. 1994. *Sordes pilosus* and the nature of the pterosaur flight apparatus. *Nature* 371: 62-64.
- Unwin, D.M., and Bakhurina, N.N. 1995. Wing shape in pterosaurs. *Nature* 374: 315-316.
- Unwin, D.M., Frey, E., Martill, D.M., Clarke, J.B., and Reib, J. 1996. On the nature of the pteroid in pterosaurs. *Proceedings of the Royal Society of London, B* 263: 45-52.
- Unwin, D.M and Martill, D.M. 2007. Pterosaurs of the Crato Formation. 475-524. In: D.M., Martill, G., Bechly, and R.F., Loveridge, (eds.) *The Crato Fossil Beds of Brazil*. Cambridge University Press. 625pp.
- Veldmeijer, A.J., 2003. Description of *Coloborhynchus spielbergi* sp.nov. (Pterodactyloidea) from Brazil in the collection of the National Museum of Natural History (Naturalis), Leiden, the Netherlands - *Scripta Geologica* 125: 35-139.
- Veldmeijer, A. J. 2006. Toothed pterosaurs from the Santana Formation (Cretaceous; Aptian – Albian) of northeastern Brazil. A reappraisal on the basis of newly described material. Unpublished PhD Thesis. Utrecht University, the Netherlands. 269pp.
- Veldmeijer, A.J., Signore, M., and Meijer, H.J.M. 2006. Description of two pterosaur (Pterodactyloidea) mandibles from the Lower Cretaceous Santana Formation, Brazil. *DEINSEA* 11: 67-86.
- Veldmeijer, A.J., Signore, M., and Bucci, E. 2007. Predator-prey interaction of Brazilian Cretaceous toothed pterosaurs: a case example. In: *Predation in Organisms*, Springer Berlin Heidelberg, 295-308.

- Veldmeijer, A.J., Meijer, H.J.M., and Signore, M. 2009. Description of Pterosaurian (Pterodactyloidea: Anhangueridae, *Brasileodactylus*) remains from the Lower Cretaceous of Brazil - *DEINSEA* 13: 9-40 [ISSN 0923-9308].
- Videler, J.J., Stamhuis, E.J., and Povel, G.D.E. 2004. Leading-edge vortex lifts swifts. *Science* 306: 1960-1962.
- Wagner, A. 1858. Neue Beiträge zur Kenntniss der urweltlichen Fauna des lithographischen Schiefers. *Abh. k. bayer. Akad. Wiss. math.-phys. Kl.* 8: 413-528 and pls 12-17. pp. 439-528 and pls 15-17. [In German].
- Wang, X., and Zhou, Z. 2003. A new pterosaur (Pterodactyloidea, Tapejaridae) from the Early Cretaceous Jiufotang Formation of western Liaoning, China and its implications for biostratigraphy. *Chinese Science Bulletin* 48: 16-23.
- Wang X., and Zhou Z., 2006, Pterosaur assemblages of the Jehol Biota and their implication for the Early Cretaceous pterosaur radiation. *Geological Journal* 41: 405-418.
- Wang, X., Kellner, A.W.A., Zhou, Z., Campos, D.A. 2005. Pterosaur diversity and faunal turnover in Cretaceous terrestrial ecosystems in China. *Nature* 437: 875-879.
- Wang, X., Kellner, A.W.A., Zhou, Z., and Campos, A. 2008. Discovery of a rare arboreal forest-dwelling flying reptile (Pterosauria, Pterodactyloidea) from China. *PNAS* 105: doi:10.1073/pnas.0707728105.
- Wang, X., Kellner, A.W.A., Jiang, S., and Meng, X. 2009. An unusual long-tailed pterosaur with elongated neck from western Liaoning of China. *Anais da Academia Brasileira de Ciências* 89: 793-812.
- Wedel, M.J. 2005. Postcranial skeletal pneumaticity in sauropods and its implications for mass estimates. pp. 201-228. In Wilson, J.A., and Curry-Rogers, K. (eds.), *The Sauropods: Evolution and Paleobiology*. University of California Press, Berkeley.
- Wellnhofer, P. 1970. Die Pterodactyloidea (Pterosauria) der Oberjura-Plattenkalke Süddeutschlands. *Abhandlung der Bayerischen Akademie der Wissenschaften* 141: 1-133.
- Wellnhofer, P. 1975. Die Rhamphorhynchoidea (Pterosauria) der Oberjura-Plattenkalke Süddeutschlands. *Palaeontographica Abt. A.* 148: 1-186.
- Wellnhofer, P. 1977. *Araripedactylus dehmi* nov. gen., nov. Sp., a new pterosaur from the Lower Cretaceous of Brazil. *Mitteilungen der Bayerischen Staatssammlung für Paläontologie und historische Geologie* 17: 157-167.
- Wellnhofer, P. 1985. A new pterosaur from the Santana Formation (Aptian), Chapata do Araripe, Brazil. *Palaeontographica Abteilung. A.* 187: 105-182..
- Wellnhofer, P. 1987. New crested pterosaurs from the Lower Cretaceous of Brazil. *Mitt. Bayer. Staatsslg. Paläont. Hist. Geol.* 27: 175-186.
- Wellnhofer, P. 1988. Terrestrial locomotion in pterosaurs. *Historical Biology* 1: 3-16.
- Wellnhofer, P. 1991a. The Illustrated Encyclopedia of prehistoric flying reptiles. *Salamander Books Ltd, London, UK*.
- Wellnhofer, P. 1991b. Additional pterosaur finds from the Santana Formation (Apt) of the Chapada do Araripe, Brazil. *Palaeontographica Abteilung. A* 215: 43-101.
- Wellnhofer, P. 2003. A Late Triassic pterosaur from the Northern Calcareous Alps (Tyrol, Austria). 5-22. In: E., Buffetaut, and J-M., Mazin, (eds). *Evolution and Palaeobiology of Pterosaurs. Geological Society, London, Special Publications* 217: 247pp.
- Wellnhofer, P., Buffetaut, E., and Gigase, P. 1983. A pterosaurian notarium from the Lower Cretaceous of Brazil. *Paläontologische Zeitschrift* 57: 147-157.
- Wellnhofer, P., and Kellner, A.W.A. 1991. The skull of *Tapejara wellnhoferi* Kellner (Reptilia, Pterosauria) from the Lower Cretaceous Santana Formation of the Araripe Basin, Northeastern Brazil. *Mitt. Bayer. Staatsslg. Paläont. Hist. Geol.* 31: 89-106.
- Wild R. 1973. Die Triasfauna der Tessiner Kalkalpen. XXIII. *Tanystropheus longobardicus* (Bassani) (Neue Ergebnisse). *Abh. Schweiz. Paläont. Ges.* 95, 1-162.
- Wild, R. 1978. Die Flugsaurier (Reptilia, Pterosauria) aus der Oberen Trias von Cene bei Bergamo, Italien. *Bollettino della Società Paleontologica Italiana* 17: 176-256.
- Wild, R. 1984a. Flugsaurier aus der Obertrias von Italien. *Naturwissenschaften* 71: 1-11.
- Wild, R. 1984b. A new pterosaur (Reptilia, Pterosauria) from the Upper Triassic (Norian) of Friuli, Italy. *Atti. Museo Friul Storia Nat* 5: 45-62.
- Wild, R. 1994. A juvenile specimen of *Eudimorphodon ranzii* Zambelli (Reptilia, Riv. Mus. civ. Sc. Nat. "E. Caffi" BERGAMO Pterosauria) from the Upper Triassic (Norian) of Bergamo. 16: 95-120.

- Wilkinson, M.T. 2007. Sailing the skies: the improbable aeronautical success of the pterosaurs. *Journal of Experimental Biology* 210: doi:10.1242/jeb.000307.
- Wilkinson, M.T. 2008. Three-dimensional geometry of a pterosaur wing skeleton, and its implications for aerial and terrestrial locomotion. *Zoological Journal of the Linnean Society* 154, 27-69.
- Wilkinson, M. T., Unwin, D. M. and Ellington, C. P. 2005. Lift capability of pterosaur wings and the evolution of gigantism. *Proceedings of the Royal Society B: Biological Sciences* 273: 119-126.
- Williston, S.W. 1911. The wing finger of pterodactyls, with restoration of *Nyctosaurus*. *Journal of Geology*, p 696-705.
- Witmer, L.M., Chatterjee, S., Franzosa, J., and Rowe, T. 2003. Neuroanatomy of flying reptiles and implications for flight, posture and behaviour. *Nature* 425: 950-953.
- Witton, M.P. 2008a. A new approach to determining pterosaur body mass and its implications for pterosaur flight. *Zitteliana* B28: 143-158.
- Witton, M.P. 2008b. The palaeoecology and diversity of pterosaurs. Unpublished Ph.D. Thesis. University of Portsmouth, 307pp.
- Witton, M.P. 2009. A new species of *Tupuxuara* (Thalassodromidae, Azhdarchoidea) from the Lower Cretaceous Santana Formation of Brazil, with a note on the nomenclature of Thalassodromidae. *Cretaceous Research* 30: 1293-1300.
- Witton, M.P. and Naish, D. 2008. A Reappraisal of Azhdarchid Pterosaur Functional Morphology and Paleocology. *PLoS ONE* 3: e2271. doi:10.1371/journal.pone.0002271.
- Witton, M.P., and Habib M.B. 2010. On the size and flight diversity of giant pterosaurs, the use of birds as pterosaur analogues and comments on pterosaur flightlessness. *PLoS* 5: e13982. doi:10.1371/journal.pone.0013982
- Xing, L., Wu, J., Lu, Y., Lü, J.-C., and Ji. Q. 2009. Aerodynamic characteristics of the crest with membrane attachment on Cretaceous pterodactyloid *Nyctosaurus*. *Acta Geologica Sinica* 83: 25-32.
- Yates, D., and Elgin, R.A. 2013. Sticks v. Stones: A comparative discussion of the commercialization and regulation of palaeontological and archaeological material. *University of Massachusetts Conference 2013. "The Past For Sale? The Economic Entanglements of Cultural Heritage.*

# Zitteliana

An International Journal  
of Palaeontology and Geobiology

Series B/Reihe B  
Abhandlungen der Bayerischen Staatssammlung  
für Paläontologie und Geologie

28



DAVID W. E. HONE & ERIC BUFFETAUT (Guest Editors)

**Flugsaurier: pterosaur papers in honour of  
Peter Wellnhofer**

München 2008

# Zitteliana

An International Journal of Palaeontology and Geobiology  
Series B/Reihe B

Abhandlungen der Bayerischen Staatssammlung für Paläontologie und Geologie

## B28

DAVID W. E. HONE & ERIC BUFFETAUT (Eds)

### Flugsaurier: pterosaur papers in honour of Peter Wellnhofer

#### CONTENTS/INHALT

|  |     |
|--|-----|
| Dedication   | 3   |
| PETER WELLNHOFER<br>A short history of pterosaur research  | 7   |
| KEVIN PADIAN<br>Were pterosaur ancestors bipedal or quadrupedal?:<br>Morphometric, functional, and phylogenetic considerations   | 21  |
| DAVID W. E. HONE & MICHAEL J. BENTON<br>Contrasting supertree and total-evidence methods: the origin of the pterosaurs   | 35  |
| PAUL M. BARRETT, RICHARD J. BUTLER, NICHOLAS P. EDWARDS & ANDREW R. MILNER<br>Pterosaur distribution in time and space: an atlas   | 61  |
| LORNA STEEL<br>The palaeohistology of pterosaur bone: an overview  | 109 |
| S. CHRISTOPHER BENNETT<br>Morphological evolution of the wing of pterosaurs: myology and function  | 127 |
| MARK P. WITTON<br>A new approach to determining pterosaur body mass and its implications for pterosaur flight  | 143 |
| MICHAEL B. HABIB<br>Comparative evidence for quadrupedal launch in pterosaurs  | 159 |
| ROSS A. ELGIN, CARLOS A. GRAU, COLIN PALMER, DAVID W. E. HONE, DOUGLAS GREENWELL & MICHAEL J. BENTON<br>Aerodynamic characters of the cranial crest in <i>Pteranodon</i> | 167 |
| DAVID M. MARTILL & MARK P. WITTON<br>Catastrophic failure in a pterosaur skull from the Cretaceous Santana Formation of Brazil   | 175 |
| MARTIN LOCKLEY, JERALD D. HARRIS & LAURA MITCHELL<br>A global overview of pterosaur ichnology: tracksite distribution in space and time                                  | 185 |
| DAVID M. UNWIN & D. CHARLES DEEMING<br>Pterosaur eggshell structure and its implications for pterosaur reproductive biology  | 199 |
| DAVID M. MARTILL, MARK P. WITTON & ANDREW GALE<br>Possible azhdarchoid pterosaur remains from the Coniacian (Late Cretaceous) of England                                 | 209 |
| TAISSA RODRIGUES & ALEXANDER W. A. KELLNER<br>Review of the pterodactyloid pterosaur <i>Coloborhynchus</i>   | 219 |
| JUNCHANG LÜ, LI XU & QIANG JI<br>Restudy of <i>Liaoxipterus</i> (Istiodactylidae: Pterosauria), with comments on the Chinese istiodactylid pterosaurs                    | 229 |
| DAVID M. MARTILL<br>First pterosaur remains from the Exu Formation (Cretaceous) of the Araripe Basin, Brazil   | 243 |
| ERIC BUFFETAUT<br>Late Cretaceous pterosaurs from France: a review   | 249 |

|            |      |            |                     |                |
|------------|------|------------|---------------------|----------------|
| Zitteliana | B 28 | 255 Seiten | München, 31.12.2008 | ISSN 1612-4138 |
|------------|------|------------|---------------------|----------------|



Editors-in-Chief/Herausgeber: Michael Krings, Gert Wörheide  
Production and Layout/Bildbearbeitung und Layout: Martine Focke  
Bayerische Staatssammlung für Paläontologie und Geologie

#### Editorial Board

A. Altenbach, München  
B.J. Axsmith, Mobile, AL  
F.T. Fürsich, Erlangen  
K. Heißig, München  
H. Kerp, Münster  
J. Kriwet, Stuttgart  
J.H. Lipps, Berkeley, CA  
T. Litt, Bonn  
A. Nützel, München  
O.W.M. Rauhut, München  
B. Reichenbacher, München  
J.W. Schopf, Los Angeles, CA  
G. Schweigert, Stuttgart  
F. Steininger, Eggenburg

Richard-Wagner-Str. 10, D-80333 München, Deutschland  
<http://www.palmuc.de/zitteliana>  
email: [zitteliana@lrz.uni-muenchen.de](mailto:zitteliana@lrz.uni-muenchen.de)

Für den Inhalt der Arbeiten sind die Autoren allein verantwortlich.  
Authors are solely responsible for the contents of their articles.

Copyright © 2008 Bayerische Staatssammlung für Paläontologie und Geologie, München

Die in der Zitteliana veröffentlichten Arbeiten sind urheberrechtlich geschützt.  
Nachdruck, Vervielfältigungen auf photomechanischem, elektronischem oder anderem Wege  
sowie die Anfertigung von Übersetzungen oder die Nutzung in Vorträgen, für Funk und Fernsehen  
oder im Internet bleiben – auch auszugsweise – vorbehalten und bedürfen der schriftlichen Genehmigung  
durch die Bayerische Staatssammlung für Paläontologie und Geologie, München.

ISSN 1612-4138

Druck: Gebr. Geiselberger GmbH, Altötting

**Cover Illustration:** Modell eines *Rhamphorhynchus* aus dem Oberjura von Eichstätt. Entwurf: P. Wellnhofer, Modell: R. Liebreich,  
Foto und Collage: M. Schellenberger, L. Geißler, BSPG München.

**Umschlagbild:** Reconstitution of a *Rhamphorhynchus* from the Upper Jurassic of Eichstätt, Bavaria. Concept: P. Wellnhofer;  
design: R. Liebreich; photograph and collage: M. Schellenberger, L. Geißler, BSPG Munich.

## Aerodynamic characters of the cranial crest in *Pteranodon*

By

Ross A. Elgin<sup>1\*</sup>, Carlos A. Grau<sup>2</sup>, Colin Palmer<sup>2</sup>, David W. E. Hone<sup>3</sup>,  
Douglas Greenwell<sup>4</sup> & Michael J. Benton<sup>2</sup>

<sup>1</sup>*Staatliches Museum für Naturkunde Karlsruhe, Erbprinzenstraße. 13, 76133 Karlsruhe, Germany*

<sup>2</sup>*Department of Earth Sciences, University of Bristol, Bristol, BS8 1RJ, UK*

<sup>3</sup>*Institute of Vertebrate Palaeontology and Palaeoanthropology, Xizhimenwai Dajie 142,  
Beijing 100044, P. R. China*

<sup>4</sup>*Centre for Aeronautics, School of Engineering & Mathematical Sciences, City University,  
Northampton Square, London, EC1V 0HB, UK*

Manuscript received October 30, 2007; revised manuscript accepted February 11, 2008.

### Abstract

Perhaps the most iconic of pterosaurs is the Late Cretaceous *Pteranodon*, known for its large wing span of up to 5.6 m or more and a remarkable long bony crest at the back of the head. The function of this crest has been the subject of much controversy, having been interpreted as an aerodynamically beneficial structure, perhaps acting as an airbrake, a forward rudder, or a counterbalance to the beak. In this paper these hypotheses are tested by experimenting on cranial models of both *P. longiceps* and its close relative *P. sternbergi* in a wind tunnel and comparing the results against a crestless control model. The results show that, while a crest assists in lowering the yawing moment of the head and limiting the movement of the centre of pressure, the overall aerodynamic effect is modest. The crest most probably evolved independently of any aerodynamic function, other than to maintain their streamlined profile for reducing drag, and presumably served primarily in either intraspecific sexual displays and/or species recognition.

**Key words:** pterosaurs, aerodynamics, flight, Cretaceous, biomechanics.

### Zusammenfassung

Mit seiner Flügelspanne von bis zu 5,6 m und dem markanten knöchernen Hinterhauptskamm gehört *Pteranodon* aus der Oberkreide zu den bekanntesten und beliebtesten Flugsauriern. Die Funktion des Scheitelkammes war Gegenstand vieler Kontroversen: Er wurde als aerodynamisch nützliche Struktur betrachtet, die möglicherweise als Luftbremse wirkte oder als Frontruder oder auch als Gegengewicht zum Schnabel.

Hier werden diese Hypothesen mit Hilfe von Kopfmodellen von *P. longiceps* und seinem nahen Verwandten *P. sternbergi* in Winkanalversuchen überprüft und mit einem kammlosen Kontrollmodell verglichen. Die Ergebnisse zeigen, dass der Kamm dazu beiträgt, das Giermoment zu senken und die Verschiebung des Druckzentrums zu begrenzen, obgleich der generelle aerodynamische Effekt eher gering ist. Die Kämmen entstanden höchst wahrscheinlich außerhalb des aerodynamischen Funktionsregimes außer dass die ein stromlinienförmiges Profil zur Reduktion des Luftwiderstandes zeigen. Die Kämmen waren entweder intraspezifische Sexualmerkmale oder dienten der Arterkennung.

**Schlüsselwörter:** Pterosauria, Aerodynamik, Flug, Kreide, Biomechanik

### 1. Introduction

Extinct organisms offer many challenges to functional interpretation, especially if there is no living animal that can act as a comparative model. The pterodactyloid pterosaur *Pteranodon* is an example of this – a flying reptile from the Late Cretaceous (100–65 million years ago) of North America, whose adult wingspan varied from 3.8–5.6 m depending on its gender, but might also have reached sizes of over 6 m (BENNETT 2001).

*Pteranodon* was named by MARSH (1876) on the basis of an isolated skull from shallow marine limestones of the Niobrara Chalk Formation (Late Cretaceous) of Kansas, USA. This pterosaur, as one of the largest animals ever to fly, has been the subject of several aerodynamic studies (HANKIN & WATSON 1914; BRAMWELL 1971; BRAMWELL & WHITFIELD 1974; BROWER 1983; CHATTERJEE & TEMPLIN 2004). The head crest has often been interpreted as an aerodynamically useful structure that may

\*Author for correspondence and reprint requests; E-mail: rosselgin@hotmail.com

have functioned as: an airbrake to slow speeds while landing (BRAMWELL & WHITFIELD 1974), a forward rudder to provide steering (HEPTONSTALL 1971; STEIN 1975), or an aerodynamic counterbalance to correct cranial movements, reducing the need for heavy neck muscles (EATON 1910; HEPTONSTALL 1971; BRAMWELL & WHITFIELD 1974). Others have postulated non-aerodynamic functions for the head crest including: a site of muscle attachment (EATON 1910), a heat loss vane (KELLNER & CAMPOS 2002; CHATTERJEE & TEMPLIN 2004), or a display structure (SHORT 1914; BENNETT 1992, 2001; CHATTERJEE & TEMPLIN 2004).

While some previous workers (BRAMWELL & WHITFIELD 1974; STEIN 1975; BROWER 1983; WILKINSON et al. 2006) have performed wind tunnel experiments on model pterosaurs, most work so far has focused on wing design and function. These earlier studies are also of limited use owing to inaccurate reconstructions of the animal, wing shape and properties, and a complete lack of taxonomic diversity. *Pteranodon longiceps* has thus commonly been used as a standard for all pterodactyloids. This is not appropriate for several reasons including: it's unusually large size, highly derived anatomical features, large crest variations among different *Pteranodon* species, and because recent finds have revealed pterosaurs with an even more remarkable array of head crests (CAMPOS & KELLNER 1997; KELLNER & CAMPOS 2002; FREY et al. 2003).

Recent studies that highlight the variability in size and shape between species (FREY et al. 2003), sexual dimorphism (BENNETT 1992, 2001) and ontogenetic variability (BENNETT 2003; MARTILL & NAISH 2006) have tended to interpret the primary function of the pterosaur crest as for display, even though experimental tests to determine the aerodynamic characteristics of different types of crested forms have never been carried out. The aim of this paper is to investigate the aerodynamic characteristics of the cranial crest of the well-studied pterosaur *Pteranodon longiceps* and its closest relative *P. sternbergi*. Calculated aerodynamic results can then be compared with theoretical assumptions to determine whether the crest acted in some aerodynamically useful manner, or was primarily a structure for display.

Institutional Abbreviations: FHSM, Fort Hays Sternberg Museum, Fort Hays State University, Hays, Kansas; KUVV, Museum of Natural History, University of Kansas; UALVP, Geology Museum, University of Alberta, Edmonton; YPM, Yale Peabody Museum.

## 2. Methodology

### 2.1 Model construction

While *Pteranodon* is one of the best-known pterosaurs, represented by hundreds of specimens, it is difficult to use these as a basis for accurate three-dimensional models because the bones are usually fragmentary and crushed (BENNETT 2001). Here the composite cranial reconstructions of *Pteranodon* by BENNETT (2001), based on specimens of *P. longiceps* (KUVV 976, 2212; YPM 1177, YPM 2473) and *P. sternbergi* (FHSM VP 339; UALVP 24238), were used to generate two-dimensional templates in both dorsal and lateral profiles. These two templates were then joined together to produce a three-dimensional structure

that, when bulked up with modelling clay, resulted in a three-dimensional model of the head. Additional bulking due to the presence of soft tissue was very limited as no heavy neck muscles could be attached to the free head and much of the rest of the skull formed the beak. For use in wind tunnel experiments, the sculpted models were then cast in polyurethane, and the crest was cut from a thin aluminium sheet (3 mm thick based on data from BRAMWELL & WHITFIELD 1974) so that it would remain rigid under load. Three scale models were built: large, crested versions of *P. longiceps* and *P. sternbergi*, and a crestless control. By using models with almost identical head shapes (excluding the crests), all aerodynamic differences can therefore be attributed to the shape and presence or absence of a cranial crest. The control model was based on BENNETT's (2001) composite reconstruction, but was scaled to around half life size because the wind tunnel was not large enough for a full-sized model (around 727 mm in this case). While the skulls of old adult males greatly exceed the size of this composite reconstruction (~1138 mm for the head of a presumed male *P. longiceps*, excluding a crest, and 1090 mm for *P. sternbergi*), the models were subject to the same requirements of space and were scaled down appropriately. Thus for large adult animals the model of *P. sternbergi* can be considered to be one third life size while the *P. longiceps* model is between half and one third life size.

As the object of these experiments was to measure the aerodynamic forces produced by the head crest configurations, it was only necessary that the models had external forms that were broadly representative of the real animals. Other characteristics such as mass and mass distribution did not have to be replicated as the model was not free flying. It was fixed to a central strut and dynamic stability was not a study variable. It was also unnecessary to attempt to reproduce the fine detail of the skin over the heads and crests as the lift and drag characteristics are insensitive to the precise form and patterns of roughness over the range of conditions of interest (HOERNER 1965). Similarly, the section shape of a thin aerofoil (the crest in these experiments) has very little effect on the profile drag at low Reynolds numbers (HOERNER 1965). However, the maximum lift coefficient achieved before stall is somewhat sensitive to the fine details of the section shape and also the Reynolds number. In our experiments these restrictions did not affect the conclusions because our main objective was to investigate the sub-stall performance characteristics.

### 2.2 Wind tunnel testing

The models were mounted in a low-speed wind tunnel in the Handley Page Wind Tunnel Laboratory at City University, London, on custom-made brackets positioned on the occipital condyle. The brackets allowed the models to be fixed in a range of 'beak down' (pitch) orientations (Fig. 1) as well as a range of yaw angles (to represent the head being turned to the side). The wind tunnel force-measuring balance and electronic data-acquisition system recorded the three principal forces produced by the models under aerodynamic loading: side force (laterally acting forces), yawing moment (the moment of the side force about the vertical axis), and drag (the force acting backwards). The balance was calibrated so as to cancel out the tare drag of the attachment strut and bracket as well as the weight of the models.

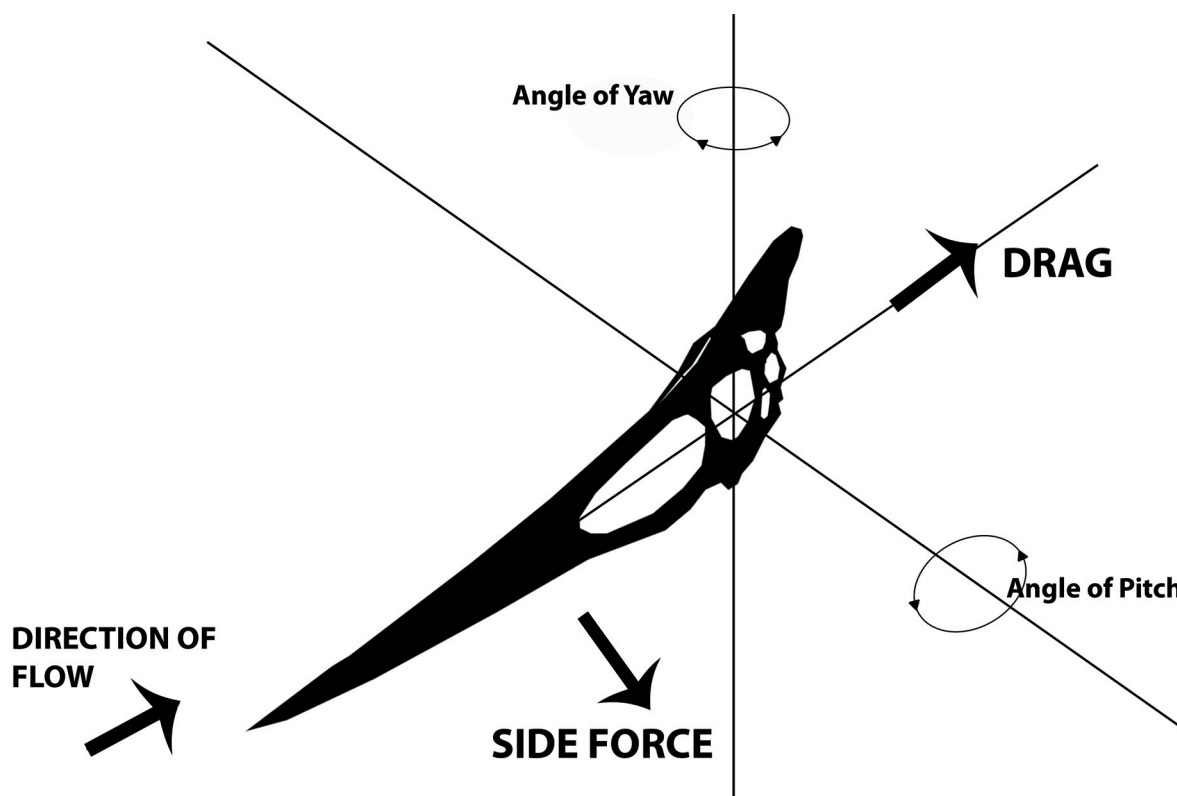


**Figure 1:** Schematic diagram of a *Pteranodon* cranium and movement about the major axes. The pitch and yaw were constantly altered to test the varying effect of model orientation on force generation while the third axis, roll, was not used in this study. The thick arrows here show the major forces acting on the model.

Experiments were run at a speed of 20 m/s, approximately twice the flight speeds calculated in previous studies for *Pteranodon*: 7 m/s (HEPTONSTALL 1971), 8 m/s (BRAMWELL & WHITFIELD 1974), 9.51 m/s (BROWER 1983), 15 m/s (STEIN 1975), or 10–15 m/s (CHATTERJEE & TEMPLIN 2004). The doubling of the tunnel velocity in this way was required to achieve dynamic similarity of the half-sized models. At this speed, the Reynolds number was 400,000 for the complete model and approximately 130,000 for the crests, both of which were expected to be below the transition point from a laminar to a turbulent flow regime. Preliminary tests at a range of air speeds confirmed the insensitivity of the non-dimensional aerodynamic characteristics to flow velocity, so a single speed could be adopted for the tests. The results were reduced to non-dimensional form, from which actual forces could then be predicted for any likely flight speed.

An examination of the osseous labyrinth from an endocast of Anhanguera by WITMER et al. (2003) indicated that pterodactyloid pterosaurs, such as *Pteranodon*, would probably have flown with a somewhat inclined cranium. As a result, side force and yawing moments were calculated for each model at head inclinations (itches) of 0°, 20° and 40° along with yaw angles ranging from -10° to 40°. While it would have been desirable to test our models at up to 90° yaw and greater degrees of pitch, the model attachment, position of the strain gauges and other aspects of the working section of the tunnel prevented this from being a possibility. At 40° pitch the range of yaw was further restricted because of interference from the

central mounting strut.

The resulting forces were then converted into their dimensionless coefficients for comparison and analysis, as follows:

- 1) Side force coefficient ( $C_Y$ ) =  $Y / q * S$ , and
- 2) Yawing moment coefficient ( $C_N$ ) =  $N / q * S * c$ ,

Where:  $Y$  = side force,  $q$  = dynamic pressure,  $S$  = Surface area (m<sup>2</sup>),  $N$  = moment, and  $c$  = reference length (m).

Owing to the unusual shape of the crest, the total head length (tip of beak to most caudal part of the cranium) was used as the model's reference length rather than the more traditional chord in the case of a wing. The yawing moment data were used to calculate the point of action of the side force (the centre of pressure), from which the turning couple applied to the heads was calculated.

### 3. Results

Results of the wind tunnel tests for each model show how variations in model pitch and yaw angle affect the side force up to a yaw angle of 40°. It is important to note that the coefficients presented are dimensionless and represent the aerodynamic characteristics of the model shape rather than any potential differences in size.

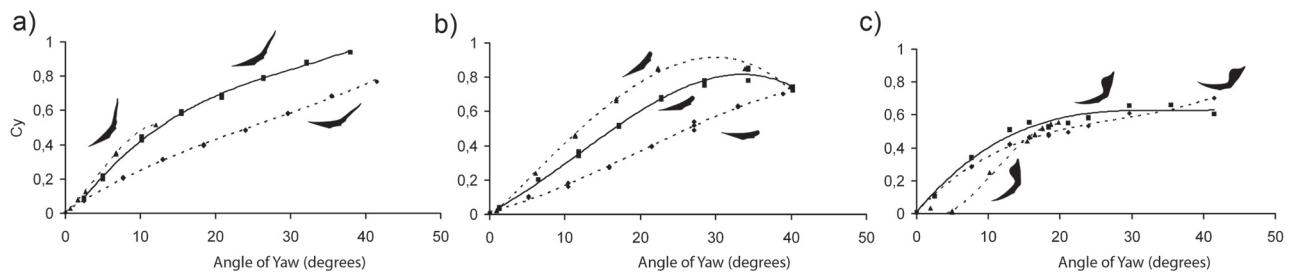


**Figure 2:** Wind tunnel results showing the lateral force ( $C_y$ ) generation characteristics of the three models over angle of yaw. The models *P. longiceps* (a), the crestless form (b), and *P. sternbergi* (c) were mounted at varying angles of cranial pitch,  $0^\circ$ ,  $20^\circ$  and  $40^\circ$ , indicated by the icons on the figure.

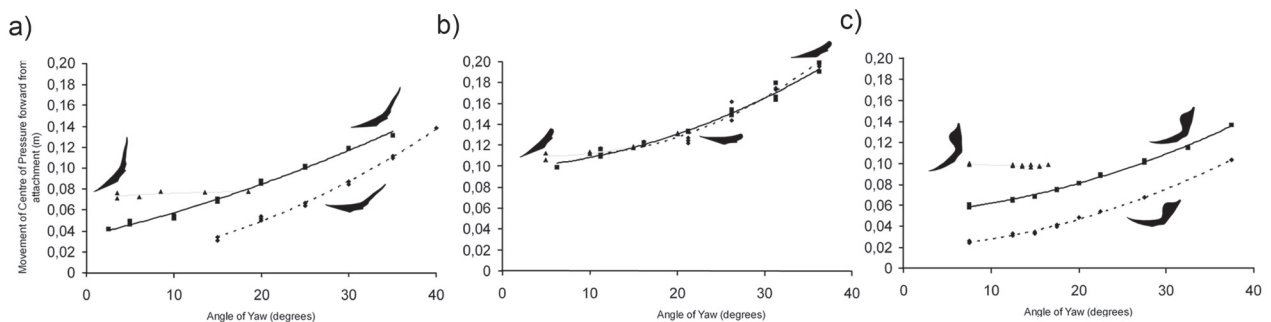


**Figure 3:** Wind tunnel results showing the displacement of the aerodynamic centre of pressure from the attachment bracket of the three models: *P. longiceps* (a), the crestless model (b), and *P. sternbergi* (c). Varying angles of cranial pitch,  $0^\circ$ ,  $20^\circ$  and  $40^\circ$  are indicated by the icons on the figure.

As was expected, there is a general trend of increasing side force with yaw angle (Fig. 2). For *P. longiceps*, (Fig. 2a) with the head horizontal, the side force coefficients increase almost linearly with angles of yaw up to the maximum value tested ( $40^\circ$ ). When the head is pitched downwards, the rate of increase of side force with yaw angle (the lift-curve slope) is initially greater, but becomes the same as for the horizontal orientation at angles of yaw greater than  $15^\circ$ . This result probably arises because the crest acts as a high aspect ratio aerofoil, which initially increases the lift-slope curve, but then experiences stall at a yaw angle of  $10^\circ$  to  $15^\circ$ . At the same time, the low aspect-ratio head, which is of greater area than the crest, can be expected to have a lower lift slope and a far less marked stall point. The combination of these two characteristics is the most likely explanation of the knee in the curve.

The crestless model (Fig. 2b) displays a similar lift slope to the crested *P. longiceps* when both are horizontal. When the head is pitched down, the lift slope increases and at  $40^\circ$  it is almost the same as for the head with a crest at the same pitch orientation. In this case, it appears that the head itself is becoming an increasingly efficient aerofoil as it is pitched down, most probably because of the increase in effective aspect ratio. With this model it was possible to test the  $40^\circ$  pitch case at yaw angles up to  $40^\circ$ , and a clear stall occurred. The angles

of stall reduce with increasing pitch angle, which is commensurate with the changing aspect ratio. However, because of the lower surface area of the crestless model, the actual forces produced will be less.

The *P. sternbergi* model (Fig. 2c) showed less variation of lift slope with pitch angle than the *P. longiceps* model. Apart from a localised reflex in the  $40^\circ$  pitch case around the zero angle of yaw, all three curves more or less collapsed into one another. They all had lift curves with a marked knee inflection at  $15^\circ$  to  $20^\circ$  angle of yaw, with maximum lift being reached by  $40^\circ$ . This is probably because the crest is a relatively large proportion of the total area of the profile of the head and crest, so tends to dominate the aerodynamic characteristics. As the head was pitched down, the effective aspect ratio did not change greatly, thus limiting the change in lift-curve slope. The marked knee inflection in the curve at an angle of yaw of approximately  $15^\circ$  most probably reflects the point at which the flow over the crest becomes stalled, while the flow around the low-aspect-ratio head remains attached and allows the lift to continue to rise with yaw angle, albeit much less rapidly.

The centres of pressure in all three models are anterior to the point of attachment (Figs 3 & 4). In the case of *P. longiceps* the centre of pressure at  $0^\circ$  and  $20^\circ$  pitch angle moves anteriorly, almost linearly with increasing yaw angle, up to the limit of the

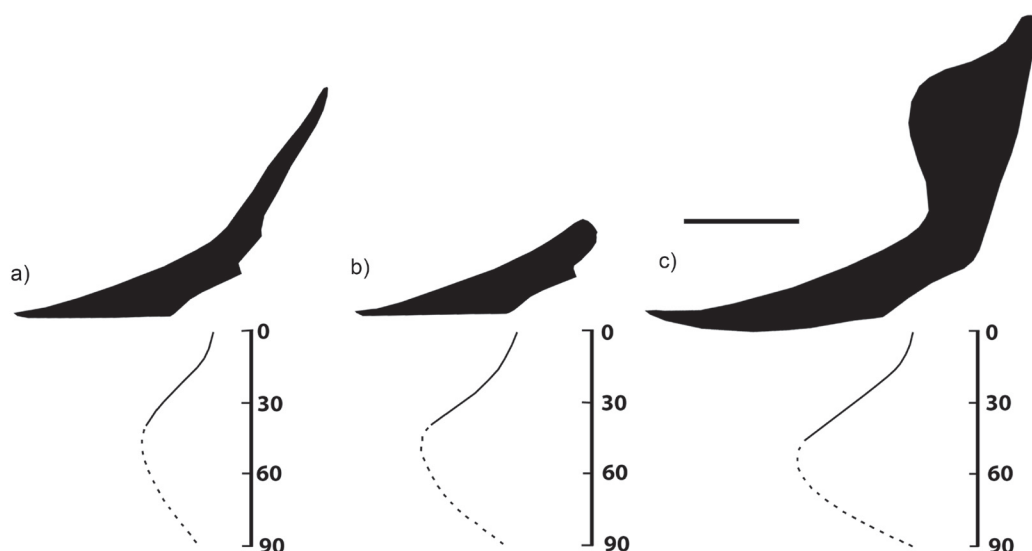


**Figure 4:** The three models: *P. longiceps* (a), the crestless model (b), and *P. sternbergi* (c) are drawn in proportion to full size along with the displacement of the aerodynamic centre of pressure off the occipital condyle for varying angles of yaw. The solid lines represent experimental data while the broken line is the predicted movement of the centre of pressure to the centre of the projected area of the head/crest at 90°. Scale bar 300 mm.

tests at 40°. The position is more anterior at 20° pitch, which may be because the model's rostrum becomes a more effective aerofoil as pitch angle increases. At 40° pitch, movement of the centre of pressure has become mostly insensitive to yaw (Fig. 3a). When the crest is removed, the results collapse onto one another and the position of the centre of pressure becomes the same regardless of the cranial pitch (Fig. 3b).

The model of *P. sternbergi* exhibits similar results to *P. longiceps*. The results for 0° and 20° pitch show almost linear increase with yaw angle, the curve for the higher pitch angle being the more anterior of the two. At 40° pitch, the centre of pressure is again constant with yaw angle (Fig. 3c).

The wind tunnel results were recorded for yaw angles up to 40°, which for the 20° and 40° pitched models was approaching the stall point, and thus the maximum side force. BRAMWELL & WHITFIELD (1974) measured similar results for *P. longiceps*, but were able to make their tests over a wider range of yaw angles. They found that stall occurred at a yaw angle of around 50° for a model in a horizontal (zero pitch) orientation.

If the model was turned to a yaw angle of 90°, the flow became fully separated and the centre of pressure coincident with the centre of area. By interpolation, this allows a good approximation of the position of the centre of pressures position for the missing angles of yaw, between 40° and 90° (Fig. 4).

The results described above show the location of the centre of pressure. However, the yawing (or twisting) moment on the attachment of the head to the neck is the product of the distance of the centre of pressure from the attachment and the actual side force being produced. Typical values of side force and yawing moment were calculated and are shown in Figure 5. As previously stated, the independence of the coefficients

from velocity allows aerodynamic forces, which are a function of the square of the flight speed, to be calculated for any desired velocity. Here, a flying speed of 14 m/s was used to facilitate direct comparison with BRAMWELL & WHITFIELD's results. The maximum value for *P. longiceps* found here was 2.5 Nm as compared to a value of 9.0 Nm reported by BRAMWELL & WHITFIELD (1974), who assumed a relatively larger head size. If the *P. longiceps* results were 'scaled up' to the size proposed by BRAMWELL & WHITFIELD (1974) a moment of 15.9 Nm is predicted – a clear disagreement between the two studies. This may be in part due to differences in the shape of the models, position of the model attachment or tunnel calibration however, in the absence of the original test data, it is not possible to comment further on this difference.

The locations of the centres of pressure in the models are shown in Figure 4. In each case the yaw scale is positioned to be in line with the neck attachment. The solid parts of the curves represent the locations calculated from the present tests. As described above, the location at a yaw angle of 90° is coincident with the centre of area and thus it is possible to construct the likely shape of the curve between yaw angles of 40° and 90°.

## 4. Discussion

Having tested our three models, we may now consider the validity of the generally assumed aerodynamic functions of the cranial crest. The depression of the head outlined by WITMER et al. (2003) tends to increase the lift-curve slope, which results in a rapid increase in lateral force with yaw angle. This force

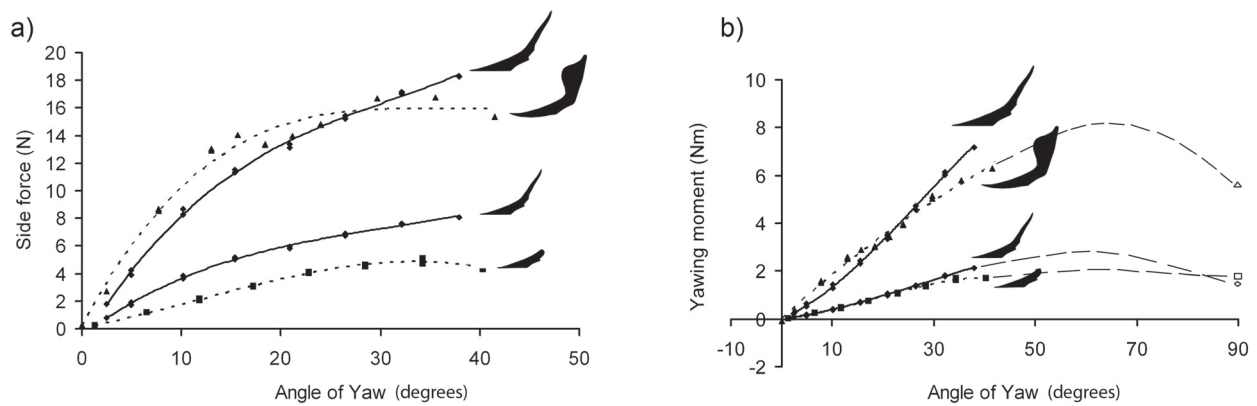


**Figure 5:** Calculated full-scale forces produced by the three models. (a) Side force over the range of tested yaw angles; and (b) yawing moment derived from the wind tunnel tests and calculation of the result at 90° yaw. The larger *P. longiceps* represents the results produced assuming the model was one third its life size. A flight speed of 14m/s was selected for ease of comparison with BRAMWELL & WHITFIELD'S (1974) results.

is, however, limited by stall, which occurs at lower yaw angles when the head is depressed, although a more abrupt stall may itself be a potential source of aerodynamic instabilities. Depression of the head also has the effect of limiting the anterior movement of the centre of pressure, which in turn limits the yawing moment acting on the attachment of the head. Thus the least destabilizing position for the head of *Pteranodon*, by which early or abrupt stall (and the associated sudden change in applied forces) can be avoided, is horizontal, while the yawing moment can be reduced by depressing the head, at the possible expense of flight stability.

#### 4.1 Airbrake

The idea that the crest acted as an airbrake, proposed by BRAMWELL & WHITFIELD (1974), relied on the generation of a large drag force as a result of turning the head through 90° in flight. While our models lacked the range of movement tested by BRAMWELL & WHITFIELD (1974), at a horizontal pitch and a maximum angle of attack of 44°, *P. longiceps* and *P. steinbergi* respectively produced around 25% and 50% more drag than the crestless model because of their crests. As the cranium was pitched down to 40°, however, the drag characteristics of the three models became much more similar. This effect is caused as the model of *P. steinbergi* generates little to no additional lift as the head is pitched downwards. In contrast, the other two models actually become better airfoils as the head is depressed and thus generate not only more lift but also additional lift-induced drag which causes the various drag profiles to converge.

Physiological arguments, as much as aerodynamic evidence, indicate that turning the head to act as an airbrake would have been a dangerous and inefficient method of slowing the animal. Turning the head fully broadside to the airflow would result in the binocular vision being diverted from the animal's flight path, a risky manoeuvre when landing. Deploying the head as an airbrake would also have required a large turn of both the head and neck and placed additional stress on to the neck muscles. It is likely that the wings would have provided a more

effective airbrake both during flight and landing in addition to the, as yet untested, braking performance of the uropatagium and webbed feet. As WILKINSON et al. (2006) have shown, the highly cambered wing membrane is capable of producing a combination of high lift and drag, a far more effective and controllable means of slowing flight than turning the head 90° to one side. The crest is thus poorly designed for an airbrake and indeed a crestless model is itself capable of producing similar values of drag compared with a crested model, provided the head could be pitched downwards during flight. The study of WITMER et al. (2003) suggests that this was the case and thus a crest is not required and, at larger values of pitch, does not enhance the production of drag.

#### 4.2 Forward Rudder

STEIN'S (1975) argument that the crest acted as a forward rudder for steering was based on the belief that a membrane joined the crest to the neck. The idea is weakened by the fact that no fossil evidence for such a membrane has been found in any pterosaur, and most significantly no evidence has been found even in specimens that preserve a gular pouch and other soft tissue structures around the head including soft-tissue crests. While a lack of evidence does not disprove the existence of such a membrane, it remains unlikely for several reasons: the dorsally, rather than caudally, directed crest of *P. steinbergi* is a poor shape to support such a membrane, neck mobility would have been hampered to an unknown degree, and large wings along with additional flight control surfaces (e.g. propatagium [WILKINSON et al. 2006] or foot rudders [FREY et al. 2003]) would almost certainly be better suited for steering.

A related idea was that the large cranium alone might have acted as a flight-control mechanism (HEPTONSTALL 1971) by generating the forces required to turn the animal. A crest would certainly have assisted in such a role, as the crested *P. longiceps* produced around twice as much side force as its crestless counterpart. It remains difficult, however, to understand why such a design would have been more efficient than the use of the animal's large wings under the control of its complex

neuroanatomy (WITMER et al. 2003). The total lift produced by the wings must equal the weight of the animal. BRAMWELL & WHITFIELD (1974) estimated a mass of 16.6 kg, so using the scaling factor deduced from the difference in head size between their reconstruction and that used for the present work, the mass of *P. longiceps* was 4.3 kg. Thus, if the animal banked at 45°, it would have produced a turning force of 30 N, more than three times the maximum generated by the head and crest at an angle of yaw of 40°, and six times that generated at 15° yaw, the probable upper limit before the onset of a potentially destabilizing stall of the crest. Thus by comparison to the wing the crest is a substantially less useful structure for generating lift. It is relevant that extant soaring bats, which do not have crests and rely on wings alone for turning, achieve tight turning circles when circling in thermal lift (NORBERG et al. 2000), as do many species of birds in same conditions.

### 4.3 Counterbalance

The final suggestion was that the crest functioned as an aerodynamic counterbalance to reduce the mass of the muscles required to resist the yawing moments of the head, by shifting the centre of pressure caudally from the attachment (EATON 1910; HEPTONSTALL 1971; BRAMWELL & WHITFIELD 1974). This reduction in the mass of the neck muscles would have had evolutionary significance through reducing the weight of the animal.

Wind tunnel experiments on *P. longiceps* by BRAMWELL & WHITFIELD (1974) showed that the crest acted as a complete counter balance only at angles of yaw greater than 70°. While this may be aerodynamically correct, it is difficult to accept that this characteristic was actually exploited by the animal. Not only is it highly unlikely that an animal in flight would ever have turned its head to such a degree, but according to BRAMWELL & WHITFIELD (1974) the margin between the aerodynamic yawing moment of the head and the restoring moment available from the neck muscles at 45–50° angle was extremely small. In practice this gives the very real possibility that the slightest increase in moment, caused for example by fluctuating air speeds (or indeed errors in their estimates), may have broken the animal's neck. This extremely low margin of safety appears implausible for a large flying animal.

While our experiments lacked this range of movement, they confirm that below a 45° turn of the head, neither crest acted as a full counterbalance, and the calculation of the result at 90° yaw indicates that even at this angle the crested forms were not fully counterbalanced. When compared to the crestless form, the *P. longiceps* model only produced a 20% higher yawing moment despite having almost 50% more total area. Thus the addition of the crest did not result in substantial increases in the yawing moment, despite increased aerodynamic forces due to its greater area.

Such an effect would have been significant since controlling lateral movements of the head was clearly important to pterosaurs, as suggested by anatomical observations. The cervical vertebrae of *Pteranodon* show a combination of condylar-cotylar, zygapophyseal, and exapophyseal articulations designed to resist twisting motions of the neck (BENNETT 2001). The location of the centre of pressure (Figs 3 & 4) in all results however suggests that the crest's primary function was not as

a full aerodynamic counterbalance.

If the crest is regarded as a sexually dimorphic feature (BENNETT 1992), the apparent absence of a major aerodynamic function might then suggest that males did not suffer a major adaptive penalty by carrying a large crest compared with the smaller-crested females. From the point of view of a sexually selected characteristic it is key that the feature impose some kind of penalty on the animal carrying it (DARWIN 1871). Although the aerodynamic effects of the crest may not have hindered the animal, a penalty, in the form of the energy devoted to both developing and carrying such a heavy structure on such a lightweight animal, must be considered. Thus the neutral aerodynamic results obtained from this study cannot rule out a sexually selective origin or function of the cranial crests in *Pteranodon*.

### 5. Conclusion

Many studies of function in animals contrast adaptations for physical activities and those for display (FARLOW & DODSON 1975; HOEFS 2000). In the case of the head crest of *Pteranodon*, and perhaps of other pterosaurs, the crest is aerodynamically streamlined, so that it does not impede flight by creating excessive drag. However our wind tunnel experiments suggest that previously proposed specific aerodynamic functions (airbrake, forward rudder, and counterbalance) are unlikely to have applied to any great extent. It is more likely that the wings could have performed any steering and balancing functions adequately, particularly with the aid of the animal's complex neuroanatomy (WITMER et al. 2003) and complex membrane (FREY et al. 2003), without the need for additional mechanical assistance from the head and its crest. A behaviour demonstrated by extant soaring bats. Our experiments suggest, in fact, that were *Pteranodon* to try to use its head to assist in steering, braking, or manoeuvring, it would have created aerodynamic instability and imposed substantial twisting loads on the neck attachment.

Sexually dimorphic traits in pterosaurs are apparently evident in the pelvic and other postcranial characters of a number of species including *Rhamphorhynchus* (WELLNHOFER 1975), *Pterodactylus* (MATEER 1976), *Quetzalcoatlus*, *Dsungaripterus* and *Anhanguera* (BENNETT 1992). The work of BENNETT (2001, 2003) has demonstrated that sexual selection and ontogenetic age are the most likely influences in determining the size and shape of the crest. In apparent male specimens of *Pteranodon* the head crest is greatly enlarged against the females, around 50% larger than in putative females (BENNETT 1992). Species could also grow through several variable crest forms throughout their development (MARTILL & NAISH 2006) and rapidly sprout massive structures upon reaching maturity (BENNETT 2003).

Palaeobiologists, and perhaps most evolutionary biologists, might feel that interpreting a complex structure as 'merely' for display is a weak line of argument. Surely something as evolutionarily costly and astounding as the head crest of *Pteranodon* must have offered some hard, biomechanical advantage? And yet, similar recent studies of the dorsal plates of *Stegosaurus* and other extinct reptiles (MAIN et al. 2005) have shown that these elaborate structures perhaps served



more for communication than for thermoregulation. A key point in understanding those animals, as here, is that many (or most) congeners seemed to survive perfectly well without the elaborate structure, be it a head crest or a dorsal plate. Animals today often sport astonishing structures for display purposes (e.g. peacock, lyrebird, red deer): providing the structure does not represent an overwhelming encumbrance, the riotous functioning of sexual selection may far outweigh the common sense of natural selection.

## Acknowledgments

We thank numerous people who collaborated on this project either by providing technical assistance, facilities, equipment, and comments. We thank members of the Centre for Aeronautics in the Bristol University Department of Engineering, including Russel EYRE, Alan BISHOP, and David DELAMORE-SUTCLIFFE. We also thank City University and its technicians both for the use of their wind tunnel facilities and invaluable aeronautic assistance. The University of Bristol Alumni Foundation provided funds to cover the costs of constructing the models. Model-making, moulding and casting were overseen by Remmert SCHOUTEN in the Palaeontology Laboratories of the Department of Earth Sciences, University of Bristol, while templates were provided by the metal workshop technicians of the same department. We also thank Gareth JONES and Colin PENNYCUICK for comments and advice.

## 6. References

- BENNETT, S. C. (1992): Sexual dimorphism of *Pteranodon* and other pterosaurs, with comments on cranial crests. – *Journal of Vertebrate Paleontology*, **12**: 422–434.
- BENNETT, S. C. (2001): The osteology and functional morphology of the Late Cretaceous pterosaur *Pteranodon*. Part 1. Part I. General description of osteology. – *Palaeontographica*, Abt. A, **260**: 1–112.
- BENNETT, S. C. (2003): New crested specimens of the Late Cretaceous pterosaur *Nyctosaurus*. – *Paläontologische Zeitschrift*, **77**: 61–75.
- BRAMWELL, C. D. (1971): Aerodynamics of *Pteranodon*. – *Biological Journal of the Linnean Society* **3**: 313–328.
- BRAMWELL, C. D. & WHITFIELD, G. R. (1974): Biomechanics of *Pteranodon*. – *Philosophical Transactions of the Royal Society London B*, **267**: 503–581.
- BROWER, J. C. (1983): The aerodynamics of *Pteranodon* and *Nyctosaurus*, two large pterosaurs from the Upper Cretaceous of Kansas. – *Journal of Vertebrate Paleontology*, **3**: 84–124.
- CAMPOS, D. A. & KELLNER, A. W. A. (1997): Short note on the first occurrence of Tapejaridae in the Crato Member, (Aptian), Santana Formation, Araripe Basin, Northeastern Brazil. – *Anais da Academia Brasileira de Ciências* **69**: 83–87.
- CHATTERJEE, S. & TEMPLIN, R. J. (2004): Posture, locomotion, and paleoecology of pterosaurs. – *Geological Society of America, Special Papers*, **376**: 1–64.
- DARWIN, C. (1871): *The Descent of Man and Selection in Relation to Sex*; New York (Appleton), 864 pp.
- EATON, G. F. (1910): Osteology of *Pteranodon*. – *Memoirs of the Connecticut Academy of Arts and Science*, **2**: 1–38.
- FARLOW, J. O. & DODSON, P. (1975): The behavioural significance of frill and horn morphology in ceratopsians dinosaurs. – *Evolution*, **29**: 353–361.
- FREY, E., TISCHLINGER, H., BUCHY, M.-C. & MARTILL, C. M. (2003): New specimens of Pterosauria (Reptilia) with soft parts with implications for pterosaurian anatomy and locomotion. – In: E. BUFFETAUT & J.-M. MAZIN (Eds), *Evolution and Palaeobiology of Pterosaurs*. – Geological Society, London, Special Publications **217**: 233–282.
- HANKIN, E. H. & WATSON, D. M. S. (1914): On the flight of pterodactyls. – *Aeronautical Journal*, **18**: 324–335.
- HEPTONSTALL, W. B. (1971): An analysis of the flight of the Cretaceous pterodactyl *Pteranodon ingens* (Marsh). – *Scottish Journal of Geology*, **7**: 61–78.
- HOEFS, M. (2000): The thermoregulatory potential of *Ovis* horn cores. – *Canadian Journal of Zoology* **78**: 1419–1426.
- HOERNER, S. F. (1965): Fluid-dynamic drag. *Hoerner Fluid Dynamics*.
- KELLNER, A. W. A. & CAMPOS, D. A. (2002): The function of the cranial crest and jaws of a unique pterosaur from the early Cretaceous of Brazil. – *Science* **297**: 389–392.
- MAIN, R. P., RICQLÉS, A. DE, HORNER, J. R. & PADIAN, K. (2005): The evolution and function of thyreophoran dinosaur scutes: implications for plate function in stegosaurs. – *Paleobiology* **31**: 291–314.
- MARSH, O. C. (1876): Notice of a new sub-order of Pterosauria. – *American Journal of Science*, **11**: 507–509.
- MATEER, N. J. (1976): A study of *Pteranodon*. – *Bulletin of Geological Institutions of the University of Uppsala, N.S.*, **6**: 23–33.
- MARTILL, D. M. & NAISH, D. (2006): Cranial crest development in the azhdarchoid pterosaur *Taupuxuara*, with a review of the genus and tapejarid monophyly. – *Palaeontology*, **49**: 925–41.
- NORBERG, U. M. L., BROOKE, A. P. & TREWHELLA, W. J. (2000): Soaring and non-soaring bats of the Family Pteropodidae (flying foxes, *Pteropus* spp.): Wing morphology and flight performance. *The Journal of Experimental Biology*, **203**: 651–664.
- STEIN, R. S. (1975): Dynamic analysis of *Pteranodon ingens*: a reptilian adaptation to flight. – *Journal of Paleontology*, **49**: 534–548.
- WELLNHOFER, P. (1975): Die Rhamphorhynchoidea (Pterosauria) der Oberjura-Plattenkalke Süddeutschlands. – *Palaeontographica*, Abt. A, **148**: 1–33.
- WILKINSON, M. T., UNWIN, D. M. & ELLINGTON, C. P. (2006): High lift function of the pteroid bone and forewing of pterosaurs. – *Philosophical Transactions of the Royal Society London B*, **273**: 119–126.
- WITMER, L. M., CHATTERJEE, S., FRANZOSA, J. & ROWE, T. (2003): Neuroanatomy of flying reptiles and implications for flight, posture and behaviour. – *Nature*, **425**: 950–953.

# 空中之龙：短尾翼龙的飞行

## DRAGONS OF THE AIR: FLIGHT IN SHORT TAILED PTEROSAURS

Ross A. ELGIN\*

*Abteilung Geologie, Staatliches Museum für Naturkunde Karlsruhe, Erbprinzenstrasse 13., 76133 Karlsruhe, Germany*

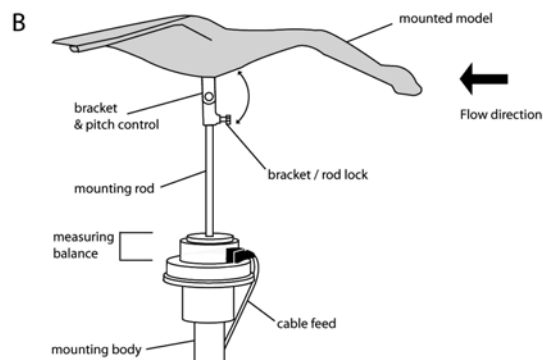
The Pterosaur Flight Dynamics Research Group was established just over three years ago as part of a Karlsruhe based initiative to investigate the aerodynamics of pterodactyloid pterosaurs. Since then, the research group has been joined by experts in the fields of aeroelastics (DLR), fluid dynamics (KIT) and textile engineering (ITV Denkendorf, BIONA project) to explore a number of aspects associated with pterosaurian flight. Models of several pterosaurian taxa, *Anurognathus*, *Coloborhynchus*, *Quetzalcoatlus*, *Sinopterus*, and an as yet unpublished azhdarchoid, were constructed and mounted in a wind tunnel at the University of Karlsruhe (Fig. 1). The results of these experiments are presented here.

The goals of this study were to utilise a number of experimental and theoretical models to record the forces and torques generated during flight; obtaining the coefficients for individual elements of the pterosaur flight apparatus (e.g., cranium, body, fore arm). The results of fixed wing models are compared to those of computerised models of the pterosaur wing (Fig. 2), while jointed models are used to trim the distal wing at higher flight velocities. The effects of altering the material properties of the wing membrane

were also investigated.

Current models of pterosaur flight are based on the use of very light mass estimations in even very large animals and a low parasite drag coefficient, with values ranging from 0.01 to 0.05, based on experiments with smooth objects. Increasing the mass of a pterosaur to match recent estimates was found to significantly increase the flight speed such that velocities attributed to adults by previous authors should instead be attributed to juveniles of the same taxon. Wind tunnel experiments of fixed wing models returned higher than expected coefficients of drag, leading to poorer gliding performances and higher sinking speeds. Such high values of total drag may perhaps be attributed to the large heads, necks and forearms of these taxa; but performance can be altered depending on the degree of streamlining of the body and the aerodynamic efficiency of the selected wing material.

The data recorded for the individual components of the flight apparatus and body will be useful for further aerodynamic analyses of low Reynolds number fliers; specifically the basal, non-pterodactyloids that remain understudied with regard to their flight dynamics.



\* Corresponding author. E-mail: rosselgin@hotmail.com.

Fig. 1 A, Wind tunnel set up with a fixed wing model mounted in the working section. B, Schematic of a model mounted above the measuring balance. Flow direction in both illustrations is from right to left.

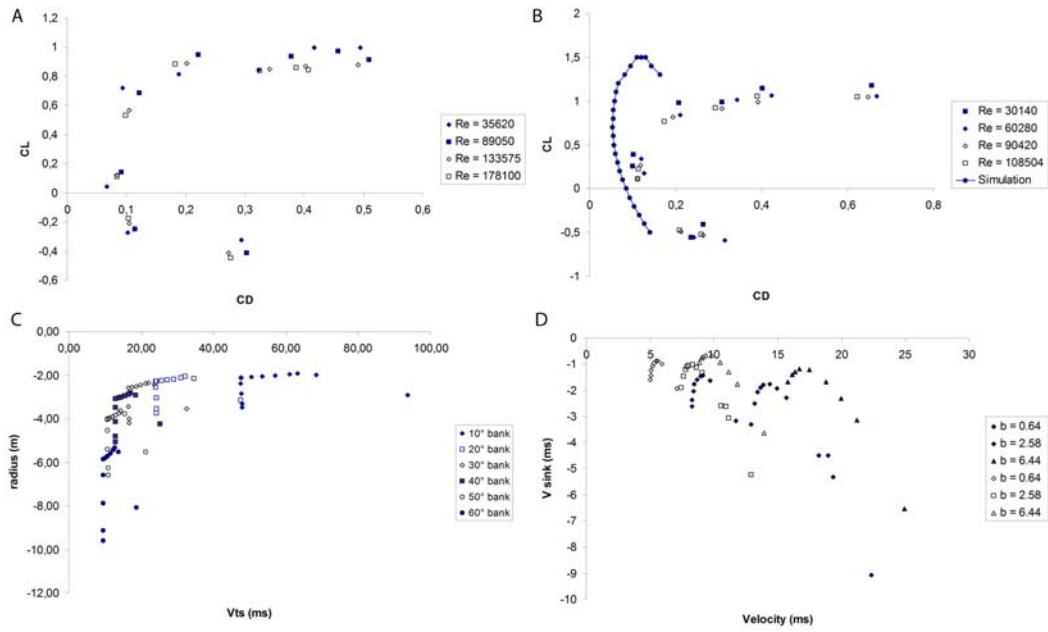


Fig. 2 Selected graphs giving an overview of the range of data gathered during the course of this project. A, Polar curve for *Sinopterus dongi*, B, Polar curves for *Coloborhynchus robustus* and a computerised simulation; C, Circling performance of *Sinopterus* based on the data presented in graph A; D, Gliding performance of *Coloborhynchus* at various stages of it's growth cycle where  $b$  = wing span, filled symbols = heavy mass estimates, open symbols = light mass estimates. CL = Coefficient of lift, CD = Coefficient of drag.

# A new ornithocheirid, *Barbosania gracilirostris* gen. et sp. nov. (Pterosauria, Pterodactyloidea) from the Santana Formation (Cretaceous) of NE Brazil

Ross A. Elgin · Eberhard Frey

Received: 15 October 2010 / Accepted: 21 March 2011  
© Akademie der Naturwissenschaften Schweiz (SCNAT) 2011

**Abstract** An almost complete, ornithocheirid pterosaur from the Romulado Member of the Santana Formation, NE Brazil is described. The specimen lacks a rostral and dentary median sagittal crest and is sufficiently distinct from other crestless taxa to warrant the erection of a new genus and species, *Barbosania gracilirostris* gen. et sp. nov. It confirms the absence of a crest as a genuine condition rather than a consequence of ontogenetic immaturity and indicates a shift from the previously observed pattern of suture closure in pterodactyloid pterosaurs, where partial fusion of the extensor tendon process has occurred at a relatively small size. Several specimens showing morphology similar to *Brasileodactylus* may instead be more closely allied to *B. gracilirostris*.

**Keywords** Barbosania · Ornithocheiridae · Pterosaur · Santana Formation

## Abbreviations

|      |  |
|------|--|
| AMNH | American Museum of Natural History, New York, USA                                    |
| BSP  | Bayerische Staatssammlung für Paläonologie und Historische Geologie, Munich, Germany |
| MHNS | Museum of Natural History Sintra, Sintra, Portugal                                   |
| NM   | Museu Nacional, Rio de Janeiro, Brazil   |
| NSM  | National Science Museum, Tokyo, Japan  |
| RGM  | Nationaal Natuurhistorisch Museum, Leiden, The Netherlands                           |

R. A. Elgin (✉) · E. Frey  
Staatliches Museum für Naturkunde Karlsruhe,  
Abteilung Geologie, Erbprinzenstraße 13,  
76133 Karlsruhe, Germany  
e-mail: rosselgin@googlemail.com

SMNK Staatliches Museum für Naturkunde Karlsruhe, Karlsruhe, Germany

## Introduction

The Romulado Member of the Santana Formation, NE Brazil, has greatly increased our understanding of the anatomy and palaeobiology of Early Cretaceous pterosaurs. Several taxa known from this locality include the ornithocheiroids: *Anhanguera santanae* (Wellnhofer 1985); *A. araripensis* (Wellnhofer 1985); *A. blittersdorffi* (Campos and Kellner 1985); *Brasileodactylus araripensis* (Kellner 1984); *Cearadactylus* (Leonardi and Borgomanero 1985; Dalla Vecchia 1993); *Coloborhynchus piscator* (Kellner and Tomida 2000); *C. robustus*; *C. spielbergi* (Wellnhofer 1987); *Santanadactylus* (Wellnhofer 1985); *Ornithocheirus mesembrinus* (Kellner and Campos 1994); and the azhdarchoids *Tapejara wellnhoferi* (Kellner 1989); *Thalassodromaeus sethi* (Kellner and Campos 2002); *Tupuxuara leonardii* (Kellner and Campos 1994); *T. longicristatus* (Kellner and Campos 1988). Despite the large number of specimens now known, various details of pterosaur systematics remain the focus of considerable debate and disagreement, foremost among them perhaps being the taxonomic composition of the Ornithocheiroidea (Kellner 2003; Unwin 2003) and the preferential use of the Ornithocheiridae or Anhangueridae; both of which are widely found within the current literature (e.g. Kellner 2003; Unwin 2003; Andres and Ji 2008; Wang et al. 2008; Lü et al. 2008). Although the purpose of this manuscript is not to debate the merits of either side, for the sake of clarity all taxonomic divisions adopted here are sensu Unwin (2003)

until a more general consensus is reached. In addition to the problems apparent at higher taxonomic levels, the diagnosis of ornithocheirid pterosaurs from the Brazilian *Lagerstätte* to a generic or species level is complicated by the presence of several taxa that are not clearly distinguished from others (e.g. *Araripedactylus*, *Araripesaurus*, *Santanadactylus*, see Kellner 1991; Kellner and Tomida 2000), the degree to which fossils from the English Greensands are represented in South American localities (Unwin 2001; Veldmeijer et al. 2005; Rodrigues and Kellner 2008), and the extent to which an ontogenetically variable cranial crest can be used to diagnose a taxon (Veldmeijer 2003; Martill and Naish 2006). Crestless materials belonging to ornithocheirid pterosaurs, primarily consisting of isolated rostral fragments, are often assigned as tentative specimens of *Brasileodactylus*, a genus known for the absence of a median crest. As such the genus is particularly controversial, having been suggested to be conspecific with either *Anhanguera* (Unwin 2001) or *Ludodactylus* (Unwin and Martill 2007). Here we present a new crestless ornithocheirid pterosaur from the Romualdo Member of the Santana Formation. The specimen is similar in morphology to those specimens assigned to *Brasileodactylus* but does not meet the current diagnostic criteria for this genus and is sufficiently distinct to warrant the erection of a new genus and species. The described specimen preserves the majority of the skull and postcranial skeleton which is unusual for crestless ornithocheirid pterosaurs from the locality. It is housed in the Museum of Natural History Sintra, Portugal, under the collection number MHNS/00/85, while a cast is held in the collections of the State Museum of Natural History Karlsruhe, Germany (SMNK).

## Preservation

The described specimen MNHS/00/85 is encased within a single large calcareous concretion as is typical of fossils from the Romualdo Member (Fig. 1). It is comprised of a mostly complete, but damaged cranium and mandible, the caudal-most cervical vertebra (c9), the dorsal vertebral column (d1–13), the first sacral vertebrae (s1), and four caudal vertebrae from the base of tail.

The skull is mostly complete, exposed in right lateral view and in natural association with the mandible, which is articulated in occlusion with the upper jaw. Due to the relief of the bone the frontal, parietal and left hand side of the skull remain buried within the matrix of the concretion after preparation. The skull has suffered lateral crushing that is particularly noticeable not only along the rostral and caudal portions of the mandible but also around of the nasoantorbital fenestra and the orbita. The bones dorsal to the nasoantorbital fenestra, such as the caudal process of

the maxilla conjoined with the frontoprefrontal complex, the nasal and the lacrimal are disarticulated along their sutures, but still lie close to their original positions. The lateral parts of the occipital, squamosal, quadrate and postorbital are eroded almost to the same level as the foramen of the n. vagus. The postorbitosquamosal arch is missing and the jugal has rotated medially with the maxillary process diving into the matrix. The transition between premaxilla and maxilla is obscured by both the overlying right humerus and sediment.

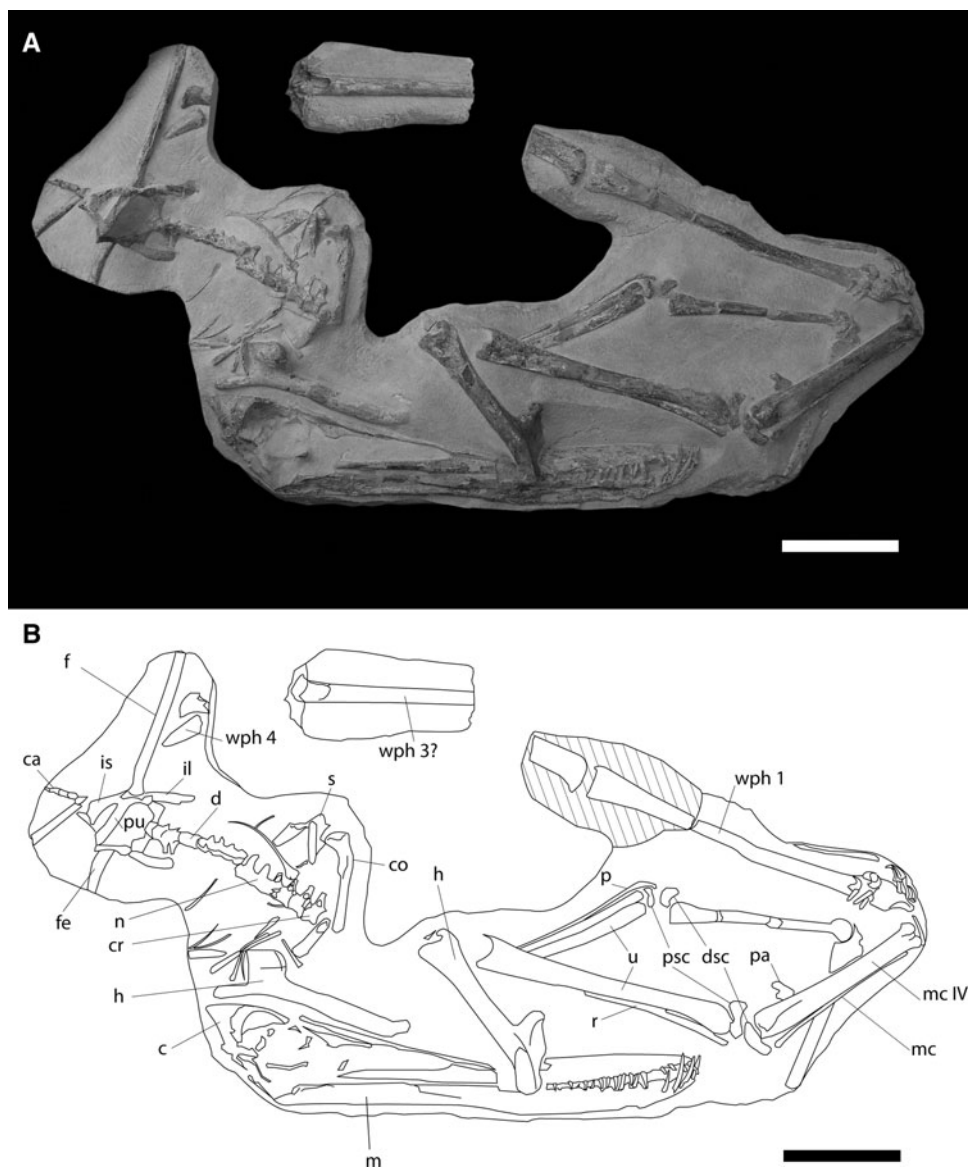
The mandible is visible in right lateral view. All parts of the mandible have been extensively crushed.

The teeth in the rostral portion of the skull show the best preservation. In both the upper and lower jaws the caudally located tooth positions are represented by empty and partially damaged alveoli. Most teeth rostral to the 12th tooth position are preserved in three dimensions with the exception of tooth positions 6 in the upper jaw and 4–5 in the lower. The crowns of the second to fifth teeth of the cranium are missing while the fourth mandibular tooth has broken off at the base of its crown. The rostral-most three of the mandible are completely preserved.

The entire vertebral column is embedded in sediment about level with the transverse processes so that the right lateral faces are only visible in the first 6 vertebrae, i.e. c9 and d1–5. Caudal to the fifth dorsal the vertebral column is offset to the right by the full diameter of a vertebral body before continuing caudally in full articulation. The bodies of the dorsal vertebrae are badly damaged and the exapophyses on the first three dorsals have broken off and are missing from the skeleton. Several disarticulated ribs and possible gastralia are scattered in the thoracic region. Only the right rib of the second dorsal retains a contact with the transverse process. Both scapulae and coracoids are preserved close to their natural positions, but only the right coracoid is almost entirely visible from its caudal aspect. The rest of the shoulder girdle is mostly camouflaged by matrix.

The majority of the skeletal elements of both wings have disarticulated from their natural position but have been displaced by only a small degree. The left humerus lies close to its natural position while the right humerus has been displaced a greater distance from the right shoulder girdle so that it is now positioned with its head across the rostrum. The right humerus and ulna are exposed in caudoventral view and make an angle of about 120° between each other. The right ulna lies along the cranial margin of the right ulna. The right wing metacarpal (mc IV) lies adjacent to the distal syncarpal although it has rotated ~90° caudally around its long axis and is viewed in its cranial aspect. Two metacarpals, associated with the first three digits, lie adjacent to its dorsal face. One is completely exposed while the

**Fig. 1** *Barbosania gracilirostris* (MHNS/00/85) gen. et sp. nov. **a** Photograph and **b** corresponding line tracing highlighting the major elements of the skeleton. *Shading* indicates material erroneously attached to the concretion. Where: *c* cranium, *ca* caudal vertebrae, *co* coracoid, *cr* cervical vertebrae, *d* dorsal vertebrae, *dsc* distal syncarpal, *f* femur, *h* humerus, *il* ilium, *is* ischium, *m* mandible, *mc* metacarpal, *n* “notarium” dorsal vertebrae 1–5, *p* pteroid, *pa* preaxial carpal, *psc* proximal syncarpal, *pu* pubis, *r* radius, *s* scapula, *sc* sacral vertebrae, *u* ulna, *wph* wing finger phalanx. *Scale* equals 100 mm



second is overlain by the first and covered by sediment so that only its distal portion is visible. The metacarpus forms an angle of about 150° with the radius/ulna. The first three digits are preserved cranial to the articulation between the wing finger metacarpal and the basal wing finger phalanx. These three digits preserve all of their elements with the exception of the disciform phalanges and lie sub-parallel to each other with the unguis facing distally. The first or basal phalanx of the right wing finger is partially preserved up until a large break in the concretion approximately 2/3rds along its length. Here a fragment of the concretion containing the articulation of two phalanges of the left wing finger has been erroneously attached. This fragment is interpreted to represent the distal portion of the left first wing finger phalanx and the proximal portion of the second wing finger phalanx.

The left humerus is visible in its ventral aspect. Of the left radius/ulna the proximal half is overlain by the elbow of the right wing and the matrix, however, the distal half is visible in its ventral aspect. The shaft of the left pteroid bone lies adjacent to the left radius. The head of the pteroid bone terminates between the proximal and the distal syncarpals. The wing finger metacarpalia and the basal wing finger phalanges are seen in their ventral aspects and remain in full articulation. A 57-mm section of the left metacarpal IV has undergone extensive repair with a large fragment of bone being glued back into place. The unguis and penultimate phalanges of the first three digits of the left wing lie perpendicular across the proximal terminus of the shaft of the right basal wing finger phalanx. The proximal elements are still covered by matrix. The angle between humerus and radius/ulna as well as that between radius/

ulna and metacarpus is about 150°, while metacarpus and the basal wing finger phalanx include an angle of about 80°. The left basal wing finger phalanx is broken at the mid shaft area at the border of the concretion.

The majority of the pelvic girdle is preserved although some damage and displacement has occurred due to lateral crushing of the specimen. The left puboischiadic plate is only slightly displaced from its natural position although its dorsal portion is obscured by sediment cover and the ventral margins of both the pubis and ilium have been broken. The right puboischiadic plate has collapsed across the sacrals and the ventral margins of the pubis and ischium lie adjacent to the broken end of the left puboischiadic elements. The majority of the right preacetabular process has been broken and crushed but remains visible. Both prepubic bones are missing.

Both femora are articulated with their respective acetabulae and are directed laterally at right angles with respect to the vertebral column. The femora terminate at the border of the concretion whereby the fragment of the right femur is three times the length of the left. Adjacent to the right femoral shaft lies the distal extremity of a wing finger phalanx, most likely wph 3 of the wing. Next to this an elongated bone is directed diagonally across the dorsal surface of the pelvic girdle and is cut by the edge of the concretion. It is uncertain whether this element represents the fourth wing finger phalanx or the tibia as the proximal margin is damaged and missing approximately half the articular surface. The distal portion of the bone does not taper or show a decrease in diameter suggesting that it is more likely to be a displaced tibia.

Although a limited amount of crushing has occurred due to compaction, principally to the skull and portions of the wing finger, the majority of the skeleton has kept its three dimensional form and many of the preserved elements show little trace of *post mortem* displacement. The dentition shows a progressively better state of preservation moving towards the rostrum. Damage from abrasion or the splitting of the concretion is more common and has been severe enough to erode through the bone surface, exposing the internal structures.

The skeleton underwent some preparation and repair prior to its arrival at the State Museum of Natural History Karlsruhe (SMNK), where the majority of preparation was completed on request from the Museum of Natural History Sintra (MHNS), Portugal. The completeness of the skeleton suggests that many more details could be uncovered with a more extensive preparation from the reverse side of the concretion. However, time constraints, a complex positioning of the bones, and a risk of damage prevented this from occurring.

## Systematic palaeontology

Pterosauria (Kaup 1834)

Ornithocheiroidea (Seeley 1870)

Ornithocheiridae (Seeley 1870)

*Barbosania* nov. gen.

*B. gracilirostris* nov. sp.

*Derivation of name* For the genus: *Barbosania* after Professor Dr. Miguel Barbosa, Sintra Museum of Natural History, a recognised local scientist, who engaged himself in bringing palaeontology to public knowledge and substantially helped to secure the specimen. For the species: *gracilirostris* (*gracilis* = lat. for slender, *rostrum* = lat. for snout): the “slender snouted” referring to the slender crestless rostrum without lateral dilatation

*Material* Holotype and only specimen MHNS/00/85 housed in the Museum Natural History Sintra, Portugal

*Locality* Unknown locality. Romualdo Member, Santana Formation, Araripe Plateau, Brazil, (Albian–?Cenomanian). The bluish colour of the concretion strongly suggests a provenance of the Sierra de Maõsina.

Diagnosis for genus and species

Ornithocheirid pterosaur with the following diagnostic features:

1. Keeled but crestless rostrum with a pointed termination.
2. Rostral-most pair of the mandibular and premaxillary alveoli positioned rostroventrally and rostr dorsally, respectively.
3. Tooth positions two and three in both jaws with teeth that are twice as long as those of the subsequent alveoli.
4. The second and third teeth are orientated cranio-laterally and together with the rostral-most teeth form a narrow rosette due to a missing expansion of the tip of the rostrum.
5. Lateral margins of the rostrum gradually converge rostrally.
6. An estimated 24 and 20 tooth positions in the upper and the lower jaw, respectively.
7. Inter-alveolar space gradually increasing caudally, alveolar diameter about constant until tooth position 13.
8. Teeth between the eighth and thirteenth tooth positions in upper and lower jaw with an almost symmetrical interdigitation.
9. Height of the nasoantorbital fenestra approximately 22% that of its length and forming ~24% of the total skull length.

10. Parietal with flat external face, dorsal margin of the short median occipital process is deflected with a triangular transversally convex dorsal face.
11. 13 trunk vertebrae.
12. Caudoventral margin of ischium concave.

While several of these features are not unique to the described specimen their presence, when combined with the other characters noted above, remains useful for the identification of this genus. Only character 12 is unique for *Barbosania*.

## Description

### Skull

The most apparent feature of the skull is the lack of any median sagittal crest on the rostrum. Both the intermaxillary region and the symphyseal area of the mandible had a tall, sub-triangular cross-section with a sharp median keel. In a rostral direction the ventral margin of the cranium is directed craniodorsally from the tenth alveolus. This is also true for the dorsal margin of the mandible although the curvature begins level with the sixth mandibular tooth. The second to seventh alveoli of the cranium counted from the tip of the rostrum are therefore positioned dorsal to and slightly lateral to those in the more caudal tooth positions.

The palate is orientated approximately 50–60° to the horizontal plane in the premaxillary portion of the cranium and is visible in lateral view, particularly by the sixth alveoli. Accounting for the compaction to the rostral region of the skull the premaxillary part of the palatine would have formed a median keel protruding into the buccal cavity.

### Premaxilla

The premaxilla is well preserved but shows an impaction groove that runs parallel to dorsal margin of the rostrum. It extends from a position level with the 4th tooth position until the 12th tooth socket. The rostral portion of the snout remains undamaged and is sub-triangular in cross section. A small discontinuous scar that may represent the remains of the suture between the premaxilla and maxilla is visible and extends to a point level with the caudal margin of the fourth tooth. Further rostrally the suture becomes vague and its exact termination cannot be reconstructed with certainty. There is no lateral expansion of the rostrum and the dorsal and ventral margins of the premaxilla converge at a steep angle, ~33.4° in lateral view. The rostrum is therefore slender with a pointed termination. The maxillary keel becomes blunt on the premaxillary part of the rostrum and merges with its slender tip (Figs. 2, 3).

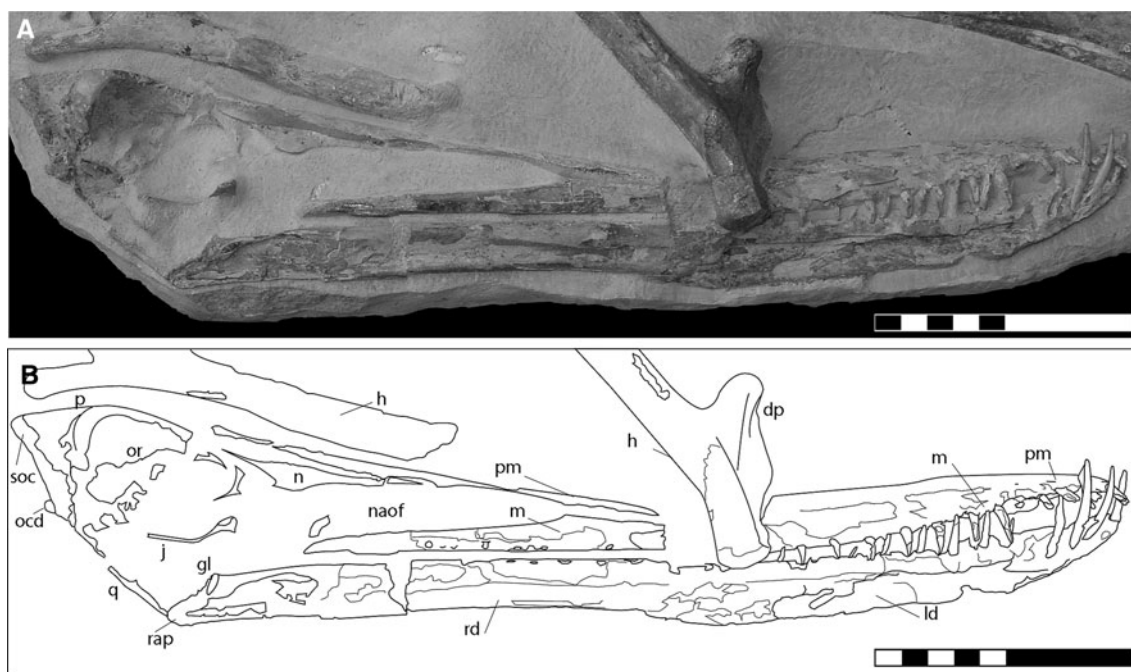


**Fig. 2** *Barbosania gracilirostris* (MHNS/00/85) gen. et sp. nov. Photograph (a) and (b) line tracing of the skull and surrounding elements: *dp* deltopectoral crest, *h* humerus, *j* jugal, *jar* jaw articulation, *ld* left dentary, *m* maxilla, *n* nasal, *naof* nasoantorbital

fenestra, *ocd* occipital condyle, *or* orbita, *p* parietal, *pm* premaxilla, *q* quadrate, *rap* retroarticular process, *rd* right dentary, *soc* supraoccipital crest. Scale equals 100 mm



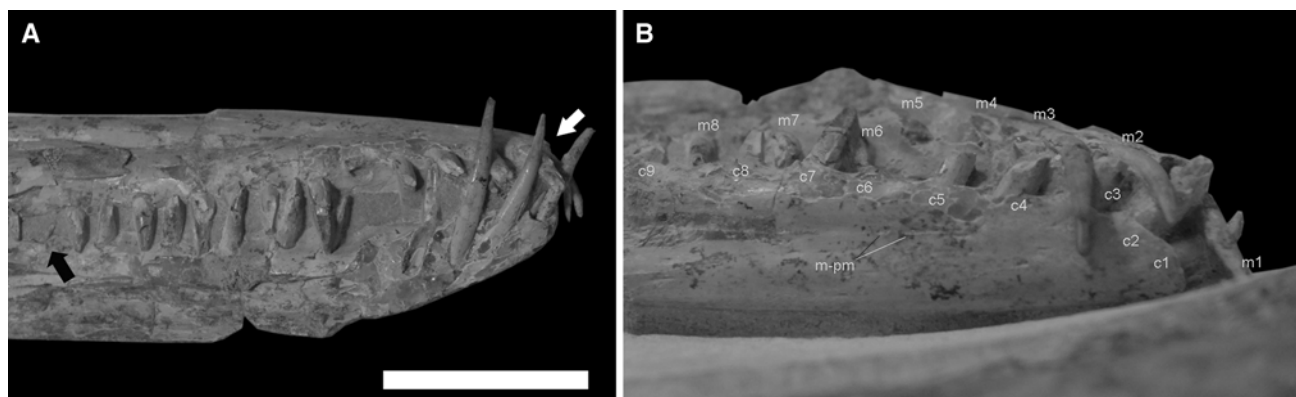


**Fig. 3** *Barbosania gracilirostris* (MHNS/00/85) gen. et sp. nov. Photographs of the rostral region of the skull in its lateral (a) and dorsal (b) aspects where: *c* cranial tooth, *m* mandibular tooth, *m-pm*

?maxilla-premaxilla suture. *White arrow* denotes the pointed rostral termination while the *black arrow* indicates an example of tooth replacement. *Scale* equals 50 mm

### Maxilla

The maxilla extends caudally forming the majority of the ventral margin of the cranium and the ventral border of the nasoantorbital fenestra. The ventral margin of the bone is straight but is deflected dorsally at an angle of about 10° around the tenth tooth position. The caudoventral portion of the bone is damaged and the compacta is missing. The caudal extent of the maxilla and its relationship with the jugal is therefore unclear.

### Nasal

The nasal lies loose from its surrounding elements and is complete with the exception of a small break in the cranial portion of the bone. In its lateral aspect the bone shows its maximum dorsoventral extension just dorsal to the articular surface with the lacrimal while the rostral and caudal processes of the nasal taper away from this point. The rostral process of the bone extends ventral to the premaxilla and forms ~48% of the dorsal margin of the nasoantorbital fenestra. Likely the caudal process of the premaxilla has merged with the rostral process of the nasal. The caudal process of the nasal is one-third the length of the rostral process and displays a more pronounced convex ventral margin. The bone margin is recurved just dorsal to the caudoventral margin of the lacrimal articulation where it would have acted as the articular surface for the rostro-dorsal margin of the prefrontal. The articular surface on the ventral margin of the nasal, where it would have articulated with the lacrimal, is flat.

### Prefrontal, frontal and parietal

These three bones form the caudodorsal roof of the skull but are mostly embedded within the concretion. No suture

dividing the three elements can be identified. The dorsal face of the parietal is transversely concave and is confluent with the supraoccipital crest.

### Jugal

The jugal is a triradiate bone that forms the caudal and caudoventral margins of the nasoantorbital fenestra, the cranioventral, caudoventral margins of the orbita and the cranial border of the infratemporal fenestra. Although it appears mostly intact in MNHS/00/85, the bone has been displaced and rotated into the skull cavity such that only the quadratojugal/postorbital and the lacrimal processes are visible but broken. The maxillary process is buried in the matrix. At the break the lacrimal process of the jugal is teardrop shaped in cross-section and tapers towards its caudal margin.

### Supraoccipital

The prominent feature of this bone is the blunt median supraoccipital crest that is elongated and triangular in lateral view. It commences as a low ridge on the mid dorsal margin of the foramen magnum and from there extends dorsally, gradually increasing in both width and prominence. At its dorsal extremity the supraoccipital crest forms a caudoventrally inclined transversally convex face that is cranially confluent with the parietal. Lateral to the supraoccipital crest the supraoccipital is vertically concave while the lateral margins of this bone are either broken or obscured by sediment. The supraoccipital forms the dorsal margin of the foramen magnum. A large oval pneumatic foramen, 3 mm by 5 mm, perforates the caudolateral face of the supraoccipital near the deepest point of the concavity. A straight, medially serrated suture separates the supraoccipital from the exoccipitobasioccipital complex.

The suture runs from the middle of the lateral margin of the foramen magnum dorsolaterally at an angle of about 20° against the horizontal plane. On the ventromedial corner of the supraoccipital a foramen is visible.

#### *Exoccipital, basioccipital and basisphenoid*

These bones make a fused complex that forms the ventrolateral and ventral margins of the foramen magnum. The foramen itself is sub-circular in outline, being slightly broader at its base than dorsally. In lateral view the occipital condyle is orientated caudoventrally at an angle of ~40° against the horizontal plane. The condyle is regularly rounded in its lateral aspect and has an oval outline in caudal view. The vagus foramen, which lies immediately lateroventrally to the occipital condyle, is orientated dorsoventrally but continues as a short ventrally directed sulcus. Directly ventral to the vagus foramen the smooth and vertically concave basioccipital part of the bone complex is exposed, forming the dorsolateral margin of the posterior cranial fenestra. Ventral to the basioccipital flange a fragment of the basisphenoid is separated from the latter by a smooth, ventrolaterally directed, shallow, and sinusoid suture that merges with the ventral margin of the posterior cranial fenestra.

#### *The mandible*

The dentary is straight with a constant height except in places where compaction has distorted the bone. A short but pronounced crest on the labial surface of the dentary, forming the lateral margin of a midline groove, is visible 2–4 mm dorsal to the level of the tooth row. Rostrally, the dentary is broken in such a way that the right lateral face is mostly missing and the medial face of the left dentary is exposed. The ventral part of the symphysis is eroded. On the rostral face of the mandible, two small, slit-like foramina, ~3 mm in length, are observed between the first tooth position and the median line. Cranial of the sixth tooth position, the ventral surface of the dentary is deflected upwards at an angle of ~23° to the long axis of the mandible. Here, the symphysis has formed as a rounded keel suggesting that no sagittal crest was present.

No suture lines defining the angular, surangular or articular are visible, suggesting that these elements may have already fused together. The articular facet for the quadrate forms as an extended, mediolaterally directed oval depression. The retroarticular process is short, 15 mm in length, and directed slightly caudoventrally.

#### *Dentition*

The number of alveoli present in the cranium and dentary is uncertain due to a combination of poor preservation,

particularly about the middle portion of the skull, and the position of the overlying right humerus. In the cranium 13 alveoli are present cranial to the right humerus and 8 poorly preserved ones caudal to this. Two tooth positions are estimated to be present below the humerus and another tooth position likely was present in the caudal portion of the tooth row where the compacta is missing. In total, a minimum of 24 tooth positions are therefore reconstructed for the cranium. As with the cranium, 13 mandibular tooth positions are also preserved rostral to the overlying humerus. A single tooth is visible adjacent to the humeral head while 5 alveoli are visible caudally. One, or perhaps two, tooth positions are likely obscured by damage or the humerus. A minimum of 20 tooth positions are therefore reconstructed for the mandible. The caudal-most alveolus of the mandible is positioned 29 mm rostral to that of the cranium. The three rostral-most teeth of the mandible are completely preserved and show mesiolingual compression and a slight mesial curvature. The crowns of first and third mandibular teeth bear a finely striated enamel cap.

Replacement teeth are observed in the third alveolus of the cranium as well as the first alveolus of the mandible, where it is <29% in size of the active tooth (Fig. 3). The fourth tooth of the cranium and the 11th of the mandible do not completely fill their alveoli indicating that they have not yet grown to their full size.

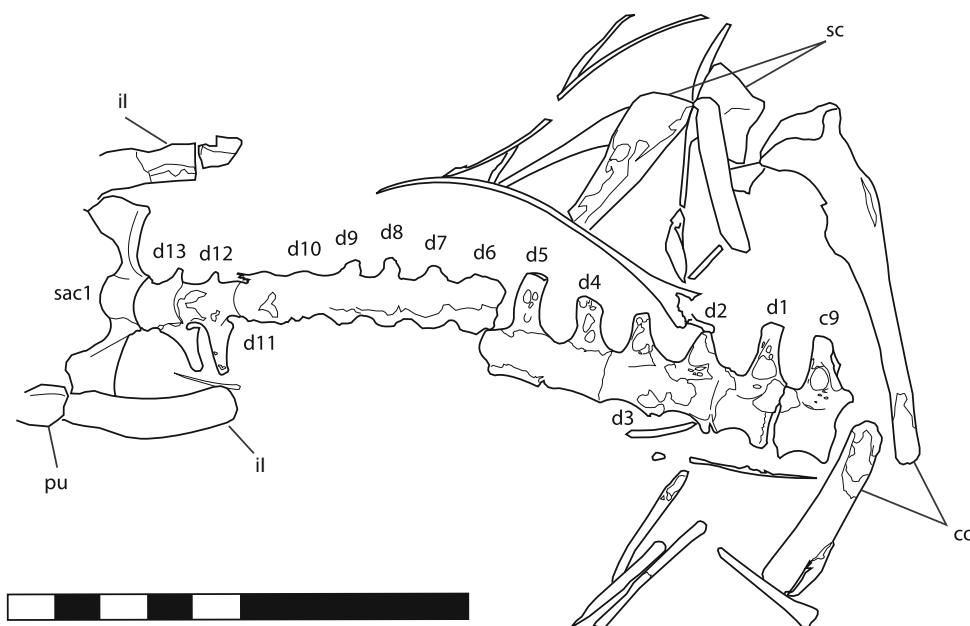
The first pair of teeth of the cranium are orientated rostroventrally, while those of alveoli 2–5 are orientated more rostromedially, as are alveoli 6 and 7 to a lesser extent. Those teeth caudal to the seventh alveoli are directed ventrally.

On the mandible the first tooth is inclined rostradorsally while the second and third are orientated rostromedially. Caudal to these the teeth have a slight dorsolateral inclination. A dentition pattern common in all ornithocheiroids is seen, where the diameter of the alveoli increases caudally until the fourth tooth, which is the largest. The fifth tooth is smaller than the fourth and while the subsequent tooth sockets (alveoli 5–11) are sub-equal in diameter they increase slightly in size up to the ninth tooth position. Caudal to the ninth tooth position the diameter appears to decline. On the mandible the first alveolus is the largest and the diameter of the subsequent alveoli decrease steadily. The interalveolar spaces are gradually increasing from rostrally to caudally, whereby the teeth from position 5 through 12 are straight and form a regular occlusion pattern with an even spacing.

#### *Vertebral column*

The vertebral column is well preserved in ventral view but missing the majority of the cervicals and terminal caudals. In total 19 vertebrae are visible, corresponding to the

**Fig. 4** *Barbosania gracilirostris* (MHNS/00/85) gen. et sp. nov. Line tracing of the axial skeleton: *c* cervical vertebrae *co* coracoid, *d* dorsal vertebrae, *il* ilium, *pu* pubis, *sac* sacral vertebrae, *sc* scapula. Scale equals 100 mm



caudal-most cervical (c9); 13 dorsals (d1–13); the cranial-most sacral (sc1), the rest of the sacrum being covered by sediment and the puboischiadic plate; and 4 caudals. An additional caudal is preserved as a fragment. Within the vertebral column four clearly defined associations are identified: (1) the neck, consisting of only a single disarticulated cervical (c9); (2) the “notarium”, comprised of the first 5 dorsals; (3) the free dorsals and sacrals, a single uninterrupted unit comprised of dorsal vertebrae 6–13 and the first sacral; (4) the four caudal vertebrae (Fig. 4). Within each of the above divisions the vertebrae remain in close association, however, no fusion has occurred between the vertebral bodies. Where the transverse processes are visible they show a depression on their ventral face. In the three cranial-most vertebrae this penetrates the base of the transverse processes deeply and may represent the openings of pneumatic foramina. In d1 and 2 they are associated with 2 or 1 additional small foramina, respectively.

The last cervical (c9) is similar in appearance to the succeeding dorsals but marginally larger in size (Table 1). It lies slightly out of articulation with the first dorsal, the gap having been filled with sediment. On the ventral surface of the transverse process a single large, transverse, oval foramen transversarium pierces the bone and occupies most of the basal region of the transverse process. The corpus itself is pierced by two small oval foramina and between these and the proximal portion of the transverse process seven more are visible. The lateral face of the body of c9 as well as d1 and 2 bears longitudinally oval pleurocoels that contain numerous foramina and pits.

On each of the first five dorsals the transverse processes are large, with those of the first dorsal being sub-equal in

**Table 1** Selected long bone lengths of *Barbosania gracilirostris* (MHNS/00/85) gen. et sp. nov.

| Element                                | Length (mm)         |
|--|---------------------|
| Skull                                  |                     |
| Skull (occipital condyle—snout)        | 391                 |
| NAOF                                   | 96 <sup>a</sup>     |
| Mandible (articulation to rostral tip) | 330                 |
| Axial column                           |                     |
| Ninth cervical                         | 13                  |
| Notarium                               | 59                  |
| Body length                            | 209.5               |
| Long bones                             |                     |
| Humerus (right/left)                   | 155/162             |
| Ulna (right/left)                      | 223/>111            |
| Carpus width (right)                   | 58                  |
| Pteroid (left)                         | 129                 |
| mc III                                 | 137                 |
| Metacarpal IV (right/left)             | 155/156             |
| Digits and phalanges (right)           |                     |
| d1 p1                                  | 29                  |
| d1 u1                                  | 14                  |
| d2 p1                                  | 20                  |
| d2 p2                                  | 29.5                |
| d2 u1                                  | 15                  |
| d3 p1                                  | x                   |
| d3 p2                                  | 3                   |
| d3 p3                                  | 23                  |
| d3 u1                                  | 15                  |
| d4 p1 (right/left)                     | >191.9/>151.7       |
| Femur (right/left)                     | 127/43 <sup>a</sup> |

<sup>a</sup> Denotes a value based on an estimation or reconstruction

size to that of ninth cervical. The shortest transverse process belongs to the second dorsal although these increase in both length and distal width for subsequent vertebrae. With the single exception of the fifth dorsal the transverse processes of c9–d4 are directed slightly caudolaterally. The distal half of the transverse process of the fifth dorsal, however, curves cranially again so that its tip is directed laterally. The vertebrae remain of sub-equal length and intervertebral articulations are unfused. As such these vertebrae have not yet fully formed a mature notarium. A single, large but unfused rib lies adjacent to the transverse process of the second dorsal. The preserved length of the rib is 79 mm and it displays a shallow curvature. The capitulum and tuberculum are damaged but have a spacing of 10 mm, which corresponds to the lateral extension of the adjacent transverse process.

The third vertebral section consists of d6–d13 and the first sacral as a single articulated unit. Despite heavy damage it is clear that the intervertebral joints are open. The transverse processes of these dorsals, of which only the bases are visible, are again directed slightly caudolaterally with two exceptions. The transverse processes of the 12th dorsal are orientated laterally while those of the 13th dorsal are recurved and point craniolaterally. For both the 12th and 13th dorsals the lateral margins of the transverse processes converge, but without meeting, and terminate close to the cranial process of the ilium. There is no evidence for a cranially expanded synsacrum. The 13th dorsal and the first sacral are clearly distinct with the sacral possessing large sacral ribs. In cranial view the dorsal margin of these ribs is almost straight while the ventral margin curves ventrolaterally causing the bone to expand to twice its basal thickness. The lateral margin is divided into two articular surfaces standing at 90° to each other for the pubis and ilium. These latter elements are slightly displaced and sediment infilling between the sacrals, pubis, and ilium indicate that they are unfused. Two faint sutures are visible between the vertebral bodies and the sacral ribs suggesting that fusion has neared completion. The remainder of the sacrals are buried beneath both sediment and the right ischiopubic complex.

The final vertebral section consists of the caudal vertebrae. These are preserved together but have been displaced slightly so that they are no longer articulated. The majority are observed in their ventral aspect, however, the first visible caudal has rotated so that it is now observed in ventrolateral view. The neural spine is positioned cranially on the bone and occupies approximately 2/3rds the length of the corpora. It is not certain that this represents the first vertebrae of the caudal series, however, comparisons with other ornithocheiroids (e.g. Kellner and Tomida 2000) indicate that it must be one of the cranially positioned vertebrae due to its prominent neural spine and short body.

### *Pectoral girdle*

The remains of the left scapula and coracoid are seen in caudal view. They are unfused and lie close to their natural articulation. The shaft of the coracoid expands towards the pars glenoidalis, where it is twice as wide as in the middle of the shaft. The ventral half of the glenoid fossa is visible on the right coracoid. A single robust process is viewed on the caudolateral margin of the bone along with a deep scar located immediately ventral to it, perhaps corresponding to the insertion points of *m. coracobrachialis* (Bennett 2003a). The shaft is blade-like and offset against the body at an angle of 25°. The medial furca for the articulation with the sternum has broken away on both coracoids.

### *Humerus*

Both humeri are present with the left observed in ventral view and the right in its caudoventral aspect. They are typical of ornithocheiroid pterosaurs and preserve the characteristic short (34% of the humeral shaft length), warped, deltopectoral crest with a sub-triangular margin. The head of the humerus is kidney shaped in its medial aspect and measures 28.5 mm by 16.5 mm. The articular surface is convex. A deep concavity marks the ventral margin of the humerus adjacent to the articular head, between the caudal tuberosity and the deltopectoral crest. In caudal view the humeral head is deflected dorsally in relation to the main humeral shaft at an angle of about 10°. It is impossible to comment on the extent of the caudal tuberosity because this has broken off from the right humerus and on the left it is mostly hidden by sediment. The deltopectoral crest begins as a thin flange proximally on the base of the humeral neck where it is orientated ventrolaterally. From cranial view the flange thickens distally by forming a pronounced convex curvature. Here, the cranial margin of the crest curves ventrally and reaches its maximum thickness. A small scar is visible on the ventral surface of the left deltopectoral crest as a rough depression where it runs a short distance of ~6 mm towards the proximal portion of the humerus. On the shaft of the humerus a large solitary scar is visible on the caudoventral margin of the humerus and extends for a distance of 21 mm. This would represent the insertion point for the medial head of *m. triceps* (Bennett 2003a) or *m. latissimus dorsi* (Bonde and Christiansen 2003). An isolated bone fragment lying off the distal margin of the right humerus, adjacent to a large oval excavation of the distal margin of the bone, is interpreted as an unfused epiphysis.

### *Radius and ulna*

The radii/ulnae are preserved in their ventral aspects where the right has been displaced so that it now overlies the

proximal half of the left. Much of the bone surface has been damaged and because of some clumsy restoration attempts during its initial preparation few details are observed. A large concave recess on the proximal articulation surface of the right ulna indicates that the now missing epiphysis was unfused. Additionally a small ridge is viewed on the ventral side of the bone. While this was probably an extensive feature only the most distal portion is visible as the compacta is missing, revealing a calcite-filled core.

### *Carpals*

The carpal regions of both forearms are well preserved in ventral view and between them show both the preaxial carpal and the pteroid bone. The two carpal blocks lie close to their natural positions but in both cases the distal syncarpal has rotated against the proximal one and now lies in disarticulation. A thin suture runs across both proximal and distal syncarpals indicating that fusion of the carpals is incomplete, however, the lateral part of the suture on the proximal syncarpal is partially closed. The distal syncarpal is semi-lunate in outline with a strong convex curvature along its proximal margin. The distal margin of the proximal syncarpal is concave to an equal degree, matching its counterpart on the distal syncarpal. A number of pneumatic foramina are visible on the carpals. The right proximal syncarpal is observed in ventral, cranial and cranio-lateral orientations where one oval foramen is located on the caudal portion of the ventral surface while another spans the cranial and distal surfaces towards the ventral margin of the bone. Only a single large depression is observed on the left distal syncarpal, located on the proximal articular face and occupying the cranial portion of the bone.

The right preaxial carpal has been displaced distally from the carpus, is partially overlain by metacarpal IV and has rotated so that it is now visible in lateral view. A large fovea filled with sediment occupies the majority of the craniodorsal surface of the bone.

The articular surface of the left pteroid is thin and is transversely compressed. Moving medially, the strongly curved neck expands to about twice its diameter at the articular end. The shaft, which is directed towards the body stands at an angle of about  $75^\circ$  to the neck. The distal half of the shaft curves slightly cranially. Restoring the pteroid to its natural position this sigmoid curve would have directed the medial end of the pteroid slightly cranially and extended the propatagium to the base of the neck. The right pteroid bone is visible for a total length of 129 mm before it is obscured by sediment and by the right ulna.

### *Metacarpalia*

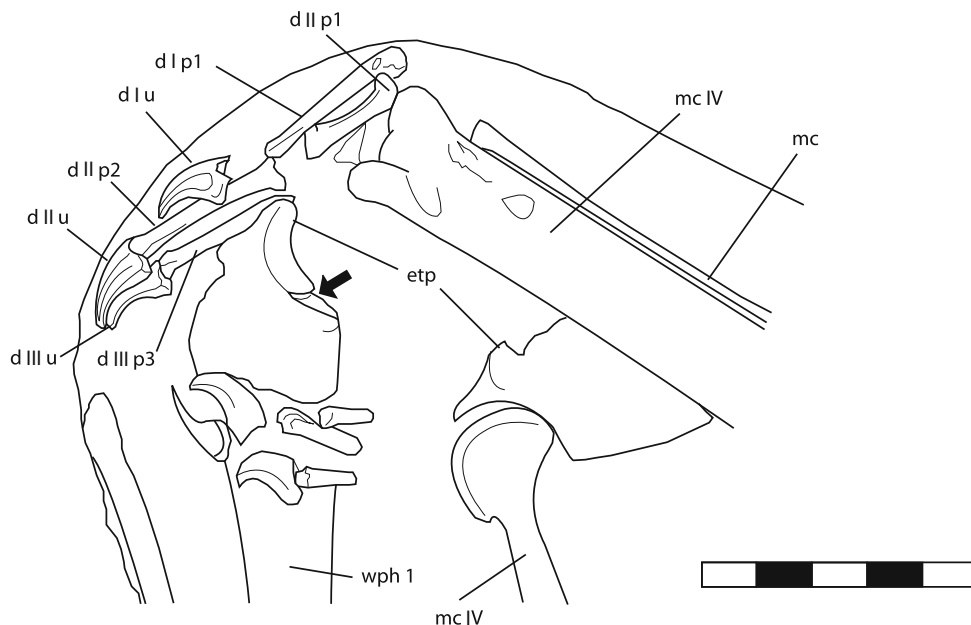
The fourth metacarpal is sub-equal in length to the humerus (Table 1). The bone is widest at its proximal articulation face with the shaft of the bone becoming gradually narrower distally and terminates in a double roller joint with the wing finger. The ventral condyle is directed only slightly ventrally and extends further onto the cranial surface of fourth metacarpal than the dorsal condyle (Fig. 5). The dorsal condyle slants steeply dorsally at an angle of  $\sim 30^\circ$  against the long axis of metacarpal IV, creating a slightly oblique sulcus. A large depression at the cranial termination of the dorsal condyle was presumably for the insertion of muscles or ligaments associated with the first three metacarpalia. Arising from the proximal articulation a short dorsoventrally compressed ridge is observed that extends for  $\sim 16\%$  of the metacarpal length distally along the cranioventral margin of the bone.

An isolated metacarpal (mc 1) is preserved along the dorsal margin of the cranial face of the fourth metacarpal. This bears a bulbous termination at both its proximal and distal ends, which lie adjacent to the distal syncarpal and the first three digits, respectively, and indicates that the shaft of the metacarpal would have extended the full distance from the digits to the carpus. Of the second metacarpal only the distal portion is visible, which shows a slight expansion towards its articular face. As is seen on the left metacarpal IV the ventral roller develops its strongest convexity at its craniodistal margin. The caudal margin is nearly straight but curves sharply caudally in its proximal-most fifth where it is off set from the shaft by a notch. Cranially the roller merges with the shaft in an even concavity. The ventral face of the roller is slightly depressed and shows a circumferential rugosity that accommodated the capsular ligaments of the joint.

### *Digits*

The digits of both arms are well preserved although with the exception of the unguals of the right manus, few of these bones are preserved in their natural articulations. As in all pterosaurs the phalangeal formula is 2-3-4-4 for digits I–IV with each of the first three digits terminating in a short cranially curving ungual (Fig. 5). Each ungual bears a deep sulcus that extends almost the whole length from the tip to the base and covers approximately a third of the bone's surface. The tip of each ungual is pointed and strongly curved in palmar direction. The individual phalanges are about twice as broad as the shaft at their proximal articulations and narrow distally as the cranial margin of the bone curves caudally for a short distance before the shaft adopts a uniform diameter for the remainder of its length.

**Fig. 5** *Barbosania gracilirostris* (MHNS/00/85) gen. et sp. nov. Line tracing centred on the fourth metacarpophalangeal joint where: *d* digit; *d-p* digit and phalanx; *mc* metacarpal, *u* ungula, *wph* wing finger phalanx (d4). Arrow indicates a partially open suture between the first wing finger phalanx and the extensor tendon process. Scale equals 50 mm



A pronounced ridge runs along most of the length of the cranial surface of digit II phalanx 2 presumably for the attachment of flexor muscles.

#### *Wing finger (digit 4)*

The extensor tendon process is preserved in situ for both left and right wing fingers. In places the suture with the corpus of the first phalanx is open but some closure has occurred. On the left first wing finger phalanx (wph 1) this suture is laterally discontinuous but extends approximately 2/3rds across the ventral surface of wph 1. On the right wph 1 the extensor tendon process is exposed in both ventral and lateral aspect. While the suture is still fully open against the proximal articular surface of wph 1 it does not extend onto the ventral surface.

The shaft of wph 1 is typical of other pterosaurs in that its width initially converges towards the middle of the shaft before expanding again to form the distal articulation surface. A fragment of bone containing a distal articular surface adjacent to the femur is interpreted as that of the third phalanx of the right wing.

#### *Pelvic girdle*

All the individual elements of the pelvic girdle remain unfused. In cranial view this is indicated by open sutures between the ilium and pubis, as well as between the sacral ribs and the ilium. In lateral view a large gap separates the caudoventral margin of the pubis from the cranioventral margin of the ischium. An open suture between the two elements extends dorsally until the ventral margin of the

acetabulum where it is lost due to poor preservation and obstruction by the femur.

Due to damage and sediment cover only a small portion of the left ischiopubis is useful for describing the external morphology. In cranial view the pubis is a medially curving, transversally compressed bone that is thickest at its articulation with the ilium and ischium, forming the cranial margin of the acetabulum. Moving ventrally the pubis is twisted so that the ventral blade is aligned in a craniolateral direction. In lateral view the cranial margin of the left pubis is slightly concave while that of the right is indeterminate due to damage to the compacta. The ventromedial margin of the pubis is straight. The high oval obturator foramen separates the pubis from the ischium.

In lateral view, the cranial margin of the ischium is strongly concave for much of its length, while the caudal margin is shallowly concave, constricting the width of the bone. The ventral margin of the ischium is straight while the cranioventral margin is convex. The caudoventral margin of the bone, however, is strongly concave. The ventral edge of the right ischium lies adjacent to the preserved ventral margin of the left, which has broken and is ~5 mm shorter than that of the right. Sediment infill between the pubis and its articular surface on the first sacral suggest that the left ischiopubic plate may have been slightly displaced laterally, likely due to the collapsing right plate. Restoring the pubis and ischium to their original positions indicates that their ventral margins would have sat close to the midline of the body but would have been sufficiently distant from the opposite elements to prevent the formation of a symphysis.

## Femur

The femoral head is offset against the shaft of the femur at an angle of approximately  $153^\circ$ . The greater trochanter is preserved as a weakly developed ridge along the lateral and dorsal margins of the bone while a large scar, approximately 9 mm in length, is located directly ventral to this.

## Discussion

### Systematic palaeontology

Specimen MNHS/00/85 is placed within the Ornithocheiroidea by preserving a notarium, a humerus with a warped, sub-triangular deltopectoral crest, an ornithocheiroid carpus, and a reduction of the metacarpalia where only one of the first three would have made contact the distal face of the carpus (see Unwin 2003). It is distinguished from the Istiodactylidae (e.g. Anders and Ji 2006; Wang et al. 2005) on the basis of a relatively short nasoantorbital fenestra, making up only  $\sim 24\%$  of the skull length, a rostrum with triangular cross-section, and narrow, elongated teeth that extend caudally for more than 50% the length of the skull. The specimen therefore ranks within the Ornithocheiridae where it is referred to a new genus and species.

The cranium and mandible of *Barbosania gracilirostris* clearly lack a median sagittal crest and as such the described specimen is considered distinct from those ornithocheirids known to possess large rostral crests e.g. *Anhanguera*, *Coloborhynchus*. While the absence of a crest may perhaps be considered an insufficient reason for distinguishing MNHS/00/85, due to ontogenetic variability or sexual dimorphism, it differs from specimens of *Coloborhynchus* by the lack of a palate turned  $90^\circ$  at the tip of the rostrum, two small teeth positioned on the rostral face of the skull, and a robust lateral expansion of the rostrum. Despite a similar appearance to specimens of *Anhanguera*, which also developed a more pointed rostrum, *B. gracilirostris* does not possess parietal crest, considered a synapomorphy of the genus (Kellner and Tomida 2000).

*Barbosania gracilirostris* shares the absence of a median sagittal crest with several other taxa including: *Anhanguera fittoni* (Owen 1859), *Brasileodactylus araripensis* (Kellner 1984; Veldmeijer et al. 2009), *Coloborhynchus sedgwickii* (Owen 1859), *Cearadactylus* (Leonardi and Borgomanero 1985; Dalla Vecchia 1993), and *Ludodactylus sibbicki* (Frey et al. 2003). A general morphological comparison with these taxa is therefore required. *Anhanguera fittoni* is superficially similar to MNHS/00/85 and also lacks a lateral rostral expansion but the specimen is limited to an isolated rostral fragment and a full comparison of the two is therefore impossible. Owen (1859)

founded the species due to its clear distinction with *Coloborhynchus sedgwickii* where the diagnosis was restricted to the interalveolar spacing of the first three tooth sockets, the lesser degree of the rostral expansion, and the presence of a shallow longitudinal groove on the palate, three characters that are no longer considered distinct. Differences between the rostral portions of the skull of *A. fittoni* and *B. gracilirostris* are limited to a slightly more rounded rostral termination in *A. fittoni* where the largest alveolus is the fourth, rather than the third as in MNHS/00/85. The pattern of the interalveolar spaces also differs between the two specimens where the interalveolar distance increases rapidly caudal to the 8th alveolus in *A. fittoni*, while in MNHS/00/85 this occurs caudal to the 13th. Without clearer indication of the diagnostic features of *A. fittoni* and a better understanding of the relationships between Brazilian and English ornithocheirid pterosaurs, the limited preservation of this specimen prevents any further consideration.

*Coloborhynchus sedgwickii* is distinguished from the MNHS/00/85 by possessing a flat, vertically orientated, triangular shaped rostral termination, which bears two rostrally directed teeth.

*Ludodactylus sibbicki* bears a blade-like, caudally directed parietooccipital crest similar to *Pteranodon longiceps* (Frey et al. 2003) and as such is clearly distinct from MNHS/00/85, where the supraoccipital process is deflected and the caudal face of the parietal is flat.

*Cearadactylus atrox* may have lacked a rostral crest, however, the dorsal part of the skull terminates with the edge of the concretion. The dorsal aspect of the specimen has neither been described nor depicted, and therefore the presence or absence of a crest remains doubtful. Furthermore, *Cearadactylus atrox* is characterized by notch in the premaxillomaxillary transition, which is missing in MNHS/00/85, and the dentition is different in both count and arrangement. A second specimen "*C.*" *ligabuei* is also distinct from MNHS/00/85 by a thick and robust rostrum. This has a rounded termination with larger and more pronounced premaxillary tooth sockets relative to the more caudally located alveoli, and a pronounced lateral expansion beginning level with the fourth alveolus.

The general morphology of the described specimen is most similar to that of *Brasileodactylus*. Although the taxonomic validity of this genus has been questioned by several authors, such interpretations have been challenged by Kellner and Tomida (2000) and Veldmeijer et al. (2009) who redefined the synapomorphies or better diagnostic features of *Brasileodactylus* as:

1. A slight expansion of the rostrum.
2. A deep groove on the dorsal surface of the mandible extending to the rostral margin of the dentary.

3. The presence of paired side branches off the primary dentary groove.
4. The rostral, rostrolateral, and lateral orientation of the first three alveoli of the mandible.

The diagnostic value of several of these characters remain questionable because the position and extent of the lateral expansion of the rostrum is not constant even between those specimens attributed to the genus, Kellner and Tomida (2000) reported this as beginning between the third and fourth alveolus of the mandible in MN 4804-V, while Veldmeijer et al. (2009) noted that it occurred between the fourth and fifth alveolus in SMNS 55414. Furthermore, the size of the expansion is not sufficiently distinct from specimens of *Anhanguera* and is also likely to be linked to ontogenetic age.

Likewise the presence of laterally directed branches of the median mandibular sulcus is also not unique to *Brasileodactylus* but is present in the large crested specimens of *Coloborhynchus* (SMNK PAL 2302), where they are restricted to the rostral-most part of the dentary, and in a skull of *Anhanguera* (SMNK PAL 1281). The median mandibular sulcus of SMNK PAL 2302 terminates 7.9 mm caudal to the rostral margin of the bone while in the latter specimen it extends to the rostral margin, bifurcating at the very tip of the rostrum. The role of these mandibular sulci is unknown, but likely they represent canals for blood and nervous supply the buccal lining of the mandibular rostrum and should not be considered unique to any particular genus. The final character, however, the positioning of the first mandibular alveolus on the rostral face of the dentary, is regarded as a valid character for diagnosis.

Regardless of the issues noted above two of the cited characters cannot be observed due to the occluded resting position of the upper and lower jaws (characters 2, 3), while the premaxillary part of the rostrum is gradually converging and does not show any lateral expansion (character 1). Finally, the rostral-most pair of mandibular teeth is positioned rostradorsally and not rostrally (character 2) and as such MNHS/00/85 fails to meet any of these diagnostic features of Veldmeijer et al. (2009). MNHS/00/85 must therefore be distinguished from *Brasileodactylus*.

Several isolated rostral fragments known from the Nova Olinda Member of the Crato Formation are superficially similar in appearance to *B. gracilirostris*, in that they lack a medial crest and possess a pointed rostral termination in lateral view (Unwin and Martill 2007, pp. 492–493; Sayão and Kellner 2000). Although these specimens have been tentatively referred to the genus *Brasileodactylus*, the first pair of alveoli on the mandible appear to be orientated rostradorsally as in MNHS/00/85 and thus should be re-investigated based on the data presented here.

## Dentition

The estimated number of teeth per half jaw in MHNS/00/85 are >24 and >20 in the upper and lower jaws, respectively, and is therefore similar to that of *Coloborhynchus piscator* (Kellner and Tomida 2000; 25 upper and 18–19 lower). Given that these are minimum estimates the dentition number is distinct from several other ornithocheirid specimens e.g. *C. robustus* (~18, lower jaw), *A. santanae* (20, upper jaw) and *Ornithocheirus mesembrinus* with 13 and 11 alveoli in the upper and lower jaws, respectively. The largest tooth in *B. gracilirostris* is the fourth which also holds true for *Cearadactylus araripensis*, *Anhanguera fittoni*, *Anhanguera blitterdorffi*, *Anganguera santanae*. However, the second largest tooth caudal to this in the above taxa is the eighth rather than the ninth for MHNS/00/85. In other taxa the largest tooth is either the second (*Brasileodactylus* SMNS 55414, Veldmeijer et al. 2009) or the third (*Coloborhynchus piscator*; *Coloborhynchus clavirostris*; *Coloborhynchus robustus*; *Anhanguera blitterdorffi*) and the second largest tooth varies between the eighth and the tenth.

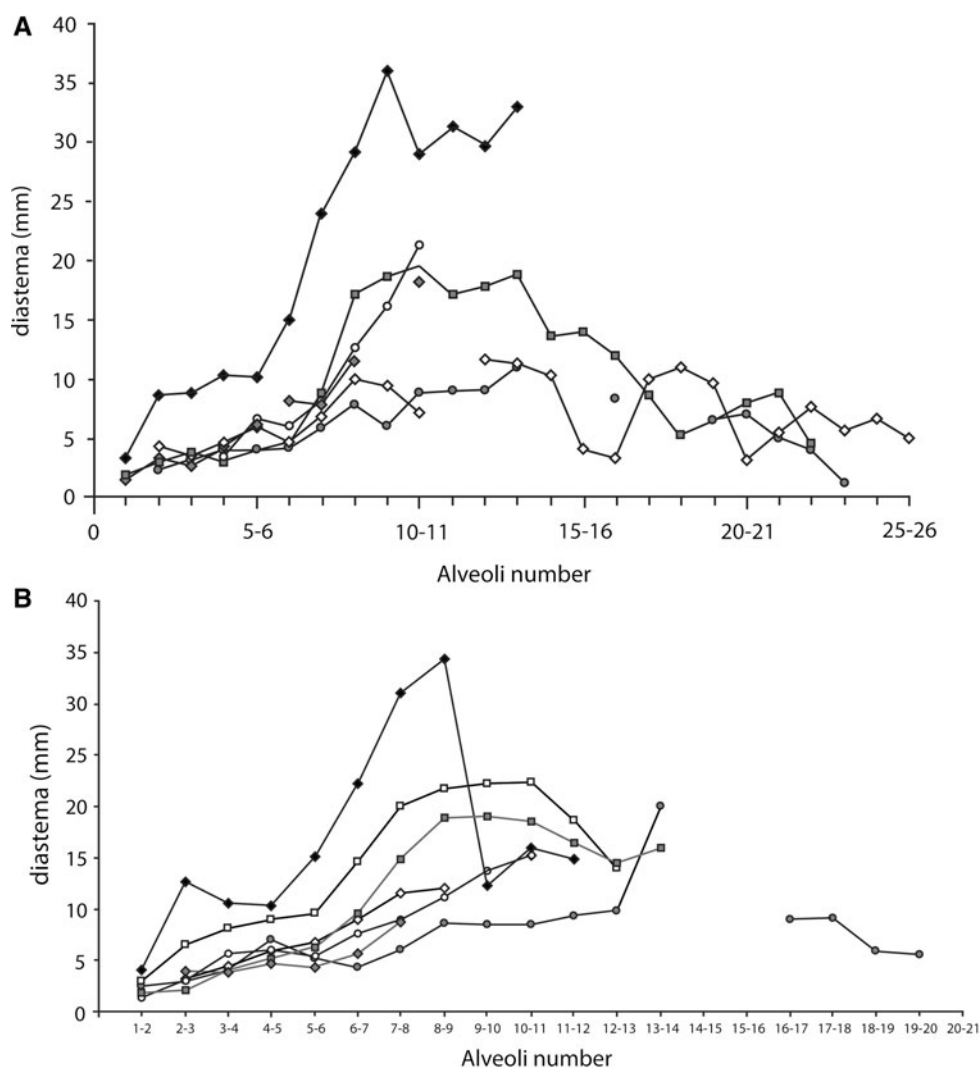
Figure 6 records the diameter of the premaxillomaxillary and mandibular alveoli and interalveolar spaces for a number of ornithocheirid pterosaurs. Several taxa e.g. *Coloborhynchus* and *Ornithocheirus* are clearly distinct from *Anhanguera*, *Brasileodactylus* and *Ludodactylus* with regard to the dentition pattern. Although the general patterns observed in these latter taxa are similar, there are a number of observations to be discussed. The cranial interalveolar space pattern of MNHS/00/85 is most similar to that of *Brasileodactylus* indet. (AMNH 24444) that differs from other *Brasileodactylus* specimens where the interalveolar space rapidly increases caudal to the sixth or seventh alveolus. The interalveolar space patterns of the two unidentified *Brasileodactylus* specimens AMNH 24444 and BSP 191 I 27 are so distinct that they must represent either different species or that a large range of dentition patterns existed for this genus. No specimen shows an exact match to the pattern observed in *Ludodactylus* and it is thus not possible to comment on the possibility that isolated and crestless rostral fragments also known from the Brazilian deposits may be conspecific.

## Postcranium

The general morphology of the ornithocheirid postcranial skeleton is almost identical between species and few features are useful for differential diagnostics. The postcranial remains of crestless specimens are rare, however, two are known (AMNH 24444 and BSP 191 I 27). The former of these is still under preparation and therefore little



**Fig. 6** Comparison of the intervalveolar spacing in selected taxa where: **a** cranium, *closed diamond*, *Ornithocheirus mesembrinus* (BSP 1987 I 46); *grey diamond*, *Barbosania gracilirostris* (MNHS/00/85); *open diamond*, *Anhanguera* sp. (SMNK PAL 1281); *closed triangle*, *Brasileodactylus araripensis* (MN 4804-V); *open triangle*, *Brasileodactylus araripensis* (MN 4797-V); **b** mandible, *closed triangle*, *Ludodactylus sibbicki*, (SMNK PAL 3828); *grey triangle*, *Brasileodactylus* sp. (BSP 191 I 27); *open triangle*, *Brasileodactylus* sp. (AMNH 24444); *closed diamond*, *Ornithocheirus mesembrinus*, (BSP 1987 I 46); *grey diamond*, *Barbosania gracilirostris* (MNHS/00/85); *open diamond*, *Coloborhynchus robustus* (SMNK PAL 2302)



information is available (Veldmeijer et al. 2009) making BSP 191 I 27 the only comparable specimen. MNHS/00/85 and BSP 191 I 27 share only a limited number of elements including the cervical and dorsal vertebrae, the humerus, and the pubis. The majority of these elements are almost identical in their morphology and as such few differences can be observed although a single pneumatic foramen on the ventral face of the transverse process of the ninth cervical is significantly smaller in MNHS/00/85 while in BSP 191 I 27 it encompasses the majority of the bone surface. The transverse processes of the fifth dorsal are significantly more elongated in MNHS/00/85, where the transverse processes are low on the neural arch, which apparently reaches ventrally onto the lateral face of the respective vertebral dorsoventrally compress corpus. The number of dorsal vertebrae present in MNHS/00/85 is 13, suggesting that variable counts of vertebrae existed within the Ornithocheiridae, where *Coloborhynchus* is known to have only 12 (Veldmeijer 2003, 2006) while *Anhanguera* (AMNH 22555) preserves 13.

The ischium of BSP 191 I 27 and MNHS/00/85 differ in the concavity of the cranial margin, which is more pronounced in the former and terminates at a relatively more ventral position on the bone. The caudal margin in BSP 191 I 27 it is almost straight whereas in MNHS/00/85 it is concave. The caudoventral margin of the bone is MNHS/00/85 is strongly concave, which is contrasted against other ornithocheiroids, where the entire caudal margin of the ischium is gently convex (Fig. 7).

#### Ontogenetic maturity

While elements of the cranium appear to suture very early in ontogeny (Kellner and Tomida 2000) all ornithocheiroids recovered from the Romualdo Member of the Santana Formation are considered to be ontogenetically immature based on the lack of fusion in the postcranial skeleton. Such findings are contrary to ornithocheiroids from the Nova Olinda Member of the Crato Formation that preserve a more mature state of suturing e.g. *Arthurodactylus*

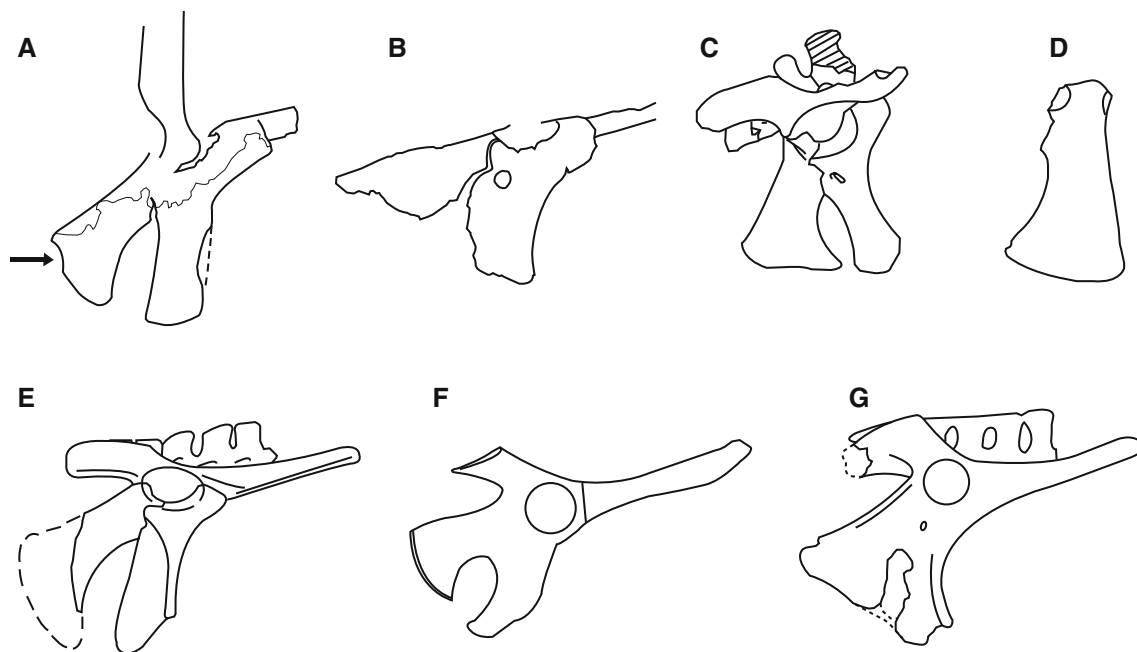


**Fig. 7** Comparison of the pelvic plate in selected ornithocheiroid pterosaurs. **a** Right puboischiadic plate of *Barbosania gracilirostris* gen. et sp. nov; **b** left puboischiadic plate of *B. gracilirostris*, clearly showing the suture between the pubis and ischium; **c** *Brasileodactylus*, left ischium (BSP 191 I 27, Veldmeijer et al. 2009); **d** *Coloborhynchus*

*piscator* (NSM-PV 19892, Kellner and Tomida 2000); **e** AMNH 22569 (Bennett 1990); **f** *Arthurdactylus conandoylei* (SMNK PAL 1132, Frey and Martill 1994); **g** *Coloborhynchus spielbergi* (RGM 401880)

*conandoylei* (Frey and Martill 1994) and azhdarchoids of the Romulada Member, e.g. SMNK-PAL 6607, a putative azhdarchoid where tendons and ligaments have mineralized along the lateral margin of the supraneural plate.

While little is known about the condition of the skull of MNHS/00/85 except that the premaxillomaxillary suture has mostly closed, the specimen must also be considered immature because the thoracic ribs have not fused to the transverse processes, the scapula and coracoid lie apart, the epiphyseal gap of the humerus is open, and large open sutures are visible between the elements of the pelvic girdle. In contrast to other ornithocheiroids from the Santana Formation (e.g. SMNK PAL 1133), MNHS/00/85 has partially closed sutures between the carpals and the extensor tendon process to the cranioproximal face of the first wing finger phalanx. As the latter of these is considered an indicator of late ontogeny in pterosaurs (Bennett 1992; Frey and Martill 1994, 1998; Kellner and Tomida 2000), it is unusual to observe this in an otherwise morphologically immature skeleton. The specimen is therefore considered as having died in a more advanced ontogenetic state than other complete Santana pterosaurs (e.g. *A. santanae*; *C. piscator*) and indicates either the onset of late fusing features at a relatively small size (i.e. dwarfism) or a significant deviation from the previously observed pattern of suture development in ornithocheirids.

#### Comments on the cranial crest

The cranial crest has been associated with a wide variety of roles including thermoregulation (Kellner and Campos 2002), an aerodynamic rudder and/or counterbalance (Bramwell and Whitfield 1974), a means to stabilise the head during prey capture (Veldmeijer et al. 2006), or a sexual display. The large variety that exists within the size, shape and position of the crest across the Pterosauria and the differences between closely related taxa argue strongly in favour of a sexually selected trait, a position reinforced by the appearance of sexually dimorphic crests in *Pteranodon* (Bennett 1992) and its strong allometric growth (Tomkins et al. 2010).

The crest as a diagnostically useful feature is problematic as the degree of intraspecific variation is unknown in pterosaurs, while the size, shape and position of the crest are also likely to change during ontogeny (Martill and Naish 2006) and must be considered with respect to the morphological maturity of the specimen. Likewise the differences between male and female animals are uncertain; while the crest of putative female specimens of *Pteranodon* are smaller than those of their male counterparts they are nonetheless present (Bennett 1992, 2001), but the exaggerated crest of *Nyctosaurus* appears to be present only beyond a specific point in their development

(Bennett 2003b). It is this uncertainty that prevents a consensus of whether specimens distinguished almost exclusively by the absence of a crest should be regarded as sexual morphs of a single species (e.g. *Colobrhynchus sedgwickii* and *C. capito*, Unwin 2001). Within the Ornithocheiridae, however, a number of ontogenetically immature specimens are known to possess a well-developed median sagittal crest (e.g. *C. piscator*, *Santana-dactylus*, AMNH 22555) suggesting that this feature formed relatively early in ontogeny. The absence of the crest in MHNS/00/85 should therefore not be considered a product of its morphologically immature status, particularly considering the partial fusion of the extensor tendon process to the first wing finger phalanx.

The lack of a rostral median crest in MNHS/00/85 is aligned with another feature, a caudoventrally deflected supraoccipital process combined with a lack of a short parietal crest that characterizes the skull of other ornithocheirids e.g., *Anhanguera blittersdorffi*. The narrow and slender rostrum of MNHS/00/85 could probably be operated with less muscular power than in *Anhanguera*, in which the crest added to the weight of the rostrum with a long lever action on the occipitoatlantal articulation. The same holds true for the cervicooccipital musculature, which in MNHS/00/85 had a relatively smaller momentum to handle compared with a similar sized, crested species. This would explain the small supraoccipital process.

As the cranial crest appears to develop relatively early during ontogeny and with no evidence to suggest that putative females should be regarded as completely crestless the lack of a rostral and dentary median crest in MNHS/00/85 is argued to be regarded as a genuine and diagnostic character. Veldmeijer et al. (2009) previously argued that in the absence of additional specimens, or until more information becomes available, crestless specimens must be regarded as separate taxa rather than juvenile members of pre-established genera. We follow them in this respect.

## Conclusions

*Barbosania gracilirostris* represents the most complete skeleton of a crestless ornithocheirid known from the Santana Formation of NE Brazil and is distinguished from the morphologically similar *Brasileodactylus* by the rostradorsal position of the first mandibular alveoli. Although they are also not observed in the described specimen, the remaining apomorphies listed for *Brasileodactylus* are dubious, because the size and position of the rostral expansion is variable and may itself develop later in ontogeny with the appearance of larger teeth and alveoli. The appearance of a long median sulcus and the presence of paired lateral branches in *Anhanguera* (SMNK PAL

1281) and *Coloborhynchus* (SMNK PAL 2303) also cast sufficient doubt on the diagnostic use of these features.

MHNS/00/85 shares 13 dorsal vertebrae with *Anhanguera* (AMNH 22555), deviating from the 12 dorsal conditions observed in other derived pterodactyloid pterosaurs. A brief comparison of the interalveolar spaces between the cranial alveoli finds two patterns within specimens assigned to *Brasileodactylus* where BSP 191 I 27 differs from AMNH 22444 and MHNS/00/85 by a significant increase of the interalveolar spacing caudal to the eighth alveolus. MHNS/00/85 strongly suggests that the absence of the cranial crest is a genuine character rather than an ontogenetic feature due to the advanced state of skeletal fusion relative to other immature, crested pterosaurs from the same locality.

Several specimens that have been possibly referred to *Brasileodactylus* but lack a rostrally positioned first mandibular pair of alveoli might instead be considered as *B. gracilirostris* (e.g. Unwin and Martill 2007, pp. 492–493; Sayão and Kellner 2000).

**Acknowledgments** The authors thank the Sintra Museum of Natural History for permission to work on this specimen, V. Griener for photography, André Veldmeijer for extensive and fruitful discussions on ornithocheirid taxonomy, and David Martill for helping with an earlier draft of the manuscript.

## References

- Anders, B., & Ji, Q. (2006). A new species of *Istiodactylus* (Pterosauria, Pterodactyloidea) from the Lower Cretaceous of Liaoning, China. *Journal of Vertebrate Paleontology*, 26, 70–78.
- Anders, B., & Ji, Q. (2008). A new pterosaur from the Liaoning province of China, the phylogeny of the Pterodactyloidea, and the convergence in their cervical vertebrae. *Palaeontology*, 51, 453–469.
- Bennett, S. C. (1990). A pterodactyloid pterosaur pelvis from the Santana Formation of Brazil: Implications for terrestrial locomotion. *Journal of Vertebrate Paleontology*, 10, 80–85.
- Bennett, S. C. (1992). Sexual dimorphism of *Pteranodon* and other pterosaurs with comments on cranial crests. *Journal of Vertebrate Paleontology*, 12, 422–434.
- Bennett, S. C. (2003a). Morphological evolution of the pectoral girdle of pterosaurs: myology and function. In E. Buffetaut & J. -M. Mazin (Eds.), *Evolution and Palaeobiology of Pterosaurs* (Vol. 217, pp. 191–215). London: Geological Society, Special Publications.
- Bennett, S. C. (2003b). New crested specimens of the Late Cretaceous pterosaur *Nyctosaurus*. *Paläontologisch Zeitschrift*, 77, 61–75.
- Bonde, N., & Christiansen, P. (2003). The detailed anatomy of *Rhamphorhynchus*: Axial pneumaticity and its implications. In E. Buffetaut & J. -M. Mazin (Eds.), *Evolution and palaeobiology of pterosaurs* (Vol. 217, pp. 217–232). London: Geological Society, Special Publications.
- Bramwell, C. D., & Whitfield, G. R. (1974). Biomechanics of *Pteranodon*. *Philosophical Transactions of the Royal Society of London B.*, 267, 503–581.
- Campos, D. A., & Kellner, A. W. A. (1985). Panorama of the Flying Reptiles Study in Brazil and South America. *Anais da Academia Brasileira de Ciências*, 57, 453–466.

- Dalla Vecchia, F. M. (1993). *Cearadactylus? ligabuei* nov sp., a new early Cretaceous (Aptian) pterosaur from the Chapada do Araripe (Northeastern Brazil). *Bollettino della Società Paleontologica Italiana*, 33, 401–409.
- Frey, E., & Martill, D. M. (1994). A new Pterosaur from the Crato Formation (Lower Cretaceous, Aptian) of Brazil. *N. Jb. Geol. Paläont. Abh.*, 194, 379–412.
- Frey, E., & Martill, D. M. (1998). Late ontogenetic fusion of the processus tendinis extensoris in Cretaceous pterosaurs from Brazil. *Neues Jahrbuch für Geologie und Paläontologie, Monatshefte*, 1998(10), 587–594.
- Frey, E., Martill, D. M., & Buchy, M. -C. (2003). A new crested ornithocheirid from the Lower Cretaceous of northeastern Brazil and the unusual death of an unusual pterosaur. In E. Buffetaut & J. -M. Mazin (Eds.), *Evolution and palaeobiology of pterosaurs* (Vol. 217, pp. 55–63). London: Geological Society, Special Publications.
- Kaup, J. (1834). Versuch einer Eintheilung der Säugethiere in 6 Stämme und der Amphibien in 6 Ordnungen. *Isis*, 3, 311–315.
- Kellner, A. W. A. (1984). Ocorrência de uma mandibular de Pterosauria (*Brasileodactylus araripensis* nov. gen.; nov. sp.) na formação Santana, Cretáceo da chapada do Araripe, Ceará-Brasil. 33º Congresso Brasileiro de Geologia, Anais, 2, 578–590
- Kellner, A. W. A. (1989). A new edentate Pterosaur of the Lower Cretaceous from the Araripe Basin, Northeast Brazil. *Anais da Academia Brasileira Ciências*, 61, 439–446.
- Kellner, A.W.A. (1991). Pterossauros do Brasil. Unpublished M. Sc. Thesis, Rio de Janeiro: Universidade Federal do Rio de Janeiro.
- Kellner, A.W.A. (2003). Pterosaur phylogeny and comments on the evolutionary history of the group. In E. Buffetaut & J. M. Mazin (Eds.), *Evolution and palaeobiology of pterosaurs* (Vol. 217, pp. 105–137). London: Geological Society, Special Publications.
- Kellner, A. W. A., & Campos, D. A. (1988). Sobre um Novo Pterossauro com Crista Sagital da Bacia do Araripe, Cretáceo Inferior do Nordeste do Brasil. *Anais da Academia Brasileira de Ciências*, 60, 459–469.
- Kellner, A. W. A., & Campos, D. A. (1994). A new Species of *Tupuxuara* (Pterosauria, Tapejaridae) from the Early Cretaceous of Brazil. *Anais da Academia Brasileira de Ciências*, 66, 467–473.
- Kellner, A. W. A., & Campos, D. A. (2002). The function of the cranial crest and jaws of a unique pterosaur from the Early Cretaceous of Brazil. *Science*, 297, 389–392.
- Kellner, A. W. A., & Tomida, Y. (2000). Description of a new species of Anhangueridae (Pterodactyloidea) with comments on the pterosaur fauna from the Santana Formation (Aptian–Albian), Northeastern Brazil. *National Science Museum Monographs*, 17, 1–135.
- Leonardi, G., & Borgomanero, G. (1985). *Cearadactylus atrox* nov. gen., nov sp.: novo pterosauria (Pterodactyloidea) da Chapada do Araripe, Ceara, Brasil. In D. A. Campos, et al. (Eds.), *Coletânea de Trabalhos Paleontológicos* (pp. 75–80). Brasília: Série Geologia.
- Lü, J., Unwin, D. M., Xu, L., & Zhang, X. (2008). A new azhdarchoid pterosaur from the Lower Cretaceous of China and its implications for pterosaur phylogeny and evolution. *Naturwissenschaften*, 95, 891–897.
- Martill, D. M., & Naish, D. (2006). Cranial crest development in the azhdarchoid pterosaur *Tupuxuara*, with a review of the genus and tapejarid monophyly. *Palaeontology*, 49, 925–941.
- Owen, R. (1859). On remains of new and gigantic species of pterodactyle (*Pter. Fittoni* and *Pter. Sedgwickii*) from the Upper Greensand near Cambridge. *Reports of the British association for the Advancement of Science*, 28, 98–103.
- Rodrigues, T., & Kellner, A. W. A. (2008). Review of the pterodactyloid pterosaur *Coloborhynchus*. *Zitteliana*, B28, 219–228.
- Sayão, J. M., & Kellner, A. W. A. (2000). Description of a Pterosaur Rostrum from the Crato Member, Santana Formation (Aptian–Albian) Northeastern, Brazil. *Boletim do Museu Nacional*, 54, 1–8.
- Seeley, H. G. (1870). *The ornithosauria: An elementary study of the bones of pterodactyles*. Cambridge: Deighton, Bell & Co.
- Tomkins, J. L., LeBas, N. R., Witton, M. P., Martill, D. M., & Humphries, S. (2010). Positive allometry and the prehistory of sexual selection. *The American Naturalist*, doi:10.1086/653001.
- Unwin, D. M. (2001). An overview of the pterosaur assemblage from the Cambridge Greensand (Cretaceous) of Eastern England. *Mitteilung aus dem Museum für Naturkunde Berlin - Geowissenschaftliche Reihe*, 4, 189–221.
- Unwin, D. M. (2003). On the phylogeny and evolutionary history of pterosaurs. In E. Buffetaut & J.-M. Mazin (Eds.), *Evolution and palaeobiology of pterosaurs* (Vol. 217, pp. 139–190). London: Geological Society, Special Publications.
- Unwin, D. M., & Martill, D. M. (2007). Pterosaurs of the Crato Formation. In D. M. Martill, G. Bechly, & R. F. Loveridge (Eds.), *The crato fossil beds of Brazil* (pp. 475–524). Cambridge: Cambridge University Press.
- Veldmeijer, A. J. (2003). Description of *Coloborhynchus speilbergi* sp nov. (Pterodactyloidea) from Brazil in the collection of the National Museum of Natural History (Naturalis), Leiden, the Netherlands. *Scripta Geologica*, 125, 35–139.
- Veldmeijer, A. J. (2006). Toothed pterosaurs from the Santana Formation (Cretaceous; Aptian–Albian) of northeastern Brazil. A reappraisal on the basis of newly described material. Unpublished PhD Thesis, Utrecht: Utrecht University.
- Veldmeijer, A. J., Signore, M., & Meijer, H. J. M. (2005). Description of two pterosaur (Pterodactyloidea) mandibles from the Lower Cretaceous Santana Formation, Brazil. *DEINSEA*, 11, 67–86.
- Veldmeijer, A. J., Signore, M., & Bucci, E. (2006). Predator-prey interaction of Brazilian Cretaceous toothed pterosaurs: a case example. In A. M. T. Elewa (Ed.), *Predation in organisms, a distinct phenomenon* (pp. 295–308). Berlin: Springer.
- Veldmeijer, A. J., Meijer, H. J. M., & Signore, M. (2009). Description of Pterosaurian (Pterodactyloidea: Anhangueridae, *Brasileodactylus*) remains from the Lower Cretaceous of Brazil. *DEINSEA*, 13, 9–40.
- Wang, X., Kellner, A. W. A., Zhou, Z., & Campos, D. A. (2005). Pterosaur diversity and faunal turnover in Cretaceous terrestrial ecosystems in China. *Nature*, 437, 875–879.
- Wang, X., Kellner, A. W. A., Zhou, Z., & Campos, D. A. (2008). Discovery of a rare arboreal forest-dwelling flying reptile (Pterosauria, Pterodactyloidea) from China. *PNAS*, 105, 1983–1987.
- Wellnhofer, P. (1985). Neue Pterosaurier aus der Santana Formation (Apt) der Chapada do Araripe, Brasilien. *Palaeontographica Abt A.*, 187, 105–182.
- Wellnhofer, P. (1987). New Crested Pterosaurs from the Lower Cretaceous of Brazil. *Mitteilungen der Bayerischen Statssammlung für Paläontologie und historische Geologie*, 27, 175–186.

## A new specimen of the azhdarchoid pterosaur *Tapejara wellnhoferi*

R.A. Elgin<sup>a\*</sup> and H.B.N. Campos<sup>b</sup>

<sup>a</sup>Staatliches Museum für Naturkunde Karlsruhe, Erbprinzenstraße 13, 76133, Karlsruhe, Germany; <sup>b</sup>Campina Grande, Paraíba 58406-025, Brazil

(Received 24 May 2011; final version received 8 August 2011)

A new specimen of the Early Cretaceous azhdarchoid *Tapejara wellnhoferi* is described from the Romualdo Member of the Santana Formation, NE Brazil, providing the first detailed account of the postcranial skeleton. Although limited in its preservation, the osteology is typical of other azhdarchoid pterosaurs from these deposits and represents a juvenile animal with a relatively small wing span of <1.5 m. The ratios of the pedal elements are identical to those noted for larger, indeterminate azhdarchoids of the Nova Olinda Member of the Crato Formation, where the unguals of the pes are greatly enlarged relative to those of the ornithocheiroids that co-inhabited the Santana lagoon. The ratios of these elements suggest that, as part of a larger suite of characters, these animals were likely better adapted for life on the ground than their ornithocheiroid relatives.

**Keywords:** pterosaur; Azhdarchoidea; *Tapejara*; Santana Formation

### Institutional abbreviations:

AMNH, American Museum of Natural History, New York, USA; CPCA, Centro de Pesquisas Paleontológicas da Chapada do Araripe, Crato, Brazil; IMNH, Iwaki City Museum of Coal and Fossils, Iwaki, Japan; MCT, Palaeontology section of the Department Nacional da Produção (Museu de Ciências da Terra), Rio de Janeiro, Brazil; MN, Museu Nacional, Rio de Janeiro, Brazil; SMNK, Staatliches Museum für Naturkunde Karlsruhe, Germany; SAO, Collection of Urs Oberli, St Gallen, Switzerland.

### Introduction

The Early Cretaceous azhdarchoid *Tapejara wellnhoferi* is well represented by several excellent cranial examples recovered from the Romualdo Member of the Santana Formation, NE Brazil (AMNH 24440, Wellnhofer and Kellner 1991; MN 6595-V, Kellner 1989; MCT 1500-R, Kellner 1996; SAO 12891, Wellnhofer and Kellner 1991; SMNK PAL 1137, personal observation, RAE). In spite of this, specimens preserving an association between the cranial and postcranial elements are rare, where the skull appears to have detached from the body early in the decay process and settled separate from the torso or wings (Unwin and Martill 2007). Although more recent acquisitions (i.e. SMNK PAL 1137 and IMNH 1053) preserve significant portions of the postcranial skeleton, and may yet provide a more robust diagnosis based on non-cranial characters, this material remains to be

formally published. Herein, a new specimen of *Tapejara wellnhoferi* that preserves elements of both the cranial and postcranial skeleton is figured and formally described. The material is listed under the collection number of SMNK PAL 3986.

### Description

#### *Preservation and provenance*

The fossil was unearthed from the concretion-bearing unit within the Chapata do Araripe, NE Brazil, commonly referred to as Romualdo Member of the Santana Formation (e.g. Kellner and Tomida 2000; Martill 2007; but see Neumann and Cabrera 1999 for an alternative stratigraphical framework), and deposited during the Early Cretaceous, Albian (e.g. Pons et al. 1990, 1996). This fossil is preserved on a single split concretion, typical of fossils unearthed from this unit, and preserves the remains of two isolated cranial elements (jugal and quadrate), the mandible, two cervical vertebrae, the radii and ulnae, metacarpals, the first wing finger phalanges, in addition to three metatarsals and six phalanges of the first four digits of the left pes (Figure 1). Only digit I is complete and preserves the ungual. The skeleton was disturbed as indicated by several small and indeterminate fragments of bone scattered about the concretion and the juxtaposition of the pes against the cervical vertebrae. The bones are 3D in form and although they remain in a generally good state of preservation many have been damaged, where the concretion was split and portions of the compacta were

\*Corresponding author. Email: rosselgin@hotmail.com

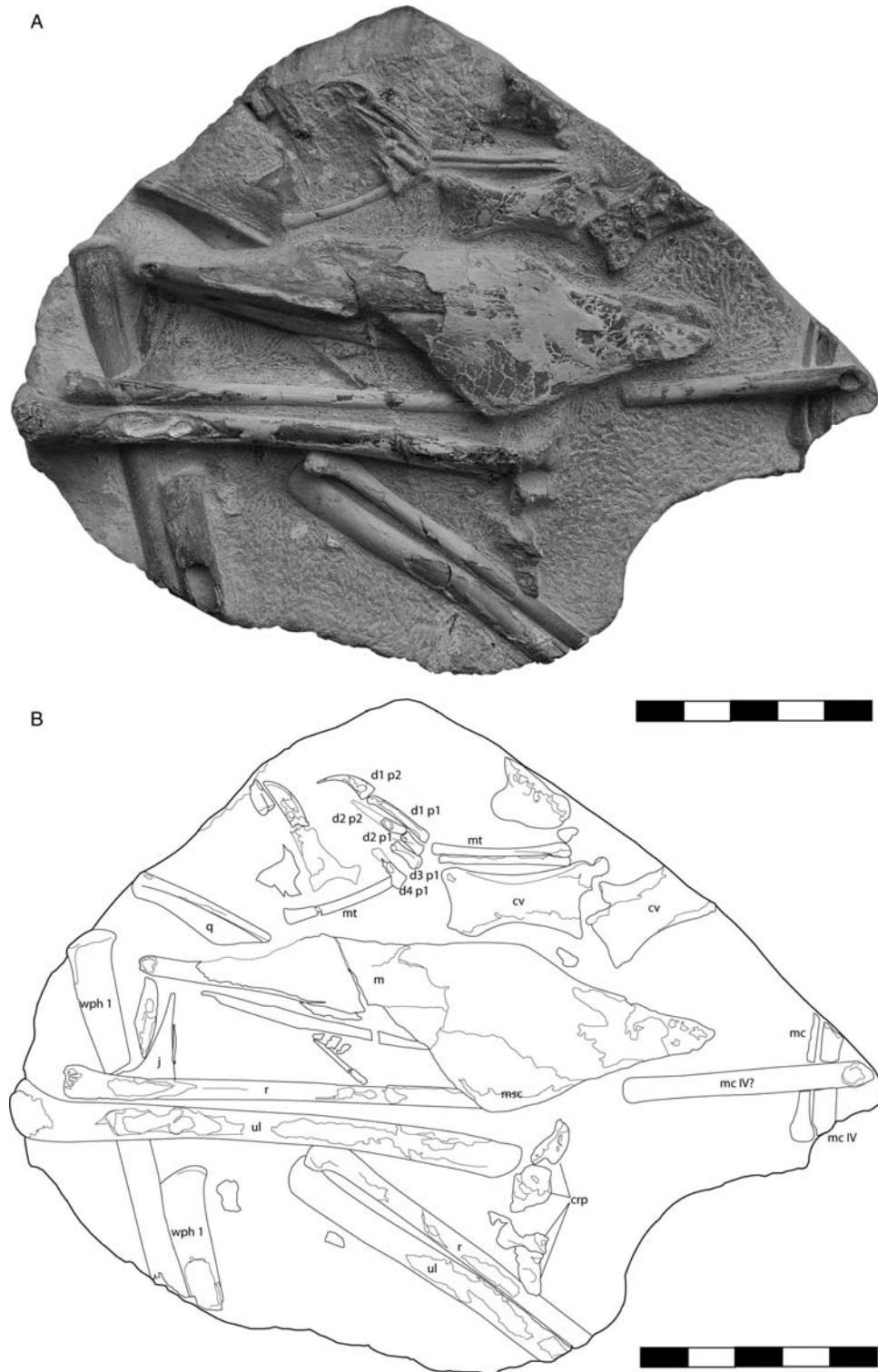


Figure 1. (A) Photograph and (B) line tracing of *T. wellhoferi*, SMNK PAL 3986; cv, cervical vertebra; crp, carpal elements; m, mandible; msc, mandibular sagittal crest; r, radius; ul, ulna; wph 1, wing finger-phalanx; j, jugal; q, quadrate; mc, metacarpal; mt, metatarsal; d?p?, digit and phalanx number. Scale bars represent 50 mm.

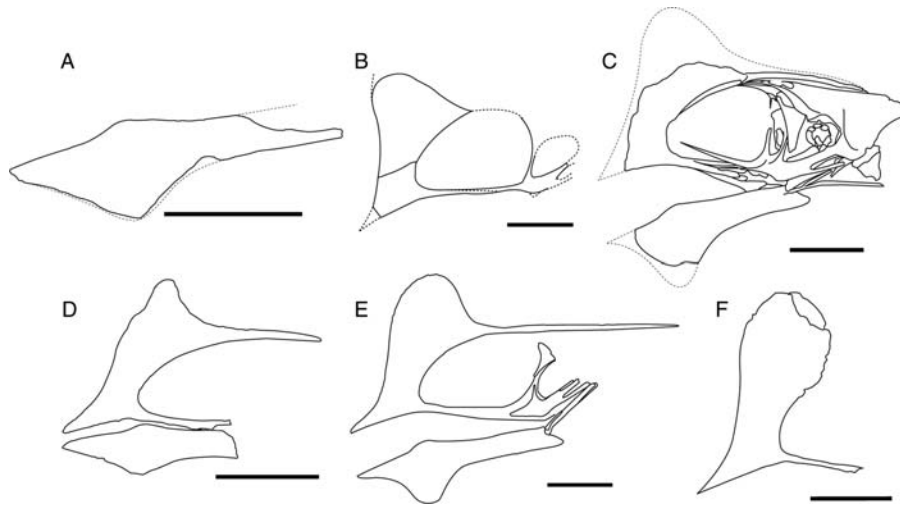


Figure 2. Cranial morphology of several specimens attributed to *T. wellnhoferi*. A, SMNK PAL 3986; B, MCT 1500-R (Kellner 1989); C, AMNH 24440 (Wellnhofer and Kellner 1991); D, SMNK PAL 1137; E, IMNH 1053; F, SAO 12891 (Wellnhofer and Kellner 1991). Dashed lines represent reconstructed portions of the cranium. Scale bars represent 50 mm.

lost from the top (i.e. visible) surface. Several of the long bones are cut by the margin of the concretion indicating that the remains were originally more extensive. No counter slab is known for this specimen.

### Anatomy

Two elements of the skull can be clearly identified, these being the dorsally directed branch of jugal, which would have articulated with the lacrimal in life and formed the caudal/caudoventral margin of the nasoantorbital fenestra, and the dorsal half of right quadrate. The jugal element is very thin and blade-like, the cranial and caudal margins of which are gently concave. In its lateral aspect, the bone has broad ventral base that tapers dorsally. The quadrate, which is observed in its caudal aspect, terminates naturally by the margin of the concretion. The dorsal articular face of the bone is small and oval in cross section, with a smoothly convex termination. Ventral to this, a dorsoventrally orientated concave depression has developed on the caudomedial face of the bone, becoming gradually more pronounced towards the ventral portion of the quadrate. The cross section of the ventral half of the bone is L-shaped, formed by the presence of a medially and caudally directed blade.

### Mandible

The edentulous mandible is visible in its right lateral aspect. The dorsal margin is typically straight with the rostral portion of the bone deflected ventrally at an angle of  $13^\circ$ , beginning at a position 42 mm short of the rostral tip. The dorsal margin of this deflection is weakly concave and merges with the rostral tip of the bone, which is

rounded. The ventral margin of the mandible supports a median sagittal crest that reaches a maximum depth of 35 mm directly ventral to the initial point of deflection. Rostral to the apex of the dentary crest, the ventral margin of the bone is weakly concave when viewed from its lateral aspect (Figures 1 and 2(A)).

### Cervical vertebrae

Two cervical vertebrae are observed in their ventrolateral aspects and represent elements from the middle of the cervical column, likely cervicals four and five. The bones are long and narrow, being 3.8 times longer than the narrowest point at the middle shaft (based on the caudalmost element), and display wide blunt postzygapophyses. The lateral margins of the corpora are concave in profile and, in the cranialmost element, are pierced by two small foramina.

### Radius and ulna

The radii and ulnae are long and narrow bones, observed in their ventral aspects, and preserve a circular cross section of 4 mm in diameter at the middle portion of the shaft. The elements from both left and right sides of the wing are present; however, only the left ulna is complete with a total length of 107 mm. The shaft of the ulna curves caudally and becomes craniocaudally compressed towards the distal articulation. A pronounced tubercle is observed on the dorsal margin of the right radius and left ulna that would have braced against the capitulum of the humerus during life. A small pneumatic foramen is observed on the ventral half of the cranial face of the ulna, immediately adjacent to the proximal articular surface. An elongate

depression, presumably for the attachment of antebrachial muscles, is visible on the cranioventral margin of the bone.

### ***Carpus***

Immediately adjacent to the distal margin of the left ulna, two carpal bones are observed, which are still partially buried within the concretion. Their visible surfaces are transversely concave and pierced by two foramina. Adjacent to the left carpals, two partially preserved bones are regarded as the displaced carpals of the right carpus due to the similarities in size and form when compared with the left carpal elements. Sediment cover prevents any further description.

### ***Metacarpals***

A single long bone aligned with the left radius is regarded as the fourth metacarpal based on its position and circular cross section. The element, however, is cut by the margin of the concretion after a length of 54 mm and the proximal portion of the shaft is covered by sediment, making this diagnosis uncertain. Two elements underlie the distal portion of this bone and are regarded as the wing metacarpal of the right arm and one of the three preaxial metacarpals. The smaller metacarpal craniocaudally compresses and expands dorsoventrally towards its distal termination to create the articular surface for the manual digits.

### ***Wing finger phalanges***

The distal ends of both first wing finger phalanges lie parallel to one another with their shafts displaying a circular cross section about the middle shaft that becomes dorsoventrally compressed towards the distal termination. The caudal margins of the phalanges curve caudally to create an expanded articular surface, convex in profile and 10 mm in width craniocaudally.

### ***Pes***

The left pes preserves three metatarsals and six elements of the first four digits. The metatarsals are long and narrow with mediolaterally compressed proximal margins. The bones become more circular in section towards their midpoints and have a diameter of 1.7 mm. All metatarsals are at least 28 mm in length and preserve a slight ventral curvature. The first phalanx of digit one is complete and preserves a length of 15 mm, along with a very slight ventral curvature of the shaft. The phalanx terminates in a weak condyle, lying in natural articulation with its ungual which itself is 11 mm in length. In its lateral aspect, the proximal half of the ungual is almost

trapezoidal in its outline while that of the distal half is curved strongly in a ventral direction and compressed dorsoventrally. The first phalanx of the second digit is 4.5 mm in length and lies in natural articulation with the second phalanx, which is estimated to have been 13 mm in length. The first phalanx of the third digit is 6 mm in length and lies in articulation with the second phalanx. The phalanx of the fourth digit is broken after only 5 mm but was at least 9 mm long.

### **Discussion**

The specimen described herein does not preserve the cranium and the high sagittal crest on its rostral margin that are diagnostic for *T. wellnhoferi*; however, the form of the mandible matches perfectly the amended diagnosis of Wellnhofer and Kellner (1991, p. 101), 'Lower jaw ventrally with sagittal crest on the symphysis. Upper margin of symphysis inclined downwards [ventrally] with concave depression dorsally.' The upper margin of the symphysis is turned ventrally at an angle of 13° relative to the dorsal margin of the ramus and is sufficiently similar to that noted in other examples of the *T. wellnhoferi* (i.e. 16°, AMNH 24440; 12°, SMNK PAL 1137; 14°, IMNH 1053) for the mandible to be considered complementary (Figure 2). Although a similar mandible is also noted for *Tupandactylus imperator* (CPCA 3590, Pinheiro et al. 2011), the ventral deflection is flat not concave, and the cranial margin of the mandibular crest is dominantly convex rather than concave, as noted in all individuals of *T. wellnhoferi*. The form of the mandibular crest in *Tupandactylus navigans* (Frey et al. 2003b) is unknown.

The shape of the ventral margin of the mandible is noteworthy in that the cranial and caudal margins of the crest show a shallow concave curvature relative to IMNH 1053 and the reconstructed margins of AMNH 24440. As such the profile of SMNK PAL 3986 is more comparable to that of SMNK PAL 1137, which also preserves a more gentle convex curvature (Figure 2D). There is, however, little reason to consider such a small divergence in crest morphology to be of taxonomic significance and it is instead likely to be the result of intraspecific variation or perhaps even slight differences in development or relative ontogenetic age. With regard to the latter point, the described specimen is relatively ontogenetically immature based on the lack of fusion between the cranial elements, which are found isolated, and the individual carpals, which have been disassociated from one another.

Although very little work has focused on the postcranial remains of azhdarchoid pterosaurs, any comparison of the described specimen with those of more complete azhdarchoids is restricted owing to a lack of preserved elements. The radius and ulna, which here represent the most complete long bones, are identical in



form to that of all derived pterosaurs with the exception of the size and position of pneumatic features. A large pneumatopore positioned on the cranial face of the ulna is known in other indeterminate azhdarchoids from NE Brazil (e.g. SMNK PAL 3985); however, no reference is made to such a feature in Chinese azhdarchoids (e.g. *Sinopterus*, Wang and Zhou 2003), largely due to the preserved orientation of the specimens and the degree of lateral compression. The form of the ungual is identical to that of *Sinopterus dongi* (IVPP V 13363), where the distal half is very narrow and ventrally curved. It is not possible to comment on the degree of mobility available to the ungual of SMNK PAL 3986 as the proximal margin is slightly convex with no presence of a large dorsally located cotyle as observed in other taxa (e.g. SMNK PAL 3830, 3900, 6409).

The ratio of the ungual to the length of the preceding phalanx in digit one of the pes is similar to that observed in larger and more mature azhdarchoids (i.e. 0.67 versus 0.62 in the azhdarchoid SMNK PAL 3830), and as such is sufficiently distinct from other pterodactyloids (e.g. 0.4 for the ornithocheiroid SMNK PAL 3854). The development of large unguals in *T. wellnhoferi* and the likely presence of large claw sheaths as demonstrated by Frey et al. (2003a; SMNK PAL 3830) form a part of a broader suite of characters (including the elongate femur/tibiotarsus and the increased development of the greater trochanter), suggesting that azhdarchoids were well adapted to life both on the ground and in the air.

Based on the size of the mandible, the described specimen was larger than that of SMNK PAL 1137 but slightly smaller than AMNH 24440 and SAO 12891, the latter specimens having an estimated wing span of 1.35–1.5 m (Wellnhofer and Kellner 1991). Although the only complete long bone observed herein is the ulna, regression relationships are fairly well established in pterosaurs such that wing length can be calculated from the comparison of additional azhdarchoid specimens, where  $ulna\ length = 1.5789 \times humerus\ length - 7.615$  ( $R^2 = 0.97$  based on 14 azhdarchoid specimens from 10 genera) and  $total\ span = 14.485 \times humerus\ length + 413.94$  ( $R^2 = 0.76$  based on six azhdarchoid specimens from four genera). Despite the relatively low confidence coefficient for total span, the estimated wing span between 1.15 and 1.47 m agrees well with those estimates of other specimens (Wellnhofer and Kellner 1991).

Although the chaotic displacement of several bone elements indicates that the specimen was disturbed after settling, the presence of delicate bones that remained *in situ* (i.e. metacarpalia, elements of the pes) indicates that at least parts of the soft tissue remained viable for a prolonged period following death.

## Conclusions

The specimen described herein represents a small and ontogenetically immature azhdarchoid pterosaur of the genus *Tapejara wellnhoferi* along with the partial remains of the postcranial skeleton. This individual developed the large curved unguals of the pes noted for other tapejarid examples (e.g. SMNK PAL 3830, 3900) and is inferred to have spent substantially more time on the ground than the ornithocheiroids, with whom they co-inhabited the Santana locality. The relatively small wing span compared to other pterosaurs known from the *Lagerstätten* deposits of NE Brazil is interpreted as a result from the morphologically immature nature of the skeleton and it is likely that it would have grown to have become much larger in size.

## Acknowledgements

Thanks are extended to Eberhard 'Dino' Frey and the SMNK for access to the described specimen and Urs Oberli for access to both SAO 12891 and other material within his collection.

## References

- Frey E, Buchy MC, Martill DM. 2003a. New specimens of Pterosauria (Reptilia) with soft parts with implications for pterosaurian anatomy. In: Buffetaut E, Mazin JM, editors. Evolution and palaeobiology of pterosaurs. Special Publications, Vol. 217. Geological Society London. p. 233–266.
- Frey E, Buchy MC, Martill DM. 2003b. A new species of tapejarid pterosaur with soft-tissue head crest. In: Buffetaut E, Mazin JM, editors. Evolution and palaeobiology of pterosaurs. Special Publications, Vol. 217. Geological Society London. p. 65–72.
- Kellner AWA. 1989. A new edentate pterosaur of the Lower Cretaceous from the Araripe Basin, Northeast Brazil. *Anais Acad Bras Ci.* 61:439–445.
- Kellner AWA. 1996. Description of the Braincase of two Early Cretaceous pterosaurs (Pterodactyloidea) from Brazil. *Am Museum Nov.* 3175:1–34.
- Kellner AWA, Tomida Y. 2000. Description of a new species of Anhangueridae (Pterodactyloidea) with comments on the pterosaur fauna from the Santana Formation (Aptian/Albian), northeastern Brazil. *Nat Sci Museum Mon, Tokyo.* 17:135 pp.
- Martill DM. 2007. The age of the Cretaceous Santana Formation fossil Konservat Lagerstätte of north-east Brazil: a historical review and an appraisal of the biostratigraphic utility of its palaeobiota. *Cret Res.* 28:895–920.
- Neumann VH, Cabrera L. 1999. Una nueva propuesta estratigráfica para la tectonosecuencia post-rifte de la cuenca de Araripe, noreste de Brasil. In: *Bol. 5<sup>th</sup> \_ Simp. Sob. Cret. Bras.* 1999. Campos de Rio Claro, Sao Paulo: UNESP. p. 279–285.
- Pinheiro FL, Fortier DC, Schultz CL, Artur J, Andrade FG, Bantim RAM. 2011. New information on *Tupandactylus imperator*, with comments on the relationships of the Tapejaridae (Pterosauria). *Acta Pal Pol.* doi:10.4202/app.2010.0057.
- Pons D, Berthou PY, Campos DA. 1990. Quelques observations sur la palynologie de l'Aptien superieur et de l'Albien du Bassin d'Araripe. In: Campos DA, Viana MSS, Brito PM, Beurlen G, editors. Atas do Simpósio Sobre a Bacia do Araripe e Bacias Interiores do Nordeste, Crato, 14–16 de Junho de 1990. p. 241–252.
- Pons D, Berthou PY, Melo Filgueira JB, Alcantara Sampaio JJ. 1996. Palynologie des unités lithostratigraphique "Fundao", "Crato" et Ipubi (Aptien supérieur à Albien inférieur-moyen, Bassin d'Araripe, NE du Brésil): enseignements paléoécologiques, stratigraphiques et climatologiques. In: Jardine S, Klasz I, Debenet J-P, editors.

- Géologie de l'Afrique et de l'Antique Sud. Compte-Rendu des Colloques de Géologie d'Angers, 16–20 July 1994. Vol. 16. Pau, Mémoire: Elf Aquitaine. p. 383–401.
- Unwin DM, Martill DM. 2007. Pterosaurs of the Crato Formation. In: Martill DM, Bechly G, Loveridge RF, editors. *The Crato Fossil Beds of Brazil: Window into an Ancient World*. Cambridge: Cambridge University Press. p. 475–524.
- Wang X, Zhou Z. 2003. A new pterosaur (Pterodactyloidea, Tapejaridae) from the Early Cretaceous Jiufotang Formation of western Liaoning, China and its implications for biostratigraphy. *Chin Sci Bull.* 48:16–23.
- Wellnhofer P, Kellner AWA. 1991. The skull of *Tapejara wellnhoferi* Kellner (Reptilia, Pterosauria) from the Lower Cretaceous Santana Formation of the Araripe Basin, Northeastern Brazil. *Mitt Bayer Staat Paläon Hist Geo.* 31:89–106.

# A nearly complete ornithocheirid pterosaur from the Aptian (Early Cretaceous) Crato Formation of NE Brazil

ROSS A. ELGIN and EBERHARD FREY



Elgin, R.A. and Frey, E. 2012. A nearly complete ornithocheirid pterosaur from the Aptian (Early Cretaceous) Crato Formation of NE Brazil. *Acta Palaeontologica Polonica* 57 (1): 101–110.

A partial ornithocheirid, representing a rare example of a pterosaurian body fossil from the Nova Olinda Member of the Crato Formation, NE Brazil, is described from the collections of the State Museum of Natural History, Karlsruhe. While similar in preservation and taphonomy to *Arthurdactylus conandoylei*, it is distinguished by slight differences in biometric ratios, but the absence of a skull prevents closer identification. Mostly complete body fossils belonging to ornithocheiroid pterosaurs appear to be relatively more abundant in the younger Romualdo Member of the Santana Formation, making the described specimen one of only two well documented ornithocheiroids known from the Nova Olinda Lagerstätte.

Key words: Ornithocheiroidea, pterosaur, taphonomy, Aptian, Cretaceous, Crato Formation, Brazil.

Ross A. Elgin [rosselgin@hotmail.com] and Eberhard Frey [dinofrey@aol.com], Staatliches Museum für Naturkunde Karlsruhe (SMNK), Abteilung Geologie, Erbprinzenstraße 13, 76133 Karlsruhe, Germany.

Received 4 August 2010, accepted 17 March 2011, available online 31 March 2011.

## Introduction

The Araripe Basin of NE Brazil contains two Early Cretaceous Lagerstätten that are world renowned for their exceptional preservation of insects and vertebrate fossils (Unwin 1988; Unwin and Martill 2007). Pterosaurs from the Aptian/Albian-aged Crato Formation and Albian/?Cenomanian-aged Santana Formation (Martill 2007) confirm that taxa attributed to both the Ornithocheiroidea (sensu Unwin 2003) and Azhdarchoidea inhabited the area of this inland lagoon, a setting in which marine influences became more dominant towards the end of the Albian after the formation of the Santana sea (Kellner and Tomida 2000).

Despite ongoing debates on taxonomic validity, a number of ornithocheiroid pterosaurs are known from the Santana Formation including *Anhangueira/Coloborhynchus* (Wellnhofer 1991; Kellner and Tomida 2000; Fastnacht 2001), *Araucarioactylus* (Price 1971; Wellnhofer 1977), *Brasileodactylus* (Kellner 1984; Veldmeijer et al. 2009), *Cearadactylus* (Leonardi and Borgomanero 1983; Dalla Vecchia 1993; Vila Nova et al. 2011), *Ornithocheirus* (Wellnhofer 1987), and *Santandactylus* (Buissonjé 1980; Wellnhofer 1985). In contrast, relatively few ornithocheiroid specimens have been described from the older Nova Olinda Member of the Crato Formation (e.g., *Arthurdactylus conandoylei*, SMNK PAL 1132, Frey and Martill 1994; *Ludodactylus sibbicki*, SMNK PAL 3828, Frey et al. 2003a; cf. *Brasileodactylus*, Sayão and Kellner 2000) and isolated crania or headless postcranial skeletons attributed to azhdarchoid taxa are instead better represented in the literature (Sayão and Kellner 2007; Martill and Frey 1999; Frey et al. 2003b; Kellner 2004).

A new specimen from the Nova Olinda Member in the collections of the State Museum of Natural History, Karlsruhe (SMNK PAL 3854), is described here, representing the rare occurrence of a largely complete ornithocheirid pterosaur from this locality. The specimen is taxonomically indeterminate, missing the skull, cranially located elements of the cervical column and the second to fourth phalanges of the wing-fingers, but is otherwise in a fairly good state of preservation. As is typical of fossils from the Crato Lagerstätte, the bones are crushed and few three-dimensional details can be observed. A greater degree of damage is observed along the caudally located thoracic vertebrae and the pelvic girdle. The skeleton has collapsed upon itself following contact with the lagoon floor, exposing the majority of bones in their dorsal or dorsolateral aspects (Fig. 1).

*Institutional abbreviations.*—AMNH, American Museum of Natural History, New York, USA; BMNH, British Museum of Natural History, London, UK; IVPP, Institute for Palaeontology and Palaeoanthropology, Beijing, People's Republic of China; JZMP, Jinzhou Paleontological Museum, Jinzhou, Liaoning Province, China; LPM, Liaoning Paleontological Museum, Western Liaoning Institute of Mesozoic Paleontology, Shenyang Normal University, Liaoning, China; MPSC, Museu de Paleontologia de Santana do Cariri, Santana do Cariri, Brazil; NGMC, National Geological Museum of China, Beijing, People's Republic of China; NSM, National Museum of Nature and Science, Tokyo, Japan; RGM, Nationaal Natuurhistorisch Museum (Naturalis), Leiden, the Netherlands; SMNK, Staatliches Museum für Naturkunde Karlsruhe, Karlsruhe, Germany.

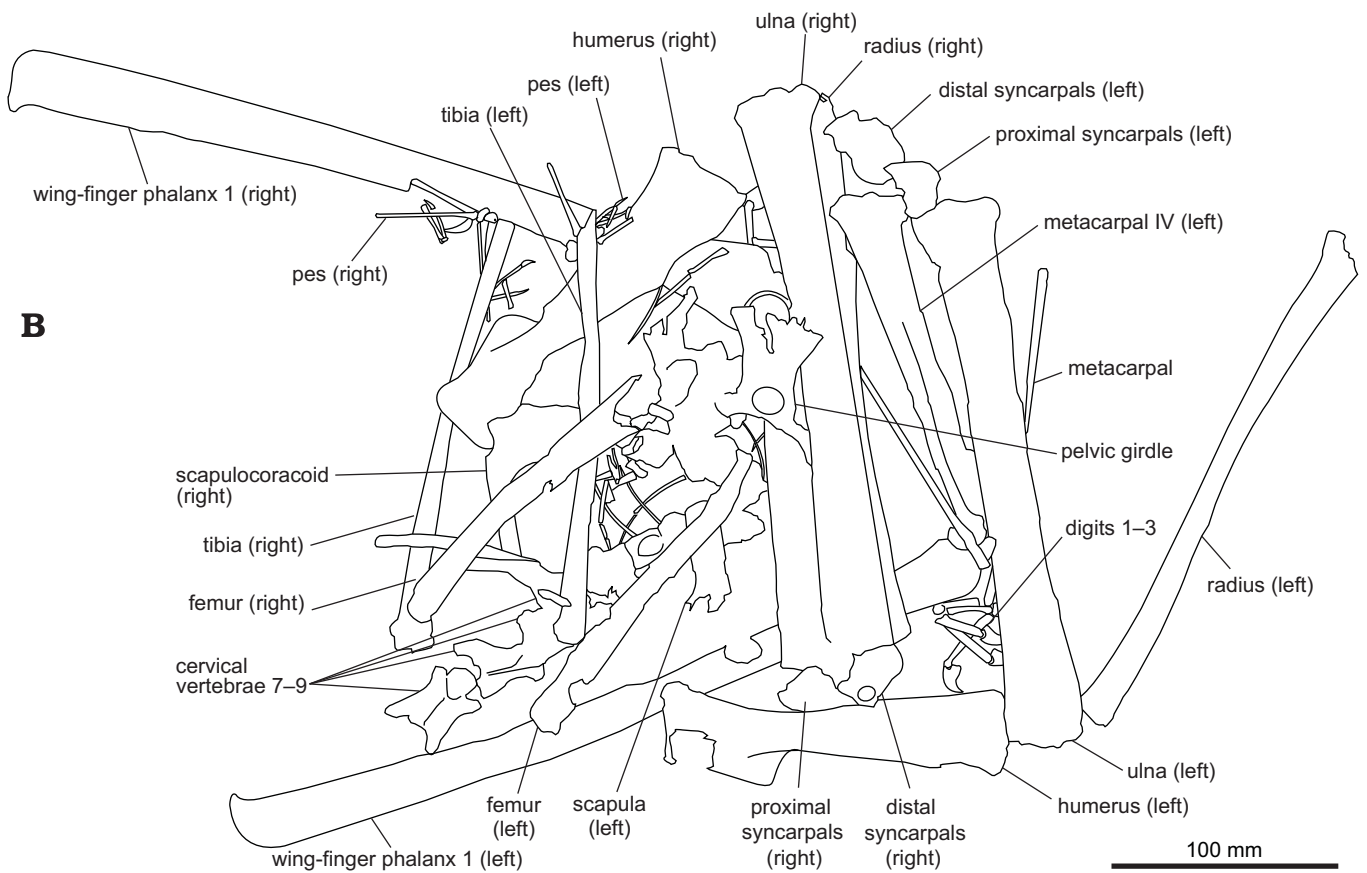


Fig. 1. New ornithocheirid pterosaur specimen (SMNK PAL 3854) from the Nova Olinda Formation, Crato Basin, Brazil. Photograph (A) and corresponding line tracing (B).

## Systematic palaeontology

Order Pterosauria Kaup, 1834

Superfamily Ornithocheiroidea Seeley, 1876

Family Ornithocheiridae Seeley, 1870

Genus and species indet.

*Description.*—The cervical column is represented by four vertebrae, identified as cervicals 5–8 (C5–8) (Figs. 2, 3). The morphology of these vertebrae is typical for ornithocheirid taxa (Table 1), in that the cervical vertebrae are 2–2.7 times as long as they are wide, they have a wide neural canal and widely diverging pre- and postzygapophyses, and the prezygapophyses are located lateral to the postzygapophyses (Bennett 2001). The neural spines of C5–6 are broken and no comment can be made on their relative height. Caudal to the 6<sup>th</sup> cervical vertebrae the remaining cervicals have been displaced from their natural position and are now visible in their craniolateral (C7) and cranial (C8) aspects. The neural spine of the 7<sup>th</sup> cervical is tall and thin with respect to the vertebral body while the most caudally located cervical vertebrae (i.e., C8–9) preserve large robust ribs that remained in situ, suggesting that these had fused to the transverse processes. Although the 9<sup>th</sup> cervical itself is not visible, being overlain by the 8<sup>th</sup>, its presence is confirmed by a single large rib situated caudal to that of the 8<sup>th</sup> cervical (Fig. 3C). The capitulum and tuberculum are widely spaced, by approximately 16 mm, and the shaft is narrow, decreasing rapidly to 6 mm by the mid corpus. The rib of the 9<sup>th</sup> cervical is complete and terminates in a robust, slightly convex surface after a length of 89 mm.

The centra of the thoracic vertebrae are missing, buried and/or badly damaged such that the description of these elements is restricted to the neural spines, three of which are

Table 1. Skeletal measurements of the new unidentified ornithocheirid from Brazil. SMNK PAL 3854. Measurements of selected bone elements. All values are in mm, where \* denotes an approximate or estimated value.

| Element            | mm   | Element       | mm   |
|--------------------|------|---------------|------|
| cervical vertebrae |      | scapula       | 73.5 |
| C5 length          | 37   | coracoid      | >61  |
| C5 mid width       | 28   | humerus       |      |
| C6 length          | 33*  | left          | 157  |
| C6 mid width       | –    | right         | 160  |
| C7 length          | >25  | ulna          |      |
| C7 mid width       | –    | left          | 252  |
| caudal vertebrae   |      | right         | 253  |
| 1                  | 10   | metacarpal IV |      |
| 2                  | 11*  | left          | 169  |
| 3                  | 10.5 | right         | 169  |
| 4                  | 12   | Wph 1         |      |
| 5                  | 12   | left          | 383  |
| 6                  | 11   | right         | 381  |
| 7                  | >6.9 | femur         |      |
| 8                  | 12   | left          | 161  |
| 9                  | 10   | right         | >150 |
| 10                 | 6.2  | tibia         |      |
| 11                 | >5   | left          | >197 |
|                    |      | right         | 202  |

partially fused and form a supraneural plate. Thin suture lines separating the individual neural spines are visible (Fig. 2). The neural spine of the first visible thoracic vertebra lies separate from the supraneural plate, although it is uncertain whether this is due to damage or displacement of the skeleton, or whether the neural spine simply did not form part of this structure. A large oval depression with a raised rim occu-

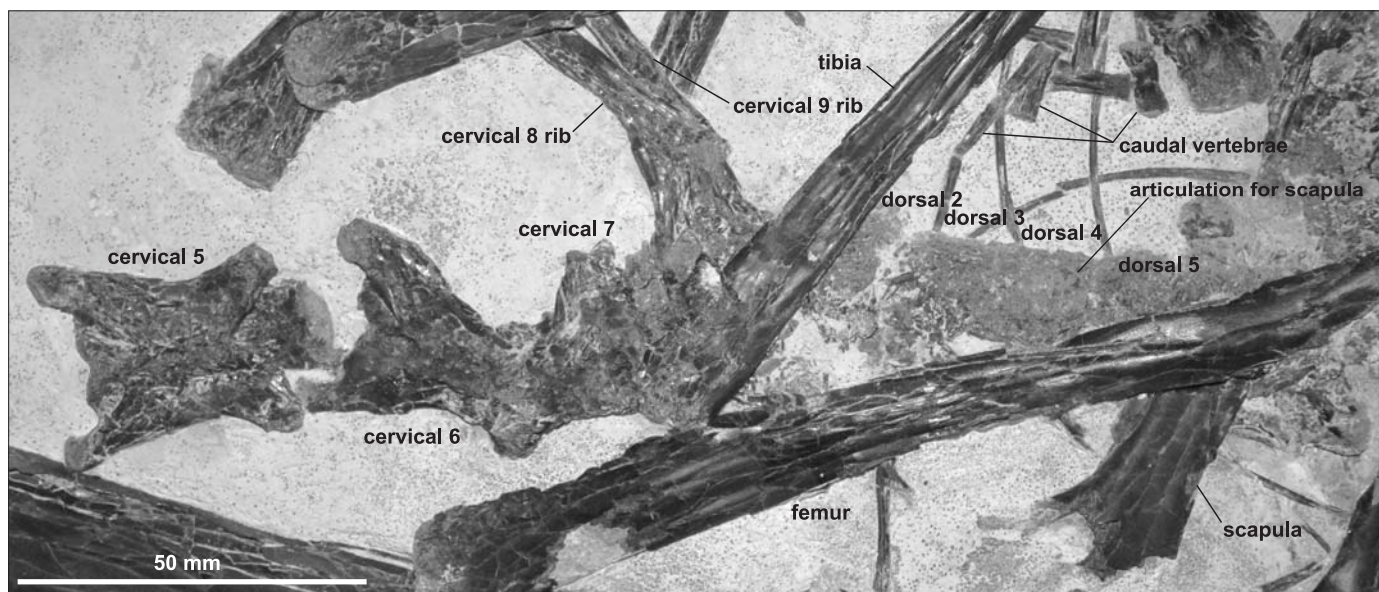


Fig. 2. New ornithocheirid pterosaur specimen (SMNK PAL 3854) from the Nova Olinda Formation, Crato Basin, Brazil. Photograph detailing the cervical, notarial thoracic and terminal caudal vertebrae.

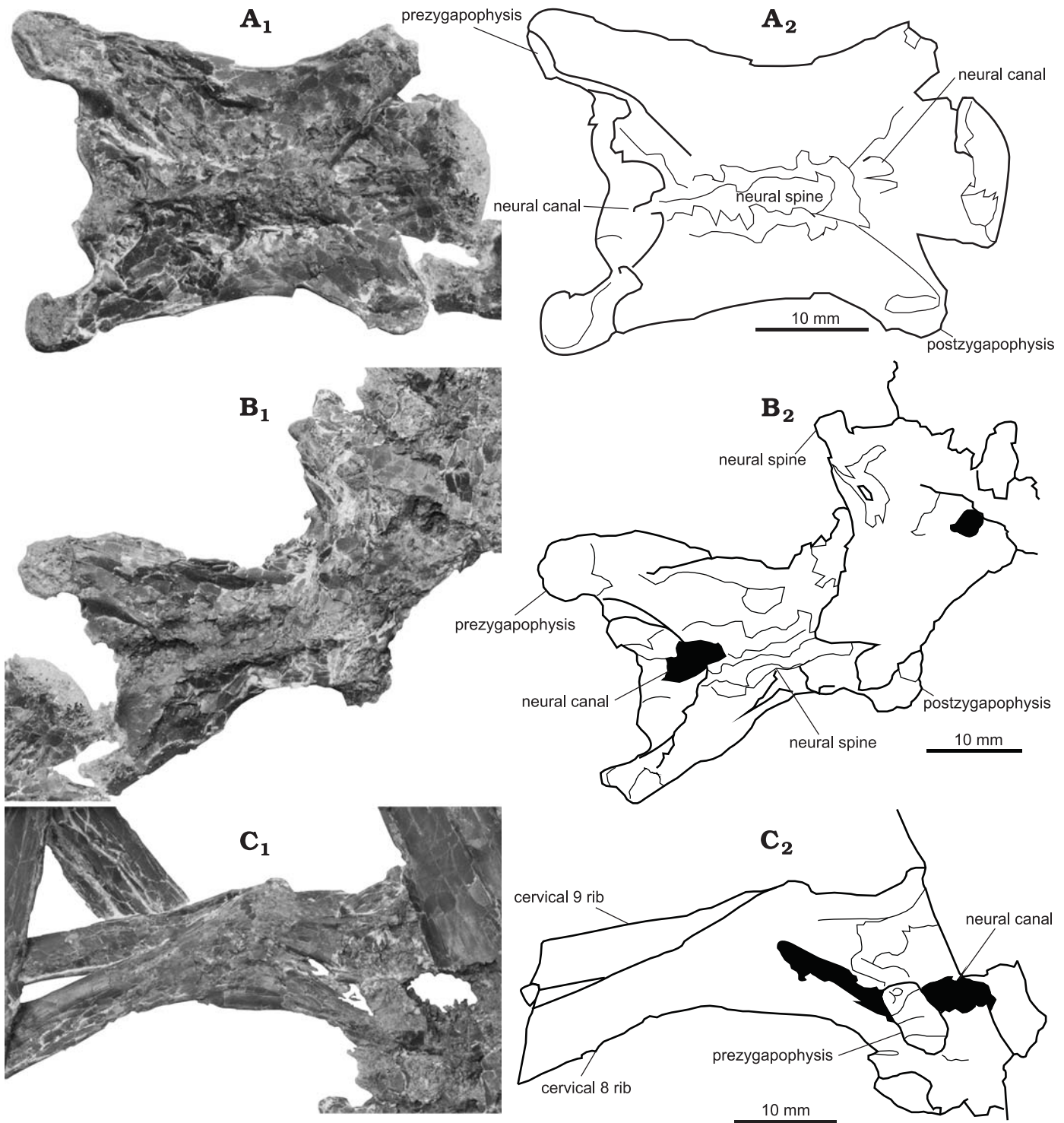


Fig. 3. New ornithocheirid pterosaur specimen (SMNK PAL 3854) from the Nova Olinda Formation, Crato Basin, Brazil. **A.** 5<sup>th</sup> cervical vertebrae. **B.** 6<sup>th</sup> and 7<sup>th</sup> cervical vertebrae. **C.** 8<sup>th</sup> and 9<sup>th</sup> cervical ribs. Photographs (A<sub>1</sub>, B<sub>1</sub>, C<sub>1</sub>) and explanatory drawings (A<sub>2</sub>, B<sub>2</sub>, C<sub>2</sub>). Black shading highlights gaps/foramina with the bone and the collapsed neurocentral canal.

pies the lateral flank of the third visible thoracic vertebra, forming the articulation for the medial articular surface of the scapula. Caudal to the notarial vertebrae the vertebral column is kinked and the more caudal thoracic vertebrae are badly damaged, indistinct and partly overlain by the left femur. These are also seen in lateral aspect and they have a

maximum height of 19 mm from the base of the centrum to the top of the neural spine.

Nothing can be said about the sacral vertebrae, which are obscured from view by the overlying pelvic girdle. At least six gastralia have separated from the main body of the fossil and were displaced to overlie the distal portion of the right

ulna following the disintegration of the dorsal column. These gastralria are preserved as three opposing sets and are associated with a limited amount of mineralised tissue. Eleven caudal vertebrae lie loose from the axial column and are scattered between the notarial vertebrae and the right scapulocoracoid. These are identical in appearance to those of *C. piscator* (Kellner and Tomida 2000), being long and narrow, typically between 2 and 4 times as long as they are wide. Where visible, the neural spines are positioned cranially and protrude past the cranial margin of the vertebrae, indicating that these bones belong to the middle portion of the tail. The terminal-most caudal vertebrae remain in articulation and are mediolaterally compressed to a greater degree than the other caudals. These are conical in form and do not expand at their articular surfaces (Fig. 2).

The right scapulocoracoid is preserved in cranial view. No suture line between the two elements is visible, indicating that the structure was fully fused. The glenoid body measures 23 mm across its widest part and the scapula is shorter than the coracoid, the condition typical of ornithocheiroids (Frey et al. 2003c; Kellner 2003; Unwin 2003). The scapula is offset against the glenoid body at an angle of  $121^\circ$  and the dorsal rim of the articular surface is visible as a flat, slightly convex surface that would have braced against the sub-oval facet of the notarium. The coracoid is about half as thick as the scapula in the mid-shaft region and forms an angle of  $60^\circ$  against the scapula. The proximal portion of the coracoid, where it would have articulated with the sternum is obscured by overlying sediment. The vertical distance between the dorsal surface of the scapula articular surface and the sternocoracoid articulation is estimated to have been no greater than 100 mm.

The individual bones of the forearm are mostly preserved in either near articulation or bent beyond bone lock. Both humeri are visible in dorsal aspect and preserve a short, warped, sub-triangular deltopectoral crest that is approximately one third of the total humeral length. The caudal tuberosity is short, and no pneumatic foramina are observed where it converges with the shaft of the humerus, although the compacta of these surfaces is slightly damaged. On the distal portion of the left humerus, along the craniodorsal margin of the shaft, a pronounced flange, 15% the humeral length, may be the insertion for the flexor muscles of the carpus (Bennett 2003). Towards the distal margin of the humerus, the humeral shaft expands to about twice its width at the elbow joint, preserving an almost straight dorsal margin perpendicular to the long axis of the shaft. The epiphyseal gap is partially open.

The left ulna lies at an angle of  $72^\circ$  to the humerus while the right makes an angle of  $53^\circ$ . Both have become slightly disarticulated from their natural positions. Both ulnae are about six times longer than they are wide and preserve no obvious muscle scars. While the right radius lies in situ along the right ulna the left radius has separated from the ulna and preserves a mid shaft width of 10–13 mm.

The carpals have fused to form two distinct syncarpal

blocks but these have disarticulated from one another and are badly damaged so that no anatomical details can be observed.

The fourth metacarpals have been displaced by approximately  $180^\circ$  and lie sub-parallel to the ulnae; the distal roller joints are located near the proximal ends of the ulnae. Both wing metacarpals are also preserved in ventral view, with the ventral part of the roller joint measuring 16 mm across at its widest point, and they retain a natural articulation with the first phalanges of the wing finger. At least two additional metacarpals, presumably belonging to the left wing, are also preserved. Both are long and narrow and at least one would have made contact with the distal syncarpal during life.

The digits of the left manus are well preserved, and although the individual phalanges have disarticulated from each other they have not been displaced any great distance. The distal bones retain a contact with their respective unguals. The phalanges are about half as wide as the proximal margins of the unguals and slightly curved, with expanded proximal and distal margins at the articular facets to accommodate the neighbouring elements. The unguals are slightly curved with longitudinally concave ventral faces, forming a sulcus that extends almost the entire length of the bone. The phalanges of the right manus are mainly obscured and only two partial phalanges and one ungual are visible.

Only the first phalanges of the wing fingers are preserved and lie in natural articulation with the fourth metacarpals, making angles of  $89^\circ$  and  $68^\circ$  against the long axis of the left and right metacarpals respectively. The extensor tendon process has fused to the proximal face of the first phalanx and a large pneumatic foramen is present on the caudoventral surface of the right phalanx, adjacent to the proximal articulation. At its distal terminus the cranial margin of the first wing finger phalanx gradually merges with the gently convex distal articulation. Caudally this articulation facet forms a sharp caudally directed process that is formed by the steeply convex caudodistal margin of the shaft. This creates an expanded surface for the second wing phalanx that would have directed the distal phalanges caudally.

The individual elements of the pelvis have fully fused to form two complete pelvic plates, although these are in a poor condition. The compacta is damaged and the bone itself is crushed over several underlying elements. The left ischio-pubic plate is observed in lateral view while the right is seen in caudolateral aspect, the acetabulum dominating the lateral faces of each and the obturator foramen being fully enclosed within the pubis. The cranial and caudal margins of the left pubis are shallowly concave, being almost symmetrical about the long axis of the bone. The bone is narrowest about its mid point before expanding towards its ventral margin, however, the ventral margin of the pubis is broken and its original shape cannot be determined. While the long axis of the pubis is directed ventrally, that of the ischium is directed caudoventrally at an angle of  $46^\circ$  against the pubis. As with the pubis, it is narrowest about its mid point and expands towards its ventral margin. Approximately half the caudal portion of the left ischium has been broken and lost from the

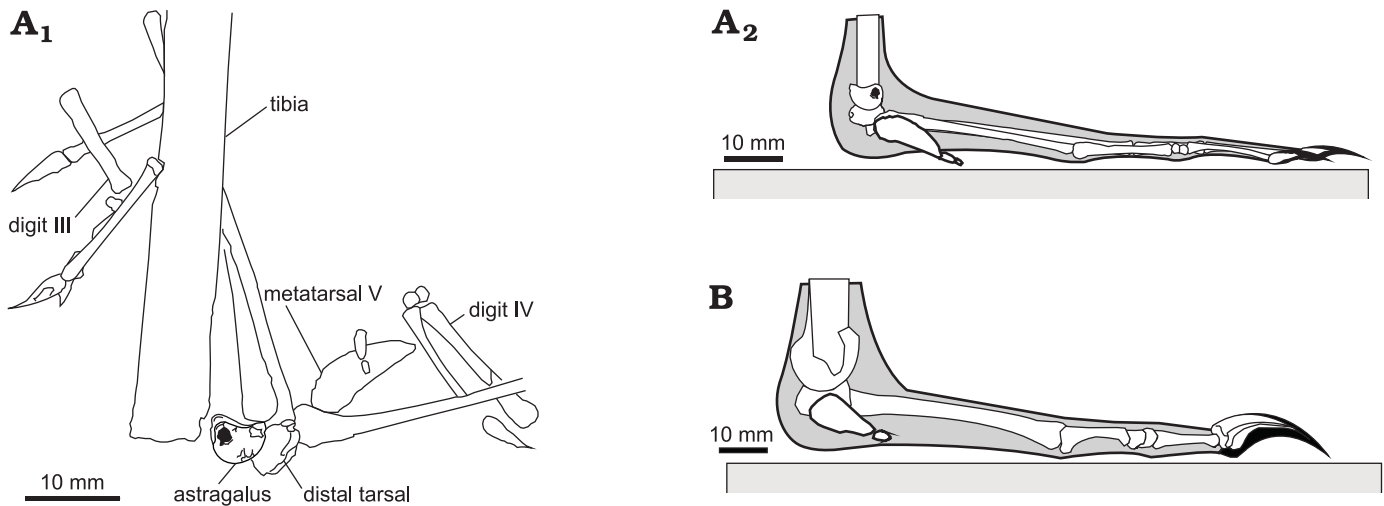


Fig. 4. The foot and pedal function of the new ornithocheiroid pterosaur from the Nova Olinda Formation, Crato Basin, Brazil. **A.** SMNK PAL 3854. Line tracing of the ankle region ( $A_1$ ) and reconstructions of the ornithocheiroid pes, based on the described specimen ( $A_2$ ). **B.** The azhdarchoid pes, based on SMNK PAL 3900. Both reconstructions are scaled to a common humeral length.

specimen while the right has been distorted and is directed through the bedding plane of the slab. The preacetabular process of the ilium is long and thin but its cranial portion is either overlain by the ulna (left) or broken (right). The postacetabular process of the right pelvic plate partially overlies that of the left, which in turn has been crushed over the remains of the sacral vertebrae. The postacetabular process expands caudodorsally for approximately one quarter of its total length due to the curvature of the dorsal margin of the bone. Caudal to this expansion, the dorsal and ventral margins are directed caudoventrally, creating a caudoventrally directed process more or less uniform in width.

The femora lie adjacent to the pelvis and preserve a long, narrow femoral collum femoris, approximately 17 mm long, and a moderately bowed, laterally curving shaft. The femoral head is offset against the shaft at an angle of  $20^\circ$ . Although both tibiae have disarticulated from their respective femurs, they have not been displaced much. The tibia is long and slender, becoming increasingly narrow towards its distal articulation. Neither fibula is preserved. The distal articulation of the left tibia is broken and missing but the right is complete and terminates as a flat surface, 7.5 mm in width, indicating that the calcaneum and astragalus had not fused with this bone to create a tibiotarsus (Fig. 4). Two tarsals, the astragalus and a distal tarsal, lie level with the distal margin of the tibia but off to one side. The astragalus is weakly crescentic in shape and is observed in medial aspect. A large foramen pierces the craniomedial portion of the bone. Although its caudomedial face is damaged, the preserved remains suggest that the medial surface was convex, projecting medially as described by Kellner (2004). The dorsal margin of the astragalus is concave to form the articulation with the distal surface of the tibia, while the ventral margin is strongly convex. The distal tarsal is as large as the astragalus itself, with a generally smooth convex surface and lies in contact with three of the four metatarsals.

The right metatarsals are very long and thin, the longest reaching a length of 58 mm with a mid-shaft diameter of only 1 mm. The length of these bones ranges from 54–58 mm, but at least one of the first four metatarsals is noticeably shorter with a length of only 45 mm. The fifth metatarsal is clearly distinct from the others, and is about one fourth to one fifth the length of metatarsals I–IV and has a sub-triangular outline with slightly convex medial and lateral margins.

The pedal phalanges are delicate and show only slight curvature. Their proximal and distal margins are slightly expanded at the interphalangeal articulations and in all cases the unguals maintain a natural articulation with the penultimate phalanx. The unguals themselves are equal in width to the preceding phalanges and are only slightly curved.

## Discussion

Largely complete ornithocheiroid pterosaurs appear to be much less common in the Nova Olinda Lagerstätte than in the geologically younger Romulado Member of the Santana Formation, NE Brazil. A thorough review of these was provided by Unwin and Martill (2007), who noted that specimens from the Crato Formation attributed to the Ornithocheiroidea are limited to SMNK PAL 1132 (*Arthurdactylus conandoylei*, Frey and Martill 1994), a headless skeleton preserving the majority of the postcranial elements; the proximal part of a wing belonging to an indeterminate ornithocheiroid (SNMK PAL 3842); an isolated tooth (Sayão and Kellner 2000); the complete cranium of SMNK PAL 3828 (*Ludodactylus sibbicki*, Frey et al. 2003a); and the rostral fragments of cf. *Brasileodactylus* (Sayão and Kellner 2000). Unwin and Martill (2007) include two further specimens, MPSC R-739 and MPSC R-779 (Nuvens et al. 2002) in the Ornithocheiroidea. A comparison of the present specimen with these other named taxa from the same locality, however, is problematic because no



Table 2. Selected long bone ratios of ornithocheiroid taxa. Abbreviations: fe, femur; FL, fore limb (humerus + ulna + metacarpal IV); HL, hind limb (femur + tibia); hu, humerus; mc IV, wing metacarpal; wph 1, first wing finger phalanx; ti, tibia; ul, ulna.

| Taxon                              | FL/HL          | hu/ul | hu/mc IV | hu/wph1 | hu/fe | hu/ti | fe/ti |
|------------------------------------|----------------|-------|----------|---------|-------|-------|-------|
| <i>Boreopterus cuiaie</i>          | JZMP-04-07-3   | 1.73  | 0.72     | 0.84    | 0.58  | 0.96  | 1.00  |
| <i>Nurhachius ignaciobritoi</i>    | LPM 0003       | –     | 0.57     | 0.87    | 0.47  | –     | –     |
| <i>Istiodactylus sinensis</i>      | NGMC 99-07-011 | –     | 0.57     | 0.82    | 0.50  | –     | –     |
| <i>Istiodactylus latidens</i>      | BMNH R 3877    | –     | 0.58     | –       | 0.56  | 1.10  | –     |
| ornithocheirid indet. (this study) | SMNK PAL 3854  | 1.48  | 0.63     | 0.94    | 0.41  | 0.98  | 0.79  |
| ? <i>Santanadactylus</i>           | SMNK PAL 1250  | –     | 0.65     | 0.93    | 0.45  | –     | –     |
| <i>Coloborhynchus robustus</i>     | SMNK PAL 1133  | 1.57  | 0.74     | 1.02    | 0.47  | 1.05  | 0.82  |
| <i>Arthurhynchus conandoylei</i>   | SMNK 1132 PAL  | 1.81  | 0.74     | 1.01    | 0.52  | 1.21  | 0.81  |
| <i>Coloborhynchus spielbergi</i>   | RGM 401880     | 1.49  | 0.71     | 1.23    | –     | 1.04  | 0.79  |
| <i>Pteranodon</i> sp.              | AMNH 4908      | 1.77  | 0.68     | 0.46    | 0.39  | 0.96  | 0.65  |

postcranial elements are known for *L. sibbicki*, while the taxonomic validity of *Brasileodactylus* is uncertain (Unwin and Martill 2007) and diagnostic features are restricted to the skull (Veldmeijer et al. 2009).

It is fortunate that pterosaurs generally display isometric growth, in which individual bones grow at the same relative rate through ontogeny, and this allows the calculation of biometric ratios to distinguish taxa. Omitting the pteranodontids (studied by Bennett 2001) and nyctosaurids, the wing metacarpal and femur of the Ornithocheiridae + Istiodactylidae show significantly negative allometric relationships, so that the ratios of lengths of these elements to humerus length increase at larger sizes (see Appendix 1). Limb bone proportions place SMNK PAL 3854 within the Ornithocheiroidea (Table 2) where it is distinguished from pteranodontid and nyctosaurid pterosaurs by the relative shortness of the wing metacarpal, and from the Istiodactylidae by a set of ratios that lie outwith the observed range of values known for these taxa. This suggests that the current specimen may be tentatively assigned to the Ornithocheiridae. Despite the similarities in preservation and taphonomy between SMNK PAL 3854 and SMNK PAL 1132, the described specimen is distinguished from *A. conandoylei* through biometric ratios, where its humerus is relatively longer, forming ratios of 0.63 and 0.41 with the ulna and first wing-finger phalanx respectively (0.74 and 0.52 for SMNK PAL 1132). A more distinct ratio is observed in the hind limb, where the femur is substantially shorter, based on a large difference in the forelimb/hindlimb ratio (1.48 for SMNK PAL 3854 versus 1.81 for SMNK PAL 1132). A possible relationship is suggested with a larger specimen attributed to *Santanadactylus* sp. (SMNK PAL 1250) by an almost identical suite of bone ratios (note that this latter fossil is in a private collection and has not been described or diagnosed; Frey and Martill 1994).

SMNK PAL 3854 is estimated to have had a wing span of 3.4 m, based on the observations of Veldmeijer (2003), who noted that in *Santanadactylus pricei* (Wellnhofer 1991) the ratio between the total length of the wing finger and the humerus plus radius/ulna is 2.7. A similar ratio is also recorded for *A. conandoylei*, suggesting that this relationship is useful across a range of ornithocheirid taxa. The length of the torso,

measured from the first thoracic vertebra to the caudal margin of the ilium, is 140 mm, namely 4% of the total wingspan.

**Ontogenetic age.**—Despite the relatively advanced state of suture closure in parts of SMNK PAL 3854 shows no fusion between the astragalus and the tibia, and so is not yet at maximum age. The relative timings of suture closure in pterosaurs have been briefly reviewed by Bennett (1993) and Kellner and Tomida (2000), and the former tentatively proposed that for *Pteranodon* the atlas-axis complex, scapulocoracoid, secondary centres of ossification in the humerus, the cranial-most notarial vertebrae and ribs appear to precede all others. The suture between the extensor tendon process and the first wing finger phalanx appears to close shortly before skeletal maturity is reached. An examination of the suture states in SMNK PAL 3854 indicates that fusion of the tibia and proximal tarsals, the caudal thoracic ribs and their respective vertebrae, complete suturing of the notarium, and fusion of the humeral epiphyses to the humerus itself should all be considered indicators of late ontogeny and are preceded by the closure of the suture between the extensor tendon process and the first wing-finger phalanx and elements of the pelvic plate. Such observations do not contradict the proposals of Bennett (1993) and Kellner and Tomida (2000) but rather provide an example of interspecific variation in developmental timings that likely existed even between closely related taxa.

**Life style.**—The estimated length of the wing spar combined with the short length of the torso and hind limbs indicates that SMNK PAL 3854 developed the high aspect-ratio configuration noted for other ornithocheiroids and likely shared their interpreted lifestyle, being a relatively fast, open water glider, using dynamic or thermal soaring (e.g., Chatterjee and Templin 2004). The view that such taxa spent most of their life on the wing is further supported by the structure and relative size of the pes with respect to the wings; these bones in SMNK PAL 3854 are exceedingly thin compared with the pedal elements of azhdarchoid pterosaurs with which they shared the Cretaceous Crato lagoon. The comparison of a similar-sized azhdarchoid, SMNK PAL 3900, effectively illustrates this difference where the mid-shaft diameter of the phalanges ranges between 2–2.5 mm, with the unguals being

17 mm long (Fig. 4A<sub>2</sub>, B). Similar values are also noted for the medium-sized azhdarchoids SMNK PAL 3830 and 6409, and the former demonstrates that sharp keratinous sheaths doubled the total length of the pedal claws. In contrast, the phalanges of SMNK PAL 3854 are only 1 mm in diameter with a length of 7 mm. The delicate nature of the pes in SMNK PAL 3854 therefore suggests that it was predominantly a soaring animal that spent little time on the ground. While one reviewer noted that blunted claws would be more in keeping with a terrestrially active lifestyle, it is difficult to explain the long, sharp keratinous sheaths of azhdarchoids without invoking a role in terrestrial support, as pterosaurs did not utilise their pedal claws for either the manipulation of prey or arboreal perching. Nonetheless, the lack of wear on the unguis sheaths of SMNK PAL 3830, a morphologically mature individual, perhaps indicates that these animals spent a significant portion of their life on the wing, while still being more terrestrially competent than ornithocheirids such as that described here.

**Taphonomy.**—The resting position and taphonomy of SMNK PAL 3854 strongly resembles SMNK PAL 1132, where the skeleton has collapsed upon itself following the destruction of the ventral body wall and the subsequent release of air from the pneumatic system. In both individuals, the lack of a preferred orientation indicates that bottom currents were absent, while the overlapping bones indicate that the carcass sank left wing first, and the hind limbs were the last elements to settle. In contrast to SMNK PAL 1132, the neck did not detach at its base but between the 4<sup>th</sup> and 5<sup>th</sup> cervicals (Frey and Martill 1994). The sternum is also missing from SMNK PAL 3854, the reason perhaps being the rapid bacterial degradation of the large pectoral muscle mass. While the pectoral muscles insert at the humerus with massive tendons, their origin on the sternum is fleshy and thus subject to more rapid decay and earlier detachment of the sternum, where the sternocostal and sternocoracoideal articulations must have been weak. The carcasses of ornithocheiroid pterosaurs likely followed the pattern of decay observed in birds and mammals (Oliver and Graham 1994; Davis and Briggs 1998), in which the head detaches first from the body, followed by the sternum.

Long-term floating at the water surface is typical for highly pneumatised tetrapods (Schäfer 1962, 1972), buoyed up by their air sacs. The state of decomposition when the specimen settled on the lagoon floor was probably relatively advanced, based on the degree of disarticulation. While this indicates that the interarticular ligaments had largely lost their ability to restrict the mobility of the bones, the carcass nonetheless must have been largely intact when it settled, as is shown by the preservation of easily displaced elements, such as manual and pedal phalanges. It then seems likely that the larger elements missing from the slab, such as the head and neck and the distal wing phalanges, were likely lost during sedimentary transport rather than during collection.

## Conclusions

A new specimen from the Crato Formation of NE Brazil is an ornithocheiroid pterosaur, distinguishable from *Arthurducatylus conandolei*, the only other nearly complete postcranial skeleton from the Crato locality, by biometrics of the long bones. Almost identical bone ratios indicate possible relationship with a specimen of ?*Santanadactylus* sp. (Frey and Martill 1994), but the lack of a formal description of the latter prevents a taxonomically useful comparison.

The inferred high aspect ratio of the wing, combined with a delicate pes, supports the established hypothesis that ornithocheiroids spent the majority of their life in the air and that, while fully capable of terrestrial locomotion, spent little time on the ground when compared to other pterosaurs.

The animal was ontogenetically relatively mature when it died, based on the state of its sutures, which include fusion of the extensor tendon process to the first wing-finger phalanx, the scapula to the coracoid, the proximal and distal syncarpals of the wrist, the ischiopubic plate, and a partial notarium. The animal was not fully mature, however, because a tibiotarsus had not yet formed, and suture lines separate the epiphyses from the humerus. These elements can therefore be regarded as late-forming structures and may be of use in diagnosing the relative ontogenetic maturity of pterosaurs in future studies.

## Acknowledgements

The authors thank René Kastner (SMNK) for preparation of the specimen and V. Griener for contributing to the photography. Comments and criticisms supplied by Chris Bennett (Fort Hays State University, Kansas, USA), Colin Palmer (University of Bristol, UK), and Mark Witton (University of Portsmouth, UK) greatly improved the quality and content of this manuscript. RAE and EF are supported by DFG grant FR1314/15-2.

## References

- Bennett, S.C. 1993. The ontogeny of *Pteranodon* and other pterosaurs. *Paleobiology* 19: 92–106.
- Bennett, S.C. 2001. The osteology and functional morphology of the Late Cretaceous pterosaur *Pteranodon*, Part 1. General description of osteology. *Palaeontographica, Abteilung A* 260: 1–112.
- Bennett, S.C. 2003. Morphological evolution of the pectoral girdle of pterosaurs: myology and function. In: E. Buffetaut and J.-M. Mazin (eds.), *Evolution and Palaeobiology of Pterosaurs*. *Geological Society, London, Special Publications* 217: 191–215.
- Buissonjé, P.H. 1980. *Santanadactylus brasiliensis* nov. gen., nov. sp., a long necked large pterosaur from the Aptian of Brasil. *Koninklijke Nederlandse Akademie van Wetenschappen (B)* 83: 145–172.
- Chatterjee, S. and Templin, R.J. 2004. Posture, locomotion, and paleoecology of pterosaurs. *Geological Society of America, Special Paper* 376: 1–64.
- Dalla Vecchia, F. 1993. *Cearadactylus? ligabuei*, nov. sp., a new Early Cretaceous (Aptian) pterosaur from Chapada do Araripe (Northeastern Brazil). *Bollettino della Società Paleontologica Italiana* 32: 401–409.

- Davis, P.G. and Briggs, D.E.G. 1998. The impact of decay and disarticulation on the preservation of fossil birds. *Palaos* 13: 3–13.
- Fastnacht, M. 2001. First record of *Coloborhynchus* (Pterosauria) from the Sanana Formation (Lower Cretaceous) of the Chapada do Araripe, Brazil. *Paläontologische Zeitschrift* 75: 23–26.
- Frey, E. and Martill, D.M. 1994. A new pterosaur from the Crato Formation (Lower Cretaceous, Aptian) of Brazil. *Neues Jahrbuch für Geologie und Paläontologie, Abhandlungen* 194: 379–412.
- Frey, E., Martill, D.M., and Buchy, M.-C. 2003a. A new crested ornithocheirid from the Lower Cretaceous of northeastern Brazil and the unusual death of an unusual pterosaur. In: E. Buffetaut and J.-M. Mazin (eds.), *Evolution and Palaeobiology of Pterosaurs*. *Geological Society, London, Special Publications* 217: 55–63.
- Frey, E., Tischlinger, H., Buchy, M.-C. and Martill, D.M. 2003b. New specimens of Pterosauria (Reptilia) with soft parts with implications for pterosaurian anatomy and locomotion. In: E. Buffetaut and J.-M. Mazin (eds.), *Evolution and Palaeobiology of Pterosaurs*. *Geological Society, London, Special Publications* 217: 233–266.
- Frey, E., Buchy, M.-C., and Martill, D.M. 2003c. Middle- and Bottom-decker Cretaceous pterosaurs: unique designs in active flying vertebrates. In: E. Buffetaut and J.-M. Mazin (eds.), *Evolution and Palaeobiology of Pterosaurs*. *Geological Society, London, Special Publications* 217: 267–274.
- Kaup, J. 1834. Versuch einer Eintheilung der Säugethiere in 6 Stämme und der Amphibien in 6 Ordnung. *Isis* 3: 311–315.
- Kellner, A.W.A. 1984. Ocorrência de uma mandibular de Pterosauria (*Brasileodactylus araripeensis* nov. gen.; nov. sp.) na formação Santana, Cretáceo da chapada do Araripe, Ceará, Brasil. *33º Congresso Brasileiro de Geologia, Anais* 2: 578–590.
- Kellner, A.W.A. 2003. Pterosaur phylogeny and comments on the evolutionary history of the group. In: E. Buffetaut and J.-M. Mazin (eds.), *Evolution and Palaeobiology of Pterosaurs*. *Geological Society, London, Special Publications* 217: 105–137.
- Kellner, A.W.A. 2004. New information on the Tapejaridae (Pterosauria, Pterodactyloidea) and discussion of the relationships of this clade. *Ameghiniana* 41: 521–534.
- Kellner, A.W.A. and Tomida, Y. 2000. Description of a new species of Anhangueridae (Pterodactyloidea) with comments on the pterosaur fauna from the Santana Formation (Aptian–Albian), northeastern Brazil. *National Science Museum Monographs, Tokyo* 17: 1–138.
- Leonardi, G. and Borgomanero, G. 1983. *Cearadactylus atrox* nov. gen., nov. sp. Novo Pterosauria (Pterodactyloidea) da Chapada do Araripe, Ceara, Brasil. In: D. A. Campos, C.S. Ferreira, I.M. Brito, and C.F. Viana (eds.), *Coletânea de Trabalhos Paleontológicos, Série Geologia*, 75–80. Ministerio das Minas e Energia-DNPM, Rio de Janeiro.
- Martill, D.M. 2007. The age of the Cretaceous Santana Fossil Konservat Lagerstätte of north-east Brazil: a historical review and an appraisal of the biostratigraphic utility of its palaeobiota. *Cretaceous Research* 28: 895–920.
- Martill, D.M. and Frey, E. 1999. A possible azhdarchid pterosaur from the Crato Formation (Early Cretaceous, Aptian) of northeast Brazil. *Geologie en Mijnbouw* 78: 315–318.
- Nuvens, P.C., Sayão, J.M., Silva, H.P., Saraiva, A.A., and Kellner, A.W.A. 2002. A coleção de pterossauros do Museu de Paleontologia de Santana do Cariri, Nordeste do Brasil. *Arquivos do Museu Nacional, Rio de Janeiro* 60: 235–240.
- Oliver, J.S. and Graham, R.W. 1994. A catastrophic kill of ice-trapped coots: time-averaged versus scavenger-specific disarticulation patterns. *Paleobiology* 20: 229–244.
- Price, L.I. 1971. A presença de Pterosauria no Cretáceo Inferior da Chapada do Araripe, Brasil. *Anais da Academia Brasileira de Ciências* 43 (Supplement): 451–461.
- Sayão, J.M. and Kellner, A.W.A. 2000. Description of a pterosaur rostrum from the Crato Member of the Santana Formation (Aptian–Albian) northeastern Brazil. *Boletim do Museu Nacional Nova Serie Rio de Janeiro–Brasil, Geologia* 54: 1–8.
- Sayão, J.M. and Kellner, A.W.A. 2007. Novo esqueleto parcial de pterossauro (Pterodactyloidea, Tapejaridae) do Membo Crato (Aptiano), Formação Santana, Bacia do Araripe, nordeste do Brasil. *Estudos Geológicos* 16: 16–40.
- Schäfer, W. 1962. *Aktuo-paläontologie nach Studien in der Nordsee*. 666 pp. Kramer, Frankfurt.
- Schäfer, W. 1972. *Ecology and Palaeoecology of Marine Environments*. 568 pp. University of Chicago Press, Chicago.
- Seeley, H.G. 1891. On the shoulder girdle in Cretaceous Ornithosauria. *Annals and Magazine of Natural History* 6: 438–445.
- Unwin, D.M. 1988. New pterosaurs from Brazil. *Nature* 332: 398–399.
- Unwin, D.M. 2003. On the phylogeny and evolutionary history of pterosaurs. In: E. Buffetaut and J.-M. Mazin (eds.), *Evolution and Palaeobiology of Pterosaurs*. *Geological Society, London, Special Publications* 217: 139–190.
- Unwin, D.M. and Martill, D.M. 2007. Pterosaurs of the Crato Formation. In: D.M. Martill, G. Bechly, and R.F. Loveridge (eds.), *The Crato Fossil Beds of Brazil*, 475–524. Cambridge University Press, Cambridge.
- Veldmeijer, A.J. 2003. Description of *Coloborhynchus spielbergi* sp.nov. (Pterodactyloidea) from Brazil in the collection of the National Museum of Natural History (Naturalis), Leiden, the Netherlands. *Scripta Geologica* 125: 35–139.
- Veldmeijer, A.J., Meijer, H.J.M., and Signore, M. 2009. Description of Pterosaurian (Pterodactyloidea: Anhangueridae, *Brasileodactylus*) remains from the Lower Cretaceous of Brazil. *Deinsea* 13: 9–40.
- Vila Nova, B.C., Saraiva, A.A.F., Moreira, J.K.R., and Sayão, J.M. 2011. Controlled excavations in the Romualdo Formation Lagerstätte (Araripe Basin, Brazil) and pterosaur diversity: remarks based on new findings. *Palaos* 26: 173–179.
- Wellnhofer, P. 1977. *Araripedactylus dehmi* nov. gen., nov. sp., ein neuer Flugsaurier aus der Unterkreide von Brasilien. *Mitteilungen der Bayerischen Staatssammlung für Paläontologie und historische Geologie* 17: 157–167.
- Wellnhofer, P. 1985. Neue Pterosaurier aus der Santana Formation (Apt) der Chapada do Araripe, Brasilien. *Palaeontographica, Abteilung A* 187: 105–182.
- Wellnhofer, P. 1987. New crested pterosaurs from the Lower Cretaceous of Brazil. *Mitteilungen der Bayerischen Staatssammlung für Paläontologie und historische Geologie* 27: 175–186.
- Wellnhofer, P. 1991. Weitere Pterosaurierfunde aus der Santana Formation (Apt) der Chapada do Araripe, Brasilien. *Palaeontographica, Abteilung A* 215: 43–101.

## Appendix 1

Long bone measurements of ornithocheiroid specimens used for calculating ratios and isometric/allometric relationships in this paper, where “R” denotes a value reconstructed from personal observations or the source literature. At the 95% CI with the humerus acting as the independent variable, the relationships of selected bone elements are defined as: ulna =  $0.325 * x^{0.936} \pm 0.119$  ( $R^2 = 0.96$ ); mc IV =  $0.493 * x^{0.789} \pm 0.082$  ( $R^2 = 0.97$ ); femur =  $0.444 * x^{0.798} \pm 0.183$  ( $R^2 = 0.93$ ); and wph 1 =  $0.16 * x^{1.071} \pm 0.13$  ( $R^2 = 0.97$ ). With respect to the humerus, the wing metacarpal and femur show a significantly negative deviation from isometry. Specimens attributed to pteranodontids and nyctosaurid pterosaurs were omitted for several reasons: the elongation of the wing metacarpal in relation to the humerus is unusual for ornithocheiroids; certain bone relationships e.g. ulna/mc IV appear to be different between *Pteranodon/Nyctosaurus* and the remainder of the Ornithocheiroidea; the large number of specimens known for *Pteranodon* would unduly bias the regression relationships towards this single genus rather than the broader trend across the entire division. The observed taxonomic level of regression relationships is thusly important and the state at one level need not be directly applicable to others.

| Taxon (Collection Nr.)                            | hu     | ul     | mc IV  | wph 1  | wph 2  | wph 3  | wph 4  | fe     | ti     |
|---|--------|--------|--------|--------|--------|--------|--------|--------|--------|
| ornithocheiroid indet. (SMNK PAL 1135)            | 172.0  | 263.0  | 179.0  | 383.0  | –      | –      | –      | –      | –      |
| ornithocheiroid indet. (SMNK PAL 1134)            | –      | 239.0  | 165.0  | 357.0  | –      | –      | –      | –      | –      |
| ornithocheiroid indet. (SMNK PAL 3854)            | 159    | 253    | 169    | 382    | –      | –      | –      | 161    | 230    |
| <i>Boreopterus cuiaie</i> (JZMP-04-07-3)          | 79.0   | 110.0  | 94.0   | 137.0  | 122.5  | 98.0   | 87.0   | 82.0   | 82.0   |
| <i>Istiodactylus sinensis</i> (NGMC 99-07-011)    | 133.5  | 233.7  | 162.7  | 268.2  | 243.5  | 195.4  | >32.9  | >139.5 | 182.5  |
| <i>Istiodactylus latiden</i> (BMNH R 3877)        | 220.0  | 381R   | –      | 393R   | 388R   | –      | –      | 200.0  | –      |
| <i>Nurhachius ignaciobritoi</i> (IVPP V-13288)    | 110.5  | 192.8  | 132.6  | 226.5  | 165.7  | –      | –      | 146.4  | >118.2 |
| <i>Nurhachius ignaciobritoi</i> (LPM0003)         | 88.3   | 156    | 101    | 188.0  | 157    | 120    | –      | 100    | –      |
| <i>Haopterus gracilis</i> (IVPP V11726)           | 70.0   | 101.5  | 90.0   | 134.5  | 119.0  | 95.5   | >45.0  | –      | –      |
| <i>Anhanguera santanae</i> (AMNH 225555)          | 204.0R | 291.0R | 206.0R | 446.0R | 389.0R | 302.0R | 192.0R | 165.0R | 287.0R |
| <i>Arthurdactylus conandoylei</i> (SMNK PAL 1132) | 230.0  | 312.0  | 227.0  | 445.0  | 402.0  | 312.0  | 275.0  | 190.0  | 234.0  |
| <i>Coloborhynchus piscator</i> (NSM-PV 19892)     | 255.0  | 390.0  | 256.0  | > 120  | –      | –      | –      | 234.0  | > 256  |
| <i>Coloborhynchus robustus</i> (SMNK 1133 PAL)    | 290.0  | 390.0  | 285.0  | 620.0R | 566.0R | 460.0R | 330.0R | 277.0  | 338.0  |
| <i>Coloborhynchus spielbergi</i> (RGM 401880)     | 290.0  | 410.0  | 235.0  | –      | –      | –      | –      | 277.8  | 351.8  |
| <i>Gegepterus change</i> (IVPP V 11981)           | –      | –      | 52.7*  | 69.3   | 68.3   | –      | >38.0  | –      | –      |
| <i>Santanadactylus pricei</i> (AMNH 22552)        | 170.0  | 242.5  | 172.0  | 372.0  | 324.0  | 252.0  | 160R   |        |        |
| ? <i>Santanadactylus</i> (SMNK PAL 1250)          | 230.0  | 353.0  | 248.0  | 515.0  | –      | –      | –      | –      | –      |

# A new azhdarchoid pterosaur from the Cenomanian (Late Cretaceous) of Lebanon

Ross A. Elgin · Eberhard Frey

Received: 16 September 2010 / Accepted: 7 October 2011  
© Swiss Geological Society 2011

**Abstract** A new pterosaur, *Microtuban altivolans* gen. et sp. nov., is described from the Sannine Formation of northern Lebanon. The specimen is the first pterosaur from the Early Cenomanian (Late Cretaceous) locality of Hjoûla and is regarded as the most complete pterosaur fossil discovered from Africa. While postcranial characters indicate a possible relationship with members of the Thalassodromidae or Chaoyangopteridae, the specimen possesses an exceptionally short wing-finger phalanx 4, forming only 1.1% of the total length of the wing-finger. Its appearance along with an unnamed ornithocheiroid from the slightly younger locality of Hâqel suggests that a number of pterosaur taxa existed within the local area, perhaps living on exposed carbonate platforms.

**Keywords** Pterosaur · Azhdarchoidea · *Microtuban* · Cretaceous · Lebanon

## Abbreviations

GMN Geological Museum of Nanjing (China)  
HGM Henan Geological Museum, Zhenzhou (China)  
IMCF Iwaki Coal and Fossil Museum (Japan)  
MN Museu Nacional, Rio de Janeiro (Brazil)  
SMNK Staatliches Museum für Naturkunde Karlsruhe (Germany)  
TMM Texas Memorial Museum (USA)

---

Editorial handling: Jean-Paul Billon-Bruyat.

---

R. A. Elgin (✉) · E. Frey  
Staatliches Museum für Naturkunde Karlsruhe,  
Abteilung Geologie, 13 Erbprinzenstraße,  
76133 Karlsruhe, Germany  
e-mail: rosselgin@hotmail.com

ZHNM Zhejiang Museum of Natural History, Hanzhou (China)

## Introduction

While the Late Cretaceous Lagerstätten deposits of northern Lebanon are famous for the exceptional preservation of their invertebrate and fish faunas, the remains of higher vertebrates are rare. Although pterosaurs, a group of aerial archosauromorphs, had effectively achieved a world wide distribution during the latter part of the Mesozoic, the first pterosaur specimen from the Lebanese carbonates was only recently described by Dalla Vecchia et al. (2001), consisting of a single isolated forearm of a Late Cretaceous ornithocheiroid. The deposits of northern Lebanon therefore follow a more general pattern observed across the whole of the African plate, where pterosaur material is both rare and consists of a rather sparse collection of fragmented bones or teeth. To date, fossil discoveries have included: “rhamphorhynchoids” (Unwin and Heinrich 1999); ornithocheiroids, anhanguerids and pteranodontids (Swinton 1948; Mader and Kellner 1999; Wellnhofer and Buffetaut 1999); the dsungaripteroid *Tendaguripterus recki* (Unwin and Heinrich 1999) from the Upper Jurassic of Tendaguru, Tanzania; and several members of the Azhdarchoidea (Wellnhofer and Buffetaut 1999), including the azhdarchids *Arambourgia philadelphiae* (Arambourg 1954) and *Phosphatodraco mauritanicus* (Suberbiola et al. 2003). Recent additions to these also include two humeri belonging to pterosaurs of the Dsungaripteroidea and the Archaeopterodactyloidea from the Upper Jurassic of Tendaguru (Costa and Kellner 2009), and the aforementioned specimen from northern Lebanon (Dalla Vecchia et al.

2001). Therefore, in spite of their condition and relative rarity, this collection of elements illustrates that Gondwanaland supported a diverse number of pterosaur taxa throughout its geological history.

This paper describes a second pterosaur from the Late Cretaceous (Cenomanian) limestone of northern Lebanon, originating from the locality of Hjoûla (Fig. 1). The specimen is preserved on a single oval slab of limestone and is partially complete, consisting of: the most posterior cervicals and anterior dorsal vertebrae, the pectoral girdle, a complete left wing, and the fragmented remains of the hindlimbs (Fig. 2). It is relatively more complete than that described by Dalla Vecchia et al. (2001) and is therefore regarded as the most complete pterosaur yet discovered from the African plate. The described specimen is housed at the State Museum of Natural History Karlsruhe in Germany under the collection number SMNK PAL 6595.

### Geological setting

The regional tectonic history of Lebanon has been the focus of several studies (e.g., Butler and Spencer 1999; Brew et al. 2001) where the prominent Yammouneh Fault, along with several smaller structures, represents the northern extension of the Dead Sea fault system (Fig. 1a; Abdel-Rahman and Nader 2002). During the Cretaceous Period the majority of the sediments were deposited within

the Palmyride Basin, a large NNE–SSW trending intraplate trough, which persisted until the end of the Cretaceous when it was destroyed by regional compression. Within this basin the sediments slope westwards to form a single large monoclinical structure and the depositional environments are split between a western, open marine facies and an eastern, coastal facies (Nader et al. 2006).

Of significant palaeontological interest are the Konservat Lagerstätten that consist of four major fossiliferous localities: Sâhel Aalma, Nammoûra, Hâqel, and Hjoûla, each of which are famous for their exceptional preservation of Late Cretaceous invertebrates and fishes (e.g., Forey et al. 2003; Hay 1903; Woodward 1942). The youngest of these localities is Sâhel Aalma, which is Santonian in age (Garassino 1994) while the others are Cenomanian and deposited as part of the Sannine Formation (Fig. 1b), which itself appears to have been created during a period of relative stability and low sea levels (Nader et al. 2006). The Nammoûra is regarded as late to mid Cenomanian in age (Dalla Vecchia and Venturini 1999) while the localities of Hâqel and Hjoûla are both Early Cenomanian (Saint-Marc 1974); with the locality of Hâqel occupying a position approximately 20 m stratigraphically higher than that of Hjoûla (Hückel 1970). Other than fish, fossil vertebrates at all of these localities are rare, however, birds (Dalla Vecchia and Chiappe 2002), turtles, dolichosaurs and marine varanoids (Dalla Vecchia and Venturini 1999; Dal Sasso and Renesto 1999) have nonetheless been described from

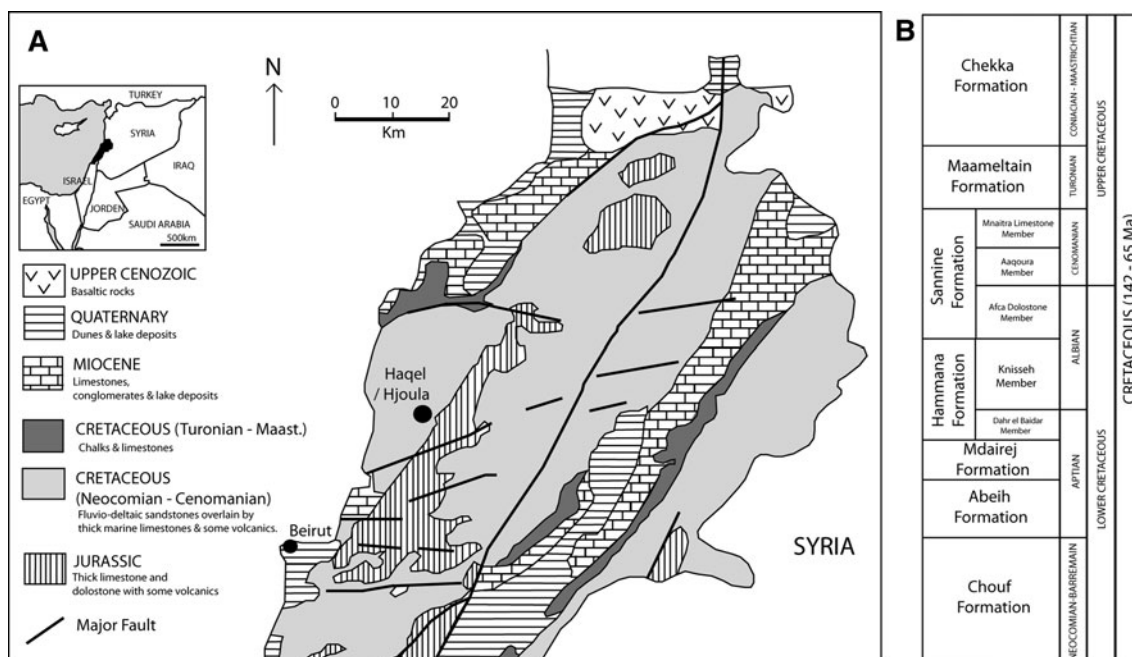


**Fig. 1** a Geological map of northern Lebanon showing the localities of Hâqel and Hjoûla. b Relative position of the Sannine Formation within the Cretaceous strata of Lebanon. Figures adapted after Abdel-Rahman and Nader (2002)

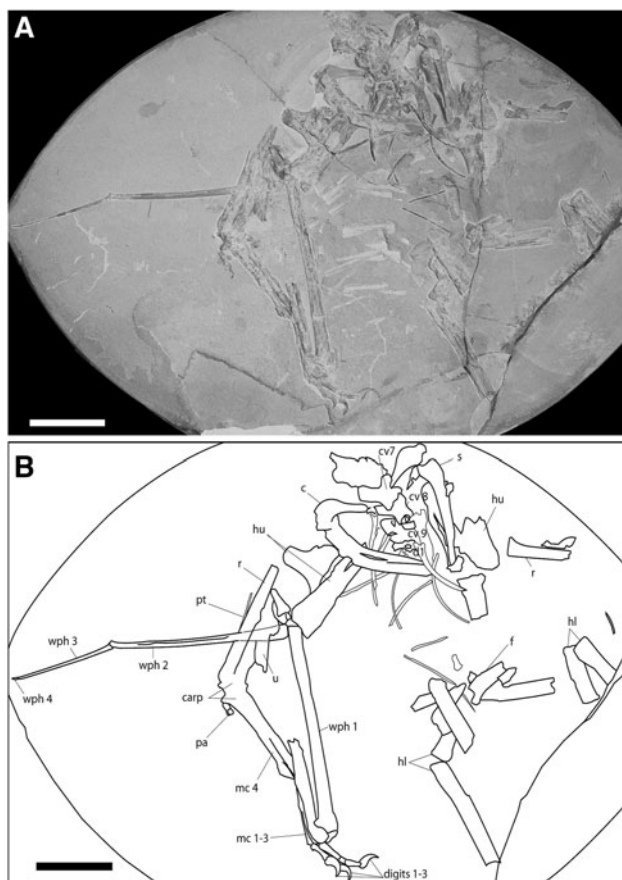


**Fig. 2** *Microtuban altivolans* (SMNK PAL 6595) gen. et sp. nov. **a** Photograph, **b** line tracing corresponding to photograph in **a**. Scale bars 50 mm. *c* coracoid, *carp* carpus, *cv* cervical vertebrae, *d* dorsal vertebrae, *digits* digits 1–3, *f* femur, *hl* fragments of the hindlimb, *hu* humerus, *mc* metacarpal, *pa* preaxial carpal, *pt* pteroid, *r* radius, *s* scapula, *u* ulna, *wph* wing-finger phalanges (digit 4)

the limestone of Nammoûra. In contrast to the older localities of Hâqel and Hjoûla, terrestrial plant remains are also common at Nammoûra (Dalla Vecchia and Venturini 1999), including a diverse selection of ferns, gymnosperms and angiosperms. Some of these share an affinity with similar aged flora in North America, central Europe and the Crimea, suggesting a palaeoclimate similar to the present day Mediterranean (Krassilov and Bacchia 2000). The occurrence of these well preserved plant materials within marine sediments indicates the proximity of the region to a palaeoshoreline. In comparison to Nammoûra, indeterminate plant material (Krassilov and Bacchia 2000) and algae (Basson 1972) are also known from Hâqel, where fossil reptiles are represented by a single ornithocheiroid pterosaur (Dalla Vecchia et al. 2001). Prior to this study, fossil reptiles were unknown from the locality of Hjoûla. Saint-Marc (1974) described the palaeoenvironments of both Hâqel and Hjoûla during the Cenomanian as a small, oxygen depleted, marine basin, with the major land mass

being located in the present WSW portion of the Arabian Peninsula. Nader et al. (2006) later described the depositional environment in the frame of a carbonate ramp model with shallower waters prevailing to the far east of Lebanon.

### Lithology and provenance

The specimen was purchased by the SMNK from a fossil dealer with local contacts and thus the exact provenance of the specimen is uncertain and worthy of discussion. The SMNK was initially told that the pterosaur originated from a quarry at Hâqel, although doubts were raised during discussions with another local dealer. We were later informed that this fossil had probably not been removed from the quarry of Hâqel but was likely from the nearby locality of Hjoûla (Roy Nohra, personal communication). As Hjoûla is only ~4 km south of Hâqel it is conceivable that the fossil dealers and middle men were uncertain as to the specimen's exact provenance. The sediments of Hâqel, however, contain a moderate amount of bioclasts and are noticeably whiter in colouration than those of Hjoûla, which are more micritic. A comparison of the grey limestone slab with other specimens housed at the SMNK leads us to propose the Early Cenomanian locality of Hjoûla as the true provenance of this specimen. This conclusion could be further confirmed by a thin section or petrographic analysis, but these were beyond the scope of this investigation.

### Systematic palaeontology

|             |  |
|-------------|--|
| Order       | Pterosauria KAUP 1834                              |
| Suborder    | Pterodactyloidea PLIENINGER 1901                   |
| Superfamily | Azhdarchoidea NESSOV 1984; <i>sensu</i> UNWIN 2003 |

#### Genus *Microtuban* gen. nov.

*Etymology* Greek μικρός = micros, for small; Arabic ثعبان = tu'bân, for basilisk, dragon, a star in the constellation *Draco*.

*Diagnosis* As for type species.

**Type species. *Microtuban altivolans* gen. et sp. nov.** (Figs. 2, 3)

*Etymology altivolans*: Latin altivolans = soaring/high flyer.

*Diagnosis* An azhdarchoid pterosaur distinguishable by an unusually high ratio of the first and second wing-finger phalanges ( $wph\ 2/wph\ 1 = 0.85$ ) and a hyper-reduced fourth wing-finger phalanx, accounting for 1.1% of the total wing-finger length.

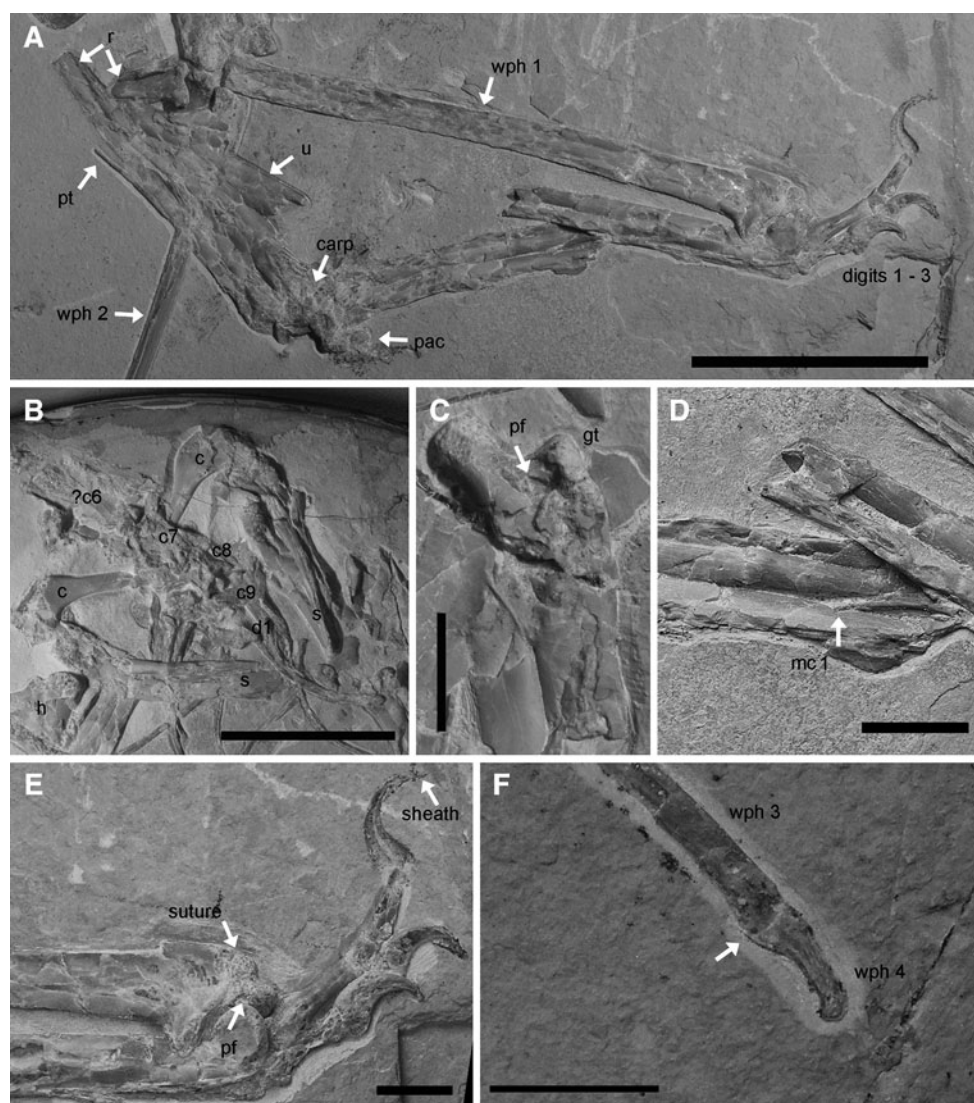


**Fig. 3** Selected elements of *Microtuban altivolans* gen. et sp. nov. with specific points of interest. **a** Overview of the forearm, **b** the cranial aspect of the pectoral girdle and cervical/dorsal series in dorsal view, **c** the right femur in dorsal view, **d** fracture across the shaft of mc IV in cranial view (*arrow* indicates the termination of metacarpal ?1), **e** close up of the left manus and first wing-finger phalanx in dorsal view, **f** the fourth wing-finger phalanx in ventral view (*arrow*

indicating the articulation between wph 3 and 4). *Scale bars a* 50 mm, *b* 50 mm, *c* 10 mm, *d* 10 mm, *e* 10 mm, *f* 5 mm. *c* coracoid, *cX* cervical vertebra X, *carp* carpus, *dX* dorsal vertebra X, *gt* greater trochanter, *h* humerus, *mc* metacarpal, *pac* preaxial carpal, *pf* pneumatic foramen, *pt* pteroid, *r* radius, *u* ulna, *wph* wing-finger phalanx

**Holotype** The holotype specimen is housed in the Staatliches Museum für Naturkunde Karlsruhe (Germany) under the collection number SMNK PAL 6595.

**Locality** ?Hjoûla (= Hadjoula), town and region 35 km NNE of Beirut (Lebanon).

**Horizon** Sannine Formation, Late Cretaceous (Early Cenomanian).

#### Description

**Cervical vertebrae and associated ribs** At least three crushed cervicals are preserved in dorsolateral view while

incomplete fragments of bone, cranial to the seventh cervical, may represent the remains of the sixth cervical vertebra. The seventh and eighth cervicals are in natural articulation, where the postzygapophyses of the former overlie the latter vertebra. The ninth cervical is in natural articulation with the first thoracic vertebra (d1). The neural spines of all the vertebrae except that of the ninth cervical are broken and missing. The seventh cervical is longer than that of the eighth (Table 1) and the prezygapophyses of both are widely splayed, lying lateral to the postzygapophyses. The prezygapophyses of the seventh cervical are orientated craniolaterally at an angle of  $\sim 45^\circ$  to the



**Table 1** Selected bone measurements in *Microtuban altivolans* gen. et sp. nov.

| Selected elements | Length (mm)            |
|-------------------|------------------------|
| Cervical 7        | 23.6                   |
| Cervical 8        | 21.1                   |
| Cervical 9        | ~9.0                   |
| Dorsal 1          | ~10.0                  |
| Humerus           | 61.6–73.3 <sup>a</sup> |
| Radius            | 92.0 <sup>a</sup>      |
| Carpus            | 13.0                   |
| pteroideum        | >38.0                  |
| mc IV             | 122.0 <sup>a</sup>     |
| mcIII?            | 50.0                   |
| dI p1             | 12.5                   |
| dIu               | 11.0                   |
| dIIu              | 11.0                   |
| dIIIp1            | 17.0                   |
| dIIIp2            | 3.0                    |
| dIIIp3            | 10.5                   |
| dIIIu             | 11.0                   |
| wph 1             | 135.0                  |
| wph 2             | 114.5                  |
| wph 3             | 63.5                   |
| wph 4             | 3.5                    |

*d* digit, *etp* extensor tendon process, *mc* metacarpal, *ph* phalanx, *postzy* postzygapophyses, *prezy* prezygapophysis

<sup>a</sup> Estimated values

midline. The left prezygapophysis of the ninth cervical face dorsomedially although at what angle remains uncertain. Double-headed ribs are visible in close association with the last two cervical vertebrae. In cervical 8 these are long (>19 mm in length) but thin, and while one lies adjacent, though un-fused, to the left prezygapophysis, another can be tentatively traced to the opposite side. More ribs also lie adjacent but un-fused to the transverse processes of the ninth cervical; however, they are significantly larger and more robust than those of the preceding vertebra.

**Thoracic vertebrae and associated ribs** A single thoracic vertebra is preserved in natural articulation with the ninth cervical, flanked by two large and robust double-headed ribs. A loose pair caudal to these suggests that they were present up to and including the second thoracic vertebrae. The neural spine is broken but must have run for a length of 8 mm along the dorsal portion of the centrum. The absence of any axial elements caudal to the first thoracic vertebrae indicates that no notarium was originally present. The caudally positioned thoracic ribs are thin, strongly curved and loosely positioned along with the imagined midline of the axial skeleton.

**Pectoral girdle** Both left and right scapulae and coracoids are unfused but the similarity in their resting positions

indicates little *post mortem* displacement (Fig. 3b). The scapula consists of a caudomedially directed blade, which ventrally diverges into a scapular body bearing the glenoid fossa. The angle between body and blade is approximately 145°. The scapular blade is straight, most likely long ovoid in cross-section as can be concluded from the right scapula, and is approximately five times longer than it is wide. The cranial edge appears to have been a little more massive than the caudal one. Towards its median terminus it tapers to a sharp median margin with a rounded outline. The two contralateral scapular blades are angled in a craniolateral direction at an angle of ~45° against the median plane. The scapular body curves medially at an angle of about 145° measured against the long axis of the blade and while crushed, was likely sub-triangular in cross-section. From their articulation with the scapulae both coracoids point medially, forming an angle of about 50° with the body of their respective scapulae. The glenoid head of the coracoid is angled against the shaft at about 80° and has three times the diameter of the medially most preserved part of the shaft. Cranioventrally the glenoid head is marked by a blunt crest that medially merges with the cranioventral face of the shaft. Nothing can be said about the morphology of the glenoid fossa because it is either covered by sediment and overlying bone, or is damaged. The coracoid shaft is almost circular in cross-section at its midpoint and preserves no trace of a medial divergence towards the furca. On the right coracoid the ventral process of the furca is visible at the left hand margin of the vertebral complex; giving a ratio of 1:0.78 between scapula and coracoid.

**Humerus** Both humeri have been broken into two large proximal and distal fragments with only the left humerus preserving any osteological details. The proximal fragment of this is preserved in its cranial aspect and consists of the humeral head, which lies slightly disarticulated from the lateral margin of the left scapular body. The collum of the humeral head is dorsocaudally concave and bears the deltopectoral crest; the proximal margin is regularly concave and would have been confluent with the cranial corner of the articular surface of the humeral head if not for a small break in the bone. The cranial margin of the deltopectoral crest is convex, whereby the convexity is a little stronger at the cranioproximal corner than at the craniodistal one. At the mid part of the deltopectoral crest the proximal and caudal margins run almost parallel to each other. Close to the collum, the distal margin of the deltopectoral crest curves distally and merges with the humeral shaft. The deltopectoral crest is almost flat, about 1.5 times as long as it is wide, and the collum itself is inclined caudally at an angle of about 43°. Near the break on the distal humeral fragment there is an elongate, oval scar that probably acted as the insertion point for a muscle; possibly *m. triceps* or *m. brachialis* (Bennett 2003a). The distal fragment is observed

in cranial view, the length of which suggests that a degree of overlap likely existed between the two fragments and a middle estimate of 67.5 mm is adopted for this study (Table 1).

*Radius/ulna* The bones of the antebrachium have been badly crushed and the compacta fragmented. The left antebrachium has fractured into at least one proximal and one distal portion, each of which preserves their respective articular surfaces. The proximal radial fragments, identified by their proximodorsal tubercle, lie almost perpendicular to the distal articular face of the left humerus. The proximal fragments are overlain by their distal fragments, the latter of which are orientated almost perpendicular to the former. An exception occurs where a further fragment of bone, attributed to the middle portion of the ulna, overlies and converges with the proximal end of the distal ulnar fragment (Fig. 3a). The distal fragments of the ulna and radius run parallel to each other, the diameter of bones approaching a ratio of 1:0.7 towards the midpoint of the shaft. The preserved diameter is fairly reliable because of the late diagenetic compaction, which preserved the actual diameter of the bones in the bedding plane.

*Carpus* Both proximal and distal elements are present and preserved in craniodorsal view, although abrasion of the compacta limits the observed articulation between the proximal and distal blocks to the cranial third of the carpus. It is thus not possible to identify the presence of a syncarpal, although given the general completeness of the carpus this appears to be likely and the term is adopted here. The left carpus remains in situ and forms an angle of  $116.5^\circ$  between the radius/ulna and the fourth metacarpal (Fig. 3a). The cranial aspect of the proximal syncarpal is cuboid in appearance while that of the distal syncarpal cannot be determined. A large, longitudinally ovoid excavation, preserving slightly broken margins, is located in a patch of predominantly intact compacta on the dorsal surface of the distal syncarpal, close to the cranial margin. Within this depression three smaller, presumably pneumatic, foramina pierce the distal syncarpal. The left pteroid and the preaxial carpal are preserved close to their natural positions (Fig. 3a). The pteroid is long and slender, about 0.75 mm wide at its distal terminus, but has been displaced medially so that the proximal portion is hidden by the overlying radius; the exact length of the element is thus unknown. The distal end does not taper but shows a rounded knob-like termination that is slightly kinked in the direction of the antebrachium. In the proximal third of the pteroid, a piece of the compacta is missing, revealing the hollow interior of the bone. The preaxial carpal has rotated over the distal margin of its articular face on the distal carpal block and now lies parallel to the fourth metacarpal. An oval sesamoid with an evenly convex surface (“Sesamoid A” = pisiform after Bennett 2008) sits within the fovea of the preaxial carpal.

*Metacarpals* The wing metacarpal is broken about halfway along its length (Fig. 3a), the proximal and distal fragments of which are displaced slightly. The shaft of the metacarpal narrows distally but then expands caudally at its most distal margin, forming a pair of condyles for the articulation of the first wing-finger phalanx. The distal dorsal condyle shows only a slight compaction and is thus well preserved in three dimensions; the dorsal surface of which is slightly concave with a shallow elevation in the centre. In cranial view the condyle is directed slightly dorsolaterally at an angle of  $\sim 20^\circ$ . Caudoproximally the rim of the dorsal condyle terminates abruptly, forming a short concavity that borders the condylar neck caudally. All three remaining metacarpals can be observed in situ along the craniodistal face of the wing metacarpal and form a natural contact with the digits. These can be traced proximally only as far as the large break across the fourth metacarpal, with the exception of a single metacarpal (mc ?I), which is preserved on the proximal fragment of the wing metacarpal and tapers to a natural termination some 48 mm distal to the carpometacarpal articulation (Fig. 3d). Damage to the metacarpals indicates that even these slender bones were hollow.

*Digits* The left manus is preserved in a slightly hyper-extended position. Digit I overlies digit II, however, digit III has been displaced slightly caudally with the palmer part of the proximal articulation condyle of its first phalanx now overlying the dorsal margin of the first phalanx of digit I (Fig. 3e). All of the elements belonging to the digits are in full articulation. The dorsally facing compacta of the phalanges of digit I are mostly eroded and the first phalanx shows signs of compaction along the mid-part of its shaft; the palmer face of which is concave between the articulation heads. A narrow trace, most likely the remnants of a claw sheath, is present, adjacent to the tip, along the caudal margin of the unguis phalanx. Of digit II only the unguis phalanx is visible. Distal to the tip of the unguis phalanx the keratinous claw sheath is visible as a yellowish buff trace that extends the tip of the unguis by at least 2 mm. Compared with the first phalanx of digit I the concavity of the shaft of the first phalanx of digit III is shallow. Phalanx 2 of digit III has barely one-fourth of the length of the first phalanx and is marked by a deep palmer notch and a dorsal styloid process that has one-third of the length of that phalanx. This process forms a bone lock that hinders a hyper-extension of the third phalanx of digit III. The third phalanx is almost conical with a very shallow circumferential concavity in its distal two-thirds. According to its external mould, the distal articular condyle with the unguis phalanx was almost confluent with the shaft. The unguis phalanx of digit III is preserved predominantly as an impression, lined with some remnants of the compacta along the lateral sulcus and the very tip. This tip is

prolonged by a black pyrolusite or goethite stain, 3 mm in length, which represents the remains of a keratinous sheath. All ungual phalanges are—or in the case of digit III were—11 mm long.

*Wing-finger* Only those elements belonging to the left wing-finger can be identified and preserve the fourth digit in its entirety. With the exception of the third and fourth phalanges these have been displaced and lie slightly out of natural articulation with their neighbouring elements. The first wing-finger phalanx is preserved in partial articulation with the fourth metacarpal and lies flexed back to such an extent that the caudal process now overlies the dorsocaudal surface of metacarpal IV, forming an angle of  $3.5^\circ$  between the two bones. This flexion has separated the metacarpal IV and the first wing-finger phalanx so that only the extensor tendon process still lies between the condyles of the metacarpal. The lack of contact between the two elements suggests that the metacarpophalangeal articulation is likely hyper-flexed. The distal terminus of the phalanx shows some surface erosion as does the dorsal margin of the proximal cotyle, but the margin of the gently convex articulation with phalanx 2 is still visible. The extensor tendon process is not fused to the first wing phalanx and is sub-triangular outline with a deeply concave cranial margin. Caudally this rises into a blunt ridge and becomes confluent with the proximal ridge above the articular face. This latter ridge tapers caudally and is perforated by a pneumatic foramen that is partly obscured by the dorsal condyle. The remaining three phalanges of the wing-finger lie adjacent to each other and display a shallow caudally directed curvature. In contrast to the other elements of the wing these are exposed in ventral view. The second wing-finger phalanx is 85% of the length of the first wing-finger phalanx and preserves a gentle, caudally directed curvature. The bone formed a long oval in cross-sectional view. The third wing-finger phalanx is missing most of the compacta and is around half the size of the second (i.e., 55%). The distal articulation face is only one-fourth the size of the proximal one. The fourth wing-finger phalanx is a tiny element about 3.5 mm in length and shows three shallow, distally converging striae on its dorsal face (Fig. 3f). The caudal margin of the bone is concave and terminates in a blunt, slightly re-curved tip with a flat distal surface.

*Hindlimbs* The hindlimbs have been crushed and broken into several mostly indeterminable elements. The right femur is preserved in its caudal aspect where the femoral neck is offset from the shaft at an angle of  $41^\circ$  (Fig. 3c). The greater trochanter is observed as a prominent, cranially directed triangular process, the caudal margin of which is slightly convex and marked by a blunt ridge that merges distally with the femoral shaft. Between the trochanteric ridge and the femoral neck a large, pneumatic, trabeculae-

lined opening pierces the shaft. Immediately distal to the trochanteric area, portions of the femur were broken and re-attached with a loss of some bone material.

## Discussion

### Ontogenetic age

The identification of unfused sutures in the skeleton, and the sequence in which they occur, has proven useful to determine the morphological age of a variety of arch-osauromorphs (Brochu 1995, 1996; Irmis 2007), included pterosaurs (e.g., Bennett 1993; Kellner and Tomida 2000). While Bennett (1993) further noted an immature bone grain, and pitting about the articular extremities as being indicative of osteological immaturity in pterosaurs, the bone grain of *M. altivolans* appears to be well developed. Immaturity is however indicated by the lack of skeletal fusion where the cervical and thoracic ribs are separate from their respective vertebrae, the scapula and coracoid have not formed a scapulocoracoid, and the presence of a large suture between the extensor tendon process and the first wing-finger phalanx. As such the animal did not live to a late ontogenetic state and is inferred as being juvenile or sub-adult.

### Taphonomy

The skeleton of *M. altivolans* shows some unusual features in that while almost all the long bones have been badly fractured (Fig. 3a), many of these elements have remained in close association or lie just beyond bone lock. Fragile elements that are easily displaced by *post mortem* movement, including the pteroid, preaxial carpal, metacarpalia, and digits I–III, are also preserved in situ or with only minor displacement. The humerus, radius, ulna and metacarpal IV were broken transversely by a single event and although one fragment of the bone often overlies the other, there has been little actual displacement. It is difficult to explain these fracture patterns as a result of a natural decay process. The sediment indicates that stagnant, and possibly hostile, seafloor conditions persisted in the local environment while disruption by sediment activities or high-energy currents is unlikely based on the lithology. The lack of any trace of bioturbation excludes any benthic or endobenthic scavengers as the cause of the given breakage pattern, thus the carcass of the pterosaur encountered a violent traumatic encounter of an unknown origin. The fact that most of the broken bones are still aligned can only be explained by the presence of soft tissues that held the fractured elements together to a large degree. The breakage of the bones must have occurred when the pterosaur was

either still alive or freshly dead and in a very early stage of decay.

### Systematic palaeontology

The presence of an elongate wing metacarpal identifies *M. altivolans* as a pterodactyloid, but it is more specifically diagnosed as an azhdarchoid by a relatively short wing-finger with a rapid decline of phalanx length distally (Lü et al. 2008), an elongated wing-finger phalanx 1 being >40% of the entire wing finger (Kellner 2003), and a well developed tubercle on the caudoventral margin of the coracoid (Kellner 2004). The pneumatization of the hindlimb and the presence of a well developed greater trochanter further support this conclusion, where the former has been demonstrated to be widespread throughout the Azhdarchoidea by means of a large excavation on the craniodorsal face of the femur (e.g., Claessens et al. 2009; Eck et al. 2011).

The Azhdarchoidea itself is comprised of four families, the Tapejaridae, the Thalassodromidae, the Chaoyangopteridae, and the Azhdarchidae (see Lü et al. 2008), along with the Protoazhdarchidae as a potential fifth (Frey et al. 2011). The assignment of *M. altivolans* to one of these families is complicated as the majority of diagnostic characters are restricted to the cranium and the middle cervicals (e.g., Kellner and Langston 1996; Kellner 2003; Unwin 2003; Suberbiola et al. 2003; Witton 2008); none of which can be observed in the described specimen. Of the few remaining elements of the axial column, only the posterior cervicals 7–9 and the first dorsal vertebrae are identified. The lack of the mid cervical vertebrae and the poor preservation of any diagnostic features on the remaining elements prevent an extensive comparison with other azhdarchoids. The posterior cervicals of the Moroccan azhdarchid *Phosphatodraco mauritanicus* (Suberbiola et al. 2003), which has an unusually elongated seventh vertebrae, are distinct from those of *M. altivolans*, whose own cervicals more closely resemble those of other pterodactyloid pterosaurs. Fortunately additional postcranial characters can be used for a more refined diagnosis. The configuration of the metacarpals for example, whereby the preaxial metacarpals appear to terminate distal to the carpus is used to distinguish the described specimen from the Tapejaridae, where a single preaxial metacarpal is known to contact the wrist. While the hyper-reduction, without loss, of the fourth phalanx to <5% that of the total length of the wing-finger is known only for *Quetzalcoatlus* (Kellner and Langston 1996; Fig. 4), an azhdarchid affinity is rejected by a further comparison of postcranial elements. Here the scapula and coracoid preserve a ratio of 1.30, more comparable to that of non-azhdarchid azhdarchoids, e.g., MN 6588-V (1.27); SMNK PAL 3843 (1.39), and an

unnumbered specimen at the SMNK (1.42, RAE, personal observation), than that of *Quetzalcoatlus* (1.01) or even the chaoyangopterid *Shenzhoupterus chaoyangensis* (1.00, Lü et al. 2008), while *M. altivolans* further lacks the well developed ventral flange to the coracoid (Fig. 5). Unwin and Martill (2007) described a number of postcranial azhdarchid apomorphies that include: a highly elongated wing metacarpal (i.e., mc IV > wph 1); and a wing-finger forming <50% the total forelimb length. Lü et al. (2008) later included a mc IV/humerus ratio of >2.2. In *M. altivolans* the wing metacarpal is slightly less than that of the first wing-finger phalanx (i.e., mc IV/wph 1 = 0.9), the wing-finger forms 51–52% of the total forelimb length and the mc IV/humerus ratio is between 1.7 and 2.0. Under these qualifiers, *M. altivolans* is excluded from the Azhdarchidae.

Despite the lack of a skull and the general state of preservation, postcranial features can be used to exclude *M. altivolans* from a placement within the Tapejaridae and Azhdarchidae, however, its assignment to either the Thalassodromidae or the Chaoyangopteridae is complicated by the fact that both of these families are defined by their cranial characteristics alone (e.g., Kellner 2004; Lü et al. 2008; Witton 2008). While a tentative similarity with *Shenzhoupterus chaoyangensis* (Lü et al. 2008) is noted from ratios of the mc IV/hu and mc IV/wph 1, the majority of body proportions do not differ substantially from those of other derived azhdarchoids (Table 2). Furthermore those elements that do, i.e., phalanx proportion in the wing-finger, differ considerably and isolate *M. altivolans* from other azhdarchoids. The high ratio of the second wing-finger phalanx to that of the first is greater than the range of values observed for other azhdarchoids; *contra* to the synapomorphy stated by Kellner (2003) for the Azhdarchoidea where by the second wing-finger phalanx is always more than 1/3rd smaller than the first wing-finger phalanx (i.e., wph 2/wph 1 < 0.7). While similar ratios are observed in other pterodactyloid pterosaurs, e.g., *Pteranodon*, *Nyctosaurus*, *Germanodactylus* and several selected ornithocheiroids, all of which are readily distinguished from the described specimen.

The phylogenetic placement of *M. altivolans* within the Azhdarchoidea therefore remains uncertain and while postcranial characteristics support the erection of a new genus within either the Thalassodromidae (Witton 2009) or Chaoyangopteridae (Lü et al. 2008), no more specific a diagnosis can, or should, be reliably made at this time.

### General discussion

The placement of *M. altivolans* within the Thalassodromidae/Chaoyangopteridae highlights the degree of to which variations in wing phalanx length can occur, along

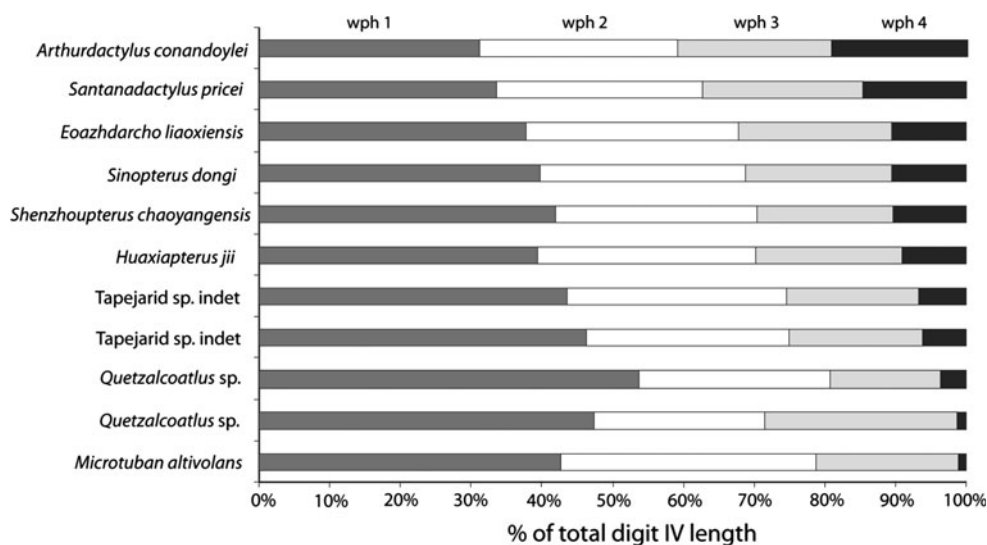


**Fig. 4** Bar chart illustrating the percentage of the total length of the fourth digit formed by each phalanx. Hyper-reduction of the terminal wing-finger phalanx is typically restricted to the Azhdarchidae and distinguishes them from other members of the Azhdarchidae. List of taxa from top to bottom: *Arthurdactylus conandoylei* (SMNK PAL 1132); *Santanadactylus pricei* (AMNH 22552); *Eoazhdarcho*

*liaoxiensis* (GMN-03-11-002); *Sinopterus dongi* (IVPP V 13363); *Shenzhoupterus chaoyangensis* (HGM 41HIII-305A); *Huaxiapterus jii* (GMN-03-11-001); tapejarid indet. (SMNK PAL 6409); tapejarid indet. (SMNK PAL 3900); *Quetzalcoatlus northropi* (TMM 41450); *Quetzalcoatlus* sp. (TMM 41961); *Microtuban altivolans* (SMNK PAL 6595)

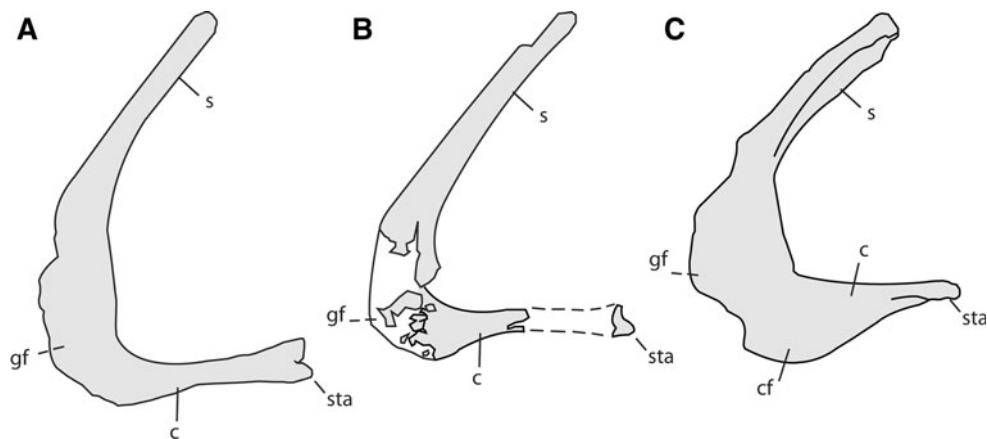


**Fig. 5** Comparison of the scapula and coracoid elements from **a** an un-named tapejarid (SMNK PAL 3843). **b** *Microtuban altivolans* (SMNK PAL 6595). **c** *Quetzalcoatlus* sp. (TMM 42138-1). All line tracings have been scaled to the same size, based on the coracoid length. The coracoid: scapula ratio of 1.30 in *M. altivolans* is similar to that of other azhdarchoid pterosaurs e.g., SMNK PAL 3843, 1:1.39;

unlabelled azhdarchoid indet. (SMNK), 1.27; MN 6588-V, 1:1.27 and is clearly distinct from that of other more derived pterosaurs, e.g., *Shenzhoupterus chaoyangensis* (1:1) and *Quetzalcoatlus* sp. (1:1). *c* coracoid, *cf* coracoid flange, *gf* glenoid fossa, *approximate location*, *s* scapula, *sta* sternal articulation

with the problems involved with identifying taxa from their biometric proportions alone. Although the ratio of the first and second wing-finger phalanges of the described specimen exceeds the range of values regarded as a synapomorphy of the Azhdarchoidea (Kellner 2003), this is not problematic as a suite of additional characters readily support its position within the group. Defining pterosaurs in absolute values is problematic as taxa or individuals (as a result of natural intraspecific variations) will occasionally fall outside the range covered by previously known

specimens. Indeed *Sinopterus dongi* (Wang and Zhou 2003) and a ?tapejarid specimen (SMNK PAL 6900, Unwin and Martill 2007) also exceed the absolute value given by Kellner (2003), although to a much smaller degree, and indicate that such practices can often fail to encompass the full range of values of the desired group.

The second unusual feature of the described specimen also relates to the wing phalanges and the size of the terminal wing-finger phalanx. While a reduction in the length of the fourth wing-finger phalanx is observed in a number

**Table 2** Ratios of selected long bone elements in various pterosaur taxa

| Taxa                                | Specimen number | wph 2/wph 1 | mc IV/hu          | mc IV/wph 1 |
|-------------------------------------|-----------------|-------------|-------------------|-------------|
| Azhdarchidae                        |                 |             |                   |             |
| <i>Zhejiangopterus linhaiensis</i>  | ZHNM M1323      | 0.66        | 2.45              | 1.04        |
| <i>Quetzalcoatlus</i> sp.           | TMM 41961       | 0.51        | ×                 | 0.81        |
| <i>Quetzalcoatlus</i> sp.           | TMM 42422       | 0.51        | 2.48              | 1.03        |
| <i>Q. northropi</i>                 | TMM 41450       | ×           | 1.79 <sup>a</sup> | ×           |
| Chaoyangopteridae                   |                 |             |                   |             |
| <i>Shenzhoupterus chaoyangensis</i> | HGM41HIII-305A  | 0.68        | 2.12              | 0.95        |
| <i>Eoazhdarcho liaoxiensis</i>      | GMN-03-11-002   | 0.78        | 1.50              | 0.76        |
| Thalassodromidae                    |                 |             |                   |             |
| <i>Tupuxuara longicristatus</i>     | IMCF 1052       | 0.60        | 1.53              | 0.71        |
| Tapejaridae                         |                 |             |                   |             |
| <i>Huaxiapterus jii</i>             | GMN-03-11-001   | 0.79        | 1.67              | 0.81        |
| tapejarid sp. indet.                | SMNK PAL 6409   | 0.71        | ×                 | ×           |
| tapejarid sp. indet.                | SMNK PAL 3900   | 0.62        | 1.39              | 0.62        |
| <i>Sinopterus dongi</i>             | IVPP V 13363    | 0.73        | 1.63              | 0.79        |
| <i>Microtuban altivolans</i>        | SMNK PAL 6595   | 0.85        | 1.81 <sup>a</sup> | 0.90        |

<sup>a</sup> Estimated values

of taxa, specifically those within the Azhdarchoidea, the actual loss of the phalanx is rare; having only been documented in specimens of *Anurognathus*, *Beipiaopterus* and *Nyctosaurus* (Bennett 2003b, 2007; Lü 2003). Even within the Azhdarchoidea the reduction of the fourth phalanx to a length <5% that of the total wing finger is known only for *Quetzalcoatlus*. Its presence here is therefore unusual and extends the range of this feature to encompass non-azhdarchid azhdarchoids. The biomechanical reasoning behind the extreme reduction or loss of the fourth phalanx remains uncertain but must have been linked to either the aerodynamic forces acting on the distal section of the wing, and the subsequent deformation of the leading edge spar/membrane, or acted as one possible means of lowering the overall aspect ratio.

The presence of *M. altivolans* within the Cenomanian aged deposits of Lebanon represents one of the few non-azhdarchid azhdarchoids known from the Late Cretaceous. Members of the Chaoyangopteridae such as *Shenzhoupterus chaoyangensis* and *Chaoyangopterus zhangii* from the Jiufotang Formation of Liaoning Province, are dated as Early Aptian, while *Eopteranodon* was uncovered from Barremian–Early Aptian deposits (Swisher et al. 1999). Members of the Thalassodromidae are known chiefly from the NE of Brazil, the two major fossiliferous deposits are both regarded as Early Cretaceous in age (Kellner and Campos 2002; Unwin and Martill 2007; Witton 2009). An isolated rostrum and mandible from the Javelina Formation of North America (Wellnhofer 1991; Kellner 2004) therefore appears to represent the sole member of the Thalassodromidae known from the Late Cretaceous (Martill and Naish 2006). The confirmation of *M. altivolans* as a thalassodromid or chaoyangopterid pterosaur within the

Early Cenomanian Lagerstätten of Lebanon therefore reveals only a minor portion of the ghost lineage available to these taxa, but it is significant as the dating of these deposits appears to be uncontroversial. Azhdarchoid remains are also known from the Cenomanian Kem Kem locality of Morocco, but are regarded as either tapejarid or azhdarchid pterosaurs (Kellner and Mader 1997; Wellnhofer and Buffetaut 1999) and as such are not directly comparable to *M. altivolans*. A similar situation is found in the Cenomanian chalk of England that yields specimens of *Anhanguera* and *Lonchodectes* (Unwin 2000), while substantial material recovered from the Cenomanian aged Cambridge Greensand of England is likewise incomparable and thought to have been reworked from the older Albian deposits (Wellnhofer 1991; Dalla Vecchia et al. 2001). *Microtuban altivolans* therefore represents one of the youngest confirmed thalassodromid/chaoyangopterid pterosaurs, perhaps the only one of a known Cenomanian age, and indicates a greater geographical distribution existed than the immediate localities encompassed by the Lagerstätten deposits of Brazil and China.

Pterosaurs from the eastern edge of the African Plate remain exceedingly rare and those belonging to the portion that now forms the Middle East are restricted to the Early Cenomanian *M. altivolans*, an indeterminate ornithocheiroid (Dalla Vecchia et al. 2001), and a “pterodactylid” hindlimb (Tchernov et al. 1996). As azhdarchid pterosaurs are known from the upper Campanian of Israel and the upper Maastrichtian of Jordan (*Arambourgiania philadelphiae*, Arambourg 1954; Frey and Martill 1996), the region was undoubtedly inhabited by a variety of pterosaurs more or less continuously throughout the Late Cretaceous. If pterosaurs formed a major portion of the local ecosystem

during the Cenomanian then it is surprising that so few of their remains have been uncovered as, unlike many localities, the Lagerstätten of Hâqel and Hjoûla are quarried exclusively for their fossils contents. The palaeogeographical reconstructions of northern Lebanon during the Cenomanian indicate that an open marine setting prevailed in the west of the country and the appearance of pterosaurs here, several hundred km from the nearest inferred palaeo-coastline, inevitably raises questions as to how they came to rest in this setting. The animal perhaps died migrating between landmasses, drifted into the region on the ocean currents, or have inhabited any palaeoislands that existed within the immediate region. Dalla Vecchia et al. (2001) suggested that the pterosaurs of the Cenomanian inhabited small islands composed of carbonate exposures, a hypothesis supported by the presence of sub-aerially exposed carbonate reefs, with palaeochannels, within the Early Cenomanian lithologies (Nader et al. 2006). Terrestrial plant deposits are also known from these localities indicating that material from colonised islands in the local area, or the nearest landmass, were occasionally swept into the region. As this input of material is of a poorer quality than that found at younger localities the source is regarded as being more distant than that of the upper Cenomanian locality of Nammoûra. The presence of these small pterosaurs so far from the nearest major landmass, along with the generally good preservation observed within the specimen, suggests that Early Cenomanian pterosaurs probably did inhabit exposed carbonate islands within the local region. Any such platforms however were located more distant in the Early Cenomanian localities when compared to these of the Late Cenomanian. The relative lack of any teeth or bone fragments attributed to pterosaurs, despite the extensive quarrying of these localities for commercial fossils suggests that pterosaurs either did not reside close by in great numbers, or unknown conditions prevented their preservation in a locality famous for its spectacular preservation of fossil fish.

## Conclusions

*Microtuban altivolans* represents a small, ontogenetically immature azhdarchoid pterosaur tentatively associated with the Thalassodromidae or Choayangopteridae. Differentiating between taxa of either group based on postcranial remains or biometric data and ratios is currently not possible and no more a specific diagnosis can be made. The unusual ratios formed by the second and fourth wing finger phalanges highlight some of the problems with using biometry to identify pterosaur taxa, indicating that the lengths of the individual wing elements are often highly variable. Additionally some ratios that are generally useful,

e.g.,  $wph\ 2/wph\ 1 < 0.7$  (Kellner 2003) or  $mc\ IV > wph\ 1$  (Unwin and Martill 2007), can ultimately fail to encompass the diversity of a desired group. The hyper-reduction without loss of the fourth wing-finger phalanx within *M. altivolans* indicates that this feature was present throughout the Azhdarchoidea and was not solely restricted to the largest azhdarchids.

While African pterosaurs remain exceedingly rare the discovery of *M. altivolans* from the Cenomanian deposits of Lebanon, and the first from Hjoûla, fills in the earliest part of the Thalassodromidae/Choayangopteridae ghost lineage in the Late Cretaceous, indicating that these pterosaurs were more geographically widespread than the immediate localities covered by the Crato/Santana and Jehol Formations of Brazil and China. Although the exact provenance of the described specimen is uncertain, the only alternative site (i.e., Hâqel) is also Cenomanian and would indicate an even younger age than we have suggested here. As such, no conclusions presented in this manuscript will become void if the specimen is later proved to have originated from a neighbouring locality. The presence of this small pterosaur in an open marine setting, many hundreds of kilometres from the nearest palaeoshoreline, supports the idea that pterosaurs of the Cenomanian of Lebanon inhabited exposed carbonate islands (Dalla Vecchia et al. 2001). Given the rarity of these specimens it is unlikely that Hjoûla will ever be as important to pterosaur workers as other European, Asian and South American Lagerstätten localities, however, it does promise the prospect of future finds from a little known Cretaceous age of pterosaur evolution.

**Acknowledgments** The authors extend their thanks to Roy Nohra for several discussions on the possible provenance of the specimen, Volker Griener (SMNK) for assisting with the photography, and Chris Bennett, David Unwin, David Martill, and Alex Kellner for their valuable and helpful comments on an earlier version of the manuscript. Also we thank two anonymous reviewers. This research was supported by the DFG, Deutsche Forschungsgemeinschaft (FR1314/15-1).

## References

- Abdel-Rahman, A.-F. M., & Nader, F. H. (2002). Characterization of the Lebanese Jurassic–Cretaceous carbonate stratigraphic sequence: A geochemical approach. *Geological Journal*, 37, 69–91.
- Arambourg, C. (1954). On the presence of a gigantic pterosaur from the phosphates of Jordan. *Canadian Royal Academy of Science, Paris*, 283, 133–134 (in French).
- Basson, P. W. (1972). *Algites hakelensis* sp. nov. a Cretaceous foliose alga from Lebanon. *American Midland Naturalist*, 88, 506–511.
- Bennett, S. C. (1993). The ontogeny of *Pteranodon* and other pterosaurs. *Paleobiology*, 19, 92–106.
- Bennett, S. C. (2003a). Morphological evolution of the pectoral girdle of pterosaurs: Myology and function. In E. Buffetaut & J.-M. Mazin (Eds.), *Evolution and palaeobiology of pterosaurs* (pp. 191–215). London: Geological Society, Special Publications 17.

- Bennett, S. C. (2003b). New crested specimens of the Late Cretaceous pterosaur *Nyctosaurus*. *Paläontologische Zeitschrift*, 77, 61–75.
- Bennett, S. C. (2007). A second specimen of the pterosaur *Anurognathus ammoni*. *Paläontologische Zeitschrift*, 81, 376–398.
- Bennett, S. C. (2008). Morphological evolution of the wing of pterosaurs: Myology and function. In E. Buffetaut & D. W. E. Hone (Eds.), *Flugsaurier: Pterosaur papers in honour of Peter Wellnhofer*. *Zitteliana B*, 28, 127–141.
- Brew, G., Barazangi, M., Al-Maleh, A. K., & Sawaf, T. (2001). Tectonic and geologic evolution of Syria. *GeoArabia*, 6, 573–615.
- Brochu, C. A. (1995). Heterochrony in the crocodylian scapulocoracoid. *Journal of Herpetology*, 29, 464–468.
- Brochu, C. A. (1996). Closure of neurocentral sutures during crocodylian ontogeny: Implications for maturity assessment in fossil archosaurs. *Journal of Vertebrate Paleontology*, 16, 49–62.
- Butler, R. W. H., & Spencer, S. (1999). Landscape evolution and the preservation of tectonic landforms along the northern Yammouneh Fault, Lebanon. *Geological Society, London, Special Publication*, 162, 1–14.
- Claessens, L. P. A. M., O'Connor, P. M., & Unwin, D. M. (2009). Respiratory evolution facilitated the origin of pterosaur flight and aerial gigantism. *PLoS ONE*, 4, e4497. doi:10.1371/journal.pone.0004497.
- Costa, F. R., & Kellner, A. W. A. (2009). On two pterosaur humeri from the Tendaguru beds (Upper Jurassic, Tanzania). *Anais da Academia Brasileira de Ciências*, 81, 813–818.
- Dal Sasso, C., & Renesto, S. (1999). Aquatic varanoid reptiles from the Cenomanian (Upper Cretaceous) lithographic limestones of Lebanon. III international symposium on lithographic limestones, extended abstracts. *Rivista del Museo Civico di Scienze Naturali di Bergamo "E. Caffi"*, 20, 63–69.
- Dalla Vecchia, F. M., Arduini, P., & Kellner, A. W. A. (2001). The first pterosaur from the Cenomanian (Late Cretaceous) Lagerstätten of Lebanon. *Cretaceous Research*, 22, 219–225.
- Dalla Vecchia, F. M., & Chiappe, L. M. (2002). First avian skeleton from the Mesozoic of northern Gondwana. *Journal of Vertebrate Paleontology*, 22, 856–860.
- Dalla Vecchia, F. M., & Venturini, S. (1999). The Middle Cenomanian Lagerstätte of Al Nammoura (Kesrouâne Caza, N. Lebanon). III international symposium on lithographic limestones, extended abstracts. *Rivista del Museo Civico di Scienze Naturali di Bergamo "E. Caffi"*, 20, 75–78.
- Eck, K., Elgin, R. A., & Frey, E. (2011). On the osteology of *Tapejara wellnhoferi* KELLNER 1989 and the first occurrence of a multiple specimen assemblage from the Santana Formation, Araripe Basin, NE-Brazil. *Swiss Journal of Palaeontology*. doi:10.1007/s13358-011-0024-5.
- Forey, P. L., Yi, L., Patterson, C., & Davies, C. E. (2003). Fossil fishes from the Cenomanian (Upper Cretaceous) of Namoura, Lebanon. *Journal of Systematic Palaeontology*, 1, 227–330.
- Frey, E., & Martill, D. M. (1996). A reappraisal of Arambourgiania (Pterosauria, Pterodactyloidea): One of the world's largest flying animals. *Neues Jahrbuch für Geologie und Paläontologie, Abh*, 199, 221–247.
- Frey, E., Meyer, C. A., & Tischlinger, H. (2011). The oldest azhdarchoid pterosaur from the Late Jurassic Solnhofen Limestone (Early Tithonian) of Southern Germany. *Swiss Journal of Geosciences*. doi:10.1007/s00015-011-0073-1.
- Garassino, A. (1994). The macruran decapod crustaceans of the Upper Cretaceous of Lebanon. *Paleontologia Lombarda*, 3, 1–40.
- Hay, O. P. (1903). On a collection of Upper Cretaceous fishes from Mount Lebanon, Syria, with descriptions of four new Genera and nineteen new species. *Bulletin of the American Museum of Natural History, New York*, 138, 395–452.
- Hückel, U. (1970). The fish beds of Haqel and Hjoula from the Upper Cretaceous of Lebanon. *Neues Jahrbuch für Geologie und Paläontologie, Abhandlungen*, 135, 113–149 (in German).
- Irmis, R. B. (2007). Axial skeleton ontogeny in the Parasuchia (Archosauria: Pseudosuchia) and its implications for ontogenetic determination in archosaurs. *Journal of Vertebrate Paleontology*, 27, 350–361.
- Kellner, A. W. A. (2003). Pterosaur phylogeny and comments on the evolutionary history of the group. In E. Buffetaut & J.-M. Mazin (Eds.), *Evolution and palaeobiology of pterosaurs* (pp. 105–137). London: Geological Society, Special Publications 17.
- Kellner, A. W. A. (2004). New information on the Tapejaridae (Pterosauria, Pterodactyloidea) and discussion of the relationships of this clade. *Ameghiniana*, 41, 521–534.
- Kellner, A. W. A., & Campos, D. A. (2002). The function of the cranial crest and jaws of a unique pterosaur from the early Cretaceous of Brazil. *Science*, 297, 389–392.
- Kellner, A. W. A., & Langston, W. (1996). Cranial remains of *Quetzalcoatlus* (Pterosauria, Azhdarchidae) from Late Cretaceous Sediments of Big Bend National Park, Texas. *Journal of Vertebrate Paleontology*, 16, 222–231.
- Kellner, A. W. A., & Mader, B. J. (1997). Archosaur teeth from the Cretaceous of Morocco. *Journal of Paleontology*, 17, 525–527.
- Kellner, A. W. A., & Tomida, R. (2000). Description of a new species of Anhangueridae (Pterodactyloidea) with comments on the pterosaur fauna from the Santana Formation (Aptian–Albian), northeastern Brazil. *National Science Museum Tokyo, Monographs*, 17, 1–135.
- Krassilov, V., & Bacchia, F. (2000). Cenomanian florule of Nammoura, Lebanon. *Cretaceous Research*, 21, 785–799.
- Lü, J.-C. (2003). A new pterosaur: *Beipiaopterus chenianus*, gen. et sp. nov. (Reptilia: Pterosauria) from western Liaoning province of China. *Memoir of the Fukui Prefectural Dinosaur Museum*, 2, 153–160.
- Lü, J., Unwin, D. M., Xu, L., & Zhang, X. (2008). A new azhdarchoid pterosaur from the Lower Cretaceous of China and its implications for pterosaur phylogeny and evolution. *Naturwissenschaften*, 95, 891–897.
- Mader, B. J., & Kellner, A. W. A. (1999). A new Anhanguerid pterosaur from the Cretaceous of Morocco. *Geologia*, 45, 1–11.
- Martill, D. M., & Naish, D. (2006). Cranial crest development in the azhdarchoid pterosaur *Tupuxuara*, with a review of the genus and tapejarid monophyly. *Palaeontology*, 49, 925–941.
- Nader, F. H., Abdel-Rahman, A.-F. M., & Haidar, A. T. (2006). Petrographic and chemical traits of Cenomanian platform carbonates (central Lebanon): Implications for depositional environments. *Cretaceous Research*, 27, 689–706.
- Saint-Marc, P. (1974). Study of the stratigraphy and micropalaeontology of the Albian, Cenomanian and Turonian of Lebanon. *Notes et Mémoires du Moyen-Orient*, 13, 8–342 (in French).
- Suberbiola, X. P., Bardet, N., Jouve, S., Iarochène, M., Bouya, B., & Amaghazaz, M. (2003). A new azhdarchoid pterosaur from the Cretaceous phosphates of Morocco. In E. Buffetaut & J.-M. Mazin (Eds.), *Evolution and palaeobiology of pterosaurs* (pp. 79–90). London: Geological Society, Special Publications 17.
- Swinton, W. E. (1948). A Cretaceous pterosaur from the Belgian Congo. *Bulletin Société Belge de Géologie, de Paléontologie et d'Hydrologie, Liège*, 77, 234–238.
- Swisher, C. C., Wang, Y., Wang, X., Xu, X., & Wang, Y. (1999). Cretaceous age for feathered dinosaurs of Liaoning, China. *Nature*, 400, 58–61.
- Tchernov, E., Polcyn, M. J., & Jacobs, L. L. (1996). Snakes with legs: The Cenomanian fauna of 'Ein Yabrud, Israel. *Journal of Vertebrate Paleontology* 16 (Suppl. to no. 3), Abstracts, 68A.
- Unwin, D. M. (2000). An overview of the pterosaur assemblage from the Cambridge Greensand (Cretaceous) of Eastern England.



- Mitteilungen aus dem Museum für Naturkunde Berlin, Geowissenschaftliche Reihe, 4*, 189–221.
- Unwin, D. M. (2003). On the phylogeny and evolutionary history of pterosaurs. In E. Buffetaut & J.-M. Mazin (Eds.), *Evolution and palaeobiology of pterosaurs* (pp. 139–190). London: Geological Society, Special Publications 17.
- Unwin, D. M., & Heinrich, W.-D. (1999). On a pterosaur jaw from the Upper Jurassic of Tendaguru (Tanzania). *Mitteilungen aus dem Museum für Naturkunde Berlin, Geowissenschaftliche Reihe, 2*, 121–134.
- Unwin, D. M., & Martill, D. M. (2007). Pterosaurs of the Crato Formation. In D. M. Martill, D. M. Bechly, & R. F. Loveridge (Eds.), *The Crato Fossil Beds of Brazil* (pp. 475–524). Cambridge: Cambridge University Press.
- Wang, X., & Zhou, Z. (2003). A new pterosaur (Pterodactyloidea, Tapejaridae) from the Early Cretaceous of western Liaoning, China and its implications for biostratigraphy. *Chinese Science Bulletin, 48*, 16–23.
- Wellnhofer, P. (1991). *The illustrated encyclopedia of pterosaurs*. London: Salamander Books.
- Wellnhofer, P., & Buffetaut, E. (1999). Pterosaur remains from the Cretaceous of Morocco. *Paläontologische Zeitschrift, 73*, 133–142.
- Witton, M. (2008). A new azhdarchoid pterosaur from the Crato Formation (Lower Cretaceous, Aptian?) of Brazil. *Palaeontology, 51*, 1289–1300.
- Witton, M. (2009). A new species of *Tupuxuara* (Thalassodromidae, Azhdarchoidea) from the Lower Cretaceous Santana Formation of Brazil, with a note on the nomenclature of Thalassodromidae. *Cretaceous Research, 30*, 1293–1300.
- Woodward, A. S. (1942). Some new and little-known Upper Cretaceous Fishes from Mount Lebanon. *The Annals and Magazine of Natural History, Series, 11*(38), 537–568.

# The extent of the pterosaur flight membrane

ROSS A. ELGIN, DAVID W.E. HONE, and EBERHARD FREY



Elgin, R.A., Hone, D.W.E., and Frey, E. 2011. The extent of the pterosaur flight membrane. *Acta Palaeontologica Polonica* 56 (1): 99–111.

The shape and extent of the membranous brachioptagium in pterosaurs remains a controversial topic for those attempting to determine the aerodynamic performance of the first vertebrate fliers. Various arguments in favour of the trailing edge terminating against either the torso or hip, the femur, the ankle, or different locations for various taxa, has resulted in several published reconstructions. Uncertainty over the correct model is detrimental to both aerodynamic and palaeoecological studies that are forced to simultaneously consider multiple and highly variable configurations for individual taxa. A review of relevant pterosaur specimens with preserved soft tissues or impressions of the wing membrane, however, strongly suggests that the trailing edge of the wing extended down to the lower leg or ankle in all specimens where the brachioptagium is completely preserved. This configuration is seen across a phylogenetically broad range of pterosaurs and is thus likely to have been universally present throughout the Pterosauria. Support for opposing hypotheses where the trailing edge terminates against the body, hip, or knee are based on several specimens where the wing membrane is either incomplete or has undergone post-mortem contraction. An ankle attachment does not rule out a high aspect ratio wing as the curvature of the trailing edge and the ratio of the fore to hind limbs also play a major role in determining the final shape of the membrane.

Key words: Reptilia, Pterosauria, flight, wings, patagium, Mesozoic.

Ross A. Elgin [rosselgin@hotmail.com] and Eberhard Frey [dinofrey@aol.com], Staatliches Museum für Naturkunde Karlsruhe (SMNK), Erbprinzenstraße 13, 76133 Karlsruhe, Germany;

David W.E. Hone [dhone@ivpp.ac.cn], Institute of Vertebrate Palaeontology and Palaeoanthropology (IVPP), Xizhimenwai Dajie 142, Beijing 100044, P.R. China.

Received 8 December 2009, accepted 2 August 2010, available online 14 September 2010.

## Introduction

The pterosaurs were prehistoric flying reptiles that dominated the skies for much of the Mesozoic Era (Late Triassic to the end Cretaceous). They were the first vertebrates to develop true powered flight and included the largest flying animals of all time, with wing spans in excess of 10 metres (Witton 2008). While several studies have considered the aerodynamic characteristics of the group (e.g., Bramwell and Whitfield 1974; Stein 1975; Brower 1980, 1982, 1983; Chatterjee and Templin 2004) further work is required to better understand the aerodynamics of the pterosaurian wing and the consequences of altering its material and structural compositions. Such studies, however, cannot proceed in the absence of a consensus on the shape and extent of the wings.

Previous aerodynamic and palaeoecological based studies have been divided over the shape and surface area of the main wing membrane by the use of either a “bird-like” model, where the proximal portion of the trailing edge attaches to the body, or a “bat-like” model where it is integrated with the hind limbs. The result of this divergence is that the conclusions of aerodynamic studies utilising a narrow chord (Brower 1980, 1982, 1983; Chatterjee and Templin 2004) will differ from those with a broader chord (Hankin and Watson 1914; Kripp 1941; Heptonstall 1971; Bramwell and Whitfield 1974; Stein

1975; Wilkinson et al. 2005) regardless of any other similarities between the methods or taxa under investigation. As both aspect ratio and wing load have important implications for ecology in bats and birds (Hazelhurst and Rayner 1992), which can be equally applied to pterosaurs (McGowan and Dyke 2009; Witton 2008), the resolution of the wing shape in pterosaurs benefits not only those seeking to investigate their aerodynamic characteristic but also those with an interest in determining pterosaur life habits.

Powered flight appears to have been the primary method of locomotion in all pterosaurs where the flight surface is primarily comprised of a single uninterrupted membrane, the “brachioptagium,” with the leading edge being formed by the bones of the forelimb (Fig. 1). Within the context of this manuscript we use the term wings inclusively to refer to all the bones of the forearm and the primary flight membrane that spans between the most distal point of the forearm to where it is associated with the lateral margin of the body or hind limb. The distal portion of the brachioptagium was controlled by the elongated fourth digit (wing-finger) that was able to flex anterioposteriorly about the wing metacarpal, folding the wing during terrestrial locomotion, diving, or fast gliding flight. For the purpose of this study all orientations are given for an animal in its estimated gliding position, with the wing fully extended as illustrated in Fig. 1. Within the patagia itself a radiat-

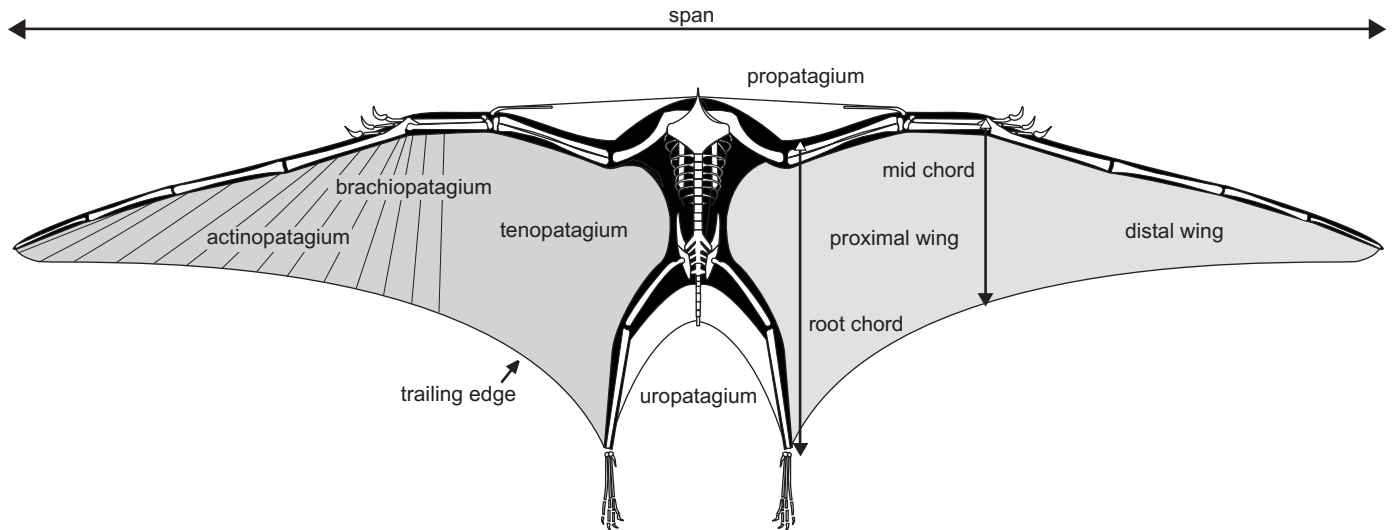


Fig. 1. Schematic sketch of *Pterodactylus* as viewed in its inferred flight position from ventral view (adapted from Wellnhofer 1970). The three flight membranes are illustrated with the brachiopatagium, the focus of this work, being shaded in grey. All terminology is applied to the animal in this position and the size of any specific chord is here generally defined as being narrow or broad, large or small. While the root chord should generally also include the chord of the propatagium for the purpose of this paper it is restricted to the brachiopatagium.

ing pattern of structural actinofibrils developed for both controlling the local camber and spreading the wing distally (Bennett 2000). The distribution of these elements gives rise to the major divisions of the brachiopatagium, the distal, fibril dense actinopatagium, and the proximal tenopatagium, containing fewer fibrils (Schaller 1985).

In addition to the brachiopatagium two separate, and much smaller, membranes are also proposed to take an active role in flight, these being the fore-wing or “propatagium” and the tail wing or “uropatagium” (also sometimes referred to as the “cruorpatagium”). While the shape of the pro- and uropatagia may also be considered controversial, the former is reliant on the orientation and mobility of the pteroid bone (see Bennett 2007a; Palmer and Dyke 2009; and Wilkinson 2008 for contrasting interpretations), while the latter also hinges on the use of an important skeletal element, the fifth pedal digit. While the authors acknowledge that both the propatagia and uropatagia are important for the construction of an accurate flying model of a pterosaur, they are not considered further here.

The primary focus of this paper is thus to evaluate the fossil evidence and identify the proximal attachment of the brachiopatagium so that future aerodynamic studies do not have to simultaneously consider radically different wing configurations. It also aims to ensure that unsupported wing reconstructions, common throughout the current literature, are not repeated in future works.

*Institutional abbreviations.*—BPM, Beipao Paleontological Museum, Beipao, China; BSPG, Bayerische Staatssammlung für Paläontologie und Geologie, Munich, Germany; GMV, Geological Museum of Nanjing, Nanjing, China; IGM, Universidad Nacional Autónoma de México Instituto Geología de Mexico, Mexico City, Mexico; IVPP Institute of Vertebrate Palaeontology and Palaeoanthropology, Beijing, China; JME,

Jura-Museum, Eichstätt, Germany; MCSNB, Museo Civico di Scienze Naturali Bergamo, Bergamo, Italy; NHMW, Naturhistorisches Museum Wien, Vienna, Austria; SMNK, Staatliches Museum für Naturkunde Karlsruhe, Karlsruhe, Germany; YPM, Yale Peabody Museum, New Haven, USA.

## Current problems: “bird” versus “bat”-like wings

Reconstructions of the wing membrane are divided between the so called “bird” (narrow chord) and “bat-like,” (broad/ankle chord) configurations (Fig. 2). In the former the membrane extends to the torso or hip (Brower 1980, 1982, 1983; Padian and Rayner 1993; Peters 2001), while in the latter it is associated with the hind limb at about the knee (Martill and Unwin 1989) or ankle (e.g., Unwin and Bakhurina 1994; Frey and Martill 1998; Frey and Tischlinger 2000; Tischlinger and Frey 2002; Frey et al. 2003; Witton 2008). Variable configurations for individual species must also remain a possibility (Wellnhofer 1991; Dyke et al. 2006). The inferred extent of the wing has been influenced by a number of factors including historical interpretations, the mode of terrestrial locomotion, and the degree of soft tissue preservation in specimens; each of which will be considered separately.

## Historical considerations

Although life restorations of pterosaurs are known as early as 1800 (Taquet and Padian 2004) it was the reconstruction of Sömmerring (1812) that was to become the best known and most widely circulated in the early years of pterosaur re-

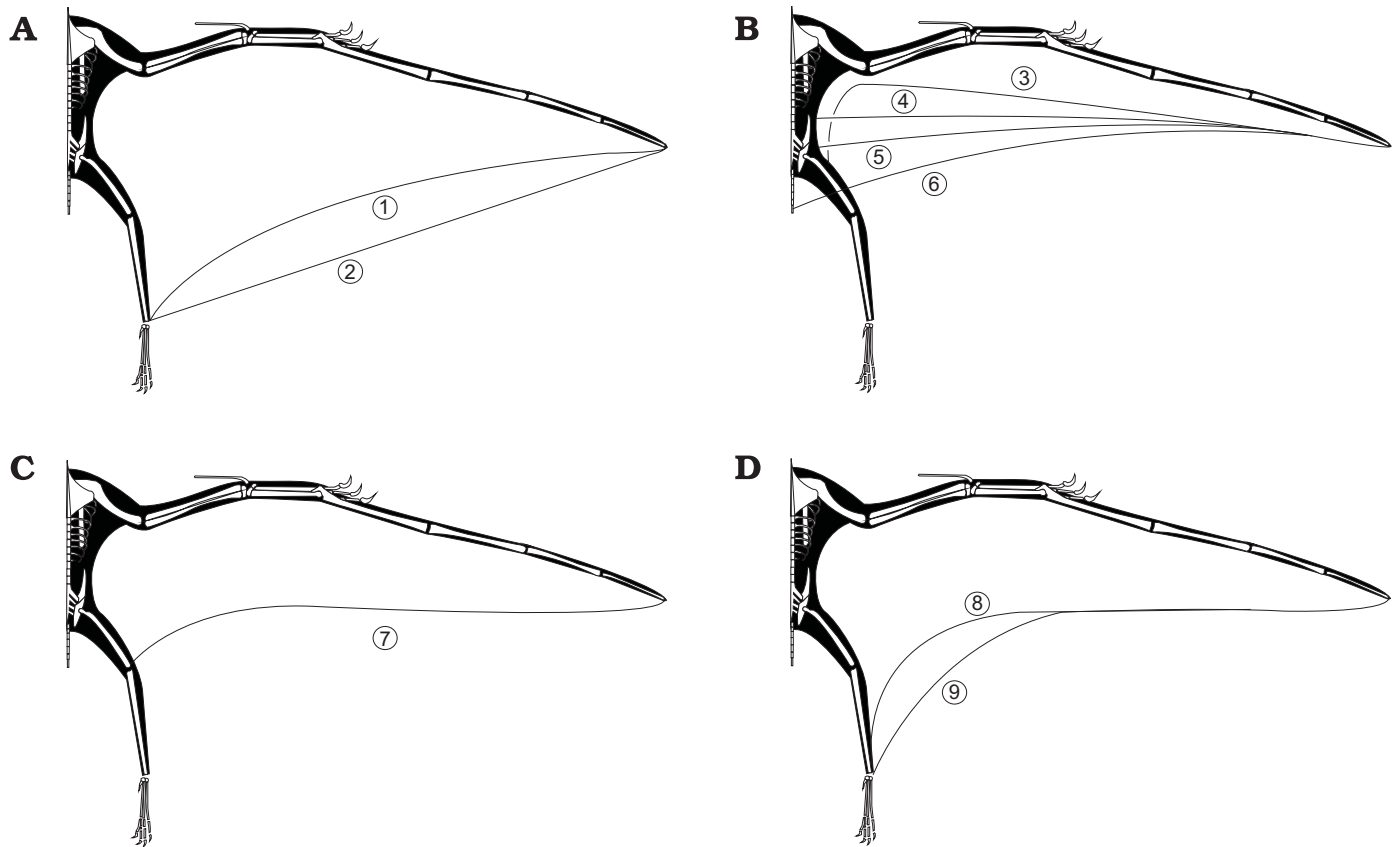


Fig. 2. Various configurations of the pterosaur main wing. **A.** The traditional “bat-like” interpretation adopted by Sömmerring 1812 (1) and Marsh 1888 (2). **B.** The “bird-like” model where the membrane was free of the legs and attached to the body after Peters 2001(3), Padian and Rayner 1993 (4, 5), or tail Bennett 1987(6). **C.** The “*Pterodactylus* model” where the membrane, based on specimen NHMW 1975/1756, attached around the knee (7). **D.** A more recent “bat-like” wing model (8, 9) where the membrane attaches to the ankle (Unwin and Bakhurina 1994; Frey and Martill 1998; Frey and Tischlinger 2000; Tischlinger and Frey 2002; Frey et al. 2003).

search. His belief that pterosaurs were a form of extinct bat, ignoring the fossil evidence laid down by Collini (1784) and Cuvier (1801)—dismissing the reptilian quadrate, the elongated fourth metacarpal and reconstructing the thorax and pelvis based on the skeleton of a bat—must have been the dominant reason why the wing membrane extended to the hind limbs in his restoration. While later authors would accept the reptilian nature of pterosaurs contra to that of Sömmerring (1812), his illustration of a “bat-like” membrane remained the accepted configuration for much of the 19<sup>th</sup> and 20<sup>th</sup> centuries.

The appearance of the first fossils preserving part of the membranous wing seventy years later did little to alter this view when in 1882 Zittel and Marsh each independently published on different exceptionally preserved fossils of *Rhamphorhynchus*. Despite the absence of the body, Zittel (1882) interpreted the membrane in his specimen as being associated with the hind limbs during life. Restorations from the 19<sup>th</sup> century illustrate that the flight apparatus in pterosaurs was more or less universally accepted to have been “bat-like” (e.g., Marsh 1882; Zittel 1882; Williston 1897; also see Seeley 1901: fig. 58). However, in his classic book “Dragons of the Air,” Seeley (1901) criticised his colleagues for restor-

ing more of the wing membrane than the fossil specimens preserved, stating that “I should have preferred to carry it [brachiopatagium] no further down the body than the lower part of the back there being no fossil evidence in favour of this extension so far as specimens have been described” (Seeley 1901: 165). Although later works such as Jaekel (1910) and Strömer (1913) also kept the hind limbs of *Rhamphorhynchus* free from the brachiopatagium, a majority of restorations produced during the first quarter of the 20<sup>th</sup> century continued to carry the membrane down to the lower hind limb or ankle (e.g., Abel 1919, 1925; Hankin and Watson 1914—*Pteranodon*; Stieler 1922—*Dorygnathus*; Wiman 1923—*Dorygnathus*; Wiman 1925—*Pterodactylus*). Williston, in his 1911 paper, included an extensive wing surface for *Nyctosaurus*, which stretched from the ankle as far forwards as the head, and stated “that the membrane extended to the tarsus on the peroneal side of the legs I think now hardly admits of doubt; the animals would hardly have been “flugfähig [volant]” were the legs wholly free, since the membrane would have been too narrow to serve as a parachute....” (Williston 1911: 704).

Although this ankle chord configuration was widely accepted and would later be adopted by several studies into

pterosaur flight dynamics (e.g., Bramwell and Whitfield 1974; Stein 1975) there was little fossil evidence during this period to suggest that this, or indeed any other model, was correct. The holotype of *Pterodactylus antiquus* preserves no trace of a membrane and therefore the restorations of Hermann (Taquet and Padian 2004) and Sömmerring (1812), amongst others, are fictional. Neither were the first specimens preserving a membrane of much assistance, as the “Zittel Wing” (BSPG 1880 II 8) is an isolated wing with no trace of the body, though Padian and Rayner (1993) argued that it would have extended no further caudally than the hip. The *Rhamphorhynchus* specimen (YPM 1778) of Marsh (1882) is also of little use as the proximal portion of the membrane is not preserved. No traces of a membrane have ever been found in any specimen of *Dorygnathus*, *Pteranodon* or *Nyctosaurus* and therefore the early reconstructions of Marsh (1882) and Williston (1897) cannot be tied to any fossil evidence. Lastly Williston’s (1911) assumptions that pterosaurs would not have been flight worthy were the legs free of the flight membrane is also untrue, as has been demonstrated by a significant increase in our understanding of aerodynamics and several recent studies on the subject (e.g., Brower 1980, 1982, 1983; MacCready 1985; Chatterjee and Templin 2004). Therefore while a “bat-like” configuration has historically been the accepted model it was not explicitly tied to any fossil evidence and appears to have been sustained primarily through a historical bias and a lack of any evidence to the contrary.

## “Bird-like” configuration

Many of these points were raised by Padian (1983, 1985, 1987) who challenged the traditional “bat-like” model and argued that the wing was far less extensive and more “bird-like” in profile. Padian (1983) supported this by observing that several fossils of *Rhamphorhynchus* “clearly show that the hind limb was free of the wing and that the wing extended no further back along the body wall than the pelvis” (Padian 1983: 219); reiterating the concerns of Seeley (1901). It was subsequently argued that previous workers were misled into reconstructing an ankle chord as post-mortem contractions had caused the trailing edge of the membrane to coincidentally lie in the same plane as the wing (Padian and Rayner 1993). Padian and Rayner (1993) also noted that an ankle membrane would have required a trailing edge structure, a feature which has never been identified, and that with an appropriate form and the actinofibrils providing a sufficient camber there was no need for the brachiopatagium to attach to the hind limbs. The hind limbs would have been of limited use in cambering a high aspect ratio wing as their influence would have been restricted to only the most proximal region of the membrane.

The narrow chorded configuration was adopted by Rayner (1990) and was also incorporated into several aerodynamic experiments (Brower 1980, 1982, 1983; MacCready 1985;

Chatterjee and Templin 2004). It was also used, along with other configurations, by Hazlehurst and Rayner (1992) in their study of pterosaur ecology. Other studies followed in a similar style by presenting a model where the hind limbs were also free from any role in flight. Bennett (1987) argued that the brachiopatagium might have attached to the lateral face of the tail, having found a pair of elongate caudal rods in *Pteranodon* and possibly *Nyctosaurus* too, although he subsequently rejected this idea (Bennett 2001). Peters (2001), based on his own photographic observations, reconstructed the trailing edge of the brachiopatagium as extending only slightly caudal to the elbow before turning sharply and attaching to the femur (Fig. 2B, configuration 3).

Due to their common association, a narrow chorded model may perhaps be viewed as being inseparable from bipedal locomotion in pterosaurs although this is not suggested to be the case. Bipedal locomotion in pterosaurs was argued for by Padian (1983) but this has been challenged and rejected by several workers (e.g., Unwin 1987, 1988; Wellnhofer 1988); although a parasagittal orientation of the hind limbs was later demonstrated to be possible (Bennett 1990, contra Wellnhofer 1988). Bennett (1997) more recently rejected bipedal locomotion in pterosaurs by noting that: the metatarsals were spreading and unfused; the foot was not symmetrical with a reduction of the medial and lateral digits, unlike other cursorial digitigrade animals; and the metatarsophalangeal joints did not permit sufficient extension. The assumption that these observations, having been made on large pterodactyls, were equally applicable to more basal pterosaurs was later confirmed by Clark et al. (1998) in a specimen of *Dimorphodon weintraubi* (IGM 3494). Although Padian (2003, 2008) subsequently acknowledged that pterodactyl pterosaurs must have adopted a quadrupedal stance as a result of ichnological evidence and the increasing length of the fourth metacarpal he argued that this evolved secondarily from a bipedal ancestry and non-pterodactyl pterosaurs may themselves have been bipedal.

The arguments for and against a bipedal mode of locomotion are not considered further here as we do not regard them as being of direct relevance in determining the extent of the main wing (for a full discussion see Padian 2008). It is sufficient to state that it is now universally accepted that pterodactyls were quadrupedal and thus would have been free to have extended a membrane to the ankle. Even if non-pterodactyl pterosaurs (or pterosaur ancestors) were bipedal it is widely accepted that the brachiopatagium was flexible, elastic and could have been folded to a large degree so there is no clear reason to expect it to hinder terrestrial locomotion to any great degree.

## Membrane-preserving fossils

The shape and extent of the brachiopatagium can only be resolved by a comprehensive review of the fossil evidence that, despite their relative rarity, contains a significant number of

specimens in which the wing membrane can be observed. Although many of these have been described individually by separate authors and used in isolation to infer details of the brachiopatagium, when considered together they present a clearer picture of the wing configuration. The most useful of these include: *Anurognathus* (private collection, see Bennett 2007b) and *Jeholopterus* (IVPP V 12705), representing the Anurognathidae; *Eudimorphodon* (MCSNB 8950a), *Rhamphorhynchus* (e.g., JME SOS 4784) and *Sordes* (PIN 2585/3) for other non-pterodactyloid pterosaurs; *Beipiaopterus* (BPM 0002), *Pterodactylus* (NHMW 1975/1756), *Eosipterus* (GMV 2117), and to a lesser degree a number of indeterminate azhdarchoids (e.g., SMNK PAL 3830, 3900, 6404) for the pterodactyloids.

The extensive preservation of soft tissue belonging to the wing appears to be relatively more common for *Rhamphorhynchus* than for any other pterosaur taxon. However, despite the relatively large number of individuals having been documented with membrane preservation, only a minority of these are of much use for the purpose of this study. These include the specimens figured by Padian and Rayner (1993: fig. 3) as contra to their claims that these clearly show the hind limb to be free of a membrane, the proximal portion of the trailing edge in each specimen is either obscured or detached. While we rightly acknowledge that these were some of the best specimens available at that time, they cannot be used to infer details of the wing other than that the distal portion of the wing was narrow, as in no specimen does the trailing edge of the membrane contact the body wall in a natural state. This is also the situation observed in the “Zittel Wing” (BSPG 1880 II 8) as despite its exceptional preservation, the absence of the body means that it is of little value for determining the extent of the wing membrane, having been interpreted as supporting a trailing edge attachment to both the ankle (Zittel 1882) and the torso (Padian and Rayner 1993). Arguably the only specimen of *Rhamphorhynchus* that preserves the proximal portion of the wing in association with the hind limb is that of *R. muensteri* (JME SOS 4784), commonly referred to as the “Dark Wing”. The detail of preservation here is superior to these other specimens and allows for ultra-violet light to pick out muscle fascia and a vascular system within the wing itself (see Frey et al. 2003). Importantly the proximal portion of the left wing is complete and demonstrates that the membrane curved sharply caudally on approaching the body to attach by the ankle (Figs. 3A, 4A).

The holotype of *Sordes pilosus* (PIN 2585/3) preserves several extensive membranous surfaces and has been the focus of a number of publications since its original description by Sharov (1971) (e.g., Unwin and Bakhurina 1994; Unwin 1999). While identifying the full length of the trailing edge of the wing in photographs is often difficult, the brachiopatagium was described as being narrow distally and becoming broader towards the proximal portion with a trailing edge that terminates about the ankles (Unwin and Bakhurina 1994: figs. 3E, 4E). Bakhurina and Unwin (2003) later reconstructed the wing membrane of *Eudimorphodon ranzii*

(MCSNB 8950a) noting that the hind limbs, foot and 5<sup>th</sup> toe, together with preserved patches of membrane, showed an almost identical disposition to that seen in the holotype of *Sordes* (Figs. 3F, 4F). The patterns of fibres observed between the hind limbs were interpreted as patagial fibres with the same orientation and spacing viewed in the uropatagium of *Sordes* and therefore the reconstruction of the wings of *E. ranzii*, and very likely all basal pterosaurs, are directly comparable to that of *S. pilosus*. The wing shape of *Sordes* was disputed by Peters (1995, 2001) who questioned the trailing edge identified by Sharov (1971), suggesting that it may have been an organic smear bounded by breaks in the bedding plane, and having identified a “possible alternate trailing edge.....just posterior to the elbows” (Peters 2001: 285). He also argued that post-mortem disturbance was evident in this specimen and that the movement of the fore and hind limbs had created the illusion of an ankle wing. Dyke et al. (2006) later cautioned against applying a *Sordes*-like configuration universally because the hind limb proportions were suggested to be atypical for even its closest relatives. The completion of more extensive databases, however, indicates that this concern is incorrect and nothing unusual is noted in its limb proportions (RAE personal observation 06/2010).

Within the Anurognathidae the exceptional preservation of the specimens of *Jeholopterus ningchengensis* (Figs. 3B, 4B) and *Anurognathus ammoni* (Figs. 3D, 4D) indicate that the membrane, or the impression of the wing and its associated fibres, were also associated with the hind limb down to the ankle (Wang et al. 2002; Bennett 2007b; Kellner et al. 2009). While a second specimen of *Jeholopterus* (Ji and Yuan 2002) is also known it does not show an ankle attachment but rather the trailing edge is clearly seen to extend from the first wing-finger phalanx to the proximal margin of the humerus (Fig. 5B). This forms a wing of an impossibly narrow chord that does not even contact much with the wing finger and is a clear example of the extent to which a flexible membrane can contract post-mortem.

The preservation of extensive wing membranes in pterodactyloid pterosaurs appears to be less common than for non-pterodactyloids taxa. In one exceptional *Pterodactylus* specimen (the “Vienna specimen”, NHMW 1975/1756) a very narrow wing membrane is preserved and implies a femoral attachment of the brachiopatagium (Figs. 3C, 4C). However, the original extent of the membrane is unclear as its narrow chord suggests a large degree of post-mortem contraction while soft tissue structures preserved adjacent to the tibia, observed under UV light (Tischlinger and Frey 2002), suggest that the trailing edge did not truly terminate about the knee. Rather it is likely that the membrane extended further distally along the limb towards, or even as far as the ankle (Helmut Tischlinger personal communication 6/2008).

The pterodactyloid *Beipiaopterus chenianus* (Lü 2002, 2003) preserves a long patch of membrane adjacent to its femur and a configuration similar to that found in non-pterodactyloid pterosaurs can be observed in the holotype specimen of *Eosipterus* (Figs. 3E, 4E; Ji and Ji 1997). Although

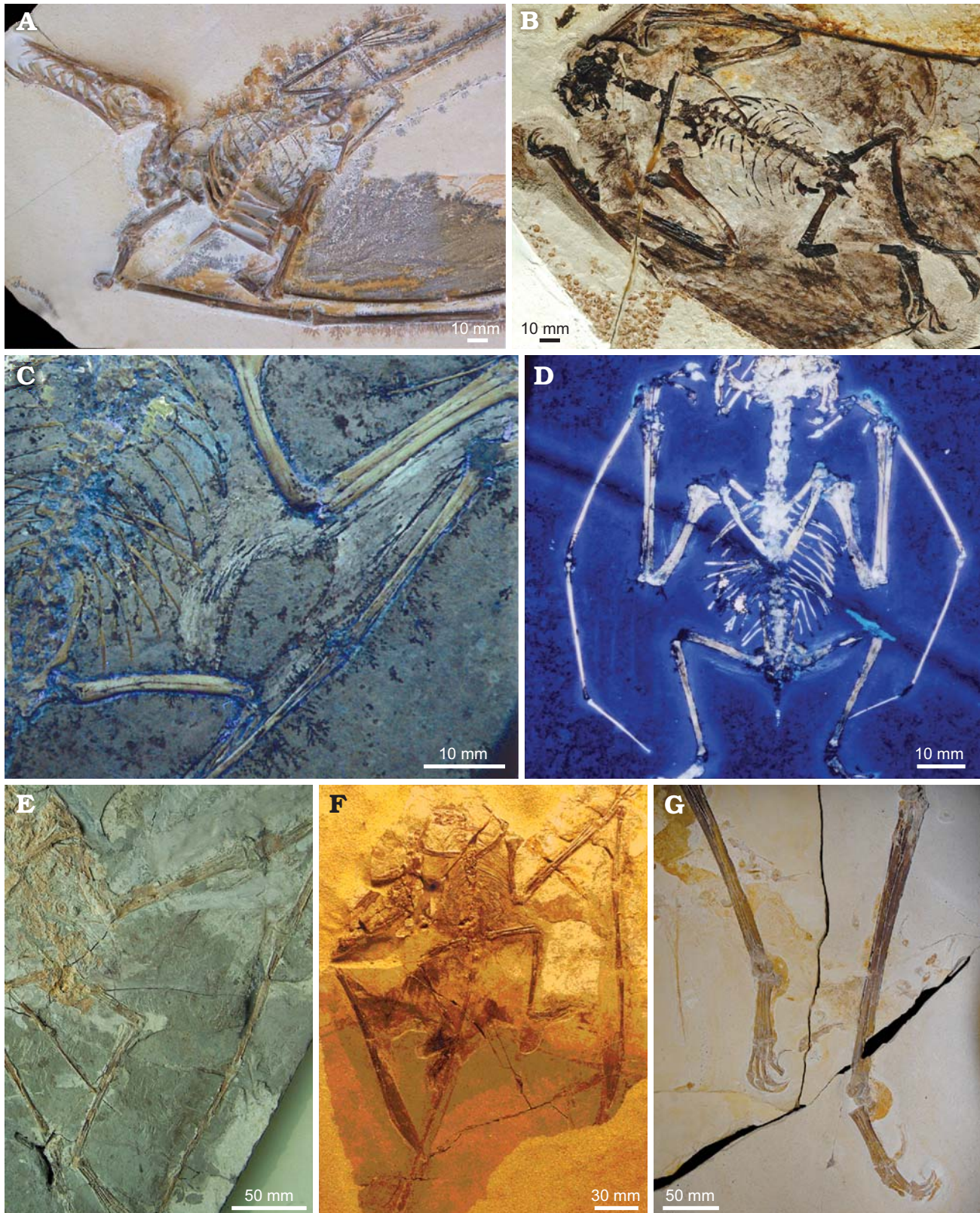


Fig. 3. Selected photographs of pterosaur specimens displaying soft tissue preservation around the hind limbs and/or ankles. **A.** *Rhamphorhynchus muensteri* (Goldfuss, 1831), the “Dark Wing”, JME SOS 4784, Eichstätt region (Upper Jurassic), Germany. **B.** *Jeholopterus ningchengensis* Wang, Zhou, Zhang, and Xu, 2002, IVPP V 12705, Lower Yixian Formation (Early Cretaceous), China. **C.** *Pterodactylus kochi* (Wagner, 1837), “Vienna specimen”, NHMW 1975/1756, Solnhofen Limestone (Upper Jurassic), Germany. **D.** *Anurognathus ammoni* Döderlein, 1923, private specimen (Bennett 2007b), Solnhofen Limestone (Upper Jurassic), Germany. **E.** *Eosipterus yangi* Ji and Ji, 1997, GMV 2117, Lower Yixian Formation (Early Cretaceous), China. **F.** *Sordes pilosus* Sharov, 1971, PIN 2585/3, Karatau Formation (Upper Jurassic), Kazakhstan. **G.** Tapejarid indet., SMNK PAL 3830, Crato Formation (Early Cretaceous), Brazil.

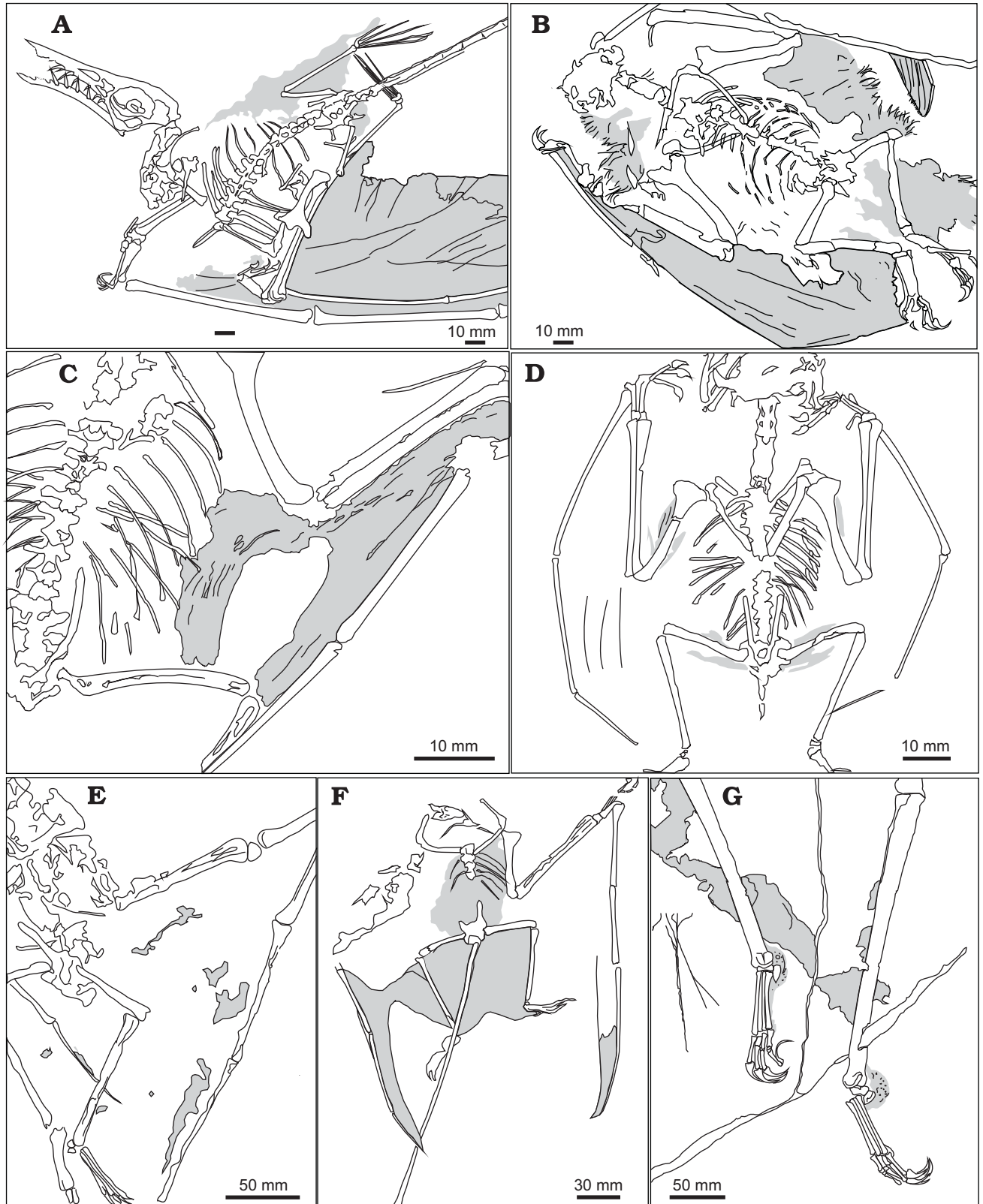


Fig. 4. Line drawings of the pterosaur specimens depicted in Fig. 3 or specific points of interest. Tissue belonging to the wings is marked in bold outlines. **A.** *Rhamphorhynchus muensteri*, the “Dark Wing”, JME SOS 4784, Eichstätt region (Upper Jurassic), Germany. **B.** *Jeholopterus ningchengensis*, IVPP V 12705, Lower Yixian Formation (Early Cretaceous), China. **C.** *Pterodactylus kochi*, “Vienna specimen”, NHMW 1975/1756, Solnhofen Limestone (Upper Jurassic), Germany. **D.** *Anurognathus ammoni*, private specimen (Bennett 2007), Solnhofen Limestone (Upper Jurassic), Germany. **E.** *Eosipterus yangi*, GMV 2117, Lower Yixian Formation (Early Cretaceous), China. **F.** *Sordes pilosus*, PIN 2585/3, Karatau Formation (Upper Jurassic), Kazakhstan. **G.** Tapejarid indet., SMNK PAL 3830, Crato Formation (Early Cretaceous), Brazil.



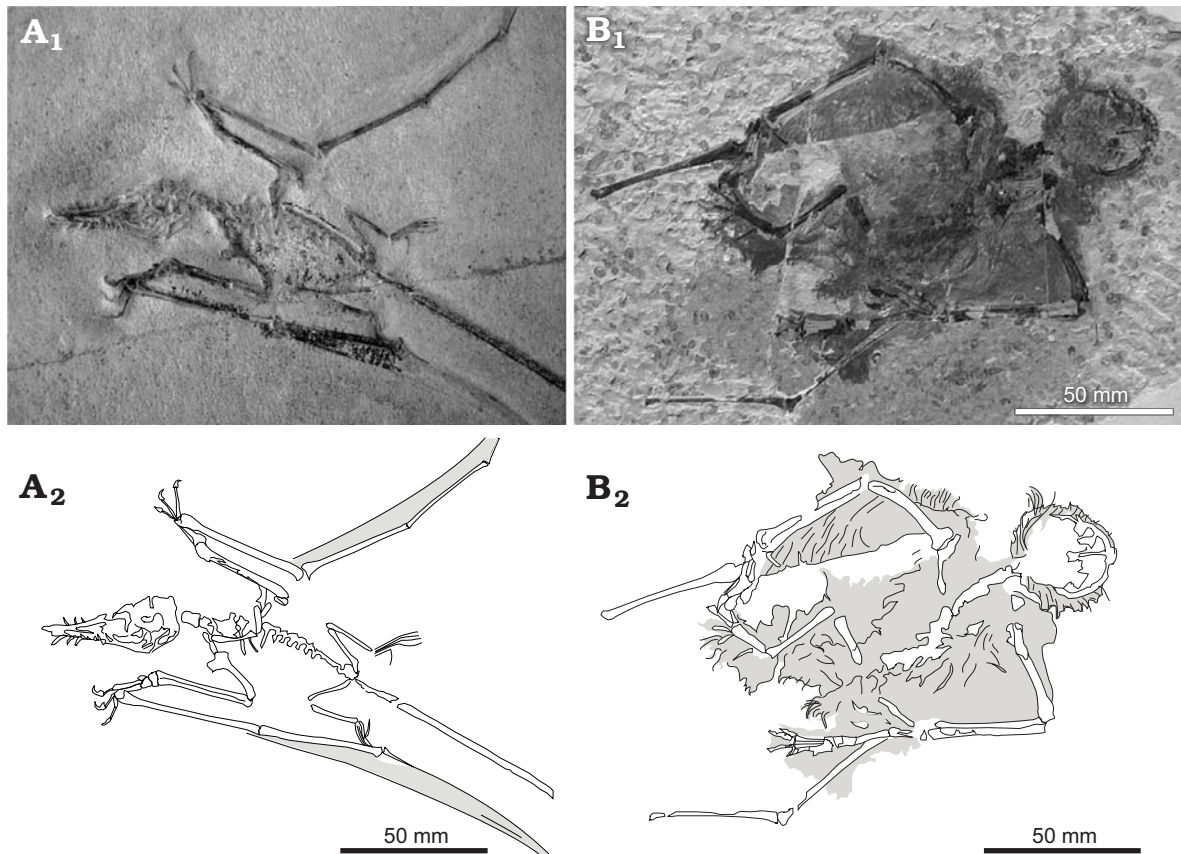


Fig. 5. Photographs and line drawings of selected specimens showing a pronounced contraction of the wing. **A.** *Rhamphorhynchus longicaudus* (Münster, 1839), BSPG 1938 I 503a, Solnhofen Limestone (Upper Jurassic), Germany; photograph (A<sub>1</sub>), explanatory drawing (A<sub>2</sub>). **B.** *Jeholopterus* sp. (Ji and Yuan 2002), Lower Yixian Formation (Early Cretaceous), China; photograph (B<sub>1</sub>), explanatory drawing (B<sub>2</sub>). Tissue belonging to the wings is marked in bold outlines in A<sub>2</sub> and B<sub>2</sub>.

the flight membrane was not specifically mentioned by Ji and Ji (1997) we confirm that the brachiopatagium extends to about the middle part of the tibia (DWEH personal observation 10/2008). However, the wing membranes of *Eosipterus* require further preparation, being partially obscured by matrix, and that exposed does not include a termination point. The attachment point of the trailing edge was thus probably located more caudally than the mid-tibia, and may well have been at the ankle.

A number of azhdarchoid limb elements from the Crato Formation of NE Brazil are associated with soft tissues from the wings but in the absence of any cranial or axial elements. Frey et al. (2003) described a basal azhdarchoid SMNK PAL 3830 (Figs. 3G, 4G) where a membrane trace extends from the metacarpal region to the ankle of the respective hind limb. Two more specimens (SMNK PAL 3900 and 6409, see Unwin and Martill 2007) also consist of the fore and hind limbs preserved in close association along with a goethitic trace representing part of the brachiopatagium. A fourth specimen (SMNK PAL 3855) preserves no visible soft tissue, however, both the fore and hind limbs are preserved in a comparable manner suggesting that they sank together. In the case of these specimens the soft tissue traces are too extensive to be regarded as anything other than the wing mem-

brane and in the SMNK PAL 3830 preserve traces of folding structures and actinobriils; known only from the brachiopatagium. Although the subsequent specimens do not preserve direct evidence about the attachment location of the tenopatagium it is difficult to explain the presence of corresponding limb elements, settling separate to the torso, without invoking a configuration where they were bound together by a flight membrane.

## Discussion

In all exceptionally preserved pterosaur specimens where the proximal portion of the membrane is present, the original descriptions confirm and/or support an attachment to the ankle (e.g., *Anurognathus ammoni*, *Beipiaopterus chenianus*, *Eosipterus yangi*, *Eudimorphodon ranzii*, *Jeholopterus ningchangensis*, *Rhamphorhynchus muensteri*, *Sordes pilosus*). Several azhdarchoid pterosaurs (i.e., SMNK PAL 3830, 3855, 3900, 6409) are also interpreted here as having their limb elements connected by an extensive membrane due to the observed state of the fossil specimens (Frey et al. 2003; Unwin and Martill 2007). Although several of these observations are in no way immune to criticism, as it can be argued that without any

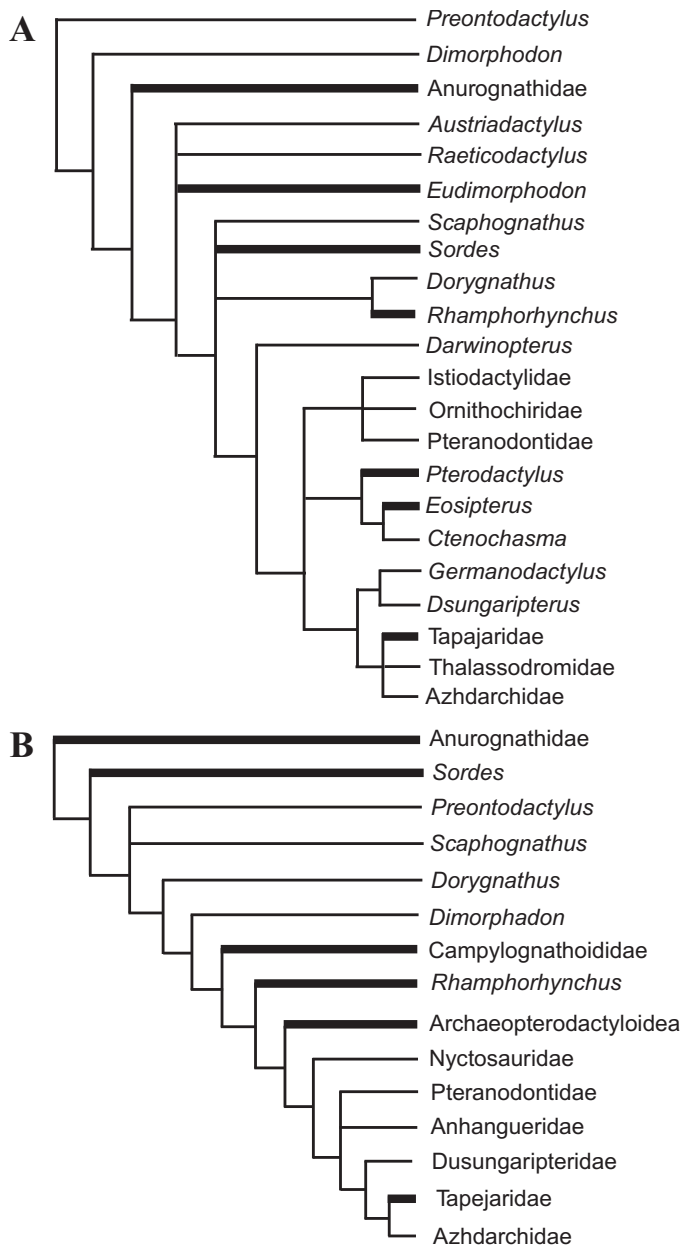


Fig. 6. Two contrasting pterosaur phylogenies. **A**. Phylogeny from Lü et al. (2009). **B**. A simplified version of that presented by Wang et al. (2005). Thick black lines indicate species or groups of taxa for which the fossil evidence supports an ankle attachment of the wing.

actinofibrils it is not always possible to know whether the tissue belongs to that of the wing of the membrane, we note that it is unlikely that tissue from the body has here been misinterpreted as belonging to the brachioptagium. The majority of the presented specimens preserve fibres and wrinkles, known only from the wing membrane, and/or a clear trailing edge that itself strongly suggests the trace must be regarded as part of the wing. Where none of these features are present the membrane traces are located lateral to the body and between the fore and hind limbs, or are too extensive in their coverage to have belonged to anything other than the flight membrane. The ankle attachment is therefore the best configuration sup-

ported by direct soft tissue evidence, although a knee attachment as suggested by the Vienna *Pterodactylus*, or tibia as with *Eosipterus* in any case confirms that the tenopatagium was associated with the hind limbs.

To the best of the authors' knowledge no specimens exist that conclusively show an attachment to the torso or hip. This is contrary to the configuration argued for by Padian and Rayner (1993) who figured several specimens of *Rhamphorhynchus* to support the hypothesis that the hind limbs were free from the wing membrane. As noted above, and is evident from their own figures, these specimens do not preserve the proximal portion of the wing membrane and thus cannot be used support a "bird-like" wing, particularly as more extensive membranes are now known (Frey et al. 2003). While Padian and Rayner (1993) had earlier argued that the post-mortem contraction of the wing membrane was responsible for the misidentification of an ankle attachment in some specimens we instead suggest that these contractions can be used to reject a hip or torso attachment. No preserved wing will ever be broader than during life, but instead may appear to be much narrower due to post-mortem effects (Fig. 5). The comparison of two specimens of *Jeholopterus* sp. (Ji and Yuan 2002; Wang et al. 2002) indicates that considerable post-mortem contraction of the flight membranes was possible and demonstrates the extent to which contractions of the membrane can deform the original shape and/or surface area of the wing (Fig. 5B). While this comparison highlights a rather extreme example of wing contraction, lesser examples are likely to be wide spread throughout the fossil record. To ensure that the most extensive membrane preserved is taken as the minimum for any particular taxa, specimens of the same genus must be compared with other, more recent discoveries whenever possible. We suggest that contraction of the membrane is also responsible for some of the exceptionally narrow chords observed in specimens of *Rhamphorhynchus* (e.g., BSPG AS I 772, BSPG 1938 I 503a; Fig. 5A) and support this by comparative observations with many other specimens of the taxon, particularly the "Dark Wing" specimen and to a lesser extent, the "Zittel Wing". We also argue that the intrinsic flexibility of the membrane (Frey et al. 2003) must be considered when confronted with a preserved wing as any folded or contracted example will inevitably produce a significant underestimate of its true extent if simply taken at face value (see e.g., Bennett 2000).

Despite continuing conflicts between major phylogenies (e.g., Kellner 2003; Unwin 2003; Wang et al. 2005, 2009; Bennett 2007b; Andres and Ji 2008, Andres et al. 2010) the presence of an ankle attachment is supported in a variety of pterosaur taxa (Fig. 6) demonstrating that an ankle attachment of the wing was widespread across the full range of the Pterosauria. Although Kellner (2003) and Bennett (2007b) both considered the anurognathids to be the most basal pterosaurs, which would confirm an ankle wing as a basal characteristic, the more recent study of Andres et al. (2010) instead places them as the sister-group to the Pterodactyloidea. Accepting a more derived placement of the Anurognathidae

does not alter the idea of a basal pterosaurian ankle wing as *Eudimorphodon ranzii* (MCSNB 8950a) occupies a position low down on the tree in all phylogenies (Kellner 2003; Andres et al. 2010) and has been inferred to have a wing extent similar to *Sordes* (Bakhurina and Unwin 2003). Although Dyke et al. (2006) voiced concern about “*Sordes*-like” pattern being universally adopted, these have proven to be unfounded and *Sordes* itself is not unusual in this respect for non-pterodactyloid pterosaurs; in any case a similar configuration can be observed in other pterodactyloid and non-pterodactyloid pterosaurs. The presence of an extensive ankle wing as a basal feature is not unexpected as such a configuration would have been beneficial to early pterosaur ancestors and an arboreal leaping origin of flight in the Pterosauria (Bennett 1997).

When considering the arguments of Padian (2008) that basal pterosaurs were bipedal rather than arboreal in habit we argue for a decoupling of the biped/quadruped hypotheses and the attachment of the trailing edge of the wing membrane. Regardless of which gait pterosaurs used, the flexibility of the brachiopatagium would not have impeded terrestrial locomotion, particularly if the wing was folded.

Additional support for a universally broad wing attachment has been suggested by an observed “high knee” style of preservation common in many pterosaurs. The suggestion here is that post mortem shrinkage of the patagium would have pulled the hind limbs upwards into its observed resting position. Although this position is commonly viewed in bats (RAE personal observation, 02/2009) it is not restricted to animals where a membrane would have attached to the hind limbs as it can also be observed in many fossil birds, including the holotype specimens of *Liaoxiornis delicatus*, *Eoenantiornis buhleri*, *Longipteryx chaoyangensis*, *Yanornis martini*, and *Prototeryx fengningensis* (Zhang et al. 2007). Furthermore this position is also observed in the carcasses of extant birds and mammals and is instead linked to damage of the proximal portion of the cerebellar cortex, where decerebellate rigidity causes the limb to flex in such a way (Faux and Padian 2007). The “high knee” style of preservation is thus the result of the central nervous system just prior to the animals’ death and not as a result of a contracting flight membrane.

One of the principle reasons for resolving the confusion surrounding the extent of the wing membrane in pterosaurs is to more accurately assess their aerodynamic performance, the results of which can vary significantly depending on the chosen configuration. Wing area, aspect ratio and wing loading are all important parts of several mathematical equations used to estimate flight performance, although more straightforward comparisons of these variables with extant animals are also useful for inferring ecological or palaeobiological aspects. When discussing the narrow chorded wing of pterosaurs Padian and Rayner (1993: 108) stated that “were the wings to extend to the ankle the animals aspect ratio and wing load would be significantly lower than those of comparable piscivorous birds”. Although a high aspect ratio wing is the most efficient configuration for fast gliding, piscivorous

birds and aerodynamic studies of pterosaurs with a “bird-like” wing have shown that they would have been slow, manoeuvrable and highly competent fliers (e.g., Brower 1980, 1982, 1983; MacCready 1985; Chatterjee and Templin 2004), experimental results should not and cannot be used to contradict the fossil evidence where it exists. As demonstrated above this provides unanimous support for the integration of the hind limbs with the tenopatagium. We also note that the above concerns of Padian and Rayner (1993) need not be problematic for pterosaurs and stress that if these taxa adopted a configuration like *Rhamphorhynchus*, where the trailing edge curved sharply to the ankle only towards the proximal most portion of the wing, then the difference in overall wing characters would not be too great (Fig. 2D, configuration 8). As previously noted the long fore arms and short hind limbs that typify these taxa would naturally result in a high aspect ratio/higher wing load configuration even if the trailing edge extended as far down as the ankle, as we argue it should be reconstructed.

## Conclusions

The resurgence of interest in the aerodynamic abilities of pterosaurs is a welcome step forward following a prolonged absence of focused research; however, future experiments must not be hampered by a lack of knowledge or uncertainty when reconstructing the flight apparatus. While some variables, such as mass and mass distribution, will invariably remain contentious, others, such as the shape and extent of the brachiopatagium can instead be resolved (or at least heavily constrained) by a review of the fossil specimens. We separate the ankle chord configuration presented here from the traditional “bat-like” reconstruction, which is now widely accepted to have lacked support from fossil specimens and to have been based on incorrect historical interpretations and a supposed aerodynamic “need” for a broad chord. By contrast the ankle chord configuration presented here is based solely on individual specimens where a clear association between the membrane and the hind limbs can be observed. Based on the available specimens the only configuration supported by fossil evidence is that of an ankle or lower hind limb attachment of the proximal trailing edge (Frey et al. 2003; Witton 2008). In the absence of conflicting evidence for specific specimens or taxa we argue that the null hypothesis should become that of an ankle attachment.

The “bird-like” model remains an unsupported interpretation of the wing shape in pterosaurs as none of the specimens cited by Padian and Rayner (1993) preserve the proximal section of the brachiopatagium. As an ankle attachment is observed in the “Dark Wing” specimen proponents of a narrow chord wing must first present fossil evidence against an ankle attachment in this specimen and why, as the most extensive membrane in the taxon, it cannot be considered the standard configuration for *Rhamphorhynchus*. While we argue that the bipedal/quadrupedal debate can be separated

from the extent of the brachiopatagium, as it would not interfere with terrestrial locomotion if it was folded, pterodactyloid pterosaurs are now universally accepted to have been quadrupedal and so would have been free to extend the membrane to their ankles. Since its proposal only the interpretations of Peters (1995, 2001) have provided any new support for the “bird-like” model based on fossil evidence. Peters’ (1995, 2001) studies of the membrane in *Jeholopterus*, *Sordes*, and *Eudimorphodon* along with their subsequent reconstructions where the trailing edge extends only just caudal to the elbow are, however, extremely controversial (Unwin and Bakhurina 1995), and appear to have been based solely on photographs rather than first hand observations. While working from photographs is not uncommon and at times unavoidable the conclusions of Peters (2001) arise from an improper use of graphic manipulation that exploits the poor resolution of photographs and allows the boundaries between blocks of pixels to be interpreted as “patterns”. This methodology is subjective and produces false and often fantastical images that have no value to science in general (see Bennett 2005). Thus without substantial evidence to the contrary, the narrow wing model must be rejected and should not be considered as a viable alternative to an ankle chord model. The presence of the brachiopatagium extending to the ankle in a variety of distantly related taxa is central to our argument that pterosaurs probably never radically altered the attachment of the trailing edge of the wing throughout their evolutionary history. In this respect the authors are in agreement with Witton (2008) that changes in the lengths of the fore and hind limbs was the driving mechanism for altering pterosaur wing shape.

## Acknowledgements

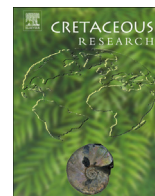
The authors wish to thank the numerous people who contributed to this paper, particularly Helmut Tischlinger, Natasha Bakhurina (both University of Bristol, Bristol, UK), Anna Paganoni (Museo Civico di Scienze Naturali, Bergamo, Italy) all of whom supplied photographs of several important specimens. Our thanks are also extended to Christopher Bennett (Fort Hays State University, Hay, USA), Mark Witton, David Martill (both University of Portsmouth, Portsmouth, UK), David Unwin (University of Leicester, Leicester, UK), Kevin Padian (University of California, Berkeley, USA) and one anonymous reviewer for their helpful comments and suggestions during previous drafts of this manuscript. DWEH is supported by the Chinese Academy of Sciences while RAE is supported the DFG funded project FR1314/15-2.

## References

- Abel, O. 1919. Neue Rekonstruktionen der flugsauriergattungen *Pterodactylus* and *Rhamphorhynchus*. *Die Naturwissenschaften* 37: 661–665. [CrossRef]
- Abel, O. 1925. *Geschichte und Methode der Rekonstruktion vorzeitlicher Wirbeltiere*. 327 pp. Gustav Fischer Verlag, Stuttgart.
- Andres, B. and Ji, Q. 2008. A new pterosaur from the Liaoning Province of China, the phylogeny of the Pterodactyloidea, and convergence in their cervical vertebrae. *Palaentology* 51: 453–469. [CrossRef]
- Andres, B., Clark, J.M., and Xing, X. 2010. A new rhamphorhynchid pterosaur from the Upper Jurassic of Xinjiang, China, and the phylogenetic relationships of basal pterosaurs. *Journal of Vertebrate Paleontology* 30: 163–187. [CrossRef]
- Bakhurina, N.N. and Unwin, D.M. 2003. Reconstructing the flight apparatus of *Eudimorphodon*. *Rivista del Museo Civico di Scienze Naturali “Enrico Caffi”* 22: 5–8.
- Bennett, S.C. 1987. New evidence on the tail of the pterosaur *Pteranodon* (Archiosauria, Pterosauria). In: P.J. Currie and E.H. Koster (eds.), Fourth Symposium On Mesozoic Terrestrial Ecosystems, Short Papers. *Occasional Papers of the Tyrrell Museum of Paleontology* 3: 18–23.
- Bennett, S.C. 1990. A pterodactyloid pterosaur pelvis from the Santana Formation of Brazil: Implications for terrestrial locomotion. *Journal of Vertebrate Paleontology* 10: 80–85. [CrossRef]
- Bennett, S.C. 1997. The arboreal leaping theory of the origin of pterosaur flight. *Historical Biology* 12: 265–290. [CrossRef]
- Bennett, S.C. 2000. Pterosaur Flight: the role of the actinofibrils in wing function. *Historical Biology* 14: 255–284. [CrossRef]
- Bennett, S.C. 2001. The osteology and functional morphology of the late cretaceous pterosaur *Pteranodon*. Part 1. General description of osteology. *Palaentographica A* 260: 1–112.
- Bennett, S.C. 2005. Pterosaur science or pterosaur fantasy? *Prehistoric Times* 70: 21–23, 40–41.
- Bennett, S.C. 2007a. Articulation and function of the pteroid bone in pterosaurs. *Journal of Vertebrate Paleontology* 27: 881–891. [CrossRef]
- Bennett, S.C. 2007b. A second specimen of the pterosaur *Anurognathus ammoni*. *Paläontologische Zeitschrift* 81: 376–398.
- Bramwell, C.D. and Whitfield, G.R. 1974. Biomechanics of *Pteranodon*. *Philosophical Transactions of the Royal Society, London B* 267: 503–581. [CrossRef]
- Brower, J.C. 1980. Pterosaurs: How they flew? *Episodes* 4: 21–24.
- Brower, J.C. 1982. The aerodynamics of an ancient flying reptile. *Syracuse Scholar* 1982: 45–57.
- Brower, J.C. 1983. The aerodynamics of *Pteranodon* and *Nyctosaurus*, two large pterosaurs from the Upper Cretaceous of Kansas. *Journal of Vertebrate Paleontology* 3: 84–124. [CrossRef]
- Chatterjee, S. and Templin, R.J. 2004. Posture, locomotion, and paleoecology of pterosaurs. *Geological Society of America, Special Paper* 376: 1–64.
- Clark, J.M., Hopson, J.A., Hernández, R.R., Fastovsky, D.E., and Montellano, M. 1998. Foot posture in a primitive pterosaur. *Nature* 391: 886–889. [CrossRef]
- Collini, C. 1784. Sur quelques Zoolithes du Cabinet d’Histoire naturelle de S.A.S.E Palatine et du Bavière, à Mannheim. *Acta Academiae Theodoro Palatinae, Mannheim, Pars Physica* 5: 58–103.
- Cuvier, G. 1801. Reptile volant. Extrait d’un ouvrage sur les espèces de quadrupèdes don’t on a trouvé les ossements dans l’intérieur de la terre. *Journal de Physique, de Chimie et d’Histoire Naturelle* 52: 253–267.
- Döderlein, L. 1923. *Anurognathus Ammoni*, ein neuer Flugsaurier. *Sitzungsberichte der Mathematisch-Naturwissenschaftlichen Abteilung der Bayerischen Akademie der Wissenschaften zu München* 1923: 306–307.
- Dyke, G.J., Nudds, R.L., and Rayner, J.M. 2006. Limb disparity and wing shape in pterosaurs. *Journal of Evolutionary Biology* 19: 1339–1342. [CrossRef]
- Faux, C.M. and Padian, K. 2007. The opisthotonic posture of vertebrate skeletons: post-mortem contraction or death throes? *Paleobiology* 32: 201–226. [CrossRef]
- Frey, E. and Martill, D.M. 1998. Soft tissue preservation in a specimen of *Pterodactylus kochi* (Wagner) from the Upper Jurassic of Germany. *Neues Jahrbuch für Geologie und Paläontologie Abhandlungen* 210: 421–441.
- Frey, E., and Tischlinger, H. 2000. Weichteil-anatomie der Flugsaurierfüße und Bau der Scheitelkämme: Neue Pterosaurierfunde aus den Solnhofener Schichten (Bayern) und der Crato-Formation. *Archaeopteryx* 18: 1–16.
- Frey, E., Tischlinger, H., Buchy, M.-C., and Martill, D.M. 2003. New speci-

- mens of Pterosauria (Reptilia) with soft parts with implications for pterosaurian anatomy and locomotion. In: E. Buffetaut and J.-M. Mazin (eds.), *Evolution and Palaeobiology of Pterosaurs. Geological Society of London, Special Publications 217*: 233–266.
- Goldfuss, G.A. 1831. Beiträge zur Kenntnis verschiedener Reptilien der Vorwelt. *Nova acta Academiae Caesareae Leopoldino-Carolinae Germanicae Naturae Curiosorum* 15: 61–128.
- Hankin, E.H. and Watson, D.S.M. 1914. On the flight of pterodactyls. *The Aeronautical Journal* 18: 324–335.
- Hazlehurst, G.A. and Rayner, J.M.V. 1992. Flight characteristics of Triassic and Jurassic Pterosauria: an appraisal based on wing shape. *Paleobiology* 18: 447–463.
- Heptonstall, W.B. 1971. An analysis of the flight of the Cretaceous pterodactyl *Pteranodon ingens* (Marsh). *Scottish Journal of Geology* 7: 61–78.
- Jaekel, O. 1910. Rekonstruktion fossiler Tiere. *Meyers Großes Konversations Lexikon* 22: 1–10.
- Ji, S.-A. and Ji, Q. 1997. Discovery of a new pterosaur from western Liaoning, China. *Acta Geologica Sinica* 71: 1–6.
- Ji, Q., and Yuan, C.X. 2002. Discovery of two kinds of protofeathered-pterosaurs in the Mesozoic Daohugou Biota in the Ningcheng region and its stratigraphic and biologic significances [in Chinese]. *Geological Review* 48: 221–224.
- Kellner, A.W.A. 2003. Pterosaur phylogeny and comments on the evolutionary history of the group. In: E. Buffetaut and J.-M. Mazin (eds.), *Evolution and Palaeobiology of Pterosaurs. Geological Society of London, Special Publications 217*: 105–137.
- Kellner, A.W.A., Wang, X., Tischlinger, H., Campos, D.A., Hone, D.W.E., and Meng, X. 2009. The soft tissue of *Jeholopterus* (Pterosauria, Anurognathidae, Batrachognathinae) and the structure of the pterosaur wing membrane. *Proceedings of the Royal Society B* 277 (1679): 321–329. [CrossRef]
- Kripp, D. 1941. Ein Lebensbild von *Pteranodon ingens* auf flugtechnischer Grundlage. *Luftwissen* 8: 217–246.
- Lü, J.-C. 2002. Soft tissue in an Early Cretaceous pterosaur from Liaoning province, China. *Memoir of the Fukui Prefectural Dinosaur Museum* 1: 19–28.
- Lü, J.-C. 2003. A new pterosaur: *Beipiaopterus chenianus*, gen. et sp. nov. (Reptilia: Pterosauria) from the Western Liaoning Province of China. *Memoir of the Fukui Prefectural Dinosaur Museum* 2: 153–160.
- Lü, J.-C., Unwin, D.M., Jin, X., Liu, Y., and Ji, Q. 2009. Evidence for modular evolution in a long-tailed pterosaur with a pterodactyloid skull. *Proceedings of the Royal Society B* 277 (1680): 383–389. [CrossRef]
- MacCready, P. 1985. The great pterodactyl project. *Engineering and Science* 49: 18–24.
- Marsh, O.C. 1882. The wings of pterodactyls. *American Journal of Science* 23: 251–256.
- Martill, D.M. and Unwin, D.M. 1989. Exceptionally well preserved pterosaur wing membrane from the Cretaceous of Brazil. *Nature* 340: 138–140. [CrossRef]
- McGowan, A.J. and Dyke, G. 2009. A morphospace-based test for competitive exclusion among flying vertebrates: did birds, bats and pterosaurs get in each other's space? *Trustees of the Natural History Museum* 20: 1230–1236.
- Münster, G.G. 1839. Ueber einige neue Versteinerungen in der lithographischen Schiefer von Baiern. *Neues Jahrbuch für Mineralogie, Geologie, und Palaeontologie* 1839: 676–682.
- Padian, K. 1983. A functional analysis of flying and walking in pterosaurs. *Paleobiology* 9: 218–239.
- Padian, K. 1985. The origins and aerodynamics of flight in extinct vertebrates. *Paleontology* 28: 423–433.
- Padian, K. 1987. The case of the bat-winged pterosaur. Typological taxonomy and the influence of pictorial representation on scientific perception. In: S.J. Czerkas and E.C. Olson (eds.), *Dinosaurs Past and Present. Vol. 2*, 65–81. Natural History Museum of Los Angeles County and University of Washington Press, Seattle.
- Padian, K. 2003. Pterosaur stance and gait and the interpretation of trackways. *Ichnos* 10: 115–126. [CrossRef]
- Padian, K. 2008. Were pterosaurs ancestors bipedal or quadrupedal?: Morphometric, functional, and phylogenetic considerations. *Zitteliana B* 28: 21–33.
- Padian, K. and Rayner, J.M.V. 1993. The wings of pterosaurs. *American Journal of Science A* 293: 91–166. [CrossRef]
- Palmer, C. and Dyke, G.J. 2009. Biomechanics of the unique pterosaur pteroid. *Proceedings of the Royal Society B* 277 (1684): 1121–1127. [CrossRef]
- Peters, D. 1995. Wing shape in pterosaurs. *Nature* 374: 315–316. [CrossRef]
- Peters, D. 2001. A new model for the evolution of the pterosaur wing—with a twist. *Historical Biology* 15: 277–301. [CrossRef]
- Rayner, J.M.V. 1990. Vertebrate flight and the origins of flying vertebrates. In: K.C. Allen and D.E.G. Briggs (eds.), *Evolution and the Fossil Record*, 188–217. Belhaven, London.
- Schaller, D. 1985. Wing evolution. In: M.K. Hecht, J.H. Ostrom, G. Viohl, and P. Wellnhofer (eds.), *The Beginning of Birds*, 333–348. Proceedings of the International Archeopteryx Conference Eichstätt, Eichstätt: Freundes Jura-Museums, Eichstätt.
- Seeley, H.G. 1901. *Dragons of the Air: an Account of Extinct Flying Reptiles*. 239 pp. Methuen, London.
- Sharov, A.G. 1971. New flying reptiles from the Mesozoic of Kazakhstan and Kirgizia [in Russian]. *Trudy Palaeontologičeskogo Instituta Akademii Nauk SSSR* 130: 104–113.
- Sömmerring, S.T. von 1812. Über einen *Ornithocephalus* oder über das unbekanntes Thier der Vorwelt, dessen Fossiles Gerippe Collini im 5. Bande der Actorum Academiae Theodoro-Palatinae nebst einer Abbildung in natürlicher Grösse im Jahre 1784 beschrieb, und welches Gerippe sich gegenwärtig in der Naturalien-Sammlung der königlichen Akademie der Wissenschaften zu München befindet. *Denkschriften der königlichen bayerischen Akademie der Wissenschaften, München: mathematisch-physikalische Classe* 3: 89–158.
- Stein, R.S. 1975. Dynamic analysis of *Pteranodon ingens*: a reptilian adaptation to flight. *Journal of Paleontology* 49: 534–548.
- Stieler, C. 1922. Neuer Rekonstruktionsversuch eines liassischen Flugsauriers. *Naturwissenschaftliche Wochenschrift* 20: 273–280.
- Strömer, E. 1913. Rekonstruktion des Flugsauriers *Rhamphorhynchus gemmingi* H. v. M. *Neues Jahrbuch für Mineralogie, Geologie und Paläontologie* 2: 49–68.
- Taquet, P. and Padian, K. 2004. The earliest known restoration of a pterosaur and the philosophical origins of Cuvier's *Ossemen Fossiles*. *Comptes Rendus Palevol* 3: 157–175. [CrossRef]
- Tischlinger, H. and Frey, E. 2002. Ein *Rhamphorhynchus* (Pterosauria, Reptilia) ungewöhnlicher Flughauterhaltung aus dem Solnhofener Plattenkalk. *Archaeopteryx* 20: 1–20.
- Unwin, D.M. 1987. Pterosaur Locomotion—joggers or waddlers? *Nature* 327: 13–14. [CrossRef]
- Unwin, D.M. 1988. A new specimen of *Dimorphodon* and the terrestrial ability of early pterosaurs. *Modern Geology* 13: 57–68.
- Unwin, D. 1999. Pterosaurs: back to the traditional model? *Trends in Ecology and Evolution* 14: 263–268. [CrossRef]
- Unwin, D.M. 2003. On the phylogeny and evolutionary history of pterosaurs. In: E. Buffetaut and J.-M. Mazin (eds.), *Evolution and Palaeobiology of Pterosaurs. Geological Society of London, Special Publications 217*: 139–190.
- Unwin, D.M. and Bakhurina, N.N. 1994. *Sordes pilosus* and the nature of the pterosaur flight apparatus. *Nature* 371: 62–64. [CrossRef]
- Unwin, D.M. and Bakhurina, N.N. 1995. Wing shape in pterosaurs. *Nature* 374: 315–316. [CrossRef]
- Unwin, D.M. and Martill, D.M. 2007. Pterosaurs of the Crato Formation. In: D.M. Martill, G. Bechly, and R.F. Loveridge (eds.), *The Crato Fossil Beds of Brazil*, 475–524. Cambridge University Press, Cambridge.
- Wang, X., Zhou, Z., Zhang, F., and Xu, X. 2002. A nearly completely articulated rhamphorhynchoid pterosaur with exceptionally well-preserved wing membranes and “hairs” from Inner Mongolia, northeast China. *Chinese Science Bulletin* 47: 226–230. [CrossRef]

- Wang, X., Kellner, A.W.A., Zhou, Z., and Campos, A. 2005. Pterosaur diversity and faunal turnover in Cretaceous terrestrial ecosystems in China. *Nature* 437: 875–879. [CrossRef]
- Wang, X., Kellner, A.W.A., Jiang, S., and Meng, X. 2009. An unusual long-tailed pterosaur with elongated neck from western Liaoning of China. *Anais da Academia Brasileira de Ciências* 89: 793–812.
- Wellnhofer, P. 1970. Die Pterodactyloidea (Pterosauria) der Oberjura-Plattenkalke Süddeutschlands. *Abhandlung der Bayerischen Akademie der Wissenschaften* 141: 1–133.
- Wellnhofer, P. 1988. Terrestrial locomotion in pterosaurs. *Historical Biology* 1: 3–16. [CrossRef]
- Wellnhofer, P. 1991. Weitere pterosaurierfunde aus der Santana-Formation (Apt) der Chapada do Araripe, Brasilien. *Palaeontographica Abteilung A* 215: 43–101.
- Wilkinson, M.T. 2008. Three-dimensional geometry of a pterosaur wing skeleton, and its implications for aerial and terrestrial locomotion. *Zoological Journal of the Linnean Society* 154: 27–69. [CrossRef]
- Wilkinson, M.T., Unwin, D.M., and Ellington, C.P. 2005. Lift capability of pterosaur wings and the evolution of gigantism. *Proceedings of the Royal Society B, Biological Sciences* 273: 119–126. [CrossRef]
- Williston, S.W. 1897. Restoration of Ornithostoma (Pteranodon). *Kansas University Quarterly* 6: 35–51.
- Williston, S.C. 1911. The wing-finger of pterodactyls, with restoration of *Nyctosaurus*. *Journal of Geology* 19: 696–705. [CrossRef]
- Wiman, C. 1923. Über *Dorygnathus* und andere Flugsaurier. *Bulletin of the Geological Institute of Upsala* 19: 23–55.
- Wiman, C. 1925. Über *Pterodactylus westimani* und andere Flugsaurier. *Bulletin of the Geological Institution of the University of Uppsala* 20: 1–38.
- Witton, M.P. 2008. A new approach to determining pterosaur body mass and its implications for pterosaur flight. *Zitteliana B* 28: 143–158.
- Zhang, F., Zhou, Z., and Hou, L. 2007. Birds. In: M.-M. Chang, P. Chen, Y. Wang, and Y. Wang (eds.), *The Jehol Fossils, the Emergence of feathered Dinosaurs, Beaked Birds and Flowering Plants*, 128–149. Academic Press, New York.
- Zittel, K.A. Von 1882. Über Flugsaurier aus dem lithographischen Schiefer Bayerns. *Paläontographica* 29: 47–80.



## Pneumatization of an immature azhdarchoid pterosaur



Ross A. Elgin<sup>a,\*</sup>, David W.E. Hone<sup>b</sup>

<sup>a</sup>Staatliches Museum für Naturkunde Karlsruhe, Erbprinzenstraße 13, 76137 Karlsruhe, Germany

<sup>b</sup>School of Biological and Chemical Sciences, Queen Mary, University of London, Mile End Road, London, UK

### ARTICLE INFO

#### Article history:

Received 6 April 2013

Accepted in revised form 24 June 2013

Available online

#### Keywords:

Air-space proportion

Azhdarchoidea

Palaeoecology

Pneumaticity

Pterosaurs

### ABSTRACT

The partial skeleton of an immature azhdarchoid pterosaur from the Santana Formation (Early Cretaceous) of NE Brazil is described, where breaks across several of the three dimensionally preserved postcranial elements have permitted the thickness of the cortex to be accurately measured. Air-space proportions (ASP) are shown to be comparable to those observed in sauropod dinosaurs. The pterosaurian pneumatic system, prevalent throughout these animals, is shown to be well developed in even non-adult animals and is inferred to have penetrated into even the smallest of bones.

© 2013 Elsevier Ltd. All rights reserved.

### 1. Introduction

The pterosaurs were a group of volant archosaurian reptiles that existed during the Mesozoic (Triassic, Norian – Cretaceous, Maastrichtian), predating birds as the earliest actively flying vertebrates by around 60 million years. While the aerodynamic prowess of the Pterosauria has been widely debated (Bramwell and Whitfield, 1974; Brower, 1980, 1983; Witton, 2008; Sato et al., 2009; Witton and Habib, 2010), numerous adaptation to active flight, including both a complex series of flight membranes (Frey et al., 2003a; Lü, 2003; Kellner et al., 2010) and an advanced neurological system (Witmer et al., 2003) are suggestive of great aerial competence and likely contributed to the diversification of the group, along with their worldwide distribution. As part of their advanced suite of adaptations to flight, the skeleton became largely hollow with paper thin compacta, braced by trabeculae, as the diverticulae of the lungs or air sacs invaded a number of skeletal elements (Claessens et al., 2009; Naish et al., 2013), creating a system of postcranial pneumaticity that may be considered analogous to (or perhaps homologous to) those of birds and, by extension, other saurischian dinosaurs (Schwarz et al., 2007; Schwarz-Wings et al., 2010; Claessens et al., 2009). The net effect of pneumatisation appears to have been a reduction in total mass by lightening the skeleton (Wedel, 2005; Witton, 2008), and a subsequent reduction in required power during flight.

This latter development, observed across both major divisions of the Pterosauria, the pterodactyloids, and the basal paraphyletic group of smaller animals, the ‘rhamphorhynchoids’ or non-pterodactyloid pterosaurs, became significantly more widespread in larger and more derived taxa (Claessens et al., 2009). In addition to the often greatly enlarged sinus cavities of the skull (e.g., *Chaoyangopterus*, Wang and Zhou, 2003; *Tapejara*, Frey et al., 2003b), elements belonging to the postcranial skeleton including the cervical and dorsal vertebrae, sternum, scapula and coracoid, humerus, radius and ulna, carpus, metacarpalia, wing-finger phalanges, pelvic girdle and proximal hind limb bones, have been confirmed as pneumatic in one or more taxa (Bonde and Christiansen, 2003; Butler et al., 2009; Claessens et al., 2009; Eck et al., 2011; Naish et al., 2013).

Although several studies have otherwise noted that the mass reduction gained from the development of hollowed out bones appears to be small (Waiser, 2007; Witton, 2008), or that these features developed as a consequence of flapping flight, where bending strength was sacrificed for torsional resistance (Cubo and Casinos, 2000), it is difficult to separate extensive pneumaticity from mass reduction given its prevalence within both birds and terrestrial animals of a very large maximum size, i.e. sauropod dinosaurs (Wedel, 2005, 2006, 2009; Schwarz et al., 2007; Schwarz-Wings et al., 2010). For palaeontologists trying to accurately reconstruct the biology of pterosaurs, the pneumatic system therefore impinges strongly on a large number of different factors, these being (among others) a key component of mass estimates (Wedel, 2005; Witton, 2008; Henderson, 2010) and by extension, flight and locomotion dynamics (Habib, 2008), physiology (Claessens et al., 2009) and histology (Steel, 2008).

\* Corresponding author.

E-mail addresses: [rosselgin@gmail.com](mailto:rosselgin@gmail.com), [rosselgin@googlemail.com](mailto:rosselgin@googlemail.com) (R.A. Elgin), [dwe@yahoo.com](mailto:dwe@yahoo.com) (D.W.E. Hone).

Herein a new specimen of a juvenile pterosaur is described where damage to the bone cortices has exposed the pneumatic cavities and their associated trabeculae. The significance of the fossil, in addition to detailing the often overlooked postcranial anatomy of the Azhdarchoidea, is that it permits observations to be made on the orientation of the internal bracing systems within several long bone elements, and the calculation of air-to-space (ASP) proportions. Accurate measurements of the bone wall thickness indicate that the compacta of pneumatic elements can be as thin as only a few hundredths of a millimetre.

**Institutional abbreviations:** BSP, Bayerische Staatsammlung für Paläontologie und Historische Geologie, Munich, Germany; SMNK, Staatliches Museum für Naturkunde Karlsruhe, Karlsruhe, Germany; YPM, Peabody Museum of Natural History, Yale University, New Haven, USA.

## 2. Taphonomy and locality information

The specimen is preserved in a concretion and originates from the Romualdo Member of the Santana Formation, an Albian–Cenomanian aged Fossil Lagerstätte in the northeast of Brazil (Kellner and Tomida, 2000; Martill, 2007), the depositional environment of which is reported as a shallow lagoon that retained an ever expanding connection to the open sea (Kellner and Tomida, 2000).

The bones are preserved in three dimensions without any apparent distortion, although several of these elements are broken at the margin of the concretion. Abrasion of the proximal and distal regions of the long bones has exposed their internal structure, allowing for the infilling of such regions by the matrix. Diagenetic calcite is limited to the distal portion of the radius and the medular cavity of the humerus. The presence of elements from various regions of the body indicates the animal was mostly complete prior to burial, an observation supported by the retention of small, easily transportable elements such as the phalanges of digits I–III. Prior to petrification, the skeleton settled in such a manner that several elements lay heaped one on top of the other and the right humerus was rotated 180° about its long axis.

## 3. Specimen description

The specimen is embedded within a small concretion (173 mm by 112 mm in plan view) that has been broken into two equally sized parts. It is housed within the State Museum of Natural History Karlsruhe under the collection number SMNK PAL 3985 (Fig. 1). The partial skeleton consists of at least five cervical vertebrae, six thoracic vertebrae, the sternum and pectoral girdles, right and left humeri, radii and ulnae, the right wing metacarpal, elements of the pelvic girdle, and the left femur, and is estimated to have possessed a wing span of approximately 1.2 m, based on comparisons of the humerus with the early complete azhdarchoid SMNK PAL 3900 (where the half span is 8.6 times the humeral length). Although only partially complete, the presence of an unwarped deltopectoral crest on the humerus (Unwin, 2003) distinguishes SMNK PAL 3985 from the numerous ornithocheiroids known to have inhabited the region (e.g., Wellnhofer, 1991; Kellner and Tomida, 2000), while large pneumatopores on the ventral and posterior faces of the humerus and femur, respectively, remain a feature only observed within the Azhdarchoidea, specifically for *Tapejara wellnhoferi* where numerous postcranial elements are known (Wang et al., 2009; Eck et al., 2011; Elgin and Campos, 2011). Beyond that of an indeterminate azhdarchoid, no further taxonomic identification is possible owing to a lack of diagnostic anatomical or morphometric characters.

The cervical series is represented by five damaged vertebrae, positioned adjacent to the left coracoid, and are distinguished by their larger size and more robust form relative to those of the thoracic series. The posterior faces of the cervical neural spines are depressed and perforated by numerous foramina. A single foramen occupies the lateral flank of the corpus. The centre of the thoracic vertebrae is 7 mm in both length and width and associated with long transverse processes (8 mm), and tall neural spines (>10 mm). Three vertebrae remain *in situ* but small sutures between the centrum and the transverse process/neural arches indicate that these elements remain osteologically immature. Several foramina are observed on the ventral surfaces of the transverse processes although their size and position are not consistent. In three vertebrae the only visible perforations are small oval foramina (1 mm by ~0.5 mm) situated on the anteroventral portion of two elements and the posteroventral portion of a third. By contrast, a more posteriorly located element preserves a larger foramen (2.5 mm by 1.5 mm) on the anteroventral portion of the transverse process that penetrates the interior of the bone. In several elements the posterior face of the neural spine is “kite-shape,” and well defined, the centre of which is deeply depressed and pierced by three large foramina that likely exited onto the anterior face (Fig. 2D). The postzygapophyses are 3 mm in length, and are angled dorsolaterally at 45° against the lateral plane in posterior view, and slightly posterolaterally in dorsal view. Directly ventral to the postzygapophyses, a pair of small foramina flank the neural canal. In the second configuration, associated with a more posterior position within the dorsal column, the posterior face of the neural spine instead develops only a slight depression and in its lateral aspect slopes gently dorsally from the ventral to dorsal margins. Several small foramina pierce the ventral portion of the neural spine but the majority of the posterior surface is occupied by a single, mediolaterally compressed foramen that appears to extend for almost the entire length of the spine. The posterolateral flanks of the spine are penetrated by tiny foramina.

Several dorsal ribs belonging to the anterior and posterior sections of the torso lie adjacent to the remains of the vertebral column. Two large, robust and double-headed ribs showing only a slight curvature must have articulated with the last cervical or one of the first two dorsal vertebrae, while those ribs associated with the more posterior dorsals are much thinner. A single dorsal rib has been damaged to reveal its internal structure and the remains of minute trabeculae are visible within the proximal part of the internal cavity.

The sternal plate is compact with no sign of a keel or any obvious muscle scars (Fig. 2A). Although damaged, the cristospine appears to have been very short. The plate itself is gently convex in all directions with the posterolateral margins lying approximately 12 mm above the lowest point of the sternum, i.e., where the plate meets the cristospine. The flanks of the cristospine are sharply concave and pierced by a small crescent-shaped foramen while the posterior margin is smooth and evenly convex.

The scapula and coracoid are unfused. The shaft of the left coracoid is long and thin (3.5 mm) with an oval-shaped cross section, that expands to a width of 9 mm towards its proximal edge where it would have articulated with the sternum. Muscle scars and attachments are clearly visible. A small tubercle on the distal edge of the shaft lies lateral to a pronounced scar, itself 12 mm in length and which occupies the posteroventral margin of the bone. A coarse series of dorsomedially orientated ridges occupy the lateral flank of the bone, ventral to the biceps tubercle. The tubercle and scar may represent the insertion points for *m. coracobrachialis* while on the series of ridges *m. supracoracoideus* originated (Bennett, 2001, 2003). The articular surface of the glenoid fossa is concave and is distinguished from the rest of the bone by both its smooth surface and lighter colouration.



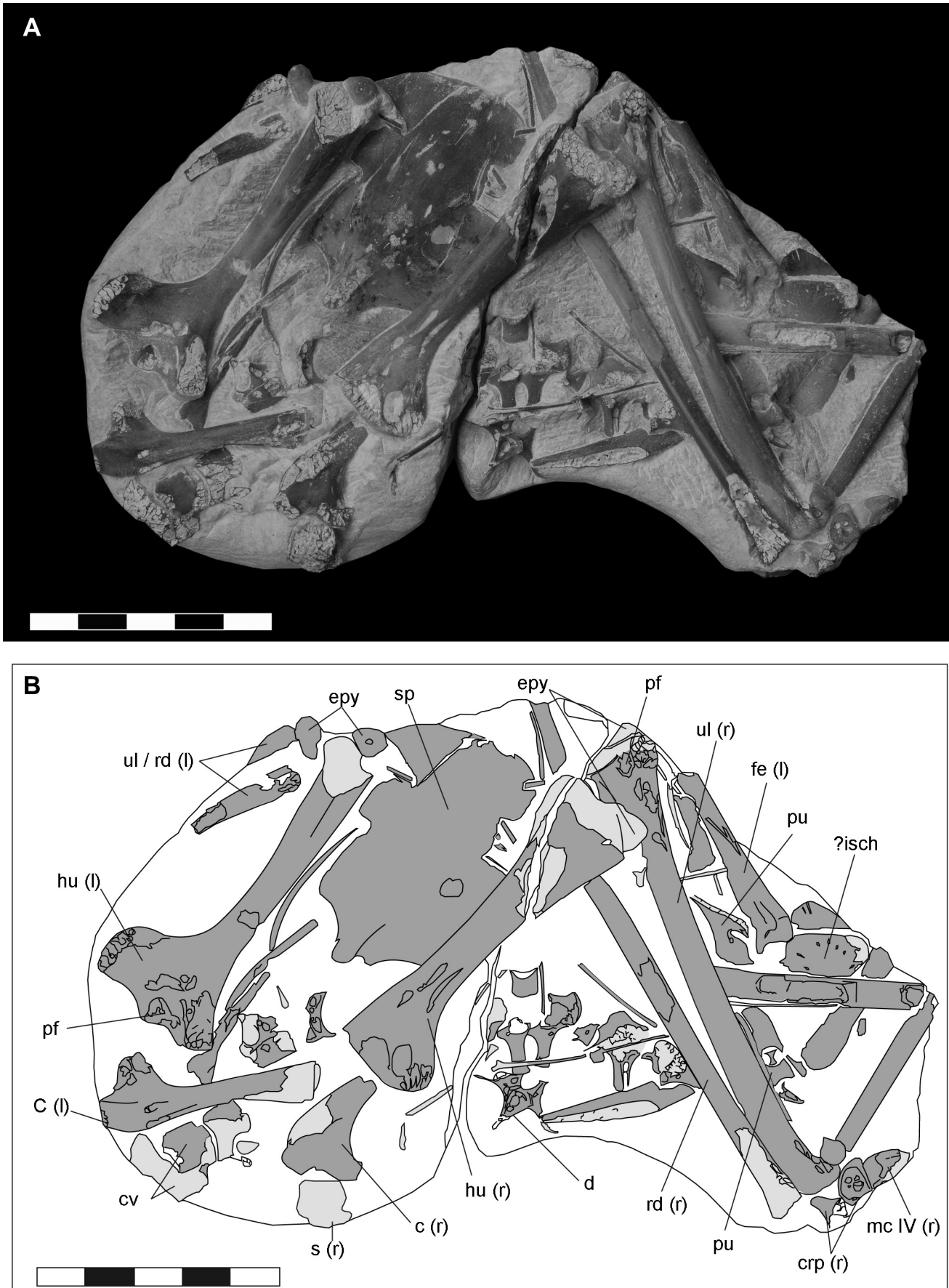


**Fig. 1.** A, Overview of the described specimen (SMNK PAL 3985); B, Corresponding line tracing. Abbreviations: cv, cervical vertebrae; d, dorsal vertebrae; sp, sternal plate; c, coracoid; s, scapula, hu, humerus, ul, ulna; rd, radius; epy, epiphysis; crp, carpals; mc IV, metacarpal IV; pu, pubis; isch, ischium; fe, femur; pf, pneumatic foramen. Scale bar = 50 mm.

Both humeri are preserved (Fig. 2C) and each measure 71 mm in length. The deltopectoral crest is unwarped with concave medial and lateral margins, preserving a number of coarse striae on its ventral face to serve as the origin of the pectoral muscles. A single large pneumatic foramen occupies the anteroventral surface of the humeral column. The column is further marked by a long scar, positioned about three quarters along the shaft on the poster-ventral margin of the bone, here considered to be the insertion point for *m. triceps* (Bennett, 2003). Two disarticulated, but well ossified, epiphyses lie adjacent to the distal margin of the bone, the first is sub-circular, located on the ventral portion of the articular surface, while the second is saddle-shaped and is located dorsal and posterior to the first.

The ulna is an elongate bone, 99.5 mm in length, with an oval cross section and a mid-shaft diameter of 5–6 mm. A single loose epiphysis lies adjacent to the proximal articular margin while adjacent to this a pneumatic foramen is observed on the anterior face of the ulna. The shaft of the ulna bows anteriorly and towards the distal margin the anterior face becomes anteroposteriorly flattened. The radius is of a similar length but is smaller and more circular in cross section, being 4.5 mm in diameter at the midpoint of the shaft.

Only two carpalia of the right carpus are present, indicating that fusion to form the proximal and distal syncarpal blocks was incomplete at the time of death. The medial side of the anterior proximal carpal acted as the articular surface with the antebrachial bones and is divided into two sub-oval concavities by a prominent anteroventrally orientated ridge. The ventral articular surface that accommodates the ulna is smaller than the dorsal one for the radius. The anterior face of the carpal is flat and perforated by foramina. The central portion of the distal ventral carpal, which is observed in ventral view, is gently concave and pierced by three large foramina. A third element by the wrist is likely not part a carpal as the shape, colour and texture of the element have more in common with the unfused epiphyses of the humeri and ulna. If this represents an epiphyseal element, then its original association remains uncertain.

Only a single element is identified as belonging to the fourth digit by its sub-triangular cross-section indicating that it represented either the second or third phalanx within the series (Martill and Frey, 1999). The bone wall is particularly thick about its anterior and posterior margins, 1.3 and 1.8 mm respectively, despite the small size of the actual element.

Elements of the pelvic girdle are unfused and lie loose about the femur. A large circular opening approximately one third along the posterior margin of the pubis represents the obturator foramen, which is fully enclosed within the ischiopubic plate later in ontogeny. A small, tear-drop shaped foramen is observed on the medial face of the pubis, directly adjacent to the obturator foramen. What little can be observed of the ischium suggest that it is largely flat, with a sub-triangular outline.

On the femur a prominent, sub-triangular development, representing the “greater” (Bennett, 2001; Kellner and Tomida, 2000) or “lesser” (Hutchinson, 2001) trochanter, is observed lateral to the femoral collum and occupies the dorsolateral margin of the shaft. The trochanter grades medially into a steep walled excavation, which represents the likely insertion of *m. iliofemoralis*, and subsequently pierces the interior of the bone.

## 4. Discussion

### 4.1. Ontogenetic status

Bennett (1993, 1995, 1996) described three indicators of ontogenetic maturity in *Pteranodon* that are equally applicable here: the

degree of skeletal fusion; degree of epiphysal ossification; and degree of pitting on the cortex (i.e. bone grain). The described specimen is considered mature by the first condition as there is no pitting and the cortex is smooth, however, the epiphyses remain unfused (but well ossified) to their associated element, and the very poor degree of skeletal fusion indicates that the animal was juvenile when it died. The relative timing of suture closure within pterosaurs remains an area that requires further exploration as only the early fusion of the cranial elements and fusion of the extensor tendon process towards the end of ontogeny appear to have been consistently reported (Eck et al., 2011). Despite this, a crocodile-like, posterior-to-anterior pattern of fusion between the neural arch and vertebral body has been demonstrated within the ornithocheirids (Kellner and Tomida, 2000), although unlike modern crocodiles the mid-cervicals (i.e. 3–7) fuse early in ontogeny. As such the presence of disarticulation between the vertebral corpora of the dorsal vertebrae and their respective neural arches within the described specimen, unfused sutures within posterior cervicals (or anterior dorsals), unfused epiphyses of the humeri and ulna, distinct scapula and coracoid elements, individual carpalia, an unformed pelvic girdle, and loose ribs are all indicative that the animal must have been relatively juvenile at the time of its death and a long way off what would be considered an osteologically mature state.

### 4.2. Trabeculae orientation

The bones of the specimen show the pattern of trabeculae orientation and distribution commonly observed within other pterosaurs, where the long bones are pneumatic with concentrations of trabeculae in the proximal and distal margins of the bone and substantially fewer in the middle. This is well illustrated by the radius, which has broken open by its distal margin. The trabeculae show a mixture of orientations, typically two perpendicular to each other but reinforced in only one direction to resist compressive loads on the bone (Habib, 2008). Examples of these reinforcement patterns are visible in Fig. 3 and illustrate that the trabeculae adopted a variety of orientations among different elements to suit the local loading conditions. The trabeculae of the humeral epiphyses (Fig. 3B) are therefore orientated mediolaterally to resist the compressive forces generated by flexion of the elbow while those of the sternal plate are orientated dorsoventrally. Within the corpora of the dorsal vertebrae the trabeculae are arranged in a fan-like pattern, roughly perpendicular to the outer bone wall (Fig. 3A).

### 4.3. Pneumatic invasions

Along with both derived saurischian dinosaurs lineages (sauropods and theropods), pterosaurs represent the only other vertebrate to have evolved an extensively pneumatic skeleton (Wedel, 2005, 2006, 2009; Butler et al., 2009). As in birds, the observed degree of pneumaticity in pterosaurs increases with body size (Bonde and Christiansen, 2003; Claessens et al., 2009), and is thus tied to some degree with phylogeny, where derived pterodactyloids become substantially larger than even the biggest of non-pterodactyloid taxa (Hone and Benton, 2007).

While O'Connor's (2006) examination of extinct archosaurs determined that a large foramen or communicating fossa that pierces the compacta and exits into a large internal chamber remains the only reliable and consistent means of diagnosing pneumaticity, distinguishing pneumatic openings from their vascular counterparts remains problematic for pterosaurs (see also Wedel, 2009). Preservational artefacts means that generally only one of two possible situations is observed: firstly where the external surface of the bone showing a penetrating pneumatopore is visible

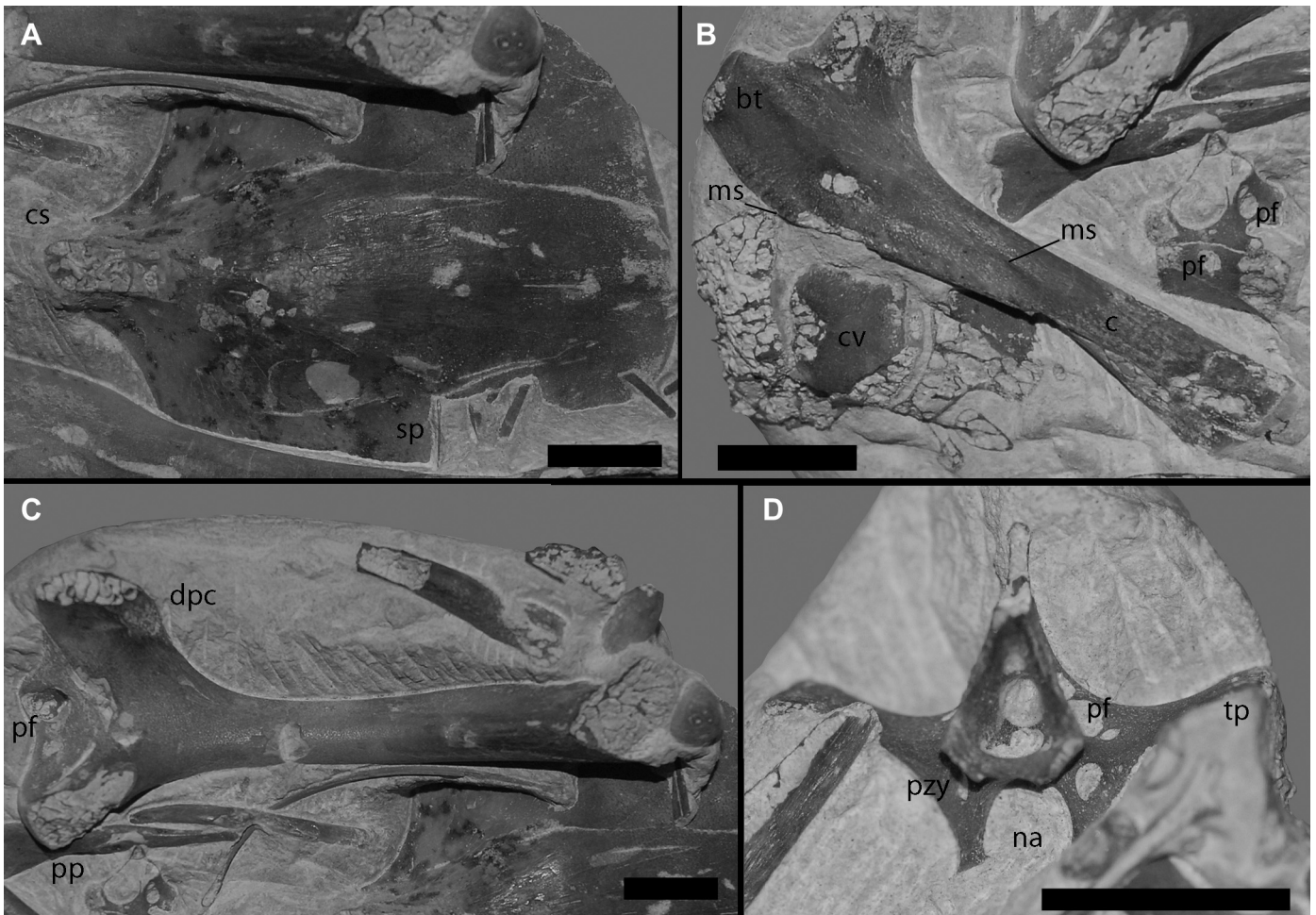


**Fig. 2.** Photographs illustrating points of anatomical interest in SMNK PAL 3985. A, sternal plate and cristospine; B, coracoid; C, left humerus and epiphyses; D, ventral aspect of a thoracic vertebrae. Abbreviations: bt, biceps tubercle; c, coracoid; cs, cristospine; cv, cervical vertebrae; dpc, deltopectoral crest; ms, muscle scar; na, neural arch; pf, pneumatic foramen; pp, posterior process; sp, sternal plate. Scale bar = 10 mm.

or, alternatively (as is the case here), erosion or damage to the internal surface exposes the internal structure at the expense of surface features. Furthermore, biological factors such as specific gravity of the bone and a reduction in oil and marrow content cannot be observed (Hunter, 1774) and the literally paper thin bones of the pterosaurian skeleton mean that almost all foramina or fossi that penetrate the cortex will inevitably open into a large internal cavity.

The confirmation of pneumatic elements from the two diagnostic criteria of O'Connor's (2006) must therefore be based on multiple specimens of a single taxon or, where these do not exist, must instead be inferred from allied or closely related specimens with differing states of preservation, the most parsimonious pneumatic state being subsequently adopted. Within pterodactyloid bones, and more specifically those attributed to the azhdarchoids, pneumatic foramina are known to pierce the sternum (SMNK PAL 1133), coracoid (SMNK PAL 1269), humerus (SMNK PAL 3985, Zhou, 2010; Eck et al., 2011), ulna (SMNK PAL 3986), distal manual carpals (Lü et al., 2006), first wing-finger phalanx (SMNK PAL 6595, Lü and Yuan, 2005), ilium (Naish et al., 2013), cervical and dorsal vertebrae, cervical and notarial ribs (SMNK PAL 3856, SMNK PAL 1133), dorsal ribs (SMNK PAL 1133), and the femur (SMNK PAL 3900; Eck et al., 2011). Pneumatic elements in SMNK PAL 3985 that are supported by the presence of pneumatic foramina are confined to the several cervical and thoracic vertebrae, the humerus, ulna, carpal

elements and femur, whilst inferred elements based on the related taxa above include the sternum, coracoid and first wing-finger phalanx, as well as many additional bones from the cervical and thoracic vertebral column (Fig. 4). A large, trabeculae-supported cavity observed within the thoracic ribs of SMNK PAL 3985 is also inferred as forming part of the pneumatic system as pneumatic foramina are known to pierce the bone between the capitulum and tuberculum on the medioventral margin of the cervical and anterior dorsal ribs (SMNK PAL 3856), and extend as far as the single headed ribs of the posterior dorsals (SMNK PAL 1133). The same principle is also applied to the pubis, which is here pierced by a small foramen and known to be pneumatic in ornithocheiroids (Claessens et al., 2009) as well as in the azhdarchoid SMNK PAL 6607 (RAE pers. obs).

Through direct observation the pneumatic system in the described specimen can thusly be traced up to the carpus in the forearm, into the posterior dorsal vertebrae of the axial column, and the femur. Whilst it is reasonable, and probably more parsimonious to therefore infer that the pneumatic system extended into the sternum, ribs, first phalanx of the wing finger and the pelvic girdle, from which the diverticulae penetrating the femur may have developed a subcutaneous connection (O'Connor, 2006), we concede that this cannot be absolutely verified for this specimen. The extent of inferred pneumatization present within SMNK PAL 3985 nonetheless agrees well with the accounts of other azhdarchoid pterosaurs.

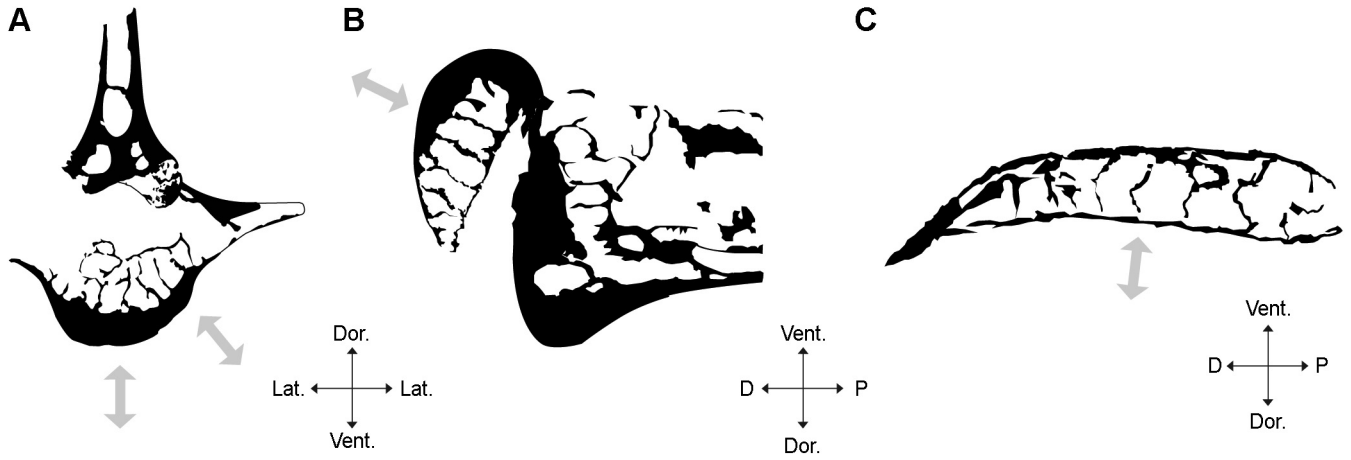


**Fig. 3.** Orientation of the trabeculae supports within three bone structures. A, dorsal vertebrae; B, humeral epiphysis; C, deltopectoral crest of the humerus. The trabeculae are reinforced primarily in a single direction to resist the local compressive loads (shown as a grey arrow). Abbreviations: D, distal; Dor., dorsal; Lat., lateral; P, proximal; Vent., ventral.

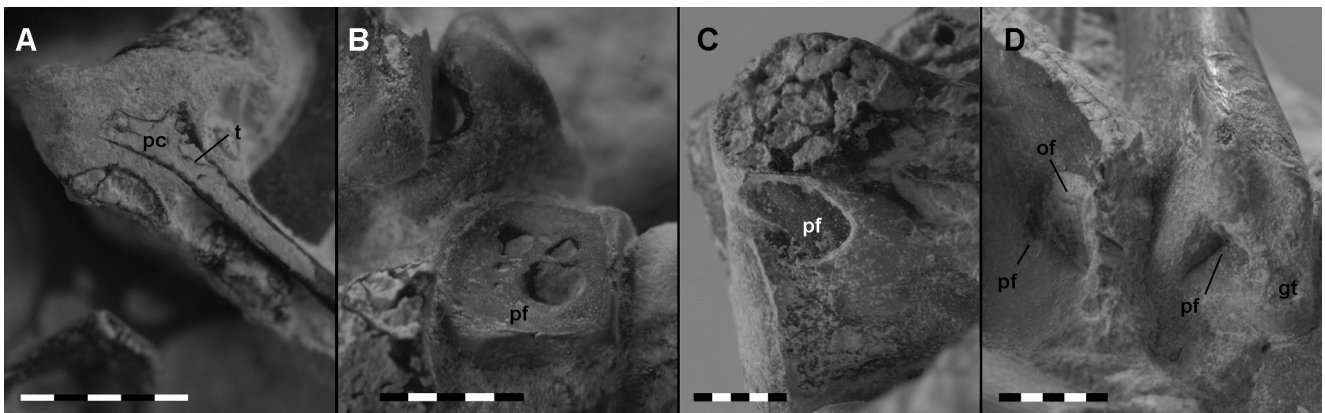


**Fig. 4.** Major pneumatopores and pneumatic cavities visible within the described specimen. A, dorsal rib and its internal pneumatic cavity; B, distal ventral carpal in ventral view; C, proximal ulna in anterior view; D, isolated pubis (left of the photograph) and the dorsal portion of the femur (right). Abbreviations: gt, greater trochanter; of, obturator foramen; pc, pneumatic cavity; pf, pneumatic foramen. All scale bars = 5 mm.

The location of pneumatic foramina in pterosaurs is notable for its variability where, despite many of the same elements being incorporated into the pneumatic system, the exact location of the pneumatopores changes between even closely related taxa. Large pterodactyls for example differ from *Rhamphorhynchus* by developing a large pneumatic foramen on the dorsal surface of the sternal plate rather than on the cristospine, but also differ from each other in the placement of the brachial and antebrachial foramina (Kellner and Tomida, 2000; Bonde and Christiansen, 2003; Lü et al., 2009). Variation of pneumatopore location within azhdarchoids (e.g. *Tupuxuara*, *Quetzalcoatlus*) and other pterodactyl taxa (e.g. *Pteranodon*, *Anhanguera*, *Coloborhynchus*), most noticeable between the humeri, lead Claessens et al. (2009) to suggest an independent origin and evolution of pneumatization within various lineages of Pterosauria. The relationships of pneumatopore development in pterosaurs, however, remain poorly understood and while the presence of a large foramen on the ventral surface of the humerus, observed in the described specimen, is a common feature of azhdarchoids, it is certainly not unique to them, being also found in *Pteranodon* (Bennett, 2001). Furthermore while the ventrally located foramen is in clear contrast to that of the ornithocheiroids, whose own humerus is pierced by a pneumatopore on its posteriodorsal surface where the posterior process merges with the neck, hybrid configurations where

pneumatopores pierce both the dorsal and ventral surfaces of the bone are also known (Wang et al., 2009; Eck et al., 2011), acting as a potential transitional state between the “ornithocheiroid” and “azhdarchoid” pneumatic configurations.

**Table 1**

Average cortex thickness and corresponding air space proportions (ASP) for selected bone elements of SMNK PAL 3985. Both bone wall thickness and the ASP were calculated from digital photographs of the individual elements using the measuring tools of Adobe Photoshop CS3 where ASP is equal to the gas filled component of the bone/total cross sectional area.

| Element                            | Average cortex thickness (mm) | ASP  |
|------------------------------------|-------------------------------|------|
| Sternal plate                      | 0.06                          | –    |
| Dorsal rib                         | 0.14                          | 0.77 |
| Left humerus (shaft)               | 0.42                          | –    |
| Left humerus (deltopectoral crest) | 0.19                          | –    |
| Right radius                       | 0.28                          | –    |
| Left radius/ulna                   | 0.32                          | –    |
| Wing-finger phalanx                | 0.65                          | 0.27 |
| Pubis                              | 0.06                          | –    |
| Ischium                            | 0.12                          | –    |
| Left femur                         | 0.53                          | –    |
| Right femur                        | 0.56                          | 0.66 |
| Right tibia                        | 0.52                          | 0.72 |

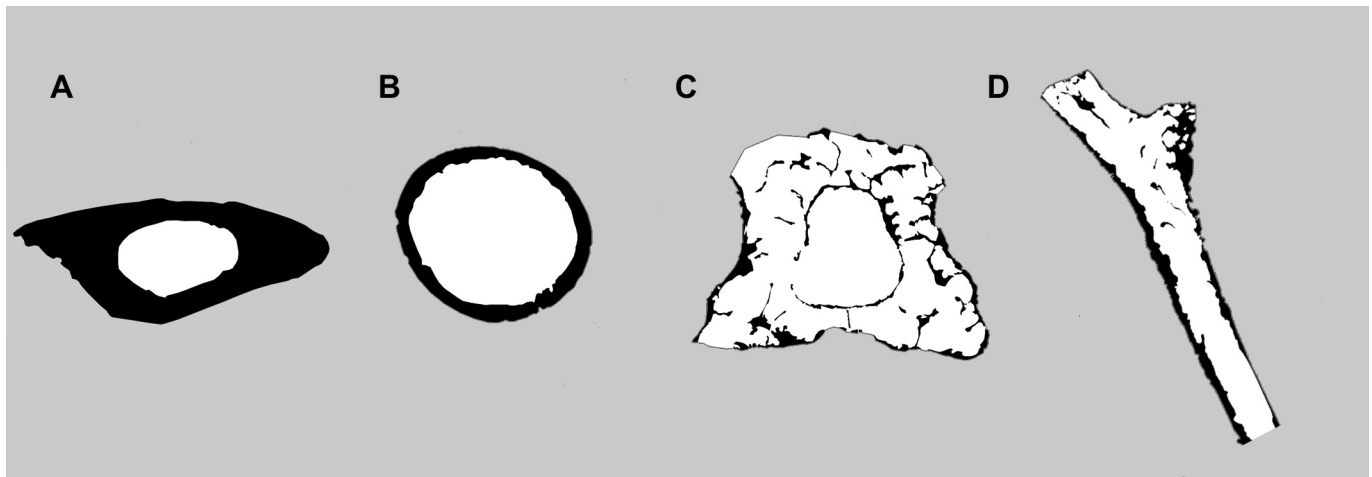


**Fig. 5.** Cross sections through several bone elements used for determining the ASP values where, black = bone; white = air space. A, 3rd phalanx of digit IV; B, right tibia; C, cervical vertebrae; D, posterior dorsal rib.

The described specimen confirms the presence of a large foramen on the anterior face of the ulna, adjacent to the proximal articulation (Fig. 4C), however, caution is advised against applying this observation too broadly as the placement of foramina on the ulna appears variable even between closely related taxa. Comparisons between *Pteranodon* specimens YPM 1181 and YPM 2767 (Bennett, 2001) highlight the degree of variation that can exist as the foramen in the former is found on the anterior face of the proximal articulation while in the latter it is found on the posterior surface. Likewise the holotype of *Anhanguera araripensis* (BSP 1982 I 89) preserves a pneumatic formation on the anterior side of the distal portion of the bone but this is not observed in any other Santana pterosaur (Kellner and Tomida, 2000).

The extent that the vertebral pneumatization invades even the smallest of elements is effectively illustrated within the dorsal ribs, where internal chambers within the head and proximal shaft are expansive (Fig. 4A) and the bone wall thickness, which averages at 0.14 mm, can shrink to a minimum of 0.03 mm (Table 1). Other thin-walled elements all with trabeculae and large pneumatic cavities include the pubis (0.06 mm), and ischium (0.12 mm), but relative measures of the degree to which the pneumatic system has hollowed out a bone is required. One method is to calculating K, or the ratio of the outer cortex circumference to that of the inner, however this is effective for only tubular bones. For the more complex geometries of bones encountered here we calculate the Air-space proportion (ASP) of the element following the methodology of Wedel (2005). Here the exposed cross sections were digitally recorded and imported into the Adobe Illustrator software package. The bone wall and empty spaces were subsequently traced, converted into black and white pixels respectively before being transferred to Adobe Photoshop. This allowed a count of the number of black to white pixels within the image, where the proportion of the element that is filled with gas would be, (number of white pixels)/(number of black + white pixels).

The highest value that was found in the specimen described here belongs to a partial cervical that scored an ASP value of 0.83 (Fig. 5, Table 1), indicating that the bones are comparable to some sauropods, whose cervical vertebrae were also highly pneumatic (Schwarz et al., 2007), and approach the maximum value calculated by Wedel (2005, i.e., 0.89 in *Sauroposeidon*). A single thoracic rib was calculated to have an ASP of 0.77, and two long bones, suggested to be the right femur and tibia based on their relative positions within the concretion, had values of 0.66 and 0.72,

respectively. The phalanx of the wing finger with its triangular cross-section and thicker cortex had the lowest observed ASP of only 0.27 (Table 1). While the limitations of this technique are apparent and the values obtained are highly dependant on which section the bone can be observed, it nonetheless provides an objective value for comparing bone space both within and between individual skeletons. The degree to which the pneumatic invasions filled these elements is central to the reduction of mass within the pterosaurs and was likely a key development that allowed them to reach giant sizes (O'Connor, 2009). Even for smaller animals the reduction in mass must have been of significant benefit and represented an energy saving in transport costs.

Although the described specimen is considered a juvenile on the basis on several unfused sutures there must have been great potential to develop postcranial air sacs in even younger animals with equally thin walled bones. In domestic fowl there is a rapid development of an extensive system of air sacs throughout their postcranial skeleton after hatching. The earliest development of this system within the humerus and cervical vertebrae occurs 28 days after hatching with the remainder of the vertebral column becoming pneumatic after 77 days, although it is noted that some synsacral vertebrae do not form part of this system until at least 182 days post hatching (Hogg, 1984). While the possible volant nature of pterosaur hatchlings (Unwin, 2006) has proven controversial (Prondvai et al., 2012), we note that juveniles below a sub-adult status may have been largely pneumatic, and the acquisition of such a system close to, or shortly after, hatching would have doubtless been of significant benefit to an animal flying for the first time.

## 5. Conclusions

The described specimen is that of an azhdarchoid pterosaur from the Santana Formation of NE Brazil where a combination of three dimensional preservation and a limited degree of cortex damage allows for an accurate determination of the bone wall thickness and confirms the extent of skeletal pneumaticity in these animals, as has been mapped by other workers (e.g., Bonde and Christiansen, 2003; Claessens et al., 2009). While the authors agree that a foramen penetrating the cortex and coinciding with a large internal cavity remains the most reliable means of determining the presence of pneumatic elements (O'Connor, 2006) it is appropriate (or indeed necessary) where the preservation of the

specimen cannot confirm to both of these requirements to infer the most parsimonious pneumatic state based on the material of closely related taxa.

The range of variation observed in the positioning of pterosaurian pneumatopores indicates that even closely allied specimens, the foramina need not be found in the same location and that inferring phylogenetic implications from this data may be problematic. While the hypothesis of an independent origin of the pneumatic system in ornithocheiroids and azhdarchoids requires further investigation (Claessens et al., 2009), the presence of intermediate forms of humeral pneumaticity suggests that the very large degree of positional variations inherently present within the Pterosauria may itself potentially account for such discrepancies (Eck et al., 2011).

SMNK PAL 3985 was still morphologically immature upon its death confirming that the pneumatic system was well developed within juvenile individuals and penetrated even some of the smallest bones of the body. The air-space proportions of these bones are typically high and fall within the range observed in sauropod dinosaurs (typically >0.50, Wedel, 2005), although these values are greatly reduced in those distal wing-finger phalanges. The increasing extent of the air sac system is generally credited with allowing derived pterosaurs to grow to large sizes but the corresponding reduction in skeletal mass may have permitted the redistribution of mass around the animal, and potentially even contributed towards the larger and more elaborate cranial crests that developed in several taxa. In addition to this, if the hypothesis of volant juveniles is accepted then the invasion of the pneumatic system into extremely thin bones may have been beneficial to very young animals.

## Acknowledgements

The authors extend their thanks to “Dino” Frey for allowing access to the described specimen and help with proof reading. Matt Wedel is thanked for discussion of pneumatic characteristics along with Patrick O’Connor and two anonymous referees for their constructive criticisms.

## References

- Bennett, S.C., 1993. The ontogeny of *Pteranodon* and other pterosaurs. *Paleobiology* 19, 92–106.
- Bennett, S.C., 1995. A Statistical study of *Rhamphorhynchus* from the Solnhofen Limestone of Germany: Year-classes of a single large species. *Journal of Palaeontology* 69, 569–580.
- Bennett, S.C., 1996. Year-classes of pterosaurs from the Solnhofen limestone of Germany: taxonomy and systematic implications. *Journal of Vertebrate Paleontology* 16, 432–444.
- Bennett, S.C., 2001. The osteology and functional morphology of the Late Cretaceous pterosaur *Pteranodon*, Part 1. General description of osteology. *Palaeontographica A* 260, 1–112.
- Bennett, S.C., 2003. Morphological evolution of the pectoral girdle of pterosaurs: myology and function. In: Buffetaut, E., Mazin, J.-M. (Eds.), *Evolution and Palaeobiology of Pterosaurs*, Geological Society, London, Special Publications 217, pp. 191–215.
- Bonde, N., Christiansen, P., 2003. The detailed anatomy of *Rhamphorhynchus*: axial pneumaticity and its implications. In: Buffetaut, E., Mazin, J.-M. (Eds.), *Evolution and Palaeobiology of Pterosaurs*, Geological Society, London, Special Publications 217, pp. 217–232.
- Bramwell, C.D., Whitfield, G.R., 1974. Biomechanics of *Pteranodon*. *Philosophical Transactions of the Royal Society, London, B* 267, 503–581.
- Brower, J.C., 1980. Pterosaurs: How they flew? *Episodes* 4, 21–24.
- Brower, J.C., 1983. The aerodynamics of *Pteranodon* and *Nyctosaurus*, two large pterosaurs from the Upper Cretaceous of Kansas. *Journal of Vertebrate Paleontology* 3, 84–124.
- Butler, R.J., Barrett, P.M., Gower, D.J., 2009. Postcranial skeletal pneumaticity and air-sacs in the earliest pterosaurs. *Biology Letters*. <http://dx.doi.org/10.1098/rsbl.2009.0139>.
- Claessens, L.P.A., O’Connor, P.M., Unwin, U.M., 2009. Respiratory evolution facilitated the origin of pterosaur flight and aerial gigantism. *PLoS One* 4. <http://dx.doi.org/10.1371/journal.pone.0004497>.
- Cubo, J., Casinos, A., 2000. Incidence and mechanical significance of pneumatization in the long bones of birds. *Zoological Journal of the Linnean Society* 130, 499–510.
- Eck, K., Elgin, R.A., Frey, E., 2011. On the osteology of *Tapejara wellnhoferi* Kellner 1989 and the first occurrence of a multiple specimen assemblage from the Santana Formation, Araripe Basin, NE-Brazil. *Swiss Journal of Palaeontology*. <http://dx.doi.org/10.1007/s13358-011-0024-5>.
- Elgin, R.A., Campos, H.B.N., 2011. A new specimen of the azhdarchoid pterosaur *Tapejara wellnhoferi*. *Historical Biology*. <http://dx.doi.org/10.1080/08912963.2011.613467>.
- Frey, E., Tischlinger, H., Buchy, M.-C., Martill, D.M., 2003a. New specimens of Pterosauria (Reptilia) with soft parts with implications for pterosaurian anatomy and locomotion. In: Buffetaut, E., Mazin, J.-M. (Eds.), *Evolution and Palaeobiology of Pterosaurs*, Geological Society, London, Special Publications 217, pp. 233–266.
- Frey, E., Martill, D.M., Buchy, M.-C., 2003b. A new species of tapejarid pterosaur with soft-tissue head crest. In: Buffetaut, E., Mazin, J.-M. (Eds.), *Evolution and Palaeobiology of Pterosaurs*, Geological Society, London, Special Publications 217, pp. 65–72.
- Habib, M.B., 2008. Comparative evidence for quadrupedal launch in pterosaurs. *Zitteliana B28*, 159–166.
- Henderson, D.M., 2010. Pterosaur body mass estimates from three-dimensional mathematical slicing. *Journal of Vertebrate Paleontology* 30, 768–785. <http://dx.doi.org/10.1080/02724631003758334>.
- Hogg, D.A., 1984. The development of pneumatization in the postcranial skeleton of the domestic fowl. *Journal of Anatomy* 139, 105–113.
- Hone, D.W.E., Benton, M.J., 2007. Cope’s Rule in the Pterosauria and differing perceptions of Cope’s Rule at different taxonomic levels. *Journal of Evolutionary Biology* 20, 1164–1170.
- Hunter, J., 1774. An account of certain receptacles of air, in birds, which communicate with the lungs, and are lodged both among the fleshy parts and in the hollow bones of those animals. *Philosophical Transactions of the Royal Society of London* 64, 205–213.
- Hutchinson, J., 2001. The evolution of femoral osteology and soft tissues on the line to extant birds (Neornithes). *Zoological Journal of the Linnean Society* 131, 169–197.
- Kellner, A.W.A., Tomida, Y., 2000. Description of a new species of Anhangueridae (Pterodactyloidea) with comments on the pterosaur fauna of the Santana Formation (Aptian-Albian), Northeastern Brazil. *National Science Museum Monographs Tokyo* 17, 1–135.
- Kellner, A.W.A., Wang, X., Tischlinger, H., Campos, D.A., Hone, D., Meng, X., 2010. The soft tissue of *Jeholopterus* (Pterosauria, Anurognathidae, Batrachognathinae) and the structure of the pterosaur wing membrane. *Proceedings of the Royal Society B*. <http://dx.doi.org/10.1098/rspb.2009.0846>.
- Lü, J.-C., 2003. A new pterosaur: *Beipiaopterus chenianus*, gen. et sp. nov. (Reptilia: Pterosauria) from the Western Liaoning Province of China. *Memoir of the Fukui Prefectural Dinosaur Museum* 2, 153–160.
- Lü, J.C., Yuan, C., 2005. New Tapejarid Pterosaur from Western Liaoning, China. *Acta Geologica Sinica* 79, 453–458.
- Lü, J.-C., Liu, J., Wang, X., Gao, C., Meng, Q., Ji, Q., 2006. New material of pterosaur *Sinopterus* (Reptilia: Pterosauria) from the Early Cretaceous Jiufotang Formation, Western Liaoning, China. *Acta Geologica Sinica* 80, 783–789.
- Lü, J.-C., Unwin, D.M., Jin, X., Liu, Y., Ji, Q., 2009. Evidence for modular evolution in a long-tailed pterosaur with a pterodactyloid skull. *Proceedings of the Royal Society B*. <http://dx.doi.org/10.1098/rspb.2009.1603>.
- Martill, D.M., Frey, E., 1999. A possible azhdarchid pterosaur from the Crato Formation (Early Cretaceous, Aptian) of northeast Brazil. *Geologie en Mijnbouw* 78, 315–318.
- Martill, D.M., 2007. The age of the Cretaceous Santana Formation fossil Konservat Lagerstätte of north-east Brazil: a historical review and an appraisal of the biostratigraphic utility of its biota. *Cretaceous Research* 29, 895–920.
- Naish, D., Simpson, M., Dyke, G., 2013. A new small-bodied azhdarchoid pterosaur from the Lower Cretaceous of England and its implications for pterosaur anatomy, diversity and phylogeny. *PLoS One* 8, e58451. <http://dx.doi.org/10.1371/journal.pone.0058451>.
- O’Connor, P.M., 2006. Postcranial Pneumaticity: An evaluation of soft-tissue influences on the postcranial skeleton and the reconstruction of pulmonary anatomy in archosaurs. *Journal of Morphology* 267, 1199–1226.
- O’Connor, P.M., 2009. Evolution of archosaurian body plans: skeletal adaptations of an air-sac-based breathing apparatus in birds and other archosaurs. *Journal of Experimental Zoology* 8, 629–646. <http://dx.doi.org/10.1002/jez.548>.
- Prondvai, E., Stein, K., Osi, A., Sander, M.P., 2012. Life history of *Rhamphorhynchus* inferred from bone histology and the diversity of pterosaurian growth strategies. *PLoS One* 7, e31392. <http://dx.doi.org/10.1371/journal.pone.0031392>.
- Sato, K., Sakamoto, K.Q., Watanuki, Y., Takahashi, A., Katsumata, N., Bost, C.-A., Weimerskirch, H., 2009. Scaling of soaring seabirds and implications for flight abilities of giant pterosaurs. *PLoS One* 4, e5400. <http://dx.doi.org/10.1371/journal.pone.0005400>.
- Schwarz, D., Frey, E., Meyer, C.A., 2007. Pneumaticity and soft-tissue reconstructions in the neck of diplodocid and dicraeosaurid sauropods. *Acta Palaeontologica Polonica* 52, 167–188.
- Schwarz-Wings, D., Meyer, C.A., Frey, E., Manz-Steiner, H.-R., Schumacher, R., 2010. Mechanical implications of pneumatic neck vertebrae in sauropod dinosaurs. *Proceedings of the Royal Society B*. <http://dx.doi.org/10.1098/rspb.2009.1275>.

- Steel, L., 2008. The palaeohistology of pterosaur bone: an overview. *Zitteliana* B28, 109–126.
- Unwin, D.M., 2003. On the phylogeny and evolutionary history of pterosaurs. In: Buffetaut, E., Mazin, J.-M. (Eds.), *Evolution and Palaeobiology of Pterosaurs*, Geological Society, London, Special Publications 217, pp. 139–190.
- Unwin, D.M., 2006. Pterosaurs: from deep time. Pi Press, 352pp.
- Wang, X., Zhou, Z., 2003. A new pterosaur (Pterodactyloidea, Tapejaridae) from the Early Cretaceous Jiufotang Formation of western Liaoning, China and its implications for biostratigraphy. *Chinese Science Bulletin* 48, 16–23.
- Wang, X., Kellner, A.W.A., Jiang, S., Meng, X., 2009. An unusual long-tailed pterosaur with elongated neck from western Liaoning of China. *Anais da Academia Brasileira de Ciências* 81, 793–812.
- Waiser, G.W., 2007. *The Inner Bird: Anatomy and Evolution*. UBC Press, Vancouver, Canada, 386pp.
- Wedel, M.J., 2005. Postcranial skeletal pneumaticity in sauropods and its implications for mass estimates. In: Curry Rogers, K.A., Wilson, J.A. (Eds.), *The Sauropods: Evolution and Paleobiology*. University of California Press, Berkeley, pp. 201–228.
- Wedel, M.J., 2006. Origin of postcranial skeletal pneumaticity in dinosaurs. *Integrative Zoology* 2, 80–85.
- Wedel, M.J., 2009. Evidence for Bird-Like Air Sacs in Saurischian Dinosaurs. *Journal of Experimental Zoology* 311A, 611–628.
- Wellnhofer, P., 1991. Weitere pterosaurierfunde aus der Santana. Formation (Apt) der Chapada do Araripe, Brasilien. *Palaeontographica A* 215, 43–101.
- Witmer, L.M., Chatterjee, S., Franzosa, J., Rowe, T., 2003. Neuroanatomy of flying reptiles and implications for flight, posture and behaviour. *Nature* 425, 950–953.
- Witton, M.P., 2008. A new approach to determining pterosaur body mass and its implications for pterosaur flight. *Zitteliana* B28, 143–158.
- Witton, M.P., Habib, M.B., 2010. On the size and flight diversity of giant pterosaurs, the use of birds as pterosaur analogues and comments on pterosaur flightlessness. *PLoS One* 5, e13982. <http://dx.doi.org/10.1371/journal.pone.013982>.
- Zhou, C.F., 2010. New material of *Chaoyangopterus* (Pterosauria: Pterodactyloidea) from the Early Cretaceous Jiufotang Formation of western Liaoning, China. *Neues Jahrbuch für Geologie und Paläontologie* 257, 341–350.

**Show me your sutures, I tell you your age: Age traces in a young *Anhanguera* skeleton.**

Ross A. Elgin & Eberhard Frey  
Staatliches Museum für Naturkunde Karlsruhe, Germany.

The reconstruction of the pterosaurian ontogenetic sequence is complicated by a number of factors including a lack of extant relatives, crushed and isolated bones and low numbers of useful specimens for each taxon. Where sufficient material is available, however, the closure of key sutures could be a good method to assess the relative morphological maturity of fossil vertebrates. Extant tetrapods may serve as a model for extinct animals. Brochu (1996) demonstrated that during crocodylian ontogeny the neurocentral sutures closed following a caudal to cranial pattern while the scapula and coracoid in extant crocodiles and alligators would reach their closed, morphologically mature state late in life (Brochu 1995).

For pterosaur, the suture/fusion state was used in conjunction with size dependant characters by Wellnhofer (1975) to distinguish between juvenile and adult specimens of *Rhamphorhynchus*. However, size dependant features are unreliable characters for determining maturity in extinct animals, because intraspecific variations in genetics, environmental conditions and the supply of food may result in similar aged individuals being of very different sizes. Thus, a calibration of the maturity based on sutures size is impossible. Bennett (1993) successfully demonstrated this in populations of *Pteranodon* where animals with juvenile characteristics, based on fusion state, epiphyseal ossification and bone grain, were not of a significantly different size to fully mature adults. Due to the fragmentary nature of the specimens Bennett (1993) stated that the exact order of element fusion could not be determined, although he did suggest that the atlas-axis complex, scapulocoracoid, secondary ossification centres of the humerus, cranial notarial vertebrae and ribs fused before other elements. The extensor tendon process (olecranon *sensu* Wellnhofer 1991), however, remained unfused in *Pteranodon* until just before skeletal maturity.

Kellner & Tomida (2000) also discussed the ontogeny of pterosaurs but based their arguments on a large juvenile specimen of *Coloborhynchus* and other well preserved members of ornithocheiroids from Brazil. Their work and conclusions form the base for this study.

Here we describe a new sub-complete specimen of ?*Anhanguera* with several enigmatic features including a relatively short first wing finger phalanx of comparable size to that of a short winged form from the Cenomanian of Lebanon (Dalla Vecchia et al 2001). Secondly while, like all previous anhanguerids, the specimen is clearly a juvenile it also displays a number of more advanced closure states and mature characteristics including a partially fused notarium and extensor tendon process. This combined with other material housed at the Staatliches Museum für Naturkunde Karlsruhe (SMNK) is used to provide the most detailed evaluation of ornithocheiroid ontogeny to date. Here we propose that suture closure follows the general pattern of:

- 1) Fusion of the cranial elements
- 2) Fusion of vertebral elements



- 3) Initial development of a notarium
- 4) Fusion of the scapulocoracoid
- 5) Fusion of the extensor tendon process to the first wing finger
- 6) Fusion of epiphyses and formation of the tibiotarsus

In a number of specimens, however, deviations from this pattern are observed, indicating that the possible stages of suture closure could overlap quite substantially or that, more likely, the order of suture closure was variable between members of the ornithocheiroids. A similar change in the onset of suture closure has been demonstrated in the scapula and coracoid of *Alligator* and *Caiman* (Brochu 1995). While this highlights the problems of determining the ontogenetic sequence in pterosaurs, even between closely related taxa, our results do provide a useful sequence and framework for dating relative maturity that can easily incorporate newly discovered specimens as they come to light.

#### References:

- Bennett, S.C. 1993. The ontogeny of *Pteranodon* and other pterosaurs. *Paleobiology* 19(1): 92-106.
- Brochu, C.A. 1995. Heterochrony in the Crocodylian Scapulocoracoid. *Journal of Herpetology* 29(3): 464-468.
- Brochu, C.A. 1996. Closure of the neurocentral sutures during crocodylian ontogeny: implications for maturity assessment in fossil archosaurs. *Journal of Vertebrate Paleontology* 16(1): 49-62.
- Dalla Vecchia, F.M., Arduini, P., & Kellner, A.W.A. 2001. The first pterosaur from the Cenomanian (LateCretaceous) *Lagerstätten* of Lebanon. *Cretaceous Research* 22: 219-225
- Kellner, A.W.A., & Tomida, Y. 2000. Description of a new species of Anhangueridae (Pterodactyloidea) with comments on the pterosaur fauna from the Santana Formation (Aptian-Albian), Northeastern Brazil. *National Science Museum Monographs* 17: 1-135.
- Wellnhofer, P. 1975. Die Rhamphorhynchoidea (Pterosauria) der Oberjura-Plattenkalke Süddeutschlands. *Palaeontographica A* 148:1-33, 148:132-186, 149:1-30.

### The problem of the pterosaur wrist.

Ross A. Elgin & Eberhard Frey

Staatliches Museum für Naturkunde Karlsruhe, Germany.

The construction of the pterosaur wrist is a familiar problem for pterosaur workers. Even the best, three dimensionally prepared materials have failed to produce a commonly accepted reconstruction of the carpus. These problems, the articulation and mobility of the pteroid and the function of the preaxial carpal and its sesamoid associated tendon, have dogged all previous reconstructions. The forward directed pteroid sitting in the fovea of the preaxial carpal (Frey & Reiß 1981, Wilkinson et al 2006) has effectively been replaced by a medially directed model (Frey et al 2006, Bennett 2007) where the fovea of the preaxial carpal holds a sesamoid associated with a tendon. Bennett (2007) has argued that the pteroid articulated on to the medial side of the preaxial carpal and the tendon that passed through its fovea inserted on to the fourth metacarpal as an extensor of the wrist, making it *M. flexor carpi ulnaris*. This interpretation is *contra* Frey et al (2006) who instead suggested that the pteroid articulated between the two syncarpal blocks and the tendon ran the length of the metacarpals distally and inserted on to the extensor tendon process of the first wing finger phalanx..

For us the arguments of Bennett (2007) are far from conclusive and in several cases are contradicted by the fossil evidence and taphonomy. We counter the notion that the pteroid articulated on the medial side of the preaxial carpal by noting that:

- i) Until now, in no specimen are the two elements ever preserved in the proposed articulation.
- ii) The articular surface of the pteroid in well preserved and relatively undisturbed specimens is commonly found resting between the proximal and distal syncarpals.
- iii) The articulation surface identified by Bennett (2007) on the preaxial carpal does not exist on any mature specimens housed in the SMNK.
- iv) The nyctosaurid pteroid requires a different explanation and a different articulation point under the model of Bennett (2007). Based on a second specimen of *Muzquizopteryx* in which the articulation surface of the pteroid is preserved it would be impossible to place this against the preaxial carpal leading to multiple points of origin which we deem unlikely.
- v) Under the configuration suggested by Bennett (2007) the pteroid and preaxial carpal would be bound together by muscles and ligaments. Thus, we might expect to find these elements in close association. This is rarely the case and in several specimens the two elements are pulled in opposite directions, the pteroid medially and the preaxial carpal laterally and up against the fourth metacarpal, sometimes very close to the distal insertion point of the tendon of *M. flexor carpi ulnaris* as reconstructed by Bennett (2007).

Reconstruction of the path taken by the tendon is more difficult as there is less taphonomic evidence on which to base any conclusion. Detailed three dimensional

reconstructions of the carpals, metacarpals I-IV and the first wing finger, however, allow the potential paths and insertion points for any long fibred muscle or tendon that passed this way to be examined. This approach is necessary to prevent interference between muscles and other structures such as in Bennett's (2007) reconstruction of the long *M flexor carpi ulnaris*, which is anchored dorsal to the path taken by metacarpals I-III.

Without good evidence, reconstructions that require the restoration of soft tissue take palaeontology to the very edge of its useful limits as a science. None the less, experimental models reconstructing the lever arms and pull of ancient muscles about a frame, based on three dimensionally preserved long bones, can be a very useful tool for the reconstruction of a musculotendinal apparatus. If the results produced can be tied together with the available taphonomy and fossil evidence and do not interfere with other structures then a fairly robust and scientific model can still be produced. Here we present our findings but also argue that the construction of the pterosaur wrist is an issue that is far from being resolved and we encourage further discussion and experimentation in this area.

#### References:

Bennett, S.C. 2007. Articulation and function of the pteroid bone in pterosaurs. *Journal of Vertebrate Paleontology* 27(4): 881-891.

Frey, E. & Riess, J. 1981. A New Reconstruction of the Pterosaur Wing. *N. Jb. Geol. Paläont. Abh.* 161(1): 1-27

Frey, E., Buchy, M-C., Stinnesbeck, W., González González, A., di Stefano, A. 2006. *Muzquizopteryx coahuilensis* n.g., n. sp., a nyctosaurid pterosaur with soft tissue preservation from the Coniacian (Late Cretaceous) of northeast Mexico (Coahuila). *ORYCTOS* 6: 19-39.

Wilkinson, M.T., Unwin, D.M., Ellington, C.P. 2006. High lift function of the pteroid bone and forewing of pterosaurs. *Proceedings of the Royal Society B: Biological Sciences* 273: 119-126.

**Testing the functional significance of cranial crests as an aerodynamic feature within the Pterosauria.**

Ross A. Elgin<sup>1</sup>, Colin Palmer<sup>2</sup>, David W.E. Hone<sup>3</sup>, Carlos A. Grau<sup>2</sup>, Eberhard Frey<sup>1</sup>, Doug Greenwell<sup>4</sup>.

<sup>1</sup>Staatliches Museum für Naturkunde Karlsruhe, Germany; <sup>2</sup>University of Bristol, UK; <sup>3</sup>Institute of Vertebrate Palaeontology and Palaeoanthropology, China; <sup>4</sup>City University, UK.

The unusual and often bizarre cranial crests sported by most pterosaurs appear to demand an unusual or extravagant explanation. Normally the cranial crests have been taken as some kind of aerodynamically beneficial structure perhaps acting as an airbrake (Bramwell & Whitfield 1947), a forward rudder (Heptonstall 1971; Stein 1975) or a means of counterbalancing the head (Eaton 1910; Heptonstall 1971; Bramwell & Whitfield 1974). Very little experimental work exists and previous studies predate the discovery of many of the most interesting and diverse specimens (Bramwell 1971; Bramwell & Whitfield 1974; Stein 1975; Brower 1983). As a result they were hampered by a compelling lack of taxonomic diversity in which the results of *Pteranodon longiceps* were applied to all pterosaurs.

Here we present the first comprehensive study that tests the aerodynamic characteristics of the most basal crested rhamphorhynchoids to the most derived and elaborate azhdarchid pterosaurs. Highly unusual forms including *Nyctosaurus gracilis*, *Tupandactylus imperator* and *Thalassodromeus sethi* are also included for the first time. Here we show that many of the previously proposed aerodynamic effects cannot apply. This gives extra weight to suggestions they were used primarily as display structures (Bennett 1992) and, bearing a streamlined profile, evolved largely independent of any aerodynamic factors. None the less in some cases they were capable of generating large forces which should be considered during future modelling of pterosaurian flight capabilities.

References:

- Eaton, G. F. 1910. Osteology of *Pteranodon*. *Memoirs of the Connecticut Academy of Arts and Science* 2: 1–38.
- Bennett, S. C. 1992. Sexual dimorphism of *Pteranodon* and other pterosaurs, with comments on cranial crests. *Journal of Vertebrate Paleontology* 12: 422–434.
- Bramwell, C. & Whitfield, G. R. 1974. Biomechanics of *Pteranodon*. *Philosophical Transactions of the Royal Society London B* 267: 503–581.
- Brower, J. C. 1983. The aerodynamics of *Pteranodon* and *Nyctosaurus*, two large pterosaurs from the Upper Cretaceous of Kansas. *Journal of Vertebrate Paleontology* 3: 84–124.
- Heptonstall, W.B. 1971. An analysis of the flight of the Cretaceous pterodactyl *Pteranodon ingens* (Marsh). *Scottish Journal of Geology* 7: 61–78.
- Stein, R. S. 1975. Dynamic analysis of *Pteranodon ingens*: a reptilian adaptation to flight. *Journal of Paleontology* 49: 534–548.

**Extreme pneumaticity in pterosaurs**

Ross A. ELGIN<sup>1</sup>, David W.E. HONE<sup>2</sup> & Eberhard FREY<sup>1</sup>.

<sup>1</sup>Staatliches Museum für Naturkunde Karlsruhe, Abteilung Geologie, Erbprinzenstraße 13. 76133 Karlsruhe, Germany. E-mail: rosselgin@hotmail.com

<sup>2</sup>Institute of Vertebrate Palaeontology and Palaeoanthropology (IVPP), Xizhimenwai Dajie 142, Beijing 100044, P. R. China.

Pterosaurs, like fossil and extant birds, developed an extensive system of air sacs within much of their skeletons. This feature appears to have been of great importance for flying animals and has been linked to roles in physiology and weight reduction or redistribution (Claessens et al 2009; Witton 2008). While the idea that dorsal ribs also formed part of the pneumatic system is not particularly novel (e.g. Bennett 2001) a new tapejarid specimen (SMNK PAL 3985) is presented here and indicates that pneumatic invasions entered even the smallest of bones, mostly filling them. The rib in question is interpreted to be one of the smallest pterosaurian elements in which a pneumatic system is visible and the bone wall thickness can be accurately measured as being 0.426mm at its thickest point, by the smaller of the two articular heads, and 0.045mm at its thinnest point, by the larger of the two heads. The rib is interpreted as belong to one of the most cranially located thoracic vertebrae and may have been expected to form part of the notarium later in life. The lack of fusion suggests that the animal was still ontogenetically immature and raises questions as to how such small, hollow ribs were capable to withstanding the large stresses that they were, presumably, subjected too (Bennett 2001, 2003). The pneumatic system thus appears to have been extensively developed in young animals and to have penetrated even the smallest bones. Further analysis is required to determine the taxonomic distribution of the pneumatic system and how it may have developed within the clade.

References:

Bennett, S.C. 2001. The Osteology and Functional Morphology of the Late Cretaceous Pterosaur *Pteranodon*. *Palaeontographica, A.*, 260, 1-153.

Bennett, S.C. 2003. Morphological evolution of the pectoral girdle of pterosaurs: myology and function. In Buffetaut, E and Mazin, J-M, eds. *Palaeobiology and Palaeoecology of Pterosaurs*. London, Geological Society, 191-215.

Claessens, L.P.A.M., O'Conner, P.M., Unwin, D.M. 2009. Respiratory Evolution Facilitated the Origin of Pterosaur Flight and Aerial Gigantism. *PLoS ONE*, 4(2): e4497.doi:10.1371/journal.pone.0004497

Witton, M.P. 2008. A new approach to determining pterosaur body mass and its implications for pterosaur flight. *Zitteliana*, B28, 143 – 158.

**Modelling pterosaur flight dynamics: Initial experimental findings**

Ross A. ELGIN

Staatliches Museum für Naturkunde Karlsruhe, Abteilung Geologie, Erbprinzenstraße 13, 76133 Karlsruhe, Germany. E-mail: [rosselgin@hotmail.com](mailto:rosselgin@hotmail.com)

Pterosaurs were the first vertebrate clade to evolve true powered flight and have attracted the attention of both palaeontologists and aerodynamicists alike. A number of issues, however, are required to be addressed prior to an investigation into their flight characteristics. As part of an ongoing investigation, the workgroup for Pterosaur Flight Dynamics presents its findings to date. We reconstruct the fore-arm and overall joint mobility based on a number of ornithocheiroid and azhdarchoid specimens along with basal taxa including *Dorygnathus*. Mass is theoretically altered so experiments can represent both the suggested “light” (e.g. Bramwell and Whitfield 1974; Brower 1983; Chatterjee and Templin 2004) and “heavy” builds (Prondvai et al. 2008; Witton 2008) attributed to these animals and the wing membrane is demonstrated to have extended to the lower leg or ankle. This pattern appears to have been universally present within the clade (Elgin et al in press).

Using the above reconstructions the flight characteristics of several pterosaurian taxa are examined through both theoretical and experimental approaches. A variety of models were flown in a wind tunnel and the resulting data was contrasted with that of other studies (e.g. Bramwell and Whitfield 1974; Brower 1983; Chatterjee and Templin 2004). Subsequent experiments will construct the wing membrane from materials of different structural properties to simulate and allow the development of more complex patagia and their associated aeroelastic characteristics. This approach is central to understanding the flight of large pterosaurs which must have encountered a range of Reynolds numbers during their development.

**References:**

- Bramwell, C.D., and Whitfield, G.R. 1974. Biomechanics of *Pteranodon*. Philosophical Transactions of the Royal Society, London, B., 267, 503 – 581.
- Brower, J.C. 1983. The Aerodynamics of *Pteranodon* and *Nyctosaurus*, two large pterosaurs from the Upper Cretaceous of Kansas. Journal of Vertebrate Paleontology, 3, 84 – 124.
- Chatterjee, S., and Templin, R.J. 2004. Posture, locomotion and paleoecology of pterosaurs. Geological Society of America, Special Paper, 376. 64pp
- Elgin, R.A., Hone, D.W.E. and Frey, E. Hip, Knee or Ankle?: the extent of the pterosaur wing. Palaeontology, (in press).
- Prondvai, E., Tanács, T., and Frey, E. 2008. Mass estimate of Pterosaurs: A case study on *Rhamphorhynchus* and the problems of finding the best method. 6th Meeting of the European Association of Vertebrate Palaeontology, Spišská Nová Ves. Abstracts.
- Witton, M.P. 2008. A new approach to determining pterosaur body mass and its implications for pterosaur flight. Zitteliana, B28,143 – 158.

**AERODYNAMICS OF PTEROSAUR HEAD CRESTS: THE PROBLEM WITH *NYCTOSAURUS*.**

Ross A. Elgin

Staatliches Museum für Naturkunde Karlsruhe (SMNK), Abteilung Geologie, Erbprinzenstraße 13., 76133 Karlsruhe, Germany. E-Mail: rosselgin@hotmail.com

Many authors have speculated on the function of the pterosaurian cranial crest; proposing that it assisted flight performance by acting as a forward rudder, an airbrake, and/or an aerodynamic counterbalance. More recently the aerodynamics of the North American pterodactyloid *Nyctosaurus* were calculated where, *contra* to fossil evidence, a membranous sail was reconstructed and interpreted as an auxiliary form of flight control. This highlights the dangers of ignoring fossil evidence and relying on aerodynamic data alone to arrive at conclusions about past performance.

The “aerodynamic benefits” of a cranial crest are difficult to disprove from numerical data alone as larger structures will naturally be correlated with an increase in both the torques and forces acting on the skull. However, the diversity in crest size, material composition, and relative location throughout the pterosaur lineage strongly suggests that the evolution of such a feature cannot be tied with a universal form of aerodynamic enhancement; “performance” must have varied greatly between taxa.

Aerodynamic studies on the crania of pterosaurs may still prove useful even when no benefits are noted as many pterodactyloids develop large skulls/crests; the acting forces and torques are unknown and are an important consideration due to yawing and pitching movements of the head. Here we report on the aerodynamic characteristics of a number of derived pterodactyloid taxa, recorded during wind tunnel experiments, as part of a larger study into the aerial characteristics of these Mesozoic fliers.

**WHEN ALL ELSE FAILS: CT SCANNING IN PTEROSAUR RESEARCH**

Ross A. Elgin

Staatliches Museum für Naturkunde Karlsruhe (SMNK), Abteilung Geologie, Erbprinzenstraße 13., 76133 Karlsruhe, Germany. E-Mail: rosselgin@hotmail.com

The Romualdo Formation of NE Brazil is well known by pterosaur researchers as an excellent source of three dimensionally material; where fossil material is encased within a protective concretion. Removing the sediment surrounding such specimens can, however, be problematic as it is both time consuming and damage can occur from either mechanical preparation, or acid seeping into the hollow interior of the bones; slowly destroying portions of the skeleton. Such a condition is found within an almost complete azhdarchoid torso housed within the collections of the SMNK. The specimen itself is scientifically important, reaching a state of morphological maturity unknown from the Romulado Formation where an epineural plate has immobilized the entirety of the vertebral column and mineralized tendons of the *m. spinoarticularis* and *m. articulospinalis* are present along the lateral margins of the neural arches and their spinous processes. Further preparation of the specimen, mechanical or acid, is unlikely to occur in the near future for the above noted reasons. Instead computed tomography (CT) scans, conducted by the Royal Veterinarian College London (RVC), provides a means to determined the three dimensional shape of the bones, observe their internal architecture, and map the extent of the pneumatic system known to have penetrated the majority of the pterodactyloid skeleton. The extent of the pneumatic system, here present throughout the vertebrae and most of the pelvic girdle, is compared with that observed in CT scans of *Anhanguera*.